Author:
Bowen, Emily E

Title:
The Role of the Podocyte in Shiga Toxin Associated Haemolytic Uraemic Syndrome

The Role of the Podocyte in Shiga Toxin Associated Haemolytic Uraemic Syndrome

Dr Emily Elizabeth Bowen

A dissertation submitted to the University of Bristol in accordance with the requirements for award of the degree of Doctor of Philosophy in the Faculty of Health Sciences.

School of Translational Health Sciences

May 2020

Word Count: 79 790

Abstract

Introduction: Haemolytic uraemic syndrome (HUS) is a thrombotic microangiopathy (TMA) that has a predilection to present in the kidney. It is a triad of microangiopathic haemolytic anaemia, thrombocytopenia, and acute kidney injury. In 90% of cases, HUS follows gastroenteritis secondary to infection with Shiga toxin (Stx) producing bacteria such as *Escherichia coli*. Stx HUS is the leading cause of acute kidney injury in children with a mortality of 5%. The precise pathophysiological mechanisms following Stx infection that lead to TMA are poorly understood.

Objective: To investigate whether Stx acts via the podocyte globotriaosylceramide (Gb3) receptor to cause HUS.

Results: To interrogate the pathways activated by Stx in podocytes, total and phospho-proteomic studies in human podocytes versus Gb3 knockout controls were performed. Ingenuity Pathway Analysis showed a significant reduction in VEGF-A signalling in wild type podocytes treated with Stx; suggesting VEGF-A maybe a critical coordinator of Stx HUS.

To illustrate that Gb3 is the receptor for Stx *in vivo*, a constitutive whole body Gb3 knockout mouse (Gb3KO) was generated. Gb3KO mice were completely protected from the toxicity of intraperitoneal Stx even at x400 the lethal dose. All wild type control mice died within 4 days of receiving Stx from extra-glomerular dehydration, as demonstrated by ATN on renal histology.

To determine the role of the podocyte Gb3 receptor *in vivo*, an inducible podocyte expressing Gb3 mouse on a Gb3 null background (PodGb3) was generated. PodGb3 mice given intraperitoneal Stx developed HUS (thrombocytopenia, haemolytic anaemia, and uraemia $p<0.05$) at day 10. Renal histology demonstrated glomerular TMA, with intracapillary thrombus on electron microscopy. Immunofluorescence demonstrated increased glomerular fibrinogen and C3b deposition vs. controls. Additionally, glomerular complement regulator factor H was significantly reduced in PodGb3 mice. Fascinatingly, administration of a C5 inhibitor in this model rescued the HUS phenotype.

Conclusions: The discovery that the podocyte is capable of causing Stx HUS, with activation of complement observed on the glomerular endothelium; is compelling evidence for the importance of glomerular cell cross-talk within the kidney in the development of the disease. This may explain why the glomerulus is the prime target of systemic Stx driven infection and lead to the development of novel therapies to help treat patients with this devastating condition.

Dedication

This thesis is dedicated to my husband James Barr, without whom completion of this PhD would not have been possible. Thank you for believing in me, accepting that we needed to live apart in our first year of marriage and moving your life to Bristol for a year. Your love and support has kept me focused and allowed me to pursue my research ambitions.

Acknowledgements

The work presented in this thesis would not have been possible without the continuous support of my supervisors: Professor Richard Coward and Professor Moin Saleem. Thank you both for all your help and guidance, from initial conception of my research hypothesis through to the design and completion of the project. Throughout the course of this PhD, you have given me invaluable advice, inspired me to achieve beyond what I thought possible and helped me to refine my research skills to become a better scientist. It has been a privilege to work for you.

I am also grateful to Dr Gavin Welsh, Professor Simon Satchell, and Dr Rebecca Foster. Thank you for your insightful and probing questions during renal laboratory meetings as well as the advice, guidance, and mentorship you have all given me over the last few years. Bristol Renal is a fantastic place to work because of your leadership and vision.

Thank you to the Coward group, in particular Dr Jenny Hurcombe and Miss Fern Barrington who have been instrumental in teaching me laboratory techniques, available for advice and discussion to help troubleshoot experimental issues and with whom I have become good friends.

Finally, I must acknowledge the financial support I have received from Kidney Research UK (KRUK) that has funded my clinical research fellowship and made this work possible. Thank you for working tirelessly to raise funds to make kidney research in the UK a priority and ensuring that basic science research remains translational and focused on the patients we hope to benefit.

Author and senior author declaration re. referencing of own published works

During the course of this PhD research project the following review article was published:

'*Bowen EE, Coward RJ. Advances in our understanding of the pathogenesis of hemolytic uremic syndromes. Am J Physiol Renal Physiol. 2018;314(3):F454-F461. doi:10.1152/ajprenal.00376.2017.'*

Text and figures directly taken from this manuscript are included in 'Chapter 1: Introduction' of this thesis. These have been clearly referenced as such. As first author of the review article, I drafted the manuscript and prepared all figures. The senior author of the review article, Professor Richard Coward edited and revised the manuscript, prior to both authors approving the final version before publication.

SIGNED:

Dr Emily Elizabeth Bowen **DATE**: 26th May 2020

(First Author of manuscript)

SIGNED:

Professor Richard Coward **DATE**: 26th May 2020

(Senior Author of manuscript)

Author's declaration

I declare that the work in this dissertation was carried out in accordance with the requirements of the University's *Regulations and Code of Practice for Research Degree Programmes* and that it has not been submitted for any other academic award. Except where indicated by specific reference in the text, the work is the candidate's own work. Work done in collaboration with, or with the assistance of, others, is indicated as such. Any views expressed in the dissertation are those of the author.

SIGNED:

Dr. Emily Elizabeth Bowen **DATE**: 29th May 2020

Table of Contents

List of Figures

List of Tables

Chapter 1 : Introduction

Haemolytic uremic syndrome (HUS) is a major global healthcare issue as it is the leading cause of acute kidney injury in children [1]. The syndrome presents clinically as a triad of acute kidney injury, microangiopathic haemolytic anaemia and thrombocytopenia. It is classified histopathologically, as a glomerular thrombotic microangiopathy (TMA) [2]. In recent years, there have been major advances in our understanding of rare, complement driven, inherited forms of HUS. However 90% of HUS cases are associated with Shiga toxin producing enteric pathogens [3]. The precise pathological pathways in this setting are yet to be elucidated. The purpose of my research is to determine the glomerular mechanisms underlying the action of Shiga toxin. Hence, an understanding of the function of the kidneys in health is required; before the effects of Shiga toxin on this vital organ are explored.

1.1 The kidney

The kidneys are a pair of two "kidney bean shaped" organs located in the retroperitoneal space within the abdominal cavity (Figure 1-1). Together they filter 180 litres of blood a day [4]. The major function of the kidneys is to remove waste products and excess water from the blood via the urine. The production of urine involves a complex series of steps of not only excretion, but also reabsorption of electrolytes and water which is critical to maintain homeostasis [5]. The kidneys also release hormones that regulate blood pressure, control erythropoiesis, maintain acid-base balance and hydroxylate vitamin D to its active form to ensure calcium homeostasis and bone health [5].

1.1.1 The nephron

The functional filtration unit of the kidney is the nephron. Each kidney contains up to 1 million nephrons that consist of a long fine tubule; closed at one end to form Bowman's capsule which encapsulate a tuft of microscopic blood vessels known as the glomerulus [6]. From the Bowman's capsule arises: the proximal tubule, the descending and ascending limbs of the Loop of Henle, the distal tubule and finally the collecting duct [7]. The glomerulus filters the blood and provides a physical barrier to prevent the passage of erythrocytes and protein into the urine. The filtrate is produced in the glomerulus and enters the tubule. As it passes through each section of the nephron the urinary filtrate is modified through reabsorption and secretion of fluid and electrolytes to maintain body

fluid homeostasis [7]. Urine then passes from the collecting ducts into papillary ducts which drain into the central renal pelvis and form here into the bladder via the ureter (Figure 1-2) [8].

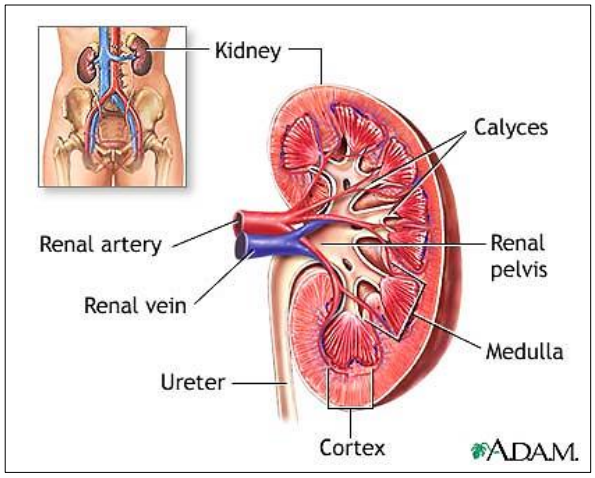

Figure 1-1: The anatomy of the kidney

The retroperitoneal anatomical location of both kidneys are shown. A coronal section through one kidney reveals the outer cortex enclosing a pyramid-shaped medulla. The apex of the medulla protrudes into the renal calyces which drain into the renal pelvis. Urine passes from the renal pelvis into the ureter and out into the bladder [8]. *Image downloaded from http://www.fitnesstipsforlife.com*.

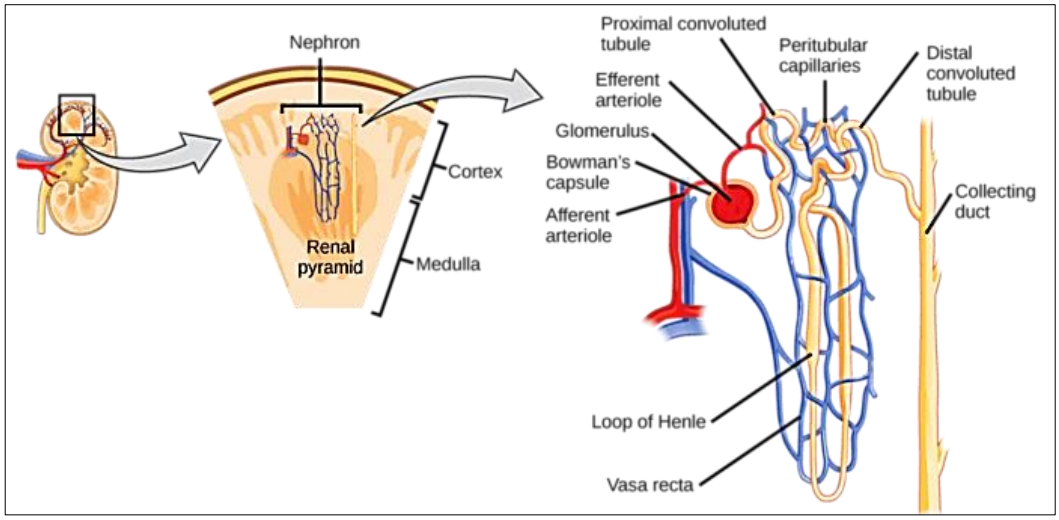

Figure 1-2: The nephron

The functional unit of the kidney is the nephron, which is shown traversing the renal cortex and medulla. The nephron consists of the glomerulus which is enclosed by Bowman's capsule. From

the Bowman's capsule arises in succession: the proximal tubule, the descending and ascending limbs of the Loop of Henle, the distal tubule and finally the collecting duct. *Figure reproduced from Field et al* [7].

1.1.2 The glomerulus

The glomerulus is a network of specialised capillaries attached to the mesangium which together are enclosed by Bowman's capsule. It is here that plasma ultrafiltration occurs to form urine [8]. The glomerular capillaries are unique as they are located between two arterioles: the afferent arteriole which supplies the glomerular tuft and the efferent arteriole that drains the glomerular capillary bed (Figure 1-3) [9]. This allows glomerular capillary pressure (via constriction of the efferent arteriole) and therefore glomerular filtration to be maintained regardless of fluctuations in blood flow to the kidney [10].

The glomerular capillaries and outer mesangium are covered by epithelial cells which form part of the visceral epithelium of Bowman's capsule. These terminally differentiated epithelial cells are known as podocytes. Separating the fenestrated glomerular endothelial cells (GEnC) and the epithelial podocyte cells is the glomerular basement membrane (GBM). Together, these three components form the glomerular filtration barrier (Figure 1-4). The integrity of the glomerular filtration barrier is maintained through chemical cross-talk between these three cell types. In the event of mutation or injury to any of these constituent parts, the glomerular filtration barrier is damaged and there is leakage of macromolecules (typically albumin). Albuminuria itself is known to correlate with kidney disease progression and cardiovascular mortality [10].

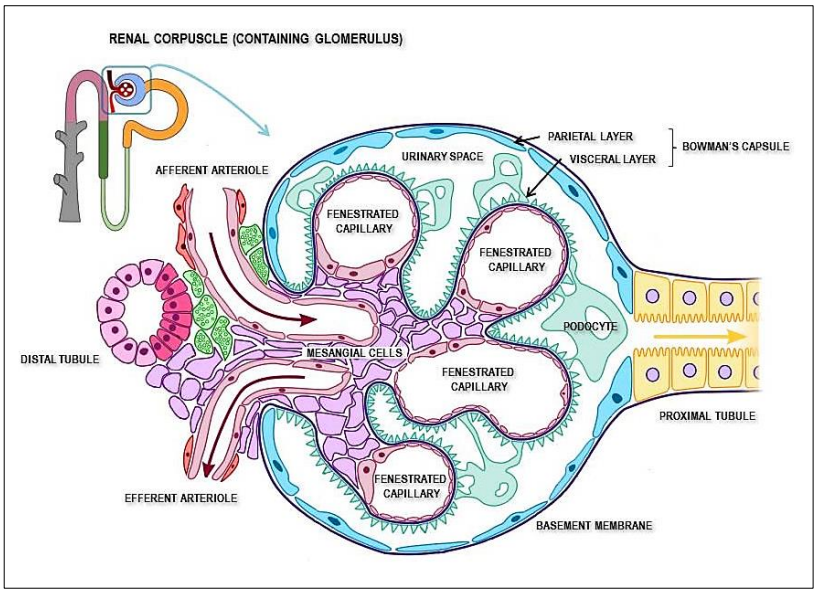

Figure 1-3: The glomerulus

The glomerulus is a network of specialised capillaries attached to the mesangium which is encapsulated by Bowman's capsule. It is here that plasma ultrafiltration occurs to form urine [8]. Together the glomerulus and Bowman's capsule are known as the renal corpuscle. The glomerular capillaries and outer mesangium are covered by epithelial cells which form part of the visceral epithelium of Bowman's capsule. These terminally differentiated epithelial cells are known as podocytes. *Image downloaded from https://www.studyblue.com.*

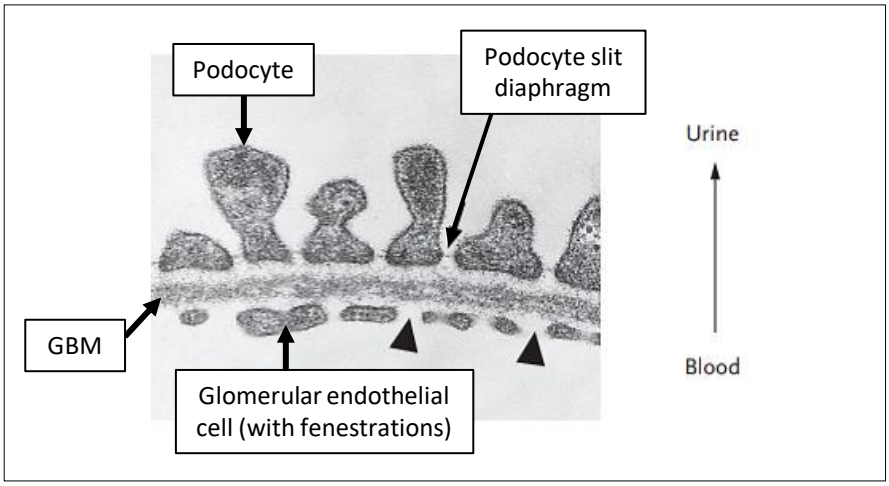

Figure 1-4: Electron Microscopy (EM) cross-sectional image of the glomerular filtration barrier

The podocyte foot processes are clearly seen on the urinary side of the lumen, with their slit diaphragms visible. The glomerular endothelial cells sit on the on the blood side with fenestrations indicated by the arrow heads. Lying between these two cells is the GBM (glomerular basement membrane). Urinary filtrate passes from the blood lumen to the urinary space. *Figure adapted from Eremina et al* [11].

1.1.3 The podocyte

Podocytes are highly specialised, terminally differentiated epithelial cells of mesenchymal origin [10]. As such they are unable to replicate and cannot be replaced after birth [8]. They constitute the visceral epithelium of Bowman's capsule and are formed of a cell body which gives rise to long extensions known as primary processes, which end in multiple interdigitating foot processes (Figure 1-5). These rest upon the basement membrane surface of the glomerular capillary [8]. The foot processes of one podocyte interact with another at specialised cell to cell junctions known as 'slit diaphragms' [12]. Several proteins (including nephrin, podocin and P-cadherin) have been shown to form the slit diaphragm. Exactly how these molecules interact to form a size-selective filtration barrier and signal to the podocyte cytoskeleton is yet to be fully determined [8].

Distortion of podocyte foot process architecture termed 'foot process effacement' due to injury or mutation in slit diaphragm proteins causes glomerular proteinuria [10]. It has been shown to be a result of active actin cytoskeleton reorganisation in response to intracellular signalling [10]. Podocyte injury is known to be the origin of many glomerular diseases [13]. However, there are a few conditions where nephrotic proteinuria occurs without evidence of foot process effacement, most notably in pre-eclampsia (a pregnancy associated TMA). Furthermore, the degree of foot process effacement quantified upon morphometry does not appear to correlate with the level of proteinuria observed in disease states [10]. This has prompted an alternative hypothesis from Kriz et al. who suggest that podocyte effacement represents an attempt to re-model and prevent detachment from the GBM [14]. This is an interesting concept, which if correct suggests podocyte effacement may not always be due to podocyte specific pathology [14].

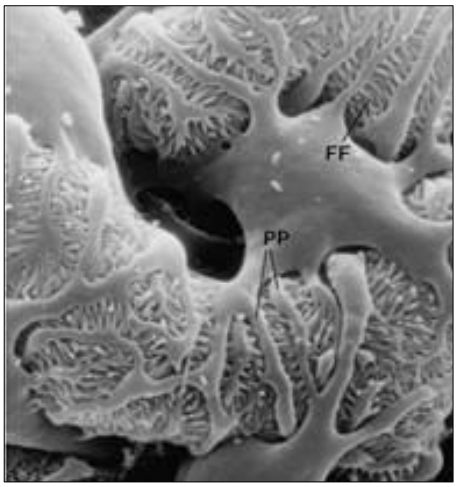

Figure 1-5: Scanning electron micrograph of the podocyte

Each podocyte consists of a cell body which gives rise to long extensions known as primary processes (PP) which end in multiple interdigitating foot processes (FP). The glomerular capillary loop is entirely covered by podocyte foot processes [12]. *Image downloaded from http://medcell.med.yale.edu.php.*

1.1.4 The glomerular basement membrane

As seen in Figure 1-4, glomerular endothelial cells line the inner surface of the glomerulus and are in direct contact with the bloodstream within the kidney [15]. At the edges of the glomerular capillary loop, these highly specialised endothelial cells are flattened and share a common glomerular basement membrane (GBM) with adjacent podocytes. Thus, the GBM is formed from the fusion of the basal laminae of the glomerular endothelium and the basal cell membrane of the podocyte foot processes [16]. The GBM consists of a complex gel meshwork consisting of laminin isotypes, type IV collagen, nidogen and heparin sulphate proteoglycans. These matrix molecules provide structural support for the glomerulus and act as ligands for receptors found on the surface of endothelial cells, podocytes and the mesangium [16][17]. The GBM is clearly an important part of the glomerular filtration barrier as genetic mutations in GBM genes are known to result in albuminuria and progress to end stage renal disease. The most well-known being Alport syndrome, caused by an X-linked mutation in the COL4A5 gene in 80% of cases [17].

1.1.5 The glomerular endothelial cell

The glomerular endothelium is characterised by the presence of large fenestrations which give it a high permeability to water and small solutes [16]. These circular transmembrane pores make up 30 to 50% of the entire endothelial cell surface, and facilitate the flow of

filtrate through the glomerular filtration barrier across the GBM to the podocyte [15]. Due to the size of these pores it was initially thought that the glomerular endothelium represented a non-selective permeable layer within the glomerular filtration barrier. However, glomerular endothelium and their fenestrae are now known to be covered in a layer of negatively charged proteins which contribute to the selective permeability of the glomerular filtration barrier [18]. These are either anchored to the cell membrane of the endothelial cell to form a glycocalyx or are non-covalently bound to associated proteins on the endothelial cell surface [16].

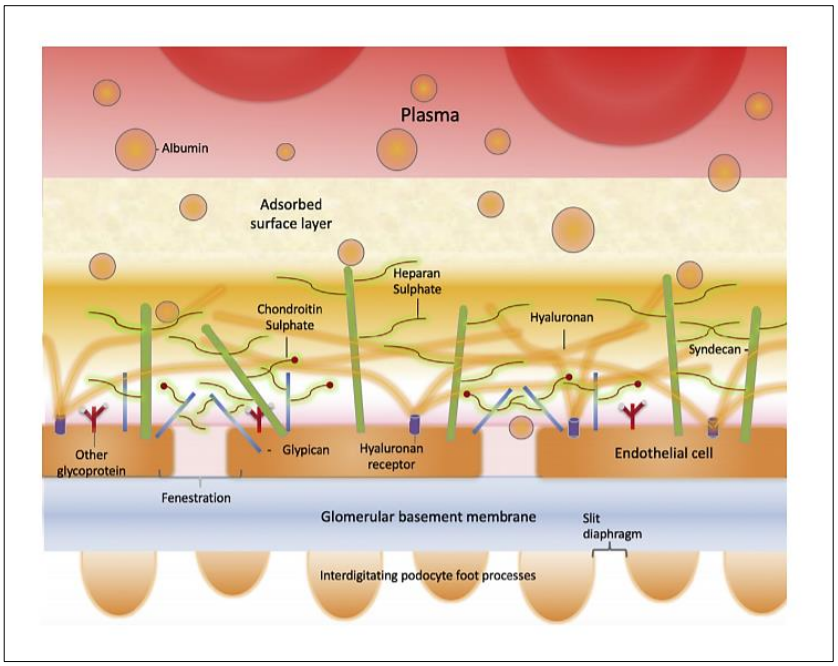

Figure 1-6: The glomerular endothelial cell and glycocalyx

The glycocalyx is a complex structure of core proteoglycans with attached hyaluronan, heparin sulphate and chondroitin sulphate chains (as shown). Circulating plasma proteins in the lumen of the glomerular capillary are adsorbed from the circulation and adhere to the surface of the glycocalyx. This generates a layer (indicated in pink) of protein deplete filtrate that is adjacent to the endothelial cell membrane. This acts to reduce the oncotic pressure across the endothelium, controlling transcapillary fluid exchange. *Figure reproduced from Butler et al.* [19].

The glycocalyx is made up of a complex structure of sulphated proteoglycans, hyaluronan, glycoproteins and various other circulating plasma proteins from the blood that adhere to the surface of the endothelium [18]. This generates a layer of protein deplete filtrate

that is adjacent to the endothelial cell membrane (Figure 1-6) [19]. It is this layer that reduces the loss of plasma macromolecules such as albumin into the urinary filtrate and that maintains oncotic pressure regulating transcapillary fluid exchange within the glomerulus [18][19].

Disruption to the glycocalyx has been shown to contribute to a number of vascular diseases including diabetic kidney disease, hypertension and atherosclerosis [20]. The Bristol Renal endothelial research group has demonstrated (both in conditionally immortalised endothelial cells *in vitro* and in murine models *in vivo)*, that loss of glycosaminoglycans occurs under diabetic conditions [21]. More recently, in a diabetic mouse model, this group has also shown that blocking matrix metalloproteinase (MMP) mediated syndecan-4 shedding restored the glomerular endothelial glycocalyx; which led to the attenuation of diabetes induced albuminuria [21]. This work highlights the importance of the glomerular endothelium and a healthy glycocalyx in maintaining the glomerular filtration barrier.

Of interest to my research, loss of endothelial cell fenestrations together with degradation of the endothelial glycocalyx have also been shown to be associated with the vascular injury of early onset pre-eclampsia (a pregnancy associated TMA) [22][23]. Furthermore, being the primary interface between the circulation and the endothelium, the glycocalyx also plays a key part in the inflammatory response within the glomerulus [18]. Indeed, it is known that the glomerular glycocalyx can inhibit leukocyte capture and extravasation, acting as a physical barrier regulating the recruitment of inflammatory cells to the kidney [18]. Moreover, the endothelial cell itself is known to be particularly susceptible to complement mediated injury and reliant upon the protection of membrane bound complement regulators (such as membrane co-factor protein: MCP) as well as fluid phase regulators such as complement factor H to maintain immune homeostasis [18]. Acquired or genetic deficiency in these complement regulators results in a wide range of glomerular diseases: from dense deposit disease (DDD) to atypical haemolytic uraemic syndrome (aHUS) [10]. Thus, although my research has focused upon the role of the podocyte in Shiga toxin HUS, the importance of the glomerular endothelial cell in the pathogenesis of this disease cannot be overlooked. As such, an increase in glomerular endothelial cell susceptibility to complement attack forms a key concept within my research hypothesis; which aims to improve understanding of the mechanisms responsible for glomerular TMA in Shiga toxin HUS.

1.1.6 Cellular interactions within the glomerulus

It is an over-simplification to think of the three major constituents of the glomerular filtration barrier as independent elements. Through recent advances in targeted cell-specific transgenic animal models there has been great advancement in the understanding of the communication and cross-talk within the glomerulus *in vivo* [24]. Key pathways that have been identified to date include: vascular endothelial and platelet derived-growth factors as well as novel paracrine pathways such as IL-6 and CXC chemokine ligand 12 signalling [24]. Indeed, there is mounting evidence in support of the glomerular filtration barrier being a fluid, constantly adapting inter-cellular communication unit to maintain glomerular function [25]. My work expands on this concept, being founded upon the hypothesis that in Shiga toxin HUS the podocyte is capable of inducing changes in neighbouring endothelium to cause a glomerular TMA (the histopathological hallmark of the disease). This hypothesis has been generated on the basis of work published by Eremina et al. that described the development of a glomerular TMA following targeted podocyte specific VEGF-A deletion *in vivo* [11]. The precise role of VEGF-A in maintaining glomerular health and its association with glomerular TMA will be re-visited in detail in subsequent sections.

1.2 Haemolytic Uraemic Syndrome

Haemolytic uremic syndrome (HUS) is the leading cause of acute kidney injury in children. It is a triad of acute kidney injury, microangiopathic haemolytic anaemia and thrombocytopenia; first described in 1955 by Gasser et al [26]. Over 90% of childhood HUS cases are associated with infection [3]. Shiga toxin-producing *Escherichia Coli* found in contaminated food and water supplies is typically the infective trigger; although HUS has also been reported following exposure to *Shigella*, *Campylobacter* and *Streptococcus Pneumoniae* [3]. In England, Shiga toxin associated HUS affects 1.8 people per 100,000 population per year. The majority of these cases are reported in children under 5 years of age in whom the incidence is considerably higher at 7.6 per 100,000 population per year [27].

The remaining 10% of HUS cases are termed ‘atypical’. These include familial cases which are due to genetic abnormalities in complement regulation and other non-infective causes such as pregnancy, drugs, malignancy, connective tissue disorders and transplantation [28]. Over the last decade there has been a renewed appreciation and

considerable interest in the role of the complement system in renal disease which has been magnified by the effectiveness of eculizumab (a monoclonal humanised antibody against C5) in the treatment of atypical HUS. Eculizumab was first used in atypical HUS in 2009 and there have been numerous case reports detailing the success of the drug in controlling the disease. A landmark prospective Phase 2 trial published in 2013, further consolidated the evidence for significant improvement in renal function in atypical HUS patients treated with eculizumab [29].

1.2.1 The classification of HUS

HUS is categorised histopathologically as a thrombotic microangiopathy (TMA). This term was first introduced in 1952 by Symmers to describe: capillary wall thickening, swelling and detachment of the endothelial cell from the basement membrane, accumulation of debris in the subendothelial space and intraluminal platelet thrombosis (Figure 1-7) [2]. The microangiopathic haemolytic anaemia that ensues is a consequence of erythrocyte sheer stress resulting in red cell fragmentation. Platelet activation and entrapment in microthrombi, as well as trafficking to the reticuloendothelial system leads to thrombocytopenia, local thrombosis and organ ischaemia [3]. When this process occurs in the microvasculature of the kidney (as is the case in HUS) renal impairment is seen due to organ ischaemia. In contrast, in thrombotic thrombocytopenic purpura (TTP) neurological impairment is observed as the predominant microvascular bed affected is the brain [3]. Therefore, TMA represents a final common pathway in a number of disease processes which amongst others include HUS and thrombotic thrombocytopenic purpura (TTP) (Figure 1-8). The clinical sequelae observed is dependent upon the vascular bed and organ affected [3].

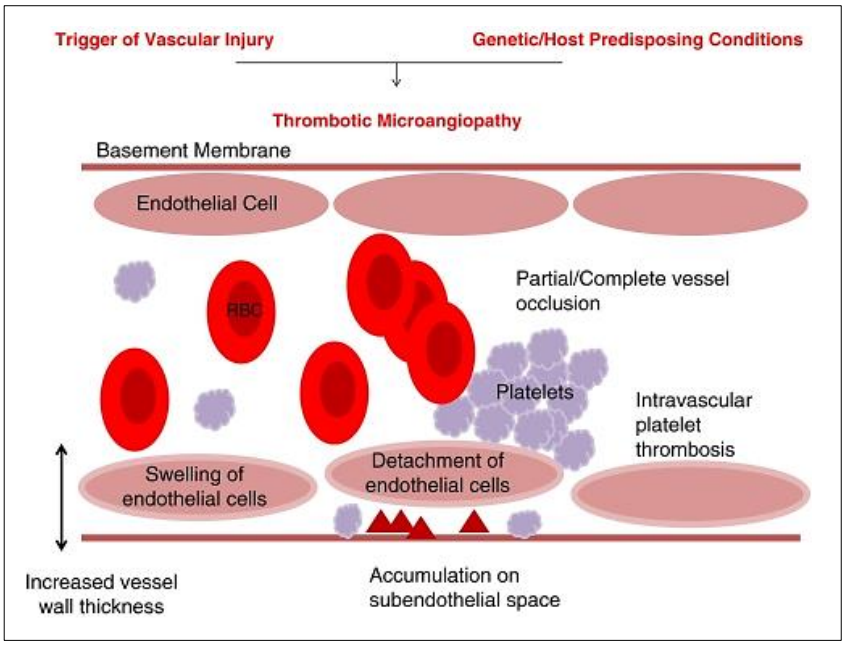

Figure 1-7: The pathophysiology of TMA

TMA is the final common pathway of many disease processes but is most often seen in the context of HUS and TTP. The pathological features of TMA include increased vessel wall thickening, swelling and detachment of endothelial cells within the target organ and platelet aggregation as shown. This leads to accumulation of debris in the subendothelial space. Clinically this presents as a consumptive thrombocytopenia, microangiopathic haemolytic anaemia and organ ischaemia. *Figure reproduced from Keir et al. with permission* [3].

Although HUS and TTP both result in TMA, they are different diseases with distinct underlying mechanisms [30]. TTP results from a deficiency in ADAMTS13 due to the presence of an acquired antibody or inherited due to an autosomal recessive mutation in the gene [31]. ADAMTS13 is a metalloproteinase enzyme that cleaves von Willebrand Factor (vWF) preventing unregulated platelet aggregation and adhesion at sites of vascular injury. When this enzyme is deficient (as is the case in TTP) vascular homeostasis is lost, large multimers of vWF form and coagulation occurs resulting in a consumptive thrombocytopenia and end organ ischaemia [31]. In TTP there is no evidence of endothelial swelling and von Willebrand factor is the primary constituent of the capillary thrombi that form in the microvasculature of the affected organs. This is in contrast to HUS where fibrin predominates in these lesions [31]. Classically, TTP is associated with a pentad of microangiopathic anaemia, thrombocytopenia and acute kidney injury (AKI), fever and neurological features [1]. However, HUS can also present with extra-renal manifestations that include neurological sequalae and fever [32]. Hence, patients need to

be tested for ADAMTS13 levels to identify those with TTP (ADAMTS13 <10%) vs. those with HUS which have normal levels and function of the ADAMTS13 metalloproteinase enzyme [31].

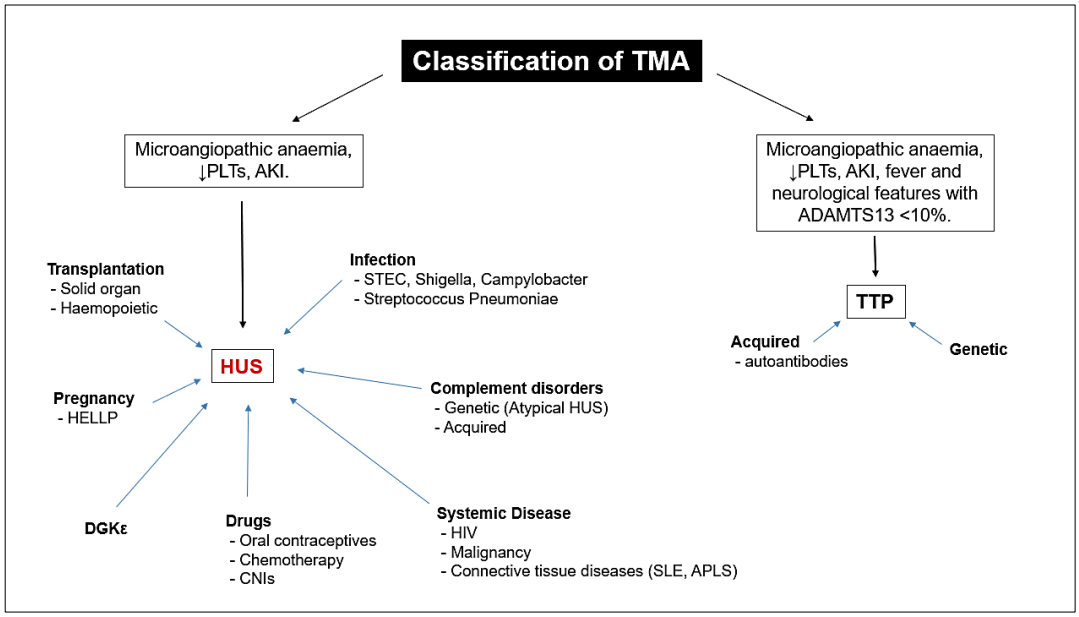

Figure 1-8: Classification of thrombotic microangiopathy

It is now widely accepted that classification of TMA according to aetiology (rather than clinical features) is a more useful guide to prognosis and treatment. TMA represents a final common pathway in many disease processes [3]. *Figure reproduced from Bowen et al. with permission* [1].

1.2.2 Infection Associated HUS

By far the commonest cause of HUS, is infection associated HUS which accounts for 90% of cases [3]. Within this group the majority follow exposure to contaminated food or water with Shiga toxin producing *Escherichia Coli* (*E.coli*) [33]. Conventionally this form of HUS has been known as 'typical' or 'diarrhoea associated'. However, these terms have proved unhelpful given that up to half of patients with atypical HUS can present with an initial diarrhoeal illness [34]. Given the need for clarity in terminology, the definition 'STEC HUS' is now used to describe HUS secondary to Shiga toxin producing *Escherichia coli*. This is distinct from other infective causes of HUS such as *Streptococcal pneumoniae*-related HUS which is considerably rarer, more severe and due to invasive pneumococcal disease [35].

Diagnosis of STEC HUS is reliant upon faecal testing in the laboratory using stool culture, serum detection of *E.coli* O157 antibodies, immunoassays, and PCR (polymerase chain reaction) assay to detect Shiga toxin genes. These tests together will identify up to 70% of cases [36]. Diagnosis of atypical HUS is therefore often implied by the absence of STEC. As a result, patients presenting with a microangiopathic anaemia, thrombocytopenia and acute kidney injury may initially be commenced on plasma exchange. Once TTP has been excluded (ADAMTS13 activity above 5-10%) and if STEC testing is negative then a diagnosis of atypical HUS is considered likely and eculizumab started; whilst levels of complement factor H, I and MCP are awaited along with subsequent targeted genetic analysis sequencing to identify specific complement mutations [37].

1.2.3 Epidemiology of STEC HUS

The latest available figures from Public Health England (PHE) report a total of 1219 confirmed cases of STEC in England and Wales in 2018 [38]. There were an additional 334 cases reported that were positive for Shiga toxin genes on PCR, but no organism was identified. As with previous years, the highest incidence of infection with was in children under 5 years of age at 3.36 per 100,000 population. The most common serogroup of STEC that caused illness in England was O157 (although other serogroups such as 026, 091 and 0146) were also detected due to more widespread use of PCR testing of stool samples. Almost one third of STEC O157 cases were hospitalised, with 2% recorded as developing HUS [38].

Prior to the introduction of PCR testing, the majority of laboratories were using culture methods to identify STEC O157 infection by its inability to ferment sorbitol on MacConkey agar. This is satisfactory for identification of STEC O157 but not for non-O157 serogroups which do ferment sorbitol. The only way to differentiate between non-O157 STEC that cause disease versus those that are non-pathogenic is to perform PCR testing. It is of no surprise therefore, that since the introduction of PCR testing in 2013 there has been an increase in the number of pathogenic non-O157 STEC cases identified in England; with 9% of these developing HUS [38]. The variation in ability to cause serious illness of each STEC serogroup is known to be due to differences in virulence. This itself is influenced by the subtype of Shiga toxin produced by *E.coli*; with the release of Shiga toxin subtype 2 known to be more likely to cause HUS [39].

The incidence of STEC O157 cases has been following a downward trajectory in England and Wales since 2015 (Figure 1-9). However, incidence in England differs according to

region. The highest incidence in 2018, was in the North East of England with 1.99 cases per 100,000 population [38]. The lowest incidence reported was in London as indicated from the map shown in Figure 1-10. Interestingly, in 2018 of the recorded STEC O157 cases in England 58% were female. In fact, across all age groups (except those over 80 years) females had a higher incidence (Figure 1-11) [38]. However, in terms of development of STEC HUS, larger pooled data retrospective studies in Europe have reported no statistically significant increase STEC HUS in women [40]. It is clear, that STEC infections follow seasonal variation and peak during the warmer summer months; a trend also observed over previous years (Figure 1-12) [38].

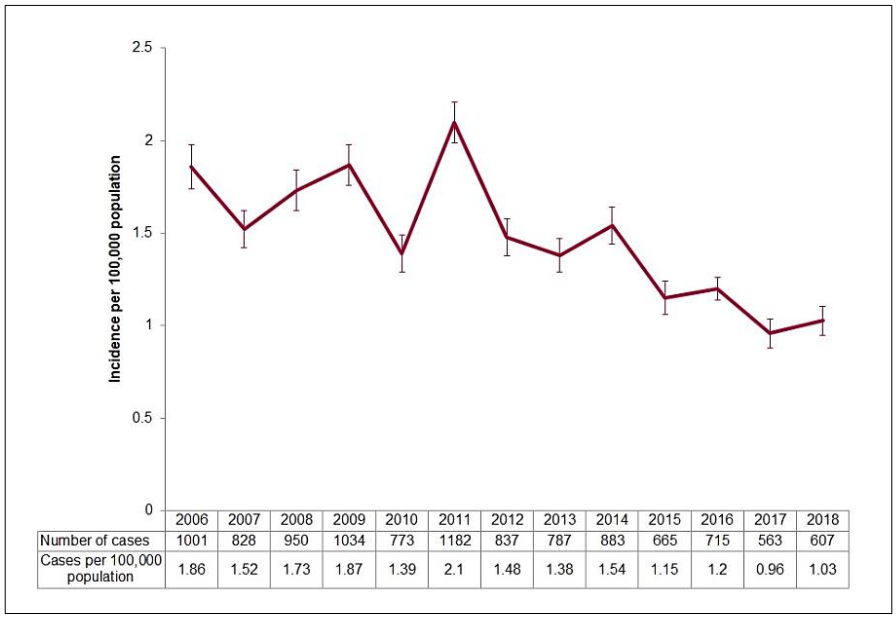

	2006	2007	2008	2009	2010	2011	2012	2013	2014	2015	2016	2017	2018
Number of cases	1001	828	950	1034	773	1182	837	787	883	665	715	563	607
Cases per 100,000 population	1.86	1.52	1.73	1.87	1.39	2.1	1.48	1.38	1.54	1.15	1.2	0.96	1.03

Figure 1-9: Incidence of STEC O157 cases in England and Wales from 2006 to 2018

The incidence of STEC O157 cases has been following a downward trajectory in England and Wales since 2015. Higher rates of STEC O157 infection correspond to higher rates of STEC HUS by definition. *Graph reproduced from https://www.gov.uk/government/publications/escherichia-coli-e-coli-o157-annual-totals* [38].

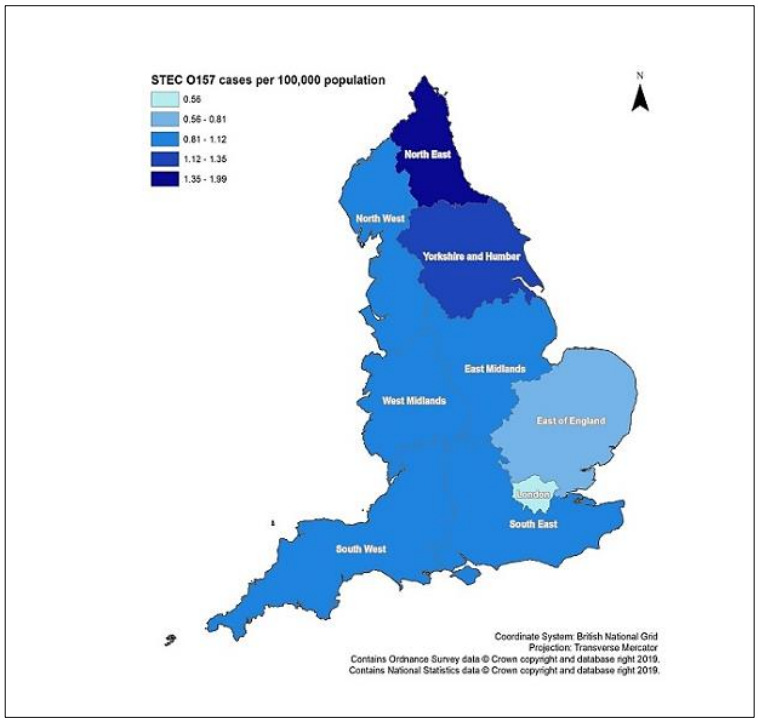

Figure 1-10: Regional incidence of STEC O157 in England

Incidence of STEC O157 infection in England differs according to region. The highest incidence in 2018, was in the North East of England with 1.99 cases per 100,000 population (dark blue on map). The lowest incidence reported was in London at 0.56 cases per 100,000 population (pale blue on map). *Map reproduced from https://www.gov.uk/government/publications/escherichia-coli-e-coli-o157-annual-totals* [38].

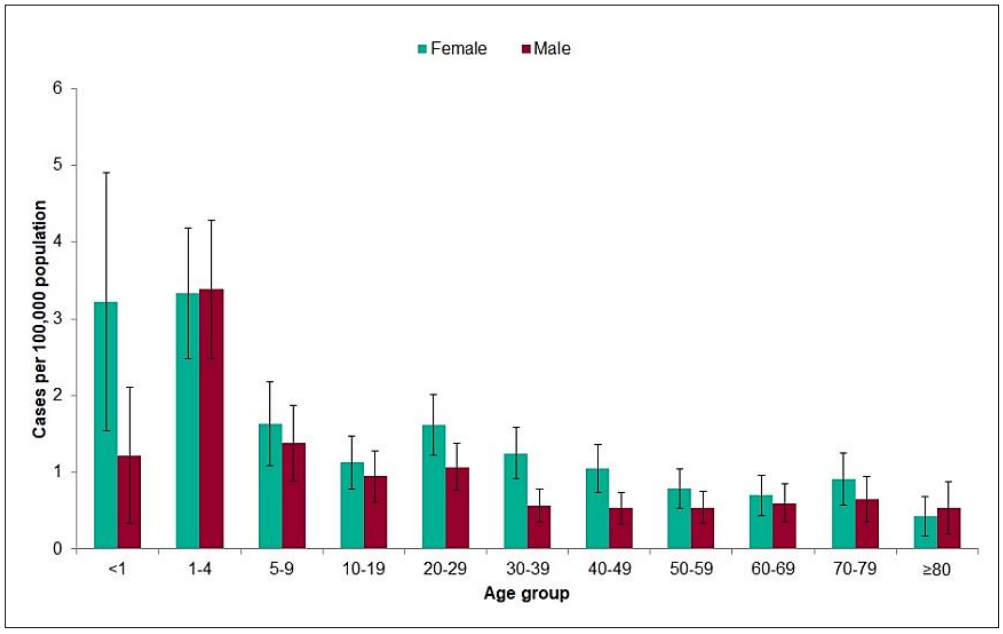

Figure 1-11: Age and gender specific incidence of STEC O157 cases in England during 2018

In 2018, of the recorded STEC O157 cases in England 58% were female. In fact, across all age groups (except those over 80 years) females had a higher incidence. As with previous years, the highest incidence of infection with was in children under 5 years of age at 3.36 per 100,000 population. *Graph reproduced from https://www.gov.uk/government/publications/escherichia-coli-e-coli-o157-annual-totals* [38].

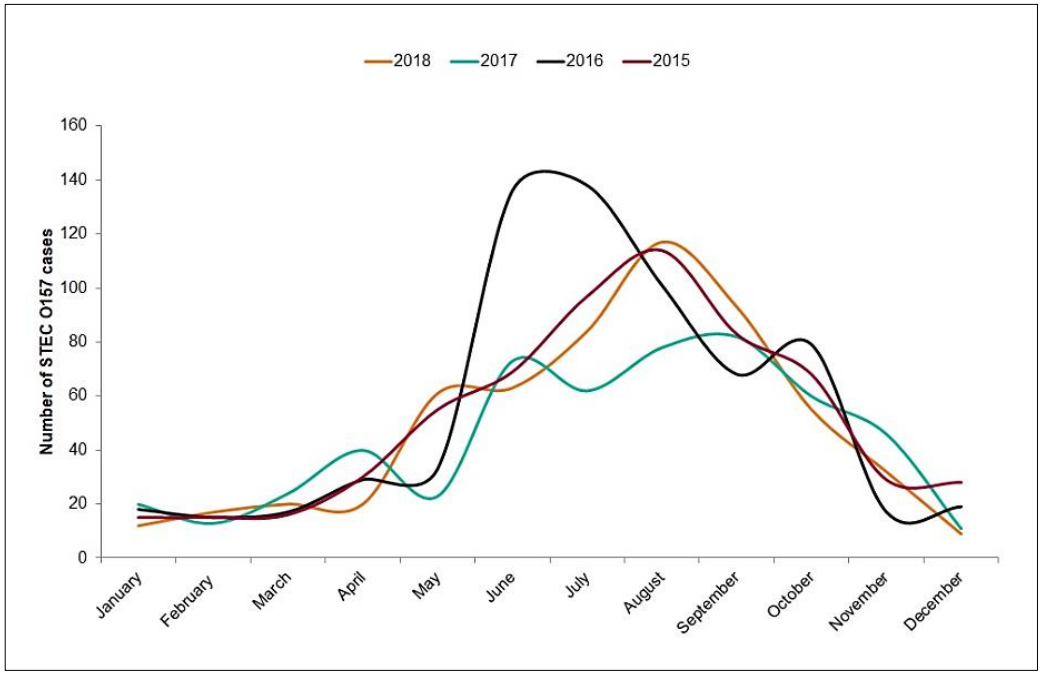

Figure 1-12: Seasonal variation in STEC O157 cases in England 2015 to 2018

Data collected by Public Health England confirms that STEC O157 infections follow seasonal variation and peak during the warner summer months. This is a trend also observed over previous years. *Graph reproduced from https://www.gov.uk/government/publications/escherichia-coli-e-coli-o157-annual-totals* [38].

1.2.4 Clinical sequelae of Shiga toxin HUS

Patients with Shiga toxin associated HUS classically present with a diarrhoeal illness, followed by the non-specific symptoms of an acute kidney injury [41]. These include pallor and breathless from anaemia as well as oliguria and oedema from acute onset renal failure [32]. The diarrhoeal prodrome of STEC HUS is bloody in nature in 80% of cases and characteristically associated with painful abdominal cramps [32]. The mean interval from exposure to the bacteria and onset of symptoms is 3 days, with almost all cases diagnosed within 2 weeks of onset of diarrhoea [31][41]. Patients may also have associated vomiting and in 30% fever is present. Blood tests reveal an elevated white cell count (leucocytosis)

in most patients and the classical HUS triad of thrombocytopenia, anaemia and uraemia [41].

In contrast to STEC HUS, atypical HUS tends to follow a history of a trigger event such as pregnancy, influenza, or viral gastroenteritis in one third of patients. Atypical HUS is seen as frequently in children as in adults, whereas Shiga toxin HUS predominates in children (usually under 3 years of age). Interestingly, in atypical HUS thrombocytopenia is less pronounced and even absent in up to 20% of cases [32]. HUS regardless of aetiology is far from benign, with 50% of patients requiring prompt initiation of renal replacement therapy at diagnosis [41]. In Shiga toxin HUS there is no specific treatment for the disease with up to 5% of patients dying during the acute phase of the illness, despite best available supportive care [41].

Although the kidney is the primary target of HUS, extra-renal manifestations including central nervous system involvement, pancreatitis, ischaemic cardiomyopathy and necrotic skin lesions are also a feature of the disease [32][42]. Thus, the symptoms apparent at presentation are dependent upon the organ systems affected by TMA. In Shiga toxin HUS neurological involvement is reported to be one of the most life-threatening complications and can be as high as 20% in paediatric populations [32]. In the infamous German STEC HUS outbreak of 2011, neurological manifestations of HUS were present in 50% of adult patients and included seizures, hemiplegia, extrapyramidal syndrome and coma [32][43].

The prognosis for STEC HUS patients is dependent upon the clinical trajectory of the disease. Acute mortality outcomes for STEC HUS have improved with the introduction of early dialysis from 30% to 5%. However, of those patients that survive the initial insult, up to 30% develop proteinuria and 18% progress to chronic renal failure [44]. Furthermore, some patients develop extra-renal sequelae such as diabetes mellitus following pancreatitis, colonic strictures due to gastrointestinal inflammation and devastating neurological disease with long term sequelae [44]. Thus, long-term follow up of all STEC HUS cases is prudent, as some patients who are apparently fully recovered from the initial insult go on to develop complications such as hypertension and proteinuria several years on from their initial diagnosis [45].

1.2.5 Source of infection in STEC HUS

Healthy cattle are the natural reservoir of Shiga toxin producing *E.coli*, although other animals such as sheep also harbour the bacteria in their intestinal tract [46]. As such under-cooked beef and unpasteurised cow's milk are the main sources of STEC infection in humans [42]. Transmission occurs through consumption of infected food and water or exposure to contamination from animal faeces. This can be either via an indirect faecal oral route e.g. unwashed vegetables and salad products; (bean sprouts were found to be the source in the 2011 German outbreak) or directly through contact with the infected animal or their environment itself [46][47]. Less than 100 *E.coli* bacteria are required to cause infection in humans, meaning outbreaks of STEC can occur with ease from person to person due to such a low infectious dose [42][46].

The seasonal variation in STEC cases (both O157 serotype as well as pathogenic non-O157 serotypes) is observed globally, with higher incidence in warmer summer months [38][48]. This is likely due to a combination of the higher level of bacterial faecal shedding from livestock in warmer climates and the increase in barbeque cooking during summertime which is known to be associated with consumption of undercooked food [49]. Preventing *E.coli* food poisoning is a priority of public health agencies worldwide. It requires vigilance and careful preparation of food and water at all stages of the food chain [42]. Although the pathogenic *E.coli* responsible for STEC HUS colonise the gut of healthy livestock animals and are resistant to acidic and high salt conditions; correct cooking procedures will destroy the bacteria and dramatically reduce the risk of infection [42]. Despite this several large outbreaks of STEC have occurred and continue to be reported across the world with devastating consequences [47][49].

1.2.6 Escherichia coli bacteria

Escherichia coli (*E.coli*) are Gram negative, rod shaped bacteria that inhabit the intestinal tract of animals and reptiles. They are the predominant aerobic bacteria in the gut of humans, being one of the first bacterial species to colonise the intestine in childhood [50]. *E.coli* is an example of a facultative anaerobe, it will generate ATP from aerobic respiration in the presence of oxygen but can switch to fermentation or anaerobic respiration should oxygen be absent [51]. The importance of the presence of non-pathogenic strains of *E.coli* in the human gut has only recently been recognised. This subgroup of *E.coli* not only provide a source of vitamin K and B12 for their human host, but are now also known to

contribute to the diversity of the human intestinal microbiome which influences our immune response, appetite and metabolism [52][53].

A lack of bacterial diversity has been reported in patients with inflammatory conditions such as Crohn's disease and psoriatic arthritis, as well as in type 1 and type 2 diabetics and those with atopic conditions such as eczema [53][54]. Moreover, in neurodegenerative conditions such as Parkinson's disease there is mounting evidence that a pro-inflammatory intestinal microbiota may act as a trigger for the condition [55]. Hence, our immune system has co-evolved to exist in a relationship of commensalism with *E.coli*, whereby the bacteria provide a healthy species-rich intestinal ecosystem preventing infection by pathogens through the production of bacteriocins; and we as the human host provide a steady supply of nutrients and a stable environment [50][53].

However, some *E.coli* strains have acquired virulence through the transfer of DNA encoded within mobile genetic elements such as bacteriophages, plasmids and transposons; to become pathogenic and cause diarrhoeal disease [56]. To assist in identification of pathogenic strains, *E.coli* has historically been classified by serotype (a system initially used in the 1940s, prior to PCR based genetic sequencing). This is based upon the presence of the major surface antigens O-polysaccharide, K-capsular and H-flagellar [50]. For example, as already eluded to the most prevalent serotype in the UK that causes HUS is *E.coli* O157 [38]. Given the vast number of different *E.coli* surface antigens and their combinations (there are 186 different O antigens alone) serotyping *E.coli* has become rather complex [57]. Additionally, in the last decade to further complicate matters, next generation sequencing technologies have made it possible to genetically subdivide *E.coli* in a more robust and discriminatory fashion. This has vastly improved our understanding of the evolutionary processes that have occurred to give rise to the variety of *E.coli* populations; as well as providing a way to investigate and contact trace to source *E.coli* food poisoning outbreaks [50][57].

For simplicity in published literature, often the terms 'extra-intestinal' and 'diarrhoeagenic' *E.coli* are used to differentiate between *E.coli* that cause disease outside the gastrointestinal tract (urinary infections and neonatal meningitis for example) and those that cause gastrointestinal infection, respectively. Diarrhoeagenic *E.coli* have been further subdivided into pathovars according to their mode of pathogenesis and the presence of typical virulence factors (Table 1) [57][58][59]. It is the Shiga toxin producing *E.coli* (STEC) pathotype that is of interest to my work. The discovery of this group of *E.coli*

can be traced back to 1927, to the description of an outbreak of *E.coli* in children associated with haemorrhagic colitis and organ failure by Albert Adam [41]. He noted that the bacterium present in these cases was unique, and that its fermentation properties varied from previously known strains of *E.coli* [41]. Indeed, until recently we still used the technique of culturing *E.coli* on MacConkey agar plates to identify *E.*coli O157 by its inability to ferment sorbitol [38].

Pathovar	Characteristics	Disease
EPEC (enteropathic E.coli)	Attaching and effacing (AE) lesions in the gut	Diarrhoea
EHEC (enterohemorrhagic E.coli)	AE lesions Shiga toxin release	Diarrhoea / HUS
STEC (Shiga toxin producing E.coli)	Shiga toxin release	HUS
ETEC (enterotoxigenic E.coli)	Heat stable and heat labile enterotoxin release	Traveller's diarrhoea
EAEC (enteroaggregative E.coli)	Intimate aggregation to give 'stacked brick appearance'	Acute or chronic diarrhoea / Urinary tract infection (UTI)
DAEC (diffuse adherent E.coli)	Heterogenous group that express Dr family of adhesins	Diarrhoea
EIEC (entero-invasive E.coli)	Closely related to Shigella and directly invasive to colon epithelial cells	Bloody diarrhoea
AIEC (adherent-invasive E.coli)	Adhere to intestinal epithelium	Possible Crohn's disease association
ExPEC (extra-intestinal pathogenic E.coli)	Responsible for infection outside of the gastrointestinal tract	Urinary tract infection (UTI) /neonatal meningitis

Table 1: *E.coli* Pathovars

Table summarising the different pathovars of *E.coli* which have been classified according to their pathogenesis and presence of typical virulence factors. Of interest to my research are the STEC pathovar group that release Shiga toxin. Of note some STEC strains are also types of EHEC, so there is an element of crossover within these groups [60]. *Table compiled from several sources* [58][59][61].

It was not until some twenty years later, that *E.coli* was noted to be present in the stool samples of 90% of children with this bloody diarrhoeal disease but never in their blood. This led to the hypothesis that a filterable agent (now known to be Shiga toxin) was being produced by this group of *E.coli* bacteria. Subsequent animal research demonstrated that

if this agent was isolated from the stool samples of affected children and injected into mice it was fatal [41]. Autopsy studies in humans with haemorrhagic colitis and organ failure later confirmed that thrombosis of capillaries was occurring and predominated in the kidney microvasculature [41]. However, it was not until many years later at the end of the 1970s, that Konowalciuck et al. discovered that these pathogenic *E.coli* released a toxin similar to that produced by the bacteria *Shigella dysenteriae* [41]. The toxin was named 'Shiga-like toxin' due to these similarities; but was also known as 'verotoxin' due to its cytotoxicity in African monkey kidney cells (Vero cells) [62]. Further support for the pathogenicity of Shiga-like toxin came from work by Karmali et al. who found a high rate of toxin activity in the faecal samples of children with *E.coli* O157 HUS and antibodies to the toxin in their blood [41].

1.2.7 Shiga toxin

Shiga toxin is an A-B exotoxin that was first isolated from *Shigella dysenteriae* in 1898 by Dr. Kiyoshi Shiga [62]. As already discussed, it was not until almost a century later that the same toxin (now known as Stx1 but initially named 'Shiga-like toxin') was found to be released from a pathogenic strain of *E.coli* [63]. This group of Shiga toxin producing *E.coli* (STEC) caused a haemorrhagic colitis and in some patients led to the development of HUS [1]. Further research led to the discovery of two main *E.coli* Shiga toxin variants Stx1 and Stx2 [63]. These are the most common types of Shiga toxin that are associated with human disease [33]. However, as more STEC serotypes were identified and the Shiga toxin strains they released sequenced, a further 10 variants of Shiga toxin were named (Table 2) [63]. Of particular interest are the variants Stx1, 1c, 2, 2c, 2d and 2e which are produced not only by *E.coli* but other bacteria including *Aeromonas hydrophila*, *Citrobacter freundii*, *Enterobacter cloacae* and *Campylobacter jejuni* [62][64]. These Shiga toxin releasing bacterial species can also cause Shiga toxin HUS, but by far the most common bacteria responsible for the disease remains *E.coli* [1].

Toxin type	Link with serious human disease?
Stx	Yes
Stx1a	Yes
Stx1c	No
Stx1d	No
Stx2a	Yes
Stx2b	No – B subunit gene not detected
Stx2c	Yes – less toxic in mice and Vero cells
Stx2d	Yes – more toxic after incubation with elastase
Stx2e	No – binds to Gb4 and associated with disease in pigs
Stx2f	No – originally isolated from STEC in pigeons
Stx2g	No

Table 2: Shiga toxin variants

Summary table of Shiga toxin (Stx) subtypes and whether they are associated with human disease. Phylogenetic analysis and PCR typing has resulted in the identification of 10 variants of Shiga toxin as shown. *Table modified from Melton-Celsa et al* [63].

1.2.7.1 Shiga toxin structure

Shiga toxins are either encoded by lambdoid bacteriophages (as is the case for Stx1 and Stx2) or chromosomal DNA (as is the case for Stx and Stx2e) [1][65]. They consist of a single 30 kDa enzymatic A subunit in non-covalent association with five identical B subunits of 7 kDa each to form a 70 kDa A-B5 holotoxin [66]. It is the B subunits of the toxin that bind to the galactose disaccharides of the Gb3 (globotriaosylceramide) receptor on target eukaryotic cells [41]. Shiga toxin encoding bacteriophage have been shown to be capable of lateral transfer of enterotoxicity to non-pathogenic *E.coli*; a process thought to be key in the evolution of new pathogens [65]. Consequently, non-pathogenic commensal *E.coli* within the gut are now thought to be potential amplifiers of Shiga toxin production within the gastrointestinal tract of susceptible patients [67]. Toxin release from *E.coli* is reliant upon phage-mediated bacterial lysis as there is no dedicated toxin secretion system in gram negative bacteria [67].

Interestingly, the nucleotide sequence homology of the A and B subunits of Stx1 and Stx2 is almost 60% with an amino acid sequence homology of 50% [41]. However, Stx1 and Stx2 are immunologically distinct, with neither being recognised by a polyclonal antibody raised to the other toxin [65]. Stx1 and Stx2 also result in a variable level of tissue damage within the host and target different organs [33]. STEC that produce Stx2 are well documented to be associated with a more severe clinical presentation and more likely to lead to the development of HUS than those that produce Stx1. This observation is also the

case in primate and mouse models of Shiga toxin HUS [41]. For this reason, Stx2 is considered to be the primary variant of Shiga toxin associated with human disease; prompting my decision to use Stx2 throughout my research project into the study of Shiga toxin HUS.

1.2.7.2 The cellular response to Shiga toxin

Irrespective of their subtype, Shiga toxins bind to the glycosphingolipid Gb3 to facilitate entry into target cell [63]. Following binding to Gb3, the Shiga toxin-receptor complex is endocytosed and transported in a retrograde manner from the endosome to the trans-Golgi network. From here it is transported to the endoplasmic reticulum (ER), where the A subunit of the toxin is cleaved by a protease produced by the ER's own degradation machinery. This results in the release of the A subunit into the host cell cytoplasm where it can enzymatically inactivate ribosomes [68]. There is also some evidence that the endocytosed Shiga toxin receptor complex can also be transported directly to the nucleus of the target cell. However, the effect of Shiga toxin in the nucleus is yet to be elucidated [33].

The three specific ways that Shiga toxin acts to affect cellular processes are as follows: firstly, it inactivates ribosomes by enzymatically removing an adenine residue from 28S ribosomal RNA. The damaged ribosome is unable to associate with elongation factor 1 resulting in cessation of protein synthesis [63]. This triggers the ribotoxic stress response leading to MAPK (mitogen-activated protein kinase) signalling and activation of cytokines and chemokines that result in pro-inflammatory and pro-apoptotic pathways [33][66]. Secondly, the unfolded protein response may be triggered by Shiga toxin unfolding within the ER. Prolonged signalling via the unfolded protein response will induce apoptosis in cells [66]. Finally, the binding of the B subunit itself can initiate a cytoplasmic transduction cascade that is distinct from the ribotoxic stress response but that also result in a pro-thrombotic, pro-inflammatory cellular environment (Figure 1-13) [33].

The precise apoptotic pathways that are triggered by Shiga toxins are thought to vary according to individual cell type [69]. Apoptosis is a specific form of programmed cell death characterised by changes in the nucleus that include chromatin condensation and DNA fragmentation [69]. The pathways that culminate in apoptosis involve sequential activation of cysteine dependent, aspartate specific proteases known as 'caspases.' For example, in monocytic THP1 cells, HeLa cells and human brain microvascular endothelial cells (HBMECs); Shiga toxin has been shown to activate similar apoptotic pathways *in vitro*

[69]. In these cells, Stx1 induces caspase 8, 6 and 3 signalling as well as expression of XIAP (a caspase 9 inhibitor of apoptosis protein). In contrast, Stx2 causes DNA fragmentation and cleavage of caspase 3, 6, 8 and 9 mediated by the upregulation of ER stress transcription factor CHOP (C/EBP homologous protein) in these cell lines [70]. Stx2 has also been shown to enhance activation of caspase 8 through complete degradation of the major anti-apoptotic protein FLIP (FLICE-like inhibitory protein) [69]. FLIP is known to be an important mediator in suppressing cytokine-induced apoptosis [71].

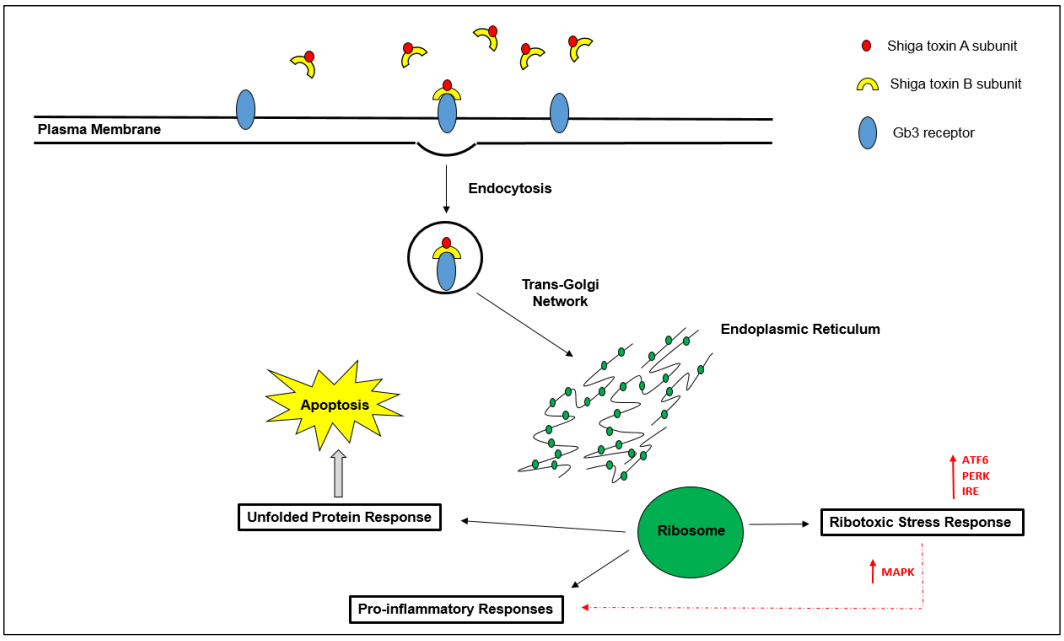

Figure 1-13: Cellular responses to Shiga toxin

The B subunit of Shiga toxin binds to the glycosphingolipid Gb3 in the target cell membrane. Following binding Shiga toxin is endocytosed and transported in a retrograde manner to the trans-Golgi network. From here it is transported to the endoplasmic reticulum (ER) where it triggers 3 responses: the ribotoxic stress response, proinflammatory cytokine release and the unfolded protein response. *ATF6=activating transcription factor 6, PERK=protein kinase R (PKR)-like endoplasmic reticulum kinase, IRE=iron-response element, MAPK=mitogen-activated protein kinase. Figure reproduced from Bowen et al. with permission* [1].

Although several studies have shown that the glomerular and tubular cells of the kidney undergo apoptosis in response to incubation with Shiga toxin, the specific apoptotic pathways activated in glomerular endothelial cells and podocytes are yet to be extensively delineated [72][73]. However, a paper published by Psotka et al. has demonstrated that

caspase 3 activity is increased in human conditionally immortalised glomerular endothelial cells and podocytes treated with Stx2 for 12 hours; suggesting that this is the major effector caspase responsible for apoptosis in these cells [74]. Hence, despite the fact that Shiga toxin does not cause apoptosis in all cell types, there is sufficient evidence to support a role for apoptosis in the generation of vascular injury and tissue damage within the human kidney due to the action of Shiga toxin in the glomerulus [69].

1.2.8 Globotriaosylceramide (Gb3)

As already established, the neutral glycosphingolipid Gb3 is the receptor for Shiga toxin and therefore of vital importance in the pathogenesis of Shiga toxin HUS [63]. Gb3 is also known as CD77, Burkitt lymphoma-associated antigen and Pk blood group antigen [75]. Glycosphingolipids consist of a carbohydrate hydrophilic moiety (containing at least one oligosaccharide residue) and a hydrophobic lipid ceramide tail [76]. The glycosphingolipid Gb3 is primarily found in the plasma membrane of eukaryotic cells, where its ceramide tail is anchored within the lipid bilayer and hydrophilic head exposed to the extracellular environment [77]. The specific physiological cellular function of Gb3 is currently unknown. However, Gb3 is thought to be involved in the maintenance of plasma membrane structure [63]. It is also known to regulate cell signalling, acting as a receptor for pathogens; not just Shiga toxin but also as a co-receptor for the gp120 envelope protein of the HIV virus, facilitating its entry into $CD4^+$ T cells [78][79].

In support of the specificity of Gb3 as the receptor for Shiga toxin, cells lacking Gb3 expression have been shown to be resistant its toxic effects [33]. Consequently, the pattern of expression of Gb3 in different cell types is a reliable predictor of the site of action of Shiga toxin [42]. However, the relationship between the amount of Gb3 present in the cell membrane and the corresponding sensitivity of the cell to Shiga toxin is not linear. This is thought to be due to the bioavailability of Gb3 within the membrane microenvironment [33]. Binding studies modelling the crystal structure of Shiga toxin, together with enzyme-linked immunosorbent assays (ELISAs) have shown that to bind to the cell membrane; the B subunit of Shiga toxin must interact with the terminal alpha-1,4 di-galactose of the trisaccharide within the Gb3 molecule [80]. This interaction is sufficient for Stx1 binding to Gb3 but Stx2 requires an additional interaction between its A subunit and the ceramide tail residue of Gb3 [81][82]. Given each Shiga toxin molecule has 5 B subunits, theoretically each B subunit could bind to one or more Gb3 receptors [33]. Crystal modelling studies have in fact shown high affinity binding with an equilibrium

dissociation constant (Kd) of 0.1nM; and 3 potential binding sites per B subunit of Shiga toxin taking this theoretical total to 15 possible binding sites in a single Shiga toxin molecule [81].

More recent Shiga toxin binding studies have demonstrated that Shiga toxin preferentially binds to Gb3 in the presence of cholesterol [81][82]. Hence, it is becoming increasingly evident that the affinity of Shiga toxin to bind to Gb3 is influenced by the plasma membrane microenvironment. This would further explain the dissociation between the amount of Gb3 extractable from a tissue and the lack of correlation in Shiga toxin sensitivity. Interestingly, Gb3 has been found to cluster within lipid raft sections of the plasma membrane *in vitro* [63]. Lipid rafts are dynamic entities formed from cholesterol and the ganglioside GM1 [80]. Assembly of lipid rafts occurs in the Golgi of the cell (cholesterol first synthesized in the ER and sphingolipids in the Golgi) before delivery to the plasma membrane. Lipid raft trafficking is under continuous endocytosis and turnover. This is one of the reasons that lipid raft existence has been so difficult to prove, along with the inability to visualise them with light microscopy [83]. What is clear from this work, is that the binding of Shiga toxin to Gb3 is complex and influenced by the specific membrane microenvironment at the time Shiga toxin is encountered by the host cell [63].

In recent years, the metabolic pathways involved in glycosphingolipid synthesis have been studied, facilitating the generation of several knockout mouse models to improve our understanding of their role *in vivo* (Figure 1-14). The synthesis of the Shiga toxin receptor Gb3, is catalysed by the enzyme Gb3 synthase also known as α-1,4-galactosyltransferase (A4GALT). Gb3 synthase is encoded by the A4GALT gene found on chromosome 22 and is responsible for catalysing the addition of an α-1,4 galactose residue to lactosylceramide to form globotriaosylceramide (Figure 1-15) [77]. In order to assess the role of Gb3 *in vivo*, Okuda et al. generated an A4GALT knockout mouse that was deficient in Gb3 using a neomycin-resistant gene targeting the open reading frame of A4GALT gene [75]. These mice did not appear to have any obvious phenotype, other than absence of Gb3 expression in their tissues [75]. These constitutive A4GALT knockout mice were found to be completely protected from the toxic effects of Shiga toxin; demonstrating for the first time that Gb3 is the endogenous ligand for Shiga toxin *in vivo* [77].

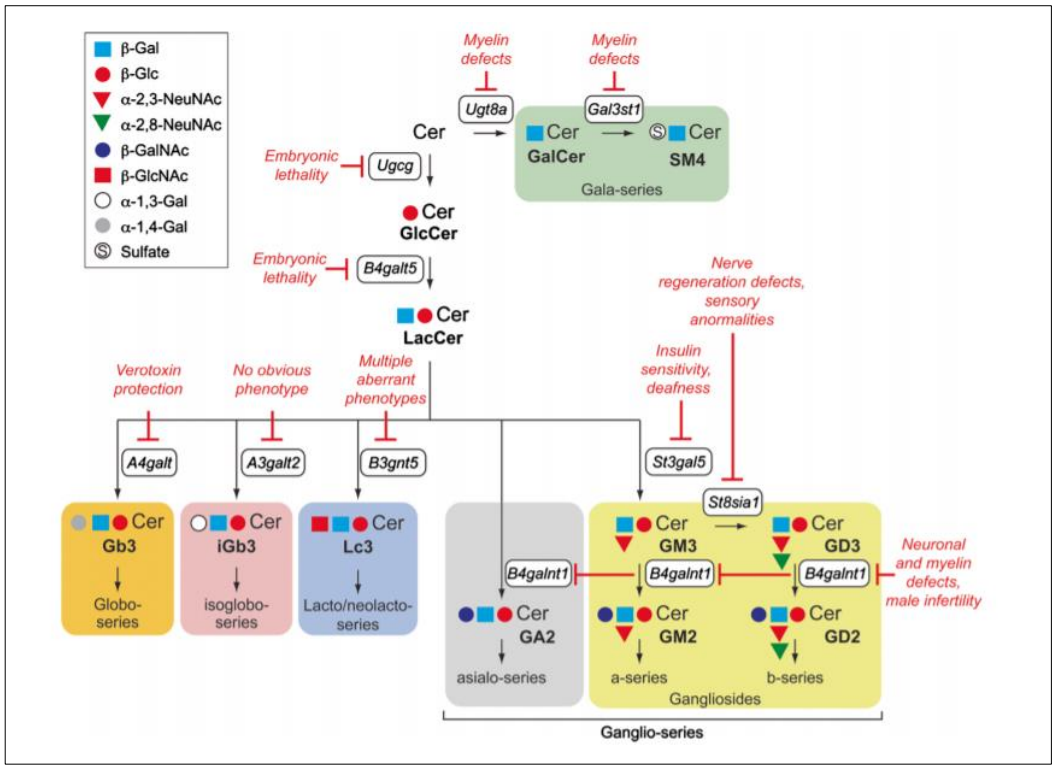

Figure 1-14: Targeted glycosphingolipid synthesis pathways in knockout mouse models

Genes that have been targeted are shown in the coloured boxes. The major mouse phenotypes due to genetic knockout in the glycosphingolipid synthesis pathway are show in red text. The only phenotype detected in A4GALT knockout mice was protection against Shiga toxin (or verotoxin) toxicity. Cer=ceramide, GalCer=galactosylceramide, GlcCer=glucosylceramide, LacCer=lactosylceramide, NeuNAc = neuraminic acid. *Figure reproduced from Allende et al.* [77].

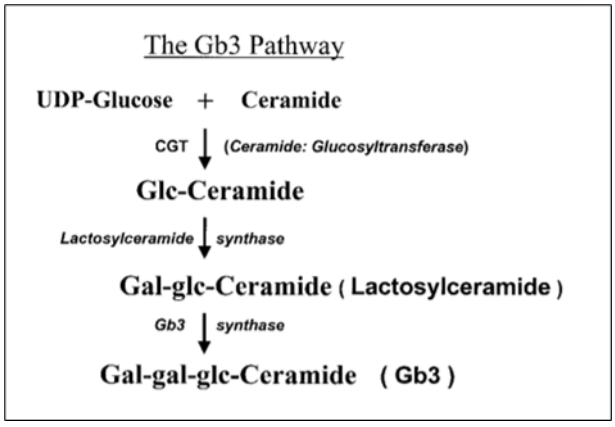

Figure 1-15: The Gb3 synthesis pathway

The biosynthetic pathway of Gb3 in eukaryotic cells is shown. The enzyme Gb3 synthase (A4GALT) is the enzyme responsible for catalysing the addition of an α-1,4 galactose residue to

lactosylceramide to form globotriaosylceramide. Gb3 is the primary receptor for Stx1 and Stx2. *Figure reproduced from Obrig et al*. [84]

Due to a number of studies reporting that a subset of immature B cells express Gb3 and that it may play a role in the differentiation of B cells; Okuda et al. also performed immunological profiling of the serum, thymus and spleen of the A4GALT knockout mice to ensure that this was not the reason for their resistance to Shiga toxin toxicity [75]. There were no significant differences in these profiles and no abnormalities evident vs. wild type age matched control mice (Table 3). Interestingly, the total neutral glycosphingolipid present in the kidney of the A4GALT knockout mice was the same as that of wild type mice, but with no Gb3 or globo-series glycosphingolipids present [75]. This suggests a possible redundancy in the glycosphingolipid synthesis pathway to facilitate the synthesis of other neutral glycosphingolipids in some sort of compensatory mechanism for the absence of Gb3. In support of this, increased ceramide monohexoside and dihexoside levels were seen in the A4GALT knockout mice [75].

Organ	Genotype	
	+/+	−/−
Spleen		
No. of cells ($\times 10^8$)	0.96 ± 0.1	1.07 ± 0.11
Population (%)		
$B220^+$	38.42 ± 5.98	38.16 ± 4.12
$CD3^+$	32.10 ± 3.45	32.00 ± 1.88
$CD4^+$	21.09 ± 4.69	23.92 ± 4.86
$CD8^+$	12.28 ± 2.8	11.41 ± 0.37
Thymus		
No. of cells ($\times 10^8$)	1.60 ± 0.08	1.58 ± 0.2
Population (%)		
$CD4^+$	7.72 ± 1.08	7.15 ± 1.15
$CD8^+$	2.69 ± 0.24	2.64 ± 1.43
$CD4^+$ $CD8^+$	83.57 ± 1.32	86.92 ± 1.17
$CD4^-$ $CD8^-$	6.72 ± 0.87	4.80 ± 1.79
Serum Igs (mg/ml)		
IgG	9.81 ± 0.66	7.81 ± 0.57
IgM	0.098 ± 0.02	0.097 ± 0.01
IgA	0.81 ± 0.04	0.83 ± 0.03

Table 3: Lymphocyte populations and serum antibody levels in A4GALT knockout mice

No significant difference in immunological profiling between the A4GALT knockout mice vs. wild type age-matched controls could be detected. This demonstrated that the protection of the A4GALT knockout mice against the lethal effects of Shiga toxin was due to the absence of Gb3 expression in the tissues and not due to the immunological profile of the mice. Data represents n=3 of each genotype (A4GALT knockout vs. wild type), mice were all female 4 weeks of age. *Table reproduced form Okuda et al.* [75].

1.2.9 Anderson-Fabry disease (over expression of Gb3)

Anderson-Fabry Disease (also known simply as Fabry disease) is an X-linked lysosomal storage disorder with an incidence of 1 in 50,000 males born in the UK [85]. In Fabry disease, there is an accumulation of Gb3 and galabiosylceramide in the lysosomes of affected organs due to deficiency in the enzyme α-galactosidase (Figure 1-16) [86]. Patients classically present with multi-system disease due to the skin, heart, nerves, brain, and kidneys all being affected. Diagnostic features include numbness of the fingers and toes, conjunctival telangiectasia, corneal opacities, angiokeratomas of the skin, anhidrosis and albuminuria [86]. Affected males usually develop cardiac abnormalities such as conduction defects or mitral valve disease by the age of 30 years; by which time they may have progressed to renal failure or suffer a stroke [86]. This pattern of symptoms reflects the distribution of Gb3 in the human body and has provided much insight into the physiological role of Gb3 and other globo-series glycosphingolipids [86].

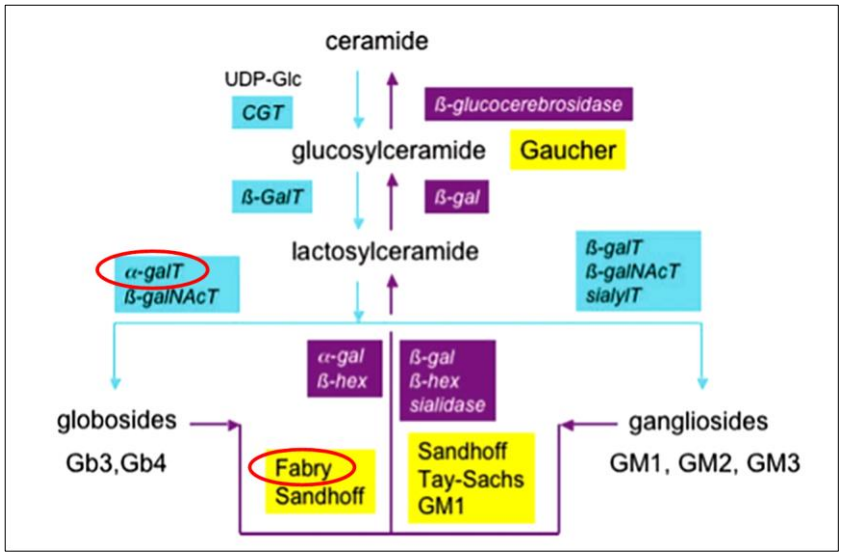

Figure 1-16: Pathways of glycosphingolipid metabolism

The biosynthesis of the carbohydrate core of glycosphingolipids from ceramide is shown by the blue arrows and catalysed by the glycosyltransferases denoted in blue boxes (α-galT=A4GALT) is circled in red. Catabolism is the reverse pathway and shown by the purple arrows, with the lysosomal enzymes denoted in purple boxes. α-gal= α-galactosidase which is deficient in Fabry disease and leads to accumulation of Gb3. Diseases that are caused by deficiency in the enzymes in the catabolic pathway are shown in yellow (Fabry disease is circled in red). CGT=ceramide glucosyltransferase; β-GalT= β-galactosyltransferase; α-galT=A4GALT; β-galNAcT=β-N-

acetylgalactosaminyltransferase; α-gal=α-galactosidase; β-gal=β-galactosidase; βhex=β-hexosaminidase; GM1= GM1 gangliosidosis. *Figure adapted from Butters et al.* [87]

There is currently no cure for Fabry disease, but intravenous recombinant α-galactosidase enzyme preparations (Fabrazyme® and Replagal®) are currently available for use in the treatment of the condition in the UK. An oral pharmacological agent migalastat hydrochloride, that facilitates trafficking of the α-galactosidase enzyme to lysosomes is also available. However, any effect of these treatments on the mortality of Fabry patients is not clear [88]. Of relevance to my work, the Fabry mouse (an α-galactosidase knockout) that over-expresses Gb3 in its organs (including the kidney) is protected from Shiga toxin toxicity, even when given a lethal dose of intraperitoneal Shiga toxin [89][90]. Furthermore, when Gb3 levels were reduced in these α-galactosidase knockout mice using an intravenous recombinant α-galactosidase enzyme, they became susceptible to the lethal effects of Shiga toxin [90].

This work clearly demonstrates that Gb3 is the receptor responsible for Shiga toxin toxicity *in vivo*. This finding is potentially explained by the accumulation of Gb3 in Fabry disease resulting in reduced delivery of Shiga toxin to target cells, due to re-direction of the toxin to multiple organs within the body, thereby neutralising its effect. However, given attempts to block Shiga toxin binding therapeutically in humans, with synthetic toxin binders such as STARFISH or Synsorb-Pk have been unsuccessful; it is unlikely that a scavenger effect is solely responsible for the observed protection of the Fabry's mouse against the lethal effects of Shiga toxin [64]. An alternative theory is that Gb3 accumulation in Fabry disease may lead to alterations in the intracellular trafficking of the toxin due to changes in Gb3 sub-populations [63][90]. Interestingly, to date there has never been a case of Shiga toxin HUS reported in a patient with Fabry disease.

1.2.10 Gb3 Expression in the kidney

From the studies discussed so far, it is clear that specific and high affinity binding of Shiga toxin to the Gb3 receptor is necessary in order for the toxin to exert its cytotoxic effects on a target cell [72]. Furthermore, the level of expression of the Gb3 receptor in a tissue correlates with the clinical manifestations of the disease even if this is not stoichiometric [33]. Methods of Gb3 detection include thin layer chromatography, lipid mass spectrometry and anti-Gb3 antibody techniques such as immunofluorescence and immunohistochemistry. These techniques have all been used to analyse the differential

expression of Gb3 *in vivo* [33]. In humans, the greatest concentration of Gb3 is found within the glomerulus of the kidney, with other cells including the colonic microvascular endothelium and the cerebellar endothelium also known to have high Gb3 expression [91]. Gb3 is also present in the lung, pancreas, heart and liver [91][92][93]. This pattern of expression could well explain the extra-renal manifestations that are known to occur in STEC HUS; although as already established the local microenvironment of the plasma membrane plays a key role in how sensitive a cell will be to the effects of Shiga toxin, not just the expression of the receptor itself [94].

1.2.10.1 Gb3 expression in glomerular endothelial cells

The general consensus amongst experts in the field of STEC HUS research is that it is a disease of the glomerular endothelium [33]. The first endothelial cells to be studied were large vessel endothelial cells from human umbilical vein endothelial cell (HUVEC) primary cultures. These were later found to be relatively resistant to the effects of Shiga toxin in comparison to microvascular glomerular endothelial cells [95]. Perhaps unsurprisingly, subsequent work found glomerular endothelial cells express 50 times more Gb3 on their cell surface than HUVECs which is thought to account for this difference in cytotoxicity [72]. Other endothelial cell types that have since been evaluated include human brain microvascular endothelial cells which apotose in response to Shiga toxin challenge; as well as dermal microvascular endothelial cells and lung microvascular endothelial cells both of which express Gb3 and are sensitive to Shiga toxin [93][96][97].

Why Shiga toxin exhibits a predilection for the kidney microvasculature remains unknown. It is likely due to a combination of factors including glomerular expression of Gb3, the specific properties of the membrane microenvironment in which Gb3 is located on the cellular surface, and local glomerular inflammatory responses to Shiga toxin. The differences in the baseline characteristics of individual endothelial cells according to both the vascular bed in which they are located and their individual gene expression profile is also likely to be of importance [98]. Together, these factors will influence glomerular endothelial extracellular matrix remodelling, angiogenesis and lipid metabolism which are all known to play a part in the cellular sensitivity and response to Shiga toxin exposure [98].

Several studies have demonstrated the importance of the host inflammatory response to infection with STEC and the development of HUS [99][100]. *In vitro* work has shown that leukocytes and monocytes release the pro-inflammatory cytokines TNFα and IL-1β in

response to Shiga toxin [101]. When glomerular endothelial cells are incubated with these cytokines, it results in upregulation of the expression of the Gb3 receptor, leading to an increase in the sensitivity of the cells to Shiga toxin. [72][98]. Interestingly, TNFα, IL-1β and bacterial LPS (lipopolysaccharide, found in the outer membrane of the cell wall of gram negative bacteria) were also found to increase the expression of Gb3 in HUVECs and increase their sensitivity to Shiga toxin *in vitro* [98]. Human *in vivo* data supports the role of inflammatory cytokines in the development of STEC HUS; with urinary levels of TNFα, IL-6 and IL-8 found to be increased in STEC HUS patients vs. healthy controls [72].

In vivo research into the role of local glomerular inflammatory responses in the kidney is somewhat limited however, due to the lack of small animal models that recapitulate STEC HUS and a paucity of human renal biopsy studies (which are rarely taken due to concomitant thrombocytopenia and the associated high risk of bleeding). *In vitro* culture of human glomerular endothelial cells under flow conditions (in an attempt to simulate the *in vivo* environment) by Zoja et al. has demonstrated that Shiga toxin stimulated leukocytes induce the upregulation of cell adhesion molecules E-selectin, ICAM-1, and VCAM-1 on the cell surface of glomerular endothelial cells [98]. The role of inflammatory cytokines, chemokines and cell adhesion molecules was further supported by gene expression studies in human glomerular endothelial cells treated with Shiga toxin, which also showed these signalling pathways were upregulated [98]. Clearly, local inflammatory responses within the kidney due to Shiga toxin play a key part in creating a local environment that favours the persistence of endothelial damage, platelet activation, and amplification of the microvascular injury within the kidney [98].

The specialised anatomy of the glomerular filtration barrier also needs to be considered in relation to development of STEC HUS. *In vitro*, human glomerular endothelial cells undergo apoptosis and are exquisitely sensitive to the cytotoxic effects of Shiga toxin [72]. In contrast damage to endothelial cells by Shiga toxin *in vivo* results in swelling and detachment of the cells from the glomerular basement membrane [33]. This type of injury is seemingly less severe than that observed *in vitro*. However, glomerular endothelium is dependent upon attachment to the basement membrane to remain viable; as well as being heavily reliant upon a supply of VEGF from neighbouring podocytes [72][102]. Thus, disruption in these survival signals will result in an increase in the glomerular endothelial susceptibility to Shiga toxin and may represent more severe injury than initially apparent. This observed discrepancy between the effects of Shiga toxin on glomerular endothelial

cells in culture vs. that observed *in vivo*, may however, suggest a protective mechanism within the glomerulus that is not present i*n vitro* [33]. Hence, the functional symbiosis and biological cross-talk known to exist between glomerular endothelial cells and podocytes within the glomerular filtration barrier *in vivo*, is likely to play a part in the pathogenesis of Shiga toxin HUS [33][102].

1.2.10.2 Gb3 expression in podocytes

Human podocytes are known to express the Gb3 receptor and are sensitive to Shiga toxin [1]. Work by Psotka et al. has confirmed that *in vitro*, human conditionally immortalised podocytes are almost as sensitive as human conditionally immortalised glomerular endothelial cells to Shiga toxin; with a CD50 (50% cytotoxic dose) of 0.5 pM versus 0.1 pM respectively [74]. However, the precise role of the podocyte in Shiga toxin HUS *in vivo* is yet to be elucidated. This is likely due to a lack of animal models of the disease, together with a general consensus that HUS is primarily an endothelial disorder.

In recent years, podocyte damage has been shown to be key in the development of a number of glomerular diseases including focal segmental glomerular sclerosis (FSGS), polycystic kidney disease (PKD) and diabetic nephropathy [33]. Furthermore, of particular relevance to my work, podocyte injury with increased podocyte turnover is now thought to be a key feature in the development of pre-eclampsia [103]. This is of interest because pre-eclampsia shares some clinical features with HUS, namely acute kidney injury and thrombocytopenia; and is also believed to be a disease of systemic endothelial dysfunction [33][104]. Further evidence in support of a key role of the podocyte in pre-eclampsia includes significant podocyturia in pre-eclamptic women compared to controls, and structural podocyte changes including down-regulation of podocyte associated proteins in human kidney biopsies at post-mortem [103][105]. In Shiga toxin HUS, markers of podocyte damage have also been detected in the urine of patients with the disease [106][107].

An interesting parallel has also been drawn between the biological features podocytes in the kidney and neurons in the brain, that has captured the attention of glomerular researchers [108]. Both cell types are terminally differentiated and are structurally similar with long microtubule protrusions and shorter actin cytoskeleton foot processes or dendritic spines. Furthermore, both podocytes and neurons express several tissue specific proteins including synaptopodin, drebin and podocin and have been shown to use glutamatergic intercellular signalling systems [108][109]. Fascinatingly, neurons and

podocytes both express the Gb3 receptor and are sensitive to Shiga toxin [72]. Indeed, the neurological sequelae seen in Shiga toxin HUS may well reflect the interaction between neurons and brain microvascular endothelial cells within the blood brain barrier; mirroring the cross-talk between podocytes and the glomerular endothelium within the glomerular filtration barrier resulting in TMA. Clearly, the interaction between these highly specialised epithelial cells and the neighbouring endothelium warrants further study to delineate the contribution of the podocyte in the pathogenesis of Shiga toxin HUS.

1.2.10.3 Gb3 expression in mesangial cells

Mesangial cells act as a glomerular scaffold, providing structural support for the glomerular capillaries and secreting a mesangial matrix of soluble factors to ensure glomerular homeostasis [110]. They are also known to regulate the glomerular filtration surface area and to phagocytose interglomerular apoptotic cells and debris [110]. Their role in Shiga toxin HUS is yet to be studied in detail. However, mesangial cells do express the Gb3 receptor and bind Shiga toxin *in vitro*. Shiga toxin acts to inhibit protein synthesis in these cells but does not result in apoptosis [72].

1.2.10.4 Extra-glomerular Gb3 expression

As already discussed, Shiga toxin HUS is a disease of the renal glomeruli, characterised by the histopathological lesion of glomerular TMA. However, the Gb3 receptor is found throughout the human nephron and highly expressed in renal tubular cells [94]. In fact *in vitro*, human proximal renal tubular cells are also sensitive to picomolar concentrations of Shiga toxin with a CD50 of 10 pM [74]. When exposed to Shiga toxin *in vitro*, proximal tubule cells release pro-inflammatory cytokines including TNFα and IL-6, chemokines, tissue factor and undergo apoptosis [33]. Shiga toxin also results in the inhibition of protein synthesis in these cells [72]. The physiological function of the proximal tubule is to reabsorb urinary filtrate solutes and water that have passed through the glomerular filtration barrier, maintaining fluid and electrolyte homeostasis [111]. Hence, proximal tubule injury from Shiga toxin may contribute to the dehydration and oliguria seen in patients with Shiga toxin HUS [72].

Similarly, human distal renal tubular cells and human collecting duct cells have also been reported to express the Gb3 receptor and bind Shiga toxin. These cell types have not been studied in significant detail in humans but again may play a part in the dehydration observed in Shiga toxin HUS patients [72]. What is interesting however, is that despite the

effects of Shiga toxin in human extra-glomerular cells *in vitro*, the disease is highly selective *in vivo* causing injury only within the glomerulus. Work by Lingwood et al. has shown that only glomerular Gb3 (not tubular epithelial cell Gb3) is detergent resistant; and that intracellular retrograde transport of the Shiga toxin-Gb3 complex is dependent upon Gb3 being located within lipid rafts (i.e. within a detergent resistant membrane) [94]. Thus, the selectivity of Shiga toxin to cause glomerular injury *in vivo*, may well be explained by the expression of glomerular Gb3 within detergent resistant membrane domains; rendering it highly susceptible to Shiga toxin toxicity [94]. Therefore, care must be taken in the interpretation of cell culture studies of Shiga toxin binding and cytotoxicity; as the plasma membrane microenvironment appears to be a significant factor in the pathogenesis of Shiga toxin HUS *in vivo*.

1.2.11 Animal models of Shiga toxin HUS

Currently, there are no small animal models that recapitulate all of the key pathological features of Shiga toxin HUS seen in human disease. Animal models of Shiga toxin HUS are needed to provide a better understanding of the mechanisms that lead to the development of acute kidney injury, in the hope of identifying new drug targets to treat the disease [112]. As already eluded to, information from human studies is limited due to the difficulty of obtaining kidney biopsies from patients due to high risk of associated bleeding from thrombocytopenia. Thus, any insight into the pathogenesis of Shiga toxin HUS in humans has been obtained from the analysis of kidney tissue at post-mortem; which represents only the final stages of the disease and is less helpful in determining important signalling pathways that result in development of the syndrome [33].

To date, the most common animal models used to study Shiga toxin HUS include those administering Shiga toxin or *E.coli* to mice, rabbits, gnotobiotic piglets and non-human primates such as the baboon [113]. Each model has a distinct response to Shiga toxin and differs in the predominant site of organ damage [33]. This observation likely reflects the species variation in Gb3 expression *in vivo*. For example, in contrast to humans, mouse and rat glomerular cells (including endothelial cells and podocytes) do not express Gb3 (Figure 1-17) [68]. Consequently, mice challenged with Shiga toxin (orally or intraperitoneally) develop lethal tubular disease without histological evidence of glomerular TMA [1]. In a mouse model reported by Keepers et al. administration of both Shiga toxin and LPS (lipopolysaccharide) was shown to cause some evidence of thrombus formation in glomeruli, but the predominant lesions were tubular and led to dehydration;

a phenomenon that is not seen in human disease [69]. Subsequent, work by Locatelli et al. in the same mouse model found C3 deposition on podocytes, which was associated with podocyte injury and loss [114]. The authors suggest that this was a consequence of alternative complement pathway activation, due to the fact that pre-treatment of the mice with a factor B inhibitory antibody prevented podocyte loss [114].

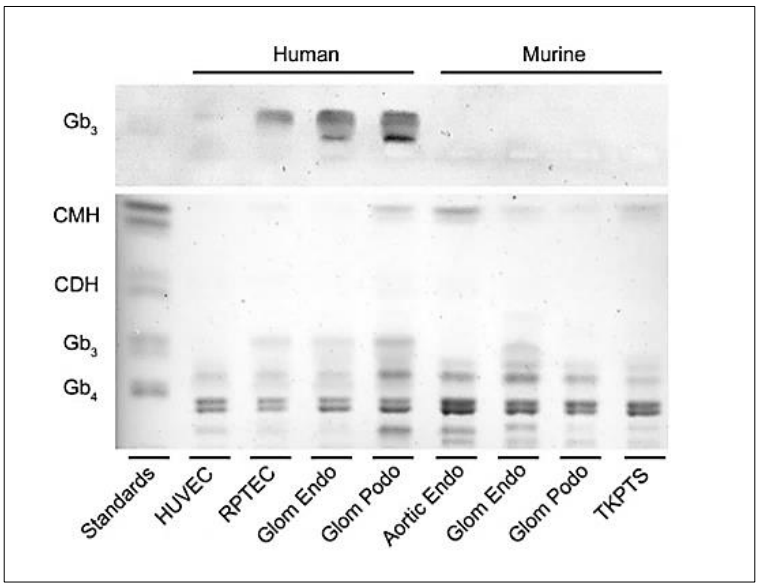

Figure 1-17: Thin layer chromatography (TLC) of neutral glycosphingolipids

Top panel shows TLC of total neutral glycosphingolipids with Shiga toxin overlay to specifically detect Gb3. Of note Gb3 is only present in human proximal tubule cells (RPTECs), glomerular endothelial cells and podocytes and is absent from mouse glomerular and renal proximal tubular cells (TKPTS). Bottom panel shows TLC with total neutral glycosphingolipids visualised with cupric acid sulphate to demonstrate loading in each lane of similar total lipid content. Lipid standards were used in the first column as a positive control for TLC with cupric acid. *HUVEC=human umbilical vein endothelial cells, CMH=ceramide monohexoside (also known as glucosylceramide), CDH=ceramide dihexoside (also known as lactosylceramide). Figure reproduced from Psotka et al* [74].

In an effort to circumvent the dehydration and tubular necrosis that occurs in rodent models; Dennhardt et al. administered intermittent subcutaneous Hartmann's solution as a volume substitute following intravenous administration of Stx2 in their 3 day and 7 day mouse models [113]. Despite this, a rise in haematocrit, profound weight loss and tubular injury remained the primary features of the disease that developed [113]. It has since

been shown that any vascular changes seen in rodent models are driven by the combined action of Shiga toxin and LPS. It is LPS that induces chemokine release (MCP-1, RANTES and MIP-1α) in the proximal tubule. If these chemokines are neutralised with monoclonal antibodies it results in the prevention of any thrombus formation and coagulation cascade activation [33][115]. Thus, at present mouse models of Shiga toxin HUS are significantly limited due to the absence of Gb3 expression in their glomeruli and as such do not recapitulate human disease.

Several other animal species have been used in an attempt to provide a more useful *in vivo* model of Shiga toxin HUS. In rabbits a naturally occurring species specific variant of STEC exists which can be used for oral inoculation. In response to this, rabbits develop acute renal failure, but this is a highly variable and inconsistent finding [33]. Porcine models have not been described in detail but, similar to murine models, tubular lesions predominate [1]. Primate studies most closely recapitulate the disease process observed in human kidneys but only following intravenous infusion with Shiga toxin [1][116]. Enteric bacterial infection with Shiga toxin-producing *E.coli* in primates does not lead to HUS, and bacterial translocation from the gut is not seen baboons [1][117][118]. This is in contrast to humans where STEC induce attaching and effacing lesions and inflammatory cytokine production in intestinal epithelial cells [1][119]. As such, non-human primate models are of use in the validation of observations in mouse studies but are expensive and impractical given the need for intravenous toxin administration. Furthermore, the lack of intestinal injury observed in baboons is a limitation of this model and suggests species-specific host factors are likely to be key in the pathogenesis of Shiga toxin HUS [1].

1.2.12 Pathogenesis of Shiga toxin HUS

The most important virulence trait of *E.coli* that leads to the development of Shiga toxin HUS is the production of a potent Shiga toxin [120]. However, this is not the only element that determines the pathogenesis of Shiga toxin HUS. It is a multi-step process, influenced by a number of both host and bacterial factors [98]. Firstly, STEC must be ingested and survive the acidic environment of the stomach to transit through the gastrointestinal tract to the large intestine. This is achieved through several mechanisms including the presence of an acid-tolerance response system (ATR) found within both *E.coli* and *Shigella* bacteria [65]. The ATR consists of a glutamate decarboxylase and glutamate/g-aminobutyrate antiporter, that facilitates transport of glutamate into the bacterium where it is decarboxylated in a reaction that requires a proton. The antiporter then expels the

reaction product to maintain a neutral pH within the bacteria [65]. A second mechanism is STEC production of the exopolysaccharide colonic acid. This enhances the buffering capacity of the bacterial cell wall through formation of a negatively charged mucoid matrix layer [65].

Upon arrival at the large intestine, STEC must compete with human commensal gut organisms to establish colonisation [120]. Colonisation involves the formation of attaching and effacing lesions (AE) between STEC and the intestinal epithelium. The genes responsible for this interaction are located within the locus of the enterocyte effacement (LEE) pathogenicity island, which has also been found within the EPEC *E.coli* pathovar [98][120]. The formation of AE lesions facilitates a non-invasive interaction between the bacteria and host, allowing STEC to remain within the colon and release Shiga toxin in to the gut lumen [120]. Shiga toxin not only causes direct damage to colonic blood vessels which results in bloody diarrhoea, but also translocate across the intestinal epithelium to enter the systemic circulation [98]. Exactly how Shiga toxin is taken up by human intestinal epithelial cells has been under much discussion, due to the fact these cells were initially thought to lack expression of the Gb3 receptor [1].

Early investigations of Gb3 expression in colonic epithelium involved thin layer chromatography analysis to determine the total glycosphingolipid content of the mucosal layer of a section of human large intestine [91]. Unfortunately, conclusive evidence could not be drawn from this work as samples were contaminated with intestinal endothelial cells which are also found within the mucosal layer of the intestine. Hence, there was considerable uncertainty as to whether the trace amounts of Gb3 that were detected were of epithelial on endothelial origin [91]. However, later work by Holgersson et al. using an anti-Gb3 antibody failed to detect any Gb3 expression on the cell surface of intestinal epithelium [121]. Several theories of Gb3 independent translocation pathways across the intestinal epithelium have subsequently been put forward as a result of this finding.

The first hypothesis is that Shiga toxin translocates through paracellular junctions, following the route of immune cell infiltrates activated by the toxin and LPS found in the cell wall of *E.coli*. The second, is that AE lesions made by STEC allow the passage of the toxin into the bloodstream via holes in the mucosa [91]. The third is that a Gb3 independent transcellular route exists, a theory supported by the finding that Shiga toxins are capable of cross-polarising intestinal epithelial cells *in vitro* despite apparent absence

of Gb3 expression in the cell line [120]. However, more recent work by Zumbrun et al. has now shown that Gb3 synthase (A4GALT) mRNA is detectable in human epithelial cells extracted from human colon tissue [91]. Through the use of laser capture microdissection, this group were able to circumvent the issue of intestinal endothelium contamination of the mucosal layer to study intestinal epithelium in isolation [91]. This finding suggests that some Gb3 is expressed on the intestinal epithelial cell surface *in vivo*, and that this may mediate Shiga toxin uptake in these cells.

To date, there is no evidence that Shiga toxin itself or the pro-inflammatory cytokines released in response to STEC infection (TNFα and IL-1β) cause upregulation of Gb3 receptor synthesis in colonic epithelium [122]. However, given the fact that Gb3 has only been found in small quantities on the surface of human intestinal epithelial cells; it is highly likely that inflammatory cell infiltrates and pro-inflammatory cytokines play a key role in priming these cells to enhance Shiga toxin translocation [65]. Certainly, in many other inflammatory diarrhoeal illnesses there is evidence of neutrophil transmigration across the intestinal epithelium with a breakdown in the epithelial barrier resulting in leakage of the contents from the gastrointestinal tract into the systemic circulation [65]. Furthermore, *in vitro* data has confirmed that STEC induced neutrophil migration augments the translocation of Shiga toxin across epithelial cells [65]. There are still many unknowns as to the mechanism of Shiga toxin uptake from the from the gut. However, much interest surrounds this area of research in the hope of finding a potential therapeutic intervention that could prevent Shiga toxin uptake from the intestinal lumen; thereby avoiding the subsequent clinical sequelae of STEC HUS [122].

1.2.13 Shiga toxin transportation to the kidney

Precisely how Shiga toxin is transported in the bloodstream to the kidney and other target organs such as the brain and pancreas is yet to be established [1]. Free Shiga toxin molecules have been isolated from the serum of human STEC HUS patients but in trace amounts only [123]. Therefore, current consensus is that that Shiga toxin prefers to circulate in Gb3 receptor cell bound complexes [123]. The interactions between Shiga toxin and human blood cell constituents, including red blood cells, platelets and monocytes have been investigated. All of these cells express Gb3 on their cell surface and are capable of binding Shiga toxin [98]. However, it is the role of neutrophils in the carriage of Shiga toxin that has generated the most interest in recent years; despite the fact these cells lack the Gb3 receptor [124]. This interest was initially prompted by *in vitro*

studies performed by te Loo et al. which demonstrated preferential binding of Shiga toxin to neutrophils in whole blood samples and in the systemic circulation of STEC HUS patients [98]. Notably, this work has never been reproduced (even by the same group); hence some uncertainty as to the validity of this finding exists [65].

Subsequent *in vitro* work has shown that direct incubation of Stx1 with neutrophils from healthy patients led to a reduction in their capacity to phagocytose pathogens but did not cause neutrophil apoptosis [125]. Incubation with Stx2, caused a delayed neutrophil apoptotic response that was abrogated by the protein kinase C inhibitor staurosporine [126]. Additionally, in human clinical observational studies, a high neutrophil count at initial presentation with STEC HUS, correlated with a worse clinical outcome [65]. Raised levels of IL-8 (a neutrophil chemoattractant) together with neutrophil activation have also been reported in patients with STEC HUS [65]. Furthermore, in the few human renal biopsy samples that are available from STEC HUS patients, a neutrophil rich glomerular inflammatory cell infiltrate has been observed early on in the disease process [127].

More recent work has identified the pattern recognition receptor, toll-like receptor 4 (TLR4) as the receptor that binds to Shiga toxin on human neutrophils [123]. Interestingly, TLR4 polymorphisms are known to influence both the frequency and severity of some other infectious diseases, including parasitic infections and urinary tract infections [128]. Hence, it is conceivable that these polymorphisms could explain the difference in individual susceptibility amongst human populations to develop STEC HUS following STEC infection [124]. Soluble forms of TLR4 have also been found to circulate in the bloodstream in humans with the capacity to bind to Shiga toxin and LPS, potentially attenuating the pro-inflammatory cytokine response of host macrophages and monocytes to STEC [129].

An alternative theory for the transport of Shiga toxin to target organs has been proposed by Stahl et al. This involves Shiga toxin containing microvesicles from infected erythrocytes, monocytes and platelets [130]. Stahl and colleagues demonstrated that these microvesicles were present in blood samples of patients with STEC HUS and generated *in vivo* by mice infected with *E.coli* O157. Moreover, they were also able to isolate Shiga toxin containing microvesicles from both human and mouse kidney tissue in these experiments [130]. Therefore, microvesicle transfer could explain the way in which STEC evades the host immune response to invade target Gb3 rich tissues. There remains much uncertainty as to the mechanism of Shiga toxin transfer to target organs in humans.

As discussed, many theories have been presented in the literature; it may be that these co-exist with each contributing to the overall pathogenicity of STEC HUS. For this reason, the generation of an animal model that recapitulates the disease would be invaluable to further dissect these mechanisms.

1.2.14 Microvascular thrombosis and fibrinolysis in Shiga toxin HUS

As previously eluded to, a key feature of Shiga toxin HUS is the formation of microvascular thrombi in the glomerulus and an impairment of fibrinolysis that results in a consumptive thrombocytopenia [72]. This process is known to be a result of an interaction between the glomerular endothelium and circulating platelets, with the role of other cell types and inflammatory cytokines yet to be fully understood. It has been established that platelet activation occurs in the early stages of the disease, with evidence of increased platelet degranulation, β thromboglobulin, platelet factor 4 and P-selectin in STEC HUS patient plasma [98]. Shiga toxin is thought to exert an indirect effect on platelets via induction of platelet stimulatory signals from monocytes. This is supported by *in vitro* studies, that have found Shiga toxin is only capable of inducing platelet aggregation in the presence of co-stimulation with thrombin or ADP [131].

The interaction between platelets and microvascular endothelial cells has also been investigated. It is now widely accepted that it is loss of endothelial cell thrombo-resistance that leads to the formation of microthrombi in target organs; rather than direct activation of platelets by Shiga toxin itself [98]. Indeed, co-culture studies performed in a high shear stress environment to mimic that of the glomerular capillaries, have confirmed that Shiga toxin acts to promote platelet adhesion in TNFα activated microvascular endothelial cells [98][132]. Von Willebrand factor has since been found to be responsible for this observation. *In vitro*, Shiga toxin induced the release of vWF multimers from endothelial cells which when pharmacokinetically blocked, reduced the formation of platelet microthrombi on the endothelium [72]. Shiga toxin has also been shown to delay the cleavage (and therefore inactivation of vWF) by ADAMTS13 *in vitro* [98]. Pro-inflammatory cytokines and chemokines produced by human endothelial cells and monocytes in response to Shiga toxin have also been reported to stimulate platelet adhesion [98]. Thus, the coagulation-inflammation-thrombosis network is likely to be of key importance in the formation of microthrombi in target organs in STEC HUS.

1.2.15 Potential treatments targeting Shiga toxin HUS

To date there are no specific treatments for Shiga toxin HUS, despite years of research to delineate the molecular pathways underlying the cellular response to Shiga toxin. Use of antibiotic treatment for STEC HUS is generally avoided at present due to lack of clinical evidence of efficacy [133]. Additionally, there is potential to worsen the clinical outcome for the patient as a result of accelerating Shiga toxin release from *E.coli* that are lysed by the antimicrobial itself [64]. Progress in development of potential pharmacological therapeutic agents has been challenging due to the sporadic, geographically dispersed nature of STEC HUS outbreaks and a lack in the availability of animal models that recapitulate the disease in which to test potential treatments. Moreover, there is little financial incentive for drug companies to develop treatments given that STEC HUS is relatively rare and affects a diverse patient population [134].

However, attempts have been made to block toxin binding with synthetic Shiga toxin binders such as STARFISH or Synsorb-Pk; and to inhibit intracellular transport of the toxin with molecules such as Exo1 and Golgicide A (Figure 1-18) [64]. Other agents have included the use of probiotic recombinant non-pathogenic *E.coli* strains with a high affinity receptor for Shiga toxin subunit B, designed to compete for Shiga toxin binding in the gut. When orally administered to mice, these bacterium efficiently neutralised the lethal effects of Shiga toxin [64]. Monoclonal antibodies targeting both Stx1 and Stx2 have also looked promising in animal models; with gnotobiotic piglets completely protected from STEC HUS when administered these antibodies 6-12 hours post Shiga toxin exposure [135].

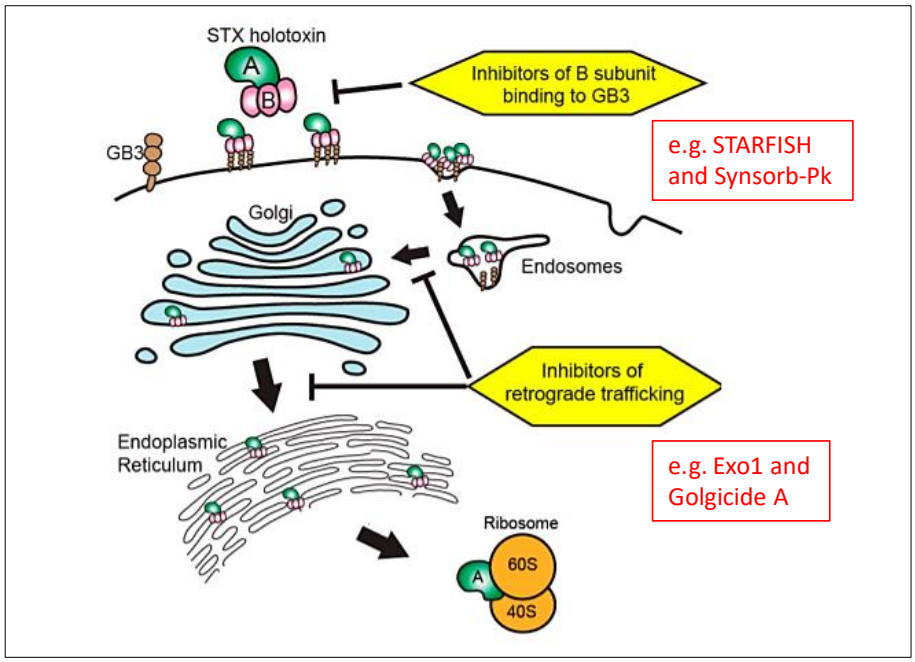

Figure 1-18: Shiga toxin treatments targeting Gb3 binding and retrograde intracellular trafficking
Therapeutic attempts have been made to neutralise Shiga toxin binding to Gb3 at the B subunit of the receptor. These include the binders STARFISH and Synsorb-Pk. Once internalised Shiga toxin undergoes retrograde trafficking from endosomes through the Golgi network to the endoplasmic reticulum (ER). The toxin is processed as a result of this trafficking to release the A subunits in to the cytoplasm which interact with ribosomes to depurinate them, resulting in ribotoxicity. Inhibitors that have been developed to target Shiga toxin trafficking include Exo1 and Golgicide A. *Figure adapted from Hall et al* [134].

A summary of therapeutic agents that have been developed as potential therapies for STEC HUS are shown in Table 4. Notably, very few treatments have made it through to clinical trial and of these (namely Synsorb-Pk and Urtoxezumab®) not one has progressed beyond Phase II [134]. In both cases this was attributable to the fact that although the drug therapy was safe to administer to humans, there was no prevention of death or serious extra-renal manifestations in STEC HUS patients seen with either treatment. Furthermore, there was no evidence for a reduction in the need or duration of renal replacement therapy for STEC HUS patients [136] [137]. The role of complement inhibitors (such as C5 inhibitor eculizumab) in STEC HUS represents an area of controversy and will be discussed in detail later in the chapter.

Therapeutic	Drug Class	Target	Mechanism of Action	Animal Models Tested	Clinical Trials Completed
Anti-sera	Polyclonal antibodies	STX, STX2	Circulating toxin neutralization	Pig, rabbit	None
Urtoxezumab®	Humanized murine monoclonal antibody	STX2	Circulating toxin neutralization	Rodent, NHP	Phase II
cαSTX1 and cαSTX2	Humanized murine monoclonal antibody	STX1, STX2	Circulating toxin neutralization	Rodent	Phase I
Murine anti-STX2	Murine monoclonal antibody	STX2	Circulating toxin neutralization	Rodent	None
Anti-STX antibodies (various clones)	Human monoclonal antibody	STX1, STX2	Circulating toxin neutralization	Rodent, pig	None
Camelid anti-STX oligomers	VHH-based neutralizing agent	STX1, STX2	Circulating toxin neutralization	Rodent	None
Adenoviral anti-STX2 construct	VHH-based neutralizing agent	STX2	Circulating toxin neutralization	Rodent, pig	None
Tetravalent peptides	Gb3 analogs	STX1, STX2	Circulating toxin neutralization	Rodent, non-human primate	None
Synsorb-Pk®	Silicon dioxide-Gb3 construct	STX1, STX2	Gastrointestinal toxin neutralization	None	Phase II (failed)
Retro 1 and Retro 2	Small molecule inhibitors	STX1, STX2	Retrograde trafficking inhibitor	Rodent	None
Manganese	Enzyme cofactor	STX1	Retrograde trafficking inhibitor	Rodent	None

Table 4: Shiga toxin therapies in early development

Many treatments are under development or in pre-clinical trials in an attempt to neutralise Shiga toxin binding or prevent retrograde intracellular trafficking once endocytosed by the cell. To date, not one of these therapies has been shown to improve outcome in patients with Shiga toxin HUS. *Table adapted from Hall et al* [134].

1.2.16 Atypical HUS

Accounting for 10% of HUS cases, atypical HUS (aHUS) is a rare condition associated with significant morbidity and mortality. In up to 50% of patients aHUS leads to end-stage renal disease [138]. Accurate estimates of the incidence of aHUS are difficult to ascertain, as many cases remain undiagnosed and the figures that are reported often include similar disorders such as STEC HUS and TTP [139]. A recent systemic review into the epidemiology of aHUS by Yan et al. has reported a worldwide incidence of between 0.23 to 1.9 per million population [140]. Interestingly, in children aHUS occurs in females and males equally, whilst in adults a female preponderance is observed [140].

Atypical HUS is known to be associated with complement pathway dysregulation, with at least 50% of cases found to be due to an underlying inherited or acquired complement gene abnormality [141]. These may be loss of function mutations in complement regulatory factors or gain of function mutations in C3 or factor B [142]. Auto-antibodies against complement regulatory factors (including the most well characterised factor H

auto-antibodies) have also been found to cause an acquired form of aHUS [1]. In aHUS patients with complement gene abnormalities, there is a loss of protection of the glomerular endothelium against complement attack and the development of glomerular TMA. Often, a trigger event is required to unmask this underlying genetic predisposition prior to clinical presentation with the disease [141]. Such trigger events include: autoimmune conditions, transplantation, pregnancy, infection, malignancy and drugs such as the oral contraceptive pill and chemotherapy agents [143].

In some patients, identifying the specific complement abnormality that has led to aHUS can be a challenge; both due to the vast number of genetic variants and risk haplotypes for complement genes that have been described, and due to the possibility of a co-existent trigger event having occurred [141]. Additional uncertainty exists as a high proportion of the mutations that are found in patients tested for aHUS, may not be of biological or clinical relevance in the development of the disease [144]. Consequently, genetic variants are now classified internationally as 'benign, variant of uncertain significance, likely pathogenic and pathogenic' to aid in this process [141]. Given the complexity of diagnosis and the requirement to identify pathogenic genetic variations, hybrid genes, and genomic rearrangements in CFH/CFHR genes with accuracy; a National rapid diagnostic genetic testing centre for aHUS has been set up in the UK [145].

Inheritance of pathogenic genetic variants in aHUS may be sporadic, autosomal recessive or autosomal dominant with incomplete penetrance [144]. Through international collaboration, the study of hundreds of aHUS patients and their underlying genetic variation in complement regulation has been made possible. This work has provided powerful prognostic information to clinicians, allowing them to give aHUS patients an indication of their individual risk of disease progression, response to therapy and post-transplantation recurrence [28][141][146]. For example, mutations in complement factor H (CFH) are known to be associated with the worst outcomes, whereas those with membrane cofactor protein (MCP) mutations do far better. This is perhaps not surprising given that MCP is a transmembrane protein which is highly expressed in the kidney; hence kidney transplantation corrects the MCP defect and restores MCP solid phase activity. This is in contrast to mutations in circulating (fluid phase) complement factors H and I, which are predominantly of hepatic origin [2].

A minority of atypical HUS cases have been attributed to dysfunction in the degradation of von Willebrand factor, thrombomodulin mutations or loss of function mutations in

diacylglycerol kinase ε (DGKε) [146]. Indeed, the discovery in 2013 by Lemaire et al. that recessive mutations in DGKε cause aHUS in a significant proportion of children; led to a conceptual change in the pathophysiology of aHUS and recognition that an inheritable, non-complement driven mechanism could cause the disease [147]. DGKε was the first gene to be associated with HUS that did not have a direct role in alternative pathway complement activation [148][149]. Diacylglycerol kinases (DGKs) are intracellular lipid kinases that phosphorylate diacylglycerol (DAG) to phosphatidic acid (PA) leading to termination of DAG signalling [148]. The DGKε isoform preferentially phosphorylates arachidonic acid containing DAG (AADAG) to PA thereby terminating AADAG signalling (Figure 1-19) [148].

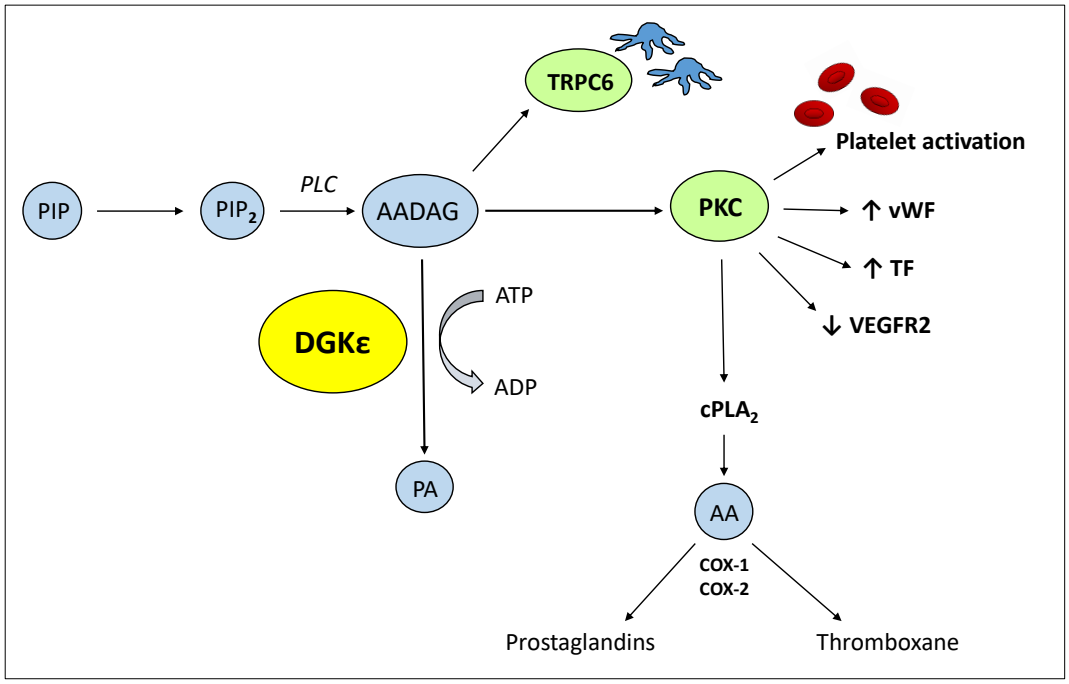

Figure 1-19: The AADAG signalling pathway

DGKε is an intracellular kinase that preferentially phosphorylates AADAG to PA which terminates AADAG signalling. Loss-of-function mutations in DGKε therefore, lead to unregulated AADAG signalling and PKC dependent platelet activation with an increase in production of prothrombotic factors including vWF and TF. *PIP=phosphatidylinositol, PIP_2=phosphatidylinositol-4,5-bisphosphate, PLC=phospholipase C, AADAG=arachidonic acid diacylglycerol, ATP=adenosine triphosphate, ADP=adenosine diphosphate, DGKε=diacylglycerol kinase ε, PA=phosphatidic acid, TRCP6=transient receptor potential cation channel 6, PKC=protein kinase C, vWF=von Willebrand factor, TF=tissue factor, VEGFR2=vascular endothelial growth factor receptor 2, $cPLA_2$=cytosolic*

phospholipase A_2, AA=arachidonic acid, COX=cyclooxygenase enzyme. Figure reproduced from Bowen et al. with permission [1].

AADAG is a key intracellular signalling molecule that activates protein kinase C (PKC). AADAG-dependent PKC signalling promotes thrombin-induced platelet activation. In endothelial cells it has been shown to increase production of prothrombotic factors such as von Willebrand factor and tissue factor; as well as downregulating VEGF receptor VEGFR2 signalling, which has been linked to TMAs previously [147][149]. Bruneau et al. have demonstrated in endothelial cells that knockdown of DGKε results in a proinflammatory and prothrombotic state via over activation of p38 and p44/42 MAP kinases [148]. In podocytes DAGs have been shown to modify slit diaphragm function and through PKC-dependent pathways downregulate expression of VEGFR2 [149]. Hence, the hypothesis that loss of function mutations in DGKε results in sustained AADAG signalling and a subsequent prothrombotic state. This finding has important implications for the management of atypical HUS, which to date have focused upon complement blockade.

1.3 The Complement Cascade

The complement system has been implicated in a number of renal diseases and represents an area of great interest amongst the nephrological community [150]. As already discussed, in the majority of cases atypical HUS is caused by impaired regulation of complement activation on glomerular endothelial cell surfaces [151][138]. Complement hyperactivation following Shiga toxin exposure has also been proposed as a mechanism in the development of infection associated HUS although this yet to be proven [2]. A recent study from Ozaki et al. has demonstrated that inhibition of the mannose binding lectin (MBL) complement pathway protected mice against renal injury due to Shiga toxin exposure [152]. Thus, an understanding of the complement pathway is essential prior to delving into the pathophysiology of HUS irrespective of aetiology.

The complement pathway forms part of the innate immune response and consists of 60 proteins which play a vital role in the host defence against pathogens and in the maintenance of tissue homeostasis [2]. These proteins can be plasmatic (fluid) or membrane bound receptors (solid) [3][153]. The complement system has several key functions which include: lysis of target cells through opsonisation, production of pro-inflammatory mediators and regulation of the adaptive immune response [154]. Three

pathways leading to activation of the complement cascade have been described: classical, lectin and alternative (Figure 1-20). All three culminate with the formation of the membrane attack complex (MAC) leading to the insertion of pores in the target cell membrane resulting in osmotic lysis and cell death [2][153].

The classical pathway is activated by binding of C1q to the Fc portion of complement-fixing antibodies (usually IgM or IgG) that are attached to the surface of a pathogen; leading to the formation of antibody-antigen immune complexes (Figure 1-20). The lectin pathway is triggered by the binding of germline encoded pattern recognition receptors (PRRs) such as MBL, ficolins and cytokeratin; to mannose containing carbohydrates on microbial surfaces which activate MASP 1 (mannan-binding lectin serine protease 1) and MASP 2 [2][155]. Mannose containing carbohydrates are an example of pathogen associated molecular patterns (PAMPs). Other examples of PAMPs recognised by the lectin pathway include: LPS found in gram negative bacterial walls, peptidoglycan, lipoteichoic acid (LTA) of gram positive bacteria and β-glucan of fungi [156].

In contrast to the incredibly diverse adaptive immune response, capable of recognising an almost infinite number of invading pathogens due to somatic gene rearrangements in lymphocyte antigen receptor gene segments; PRRs in the lectin pathway are focused on the recognition of a few highly conserved PAMPs that are present in large numbers of microorganisms [156][157]. This results in a system where a number of PRRs recognise a given pathogen to ensure a rapid and effective inflammatory response whilst maintaining some specificity [158]. Both the classical and lectin pathways lead to the generation of the same C3 convertase, C4b2a on target cell surfaces resulting in proteolytic cleavage of C3 into anaphylatoxin C3a and opsonin C3b [2][153].

The alternative pathway differs from the other two, in that it is continually active at low levels in the plasma. This is due to spontaneous hydrolysis of C3 (circulating in abundant amounts in human plasma) to C3b analogue C3(H20). This conformationally rearranged product of C3 cleavage shares functional similarity with C3b and is able to bind to Factor B, activating its cleavage into Ba and Bb by Factor D [159]. This facilitates the formation of the alternative pathway C3 convertase C3bBb. C3bBb forms the basis of a positive feedback loop, amplifying alternative complement pathway activity; which can be further potentiated by Factor P (properdin) which acts to stabilise the C3bBb complex [156]. Thus, the generation of C3 convertase is the central point at which all three sub-divisions of the complement pathway converge (Figure 1-20). The cleavage of C3 into C3b (whether by

C4b2a or C3bBb) exposes an internal thioester bond which facilitates stable covalent binding of C3b to hydroxyl groups on the target cell surface via trans-esterification [160]. This action effectively underpins the entire complement cascade; with C3b opsonisation marking pathogens as foreign, resulting in further amplification of the complement system which terminates in the assembly of the C5b-C9 MAC and cell lysis [156].

Of note, the alternative complement cascade may account for as much as 80% of MAC terminal pathway activity [155]. This is due to the efficiency of the positive feedback amplification loop within the system. Hence, the alternative complement cascade has great potential for non-specific destruction once activated; hence it is vital that host cells are protected. Under physiological conditions, complement activation is tightly regulated by a number of plasma and membrane bound factors [2][153]. As evident in atypical HUS, if these regulatory mechanisms fail there is uncontrolled alternative complement pathway activity leading to glomerular endothelial cell injury and TMA [161].

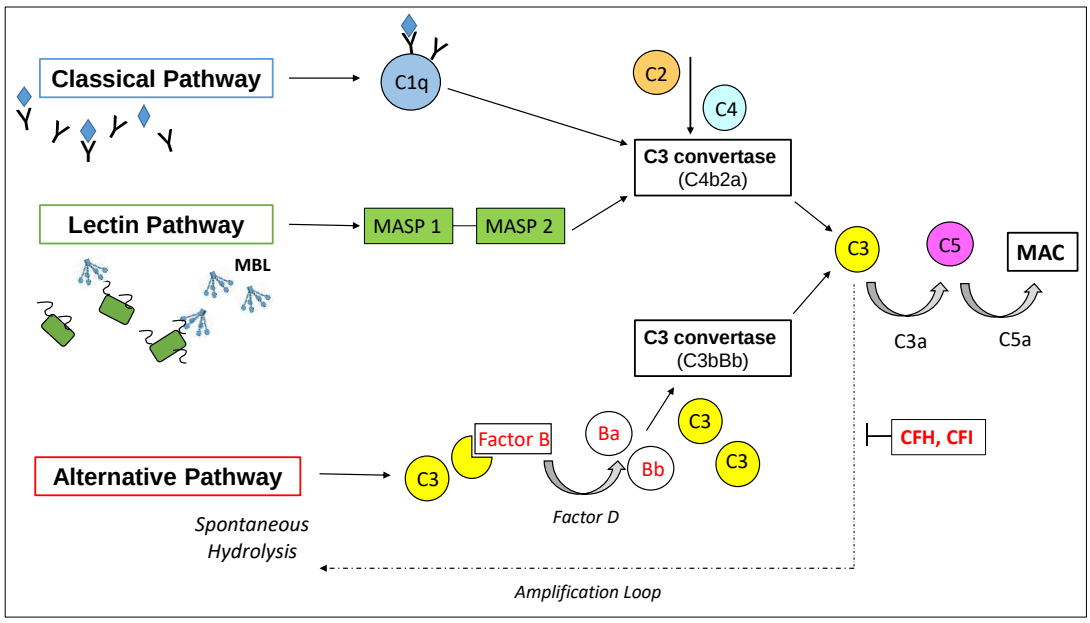

Figure 1-20 The complement cascade

Three pathways have been described leading to activation of the complement pathway; classical, lectin and alternative. All culminate with the formation of the membrane attack complex (MAC) leading to the insertion of pores into the target cell membrane resulting in osmotic lysis and cell death. The alternative pathway differs from the other two in that it is continually active at low levels in the plasma and is activated by spontaneous hydrolysis of a thioester bond in C3. To protect host cells from non-specific destruction complement activation is regulated by a number of plasma

(CFH, CFI) and membrane bound factors [2][153][155]. *Figure reproduced from Bowen et al. with permission* [1].

1.3.1 Complement Regulation

It is essential that complement activation is regulated to prevent excessive cell injury and inflammation [138][155]. Host cells are protected by surface bound and soluble plasma complement regulatory proteins. Of particular importance are the plasma proteins factor H and factor I which negatively regulate the C3b amplification loop (Figure 1-20). Although found in the plasma both can act in the fluid phase and on cellular surfaces. Their role on cell surfaces that lack membrane bound complement regulators e.g. the glomerular basement membrane in the kidney is vital as they are the only defence against complement attack and thrombus formation [138][162]. Notable membrane bound complement factors include CD46 (MCP – membrane co-factor protein), CD55 (DAF – decay activating factor), CD59 and CR1. By definition, these surface bound complement regulatory proteins are restricted in activity by their cellular expression and distribution. The exception being CR1 which is expressed by neutrophils, lymphocytes and erythrocytes which circulate throughout the body rather than being tissue bound [162]. The role of the key regulatory factors involved in the modulation of complement activation are discussed below.

1.3.1.1 Serum based complement regulator: complement factor H

Complement factor H is a 150 kDa glycoprotein, synthesized in the liver and found circulating in the serum at a high concentration [161]. It is thought to be the most important fluid phase regulator of the alternative complement pathway [163]. The structure of human factor H has been well characterised and is known to consist of 20 complement control protein domains (CCPs) (Figure 1-21) [164]. CCP domains 1-4 are located at the N-terminal of the protein forming a C3b binding site. CCP 7 contains several binding sites, recognising ligands found on host cell surfaces including: glycosaminoglycans, pentraxins and malondialdehyde epitopes that facilitate self / non-self discrimination. C-terminal CCP 19-20 regions also include binding sites for C3b (and C3d) which act to securely anchor factor H to host cell surfaces that are under complement attack and have been opsonisated with C3b [165].

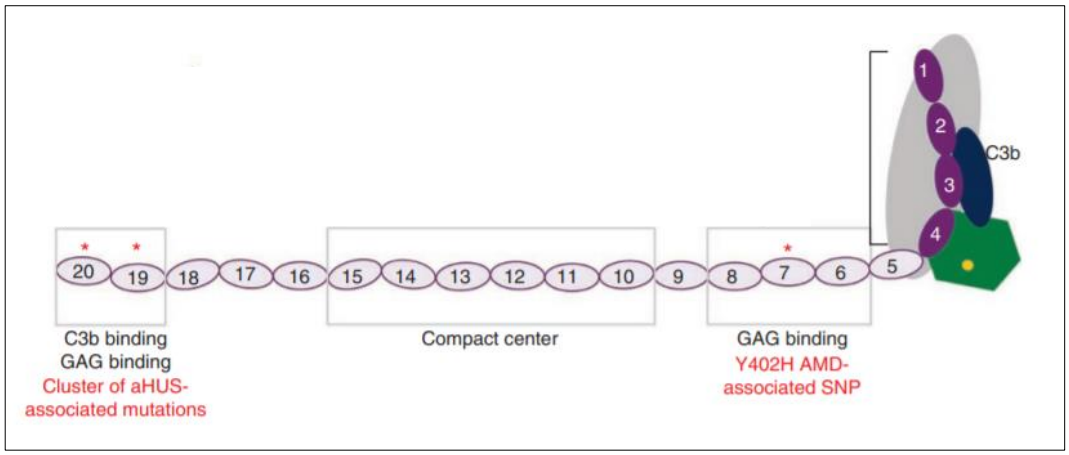

Figure 1-21: Structure of complement factor H

Complement factor H consists of 20 complement control protein domains (CCPs) outlined in purple. CCP domains 1-4 are located at the N-terminal of the protein forming a C3b binding site as indicated. CCP 7 contains several binding sites, recognising ligands found on host cell surfaces such as glycosaminoglycans (GAGs). C-terminal CCP 19-20 regions also include binding sites for C3b (and C3d) which act to securely anchor factor H to host cell surfaces that are under complement attack. Many mutations in factor H CCP domains have been reported in association with disease; * indicate the key mutation CCP sites associated with aHUS and age-related macular degeneration (AMD). *Figure adapted from Morgan et al* [164].

The regulatory activity of factor H occurs via several mechanisms. Firstly, it competes with factor B to bind to C3b preventing formation of the C3 convertase complex (C3bBb). Secondly, it accelerates the irreversible degradation of C3 convertase into its constituents. Finally, it acts as a co-factor for factor I-mediated C3b proteolytic cleavage, inactivating C3b so that it cannot bind to circulating factor B [163][164]. Interestingly, it has been demonstrated through factor H binding assays, that attachment of factor H to C3b or C3 convertase (C3bBb) is enhanced when these molecules are bound to host cell negatively charged glycosaminoglycans, sialic acid and heparin sulphate; i.e. the constituents of the glycocalyx found on many cells including the glomerular endothelium [161][166]. It is this high affinity interaction between factor H and host cell bound C3b or C3bBb, that facilitates factor H enrichment on host cells, ensuring self-recognition and protection against the innate immune system complement response [164].

The importance of factor H regulation in complement pathway activation is evident from genetic analysis of aHUS patients. Indeed, it was the finding by Warwicker et al. in 1998 that a mutation in factor H led to the development of aHUS, that prompted the search

and subsequent discovery of over 200 mutations in complement regulatory genes responsible for the disease [2]. Today, up to 60% of cases of aHUS are associated with identifiable mutations in complement cascade activation or its regulation [161]. Of these, 25% are associated with the genes encoding factor H; making it the most frequent genetic abnormality associated with the condition [161]. These mutations are usually heterozygous, with the majority affecting the C-terminus of the protein and therefore factor H protection of the host cell surface [163]. Mutations in factor H are associated with a poor prognosis, with 60-70% of patients reaching end stage renal failure or dying within one year of diagnosis [161].

The factor H mutations associated with aHUS have been extensively studied, with functional red blood cell lysis assays confirming that mutations in the C-terminal region of the protein, lead to failure to control C3 activation at the glomerular endothelial cell surface [163]. Interestingly, in the majority of patients mutations in factor H do not result in a reduction of detectable plasma levels of the protein [154]. Additional work by Stahl et al. has shown that C-terminal factor H mutations can also result in the loss of factor H protection of platelets from complement attack [167]. Consequently, platelets are activated and aggregate to form microthrombi. Combined, this loss of factor H protection on both glomerular endothelial cells and circulating platelets is thought to give rise to a pro-coagulant state which culminate in aHUS [163].

To date, *in vivo* work has centred around two transgenic genetic mouse models: the complement factor H homozygote knockout mouse (CFH -/-) and a homozygote factor H C-terminal (CCP 16-20) knockout mouse. The former has been reported to have incredibly low C3 levels as a consequence of uncontrolled alternative complement pathway activation; and displays a renal phenotype reminiscent of membranoproliferative glomerulonephritis (MPGN) i.e. accumulation of C3 and electron dense material along the renal glomerular basement membrane [163][168]. The latter spontaneously develops aHUS and has much higher levels of circulating C3. This work suggests that mutations in complement factor H C-terminal regions *in vivo*, result in local glomerular complement dysregulation but control of alternative pathway activity in the plasma [168]. Fascinatingly, crossing the factor H C-terminal knockout mouse with a C5 deficient mouse resulted in protection from the aHUS phenotype; suggesting that C5 activity is vital in the development of aHUS and perhaps explaining the success of eculizumab in treatment of the disease [169].

1.3.1.2 The factor H protein family

The complement regulator factor H is a member of the factor H protein family, which consists of 8 glycoproteins that are encoded by 6 genes [170]. All CFH family proteins are produced in the liver and consist of distinct, individual folding domains known as complement control protein domains (CCPs). The CFH family share common features which are reflected at a genomic level by the tandem arrangement of the CFH gene and the 6 factor H-related protein encoding regions which are all found within the CFH gene cluster on human chromosome 1 [171]. The CFH gene cluster itself, is located within an even larger gene cluster on chromosome 1 referred to as the 'regulators of complement activation' (RCA) cluster [172]. The RCA cluster encodes more than 60 genes, of which 15 are related to complement regulation, including not only the genes for factor H and the family of factor H proteins; but also, membrane bound complement regulators MCP, CD55 and CR1. Thus, complement regulatory genes that are encoded in the RCA share a common genetic ancestral motif from which they originated by multiple genetic duplication events [172].

Complement factor H-like protein (FHL-1) is the most similar in structure to factor H, generated from an alternatively spliced mRNA transcript derived from the CFH gene [170]. FHL-1 contains the 7 CCPs from the N terminal of factor H, together with 4 unique amino acids located at its C-terminus. Therefore, it is hardly surprising given FHL-1 shares such genetic homology with CFH, that it emulates both the complement inhibiting and C3b or C3bBb ligand binding capabilities of factor H [171]. The role of FHL-1 was largely undetermined until research by Clark et al. demonstrated that this protein is the main complement regulator of the human retinal pigment epithelium of the eye and that only in this truncated form (not the fully sized glycosylated factor H form) is it able to passively diffuse into Bruch's membrane [173]. Bruch's area is the innermost layer of the choroid of the eye and a key site at which age-related macular degeneration (AMD) occurs [174].

Factor H gene polymorphisms are known to be associated with an increased risk of AMD, a condition characterised by the formation of drusen (aggregates containing activated complement factors and inflammatory mediators) within Bruch's membrane [173]. Clark et al. went on to demonstrate that the binding of FHL-1 to retinal epithelium involved interactions between FHL-1 and heparin sulphate on the cell surface. Moreover, the commonest CFH polymorphism associated with AMD (Y402H) was shown to significantly reduce this interaction, resulting in loss of FHL-1 protection against complement attack

[173]. Interestingly, the drusen of AMD are structurally similar to the dense deposits seen in the glomerular basement membrane of the kidney in patients with MPGN type II [175]. In fact, MPGN type II patients are often found to have co-existent drusen in their eyes and may develop visual impairment alongside renal failure [176]. Together, these observations imply that dysregulation of the alternative complement pathway secondary to Factor H (or indeed FHL-1 mutations) contributes to the development of both AMD and MPGN type II [175].

The remaining members of the factor H family are known as the complement factor H related proteins (CFHR). In stark contrast to factor H, they lack potent complement regulatory activity; although some have been reported to be involved in modulatory activity as potential co-factors for factor H [171][177]. The CFHR proteins all lack the N-terminal CCPs of Factor H which is likely to account for the observed loss of C3 convertase decay accelerating activity [165]. Further work is required into the precise roles of each CFHR protein; with most recent work suggesting that some of these glycoproteins may in fact be antagonists of Factor H, acting to fine-tune the host's complement regulatory response [170].

1.3.1.3 Serum based complement regulator: complement factor I

Factor I is an 88 kDa glycoprotein predominantly synthesized in the liver; unlike the majority of other complement regulatory proteins, the factor I gene is located on chromosome 4 and not within the RCA of chromosome 1 [178]. Prior to its secretion it undergoes proteolytic cleavage of its linker protein by furin; to produce a 37 kDa enzymatic light chain bound to a 55 kDa heavy chain residue of unknown function [163][178]. However despite this post-translational processing, factor I remains proteolytically inactive and circulates in the plasma in a 'zymogen-like' state [179]. Studies by Roversi et al. mapping the crystal structure of the factor I molecule, suggest that the heavy chain allosterically inhibits the serine protease activity of the light chain until the C3b/cofactor complex engages [179].

Factor I is recruited to sites of complement activation to regulate the host immune response [178]. It requires the presence of a co-factor (such as Factor H, MCP, CR1) in order to cleave the α chains of C3b or C4b. These co-factors are either found intrinsically expressed on host cells or have mechanisms to ensure preferential recognition of host cell surfaces. The need for co-factor presence to facilitate Factor I complement regulation, ensures host tissue is protected from injury whilst preventing non-specific C3b

degradation in the context of appropriate complement activation by a microbe [156]. The proteolytic cleavage of C3b and C4b by Factor I, inactivates them and prevents the formation of C3 and C5 convertases, respectively [163]. Thus, Factor I prevents amplification of the complement cascade, regulating both the classical and alternative complement pathways [178].

Mutations in Factor I are responsible for up to 10% of aHUS cases. The majority of these are heterozygous and located in the serine protease region of the glycoprotein [161]. Factor I mutations lead to a decrease in regulatory activity and impaired degradation of C3b and C4b [154]. Serum factor I levels in these patients is usually within normal range [163]. Patients with factor I mutations have a poor prognosis, with 50% progressing to end stage renal failure or dying within 2 years of initial presentation. Often factor I mutations are present in association with other complement regulatory gene polymorphisms [161].

1.3.1.4 Membrane bound complement regulator: MCP (CD46)

Membrane bound co-factor protein (MCP) also known as CD46 is a cell surface bound glycoprotein, expressed on nucleated host cells (i.e. it is absent from red blood cells). MCP consists of 4 CCPs which form the extracellular component of the protein, a transmembrane region and an alternatively spliced cytoplasmic tail residue [163]. The MCP gene is located on chromosome 1 within the regulators of complement activation (RCA) cluster [172]. As aforementioned, MCP is a co-factor for factor I, facilitating the inactivation of C3b and C4b that has bound to host cells [163]. Mutations in MCP are identified in up to 15% of aHUS patients. These are predominantly heterozygous and located within the extracellular domain of the protein, resulting in reduced MCP activity and dysregulation of complement activation on host cell surfaces [154]. Interestingly, MCP mutations are more often reported in paediatric cohorts and are associated with a lower risk of progression to end stage renal failure than in other fluid phase complement regulatory mutations [161]. Furthermore, in those patients that do require kidney transplantation, prognosis (i.e. likelihood of recurrence of TMA) is significantly better than in aHUS patients with fluid phase complement regulator mutations [161].

1.3.1.5 Membrane bound complement regulators: CD55, CD59 and CR1

CD55 or decay activating factor (DAF) is another membrane bound complement regulator, which acts to prevent the amplification of the alternative complement cascade through inhibition of C3 convertase assembly [156]. It is a 70 kDa protein, attached to the host cell

surface by a glycophosphatidylinositol (GPI) anchor [180]. Unlike MCP, DAF is expressed on the surface of erythrocytes. In fact, the importance of DAF protection on host red blood cells is evident from the occurrence of the rare condition, paroxysmal nocturnal haemoglobinuria (PNH). In PNH, there is a reduction of DAF expression on erythrocytes (due to mutations in the enzymes required to catalyse GPI synthesis); with subsequent loss of protection from destruction by the complement system [181]. In aHUS patients, very few mutations in DAF have been described and to date these mutations have not been linked to any functional abnormalities in complement regulation [182]. Interestingly, in the DAF knockout mouse model although erythrocytes were susceptible to increased complement attack, no evidence of glomerular TMA or renal disease was reported [182][183]. These findings suggest that DAF is likely to be a key regulator of complement activation on the surface of red blood cells but is perhaps less important in the pathogenesis of aHUS.

Other membrane bound complement regulators expressed on circulating blood cells include CD59 (also known as MAC inhibitory protein) and CR1. CD59 is a GPI anchored protein that prevents the polymerisation of C9 and subsequent MAC formation [184]. As such, reduction in CD59 expression on erythrocytes (again due to mutations in the enzymes required to catalyse GPI synthesis) is also associated with PNH [185]. Currently, no functional mutations in CD59 have been identified in aHUS patient cohorts [186][187]. CR1 is a glycoprotein encoded by the RCA cluster region on chromosome 1, that is expressed by many human cells including erythrocytes, leukocytes, dendritic cells, and podocytes [188]. CR1 binds C3b to deactivate alternative complement pathway convertases and acts to accelerate the decay of the classical and lectin pathway convertases through binding of C4b. In addition to shortening the half-life of preformed C3 and C5 convertases and preventing the assembly of new C3 convertases; CR1 also acts a co-factor for the cleavage of C3b and C4b by Factor I [156].

Fascinatingly, the podocyte is the only epithelial cell that has been identified to express CR1; resulting in much interest as to its physiological role in the kidney. To date *in vitro* research in this area has been hindered by the fact that conditionally immortalised podocytes do not express CR1 (of note its expression has been demonstrated reproducibly in human kidney sections using immunohistochemistry and in human kidney biopsy samples by PCR and western blotting). To circumvent this issue, Java et al. transfected a Chinese hamster ovary epithelial cell line (CHO) with a CR1 cDNA expression vector and

assessed complement activity using flow cytometry and ELISA [189]. This study found CR1 to be a potent regulator of the alternative complement pathway, reducing C3b deposition on the cell surface by over 95% compared to CHO control cells lacking CR1 expression [189]. Further work is needed to explore the role of CR1 in glomerular disease and to improve current understanding of how a reduction in CR1 expression on the podocyte cell surface may contribute to complement mediated injury in the kidney [189]. Notably, no mutations in CR1 have been identified in aHUS patient cohorts to date, and crystal structure analysis of C3-CR1 mutant complexes against factor I activity have not shown a significant impact on regulatory activity [163][190].

1.3.2 Complement Blockade

Prior to the era of C5 inhibition with eculizumab in 2009, the gold standard treatment for aHUS had been plasma exchange [143]. This involved replacement of non-functional complement proteins and the removal of activated complement components and auto-antibodies against complement regulators with donor plasma. In many developing countries plasmapheresis remains the only treatment option available, due to the cost implications of eculizumab therapy [191]. In contrast to TTP where the response to plasma exchange is in the region of 80-90%; atypical HUS patients undergoing plasma exchange may see initial improvement in platelet count and anaemia but only transiently; with underlying TMA and complement activation persisting [37]. Indeed, end-stage renal disease or death occurs in up to 40% of atypical HUS patients at first presentation despite plasma exchange [29]. Eculizumab has transformed treatment for these patients and is increasingly being reported to be efficacious in cases of HUS associated with medications, pregnancy and connective tissue disorders such as systemic lupus erythematosus (SLE) [192][193].

Therefore, in the UK all patients with a diagnosis of aHUS should be considered for treatment with the recombinant humanised monoclonal antibody eculizumab [141]. The earlier eculizumab therapy is started the better, in terms of preservation of renal function. Hence, current recommendations are that treatment begins as soon as STEC HUS and TTP have been excluded [143][194]. Eculizumab is reported to be highly effective in aHUS, with 85% of eculizumab treated patients entering remission [143]. Eculizumab is produced from mouse myeloma cells through recombinant DNA technology [194]. It has been humanised by replacing the murine heavy chain constant region of the antibody with a human IgG2/IgG4 hybrid. The design of this humanised IgG hybrid has been

carefully considered to ensure that any inherent pro-inflammatory potential of the antibody has been minimised [191]. Through high affinity binding to C5, inhibition of C5 cleavage occurs, preventing formation of the membrane attack complex (MAC) and glomerular TMA [195]. As such it acts as a terminal complement pathway inhibitor, with proximal functions of immune clearance remaining intact [37].

The success of eculizumab in the treatment of atypical HUS is reflected in expert consensus, which includes NICE approval in the UK with eculizumab currently the most expensive treatment endorsed by this National guidance body. UK NICE guidelines advocate early use in patients with atypical HUS so as to achieve optimal chance of renal recovery [34]. The question as to whether eculizumab use should be extended to other forms of TMA remains controversial [196]. However, it should be highlighted that eculizumab treatment is not without risk of serious side effects. Several have been reported including: peritonitis, influenza, severe hypertension and the well-recognised risk of meningococcal infection [191]. Patients treated with eculizumab, therefore receive vaccination for the available serogroups of *Neisseria meningitidis* (A,C,Y,W135 and now B); with prophylactic oral penicillin cover for the duration of treatment and 3 months after discontinuation of therapy [141].

A more recent discussion amongst experts in the field of aHUS, has been surrounding the optimal duration of eculizumab therapy. Data in this area are lacking and there is considerable concern over the potential for disease recurrence and loss of patient native or transplanted kidney function if therapy is withdrawn. However, there is no evidence for lifelong treatment with eculizumab and the risks of long term C5 blockade need to be considered [141]. A recently published large, prospective long-term (over 6 years) observational study in aHUS patients treated with eculizumab was conducted by Menne et al [195]. The investigators reported eculizumab to be a safe and efficacious form of treatment for aHUS; with a higher risk of glomerular TMA and trend toward reduction in eGFR in patients that were discontinued on eculizumab [195]. However, the strength of this work (together with that of the global aHUS registry) is the insight it has provided into which aHUS patient sub-groups are at highest risk of relapse following discontinuation of eculizumab treatment. At risk aHUS sub-groups were identified as those who presented in childhood, those with identified genetic complement mutations or factor H autoantibodies and those patients with a history of multi-organ TMA [195]. Such knowledge is invaluable in determining eculizumab treatment strategies, disease

monitoring and in which patients it may be safe to withdraw treatment. Further work in this area is ongoing in the form of the multicentre prospective 'Stopping Eculizumab Treatment Safely in aHUS' (SETS) clinical trial; led by Professor Sheerin and the team at the National Renal Complement Therapeutics Centre in Newcastle [197].

1.3.3 Evidence of complement activation in STEC HUS

In the last decade, evidence has been mounting in support of a role for complement activation in the development of Shiga toxin associated HUS. *In vitro* studies have demonstrated that Shiga toxin directly activates the complement pathway, leading to increased soluble C5b-9 when incubated with normal human serum [124]. Shiga toxin has also been demonstrated to bind to factor H, reducing its cell surface co-factor activity; leading to an increase in C3b deposition and activation of the alternative complement system [124]. Additionally, in human glomerular endothelial cells treated with Shiga toxin, surface expression of CD59 was found to be lower than that of renal tubular cells cultured under the same conditions [124][198].

Most STEC HUS patients have also been found to express increased markers of compliment activation including high levels of plasma Bb and soluble C5b-9; both of which have been found to correlate with STEC HUS activity and the presence of oliguria [124]. In addition to systemic complement activation, intra-glomerular deposits of C3 and C5b-C9 have also been identified in kidney biopsies of STEC HUS patients [124]. Moreover, the detection of complement containing microvesicles within platelets, leucocytes, and erythrocytes in STEC HUS patient plasma; further supports a direct interaction between Shiga toxin and complement activation *in vivo* [198]. More recent work by Ozaki et al. has demonstrated in a humanised MBL expressing mouse model, that monoclonal antibody treatment against MBL was protective against complement activation and renal injury induced by Stx2 [152]. However, clinical validation in favour of compliment blockade with the C5 inhibitor eculizumab is inconsistent. A few case series in paediatric STEC HUS patients with neurological sequelae have suggested benefit from eculizumab treatment. Yet, retrospective analysis of eculizumab therapy in adults with STEC HUS (such as those affected by the 2011 German outbreak) has failed to demonstrate any benefit in outcome [199]. Indeed, unravelling any meaningful answers as to the effectiveness of eculizumab in such studies is difficult. Only the most severely affected patients were administered eculizumab and it is unclear as to whether they would have recovered without it [200]. Thus, despite compelling evidence that the alternative complement pathway is activated

in STEC HUS patients *in vivo*, the extent to which this activation contributes to the pathogenesis of the disease remains unclear [198].

In an attempt to address this issue a national (NIHR and MRC funded) randomised, double-blind, placebo controlled trial 'ECUSTEC' (international trial no: ISRCTN89553116) is now open and recruiting in the United Kingdom [201]. This will attempt to definitively answer whether eculizumab treatment in children with STEC HUS is of benefit. Throughout the course of my PhD, I have been involved in the analysis of patient ECUSTEC samples that were sent to Bristol Renal for exploratory studies. These were additional, optional blood and urine samples from patients who are enrolled in the study. These samples were analysed in an attempt to investigate several areas of interest including: the role of neutrophils in transport of Shiga toxin to the kidney through *in vitro* co-culture experiments; whether complement activation correlates with markers of acute kidney injury; and whether urinary VEGF-A levels are altered in STEC HUS patients compared to healthy age-matched controls. Pre-liminary results from this work are discussed in the relevant results chapters.

1.3.4 The interaction between complement and coagulation

In recent years, there have been several reports of interactions between the complement system and the coagulation cascade. Indeed, there are similarities between the two, with both pathways featuring a series of proteolytic enzyme reactions that are tightly regulated by activator and inhibitor signals which ensure physiological homeostasis [202]. The interaction of the coagulation system and complement pathway is well established in sepsis; where uncontrolled systemic activation can lead to development of disseminated intravascular coagulopathy (DIC) with multi-organ failure and death [203]. Furthermore, concept changing work by Huber-Lang et al. demonstrated that C5 can be directly activated by proteases within the coagulation system independent of the complement cascade. Through a C3 knockout mouse IgG immune complex-induced lung injury model, it was observed that kallikrein and thrombin proteolytically cleaved C5 to produce anaphylatoxin C5a. Fascinatingly, plasma thrombin activity in C3 knockout mice (compared to wild type mice) was found to be threefold higher [204].

The same group went on to perform *in vitro* and *ex-vivo* studies, in which the human coagulation factors XIa, Xa, IXa, thrombin and plasmin were all found to cleave C3 and C5 [205]. The cleavage products generated in these experiments (C3a and C5a) were subsequently shown to exhibit chemoattractant properties known to be involved in mast

cell and neutrophil recruitment [205]. Together this work has provided evidence to support a novel connection between the complement cascade and coagulation system; with the coagulation system able to provide a compensatory pathway for complement activation that is independent of the complement cascade itself [156].

Equally, the complement system has been shown to influence the activity of the coagulation cascade. The enzyme MASP-2 (generated in the initial activation stages of the lectin pathway) has been shown to generate thrombin via direct cleavage of pro-thrombin *in vitro* [206]. Notably, MASP-2 is able to facilitate this cleavage in the absence of the coagulation cascade co-factor, factor V [202]. In addition, platelets treated with purified C5b-C9 proteins have also been shown to cleave prothrombin to form thrombin, thereby promoting fibrin deposition and clot formation at sites of complement activation [202]. Furthermore, both C5a and the C5b-C9 complex, promote coagulation through upregulation of tissue factor from endothelial cells and neutrophils [207].

In STEC HUS, there is also evidence of complement cascade and coagulation system cross-talk. In vitro, Shiga toxin has been shown to increase expression of the cell adhesion molecule, P-selectin in human microvascular endothelial cells [198]. P-selectin is known to play a key role in both the recruitment of neutrophils in the presence of inflammation and in the aggregation of platelets at sites of vascular injury. Whilst inactive it is stored in granules within the endothelial cell, known as Weibel-Palade bodies (WPBs). *In vitro* work by Morigi et al. has demonstrated that P-selectin can bind to and activate C3 in human microvascular endothelial cells, leading to thrombus formation under flow conditions [208]. This group went on to show that in a STEC HUS mouse model, there was upregulation of glomerular endothelial cell P-selectin that was associated with C3 and fibrinogen deposits, platelet aggregation and a reduction in thrombomodulin. Additionally, anti-P-selectin antibody treatment led to an attenuation of these findings, with limited C3 accumulation evident in the glomerulus [208].

In contrast to these findings, Khursigara et al. have shown that in blood outgrowth endothelial cells (BOECs) derived from healthy donors, terminal complement activation led to mobilisation of WPBs and the release of vWF [209]. Interestingly, these cells were protected from complement-mediated injury; an affect that was lost in BOECs derived from patients with von Willebrand disease which lack WPB expression [209]. Hence, in BOECs the expression of P-selectin via mobilisation of WPBs to the cell surface, appears to protect the vascular endothelium from complement-mediated attack [209]. Clearly,

there is substantial experimental evidence in favour of cross-talk between the complement and coagulation cascades both in health and disease; with these data supporting further investigation into the role that this interaction may play in development of glomerular TMA in STEC HUS.

1.4 Vascular Endothelial Growth Factor (VEGF)

Human vascular endothelial growth factors (VEGFs) are a family of five related glycoproteins, that include: VEGF-A, VEGF-B, VEGF-C, VEGF-D and placental growth factor (PIGF) [210]. Each of these proteins are secreted to form covalently linked homodimers which interact with one of three cell surface tyrosine kinase VEGF receptors (VEGFRs) [16]. The VEGFRs consist of seven extracellular domains, with a transmembrane region and intracellular tyrosine kinase receptor. Each VEGF glycoprotein preferentially binds to a specific VEGFR (Figure 1-22), to induce receptor dimerization and transphosphorylation [16]. Enhancement of VEGFR signalling has been shown to occur through co-receptors neuropilin-1 and 2 upon VEGF binding; but these co-receptors do not have any independent signalling capacity [16]. The initial description of VEGF was as a regulator of microvascular vascular permeability [211]. It is now known that VEGF also acts as a vital regulator of angiogenesis [212]. It acts to stimulate endothelial cell differentiation and proliferation as well as to promote endothelial cell survival through anti-apoptotic signalling [212]. It also increases vascular permeability through an effect on endothelial fenestration density and regulates endothelial vasodilation by increasing nitric oxide production [210].

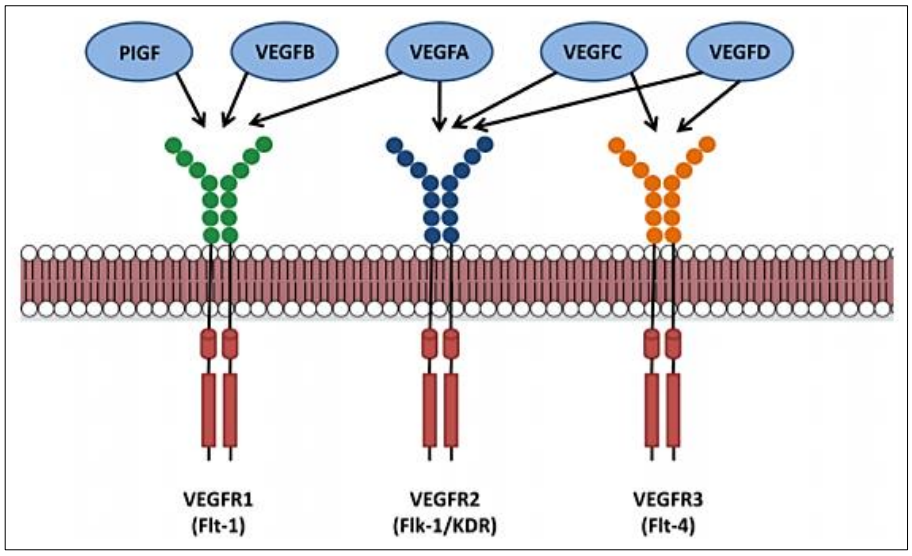

Figure 1-22: The human vascular endothelial growth factor family and receptors

Human vascular endothelial growth factors (VEGFs) are a family of five related glycoproteins, that include: VEGF-A, VEGF-B, VEGF-C, VEGF-D and placental growth factor (PIGF) [210]. Each of these proteins are secreted to form covalently linked homodimers which interact with one of three cell surface tyrosine kinase VEGF receptors known as VEGFR1, VEGFR2 and VEGFR3 (VEGFRs) [16]. As shown, VEGFR1 (also known as Flt-1) can interact with PIGF, VEGF-A and VEGF-B. VEGFR2 (also known as Flk-1 or KDR) can interact with VEGF-A, VEGF-C and VEGF-D. VEGFR3 (also known as Flt-4) can bind VEFF-C and VEGF-D. *Flt-1=fms-like tyrosine kinase 1, Flk-1=fetal liver kinase, KDR=kinase insert domain. Figure reproduced from Pandey et al* [210].

1.4.1 VEGF-A

Within the VEGF family, the glycoprotein VEGF-A is the most studied and considered to be the key stimulatory factor in both physiological and pathological angiogenesis [16]. In the kidney, podocytes are the major source of VEGF-A, which is essential for maintaining the nearby glomerular endothelium [11]. VEGF-A mRNA is also detectable in renal tubular epithelial cells to a much lesser extent; with VEGFR expression predominantly located on glomerular endothelium. This distribution of VEGF secretion and VEGFR expression supports the concept of a paracrine signalling loop within the glomerulus between the podocyte and glomerular endothelial cell [213]. The importance of VEGF-A in both glomerular development and maintenance is evident from VEGF-A mouse models. In both homozygous and heterozygous VEGF-A knockout mice, major vascular defects are observed leading to death within 10-12 days [214]. Equally, in mouse models of podocyte VEGF-A over-expression, worsening of diabetic nephropathy was reported [24]. Clearly, a

fine balance exists in the regulation of podocyte VEGF-A production, that if impaired may lead to glomerular injury.

VEGF-A is encoded by a single gene of 8 exons, with alternative mRNA splicing of the gene giving rise to at least seven different VEGF-A isoforms in humans (Figure 1-23) [215]. Each isoform has unique properties of varying diffusability and binding affinity to heparin sulphate on the cell surface and neuropilin-1 and 2; and is named after the number of amino acids (excluding the signal peptide) that it possesses [216]. For example, VEGF-A 165 isoform contains 165 amino acids and is the major VEGF-A isoform expressed in the kidney. All isoforms bind to VEGF-A receptors: VEGFR1 (also known as Flt-1) and VEGFR2 (also known as Flk-1/KDR or fetal liver kinase) [217].

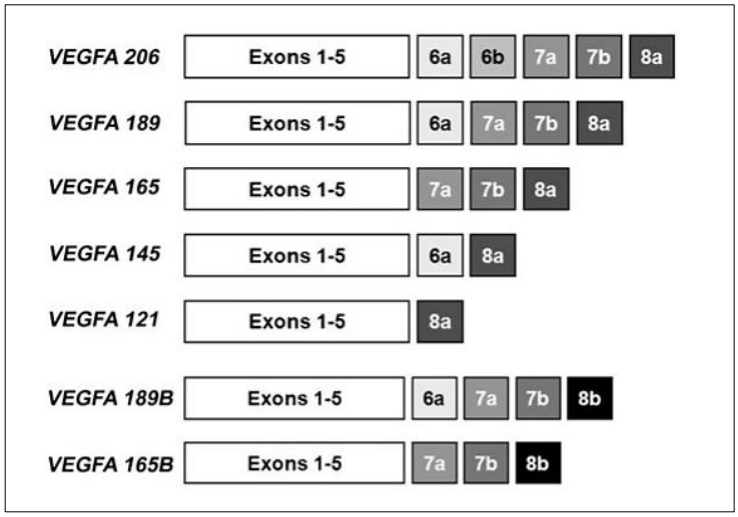

Figure 1-23: The human VEGF-A isoforms produced by alternative splicing of the VEGF-A gene
In humans VEGF-A is encoded by a single gene of 8 exons (1-8). As shown all VEGF-A isoforms contain exons 1-5 with alternative mRNA splicing of the VEGF-A gene resulting in different combinations of exons thereafter; giving rise to at least seven different VEGF-A isoforms. Alternative splicing of exon 8 results in either the generation of pro-angiogenic isoforms (exon 8a) or anti-angiogenic 'b' isoforms (exon 8b). *Figure reproduced from McFee et al* [215].

To add to the complexity of VEGF signalling, further VEGF-A isoforms have been described that originate from the alternative splicing of exon 8 of the VEGF-A gene; leading to a set of sister inhibitory VEGF-A isoforms [215]. These inhibitory or VEGF-A b isoforms vary from the pro-angiogenic VEGF-A a isoforms already described, by only six amino acids located at the C-terminus of the protein. However, this difference is enough to confer

anti-angiogenic properties to the VEGF-A b isoforms. In humans, such b isoforms constitute at least 50% of the total VEGF-A expressed in a tissue [215]. It is the careful regulation of VEGF-A pro-angiogenic isoform expression versus the inhibitory VEGF-A b isoform expression within a specific tissue that will determine the level of active angiogenesis occurring. In fact, it is well known that in some malignancies there is a down-regulation of inhibitory VEGF-A b isoform expression; which has led to the development of VEGF-A inhibitors for use in various solid tumour cancer treatments [215].

1.4.2 VEGF-A and thrombotic microangiopathy

In the last decade, advances in the generation of targeted, glomerular cell specific, genetic mouse models have greatly increased our understanding of the cellular interactions between podocytes and glomerular endothelial cells [24]. Eremina et al. have shown that post-natal disruption of VEGF-A signalling in mature, fully developed podocyte-specific VEGF-A knockout mice results in a glomerular TMA; with a phenotype that recapitulates the glomerular injury seen in HUS [11]. In further support of this finding, Eremina et al. also demonstrate the occurrence of glomerular TMA in human cancer patients treated with the VEGF-A inhibitor bevacizumab [11]. Interestingly, in these patients renal function, proteinuria and hypertension improved when bevacizumab was withdrawn. Eremina and colleagues draw parallels in this observation between VEGF-A inhibitor effects and pre-eclampsia; where delivery of the placenta (and therefore removal of the source of excess sFLT (a soluble form of the VEGFR1 receptor which binds to and inactivates VEGF-A) results in resolution of the condition [11]. No such recovery was seen in the podocyte-specific VEGF-A knockout mice in the study, even upon systemic administration of VEGF-A [11].

In further support of the complexity of local VEGF-A signalling, Jin et al. have shown that sFLT1 is not only produced by the placenta but also by podocytes [218][219]. Though the use of a specific podocyte promoter driven Cre recombinase $Flt1^{flox/flox}$ mouse model; this group went on to demonstrate that sFLT1 deletion in podocytes causes actin cytoskeleton rearrangement with damage to the glomerular filtration barrier and massive proteinuria [218]. This work not only illustrates the autocrine function of sFLT1 in the regulation of podocyte behaviour, but also highlights the complexity of VEGF-A signalling within the kidney [218].

Given these findings, the potential role of VEGF-A in the pathogenesis of Shiga toxin associated HUS cannot be overlooked. To date, this association is yet to be fully evaluated,

but there have been several studies investigating the link between VEGF-A levels and development of glomerular TMA in response to Shiga toxin. *In vitro* work by Psotka et al. has demonstrated that Shiga toxin treatment of human conditionally immortalised podocytes led to a 60% reduction of VEGF-A in expression in comparison to untreated control cells (Figure 1-24) [74]. Furthermore, in conditionally immortalised mouse podocytes (which lack the Shiga toxin receptor Gb3), no such reduction in VEGF-A was apparent, even following treatment with Shiga toxin at x1000 higher concentrations than that used in human podocyte experiments [218].

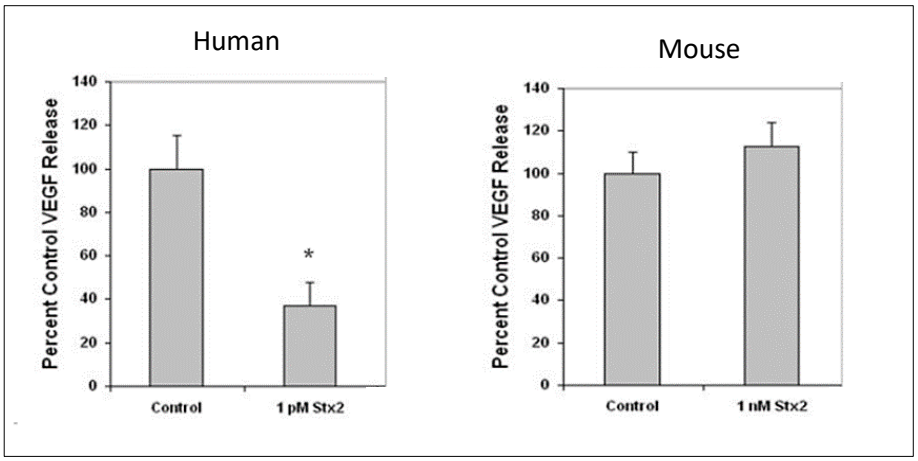

Figure 1-24: Shiga toxin treatment reduces VEGF-A expression in human podocytes

In vitro experiments performed by Psotka et al. measuring VEGF-A concentrations in human and mouse podocytes (as indicated) following 12 hr treatment with Stx2 as detected by ELISA. Control human or mouse podocytes were treated with a vehicle control for 12 hrs instead of Stx2. A statistically significant reduction (*p value <0.01) in VEGF-A release of 60% was seen in human podocytes treated with Stx2 vs. vehicle control treated human podocytes. No change was seen in mouse podocytes, despite treatment with x1000 times the dose of Stx2. *Figure reproduced from Psotka et al* [74].

In a paediatric study of 40 Shiga toxin HUS patients, immunohistochemical staining of renal biopsies revealed that glomerular VEGF-A expression was reduced; with an accompanying increase in the expression of VEGF-A receptors VEGFR1 and VEGFR2 [220]. Interestingly, plasma VEGF-A levels in the same cohort increased during the second and third weeks following STEC HUS diagnosis. The authors hypothesize this to be a marker of recovery and repair in the course of the disease [220]. In support of this notion, in a rat

model of glomerular TMA (utilising selective renal artery perfusion with an anti-endothelial cell antibody), VEGF-A treatment has been shown to accelerate recovery of renal TMA [221]. What remains unclear however, is the degree to which changes in VEGF-A are causative or simply consequential of glomerular pathological processes [212].

Finally, in more recent work performed by Keir et al. the interaction between VEGF-A and the complement cascade has been investigated. In patients with disease associated complement factor H genetic mutations (resulting in either AMD or aHUS), retinal pigment epithelial cells or podocytes, were cultured and (perhaps expectedly) shown to have more C3d cell surface deposits (indicative of alternative complement pathway activation) than controls [222]. Fascinatingly, these deposits were increased by VEGF-A antagonism with either bevacizumab or aflibercept; suggesting that VEGF-A inhibition is capable of causing a further reduction in complement regulatory activity. Keir et al. went on to show that in podocyte specific VEGF-A knockout mice, lack of podocyte VEGF-A led to a decrease in glomerular complement factor H expression by both podocytes and glomerular endothelial cells which predisposed them to complement deposition [222]. Together, these findings demonstrate a link between VEGF-A, complement regulation and the development of glomerular TMA. In light of such the podocyte may well prove to be more important in the pathogenesis of HUS than first thought.

Chapter 2 : Hypothesis

The central hypothesis of my research is that Shiga toxin produced by E.*coli* acts via the Gb3 receptor on podocytes to cause STEC HUS. Following binding of Shiga toxin to Gb3 on the podocyte there is an increase in glomerular endothelial cell susceptibility to complement attack. An acute reduction in local glomerular VEGF-A production is one possible mechanism that could be driving this; resulting in the development of a glomerular thrombotic microangiopathy (TMA). This manifests clinically as haemolytic uraemic syndrome (HUS).

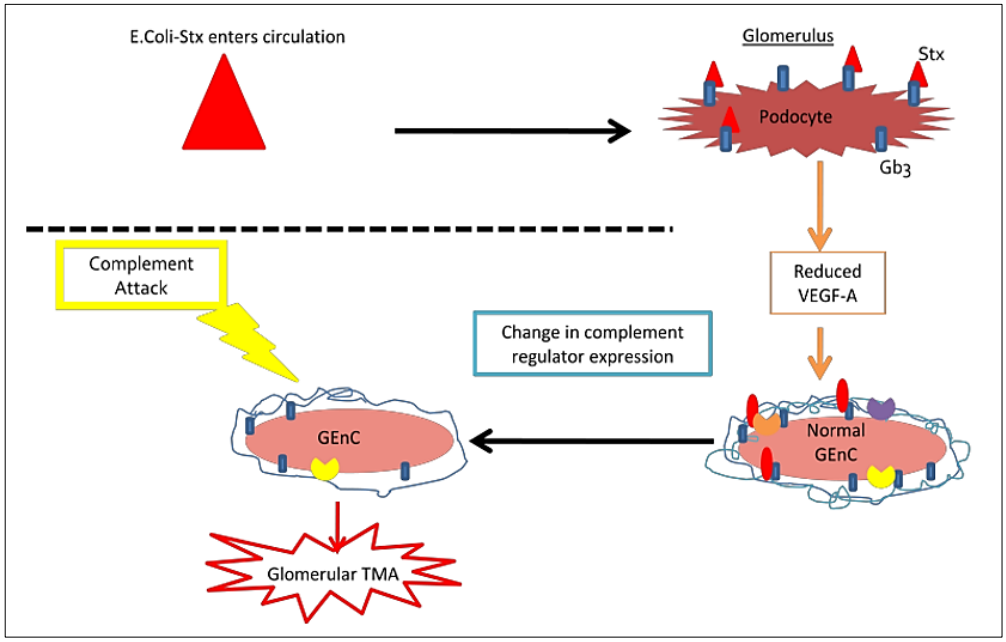

Figure 2-1: Central hypothesis

Shiga toxin enters the circulation and is transported to the glomerulus, where it targets the Gb3 receptor on the podocyte. This results in reduced VEGF-A expression which leads to glomerular TMA due to complement mediated attack on the glomerular endothelial cell surface. *Figure reproduced from Dr. Lindsay Keir PhD Thesis* [61].

I will test this hypothesis with the following research aims:

1. Prove that Shiga toxin acts through the podocyte Gb3 receptor to cause HUS.

2. Therapeutically rescue STEC-HUS with a C5 inhibitor (analogous to eculizumab).

3. Determine the cellular mechanisms underlying the action of Shiga toxin.

The summary of my experimental approach to address these aims is shown in Figure 2-2.

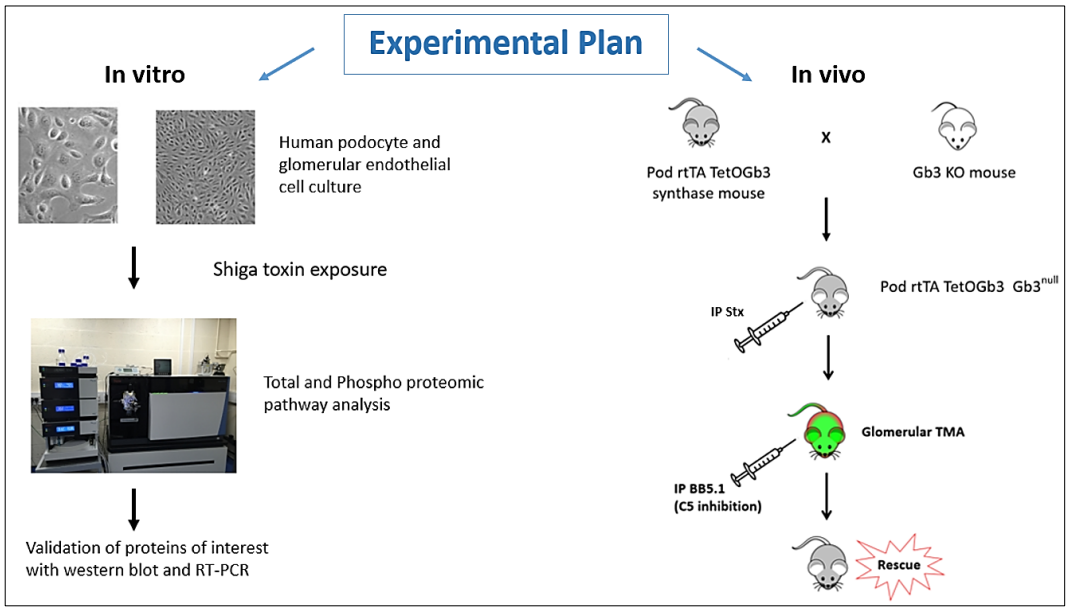

Figure 2-2: Summary of experimental plan

My experimental plan will involve both an *in vitro* and *in vivo* approach. To determine the mechanism responsible for glomerular TMA in Shiga toxin HUS, I will perform total and phospho-proteomic studies in conditionally immortalised human podocytes exposed to Shiga toxin. These experiments will be run in parallel using tandem mass tag (TMT). Any target proteins identified will be validated by western blot and phospho-protein blotting. To control for non-specific, non-Gb3 binding I will also study the proteomic changes in a human Gb3 synthase knockdown podocyte cell line. To prove that Shiga toxin acts through the podocyte Gb3 receptor to cause HUS, I will cross the podocyte expressing Gb3 synthase mouse with a constitutive Gb3 knockout mouse to produce a podocyte specific Gb3 mutant on a Gb3 null background. These mice will be given intraperitoneal Shiga toxin and their phenotype studied. Should they develop a glomerular TMA, I will attempt to rescue this phenotype with a C5 inhibitor (analogous to eculizumab in humans).

Chapter 3 : Materials and Methods

All reagents are from Sigma-Aldrich UK unless stated.

3.1 Materials and methods *in vitro*

3.1.1 Cell Culture

Human and mouse conditionally immortalised podocytes and glomerular endothelial cells have been used for my *in vitro* work [223][224][225]. They are an established resource in Bristol and considered the gold standard for the study of these specialised cells. The cells are derived from glomeruli isolated (by sieving) from nephrectomised human or mouse kidneys. Once a pure population of cells (podocytes or endothelial cells) have been isolated they are transfected with the temperature sensitive SV40 large T antigen gene construct (which also contains the hTERT telomerase gene to maintain telomere length) to immortalise them. This results in cell lines that will proliferate at 33°C and terminally differentiate at 37°C. For the specific details of this technique see the paper from Li et al [226]. All cells used were at a passage less than 20.

Conditionally immortalised podocytes were grown in humidified incubators in the presence of 5% CO_2 at 33°C in standard podocyte media: RPMI 1640 (ThermoFisher Scientific™) with 10% foetal bovine serum (FBS) and 2% penicillin and streptomycin (at 10mg/ml). They were grown until 70-80% confluent and thermo-switched to 37°C to differentiate for 10-14 days before use. Conditionally immortalised human glomerular endothelial cells (GEnCs) were also grown at 33°C in humidified incubators in the presence of 5% CO_2 in standard glomerular endothelial cell media: EGM-2MV (Lonza) with 5% FBS and additives (hEGF, hydrocortisone, hFGF-B, ascorbic acid and gentamicin – see appendix). They were grown until 70-80% confluent and thermos-switched to 37°C to differentiate for 5-7 days. All cells were used at a passage less than 25.

3.1.2 Splitting Cells

Once the conditionally immortalised cells reached confluency, in order to keep a supply of 'stock' flasks some of the cells were trypsinised (split) and re-seeded into new tissue culture flasks or cryopreserved for later use. Stock flasks were standard tissue culture T75 flasks with a vented cap purchased from Sarstedt Inc. Germany. Initially, media was removed from the cells which were then washed with sterile phosphate buffered saline

(PBS) to ensure any residual media present was removed. This is an important step as any residual media would de-activate trypsin. Trypsin-EDTA (1% for podocytes or 0.25% for GEnCs) purchased from (Lonza) was then added to the flask; just enough to coat the bottom of the T75 and the cells placed back into the incubator at 33°C to allow the trypsin to work.

After 5 minutes, light microscopy was used to ascertain whether the cells had been lifted off the bottom of the flask (visible as round cells within the trypsin suspension) and 5mls of standard cell culture media appropriate for each cell type quickly added to de-activate the trypsin which would damage the cells if left on for too long. New tissue culture flasks were then labelled with cell type, date and an increased passage number by 1; with 1ml of the trypsinised cell suspension added to each new flask and media added to give a total volume in each T75 of 12mls. A T75 flask of 70-80% confluency would usually be sufficient to seed 5 new T75 flasks.

When seeding INCell 96 well plates and six well plates for experiments, it was necessary to know the number of cells present per ml of media to ensure the same number of cells were present in each well. To achieve this, following trypsinisation as described above; the trypsin/media cell suspension was removed from the T75 flask and pipetted into a 15ml falcon tube. This was centrifuged at 1200 rpm for 5 minutes to generate a cell pellet at the bottom of the tube. The supernatant was removed, and cells resuspended in a small volume of media (typically 3-5mls). 10µl of this resuspension was then pipetted on to a Luna-FL™ automated cell counter slide from LabTech International. The cell counter calculated the number of cells present per ml. Trypan blue stain was used to give an estimation of dead cells which the cell counter also calculated. Knowing the number of viable cells present per ml allowed me to dilute the resuspension to seed the cells at the desired concentration per well for my experiments.

3.1.3 Cell cryopreservation

To ensure that I had a supply of conditionally immortalised cell lines available at a low passage, cells were cryopreserved using a freezing solution of 50% cell specific media, 40% fetal bovine serum and 10% dimethyl sulphoxide (DMSO). Cells were trypsinised as described previously and centrifuged to generate a cell pellet. The supernatant was removed, and the cells re-suspended in cell media. Equal volumes of freezing solution and cell suspension were aliquoted into cryovials (0.5mls of each) and transferred for storage at -80°C for short term purposes and liquid nitrogen for storage if required for longer than

a few months. To resuscitate cells from -80°C storage, they were thawed on ice until liquid and pipetted into a T75 flask along with 11mls of cell specific media. Cells were left to incubate at 33°C overnight to allow attachment to the tissue culture flask surface. After 12 hours cell media was refreshed so that any DMSO in the freezing solution was removed. Cells were then cultured under standard conditions.

3.1.4 Co-culture transwell experiments

Conditionally immortalised human podocytes and glomerular endothelial cells were cultured together in transwells (Corning 3µm pore Transwell® permeable supports). Endothelial cells were seeded onto coverslips at the bottom of the well and podocytes were seeded into the transwell support. Cells were cultured in standard endothelial media without VEGF and allowed to differentiate. Shiga toxin 0.1ng/ml was added to the podocyte transwell support at intervals of 30 min to 6 hours. Shiga toxin containing media was then removed and cells washed once with PBS. Human C7 deficient serum (40% in gelatine veronal buffer) was then added for 30 minutes. Cells were subsequently washed x3 before being fixed in 4% PFA and immunofluorescence performed for CFH or C3d and co-stained for DAPI (see appendix for antibody specifications). Glomerular endothelial cells were then imaged in the Wolfson Bioimaging Facility on confocal multi-laser Leica SP5II microscope.

3.1.5 Shiga toxin cell treatment

Shiga toxin was obtained commercially from the USA through List Biological Laboratories Inc. This toxin is tightly regulated and protected by anti-terrorism laws. To import Shiga toxin an export license was completed, and the anti-terrorism police informed that we would be receiving it. The toxin was stored in a labelled locked fridge, with a record kept of the volume and concentration present at all times. Access to the toxin was restricted and when the toxin was being used in the laboratory signs were displayed to warn other lab users. When using the toxin: a mask, eye protection, gloves and a protective clothing were worn at all times. All work involving the toxin was performed in a biological cabinet under category 3 facilities. Prior to any toxin work commencing, a 'control of substances hazardous to health regulations' (COSHH) risk assessment was completed which was submitted and reviewed by the biological and genetic safety committee.

Shiga toxins are classified into two major antigenic forms: Shiga toxin 1 and Shiga toxin 2 [227]. Shiga toxin 2 has been chosen for the purposes of my research as this is the subtype

that is associated with a more severe clinical phenotype and widely used in published literature [227]. Throughout the remainder of this report unless otherwise stated Shiga toxin refers to Shiga toxin 2. Upon receipt of Shiga toxin from List Labs, the lyophilized powder was reconstituted with 100µl distilled water and gently mixed by inversion in-keeping with the manufacturer's instructions. This resulted in a stock concentration of 10µg/100µls which was aliquoted into 20µl stock eppendorfs and stored at -20°C until use. The toxin was assessed for purity on 12% SDS-PAGE and was found to have two major bands at molecular weights of 33 kDa and 8 kDa corresponding to A and B toxin subunits, respectively. Purity was >98% and the endotoxin content determined on kinetic chromogenic LAL assay at List Labs was <90EU/mg.

All Shiga toxin cell treatments were performed on differentiated cells. Doses ranging from 0.01ng/ml to 100ng/ml were used. Once Shiga toxin treatment was removed (incubation period ranged from 0.5 to 72 hours) the supernatant was transferred to a waste flask of 0.1M of sodium hydroxide prior to disposal after 24 hours. Cells were then washed 3 times in PBS and this waste also disposed of in 0.1M sodium hydroxide. Filtered pipette tips were used throughout this work. Cells could then be analysed as described below.

3.1.6 Immunofluorescence on coverslips

Cells were grown in 6 well plates with glass coverslips placed in each well. Once fully differentiated cell treatments were applied, and toxin removed as described. Cells were washed 3 times in PBS and fixed with ice-cold 4% PFA (paraformaldehyde). After 10-15 minutes PFA was washed off with PBS and permeabilised with 0.3% triton for 10 minutes. All cells were blocked in 3% BSA for 30-60 minutes. Primary antibodies (see appendix for antibody details and concentrations) were then applied to the coverslips which were left at 4°C overnight. The following day, cells were washed 3 times in PBS and secondary fluorescent antibodies (see appendix) applied for 1 hour at room temperature. Coverslips were then washed again 3 times and mounted with VECTA Shield hard setting mount with DAPI nuclear stain (Vector Lab Inc H100). Slides were then imaged using the Leica DMI 6000B microscope or Leica Confocal SP5-II confocal laser scanning microscope at the Wolfson Imaging Institute, University of Bristol.

3.1.7 Immunofluorescence using the IN Cell

Cells were grown in 96 well Corning® IN Cell plates and once fully differentiated treated with Shiga toxin as described. Cells were then washed 3 times in ice cold PBS and fixed in

4% PFA for 5 minutes at 4°C. PFA was then removed and cells permeabilised with 50µl ice-cold methanol per well. Plates were placed into the freezer at -20°C for 5 minutes. Methanol was then removed and replaced with PBS. Non-specific binding sites were then blocked with 5% NGS (normal goat serum) for 1-2 hours at room temperature. Primary antibodies were then applied and left overnight at 4°C. The following day, cells were washed 3 time in PBS and secondary Alexa Fluor antibodies applied at 1:200 concentration for 90 minutes at room temperature. Cells were then washed twice in PBS and DAPI solution 1:10,000 concentration applied for 20 minutes at room temperature. DAPI was subsequently washed off with PBS and cells imaged using the IN Cell analyser 2000 (GE Healthcare).

3.1.8 Image J Analysis

To ensure that microscopy images were comparable across experimental conditions, cells were treated at the same time and immunofluorescence staining performed simultaneously. Images were taken on the same day under the same microscope settings. For each experiment, the control slide was imaged first with exposure, intensity and gain set accordingly. These parameters remained unchanged throughout image analysis. To calculate the corrected total cell fluorescence (CTCF) (or corrected total glomerular fluorescence (CTGF) for my *in vivo* work) the following formula was used:

CTCF or CTGF = integrated density – (area of selected cell or glomerulus x mean fluorescence intensity (MFI) of background).

Image J software and Fiji plugin device was used to calculate the integrated density and MFI from microscope images saved as TIFF files. DAPI nuclear stain (in cells) or nephrin (in glomeruli) were used as co-localisation markers to allow accurate measurement of total cell number or glomerular area, respectively. The use of Image J and the CTCF/CTGF formula facilitated the comparison of immunofluorescence microscopy images between different experimental conditions and subsequent statistical analysis.

3.1.9 Western Blotting

Western blotting was used to determine the protein expression of cells under different experimental conditions. To control for total protein loading differences between samples a housekeeping gene (β actin) was detected in each lysate.

3.1.9.1 Cell lysates

Cell lysates were made using radio-immunoprecipitation assay (RIPA) lysis buffer (see appendix for details). Protease inhibitor and phosphatase inhibitors (A and B) were added at a 1% concentration to RIPA buffer to prevent unregulated proteolytic and phosphorylation of the sample proteins. Cells were washed 3 times in ice cold PBS after removal of media. 500µl of lysis buffer cocktail was then added to each flask and the cells kept on ice. Cells were removed by scraping the bottom of the flask vigorously and pipetted up into eppendorfs which were centrifuged at 13,200rpm for 5 minutes at 4°C. The supernatant was then transferred to a new eppendorf and the cell pellet discarded. All cell lysates were kept at -80°C until use.

3.1.9.2 Reducing western blots

Sodium dodecyl sulphate polyacrylamide gel electrophoresis (SDS-PAGE) was used to separate proteins according to size and charge. 10 well gels were made according to the recipe given in the Appendix. Cell lysates were taken from storage at -80°C and thawed on ice. Loading buffer (containing SDS and mercaptoethanol) was added to each sample prior to boiling at 95°C on a hot block for 5-10 minutes to reduce and denature the proteins. 30 µl of each sample was loaded per well and the first well of each gel loaded with 3µl of ladder (Bio Rad). Gels were electrophoresed for 60-90 minutes at 150 mV in running buffer. Proteins were then transferred from the gel to a PVDF (polyvinylidene fluoride) membrane (Millipore) for 60-90 minutes at 250 mA in transfer buffer. Membranes were blocked in 5% BSA (bovine serum albumin) for 1 hr at room temperature. Blots were probed with primary antibodies (see appendix) in 5% BSA or 5% skimmed milk at 4°C overnight.

The following day membranes were washed 3 times in TBS-T (Tris-buffered saline with Tween 20). Then incubated with secondary HRP (horseradish peroxidase) conjugated antibodies diluted at 1:10,000 for 1 hr at room temperature; followed by 3 more washes in TBS-T and imaged using chemiluminescence (Biorad) and viewed on the Amersham 600 imager.

3.1.9.3 Non-reducing western blots

Western blotting was also performed in non-reducing conditions. The same gel recipe was followed as for reducing western blots, but no Sodium dodecyl sulphate (SDS) was added. Cell protein lysates were taken from storage at -80°C and thawed on ice. Loading buffer

was made without SDS or mercaptoethanol and the samples were not boiled on a hot block prior to being loaded on the gel. Electrophoresis was performed for 2 hours at 90 mV in running buffer, again with no addition of SDS in the buffer. Proteins were then transferred from the gel to a methanol activated PVDF membrane for 60-90 minutes at 250 mA in transfer buffer. The remainder of the western blot protocol was the same as for reducing blots. Non-reducing immunoblotting was performed when probing for the presence of complement factor H in cell lysates. This was necessary because the antibody used for human complement factor H did not recognise the protein in its reduced form (see appendix for antibody specifications).

3.1.9.4 Densitometry

Western blots (both reducing and non-reducing) were quantified using Image J software. Images of each immunoblot were saved a TIFF files and opened in Image J. No changes to the resolution or contrast of the images were made. The image transform tool was used to rotate images if they appeared to be off centre to enable the software to detect each protein band more accurately. The rectangle tool was then selected and used to draw a box around the first band on the blot. This box was duplicated and moved along the blot covering each band in turn. This set an area of analysis for the band intensity to be measured in each lane (Figure 3-1).

The same process was followed for β actin control band intensity measurements. Using the analyse tool in Image J, each box was plotted to give a single peak which was then analysed for the area under the curve as shown in Figure 3-1. The calculated densitometry measurements were then copied into a spreadsheet on Microsoft Excel and normalised to those of the corresponding β actin loading control, followed by normalisation to the experimental control to give a relative fold change. All western blots were performed as triplicate repeats to facilitate statistical analysis.

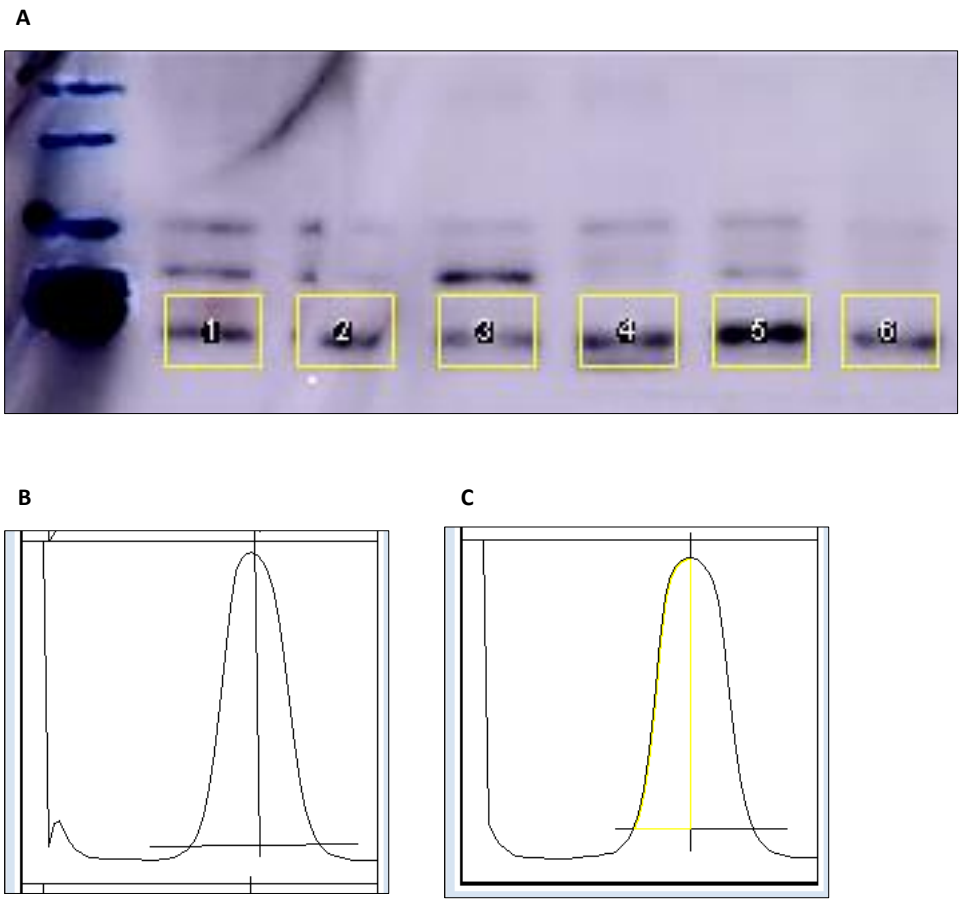

Figure 3-1: Densitometry analysis used in western blotting

Panel A shows boxes drawn around each protein band detected on western blotting, using Image J software. These boxes were drawn very carefully to ensure the entire band was contained within it and no other bands that were present included in the analysis. All boxes were of the same size to allow accurate comparison between lanes. The same process was performed for β actin loading controls (not shown). Panel B shows a representative graph plotted by the analysis tool in Image J, that gives an easily identifiable single peak. Panel C shows how the area under the curve for each graph is selected, by drawing a line across the bottom of the peak and through the middle of the peak. The area used to calculate a densitometry reading using the wand tool in Image J is highlighted in yellow. The densitometry readouts generated from Image J in this way were then copied into a Microsoft Excel worksheet for normalisation.

3.1.10 Protein Quantification Assay

Cell lysate samples and cell supernatant protein content was quantified using a Bicinchonic Acid (BCA) Thermo Scientific Protein Assay kit. BSA standards were made up with a starting solution of 1mg/ml in distilled water. From this starting solution serial dilutions of 1 in 2 were made in eppendorfs to give final concentrations of 1000µg/ml,

500µg/ml, 250µg/ml, 125µg/ml, 62.5µg/ml and so on until the final eppendorf contained only distilled water. Sample lysate or supernatant dilutions were then prepared in eppendorfs. These began at a 1 in 50 dilution, 1 in 100 dilution, 1 in 200 dilution and so on until a 1 in 32000 dilution was reached. 25µl of BSA standard or protein sample to be tested was then pipetted into a 96 well cell culture microplate (Corning®) in duplicate to give a technical repeat. Two wells per 96 well plate were used as blanks (containing just distilled water) to give a negative control.

A working assay master mix solution was made according to manufacturer's instructions. This involved mixing 50 parts reagent A with 1 part reagent B. 200µl of master mix solution was then added to each well of the 96 well plate using a multichannel pipette. The plate was wrapped in foil to protect it from the light and left for 30 minutes at room temperature. The colorimetric change was read by a plate reader using Revelation® software at a wavelength of 570nm. Protein concentrations in the samples could then be calculated using a plot of the standard curve obtained from the BSA standards on the same plate.

3.1.11 Quantitative polymerase chain reaction (qPCR) and Endpoint PCR

Polymerase chain reaction (PCR), both quantitative and endpoint was used to compare gene expression in cells and tissues. Messenger RNA (mRNA) was extracted from these samples and changes in mRNA levels used as a marker of gene transcription.

3.1.11.1 RNA extraction

Commercially available Qiagen RNeasy kits were used to extract mRNA from both cell and tissue samples. Cells were grown in T75 flasks and differentiated before treatment and mRNA extraction. Media was removed and 700µl of QIAzol lysis buffer added to each flask. After 5 minutes the cells and lysis buffer were transferred to an eppendorf and 140µl of chloroform added. Eppendorfs were shaken vigorously for 15 seconds and left at room temperature for 3-5 minutes. Samples were then centrifuged at 12000g at 4°C for 15 minutes to separate the sample into 3 phases. The upper aqueous phase contains RNA and was extracted off with a pipette being careful to avoid contamination with the interval protein phase or lower organic phase containing DNA. 100% ethanol was then added at 1.5 times the volume of RNA aqueous phase solution obtained.

A maximum of 700µl of this solution was loaded onto an RNeasy mini column (any more risks overloading the binding capacity of the column) and centrifuged at ≥8000g for 15 seconds at room temperature. The RNA binds to the column and the solvent that passes through discarded into a beaker. 500µL of RPE buffer was added to the column which was centrifuged at ≥8000g for 15 seconds, any flow through was then discarded. This step was repeated to wash out any remaining ethanol. Centrifugation was then performed for 2 minutes at ≥8000g and any flow through discarded. The RNeasy column was transferred to a new collection tube and centrifuged at ≥8000g for 1 minute to dry the membrane.

Finally, the RNeasy column was transferred to an eppendorf and 30µl of RNAse free water pipetted into the column which was centrifuged at ≥8000g for 1 minute to elute the RNA. The RNA sample was kept on ice and the concentration and purity of RNA measured using the nanophotometer 1000 Pearl machine (ThermoFisher™). An absorbance ratio of 2 at 260nm/280nm was deemed acceptable as this indicates purity of the RNA sample (free from phenol or protein contamination). A secondary measure of purity of the sample the 260/230nm absorbance ratio was deemed satisfactory if >1.6; indicating a low concentration of contaminants such as carbohydrate carry over or residual phenol [228]. All RNA samples were stored at -80°C until further use.

3.1.11.2 Complementary DNA synthesis

Before qPCR or endpoint PCR could be performed, I converted extracted mRNA to complimentary DNA (cDNA) using the AB systems high capacity mRNA to cDNA kit. This required the use of a reverse transcription enzyme and buffer. Volumes of each reagent used were dependent upon the concentration of RNA in my sample and followed the manufacturer's instructions.

3.1.11.3 Primer design

Primers were ordered from Eurofins after determining the optimal sequences for the amplification of the gene of interest from the Harvard Primer Bank: https://pga.mgh.harvard.edu/primerbank. Sequences were verified using the online National Centre for Biotechnology Information (NCBI) Primer Blast resource: https://www.ncbi.nlm.nih.gov/tools/primer-blast. Once received, primers were made up to a concentration of 10µM and kept at -20°C until use. For all new primers, a serial dilution standard curve reaction was performed with either untreated cellular cDNA or WT mouse kidney cDNA. This was to determine the optimal concentration of cDNA

required for the primers to work efficiently and to ensure that the primers could detect a product in the control samples (Figure 3-2).

A negative control sample, containing no cDNA (just RNAse free water) was also included to reveal any contamination or non-specific amplification. A standard curve was then drawn to calculate the R^2 value. The CT value should increase by 3 cycles for each ten-fold dilution so that the standard curve is a straight line with R^2 >0.95 for very good primers (i.e. the closer the R^2 value to 1 the greater the efficiency of the primers).

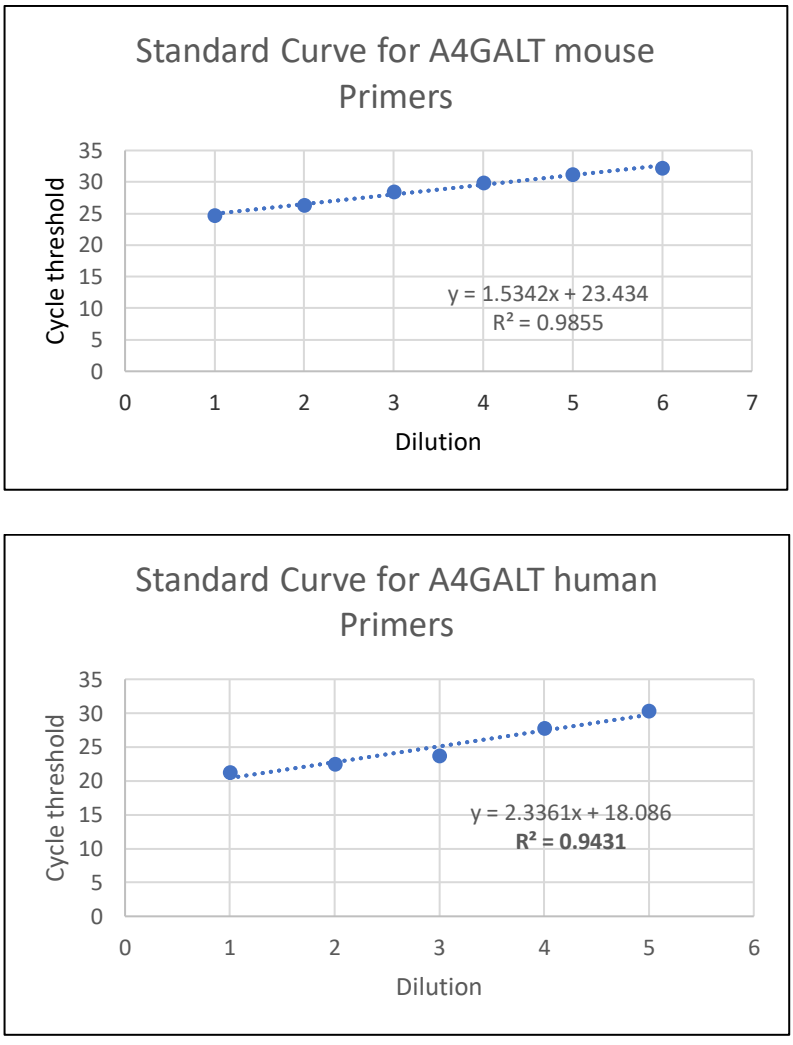

Figure 3-2: Example of standard curve analysis: A4GALT mouse and human primers

Each primer pair used for qPCR were tested for efficiency at serial dilutions of cDNA starting at a 1 in 5 dilution (dilution 1) and then serially diluted up to 6 times to give a final dilution of 1 in 5625 (dilution 6). A non-template control (containing no cDNA) was also run alongside these dilutions as a negative control. Each condition was run in triplicate. The standard curve was drawn from the

average CT (cycle threshold) value obtained from each reaction at each dilution. The example shown is for the A4GALT primer pairs using both mouse primers and human primers, respectively.

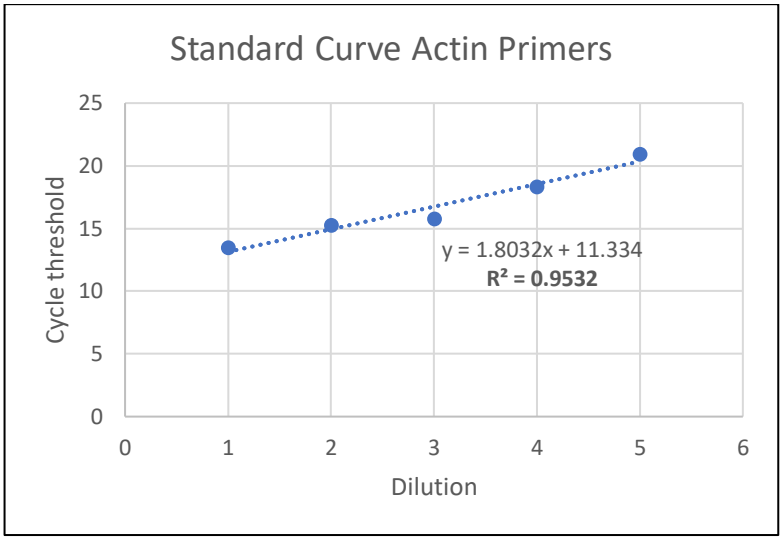

Figure 3-3: Standard curve analysis for B-actin primers (mouse and human)

β actin primers were tested in the same way as described for the A4GALT primers. An R^2 value of 0.95 equates to very good primer efficiency.

3.1.12 Quantitative PCR

QPCR was performed using SYBR green from Sigma-Aldrich according to their instructions. SYBR green is a fluorescent cyanine dye that binds to double stranded DNA between base pairs and fluoresces. This fluorescence is detected at the end of the annealing or extension step in the PCR reaction when there is maximal double stranded DNA present. This reaction is non-specific as any double stranded DNA present will be detected; therefore, the primers used must be carefully designed so as to produce a gene specific amplification product [229]. In both qPCR and endpoint PCR reactions, I sequenced the amplified product as a way of validating my results for each target gene.

QPCR was performed using the optimal cDNA concentration as determined from my standard curve for each set of primers used. Annealing temperatures were set according to the Tm (melting temperature) provided by Eurofins specific for each primer pair. All experiments included a housekeeping gene (β-actin) as a control to allow comparison between samples. Melt curves (Figure 3-4) were inspected with each experiment to ensure the cycle thresholds detected from SYBR green fluorescence were specific. The

Applied Biosystems Step One Plus real time PCR machine was used for all qPCR experiments.

The ΔΔCT method for calculating relative gene expression was used in all qPCR experiments. This first requires normalisation of all samples to β-actin (housekeeping gene) with subsequent comparison of the expression of the gene of interest under different experimental conditions to calculate a fold change or relative expression. Details of this method are found in the paper by Haimes et al [230]. Data was analysed to ensure consistency between each triplicate repeat or a single outlier that could be excluded from the dataset, a single product on the melt curve of each sample and negative control wells.

3.1.12.1 Endpoint PCR

Endpoint PCR was performed using the Hotmaster Taqman DNA kit from AB systems according to their instructions. Primers were used at a concentration of 10µM and 1µl of cDNA sample used as standard for each reaction. The Tm was set according to Eurofins data sheet which was provided with my primers (see appendix). Amplification products were run on a 2% agarose gel alongside a 100 base pair DNA ladder from New England Biolabs. Midori green (Geneflow) was added to the agarose gel to stain the DNA amplification product to enable visualisation using the Amersham 600 imager. Endpoint PCR was used to confirm the presence (or absence) of a gene of interest. This was a particularly useful technique in analysing expression of Gb3 synthase in A4GALT knockout mouse tissues. The amplification product (after PCR clean up using Qiagen PCR purification kit) was sent for sequencing to Eurofins Genomics in Germany to confirm the specificity of the primers.

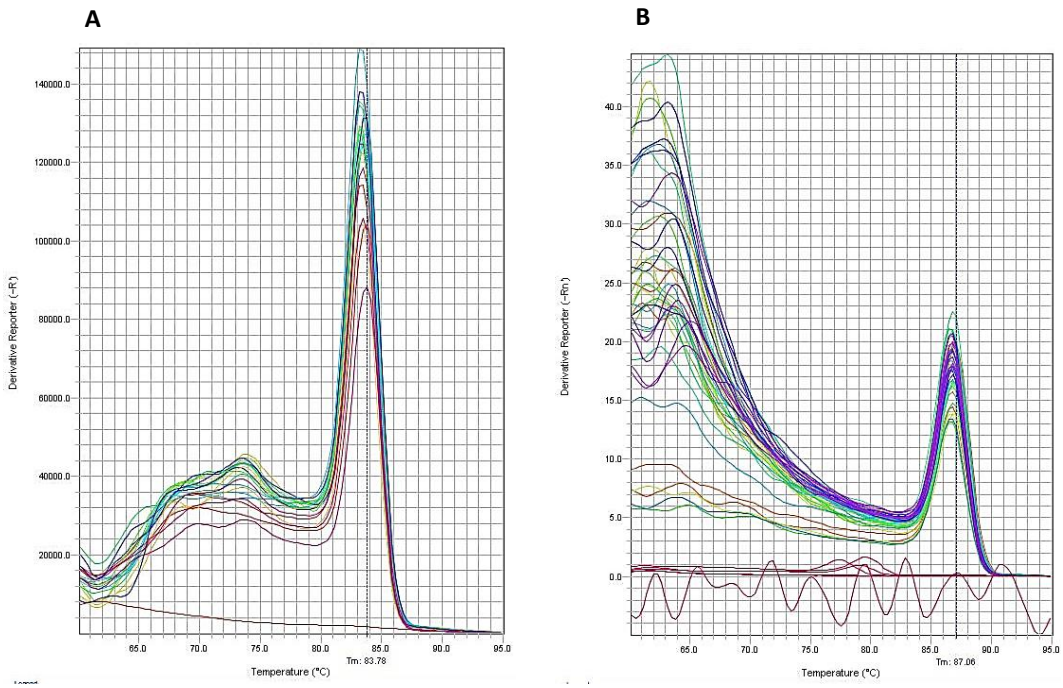

Figure 3-4: Examples of melt curves from qPCR reactions

A – shows the melt curve obtained from a qPCR reaction in glomerular isolates from mice using mouse A4GALT primers. B – shows the melt curve obtained from a qPCR reaction in human podocytes using β actin primers. The peak present in each sample tested (represented by a different colour for each) corresponds to the cycle threshold detectable from SYBR green fluorescence. Given this is a single peak it is specific for the amplification product of the primers.

3.1.13 Thin layer chromatography (TLC)

Thin layer chromatography (TLC) is a technique used to separate lipids based on their relative affinity towards the stationary and mobile phase. I went to UCL to learn this technique from lipid expert Prof. Shamshad Cockcroft.

Hela cells were radio-labelled with H^3 sphingosine for 4 hours in fatty acid free BSA DMEM media. Cells were trypsinised, washed in PBS and centrifuged at 2300 rpm for 3 minutes. The supernatant was aspirated and re-suspended in 600µl of PBS. 1.5mls of chloroform: methanol mixture (ratio of 1:2) was added to the suspension. A further 0.5mls of chloroform followed by 0.5mls of 100mM KCL and 20mM acetic acid solution was then added, and the sample mixed well. After 20 minutes at room temperature, to allow separation of the chloroform and water soluble phase the suspension was centrifuged at 8000rpm for 3 minutes. Lipid fractions (contained in the chloroform phase) were then

extracted and transferred to another eppendorf. The sample was then evaporated overnight in the Savant Speed Vac machine.

The following day, 50µl of chloroform was added to each sample and loaded on to the TLC silica glass plate. The TLC plate was run with commercially available standards from Matreya Inc. These included the following lipids: Gb3, sphingomyelin, PE (glycerophosphoethanolamine) and PC (glycerophosphocholine). This is necessary to allow identification of the lipids present in the samples. Of note, only my samples contain radio-labelled sphingosine and so these standards are not visible when the TLC plate is developed. For optimal glycosphingolipid TLC development, a chloroform: methanol: water solvent was prepared in a ratio of 65:25:4 and poured into the TLC glass column. The lipid loaded TLC plate was then placed inside and left to run for 1-2 hours. The TLC plate was then placed in iodine to confirm that separation had occurred (bands seen along the plate). The TLC plate was then placed on top of a specialised photographic film in a secure case to develop for 7-14 days. The film was then imaged using a scintillation detector.

3.1.14 Generation of an A4GALT knockdown podocyte cell line

Commercially available GIPZ lentiviral short hairpin RNA (ShRNA) particles from Dharmacon were used to create a Gb3 synthase (A4GALT) knockdown human podocyte cell line (Figure 3-6). There are several advantages of this system, firstly the ShRNA is micro-RNA adapted for specific knockdown; the transfected cells are marked by a GFP tag and a stable cell line can be maintained through the use of puromycin resistance due to presence of a puromycin resistance gene. In addition, there is experience of the use of these constructs in conditionally immortalised human podocytes in our laboratory. The manufacturer's protocol was followed as outlined below [231].

Initially, the puromycin dose response (kill curve) in wild type human conditionally immortalised podocytes was determined (Figure 3-5). Cells were plated on 6 well plates at a confluency of 80% and thermo-switched the following day and left to differentiate for 10-14 days. Podocytes were then incubated with puromycin at doses ranging from 0.1µg/ml to 5µg/ml for 24-96 hours. At each time point the cells were assessed for cell viability using the trypan blue dye exclusion test. This involved trypsinising the cells and adding 10µl of 0.4% trypan blue (Biosystems) to 10µl of cell suspension and counting the number of cells on the automated cell counter (Luna II automated cell counter, Biosytems). Cells that were viable did not take up the blue dye. This was performed in

triplicate to ensure accuracy of results. Based on these experiments the minimum amount of antibiotic to kill all wild type cells at 72 hours was 1µg/ml. Thus, the dose of puromycin used for selection of my A4GALT knockdown cells was 1µg/ml, which was added to the standard podocyte media when growing these mutant cells.

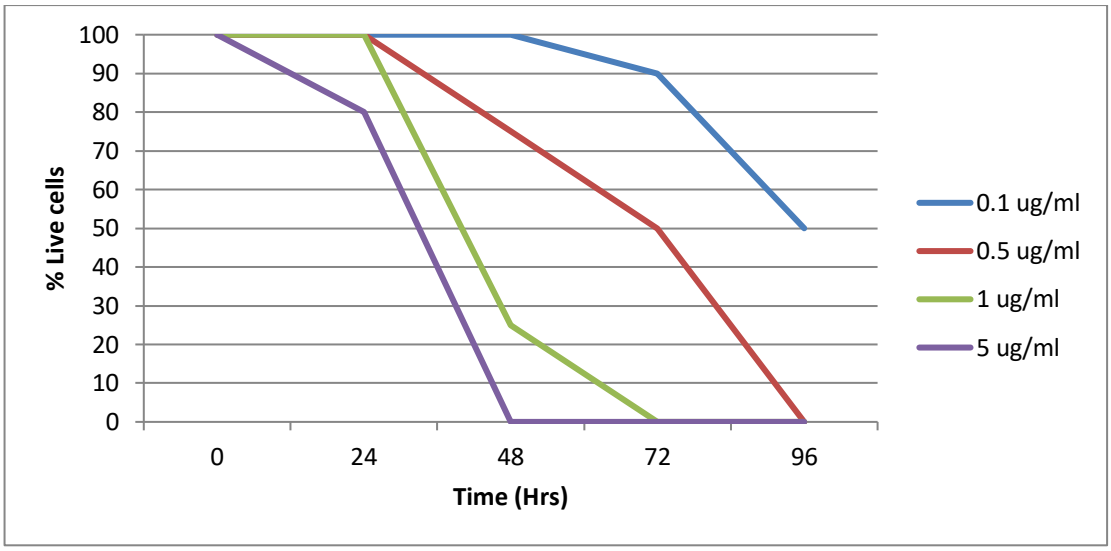

Figure 3-5: Puromycin kill curves for wild type human podocytes

As described the minimal dose of puromycin required to kill all non-transfected (i.e. wild type) human podocytes was determined. Results shown are representative of each experimental condition in triplicate. The dose chosen for selection of mutant A4GALT knockdown podocytes was 1µl/ml. At 72 hours all wild type podocytes are dead, leaving only the mutants with the puromycin resistance gene viable.

Subsequently, the titre of lentiviral stock required for transduction of human podocytes to successfully knockdown A4GALT synthase was determined. The day before transduction 6 well plates of wild type human podocytes (passage 9) were seeded at less than 50% confluency. The following day dilutions of the lentiviral stock were made in a 'working 96 well plate' using serum free media to produce a series of 5-fold dilutions reaching a final dilution of 390,625 fold. Once the serial dilutions were made, media was removed from the podocytes in the 6 well plates and replaced with 575µl of serum free media and polybrene (1 in 100 concentration). The cells were then transduced by adding 25µl of virus (or non-silencing control virus) from the 96 well plate to give a series of viral transduction dilutions. For example, 25µl of virus dilution from A2 of the 96 well plate was added to well A1 in the 6 well plate and so on [231].

Each viral transduction dilution was left on the cells for 4 hours at 33°C and then replaced with 1ml of standard podocyte media. After 3 days, standard podocyte media was replaced with media containing 1µg/ml of puromycin. Only podocytes that containing the puromycin resistance gene (i.e. successfully transduced podocytes) will survive culture in puromycin media, facilitating selection of the A4GALT synthase knockdown podocytes. The number of successfully transduced podocytes were visible under light microscopy as green cells due to their GFP tag (Figure 3-7 and Figure 3-8). Of note, the GFP tag, puromycin and ShRNA sequence were on the same CMV promoter of the GIPZ lentiviral vector.

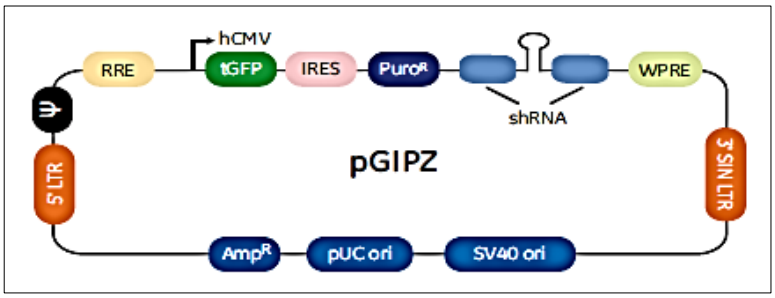

Figure 3-6: GIPZ lentiviral vector

The GIPZ lentiviral vector contains a GFP tag (tGFP) connected via an internal ribosomal entry site to allow expression of GFP and puromycin resistance genes (puroR) in a single transcript. The ShRNA sequence is driven from the same CMV promoter (hCMV). WPRE – Woodchuck hepatitis posttranscriptional regulatory element enhances transgene expression in the target cells; 5' LTR 5' - long terminal repeat; 3' SIN LTR 3' - self-inactivating long terminal repeat for increased lentivirus safety; Ψ - Psi packaging sequence; RRE - Rev response element. *Reproduced from Dharmacon GIPZ ShRNA lentiviral manual* [231].

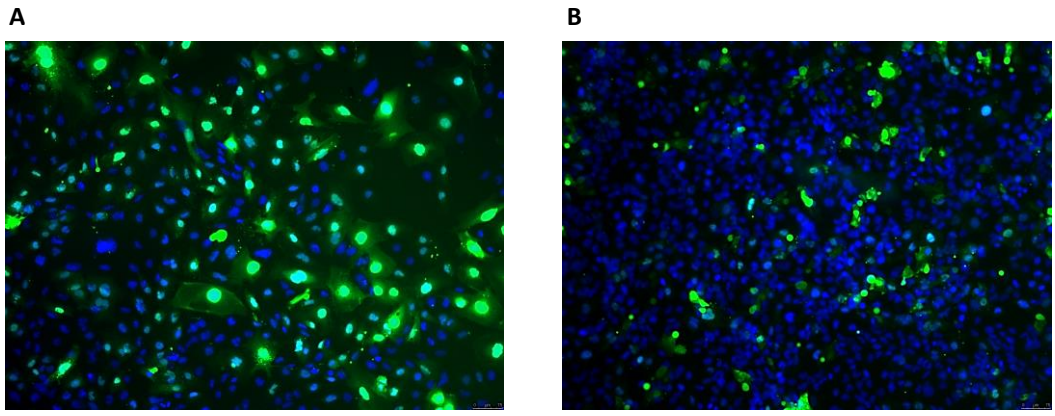

Figure 3-7: IF images in human podocytes following GIPZ ShRNA viral transduction

Panel A shows merged image of GFP (green) and DAPI (blue) transfected human podocytes achieved at a lentiviral transduction concentration of 1 in 5 at a magnification of x20. There are significantly more GFP tagged cells (i.e. transduced cells) than in panel B where a 1 in 25 dilution of lentiviral construct was used.

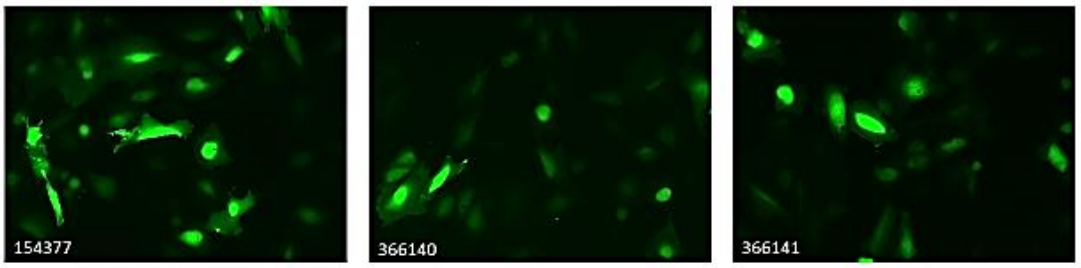

Figure 3-8: GFP tagged A4GALT knockdown human podocytes (x40 magnification)

Transfected podocytes were imaged live under fluorescent microscopy to determine whether successful transduction had taken place. All 3 mutants (sequences of ShRNA as labelled) were GFP tagged suggestive of successful transduction of the A4GALT silencing ShRNA.

The GFP tag was very useful to monitor the expression of the viral construct but there was some loss of GFP expression towards the end of differentiation in human podocytes and when these cells were resuscitated from -80°C storage. To quantify the degree of A4GALT knockdown qPCR and IF were performed. A loss of the GFP signal has been seen before in podocytes (other scientists within Bristol Renal anecdotal experience of using the same GIPZ lentiviral vectors with different ShRNA sequences). However, reassuringly this loss of signal did not correlate with any loss of expression of ShRNA silencing which was confirmed with immunofluorescence and qPCR.

3.1.15 VEGF-A ELISA

VEGF-A (165 isoform) was quantified from both conditionally immortalised podocyte and glomerular endothelial cell supernatant and from co-culture transwell experiments. Cell culture experiments were undertaken without VEGF in the media and included cells treated with 0.1ng/ml Shiga toxin and untreated controls. Patient plasma and urine samples from the ongoing ECUSTEC trial (ISRCTN89553116) were also assessed for VEGF-A levels. All experiments involved use of the R&D Systems™ human VEGF-A 165 ELISA kit (www.rndsystems.com/products/human-vegf-quantikine-elisa-kit_dve00). All samples were analysed in triplicate technical repeats and the manufacture's protocol followed.

These experiments were performed with Dr Louise Farmer a post-doctoral scientist in our laboratory.

3.2 Materials and Methods *in vivo*

3.2.1 UK Animal Care Declaration

All animal work was performed in accordance with the University of Bristol's guidelines and the Animals Scientific Procedures Act 1986. Work carried out was within the Project License of Prof. Richard Coward (no: 3003394) and approved by the UK Home Office. I obtained a personal license in order to perform the experiments detailed below. (PIL: I2780F26E).

3.2.2 Choice of genetic background

The C57BL/6 strain of mice were selected as the genetic background for use in the generation of all mouse models used in my research. This strain of mouse is commonly used in many knockout mouse models including the Gb3 null mouse generated by Okuda et al [75]. It is worth noting, that rodent models of kidney disease have conventionally avoided use of the C57BL/6 genetic background as it has been found to be relatively resistant to proteinuria, glomerulosclerosis and hypertension [232]. This is thought to be due to decreased activity of the renin-angiotensin-aldosterone system as a consequence of having only one copy of the renin gene [232].

However, arguably more important in my model, is that the C57BL/6 strain has intact complement factor 5 (C5); unlike several other commonly used mouse strains (DBA2J, A/J, AKR/J, FVB/NJ) which have a frame shift in their haemolytic complement gene (Hc) resulting in a loss of function mutation in C5 [233]. It is vital that in generating my mouse model of Shiga toxin HUS, that these complement pathways remain intact as our hypothesis seeks to determine whether complement plays a role in the pathogenesis of the disease. On balance it was decided that the C57BL/6 genetic strain was the most appropriate one to use in my model.

3.2.3 Mouse gender selection

It has been shown in some mouse models of renal disease, that male mice are more likely to develop proteinuria, ischaemic renal failure and diabetic nephropathy than female mice [232]. For this reason, male mice have been used preferentially in the majority of

published rodent models of kidney disease [232]. Renal research is not unique in this sense, use of predominantly male animals in research has been reported in many fields [234]. This has originated from concerns that the use of both sexes will mean a requirement to include more animals in the sample size, due to increased variation and reduced statistical power. However, in this project I have used both female and male mice as I did not anticipate a sizable interaction between sex and the development of Shiga toxin HUS. This decision was informed by human epidemiological data; in which large retrospective studies in Europe have shown no statistically significant difference in the incidence of STEC HUS cases according to gender [40]. Furthermore, I did not anticipate a variation between sexes in terms of the possible effects of C5 inhibition as a treatment intervention.

As a result, this work is more broadly applicable and adhered to the National Centre for the Replacement, Refinement and Reduction of Animals in Research guidelines, where by including both male and female mice I could use fewer animals to obtain comparable information from the study of male mice only. It is worth noting however, that in the C5 inhibition cohort of mouse experiments, all mice (including controls) happened to be female. There was no conscious or pre-conceived decision to use only female mice in this experiment; but merely a chance result that the mice with the required genotype were all female. All other mouse work involved both male and female mice.

3.2.4 Shiga toxin treatment in mice

All mice used during my project were between 8-12 weeks of age at the time of Shiga toxin treatment. Shiga toxin dose for each mouse was calculated based on the weight of each mouse. A dose of 10ng/g of Shiga toxin (List Biological Laboratories Inc.) diluted in sterile normal saline 0.9% (Baxter) was given to each mouse IP. Control mice were given IP 0.9% normal saline of the same volume. Prior to commencing any Shiga toxin mouse work, with each new vial of Shiga toxin 2 from E.*coli* purchased at least 2 wild type mice were given a test dose of Shiga toxin IP at 10ng/g to ensure that the toxin was virulent and there was no batch effect. This was to prevent any unnecessary use of animals in my main experiments due to failure of the toxin working in accordance with the principles of Russel and Burch [235].

Throughout the course of my animal work several batches of Shiga toxin from list labs were required. Each batch had been tested at List labs for concentration, purity, and activity. SDS-PAGE was used to assess purity and was >98% for each batch used. LPS

contamination was determined using a kinetic chromogenic LAL (Limulus amebocyte lysate) assay and found to be <90EU/ng in each vial. The toxin was stored as advised by the manufacturer at 2-8°C when a lyophilised powder and at -20°C when reconstituted in distilled water.

Shiga toxin is highly toxic and must be handled with extreme caution. In-keeping with the precautions taken during my *in vitro* work, all Shiga toxin experiments in mice were performed whilst wearing a mask, gloves, and protective clothing. Doses of Shiga toxin were made up in a biological cabinet within the animal unit and signs displayed to warn other users of the experiment being performed. Shiga toxin waste (including syringes and needles) were immediately placed in 0.1M sodium hydroxide falcons and disposed of in labelled sharps bins. Before administering IP Shiga toxin injections, I was trained to perform the procedure using normal saline in order to reduce any personal risk of needlestick injury. All experimental work was subject to authorisation by the biological and genetic safety committee at the University of Bristol.

3.2.5 Generation of a Gb3 Null mouse

Generation of a Gb3 null mouse has already been described by Okuda et al [75]. This group targeted the A4GALT gene and replaced nucleotides 68-615 within the open reading frame with a neo-resistant gene. The targeting vector was linearized and transfected into embryonic mouse embryonic stem cells and the clones containing the vector isolated. Homologous recombination was employed to facilitate targeted incorporation of the mutation into the homologous genetic locus. The generation of a Gb3 knockout mouse was confirmed by Southern blotting [75]. The Gb3 knockout mice used in my project were generated by MRC Harwell through use of the International Mouse Phenotyping Consortium (IMPC) via the European Conditional Mouse Mutatgenesis (EUCOMM) and the National Institutes of Health Knockout Mouse (KOMP) programs embryonic stem (ES) cell resource (see www.knockoutmouse.org/about/eucomm).

MRC Harwell used this repository to obtain mice containing the full Tm1a knock-out-first-reporter tagged insertion allele at the site of a critical exon within the A4GALT gene. As well as the gene specific elements this targeting cassette contains several other common components including a beta-galactosidase (lacZ gene), neomycin (neo) resistance gene and LoxP sites [236]. This mouse was subsequently crossed with mice expressing Cre recombinase. The progeny from this breeding was then genotyped (using a combination of qPCR assays) to identify the alleles generated. Only mice containing Tm1b converted

forms of the original Tm1a allele were taken forward for use in my experiments. The Tm1b allele is produced by deletion of the critical exon and the neomycin cassette (within the knock-out first mutant allele) due to Cre recombinase excision at loxP sites (Figure 3-9). As a result, the Tm1b allele is considered a true knockout as skipping over of the LacZ cassette will no longer restore gene expression (unlike in the Tm1a mutant) [237]. Mice were genotyped using primers obtained from Eurofins: www.eurofinsgenomics.eu (see appendix for details) and expression of both A4GALT and Gb3 in their tissues also assessed. The characterisation of the A4GALT knockout mice used in this project is discussed in detail in results Chapter 6.

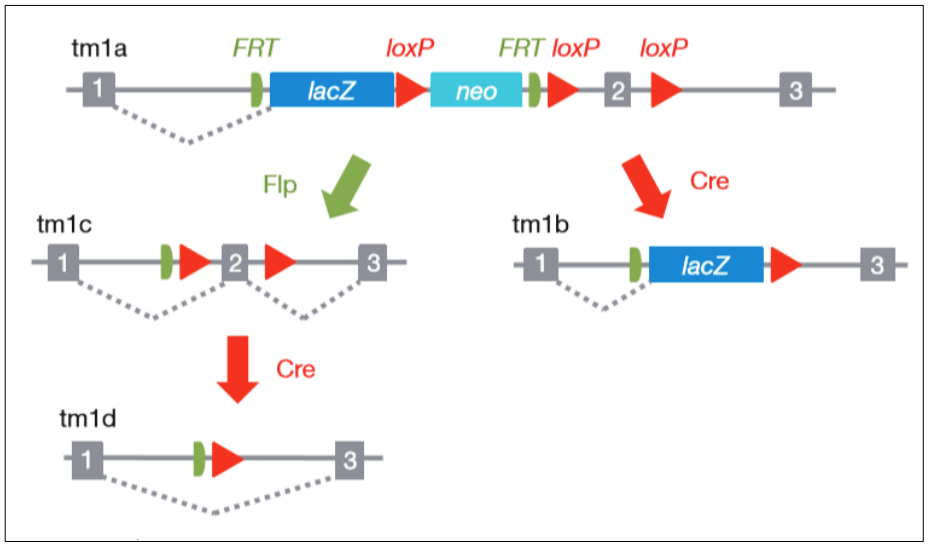

Figure 3-9: Tm1b – LacZ tagged null allele generation used to obtain A4GALT knockout mouse
The full Tm1a knockout-first-reporter tagged insertion allele, containing a lacZ trapping cassette and a floxed promoter-driven neo cassette is inserted upstream of a critical exon in the specified gene (in this case the A4GALT gene) which disrupts its function. These mice can then be crossed with mice expressing Cre recombinase. The progeny from this breeding were then genotyped (using a combination of qPCR assays) to identify the alleles generated. Cre deletes the promoter driven selection cassette and floxed exon of the Tm1a allele to generate the Tm1b allele; or deletes the floxed exon of the Tm1c allele to generate Tm1d (as shown) [227]. Only mice containing Tm1b converted forms of the original Tm1a allele were taken forward for use in my experiments. *Figure reproduced from Skarnes et al* [227].

3.2.6 Generation of an inducible podocyte specific Gb3 synthase mouse

Our laboratory has previously generated the PodrtTA-Tet-O-Gb3 mouse which uses tetracycline-controlled transcription activation of murine Gb3 synthase in the podocyte. This novel mouse model was derived from crossing the podocin rtTA (reverse tetracycline activated transactivator) mouse (a gift from Prof. Susan Quaggin in Canada); with the Tet-O-Gb3 synthase mouse generated by the company Geneta in Leicester (made using the Tet-O-Gb3 construct devised by post-doctoral scientist Dr Matt Wherlock in Bristol) [61]. The model for the generation of this complex inducible genetic mouse is shown in Figure 3-10.

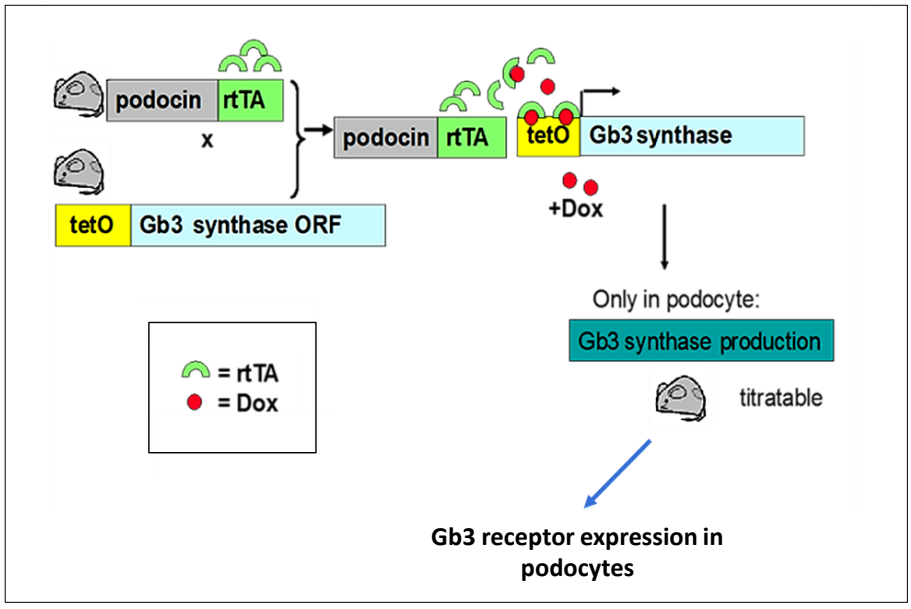

Figure 3-10: Inducible tetracycline-controlled transcription of Gb3 synthase in the podocyte
Expression of the reverse tetracycline activated transactivator (rtTA) gene is driven by the podocyte specific podocin promoter. The rtTA gene product binds doxycycline and activates transcription from the tet-O promoter. This then drives transcription of Gb3 synthase – resulting in expression of the Gb3 receptor in the podocyte. *Figure modified from Dr. Lindsay Kier PhD Thesis* [61].

The construct containing Tet-O-Gb3 synthase that was made by Dr Wherlock, originated from a Tet-O-VEGF-A construct given to our laboratory from Prof. Susan Quaggin in Canada. He designed a restriction digest to cut out VEGF-A and a ligation to insert murine Gb3 synthase (gifted by Dr T Obrig, University of Virginia). Unfortunately, the Tet-O-Gb3

mouse in our laboratory had been mistakenly culled prior to the start of my project. However, the original Tet-O-Gb3 synthase construct made by Dr Wherlock was still available. Hence, Tet-O-Gb3 synthase mice were created at the MRC Harwell through pro-nuclear injection of a single mouse embryo with this construct (Figure 3-11). This strategy resulted in the random insertion of the construct into genomic DNA.

The embryos were implanted into female mice and allowed to reach term. Once born they were genotyped to determine whether the construct had been inserted into their chromosomal DNA. Mice with the Gb3 synthase construct present were taken forward to breeding to establish a Tet-O-Gb3 synthase colony with which to cross the PodrtTA mice with. The resulting mice were PodrtTA-Tet-O-Gb3 synthase mice on a WT background. These mice were characterised prior to any further breeding to establish a PodrtTA-Tet-O-Gb3 synthase mice on a Gb3 null background. The details of this work are presented in Chapter 6.

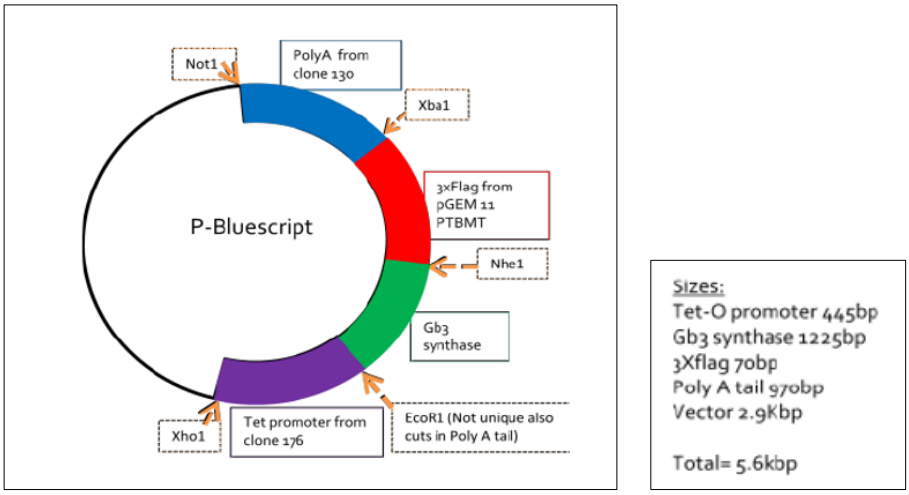

Figure 3-11: Tet-O-Gb3 synthase construct used to generate Tet-O-Gb3 mice

This Tet-O-Gb3 synthase construct was made by Dr Matt Wherlock in Bristol Renal. It was modified from a Tet-O-VEGF-A construct which originally linked the VEGF-A to a tetracycline response promoter. The flag tag sequence allows easy identification of the transgene after incorporation into the mouse genome. *Vector map supplied by Dr Lindsay Keir*.

3.2.7 Doxycycline gene induction

PodrtTA-Tet-O-Gb3 mice on either a wild type or Gb3 null background were given oral doxycycline at a dose of 2.5mg/ml in their drinking water to induce Gb3 synthase in their

podocytes. Only mice with both the PodrtTA and Tet-O-Gb3 synthase promoter should express Gb3 synthase in their podocytes as both the reverse tetracycline activated transactivator (rtTA) element and the Tet-O-Gb3 promoter need to be present (Figure 3-10). Doxycycline hyclate was purchased from Sigma-Aldrich and stored as per manufacturer instructions at 2-8°C. Doxycycline drinking water was made up fresh from this stock every 3 days and was poured into tinted water bottles to maintain the concentration of the drug which is light sensitive. Control mice receiving standard drinking water also had their water bottles changed at the same time. Doxycycline drinking water is known to taste bitter, thus mice will avoid drinking it. To circumvent this issue 5% sucrose was added to the doxycycline drinking water. Initially, 5% sucrose was also added to control drinking water, but these mice began consuming large volumes of the sweetened water which required replacing daily. This could potentially influence my experimental results, so I reverted back to using drinking water alone for my control mice.

To check that the PodrtTA-Tet-O-Gb3 system was not leaky, Tet-O-Gb3 mice were studied to ensure there was not any expression of Gb3 synthase in the absence of the podocin promoter. Furthermore, a control group of PodrtTA-Tet-O-Gb3 mice were given normal drinking water to check that Gb3 synthase was only being induced after tetracycline activation. Previous work by Dr Lindsay Keir had shown that Gb3 synthase induction required at least 10 days of oral doxycycline [61]. Therefore, in all of my experiments involving PodrtTA-Tet-O-Gb3 mice, 14 days of doxycycline treatment was administered to induce Gb3 synthase.

3.2.8 Breeding strategy for generation of the PodrtTA-Tet-O-Gb3 mouse on a null Gb3 background.

To generate an inducible podocyte specific Gb3 synthase mouse on a Gb3 null background PodrtTA-Tet-O-Gb3 mice on a wild type (C57BL/6) genetic background were back-crossed with Gb3 null mice (A4GALT KO). These mice only express the Gb3 receptor in their podocytes. This model provides temporal control over gene expression of Gb3 in the podocyte, providing invaluable insights into the role of this specialised glomerular cell in the initiation of glomerular TMA in Shiga toxin HUS. This highly complex mouse model has allowed me to test my hypothesis *in vivo* which is vital prior to any further translation into human studies and clinical application. To ensure that the minimum number of mice were used in each experiment whilst maintaining statistical significance, the intelligent breeding strategy detailed below was used:

Tet-on GB3 $^{+/+}$ pod RtTA $^{+/+}$ x GB3 $^{null/null}$ (from MRC Harwell) =

Tet-on GB3$^{+/-}$ pod RtTA$^{+/-}$ GB3 $^{+/null}$ x Tet-on GB3 $^{+/-}$ pod RtTA $^{+/-}$ GB3 $^{+/null}$

After 6 rounds of breeding the correct genotype was achieved with following cross:

Tet-on GB3 $^{+/+}$ pod RtTA $^{+/+}$ GB3 $^{null/null}$ x GB3 $^{null/null}$ =

ALL MICE: Tet-on GB3 $^{+/-}$ pod RtTA $^{+/-}$ GB3 $^{null/null}$

This process successfully generated several cohorts of PodrtTA-Tet-O-Gb3 Gb3 null mice and sufficient littermate controls for IP Shiga toxin challenge vs. sham IP injections of sterile saline as a negative control. To reduce any 'cage effects' mice of different genotypes (from the same litter) were housed together, to avoid any bias from social interactions within the cage. Mice were randomised to receive either IP Shiga toxin or saline (sham procedure) using a randomised block design. The order in which measurements were made and the way the mice were housed was also randomised to avoid any time and space variables that might influence my results.

Prior to any definitive experiments, all PodrtTA-Tet-O-Gb3 Gb3 null mice were genotyped and organs assessed for expression of Gb3 in the presence and absence of doxycycline induction using endpoint PCR and immunofluorescence techniques. Once I was satisfied that the PodrtTA-Tet-O-Gb3 system was working as expected and doxycycline was inducing the expression of the Gb3 receptor in the podocyte of the kidney only; my experiments using Shiga toxin commenced.

3.2.9 Cardiac perfusion

Cardiac perfusion of wild type mice and the inducible PodrtTA-Tet-O-Gb3 mice on a WT background was performed to clear the organs of any erythrocytes which have been shown to express Gb3 (and so can lead to contamination) [238]. Of note, A4GALT KO mice and PodrtTA-Tet-O-Gb3 Gb3 null mice did not require cardiac perfusion as they do not express Gb3 or only express Gb3 in their podocytes following doxycycline induction, respectively. Comparison of kidney tissue sections from wild type mice that were not perfused prior to tissue harvesting vs. wild type mice that underwent cardiac perfusion showed that Gb3 in the glomeruli was picked up in the non-perfused animals with immunofluorescence but not in the perfused animals (Figure 3-12 and Figure 3-13).

Mice were terminally anaesthetised via intraperitoneal injection of pentobarbital (50mg/kg). The chest cavity was opened, and anterior chest wall removed. Whilst the heart was still beating a 22-gauge butterfly needle was inserted into the left ventricle and the position of the needle checked by aspirating some blood into the syringe attached to the needle. The right atrium was then cut with scissors to release the pressure before injecting 10mls of HBSS (Hanks' buffered salt solution, ThermoFisher Scientific™). The organs (including the liver and kidneys) were observed to become pale in colour – indicating successful perfusion. The needle was removed from the left ventricle and organs dissected. Fluid leaking from the nose of the animal or the lungs increasing in size was indicative of an unsuccessful perfusion, as HBSS has entered the pulmonary circulation (rather than the systemic circulation) if this occurred. Only animals observed to be adequately perfused were used for tissue harvesting.

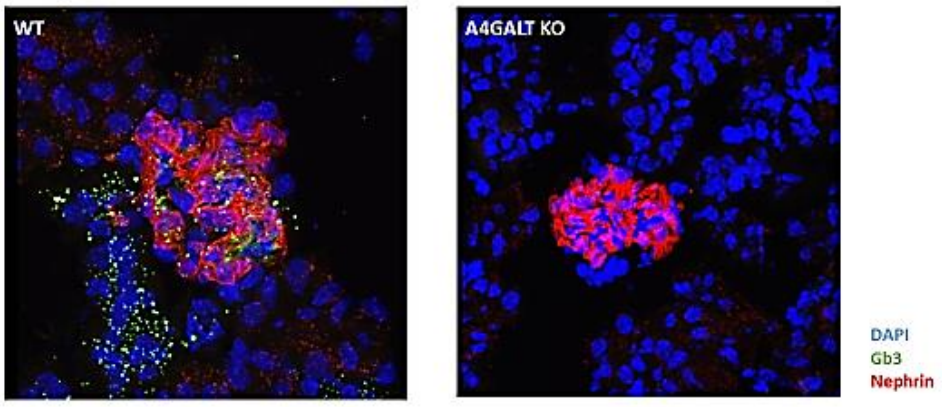

Figure 3-12: Confocal microscopy IF sections WT vs. A4GALT KO non-perfused mice (x40)

As described kidneys were harvested from WT (wild type) and A4GALT KO mice without perfusion and immunofluorescence performed to detect Gb3 (green). To determine the localisation of Gb3 in the kidney of mice nephrin was used (red) to identify podocytes. These images appear to show Gb3 expression within the glomerulus. This was unexpected as it has been well established that mouse glomeruli do not express Gb3 [61]. Red blood cell contamination was suspected; prompting the need to perfuse mice prior to organ harvest.

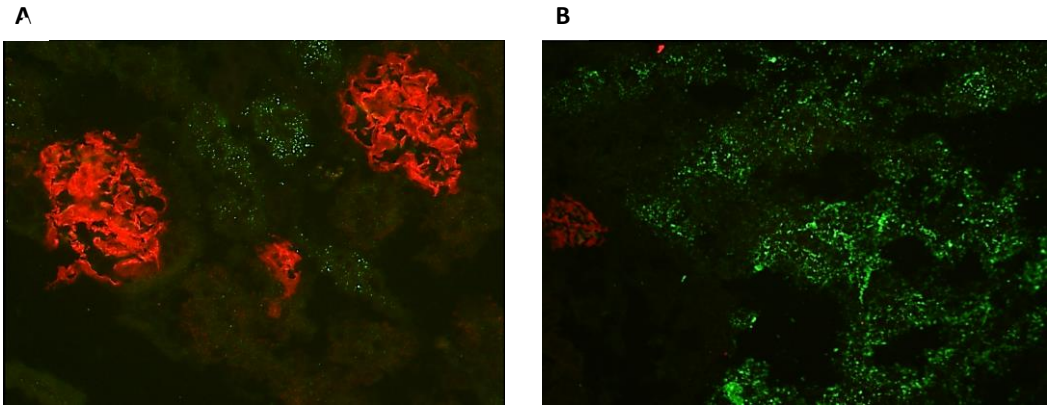

Figure 3-13: IF sections in wild type perfused mice (x40)

Images A and B are both from WT mice that have been perfused prior to kidney harvesting. There is no evidence of Gb3 expression (green) within the glomeruli (nephrin = red). There is still evidence of Gb3 expression in the tubules as seen in panel B. Therefore, as well-established WT mice do not express Gb3 in their glomeruli but do express Gb3 in their renal tubules.

3.2.10 Glomerular isolation

To specifically analyse mRNA and protein expression in the glomeruli of mice (rather than that within the whole kidney) I used a glomerular isolation technique involving Dynabeads® (ThermoFisher Scientific™). This is particularly useful when analysing tissues from PodrtTA-Tet-O-Gb3 mice on a wild type background, as these mice will express Gb3 in their renal tubules and their podocytes found within the glomeruli. Since most Gb3 in wild type mice is expressed in the renal tubules; determining whether inducible expression of Gb3 in the podocyte has occurred following oral doxycycline treatment is not possible without glomerular specific analysis.

Mice underwent cardiac perfusion as described above. Following perfusion, the syringe attached to the butterfly needle was switched to a 10ml syringe containing $8x10^7$ Dynabeads® in HBSS. The needle was then removed from the left ventricle and the kidneys dissected. Once harvested both kidneys were put into HBSS and kept on ice. In the laboratory, kidneys were minced up with scissors in a petri dish to maximise the surface area available for digestion. The minced tissue was then transferred to 1.5ml digestion buffer (1mg/ml collagenase containing 50U DNAse 1: Life Technologies) suspended in RPMI media (ThermoFisher Scientific™). This mixture was agitated at 37°C for 30 minutes.

The digested tissue was then passed through a 100µm cell strainer into a 50ml falcon tube and washed with 5mls HBSS. The strained liquid was then repassed through the cell

strainer washing again with 5mls HBSS to maximise the yield of tissue. The suspension was centrifuged at 4°C for 5 minutes at 3000g. The resulting supernatant was removed and placed in a new falcon tube. The remaining pellet (containing the glomeruli) was resuspended in 500µl of HBSS and transferred to a 1.5ml eppendorf on ice. The supernatant falcon tube was re-spun, and the pellet produced resuspended in 300µl of HBSS and transferred to an eppendorf. These eppendorfs were placed against a magnet for 1 minute, as the Dynabeads® are magnetic they collect on the side of the tube taking the glomeruli with them. The isolated glomeruli were carefully washed x3 with 500µl of HBSS ensuring that the tubes were on the magnet each time. To confirm glomerular isolation 1µl of suspension was pipetted into a microscope slide and viewed under a light microscope. The Dynabeads® were visible within the glomeruli (Figure 3-14). The glomerular isolates were transferred to RNAlater and stored at 4°C. RNA extraction was performed within 7 days of isolation.

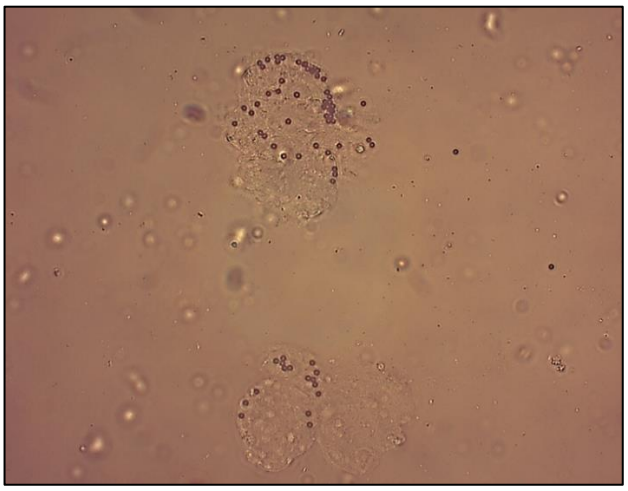

Figure 3-14: Dynabead® glomerular isolation (x40)

Mouse glomeruli are successfully isolated using cardiac perfusion and subsequent Dynabead® perfusion. Two glomeruli are visible with the Dynabead® particles visible in the capillary loops of the blood vessels of the glomeruli.

3.2.11 Organ harvesting

The kidneys, liver, heart, lung, pancreas, and brain of all mice were harvested under terminal anaesthesia (intraperitoneal injection of pentobarbital (50mg/kg). These organs were divided into two or three sections and fixed in 10% PFA, snap frozen at -80°C or

transferred to EM buffer (kidneys only). The specific fixation techniques are described below with reference to kidney tissue. Other organs in which RNA was extracted underwent the same processes. Terminal blood samples were also taken at the time of sacrifice from a cardiac puncture as well as terminal urines via a bladder puncture. An ear notch was also kept at -20°C for genotyping.

3.2.11.1 Formalin fixed kidney tissue (PAS staining)

Immediately after dissection, at least half a kidney from each mouse was preserved in 4% paraformaldehyde (Santa Cruz) and stored at 4°C. When required, kidney tissue was paraffin embedded and sectioned (3 microns thick) in the histology department at Bristol University. Sections were deparaffinised in histoclear and hydrated by immersing in serial dilutions of ethanol. Starting at 100% ethanol for 5 minutes, then 90% ethanol for 5 minutes and so on until a concentration of 50% ethanol was reached. After this the sections were transferred to distilled water for 5 minutes, followed by immersion in Periodic Acid Solution (PAS) for 5 minutes at room temperature. I used the Sigma-Aldrich PAS staining system (standard procedure 395) to staining my samples.

According to manufacturer's instructions the slides were then rinsed 3 times in distilled water and immersed in Schiff's reagent for 15 minutes at room temperature. Sections were rinsed again under running tap water for 5 minutes and counterstained with haematoxylin solution for 90 seconds. Slides were rinsed again under running tap water and dehydrated by reversing the initial hydration sequence of ethanol immersion in increasing concentrations: i.e. from 50% ethanol for 5 minutes to 70% ethanol for 5 minutes and so on. Sections were subsequently mounted, and images taken using the Leica DMI 6000B microscope. PAS positive structures stain pink to red and nuclei are blue.

3.2.11.2 Formalin fixed tissue kidney tissue (MSB trichrome staining)

The Atom Scientific Ltd. martius scarlet blue (MSB) staining kit was used as trichrome stain to differentiate fibrin, collagen, and muscle. Early fibrin and erythrocytes are also demonstrated with this technique. This is the gold standard trichrome histology stain to visualise TMA in the glomerulus. The same paraffinization procedure was performed as outlined above by the histology department in Bristol University. The sections were de-waxed in the same way as above and brought through from ethanol to water. Fresh Weigert haematoxylin was made up by adding A to B in equal volumes and pipetted on to the kidney sections and left for 10 minutes. This was rinsed off with distilled water and the slides dipped into 1% acid alcohol solution for 10 seconds.

Slides were washed under running water for 5 minutes and stained with martius yellow for 3 minutes. This was washed off under running water for 1 minute and crystal scarlet solution applied to each section of the slide with a pipette for a 5 minute incubation. Slides were washed briefly under running water for 1 minute and treated with phosphotungstic acid for 5 minutes. This was washed off in running water for 1 minute and reapplied for another 5 minutes. Slides were washed again under running water for 1 minute and methyl blue solution applied to each section for 2 minutes. This was washed off in running water for 3 minutes and blotted dry. Slides were then dehydrated in 100% ethanol for 5 minutes and immersed in histoclear for 5 minutes, prior to being mounted with DPX (Sigma-Aldrich). Slides were then imaged under light microscopy using the Leica DMI 6000B microscope.

3.2.11.3 Formalin fixed tissue kidney tissue for immunohistochemistry

Kidney sections used for immunohistochemistry (IHC) were formalin fixed and paraffin embedded as detailed above. Sections were de-paraffinised and rehydrated with histoclear and ethanol in the same way as previously described. Antigen retrieval was performed by boiling the slides in citrate buffer (10mM sodium citrate, pH6) and maintaining a sub-boiling temperature for 10 minutes using a microwave. Slides were then left to cool for 30 minutes in the buffer on the benchtop at room temperature. Once cooled, sections were removed from the buffer and washed 3 times for 5 minutes in distilled water. Sections on the slides were drawn around using an ImmEdge® hydrophobic barrier PAP pen (Vector Lab Inc.) and incubated in 3% hydrogen peroxide for 20 minutes in a humidified chamber. This is to block any endogenous peroxidase activity.

Sections were then washed with distilled water twice for 5 minutes and blocked with 5% normal goat serum (NGS) in TBST 0.1% for 30 minutes at room temperature. This was subsequently, replaced with primary antibody made up in the same blocking solution at an antibody specific concentration (see appendix) and incubated overnight a 4°C. The following day the sections were washed with 0.1% TBST three times for 5 minutes each. Each section was then covered in 1-3 drops as required of SignalStain® boost detection reagent (Cell Signalling Technologies®). This is an HRP conjugated secondary antibody to either mouse or rabbit chosen depending on the species of the primary antibody used.

The sections were incubated in a humidified chamber for 30 minutes at room temperature. They were then washed with 0.1% TBST three times for 5 minutes and SignalStain® DAB (3,3'-diaminobenzidine) substrate added to each section. This substrate

is made up freshly each time using 30µl of SignalStain® DAB chromogen concentrate to 1ml SignalStain® DAB diluent (mixed well before use). This DAB working solution reacts with the peroxidase (HRP) detection reagent to yield a brown reaction product where the primary antibody is present. To stop the reaction slides were immersed in distilled water and counterstained with haematoxylin for 10 seconds. Sections were washed under running water until the water ran clear and dehydrated through increasing concentrations of ethanol as already described. Sections were DPX mounted and visualised under light microscopy using the Leica DMI 6000B microscope.

3.2.11.4 Fresh frozen kidney tissue for PCR

Immediately after harvesting, at least half a kidney from each mouse was snap frozen on dry ice and transferred for storage at -80°C. A sample of kidney was used for RNA extraction. This was performed using the Qiagen Mini prep RNA extraction kit. The manufacturer's instructions were followed which involved use of 30mg of tissue. This was homogenised in a glass homogeniser in RLT lysis buffer supplied with the kit. A DNAse digestion step was also performed to eliminate contaminating genomic DNA in the samples. The same protocol was followed to extract RNA from the other organs harvested from the mice. This protocol is available at: www.qiagen.com/resources/download.

Once RNA had been extracted from the tissue it was quantified using the nanophotometer 1000 Pearl machine (ThermoFisher™) and stored at -80°C until needed. RNA from mouse tissues was used for endpoint and qPCR using the same methodology already described for my *in vitro* experiments. Primer sequences are listed in the appendix.

3.2.11.5 Fresh frozen kidney tissue for IF

Fresh frozen kidney tissue was sent to be sectioned by the histology department at Bristol University. Sections were cut on a cryostat to 3 microns thick. These were stored at -80°C until needed. Samples were probed to assess Gb3 expression using immunofluorescence (IF). This process was similar to that already described *in vitro*. Briefly, sections were removed from -80°C and left to air dry for 15 minutes. Each section was drawn around with an ImmEdge® hydrophobic barrier pen (Vector Labs Ltd) to prevent spill over of antibodies between sections. The sections were fixed with 4% PFA for 15 minutes at room temperature under a fume hood. Slides were then washed with PBS and blocked as well as permeabilised in 3% BSA, 0.3% Triton X 100 in PBS for 1 hour. The sections were then probed with a primary antibody (see appendix for concentrations) overnight at 4°C.

The following day the sections were washed three times in PBS and a secondary Alexa fluor antibody applied for 1 hour at room temperature. The sections were then washed again three times in PBS and VECTA Shield hard setting mount with DAPI nuclear stain applied (Vector Labs Ltd). Slides were imaged using the Leica DMI 6000B microscope or Leica Confocal SP5-II confocal laser scanning microscope at the Wolfson Imaging Institute, University of Bristol.

3.2.11.6 In situ hybridisation for VEGF-A

Fresh frozen kidney sections were sent to the histology department in Bristol university for cryostat sectioning after being put into moulds with Tissue Tek OCT compound and frozen at -80°C. New Tissue Tek OCT compound was made in histology for my in situ hybridisation so as to keep it as free of RNA contamination as possible. Sections were cut between 5-7 microns thick and placed in slides. These were stored at -80°C until needed.

In situ hybridisation uses labelled RNA probes to target the expression of a gene of interest. I was kindly given a mouse VEGF-A 164 DNA plasmid by post-doctoral scientist Dr Megan Stevens from the University of Exeter. In order to ensure an unlimited supply of plasmid for future use, a bacterial transformation was performed to increase the quantity of our stock. Competent E.*coli* (Life Technologies) were used to make copies of the plasmid. The transformation solution included competent E.*coli* and the VEGF-A plasmid which were heat shocked at 42°C for 1 minute and then placed on ice for 30 minutes. Super optimal broth media (Sigma-Aldrich) was added to the transformation solution and placed on the orbital shaker at 37°C for 1 hour.

Lysogeny Broth (LB) Agar plates with ampicillin were pre-made (see appendix for recipe) and the transformation solution added. Given the VEGF-A 164 plasmids have an ampicillin resistance gene, only E.*coli* that have taken up the plasmid should be able to colonise the plate. After being left overnight at 37°C the plate was reviewed for colony growth. Using a pipette tip over a Bunsen burner flame (to keep the atmosphere sterile), I inoculated the tip with one colony from the agar plate and dipped the pipette tip into 5mls of LB broth (Gibco, ThermoFisher Scientific™) with added ampicillin. This was then placed on the orbital shaker at 37°C overnight, but for no longer than 16 hours so as to avoid bacterial overgrowth.

A Qiagen QIAprep® miniprep kit was then used to purify the plasmid DNA from my bacterial culture by following the protocol provided with the kit. Once the plasmid DNA

had been extracted and cleaned up, it was quantified using the nanophotometer 1000 Pearl machine (ThermoFisher™). Plasmids were then stored at -80°C until further use. The plasmid was subsequently sent to Eurofins genomics for sequencing. Using the Basic Local Alignment Search Tool (BLAST) at https://blast.ncbi.nlm.nih.gov/Blast.cgi, I entered the FASTA sequence sent back to me from Eurofins which confirmed that mouse VEGF-A was the top hit for the plasmid sequence (Figure 3-15).

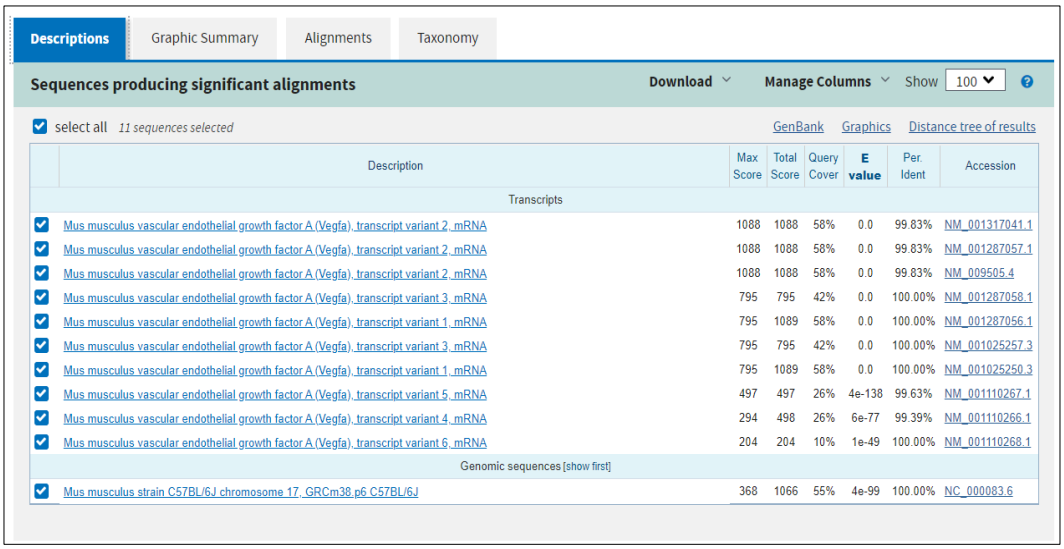

Descriptions | Graphic Summary | Alignments | Taxonomy

Sequences producing significant alignments — Download — Manage Columns — Show 100

select all *11 sequences selected* — GenBank — Graphics — Distance tree of results

Description	Max Score	Total Score	Query Cover	E value	Per. Ident	Accession
Transcripts						
Mus musculus vascular endothelial growth factor A (Vegfa), transcript variant 2, mRNA	1088	1088	58%	0.0	99.83%	NM_001317041.1
Mus musculus vascular endothelial growth factor A (Vegfa), transcript variant 2, mRNA	1088	1088	58%	0.0	99.83%	NM_001287057.1
Mus musculus vascular endothelial growth factor A (Vegfa), transcript variant 2, mRNA	1088	1088	58%	0.0	99.83%	NM_009505.4
Mus musculus vascular endothelial growth factor A (Vegfa), transcript variant 3, mRNA	795	795	42%	0.0	100.00%	NM_001287058.1
Mus musculus vascular endothelial growth factor A (Vegfa), transcript variant 1, mRNA	795	1089	58%	0.0	100.00%	NM_001287056.1
Mus musculus vascular endothelial growth factor A (Vegfa), transcript variant 3, mRNA	795	795	42%	0.0	100.00%	NM_001025257.3
Mus musculus vascular endothelial growth factor A (Vegfa), transcript variant 1, mRNA	795	1089	58%	0.0	100.00%	NM_001025250.3
Mus musculus vascular endothelial growth factor A (Vegfa), transcript variant 5, mRNA	497	497	26%	4e-138	99.63%	NM_001110267.1
Mus musculus vascular endothelial growth factor A (Vegfa), transcript variant 4, mRNA	294	498	26%	6e-77	99.39%	NM_001110266.1
Mus musculus vascular endothelial growth factor A (Vegfa), transcript variant 6, mRNA	204	204	10%	1e-49	100.00%	NM_001110268.1
Genomic sequences [show first]						
Mus musculus strain C57BL/6J chromosome 17, GRCm38.p6 C57BL/6J	368	1066	55%	4e-99	100.00%	NC_000083.6

Figure 3-15: Confirmation of mouse VEGF-A plasmid sequence from BLAST

Purified VEGF-A 164 plasmids were sent to Eurofins genomics for sequencing. Using the Basic Local Alignment Search Tool (BLAST) at https://blast.ncbi.nlm.nih.gov/Blast.cgi, I entered the FASTA sequence sent back to me from Eurofins which confirmed that mouse VEGF-A was the top hit for the plasmid sequence.

To make the RNA DIG labelled probe for in situ hybridisation, the VEGF-A plasmid needed to be linearized. Using the plasmid map provided by Dr Stevens two restriction digests were set up; one with EcoR1 restriction enzyme (New England Biolabs Ltd) to make an anti-sense probe and one with XBaI (New England Biolabs Ltd) to make a sense probe (as a negative control for VEGF-A detection). The restriction digest containing the plasmid, EcoR1 or XBaI restriction enzyme and appropriate buffer (EcoR1 buffer or CutSmart buffer respectively) was incubated at 37°C for 1 hour in a PCR machine. The reaction was stopped by heat inactivation through incubation at 65°C for 20 minutes. The digest was then run on a 1% agarose gel alongside the non-linearized plasmid to determine if the restriction digest had been successful (Figure 3-16).

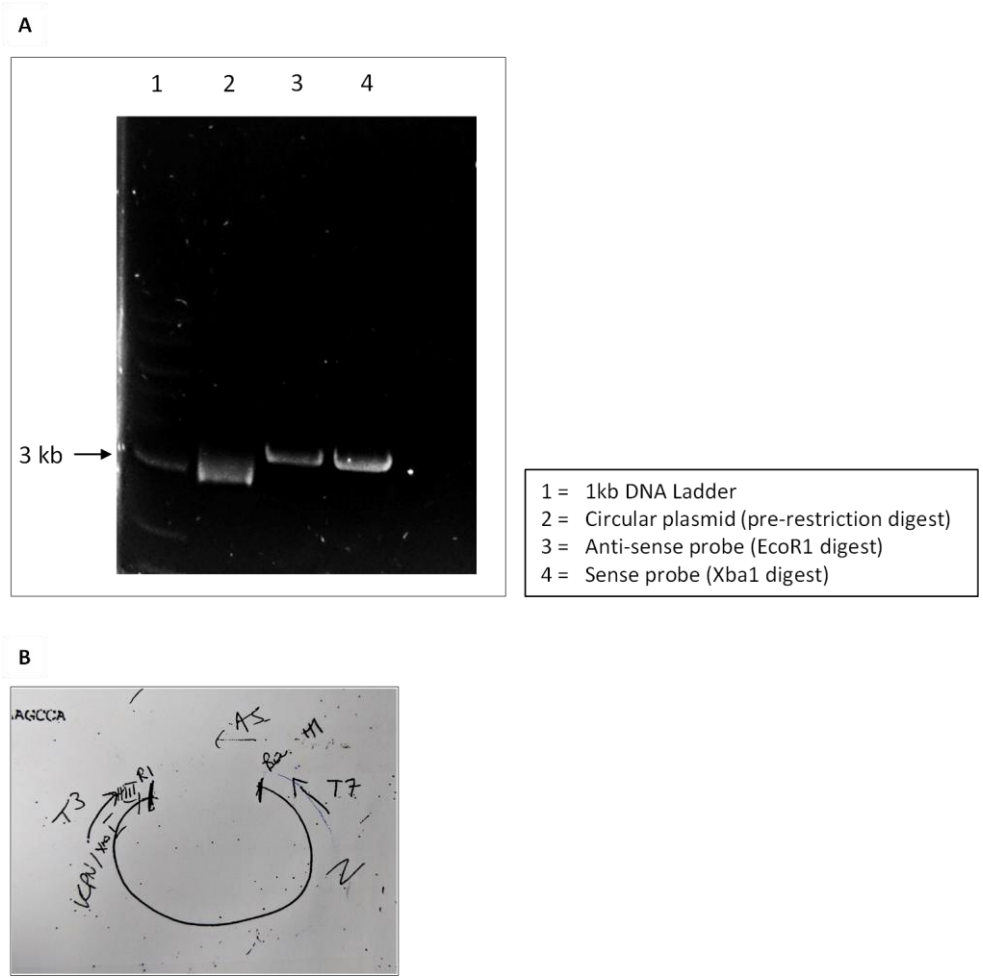

Figure 3-16: Restriction digest used to linearize the VEGF-A 164 plasmid

The VEGF-A plasmid was linearised as described to facilitate the generation of an anti-sense and sense RNA VEGF-A probe. The products of the restriction digest used to facilitate this were run on a 1% agarose gel shown in panel A. As expected, the linearised plasmid was 'heavier' than the circular plasmid which migrates more easily through the gel as it is more compact (i.e. circular plasmid will be in coiled state). The expected band size for the plasmid with the VEGF-A insert was 3.6kB as shown. Panel B shows the plasmid map supplied by Dr Megan Stevens which is a pBluescript II KS vector with mouse VEGFA 164 isoform inserted at Sma1 site. Restriction enzymes were selected on the basis of this map after cross-referencing them on the New England Biolabs website).

The linearized plasmid was then labelled by setting up a DIG labelling reaction using a DIG RNA labelling kit (Sigma-Aldrich). T3 RNA polymerase was used to label the sense probe and T7 RNA polymerase was used to label the anti-sense probe. The reaction was set up by mixing the labelling reagents (see appendix) at room temperature in an RNAse free environment (dedicated RNA free laminar flow hood) and incubating at 37°C for 4 hours.

To stop the reaction 1µl of 0.5M EDTA was added, followed by 2.5µl 4M Lithium chloride and 75µl 100% ethanol to precipitate the labelled RNA. This was then incubated at -80°C overnight.

The following day the precipitation was spun in a microfuge for 15 minutes at 4°C at top speed to generate a pellet. This pellet was washed with 500µl of 70% chilled ethanol and allowed to air dry. The pellet was then dissolved in 75µl of DEPC treated water (ThermoFisher Scientific™). 1µl of this suspension was then run on a 2% agarose gel to check the quality of the probe (Figure 3-17) and another 1µl used to estimate the concentration of the probe using the nanophotometer. The labelled probe was then stored at -80°C until further use.

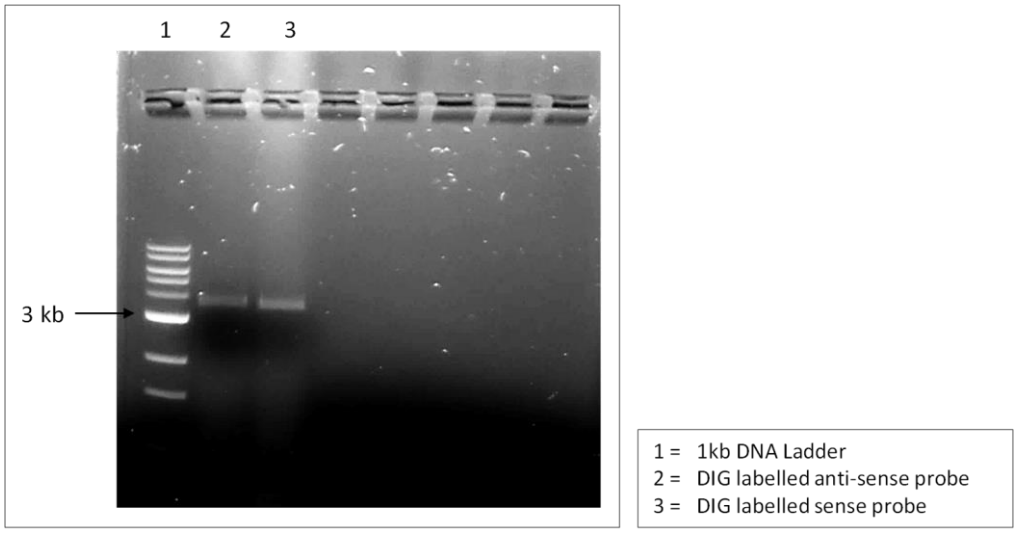

Figure 3-17: DIG labelled probes

Following DIG labelling both the anti-sense VEGF-A and sense VEGF-A probes were run on a 2% agarose gel to check that there had been no contamination during the DIG labelling process. This showed a single visible band at 3.6kB which is the expected size of the plasmid with the VEGF-A insert, confirming no contamination had occurred.

Once the RNA probes had been DIG labelled, in situ hybridisation for VEGF-A could begin. Frozen kidney sections were air dried at room temperature for 1 hour after being taken out of -80°C storage. To expose the nucleic acids in the tissue, slides were treated with 15 µg/ml proteinase K (Sigma-Aldrich) in DEPC (ThermoFisher Scientific™) PBS at 37°C for 5 minutes. Following two washes in DEPC PBS at 37°C, slides were fixed in 4% PFA at room

temperature for 7 minutes. PFA was washed off with DEPC PBS at room temperature and the slides treated with 2x saline sodium citrate (SCC) (made up from 20x SCC purchased from Sigma-Aldrich). Hybridisation buffer was made up and pre-heated to 60°C (see appendix for recipe). Slides were incubated in this buffer for 1 hour in a hybridisation oven at 60°C, within a humidified chamber. The humidified chamber was set up using 2 layers of white filter paper at the bottom, soaked in 120mls of 50% formamide (Sigma-Aldrich) in 5x SCC. This kept the chamber RNAse free. After 1 hour the hybridisation buffer was replaced with the DIG labelled RNA VEGF-A probe at a concentration of 1µg/ml (either anti-sense or sense) and incubated overnight at 60°C within the humidified chamber. To prevent the slides from drying out they were wrapped in parafilm.

The following day slides were rinsed in 2x SCC at 60°C to detach the parafilm. To remove any unbound RNA probe, slides were washed in 50% formamide in 0.2 x SCC at 60°C three times for 5 minutes. They were then washed in 2x SCC at room temperature twice before being washed in NT buffer (see appendix for recipe). Sections were drawn around using an ImmEdge® hydrophobic barrier pen (Vector Labs Ltd) and NT block solution (see appendix) applied for 30 minutes at room temperature. The sections were subsequently probed with an anti-DIG alkaline phosphatase (AP) conjugated Fab fragment antibody (1 in 2000 dilution) for 2 hours at room temperature. To block any endogenous AP activity, sections were then washed twice in TBSTL (200ml tris-buffered saline with TWEEN 20 + 200µl 2M levamisole) for 15 minutes on a rocker at room temperature. Slides were washed in freshly made up APB buffer (see appendix) for 15 minutes at room temperature on a rocker; before addition of BM purple AP precipitating substrate which was left on overnight in the dark at room temperature.

The next day, slides were washed in water twice and immersed in Fast red for 2-3 dips to stain the nuclei of the cells. Slides were washed again in running water until it ran clean and dehydrated in ethanol 50% through to 100%. Slides were immersed in histoclear twice for 2 minutes and mounted with DPX under the fume hood. Once dried they were imaged under light microscopy.

3.2.11.7 Electron Microscopy (EM) analysis

A quarter of kidney tissue harvested from mice at termination was cut up into fine pieces and preserved in EM fixative. This was freshly made up each time it was used from equal measures (1:1) of 0.2M sodium cacodylate pH 7.4, and 2.5% glutaraldehyde. 500µl of EM buffer was used for each kidney. Kidneys pieces were kept in EM buffer at 4°C for at least

48 hours before being processed by the Wolfson Bioimaging Facility at the University of Bristol. This was to ensure adequate penetration of the buffer into the tissue sections but to avoid destruction of the tissue. Samples were subsequently sectioned on an ultramicrotome, imaged and analysed by postdoctoral researcher Dr Louise Farmer. Both myself and Dr Farmer were blinded to the genotype of the mice during sample preparation and analysis. EM images were taken on the Tecnai 12 120kV BioTwin Spirit Transmission Electron Microscope scanner in the Wolfson Institute.

3.2.12 Blood sampling and analysis

Blood samples were taken from mice at the time of terminal anaesthesia via cannulation of the inferior vena cava. This technique was a new skill for our group which required training from Dr Robert Pope (a postdoctoral scientist from Prof. Alastair Poole's platelet research group). It is a technique that was used as standard in this research group that requires considerable manual dexterity but was relatively easy to pick up. The exact details of the methods involved in blood sampling, analysis of blood samples and the generation of blood films is discussed in detail in Chapter 7.

3.2.13 Urine collection and analysis

Urine was collected from all mice at several time points: at baseline (prior to induction with doxycycline), again after 14 days of doxycycline or standard drinking water prior to IP Shiga toxin or saline sham injection, and pre-termination. Mice were transferred to individual cages with hydrophobic sand placed at the bottom (LabSand® purchased from Datesand Group). This sand repels liquid, so that any urine excreted by the mice can be pipetted up from the surface without contamination. Mice were not left for more than 1 hour in these individual cages and monitored throughout. At the time of collection, each urine sample was tested for microscopic haematuria and proteinuria by urine dipstick, using Siemens Multistix 10SG Urinalysis Strips®. This gave me an estimate of whether any glomerular injury had occurred.

To quantify the amount of albumin leak into the urine, albumin creatinine ratios (ACR) were performed. Measurement of urinary albumin was performed using an albumin ELISA kit from (Bethyl Laboratories Inc). A goat anti-mouse albumin coating antibody supplied in the kit was used to coat each well and each standard or sample was run in duplicate. The recommended procedure was followed for the ELISA and absorbance was read on a plate reader at 450nm. A standard curve was plotted to allow calculation of the albumin

concentration in each urine sample. To determine the corresponding creatinine content, urine samples were sent to Kay Burt at Langford Veterinary Practice for enzymatic creatinine analysis. The ACR (µg/mg) could then be calculated by dividing the albumin concentration by the creatinine concentration for each sample.

3.3 Statistical Analysis and Data Handling

All statistics and graphical figures have been produced using GraphPad Prism V7.0 unless otherwise stated. At the beginning of my PhD, I enrolled on a 5 day 'Introduction to Statistics Course' run by the School of Social and Community Medicine at the University of Bristol. This was particularly useful to remind me of the appropriate statistical tests to apply according to the nature of the data itself. To assess if my data were normally distributed, I used the Shapiro-Wilk Test (available through Prism). If the p value of this test was greater than 0.05 a normal distribution was assumed.

Normally distributed data has been analysed by a student's unpaired T-test where the mean of two independent groups (i.e. unrelated measurements) were tested to determine if there was any significant difference between the two groups. For paired observations in the same subject paired T-tests were used. All data are presented as mean values +/- SEM (standard error of the mean) as indicated by error bars on graphs where relevant. The statistical significance has been displayed on the graphs relative to control or baseline values as indicated: *$p<0.05$, **$p<0.005$, ***$p<0.0005$. At the end of each figure legend the exact p value obtained for each statistical test is given.

For data comparisons between multiple groups (i.e. more than two groups) where data is normally distributed, a one-way ANOVA has been used. Post-hoc analysis test selection was determined by the comparisons being made and where possible Tukey's Honest Significant Difference test was performed. This post-hoc test established where the differences between groups identified by the one-way ANOVA were located. The p value results of one-way ANOVA and the type of post-hoc analysis carried out is stated in the figure legend of each graph.

Correlations were analysed using Pearson correlation on normally distributed data, and Spearman correlation where data could not be assumed to be of normal distribution as is conventional. The complex statistical methods employed in the analysis of my proteomic datasets that contain thousands of data points have been discussed separately within my

proteomic results chapter. The choice of statistical tests used in my proteomic datasets was governed by a combination of expertise from the University of Bristol Proteomics Facility, the bioinformatic service from Dr Phil Lewis, already published proteomic dataset analyses and the freely available statistical software package R. The key in analysing these data was to correct for multiple comparisons using the Bonferroni correction. As when hundreds or thousands of dependent or independent statistical tests are being performed simultaneously, the likelihood of observing a rare event simply by chance increases, thereby increasing the risk of Type 1 error (i.e. rejecting the null hypothesis incorrectly).

Chapter 4 : The molecular effects of Shiga toxin on the podocyte

4.1 Introduction

The *in vitro* study of cells in culture has a key role in advancing our understanding of the molecular pathways involved in human health and disease. There are several advantages of *in vitro* work which include: the ability to control and manipulate the environment to allow testing of a specific hypothesis; the scope to perform multiple replicates of an experiment to validate results; and the ability to drill down into the mechanistic processes occurring in the cell [239]. Historically, *in vitro* culture of podocytes has been challenging as only undifferentiated cells were available and these were of questionable purity. These cells were of limited use as they quickly lost expression of their podocyte markers (such as synaptopodin) and lost their characteristic foot processes in standard culture conditions [223].

However, in 2002, Saleem et al. developed a conditionally immortalised human podocyte cell line by transfection with the temperature sensitive SV40-T gene [223]. At 33°C these podocytes proliferate, but upon thermo-switching to 37°C they enter growth arrest and differentiate, expressing markers of differentiated human podocytes *in vivo* [223]. Subsequent work by Saleem et al. in our laboratory has led to the generation of conditionally immortalised podocyte cell lines from wild type mice [240]. These cells are now an established resource in Bristol and considered the gold standard for the *in vitro* study of podocyte biology. Using both human and mouse conditionally immortalised podocyte cell lines has allowed me to address one of the key research aims of my PhD: determining the cellular mechanisms underlying the action of Shiga toxin in the podocyte.

4.2 Detection of Gb3

Essential to this project is the ability to reliably detect Gb3 expression in tissues. Given that Gb3 is a glycosphingolipid this has proved challenging as the usual methods of detecting a receptor (most often a transmembrane protein) are redundant [241]. Furthermore, Kolling et al. have previously shown that fixation of tissues with ethanol leads to dissolution of glycosphingolipids including Gb3 [238]. Hence, tissues have been dehydrated in acetone as described in the materials and methods chapters to preserve

the receptor. As already eluded to in the introduction; it is well established that Gb3 is the receptor for Shiga toxin. It is located within host cell membranes and expression of Gb3 determines how sensitive the cell is to the effects of Shiga toxin [33]. In the following sections I will detail the four different methods I have optimised during my PhD to detect Gb3 expression both *in vitro* and *in vivo*.

4.2.1 Detection of Gb3 with immunofluorescence

Human conditionally immortalised podocytes express the Shiga toxin receptor Gb3. I have confirmed this using immunofluorescence (IF). Murine podocytes do not express the Gb3 receptor (Figure 4-1). However, Gb3 is expressed in the renal tubules of mice and has been detected in small quantities in other murine organs [242] (Figure 4-2). Gb3 expression has also been detected in other human organs including lung, brain, pancreas, heart and liver. Hence unsurprisingly, STEC HUS can be complicated by extra renal manifestations including neurological sequelae, pancreatitis and in rare cases pulmonary haemorrhage [243].

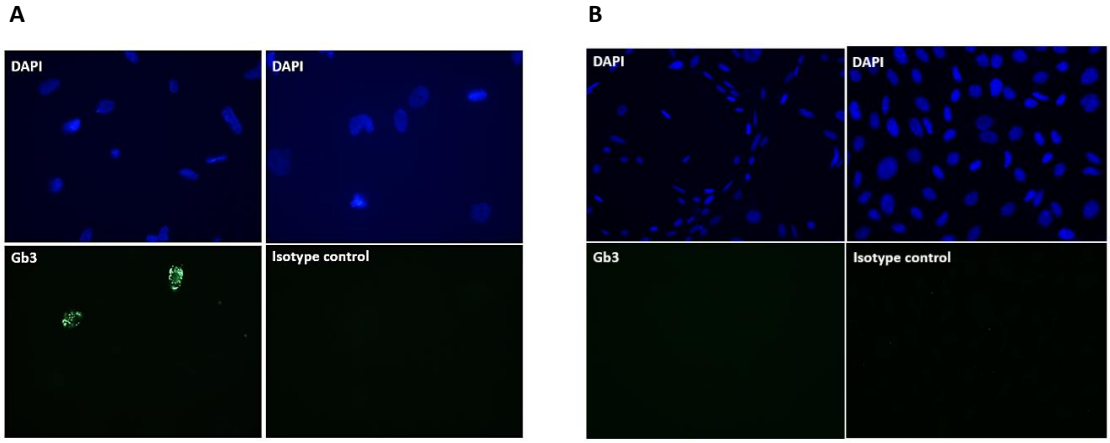

Figure 4-1: IF detection of Gb3 in human podocytes (A) vs. mouse podocytes (B)

Conditionally immortalised human or mouse podocytes were cultured and IF performed as described to detect Gb3 (green). An isotype control antibody confirms that this is specific for Gb3 expression. DAPI nuclear staining is shown in blue. There is no evidence of Gb3 expression in mouse podocytes. Images taken on the Leica DMI 6000B microscope using the same settings at x20 magnification.

Given that Gb3 is a glycosphingolipid it is unusual to have an antibody that recognises it. The antibody used has been widely cited in the literature and is a rat monoclonal anti-CD77 [238]. The immunogen of the antibody is the Daudi Cell line (Burkitt's lymphoma) (according to the antibody specifications) and so recognises part of the hydrophilic carbohydrate region of the glycosphingolipid. I was concerned that the antibody may not recognise murine Gb3 and this may lead to false negative IF staining in mouse podocytes. As a result, IF using fresh frozen mouse kidney tissue sections in wild type mice was performed which confirmed the antibody could detect murine Gb3 in the renal tubules of these mice (Figure 4-2).

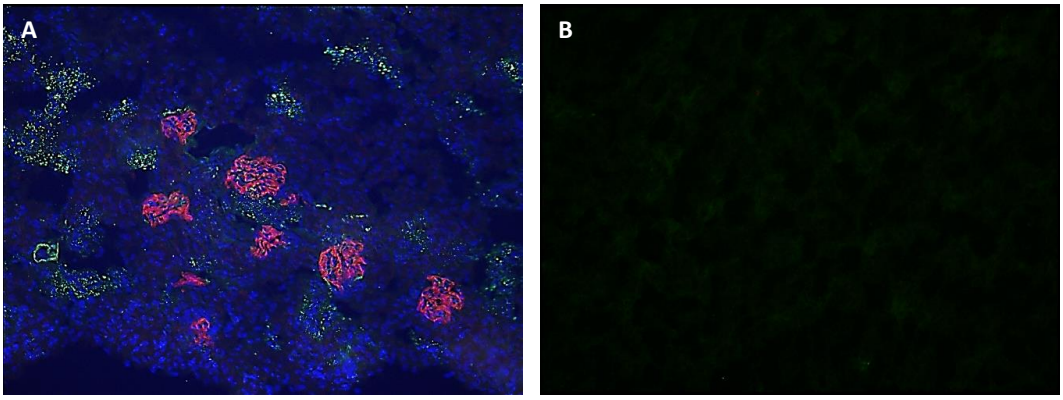

Figure 4-2: IF detection of Gb3 in wild type mouse kidney tissue

Fresh frozen kidney sections from wild type mice were prepared for IF as described and probed for Gb3 (green); nephrin (red – to identify podocytes outlining the glomeruli) and DAPI stained to identify nuclei (blue). Panel A shows Gb3 is located in the tubules of murine kidney and is absent from the glomeruli. The section in Panel B was prepared in the same way as Panel A, but without a primary antibody for Gb3/nephrin as an auto-fluorescence control for the secondary antibody.

4.2.2 Detection of Gb3 Synthase (A4GALT) with endpoint PCR

Two pairs of primers for PCR were designed (as described in my methods chapter) to identify expression of the enzyme Gb3 synthase (A4GALT) in either mouse cells or human cells. Gb3 RNA could not be detected directly by PCR because it is a glycosphingolipid. Gb3 synthase catalyses the synthesis of Gb3 from lactosyceramide (Figure 4-3). Endpoint PCR confirmed that A4GALT mRNA is present in both human and mouse podocytes (Figure 4-4). Although A4GALT is present in mouse podocytes, Gb3 itself does not appear to be expressed as it was not detectable on IF. Given I was not expecting to find A4GALT mRNA

in mouse podocytes, several different mouse cell lines were tested. Mouse podocyte cell line 2 (Figure 4-4) appeared to have very little A4GALT mRNA expression. This was a primary mouse cell line (compared to the conditionally immortalised mouse podocyte cell lines used in the other rows). Primary cell lines are known to more closely resemble cell function and morphology *in vivo* which is likely to explain the discrepancy observed in the expression of A4GALT mRNA [244]. The predicted PCR product for the A4GALT primer pairs designed was 113 base pairs. This product was subsequently sequenced to confirm that the primers were amplifying the A4GALT gene (Figure 4-5).

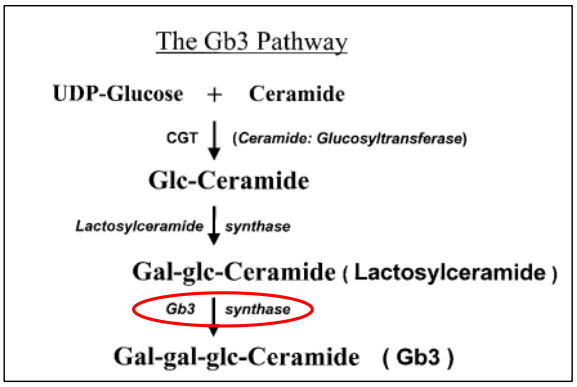

Figure 4-3: The Gb3 Pathway

Gb3 is synthesized from Lac-Cer (lactosyceramide) by the enzyme Gb3 synthase (A4GALT). All complex glycosphingolipids are formed from ceramide which is the common precursor [84].

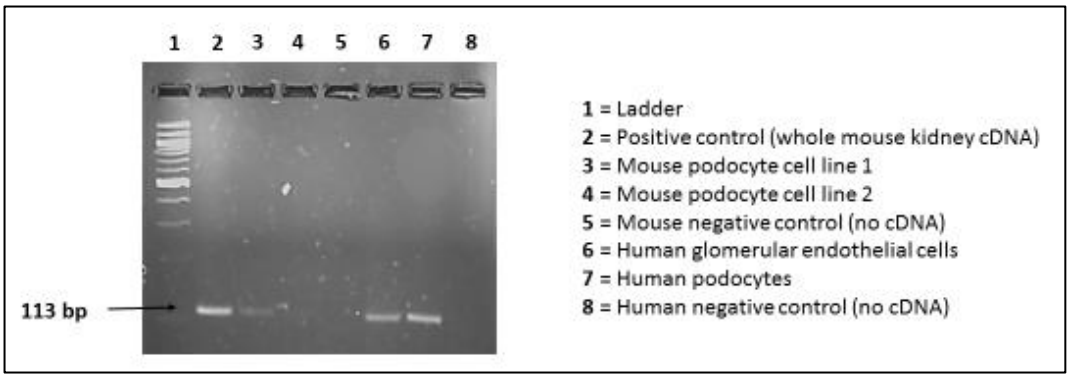

Figure 4-4: Endpoint PCR for A4GALT

Endpoint PCR demonstrates A4GALT mRNA is present in both human and murine podocytes as well as human endothelial cells. The expected PCR product size was at 113 base pairs as shown. Given A4GALT mRNA was not expected in mouse podocytes, I tested several different mouse cell lines.

Mouse podocyte cell line 2 (well 4) appeared to have very little A4GALT mRNA expression. This was a primary mouse cell line which is likely to reflect mouse podocyte expression of A4GALT mRNA more closely than conditionally immortalised cell lines which explains this difference.

Figure 4-5: Endpoint PCR product sequencing

PCR product sequencing confirmed that the A4GALT gene had been amplified by my primer pairs – both in the human (A = top panel) and mouse (B = bottom panel) cells.

4.2.3 Detection of Gb3 with thin layer chromatography

Thin layer chromatography (TLC) is considered the gold standard lipid detection method. In order to learn this technique, I collaborated with Professor Shamshad Cockcroft (a lipid expert based at University College London: UCL). Initially the assay was set up in the human cervical cancer Hela cell line, as these are the cells routinely used in the Cockcroft laboratory. The technique is dependent upon tritium labelling of sphingosine. This is then incorporated into both sphingomyelin and glucosylceramide lipids within the cell. The cellular lipid fractions are then separated on a TLC plate according to their relative affinity towards the stationary and mobile phase. The samples from the cells of interest run alongside a series of lipid standards.

The lipid fractions can be reversibly visualised (as shown in Figure 4-6) by placing the TLC plate in a bed of iodine crystals within a closed TLC tank within a fume cupboard hood. This creates an environment of iodine vapour which will saturate the plate and reveal the lipid fractions as yellow/brown bands. It is important not to expose the plate too long as iodine may covalently modify polyunsaturated fatty acids. An alternative is to use a glass Pasteur pipette with iodine crystals through which dinitrogen is blown over individual standard lanes. This circumvents the risk of oxidation of the lipid fraction. This technique confirms that separation of the lipid bands has occurred, prior to quantification using a scintillation detector. This will detect the presence of any lipids containing tritium labelled sphingosine (Figure 4-7).

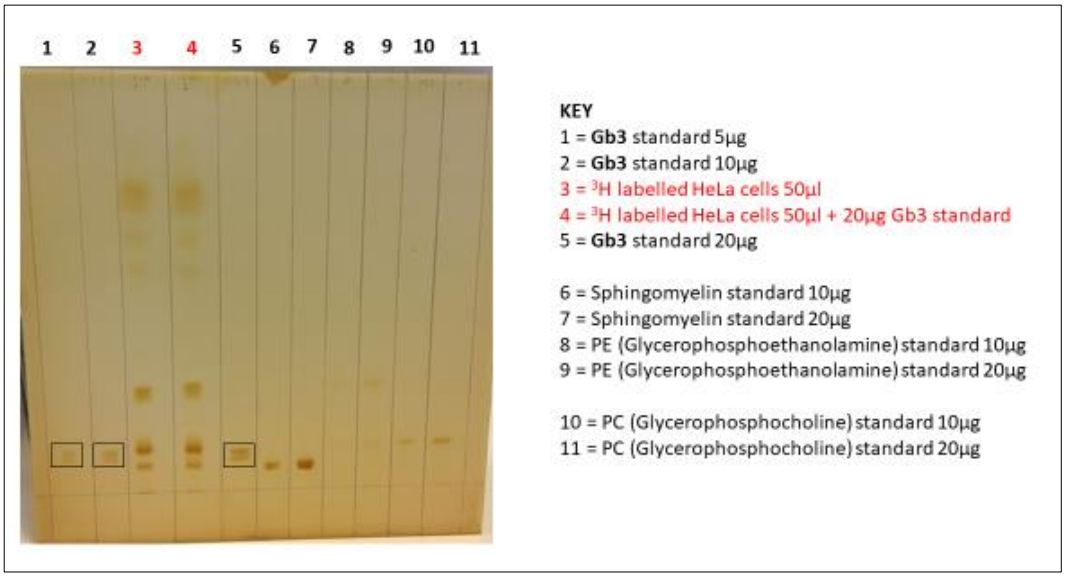

Figure 4-6: TLC plate in Hela cells: proof of concept

The Gb3 standard was run against the Tritium (3H) labelled HeLa cell samples (rows 1-5). Sphingomyelin, PE and PC standards were also run on the same plate as references. The lipid fractions can be reversibly visualised as shown here by placing the TLC plate in a bed of iodine crystals within a closed TLC tank within a fume cupboard hood. This creates an environment of iodine vapour which will saturate the plate and reveal the lipid fractions as yellow/brown bands. It is important not to expose the plate too long as iodine may covalently modify polyunsaturated fatty acids.

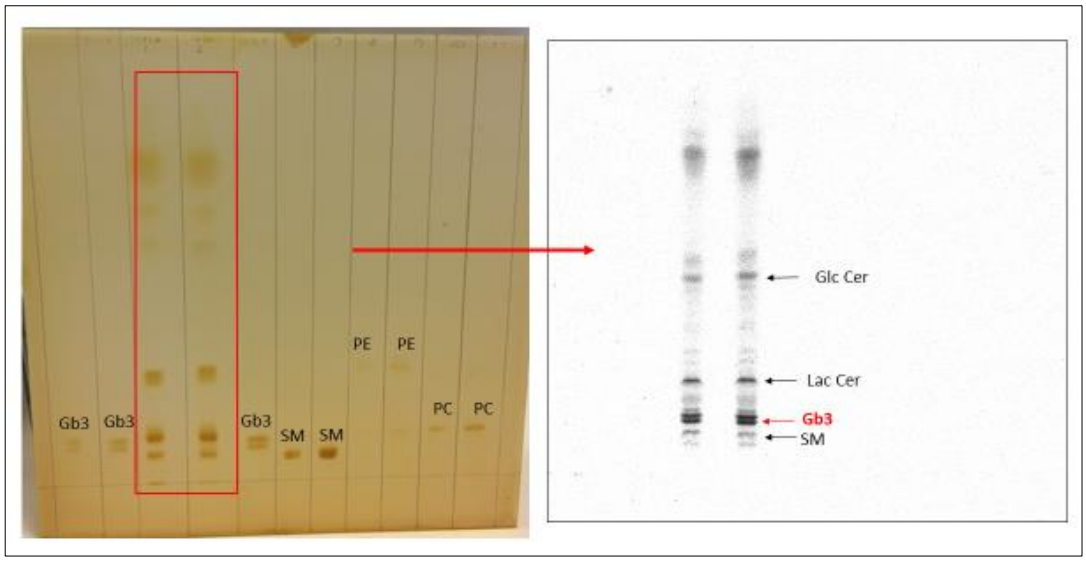

Figure 4-7: TLC plate and scintigram: Hela cells

The only samples that are visible on the scintigram are the Hela cells that have been labelled with Tritium. Hence only rows 3 and 4 (indicated by the red box) are seen on the scintigram. By overlaying the original TLC plate standards with the scintigram together with the knowledge that only complex glycosphingolipids that are synthesized from sphingosine (and therefore Tritium labelled will be visualised on the scintigram); the lipid constituents of the HeLa cells can be identified as shown: GlcCer = glucosylceramide, LacCer = lactosyceramide, Gb3 = globotriaosylceramide, SM = sphingomyelin.

This technique is reproducible and robust in HeLa cells but given podocytes are a conditionally immortalised terminally differentiated cell line, I was concerned that tritium labelling may prove difficult. Indeed, this technique has not been performed in a terminally differentiated cell line before. The cells would need to be labelled whilst proliferating prior to thermo-switching. Moreover, using TLC to analyse mouse tissues from my *in vivo* work would not be possible as there is no way of radiolabelling sphingosine: meaning a different overlay method such as orcinol spray (which is non-specific) or Shiga toxin antibody techniques would need to be utilised.

The use of a Shiga toxin antibody to detect Gb3 would involve using Shiga toxin first, to bind to Gb3 on the cell surface, followed by probing the TLC plate with an anti-Shiga toxin antibody. This has obvious safety implications (all work involving the toxin must be performed in biological cabinet under category 3 facilities due to the potential for harm). Given that Shiga toxin cannot be used on the open laboratory bench and the associated danger of spillages in placing a TLC plate in a Shiga toxin solution for several hours of

incubation; this method of Gb3 detection was decided against. However, an antibody to Shiga toxin using a dot blot protocol was tested as a proof of concept, prior to arriving at this decision.

4.2.4 Dot Blot Assay for Shiga toxin detection

A dot blot is a straightforward and relatively quick assay to ascertain whether an antibody and secondary detection system is working. It is most often employed to determine the starting concentration of a primary antibody for western blotting [245]. This assay was used as a way of testing whether a Shiga toxin 2 antibody could detect Shiga toxin in mouse tissues, as it would not be possible to radio-label Gb3 *in vivo*. Full details of the dot blot protocol used are included in my *in vitro* methods chapter. The primary antibody used was a rabbit anti-Shiga toxin 2 antibody from Quadratech®.

Lysates were blotted on a nitrocellulose membrane. These were prepared from fresh kidney tissue from mice (wild type mice with and without Shiga toxin treatment and Gb3 KO mice with and without Shiga toxin treatment) as well as a positive control of Shiga toxin 2, negative controls of untreated conditionally immortalised human podocytes and lysis buffer. To check whether there were any issues with detection from the secondary antibody, Shiga toxin 2 antibody was blotted on to the membrane as a positive control for my secondary HRP conjugated anti-rabbit antibody. The detection of the secondary antibody utilises chemiluminescent detection reagents (purchased from Bio-Rad®) which were applied to the membrane, which was subsequently viewed on the Amersham 600 imager®.

The dot blot experiment did demonstrate that Shiga toxin can be detected with Shiga toxin 2 antibody (Figure 4-8). However, in the kidney lysates prepared from mice that had been given IP Shiga toxin the antibody did not detect any toxin. This is likely due to Shiga toxin being present in too smaller a concentration to be detected in the tissue at this stage in the disease pathogenesis. Mice were injected with 10ng/g of IP Shiga toxin; the concentration of Shiga toxin reaching the kidney tissue in mice may therefore be much less than 0.1µg/ml (the concentration of Shiga toxin 2 used in the positive control that was detectable). Or it may mean that there is no longer any toxin present in the tissue once it has undergone processing to make the lysate. Reassuringly, both positive controls did show a positive result; a dark blue spot at the site of sample blot.

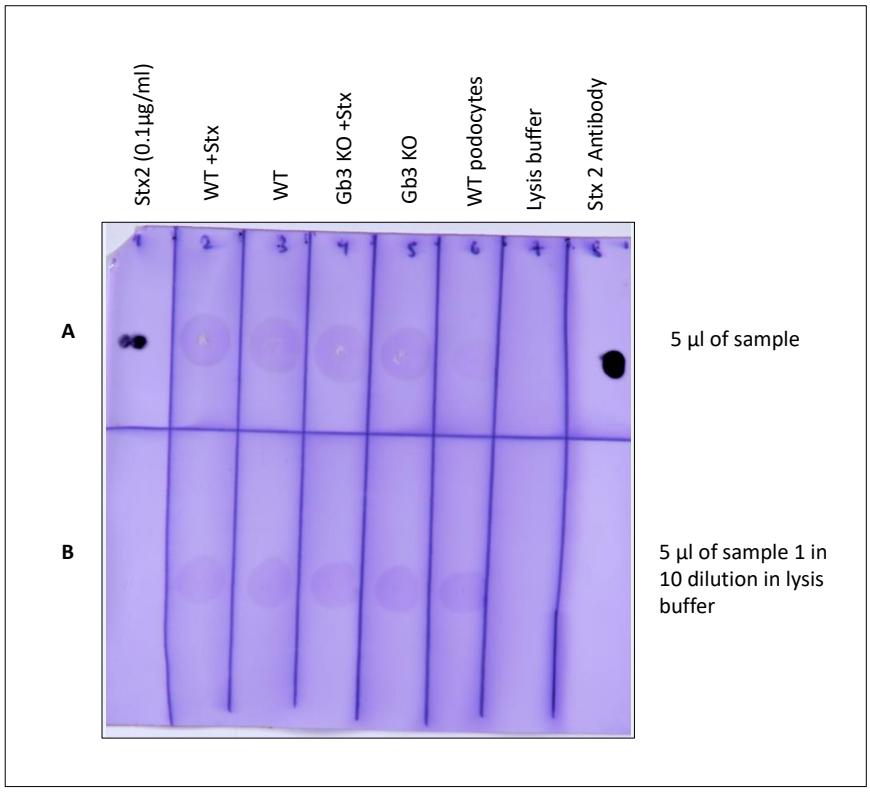

Figure 4-8: Shiga toxin 2 antibody dot blot

Shiga toxin can be detected using an anti-Shiga toxin 2 antibody as seen on this blot – dark blue spot at the site of sample blot. A nitrocellulose membrane was blotted as described with: Stx 2=Shiga toxin 2 (Stx 2 at a concentration of 0.1 µg/ml), WT+Stx =WT mouse given IP Stx kidney tissue lysate, WT=WT mouse kidney lysate untreated, Gb3 KO+Stx = Gb3 KO mouse given IP Stx kidney lysate, Gb3 KO=Gb3 KO mouse kidney lysate untreated, WT podocytes=WT human podocytes lysate, lysis buffer, and Stx 2 antibody at a concentration of 100µg/ml. Interestingly, Shiga toxin is undetectable in the kidney tissue lysate of the treated mice; which is likely due to absence (or very little) Shiga toxin being present in the tissue at this stage in the disease process. All samples at a 1 in 10 dilution of the original concentration are undetectable. Row A = 5 µl of sample blotted, Row B = 1 in 10 dilution of sample blotted.

4.2.5 Detection of Gb3 with mass spectrometry

A more modern and sensitive method of lipid detection is mass spectrometry. Professor Cockcroft suggested contacting Dr. Kevin Mills at the UCL Translational Mass Spectrometry Centre (TMSC) as his group have optimised an assay for quantifying Gb3 expression in cells and tissue. The TMSC is one of the leading mass spectrometry centres in the UK; utilising proteomic and lipidomic analysis to diagnose and monitor Fabry's disease (a lysosomal storage disorder in which Gb3 accumulates in the majority of cells

throughout the body) [246]. Cell lysates from human and mouse podocyte cell lines were prepared as detailed in my materials and methods chapter and sent to the TMSC at UCL where they were analysed for Gb3 content.

Initial results from the first set of cell lysates sent to the TMSC had much higher levels of total Gb3 than anticipated (Table 5, panel A). After discussing this with Dr Mills, it became clear that the media used to culture podocytes contained large amounts of Gb3; originating from the fetal bovine serum component and that the cells were taking up Gb3 from the media. Consequently, the experiment was repeated following serum starvation of the cells (replacing their media with sterile PBS for 4.5 hours prior to cell lysis). This timepoint was chosen because it was the maximal time that podocytes are known to tolerate incubation in serum free media before becoming stressed (anecdotal evidence from experience of Bristol Renal podocyte group); balanced against a long enough duration of serum starvation to prevent Gb3 uptake from fetal bovine serum within standard podocyte media. A sample of the podocyte media was also sent to the TMSC for mass spectrometry analysis to determine the Gb3 content and allow normalisation of the initial samples.

A

Chain length	CTH µg/mg protein	
C16-CTH	20.264	
C18-CTH	0.985	
C20-CTH	0.457	
C22:1-CTH	0.726	
C22-CTH	1.299	
C24:2-CTH	1.765	
C24:1-CTH	3.189	
C24-CTH	1.424	
C24:2-OH-CTH	0.090	
C24:1-OH-CTH	0.018	
C24-OH-CTH	0.081	
C26-CTH	0.018	
	total CTH ug/mg protein =	30.315

B

Chain length	CTH µg/ mg protein	
C16-CTH	0.2401	
C18-CTH	0.0142	
C20-CTH	0.0027	
C22:1-CTH	0.0045	
C22-CTH	0.0061	
C24:2-CTH	0.0056	
C24:1-CTH	0.0111	
C24-CTH	0.0070	
C24:2-OH-CTH	0.0007	
C24:1-OH-CTH	0.0004	
C24-OH-CTH	0.0018	
C26-CTH	0.0000	
	total CTH ug/ mg protein =	0.2941

Table 5: LC-MS/MS Results for Gb3 in human podocytes

Human podocytes were grown in podocyte media until 70-80% confluent and thermo-switched to 37°C to differentiate for 10-14 days before being lysed with RIPA buffer as detailed in the methods. Cell lysates were then sent to the TMSC for mass spectrometry analysis of Gb3 content. Each Gb3

isoform is shown in the table. The total Gb3 (CTH) content was considerably higher than expected (A). As a result, the experiment was repeated but the podocytes serum starved in PBS for 4.5 hours prior to cell lysis. This resulted in a total Gb3 level that was more in-keeping with what would be expected (B). Consequently, any further mass spectrometry analysis was performed following serum starvation for 4.5 hours to allow comparison between cell lines.

Through combining the Gb3 detection methods outlined, I have been able to confidently determine the distribution of Gb3 expression in human and mouse podocyte cell lines. These techniques were optimised *in vitro* to allow subsequent use *in vivo* to validate my mouse models.

4.3 Human podocytes are sensitive to Shiga toxin

It is well established that there is an association between the amount of Gb3 expressed on the cell membrane and its sensitivity to Shiga toxin [247]. However, increasing evidence suggests that the membrane microenvironment consisting of cholesterol, other glycolipids and fatty acids also plays a role in Gb3 receptor binding; as the amount of Gb3 extractable from a tissue does not directly correlate to its sensitivity. It is therefore vital to determine how reactive each cell type is when challenged with Shiga toxin not just the amount of Gb3 expressed [33]. Based upon previous work performed in our laboratory in human podocytes treated with Shiga toxin; the CD50 dose (dose at which 50% of the cell population exhibit cytotoxic effects) was 0.01ng/ml (Figure 4-9). Interestingly, human podocytes were shown to reduce their percentage protein synthesis to a greater extent than that observed in human glomerular endothelial cells at each Stx1 concentration. This may be explained by the fact that Shiga toxin has been shown to induce upregulation of the Gb3 receptor in podocytes *in vitro*, rendering them more susceptible to the ribotoxic effects of Shiga toxin *in vitro* (see subsequent experimental data in section 4.4); an effect that is not seen in glomerular endothelial cells. In view of these data, the effect of Shiga toxin on podocyte viability was studied at two concentrations: 0.01ng/ml (the CD50 dose) and 0.1ng/ml (10x the CD50 dose) at different time points.

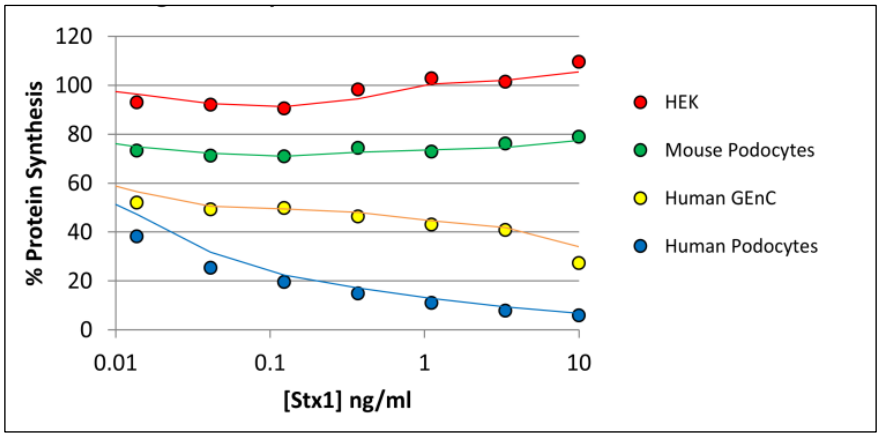

Figure 4-9: Cellular response to Shiga toxin challenge

HEK cells, mouse and human podocytes and human glomerular endothelial cells (GEnCs) were treated with Shiga toxin (concentrations of 0.01ng/ml to 10ng/ml) for 4 hours and the effect on protein synthesis determined. Of note HEK cells do not express the Gb3 receptor and so were the negative control cell line in this experiment. Interestingly, human podocytes were shown to reduce their percentage protein synthesis to a greater extent than that observed in GEnCs at each Stx1 concentration. This may be explained by the fact that Stx is known to induce upregulation of the Gb3 receptor in podocytes *in vitro*, rendering them more susceptible to the ribotoxic effects of Shiga toxin *in vitro* (see subsequent experimental data). This effect is not observed in GEnCs. *Data reproduced with permission from Dr Lindsay Keir.*

My initial experiments involved incubation of differentiated human podocytes with 0.1ng/ml of Shiga toxin in 6 well plates for up to 7 days. The cells were imaged under light microscopy on the Leica DMI 6000B microscope (Figure 4-10). The appearance of the cells suggested that they were undergoing apoptosis as fewer podocytes were present following Shiga toxin treatment. Indeed, previous work by Psotka et al. has demonstrated that Shiga toxin mediates caspase-dependent apoptosis in conditionally immortalised podocytes [74]. To assess podocyte cell viability in response to 0.1ng/ml of Shiga toxin over time triplicate repeat experiments in 96 well plates were performed, using the IN Cell Analyser. This confirmed that podocyte cell number (through the use of DAPI staining of podocyte cell nuclei) was reduced to 50% following incubation with 0.1ng/ml of Shiga toxin for 48 hours vs. media control (Figure 4-11).

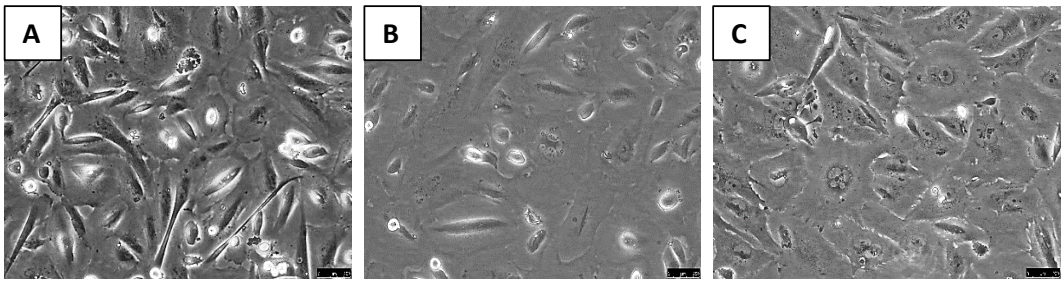

Figure 4-10: Light microscopy slides of differentiated human podocytes

Differentiated human podocytes were incubated with standard podocyte media (A); 0.1ng/ml of Shiga toxin (B); and puromycin 2µg/ml for 48 hours (C). In response to Shiga toxin and puromycin (a known ER stressor used as a positive control) the podocytes reduced in number.

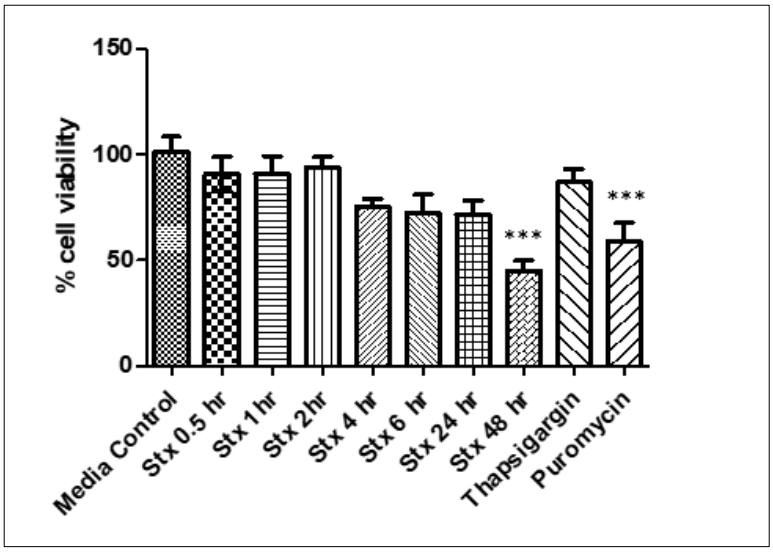

Figure 4-11: Human podocyte cell viability following 0.1ng/ml Shiga toxin treatment

Differentiated human podocytes were incubated with 0.1ng/ml of Shiga toxin for 0.5-48 hours as shown. At 48 hours of incubation cell viability was reduced to 50% vs. media control cells. Known ER stressors thapsigargin (at 1mM concentration) and puromycin (at 5µg/ml concentration) were used as positive controls with podocytes treated for 48 hours. Results pooled over three experiments. *** One way ANOVA Tukey's multiple comparison test: $p<0.0001$ vs. media control.

4.4 Shiga toxin upregulates Gb3 expression in human podocytes

Human podocytes were grown on coverslips in 6 well plates and incubated with 0.1ng/ml Shiga toxin for up to 6 hours. Immunofluorescence was then performed to assess Gb3 expression which appeared to be upregulated (Figure 4-12). In order to be able to quantify

this effect, 96 well plate experiments using the INCell microscope were performed. Human podocytes were incubated with 0.1ng/ml of Shiga toxin for time points up to 48 hours, and immunofluorescence analysis performed using an automated programme analysis on the IN Cell. This confirmed that Gb3 expression was increased in podocytes upon treatment with 0.1ng/ml of Shiga toxin (Figure 4-14). This effect has not been described in podocytes before (upon review of current literature). However, it has been seen in neuronal cells of patients with Shiga toxin HUS and in dermal microvascular endothelial cells [248][84]. Interestingly this effect was not seen in human glomerular endothelial cells [95].

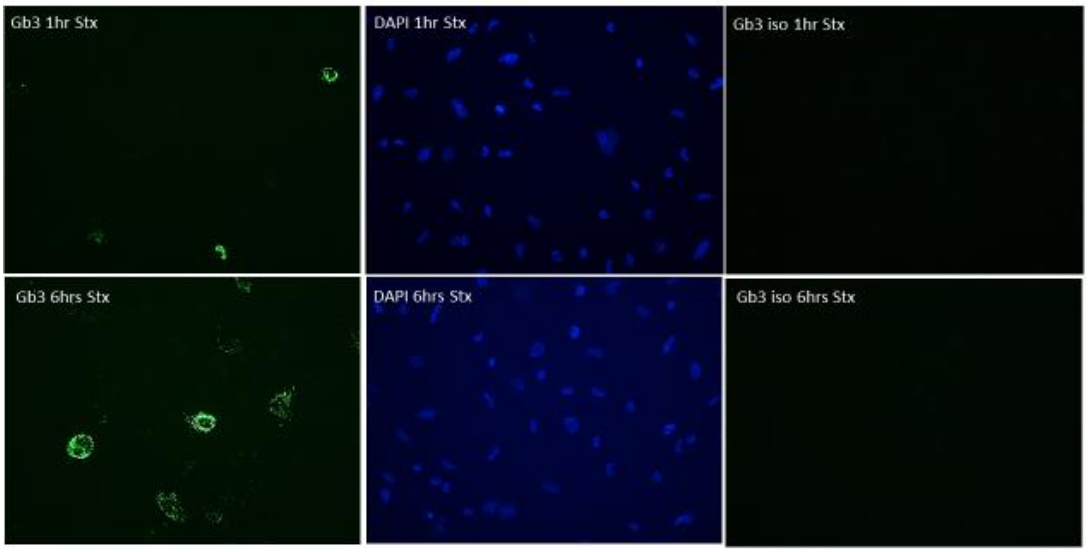

Figure 4-12: Human podocytes upregulate Gb3 expression in response to Shiga toxin challenge
Human podocytes incubated with Shiga toxin (0.1ng/ml) for 6 hours show upregulation of Gb3. Gb3 (green), DAPI (blue). IgG isotype control antibody was used to confirm primary antibody specificity. Images representative of 3 separate experiments (n=3).

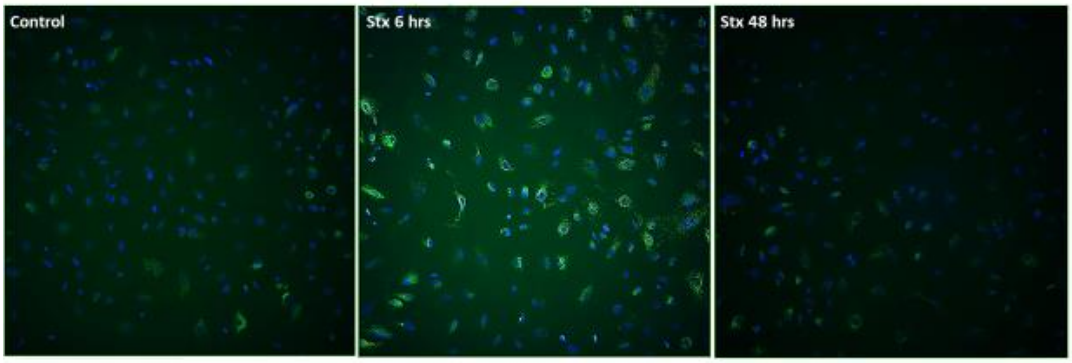

Figure 4-13: IN Cell Gb3 IF staining in human podocytes

Differentiated human podocytes incubated with Shiga toxin 0.1ng/ml at time 0 (no Shiga toxin control) 6 hours and at 48 hours. Gb3 (green), DAPI (blue).

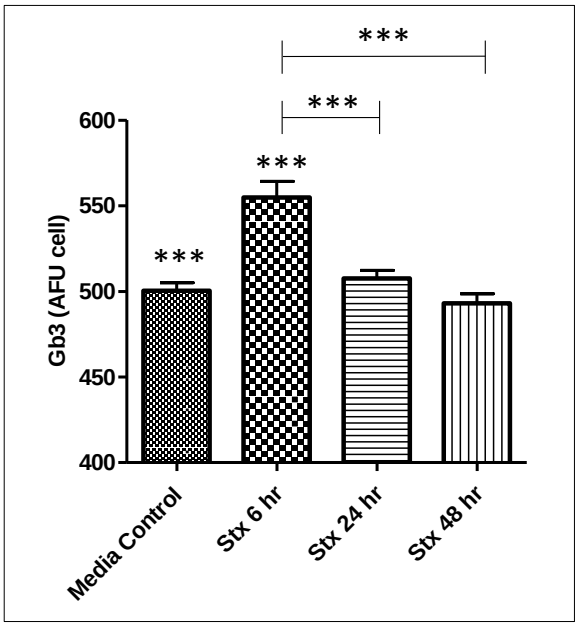

Figure 4-14: Gb3 is upregulated in human podocytes in response to treatment with Shiga toxin

Wild type human podocytes (4000 cells/well) were plated in 96 well IN Cell plates and treated with 0.1ng/ml of Shiga toxin for 6-48 hours and analysed for Gb3 expression using immunofluorescence. AFU values per cell are given. At 6 hours Gb3 expression was significantly higher vs. media control cells. Gb3 expression returns to baseline at 24 hours. ***One way ANOVA: Tukey's multiple comparison test: $p<0.001$ (n=3).

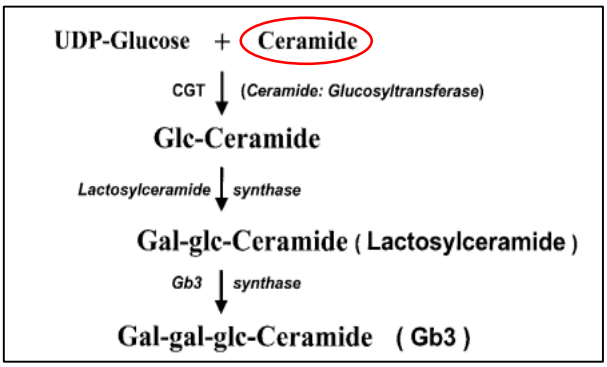

Figure 4-15: The Gb3 biosynthesis pathway

The three glucosyltransferase enzymes required at each stage of Gb3 synthesis are shown. It is thought that upregulation of the Gb3 receptor is likely due to an increase in ceramide production by the cell in response to stress with subsequent upregulation of the ceramide glucosyltransferase enzyme [84].

4.5 Generation of a stable A4GALT knockdown cell line

The precise pathophysiological mechanisms following Shiga toxin infection leading to glomerular TMA are poorly understood. In order to address this, Tandem Mass Tag (TMT) proteomic analysis of human podocyte cells exposed to Shiga toxin was performed. In order to control for non-specific Gb3 receptor binding I analysed (in parallel) the effects of Shiga toxin on an A4GALT knockdown human podocyte cell line. These podocytes were generated using ShRNA as detailed in the methods section. Six different clones were made using ShRNA and the relative expression of A4GALT in each clone versus wild type control podocytes transduced with a non-silencing ShRNA control lentiviral construct was determined using qPCR (Figure 4-16).

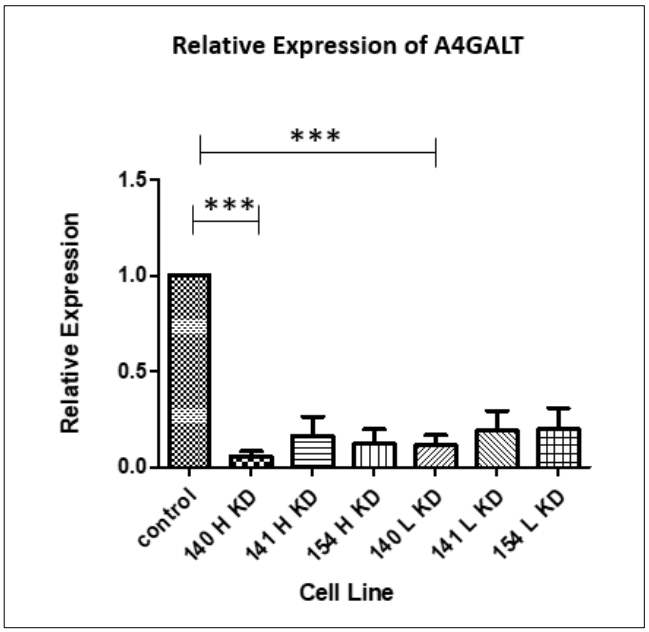

Figure 4-16: Relative expression of A4GALT in ShRNA knockdown human podocyte cell lines vs. wild type human podocytes

Across all clones knockdown of A4GALT relative to wild type human podocytes was seen. The highest knockdown was apparent in the 140H knockdown clone and so these were taken forward in all subsequent experiments. Control = wild type human conditionally immortalised podocytes transduced with a non-silencing ShRNA control scramble sequence from Dharmacon. Standard error of the mean indicated for each cell line by error bars. ***One way ANOVA, Tukey's multiple comparison test $p<0.0007$. N= 3 for each cell line.

4.5.1 Human wild type and A4GALT knockdown podocytes express podocyte markers

Prior to any further experimental work in the A4GALT knockdown cell line, western blot analysis to confirm podocyte marker expression once the cells were differentiated was performed (Figure 4-17). This confirmed that podocyte markers nephrin and synaptopodin were expressed. The second positive control was a dilution of whole mouse kidney lysate. This failed to show any bands detectable with any of the antibodies used; given that the β-actin loading control failed to show any protein loaded it is most likely that this is because of insufficient protein loaded into the well i.e. the 1 in 100 dilution was too greater a dilution to allow detection. It could also be a gel loading issue with spill over of sample into the previous well. An alternative positive control that could have been used is human whole kidney lysate or human glomerular isolates. Of note, the antibodies used were reactive in both human and mouse species (see appendix for details). In the

negative control glomerular endothelial cell line (GEnC) sample there was much less protein loaded (as evident from the β-actin loading control) but no nephrin or synaptopodin detected.

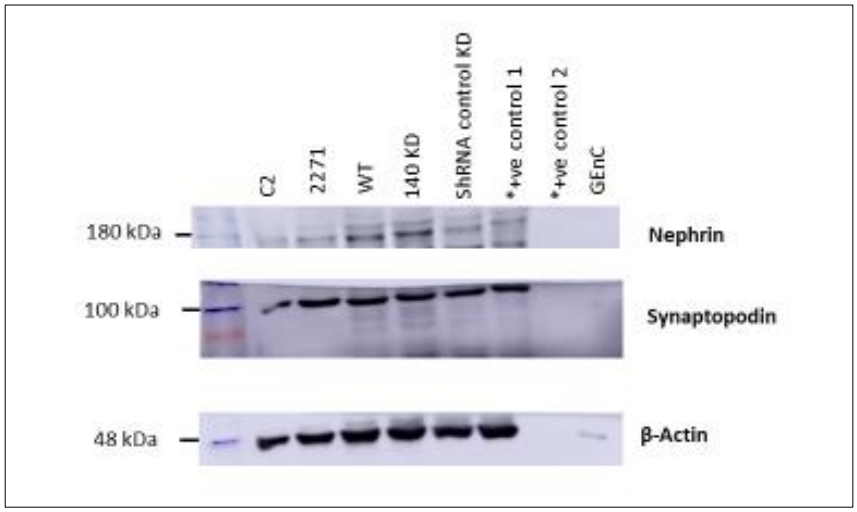

Figure 4-17: Western blot for podocyte markers in mouse and human podocyte cell lines

All cells were grown in standard culture media (appropriate for the specific cell) and thermo-switched to differentiate before protein extraction. C2 and 2271 cell lines are mouse podocyte cell lines. WT = wild type human podocyte cell line; 140 KD = human podocyte A4GALT knockdown cell line; ShRNA control knockdown = scramble ShRNA sequence control cells; +ve control = whole mouse kidney lysate at 1 in 10 dilution (1) and 1 in 100 dilution (2); GEnC = human glomerular endothelial cell line as a negative control. β-actin loading control shown. Of note, the second positive control failed to show any bands detectable with any of the antibodies used; given that the β-actin loading control failed to show any protein loaded it is most likely that this is because of insufficient protein loaded into the well. It could also be a gel loading issue with spill over of sample into the previous well.

4.5.2 A4GALT knockdown podocytes do not express Gb3

Immunofluorescence was performed on the ShRNA A4GALT knockdown mutants to confirm that they did not express Gb3. Across all three clones (only the high transfection clones were tested) immunofluorescence did not detect any Gb3 expression. The transfected cells were GFP tagged and so appear green when successfully transfected with ShRNA (Figure 4-18). Prior to A4GALT knockdown podocytes being taken forward for use

in experimental work, immunofluorescence for Gb3 was repeated alongside wild type conditionally immortalised podocytes as a positive control (see Chapter 5).

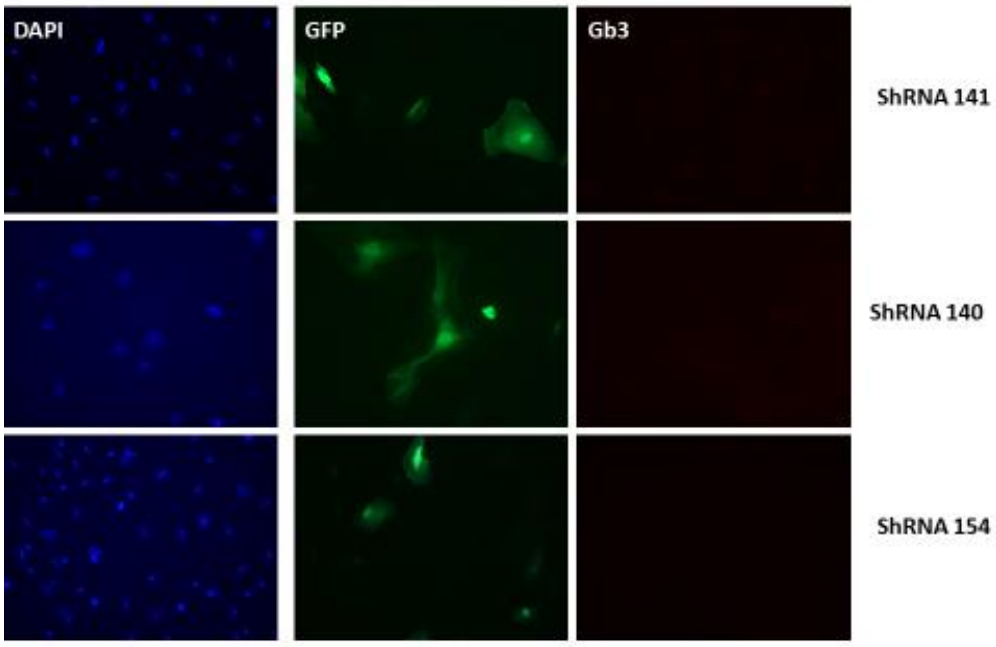

Figure 4-18: IF of A4GALT knockdown human podocytes

Cells were grown on coverslips and IF performed as described. Cells are green (GFP tagged) in the presence of transfection with the ShRNA sequence. The absence of Gb3 staining on immunofluorescence is apparent across all 3 clones of A4GALT knockdown podocytes. DAPI = Blue, Gb3 = red x40 magnification.

Cell lysates from the A4GALT knockdown cells were sent for mass spectrometry analysis at the TMSC at UCL to quantify Gb3 content. Human podocytes and wild type mouse podocytes (C2) were cultured simultaneously as controls. All podocyte cell lines were serum starved in PBS for 4.5 hours. These samples were blinded and sent to the TMSC to avoid bias. An internal standard for Gb3 was added to the cell lysate samples to quantitate against which is good practice and allows for any variation in the processing or sample analysis. My samples were analysed on the same mass spectrometry run as Fabry's patient samples, meaning that it was quality controlled as per NICE guidelines. Table 6 shows the results for each cell line (panels A-C).

Gb3 has been found to exist in several isoforms characterised by fatty acid chain modifications and different analogues denoted by modifications on the sphingosine

moiety [249]. Indeed, metabolomic studies of Fabry's patients and mice in the TMSC by Dr Mills have shown that the key biologically active isoforms are C24 and C24:1-CTH. Interestingly, in vitro studies have shown that Stx binds to C16, C22 and C24 Gb3 isoforms but not to C18 or C20 isoforms [250]. Despite total Gb3 (CTH) levels in the A4GALT KD cells being only slightly lower than in the wild type human podocytes; when comparing the C24 isoform the A4GALT knockdown podocytes contain 50% less than the wild type podocytes. Furthermore, the C24 isoform is present in even lower levels in mouse podocytes (C2). Given that A4GALT knockdown podocytes and mouse podocytes are resistant to Shiga toxin toxicity it is likely that this isoform is key in podocytes i*n vitro*.

A

Chain length	CTH µg/ mg protein	
C16-CTH	0.2401	
C18-CTH	0.0142	
C20-CTH	0.0027	
C22:1-CTH	0.0045	
C22-CTH	0.0061	
C24:2-CTH	0.0056	
C24:1-CTH	0.0111	
C24-CTH	0.0070	
C24:2-OH-CTH	0.0007	
C24:1-OH-CTH	0.0004	
C24-OH-CTH	0.0018	
C26-CTH	0.0000	
	total CTH ug/ mg protein =	0.2941

B

Chain length	CTH µg/ mg protein	
C16-CTH	0.2157	
C18-CTH	0.0106	
C20-CTH	0.0036	
C22:1-CTH	0.0044	
C22-CTH	0.0079	
C24:2-CTH	0.0065	
C24:1-CTH	0.0160	
C24-CTH	0.0039	
C24:2-OH-CTH	0.0013	
C24:1-OH-CTH	0.0009	
C24-OH-CTH	0.0008	
C26-CTH	0.0000	
	total CTH ug/ mg protein =	0.2718

C

Chain length	CTH µg/ mg protein	
C16-CTH	0.0099	
C18-CTH	0.0010	
C20-CTH	0.0001	
C22:1-CTH	0.0002	
C22-CTH	0.0000	
C24:2-CTH	0.0005	
C24:1-CTH	0.0000	
C24-CTH	0.0002	
C24:2-OH-CTH	0.0000	
C24:1-OH-CTH	0.0000	
C24-OH-CTH	0.0000	
C26-CTH	0.0000	
	total CTH ug/ mg protein =	0.0118

Table 6: Mass spectrometry analysis of wild type human podocytes vs. A4GALT knockdown podocytes vs. wild type mouse podocytes

Each cell line (A – wild type human podocytes, B – A4GALT knockdown human podocytes, and C – wild type mouse podocytes) were cultured and differentiated as described. The cells were serum

starved for 4.5 hours in sterile PBS before being lysed in RIPA buffer and sent (blinded) to the TMSC at UCL for mass spectrometry analysis of Gb3 content. Of note, total Gb3 (CTH) levels were lower in the A4GALT knockdown and mouse podocytes than wild type controls. The C24 isoform of Gb3 (circled) is 50% lower in the A4GALT knockdown cells and almost negligible in mouse podocytes.

4.5.3 A4GALT knockdown podocytes are resistant to the ribotoxic effects of Shiga toxin

To establish whether knockdown of A4GALT in human podocytes resulted in a functional resistance to Shiga toxin due to a reduction in Gb3 receptor expression; the knockdown cells were treated with Shiga toxin and the effects on cell viability determined. Wild type human podocytes and A4GALT knockdown podocytes were seeded in 96 well INCell plates at a density of 4000 cells per well, allowed to differentiate for 10-14 days and then treated with; standard podocyte media, 0.1ng/ml of Shiga toxin, 1µM of thapsigargin and 5µg/ml of puromycin. The effect of each treatment on cell survival was determined by fixing the cells and DAPI staining followed by counting total cells present in each well. All experiments were performed on three separate occasions (n=3) with technical repeats within the same plate.

Human A4GALT knockdown podocytes incubated with Shiga toxin 0.1ng/ml for 48 hours showed no statistical difference in cell viability versus media control wild type podocytes or media control A4GALT knockdown podocytes. In contrast, wild type human podocytes demonstrate a 50% reduction in viability when incubated with 0.1ng/ml Shiga toxin for 48 hours versus media control conditions. Of note, A4GALT knockdown podocytes also contain a puromycin resistance gene which accounts for the observed statistically significant difference between the knockdown cells versus wild type podocyte cell viability when treated with puromycin for 48 hours. Thapsigargin was used as a positive control for ER stress. At this dose thapsigargin did not result in a change in podocyte viability (Figure 4-19) but was shown to cause a rise in ER stress markers on western blotting (Figure 4-22).

It is an interesting observation that not all of the human wild type podocytes die (a 50% cell death rate is seen) when incubated with Shiga toxin 0.1ng/ml. These results highlight the heterogeneity of the podocyte response. This can be explained by the fact that the dose of Shiga toxin used was informed by protein synthesis assays in podocytes following Shiga toxin treatment at a range of doses. A reduction in protein synthesis does not

necessarily correlate with cell toxicity. Secondly, from my IF work, it is evident that not all podocytes appear to express Gb3 receptor at baseline; although, Gb3 expression does increase with Shiga toxin treatment. A further experiment that could be performed would be to evaluate effect of co-treatment with pro-inflammatory cytokine TNF-α and Shiga toxin on podocytes which may increase toxicity. Interestingly, previously published work has shown that in glomerular endothelial cells Shiga toxin alone or with TNF-α does not increase Gb3 receptor expression or lead to increased toxicity [95].

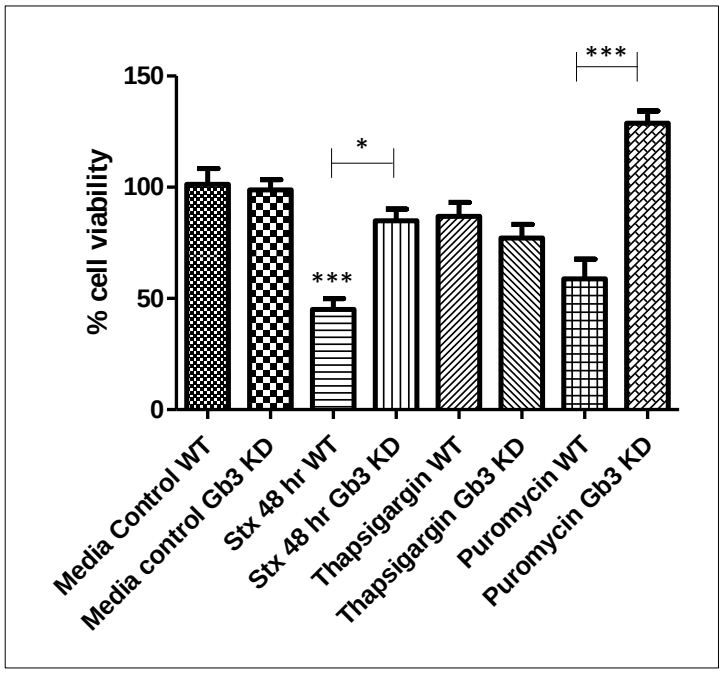

Figure 4-19: A4GALT knockdown podocytes are resistant to Shiga toxin ribotoxicity

Wild type human podocytes (WT) demonstrate a 50% reduction in cell viability vs. media control when treated with 0.1ng/ml of Shiga toxin (Stx) which is statistically significant (One way ANOVA Tukey's multiple comparison test ***p<0.0001). A4GALT knockdown podocytes (Gb3 KD) were resistant to the ribotoxic effect of Shiga toxin versus wild type podocytes (WT) and exhibit resistance to puromycin due to the presence of a puromycin resistance gene to allow selection for knockdown clones. Thapsigargin was used as a positive control for ER stress. At this dose thapsigargin did not result in a change in podocyte viability but was shown to cause a rise in ER stress markers on western blotting (Figure 4-22**Figure 4-19**). One way ANOVA Tukey's multiple comparison test: *p<0.05 *** p<0.0001. Data representative of 3 experiments performed on three separate occasions (n=3) with technical repeats within the same INCell plate.

4.5.4 A4GALT knockdown podocytes are resistant to Shiga toxin at higher doses

Given that A4GALT knockdown podocytes were resistant to 48 hours of treatment with 0.1ng/ml Shiga toxin, these cells were treated with increasing doses of Shiga toxin for 48 hours and cell viability reassessed (Figure 4-20). At all concentrations tested the A4GALT knockdown podocytes were resistant to the ribotoxicity of Shiga toxin; even at x1000 the lethal dose in podocytes (100ng/ml). These experiments were performed using the INCell analyser in triplicate.

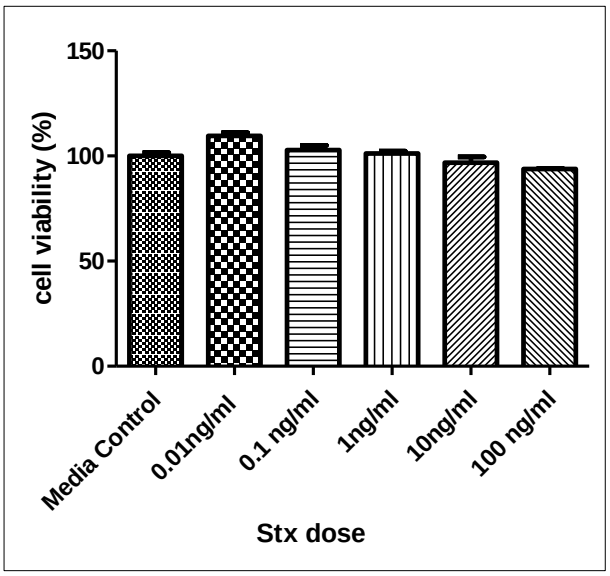

Figure 4-20: Dose response in A4GALT knockdown podocytes treated with Shiga toxin for 48 hours

At all concentrations of Shiga toxin A4GALT knockdown podocytes were resistant to toxicity at 48 hours: n=3. One way ANOVA with Tukey's multiple comparison test was not significant between all treatment groups.

4.5.5 A4GALT knockdown podocytes do not upregulate Gb3 expression following Shiga toxin treatment.

Given the observation that wild type human podocytes upregulate Gb3 expression in response to Shiga toxin treatment after 6 hours, I wanted to determine whether the A4GALT knockdown podocytes did the same. Wild type human podocytes or A4GALT knockdown podocytes were plated onto 96 well INCell plates at a density of 4000 cells per well. Cells were treated with 0.1ng/ml of Shiga toxin for 6-48 hours vs. media control and

analysed for Gb3 expression using anti-Gb3 antibody immunofluorescence as previously described. A4GALT knockdown podocytes showed 50% less Gb3 expression (quantified using AFU / cell) on the IN Cell analyser at baseline vs. wild type human podocytes. This did not change with Shiga toxin treatment (Figure 4-21).

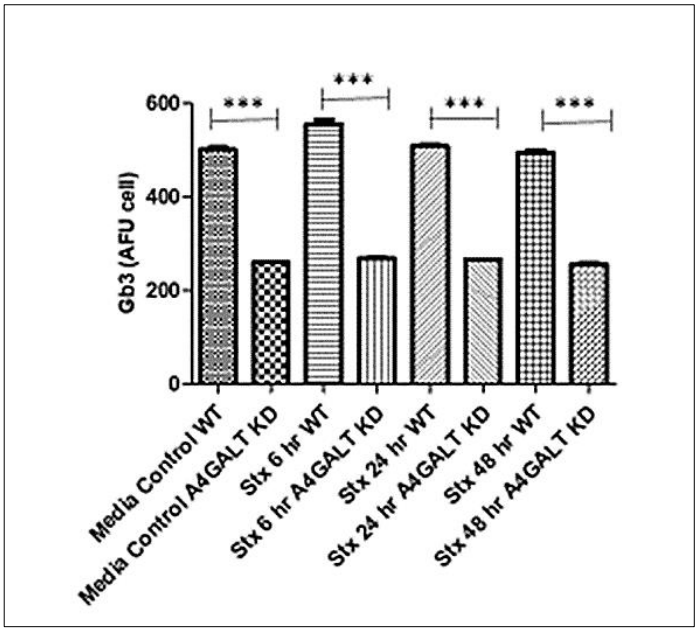

Figure 4-21: Gb3 expression in WT podocytes vs. A4GALT KD podocytes following treatment with Shiga toxin 0.1ng/ml for 6-48 hours

A4GALT knockdown podocytes show 50% less Gb3 expression (quantified using AFU / cell) on the IN Cell analyser at baseline vs. wild type human podocytes. This did not change with Shiga toxin treatment. One way ANOVA: Tukey's multiple comparison test ***p<0.001. N=3.

4.5.6 Wild type podocytes treated with Shiga toxin upregulate endoplasmic reticulum (ER) stress markers

Wild type human podocytes and A4GALT knockdown podocytes were treated with Shiga toxin 0.1ng/ml for 2 hours and 4 hours in 6 well plates. Cell lysates were obtained, and western blot analysis performed to determine the timing of ER stress responses to Shiga toxin treatment versus control media treatment for 4 hours. Antibodies for the transcription factor CHOP (CCAAT-enhancer-binding protein homologous protein) and phospho IRE were used to assess ER stress response. Western blot analysis suggests an increase in ER stress response at 4 hours with no change in ER stress response in A4GALT knockdown podocytes (Figure 4-22). The ER stress pathway response in human

conditionally immortalised podocytes treated with Shiga toxin will be discussed further in the following chapter: Proteomic analysis.

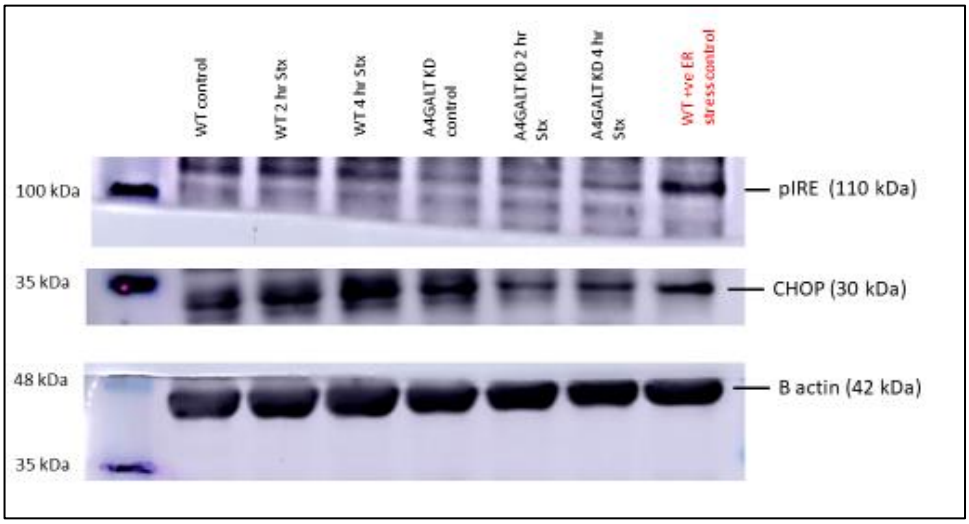

Figure 4-22: ER stress response to Shiga toxin treatment WT vs. A4GALT KD podocytes

Wild type podocytes show an increase in CHOP and phospho-IRE expression in response to treatment with Shiga toxin 0.1ng/ml at 2 and 4 hours vs. A4GALT knockdown podocytes. B actin expression is shown as a protein loading control. Wild type podocytes were treated with Thapsigargin as positive control (red) and both media control, untreated wild type podocytes and A4GALT podocytes were used as a measure of baseline ER stress activity within the cells.

4.6 Discussion

This chapter has focused upon the molecular effects of Shiga toxin on the podocyte. However, it is worth noting that human glomerular endothelial cells also express the Gb3 receptor and are sensitive to the ribotoxic effects of Shiga toxin. Gb3 immunofluorescence on human glomerular endothelial cells was performed during optimisation of the Gb3 antibody; which confirmed expression (Figure 4-23). However, mouse glomerular endothelial cells do not express Gb3 and are resistant to Shiga toxin cytotoxicity [1].

Work performed by a previous PhD student in our laboratory has already demonstrated that human podocytes are significantly more sensitive to Shiga toxin *in vitro* than human glomerular endothelial cells (Figure 4-9). Furthermore, evidence of *in vivo* damage to the podocyte in Shiga toxin HUS in humans has been suggested by the presence of

podocyturia in children with Shiga toxin HUS [251]. However, conventionally Shiga toxin HUS has been thought of as an endothelial cell disease. Central to the research hypothesis of my project is that the podocyte is an initiator of the disease process. Therefore, it is the role of the podocyte (which is exquisitely sensitive even to low doses of Shiga toxin) that will remain the central focus of this thesis.

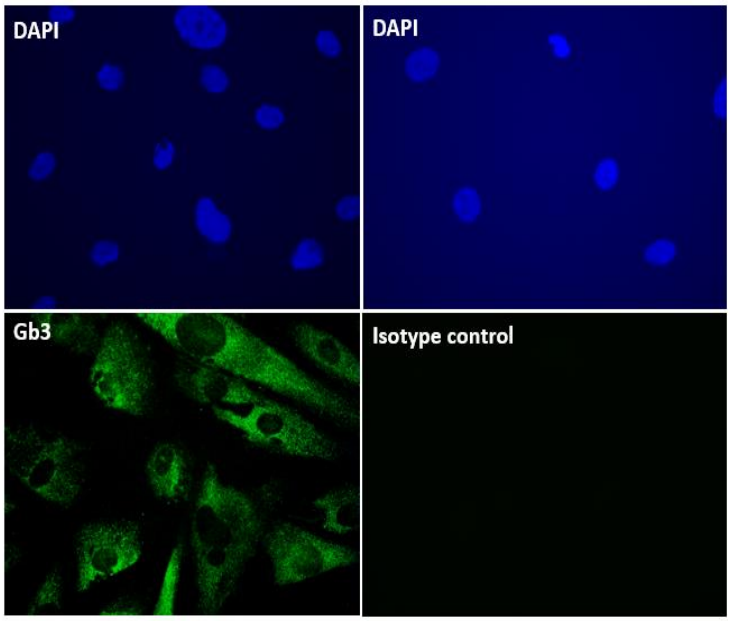

Figure 4-23: IF detection of Gb3 in human glomerular endothelial cells

Conditionally immortalised glomerular endothelial cells were cultured and Gb3 detected by IF. Gb3 is shown in green, DAPI nuclear staining is shown in blue. Isotype control antibody confirms that the staining seen is specific for Gb3 expression.

Of note, immunofluorescence for Gb3 in wild type human podocytes at baseline demonstrated that only a subset of human podocytes expressed Gb3 (Figure 4-1). This may be related to the detection method itself (Gb3 is known to cluster within lipid raft sections of the plasma membrane *in vitro*) which may have affected epitope recognition by the antibody used for immunofluorescence [63]. Or it may be representative of podocyte Gb3 expression *in vitro*; and explain the reason why only 50% of podocytes were affected in the cell viability assays performed (Figure 4-11). Fascinatingly, Shiga toxin treatment of these wild type human podocytes *in vitro* was unexpectedly found to increase Gb3 receptor expression. This effect was not seen in the A4GALT knockdown podocyte cell line. Moreover, *in vitro* studies into the effect of Shiga toxin treatment in

glomerular endothelial cells performed by Obrig et al. did not result in an upregulation of Gb3 receptor expression or lead to an increase in cytotoxicity in these cells either [95].

Through the optimisation of three different techniques, I have demonstrated that human podocytes express the Shiga toxin receptor Gb3. IN Cell experiments have provided a high-throughput, robust method to compare the effect of Shiga toxin on human podocytes and A4GALT knockdown podocytes. The generation of a novel Gb3 knockdown podocyte cell line has shown the importance of the Gb3 receptor in determining the sensitivity of a cell to Shiga toxin ribotoxicity; as podocytes lacking Gb3 are resistant to Shiga toxicity *in vitro*. Going forward, this cell line will act as a control for non-specific, non-Gb3 receptor binding in proteomic studies in wild type human podocytes; allowing further interrogation of the cellular mechanisms underlying the action of Shiga toxin in the podocyte.

Chapter 5 : Proteomic Analysis

5.1 Introduction

Proteomics is a rapidly evolving technology that involves the identification and quantification of the protein content of a cell, tissue or organism under specific experimental conditions [252]. Upon the completion of the Human Genome project in 2003, it was hoped that the complete sequencing of all 20,500 human genes would hold the key to understanding genetic inheritance and disease [253]. However, in the last few decades it has become apparent that the genotype and phenotype of an organism is not solely directed by the information contained within the genome [254][255]. Epigenetics, alternative splicing, microRNAs, and post-translational modifications are just few examples of the way in which the expression of the genome is modified without any change in the underlying DNA sequence itself [254]. Therefore, the use of proteomics to understand how cells function and communicate through protein to protein signalling networks, is arguably a much more informative method of gaining an insight into the biological processes occurring within the cell [254].

In order to elucidate the glomerular mechanisms underlying the action of Shiga toxin associated HUS; total and phospho-proteomic studies in conditionally immortalised human podocytes following incubation with 0.1ng/ml Shiga toxin at 0.5 hours and 6 hours were performed. To control for non-specific, non-Gb3 receptor binding, the proteomic changes in a stable human podocyte Gb3 receptor knockout cell line were also studied under the same experimental conditions. A4GALT knockdown cells were generated using short hairpin siRNA against Gb3 synthase as detailed in my methods. The characterisation of this cell line was described in the previous results chapter. The ultimate aim of this proteomic work was to identify novel pathways activated in the podocyte following Shiga toxin treatment using a non-biased approach. The experimental conditions, bioinformatic processes and results from my proteomic analysis are detailed below.

5.2 Methodology of proteomic analysis

The proteomic facility at the University of Bristol was used to analyse my samples. The department uses liquid chromatography mass spectrometry (LC-MS) to perform total TMT (tandem mass tag) and phospho-TMT proteomics using the Orbitrap Fusion Lumos Mass Spectrometer (Thermo Scientific®). Tandem mass tags are isobaric amine-specific

chemical tags, that allow concurrent mass spectrometry analysis of multiple samples in a single experimental run. For my experiment, the maximum available 10-Plex format was employed to analyse 10 different samples within the same TMT run. The isobaric labels used consisted of a reporter group and mass normaliser; with each reporter group having a defined mass. Once labelled all of the samples were pooled together and during liquid chromatography separation they co-elute, because they possess the same chemical properties. The samples were then fractionated using basic reverse phase chromatography and each fraction analysed by acidic reverse phase nano liquid chromatography tandem mass spectrometry (LC-MS/MS).

Fragmentation of the amine-specific chemical tag occurs releasing the reporter ions which can then be used to identify and quantify the peptides. Protein quantification is extremely accurate between samples because it is calculated using the median values of multiple peptides identified from the same protein [256][257]. The use of synchronous precursor selection triple-stage mass spectrometry (SPS-MS3) which is in-built on the Orbitrap Fusion mass spectrometer; provided additional accuracy in the quantification of proteins in my samples without reducing the number of proteins identified [257]. Indeed, SPS-MS3 has been well documented to reduce interference from reporter ion mass regions and interference from co-isolation of precursor ions [257][258].

Proteome Discoverer™ version 2 (Thermo Scientific®) was used to compare the raw data generated from my TMT proteomic analysis to several databases including FASTA and peak-finding search engines including Sequest™. This downstream data processing was performed by the University of Bristol Proteomic department, to generate an excel spreadsheet of raw data files with Uniprot™ protein accession numbers of the mass spectra digested fragments from the experiment. These raw data files were then sent to me for analysis. One issue that can be encountered with the Proteome Discoverer™ software is that some of the protein accession numbers that are generated have protein descriptions that are vague or uncharacterised; meaning they are unrecognisable by pathway analysis software used downstream. The University of Bristol Proteomic department have developed a method to streamline the annotation of the protein accession number without compromising on quantification stringency. This method was employed by the university prior to sending me the raw data files; improving protein identification from 60 to 80% and ensuring that my data was easier to interpret using pathway analysis databases.

Ingenuity Pathway Analysis software (IPA) was used to determine the biological relevance and relation between proteins identified in my proteomic experiments. Alternative software that can be used includes: DAVID, KEGG and Webgestalt; but IPA is considered the gold-standard software for pathway analysis. IPA takes into consideration the effect of each protein on cell function and predicts whether it has been activated or inhibited by the change in abundance observed. It also suggests which disease states, treatments or protein activation events may have contributed to these changes [259][260]. A series of network maps are generated by the IPA software which have been included later in this chapter. Subsequent validation of any interesting protein interactions identified by IPA using a variety of methods including western blotting, RT-PCR, IF and in-situ hybridisation were then performed.

Prior to uploading the total and phospho-proteomic dataset to IPA software, my results were filtered to include only proteins that had a false discovery rate (FDR) of 1% (i.e. a confidence interval 99%). In both datasets all proteins and phospho-proteins with empty abundance ratios were removed, along with any common contaminants. Most contaminants that were found in the proteomic dataset originated from either the reagents used to generate the samples (such as trypsin) or from the operator (such as keratin from hair / skin). These can be identified fairly easily as they are frequently found in proteomic analysis. The University of Bristol proteomic department has created a bespoke list of common contaminants that were used to identify and exclude contaminants within my dataset. This resulted in more efficient data analysis and is a well-established method that has been published by other groups [261].

5.3 Experimental design

Proteomic analysis was performed using a 10-Plex format so that all samples could be processed within a single TMT proteomic run. The benefit of this is that any differences between the samples would not be attributable to differences in TMT run. Conditionally immortalised human podocytes and A4GALT knockdown human podocytes were cultured according to standard protocol (see *in vitro* methods chapter) and thermo-switched to 37°C to differentiate for 10-14 days before experimental use. Each ‘n’ number of cells represents a different passage number of the cell lines used and a different experimental day. Wild type (WT) conditionally immortalised human podocytes and A4GALT

knockdown human podocytes were treated with 0.1ng/ml Shiga toxin for 0.5 hours or 6 hours (see Table 7 for summary of samples included in the proteomic analysis).

The A4GALT knockdown podocyte cell line was used as a control for non-specific, non-Gb3 receptor binding. To ensure these were true controls for the experiment they were treated in exactly the same way as the wild type podocytes and protein lysates taken on the same day. Ideally, as another control for this experiment, proteomic analysis of untreated WT human podocytes vs. untreated A4GALT knockdown human podocytes would have also been performed. This would help to delineate any differences due to knockdown of Gb3 vs. Shiga toxin treatment itself. However, I was limited by the number of samples possible for each TMT run (maximum of 10) and huge cost implications of multiple proteomic analysis: hence, these controls were not included in this experiment. A summary of my experimental approach is shown Figure 5-1.

Sample	Cell line	Condition
1	A4GALT KD 1	0.1ng/ml Stx 0.5 hrs
2	A4GALT KD 2	0.1ng/ml Stx 0.5 hrs
3	WT pod 1	0.1ng/ml Stx 0.5 hrs
4	WT pod 2	0.1ng/ml Stx 0.5 hrs
5	WT pod 3	0.1ng/ml Stx 0.5 hrs
6	WT pod 4	0.1ng/ml Stx 0.5 hrs
7	WT pod 5	0.1ng/ml Stx 6 hrs
8	WT pod 6	0.1ng/ml Stx 6 hrs
9	WT pod 7	0.1ng/ml Stx 6 hrs
10	WT pod 8	0.1ng/ml Stx 6 hrs

Table 7: Summary of samples included in Proteomic TMT run

Ten samples were included in a single proteomic TMT run. Each sample is shown in the table alongside the experimental condition used. Total and phospho-proteomic analysis was performed and the mean abundance for each condition calculated.

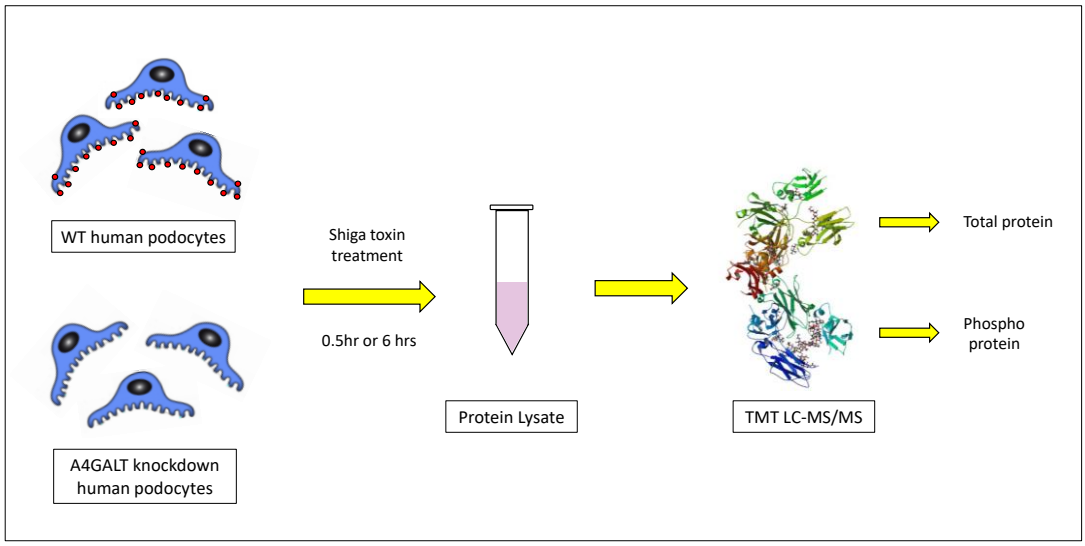

Figure 5-1: Summary of experimental design

Conditionally immortalised wild type human podocytes (with the Gb3 receptor present: red circles) and A4GALT knockdown human podocytes (no Gb3 receptor) were cultured in standard podocyte conditions and treated with 0.1ng/ml of Shiga toxin for 0.5 or 6 hours. Protein lysates were then prepared, and protein content quantified using a BCA. Sample lysates were then taken on dry ice to the University of Bristol Proteomic facility for analysis. *Podocytes from figure adapted from Kidney International article: 'From podocyte biology to novel cures for glomerular disease'* [262].

5.4 Quality control of proteomic samples

Prior to performing any proteomic analysis, a series of quality control checks were performed to ensure that the cell lines used were behaving phenotypically and functionally as intended. Protein content was also quantified in the sample lysates prior to proteomic analysis.

5.4.1 Confirmation of A4GALT knockdown

For each T175 cell culture flask of human podocytes cultured for proteomic analysis (both WT and A4GALT knockdown), two 6 well plates were simultaneously seeded. One on glass coverslips and the other without. This allowed immunofluorescence for Gb3 to be performed for each sample to be included in the proteomic analysis and treatment of the cells with Shiga toxin. This confirmed that the WT and A4GALT knockdown podocytes were responding as expected to Shiga toxin. My previous experimental work investigating the effects of Shiga toxin on the podocyte was particularly beneficial here. The A4GALT knockdown podocytes should be resistant to Shiga toxin and at a dose of 0.1ng/ml 50%

of the WT podocytes should undergo apoptosis. Once this had been confirmed that the podocyte cell lines cultured were behaving as expected, I could confidently send my protein lysates to the proteomic facility for analysis.

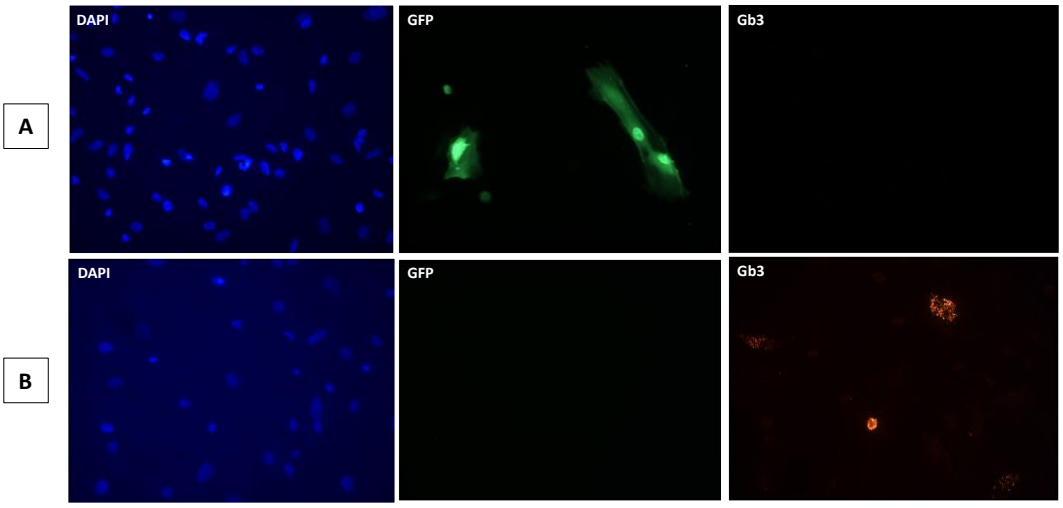

Figure 5-2: Immunofluorescence for Gb3 in A4GALT knockdown podocytes confirms Gb3 knockdown (x20) magnification

Immunofluorescence was performed in A4GALT knockdown human podocytes (A) and WT human podocytes (B) prior to samples being sent for proteomic analysis. The A4GALT knockdown cells had no identifiable expression of Gb3 using an anti-Gb3 antibody (red). A4GALT knockdown cells have a GFP tag (this is present in the lentivirus construct used to transfect the cells) and acts as a reporter to confirm the lentivirus is present. WT podocytes expressed Gb3 and did not contain a GFP tag. These images show an n of 1 for each cell line and were taken at a magnification of x20.

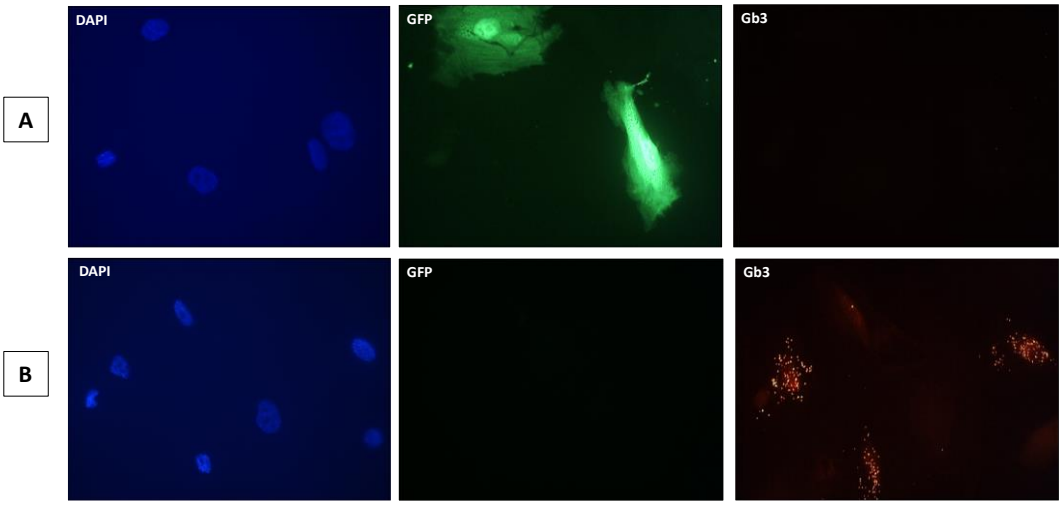

Figure 5-3: Immunofluorescence for Gb3 in A4GALT knockdown podocytes and WT podocytes (x40) magnification

Immunofluorescence was performed in A4GALT knockdown human podocytes (A) and WT human podocytes (B) prior to samples being sent for proteomic analysis. The A4GALT knockdown cells had no identifiable expression of Gb3 using an anti-Gb3 antibody (red). A4GALT knockdown cells have a GFP tag (this is present in the lentivirus construct used to transfect the cells) and acts as a reporter to confirm the lentivirus is present. WT podocytes expressed Gb3 and did not contain a GFP tag. These images are at x40 magnification and represent another n number and are representative of all samples sent for proteomics.

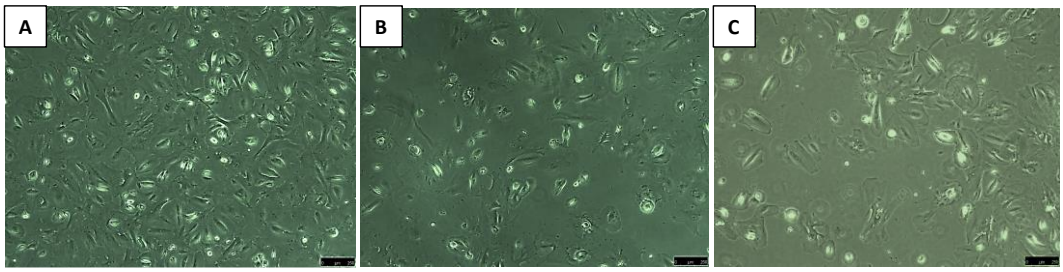

Figure 5-4: Wild type human podocytes treated with Shiga toxin undergo cell death

Six well plates confirmed that WT podocytes used in my proteomic experiment underwent apoptosis in response to Shiga toxin 0.1ng/ml. A = differentiated podocyte appearance on light microscopy at baseline prior to any Shiga toxin treatment shows the characteristic foot process extension and confluency of the cells. B = Shiga toxin (0.1ng/ml) treated podocytes after 48 hours of Shiga toxin incubation with evidence of loss of confluency and cell death. C = Shiga toxin (0.1ng/ml) treated podocytes after 7 days of incubation. Very few healthy cells left – swollen and detached cells seen on light microscopy. Images are representative of all samples sent for proteomic analysis.

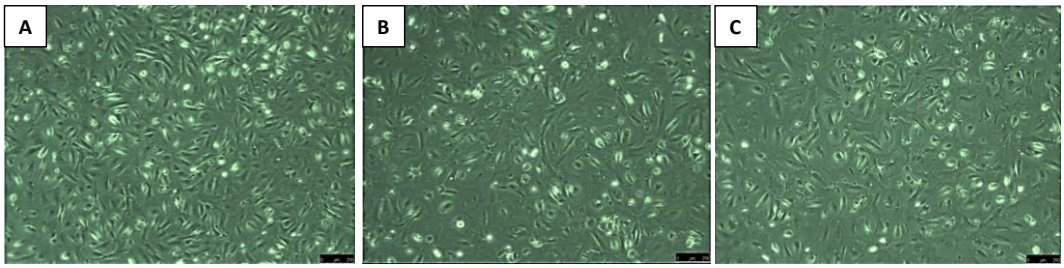

Figure 5-5: A4GALT knockdown podocytes are resistant to Shiga toxin treatment

Six well plates confirmed that A4GALT knockdown human podocytes used in my proteomic experiment were resistant to Shiga toxin incubation even following incubation with Shiga toxin for 7 days. A = differentiated A4GALT podocyte appearance on light microscopy at baseline prior to any Shiga toxin treatment shows the characteristic foot process extension and confluency of the cells. B = Shiga toxin (0.1ng/ml) treated A4GALT podocytes after 48 hours of Shiga toxin incubation with no obvious change in appearance. C = Shiga toxin (0.1ng/ml) treated podocytes after 7 days of incubation. Cells remain confluent and healthy. Images are representative of all samples sent for proteomic analysis.

5.4.2 Protein Quantification

To perform proteomic analysis the department at Bristol University requires at least 100µg of protein in each sample at a concentration of at least 2µg/µl. Prior to sending lysate samples to the proteomic department a BCA (BiCinhoninic Acid) assay was performed to estimate the protein content (see methods for details). The protein content of each sample was sent to the proteomic facility, which allowed them to ensure there was enough protein present and meant that they could adjust the volume of sample loaded to ensure the same concentration of protein in each sample in the TMT run (Table 8).

The BCA assay is one of the most sensitive commercial protein quantification assays available and has less variability than other methods (e.g. Bradford assay) [263]. However, it is known that the presence of chemical modifications such as methylation of proteins can affect the accuracy of the assay [263]. Moreover, there will be unavoidable inherent error in the loading of each sample associated into the mass spectrometer. Therefore, it is important to determine whether the protein abundance in each sample used in the proteomic analysis was similar to that of the pooled control sample and normalise accordingly. A PhD student in our group Mark Graham wrote an R script (R is a free software program for statistical computing) to assess the protein abundance in each

sample relative to the pooled sample. This R script generates a box plot for each individual sample (or n number), with the median protein abundance indicated by the line through the centre of each box. The error bars are set to the R default (Q3 upper line of box +1.5 x IQR) and (Q1 lower line of box +1.5 x IQR). Where IQR is the interquartile range. This analysis was performed post LC-MS/MS and showed minimal differences in the total protein abundance between samples; with the exception of sample 6. The same R script was run for the phospho-proteomic samples and a similar pattern was observed.

In order to achieve normalisation for the total protein samples, another R script written by Mark Graham was used to align the protein abundance for all proteins within each sample against the pooled sample median protein abundance. This statistical correction involves identifying the total amount of protein detected in each sample and calculating a 'normalisation factor' for each sample. So that the total protein in each sample is equal, each protein detected in the proteomic run is multiplied by the normalisation factor, which corrects for any errors in total protein loading. This normalisation is performed on the assumption that the total protein in each sample is the same [264].

Normalisation of phospho-proteomic samples cannot be achieved in the same way because differences are expected in phospho-peptide abundance between samples. Instead, the 'normalisation factor' calculated for the total protein is applied to the corresponding phospho-peptide. Any aberrations in the quantification of the protein will be reflected in the phospho-peptide as the TMT samples are mixed, before a portion of the sample is extracted for phospho-peptide analysis. Thus, the relative abundance of the phospho-peptide is as a fraction of the total protein i.e. the protein-normalised phospho-peptide abundance. It is vital to perform this normalisation prior to interrogation of any results to ensure each dataset has a common scale, avoiding bias by bringing all variables into the same range. Since the distribution of these data is unknown normalisation is preferable to standardisation (Figure 5-6) [264].

Sample	Cell line	Condition	Protein concentration (µg/µl)
1	A4GALT KD 1	0.1ng/ml Stx 0.5 hrs	3.09
2	A4GALT KD 2	0.1ng/ml Stx 0.5 hrs	2.98
3	WT pod 1	0.1ng/ml Stx 0.5 hrs	3.11
4	WT pod 2	0.1ng/ml Stx 0.5 hrs	3.14
5	WT pod 3	0.1ng/ml Stx 0.5 hrs	2.86
6	WT pod 4	0.1ng/ml Stx 0.5 hrs	2.64
7	WT pod 5	0.1ng/ml Stx 6 hrs	2.61
8	WT pod 6	0.1ng/ml Stx 6 hrs	2.69
9	WT pod 7	0.1ng/ml Stx 6 hrs	2.66
10	WT pod 8	0.1ng/ml Stx 6 hrs	2.77

Table 8: Protein quantification of proteomic samples by BCA assay

BCA assay was performed to quantify the protein concentration in each sample prior to proteomic analysis. To perform proteomic analysis the department at Bristol University requires at least 100µg of protein in each sample at a concentration of at least 2µg/µl. Of note the protein content of each sample was similar, with all samples containing enough protein to be included in the TMT run.

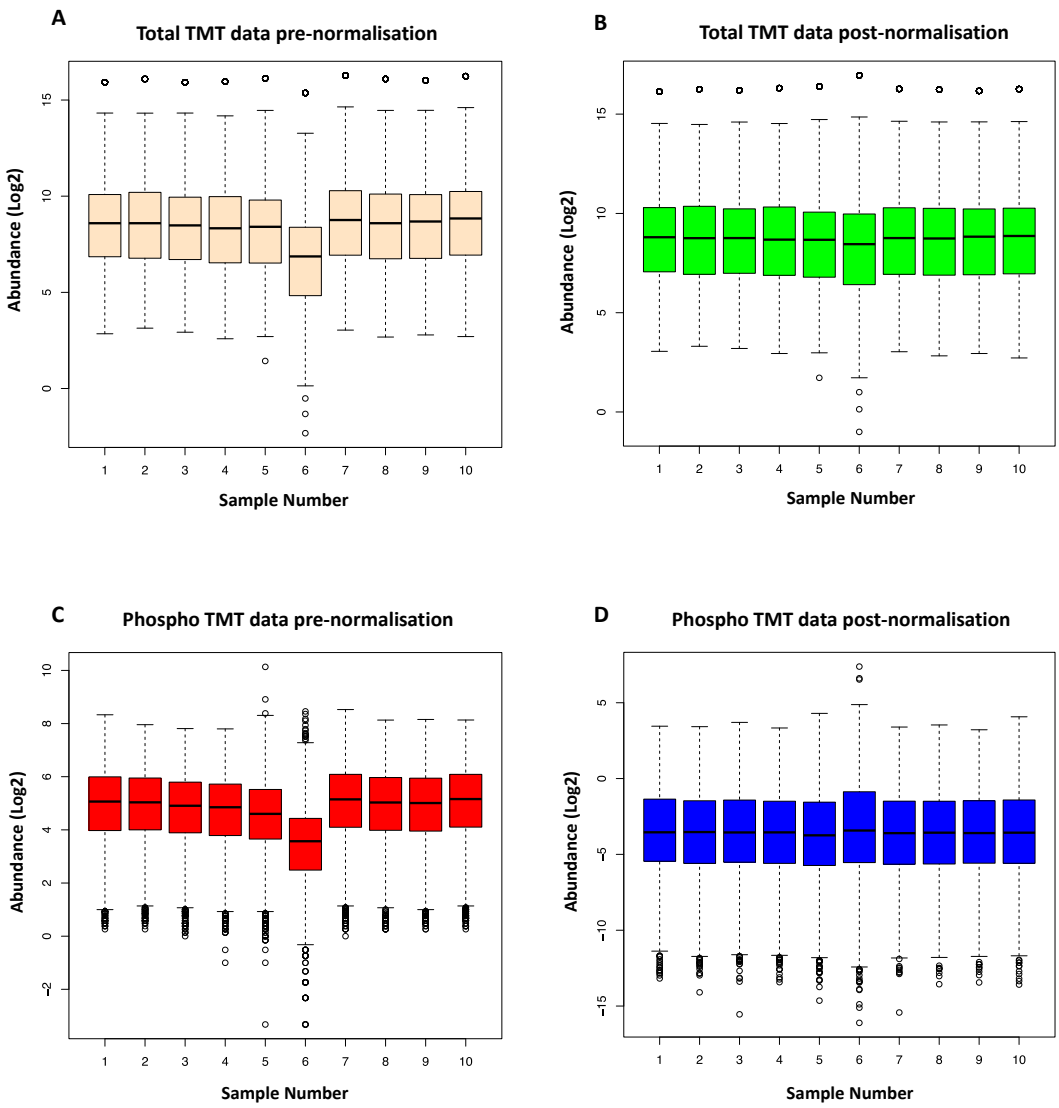

Figure 5-6: Total TMT and phospho TMT data normalisation

Boxplots generated using R script written by Mark Graham, show the total protein abundance pre-normalisation (A) and post normalisation (B). These were corrected post LC-MS/MS to allow for sample loading error. Panels C and D show the phospho TMT data pre-normalisation and post-normalisation respectively. Quantification pre-normalisation shows the samples (1-10) are fairly similar apart from sample 6. The open circles beyond each whisker (error bar) are proteins beyond the R default range: (Q3 upper line of box +1.5 x IQR) and (Q1 lower line of box +1.5 x IQR). Where IQR is the interquartile range.

5.5 Proteomic analysis results

A total of 7459 proteins and 4462 phospho-peptides were identified from my proteomic analysis. These were listed in the datasets sent to me by the University of Bristol

proteomic department. As previously eluded to, these data were then filtered to include only proteins and phospho-peptides with an FDR (false discovery rate) of 1% (i.e. confidence interval of 99%). Following normalisation of the total protein dataset (using an R script as already discussed) scaling was performed. This was performed on a protein by protein basis and uses the pool sample as a reference (where the pool is made up of each individual sample in the proteomic run added together).

Scaling expresses the protein abundances for each protein in each TMT run as relative quantities around the pool sample which is set to 100. So, by definition every pool protein is 100 across each TMT run and as such is equal. Each protein in each TMT run is scaled against the pool so that if there are any changes in the mass spectrometer's ability to identify a protein between runs this would be corrected for, as by definition it is reflected within the pool protein abundance. The scaled total protein abundance was then Log_2 transformed to bring these data closer to a normal distribution. This also makes it easier to interpret the outcome of fold change (a negative number representing downregulation and positive upregulation); rather than a ratio which is a harder concept to visualise.

In the phospho TMT dataset, phospho-peptides of proteins absent in the total protein dataset were removed, as well as peptides with empty abundance values. This simplifies downstream computational analysis. The median protein-adjusted phospho-peptide abundance was calculated by subtracting the corresponding scaled protein abundance from the scaled phospho-peptide abundance (both Log_2 transformed to bring them closer to a normal distribution). This enabled identification of genuine changes in phosphorylation rather than changes in the overall abundance of a protein whose phosphorylation level remains unchanged. There were 1946 phospho-peptides remaining in the dataset at the end of this filtering process. These data could then be represented as a fold change and charted in a volcano plot against $-Log_{10}$ p-value.

P values were calculated by Welch's t-test, used in preference to a Student's t-test as normal variance cannot be assumed in my datasets. The t-test was performed on the median protein adjusted phospho-peptide abundances of each experimental condition, e.g. WT podocytes treated with Shiga toxin for 0.5 hours vs. A4GALT knockdown podocytes treated with Shiga toxin for 0.5 hours. The same t-test was performed in the total protein TMT dataset: using the median scaled protein abundance (of the master protein identified by Uniprot) in each experimental condition. Once the p-value was calculated it was $-Log_{10}$ transformed as convention to facilitate charting in a volcano plot.

These plots allow easy visualisation of statistically significant up or downregulated proteins and phospho-peptides. In each comparison, a few proteins or phospho-peptides of potential interest have been named. These have been summarised in tables and a description of their function described.

However, given the vast number of proteins and phospho-peptides identified statistical analysis with t-tests alone results in a high false discovery rate (type 1 error) due to multi-variate analysis. To overcome this, a Benjamini Hochberg analysis was performed and used these corrected p-values to generate volcano plots. The Benjamini Hochberg method is a highly stringent tool that uses a serial modified Bonferroni correction to facilitate multiple hypothesis testing and can be used when the test statistic is known to be independent of each other as in the case of these data [265].

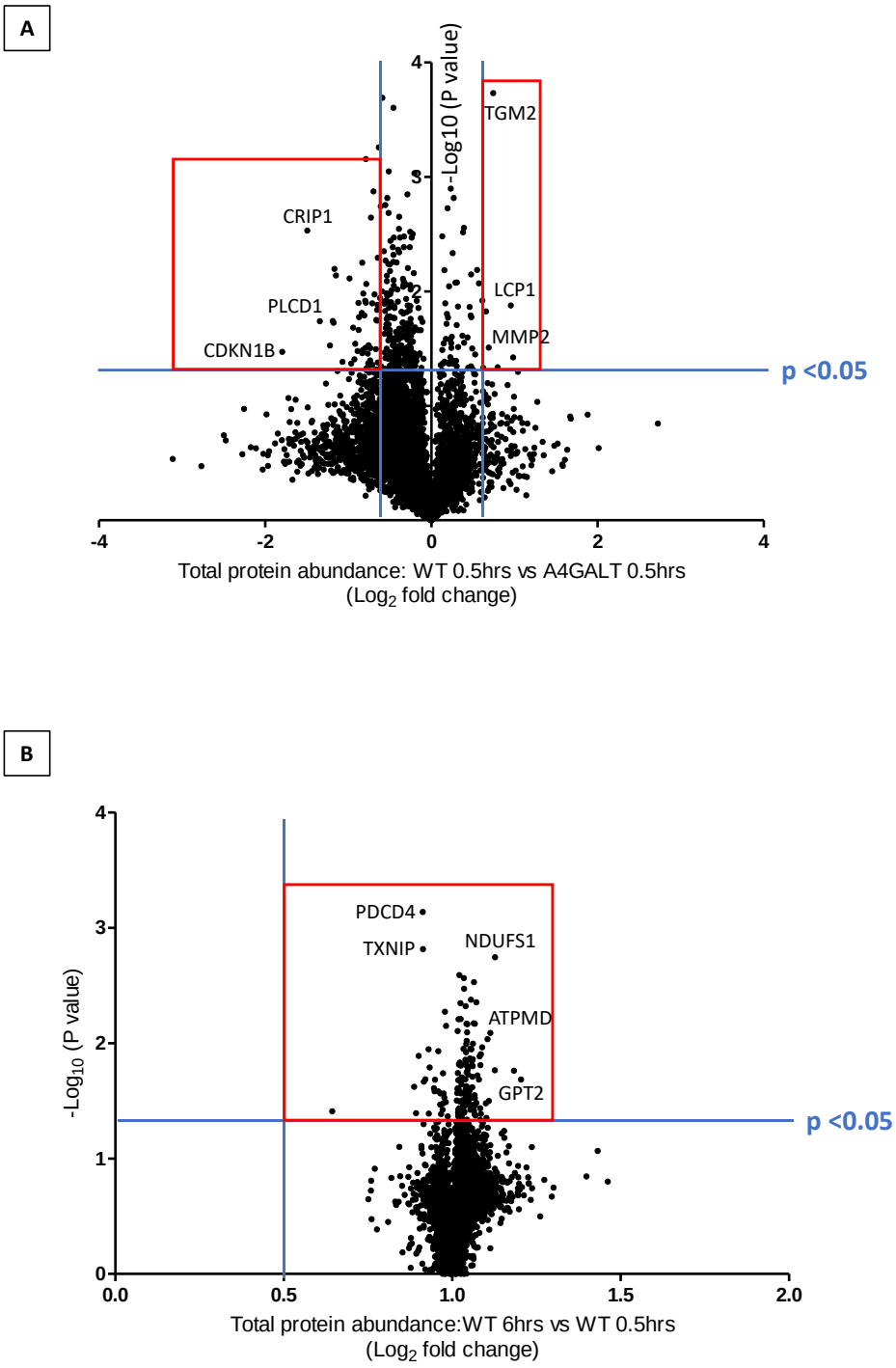

Figure 5-7: Total protein abundance volcano plots

Volcano plots showing total protein abundance changes in A - wild type (WT) podocytes vs. A4GALT knockdown podocytes, both treated with Shiga toxin for 0.5 hours; B – wild type (WT) podocytes treated with Shiga toxin for 6hrs vs. 0.5hrs. Blue vertical lines indicate Log_2 +/- 0.5 fold change and blue horizontal lines indicate the p <0.05 threshold, corrected for multiple comparisons using a Benjamini-Hochberg false discovery rate of 0.1. Red boxes indicate the proteins that are statistically significant. On each volcano plot a few proteins that reach statistical significance have been named - these are described in Table 9.

Protein (gene name)	Direction of fold change	Function
CRIP1	down	Immune response/ intracellular zinc transport
PLCD1	down	Production of DAG (diacylglycerol) and IP3 (inositol 1,4,5-trisphosphate)
CDKN1B	down	Inhibition of cell cycle
TGM2	up	Blood vessel remodelling / positive regulation of inflammatory response
LCP1	up	Activation of T cells
MMP2	up	Angiogenesis and remodelling of vasculature
PDCD4	up	Apoptosis / cellular response to LPS (lipopolysaccharide)
TXNIP	up	Transcription repressor
NDUFS1	up	Apoptotic mitochondrial changes
ATPMD	up	Mitochondrial membrane ATP synthase
GPT2	up	cellular amino acid biosynthetic processes

Table 9: Description of statistically significant proteins identified in total proteomic dataset

Statistically significant proteins identified from my total proteomic dataset volcano plots are listed. Proteins in blue are from the WT podocytes vs A4GALT knockdown podocytes treated with Stx for 0.5hr comparison. Proteins in red are from the WT podocytes treated with Stx for 6hrs vs. WT podocytes treated with Stx for 0.5hrs. Interestingly, in this dataset no proteins were statistically significantly downregulated.

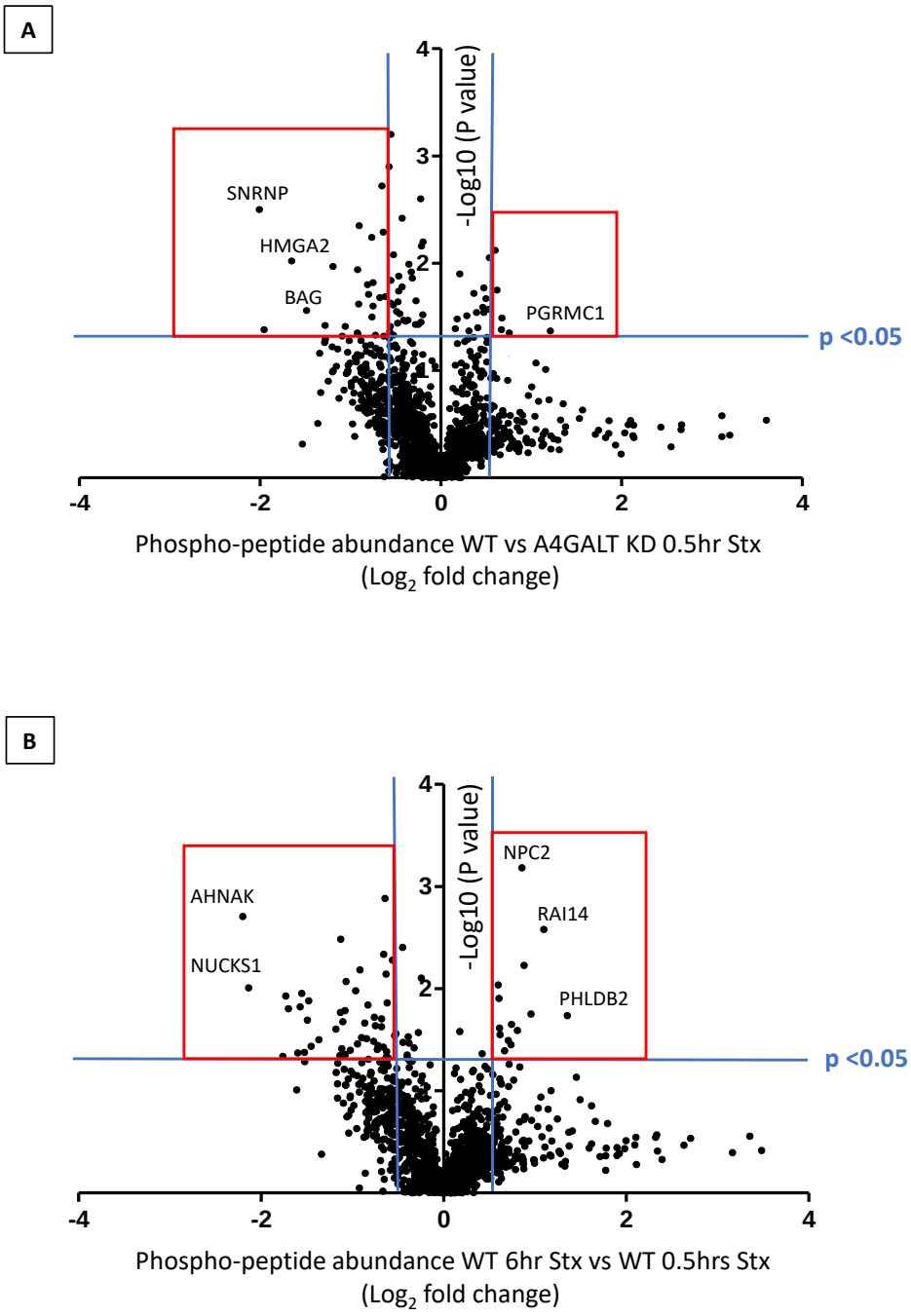

Figure 5-8: Phospho-peptide abundance volcano plots

Volcano plots showing phospho-peptide abundance changes in A - wild type (WT) podocytes vs. A4GALT knockdown podocytes, both treated with Shiga toxin for 0.5 hours; B – wild type (WT) podocytes treated with Shiga toxin for 6hrs vs. 0.5hrs. Blue vertical lines indicate Log_2 +/- 0.5 fold change and blue horizontal lines indicate the p <0.05 threshold, corrected for multiple comparisons using a Benjamini-Hochberg false discovery rate of 0.1. Red boxes indicate the phospho-peptides that are statistically significant. On each volcano plot a few phospho-peptides that reach statistical significance have been named.

Protein (gene name)	Direction of fold change	Function
SNRNP	down	mRNA splicing
HMGA2	down	Transcriptional regulator
BAG	down	Negative regulator of apoptosis
PGRMC1	up	Neutrophil degranulation
ASHNAK	down	Epithelial cell polarity
NUCKS1	down	DNA repair
NPC2	up	Cholesterol homeostasis / phospholipid transport
RAI14	up	Actin binding / cell differentiation
PHLDB2	up	Cadherin binding

Table 10: Description of statistically significant phospho-peptides in phospho-proteomic dataset
Statistically significant phospho-peptides identified from my phospho-proteomic dataset volcano plots are listed. Proteins in blue are from the WT podocytes vs A4GALT knockdown podocytes treated with Stx for 0.5hr comparison. Proteins in red are from the WT podocytes treated with Stx for 6hrs vs. WT podocytes treated with Stx for 0.5hrs.

Volcano plots are a useful way of visualising the entire total protein or phospho-peptide dataset generated from my proteomic experiment. Interestingly, the proteins up-regulated in the WT podocytes treated with Shiga toxin for 0.5 hours vs. A4GALT knockdown controls are associated with the inflammatory response and angiogenesis. WT podocytes treated with Shiga toxin for 6 hours show an increase in proteins associated with apoptosis and mitochondrial damage. These changes would be expected given the already published work investigating the effects of Shiga toxin on the kidney [33].

Interpretation of the phospho-peptide changes are slightly more complex to delineate; as phosphorylation is not always a direct measurement of protein activation, given most kinases have both activating and inhibiting phosphorylation sites. Thus, to check the effect of each phosphorylation the PhosphoSitePlus™ website was used; which also gives an indication of the most likely phosphorylation site within the peptide of interest which is useful for validation studies involving the use of antibodies (e.g. western blotting).

5.5.1 STRING pathway analysis

STRING (Search Tool for the Retrieval of Interacting Genes/Proteins) is a free web-based resource for predicting protein to protein interactions [266]. STRING version 11 (available at https://string-db.org) was used to perform pathway enrichment analysis of my datasets. STRING achieves enrichment through the use of detailed biochemical pathway databases (Gene Ontology (GO) and KEGG (Kyoto Encyclopaedia of Genes and Genomes)) but also offers new classification systems through hierarchical clustering of the identified networks themselves [266][267]. The protein interactions that are described by STRING are both direct physical interactions and indirect functional interactions [266]. These interactions are organised into one of 7 'channels' which can be enabled or disabled by the user to customise the output of the enrichment pathway analysis [266]. The protein to protein interactions are scored (taking into account the need for multiple testing correction) to generate an approximate confidence in the strength of an association. STRING uses this score to provide the user with a false discovery rate (FDR) [267].

Examples of the protein association networks generated by STRING using my datasets for total and phospho-peptide TMT proteomics are shown in Figure 5-9 to Figure 5-11. These results were filtered to include proteins or phospho-peptides with fold changes more than +/- 2; and an FDR of 1% (i.e. high confidence of the strength of the observed interaction being true). Lines connecting the protein nodes (circles) indicate predicted protein to protein interactions. Blue interconnecting lines are from existing databases and pink lines are those that have been experimentally defined. Nodes that contain drawings of proteins represent proteins that have known 3D structures [266].

STRING pathway analysis was consistent with my volcano plot data analysis. The predominant effects of Shiga toxin in the wild type vs. the A4GALT knockdown podocytes was to increase proteins and phospho-peptides associated with the immune response and apoptosis and decrease proteins and phospho-peptides associated with the cell cycle and DNA replication and repair. These findings are representative of current published literature of the effects of Shiga toxin in other cell types [33].

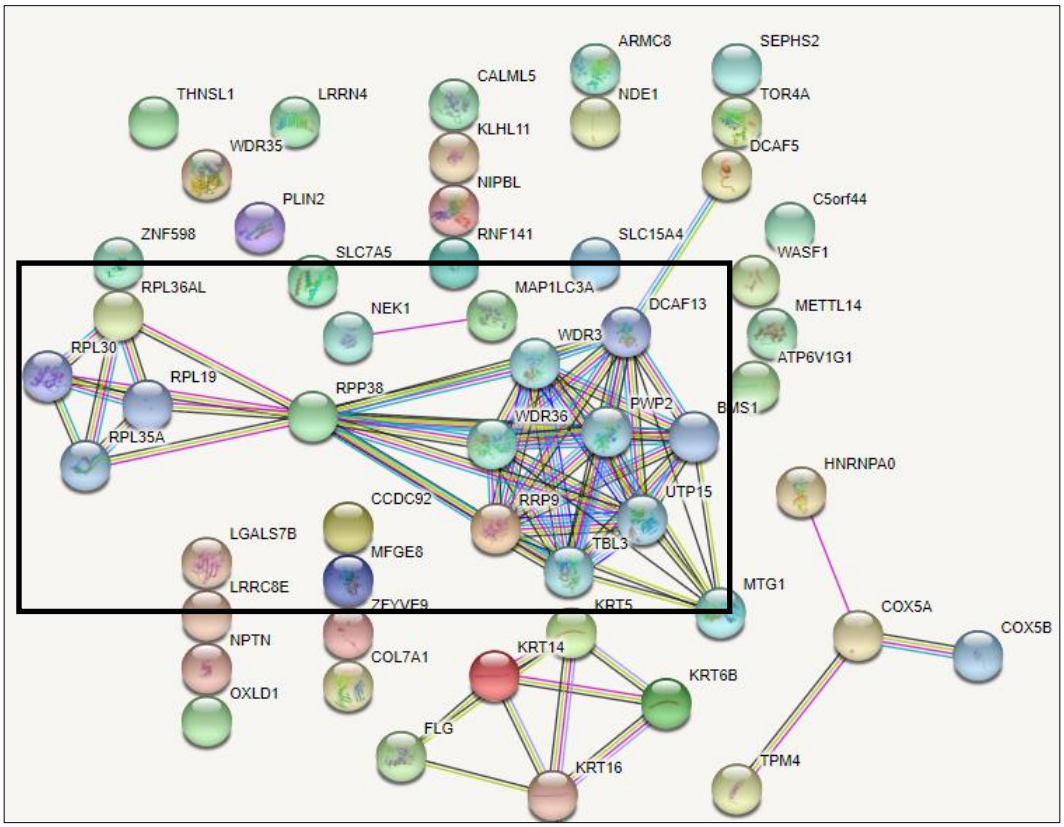

Figure 5-9: STRING network diagram of total proteins with a fold change > +2 in WT vs A4GALT knockdown podocytes treated with Stx 0.5hrs

STRING network diagram showing the significant nodes and protein interactions that are altered in the wild type podocytes vs. the A4GALT knockdown podocytes treated with Shiga toxin for 0.5hrs. Proteins were filtered on an abundance of > +2 fold change. Blue interconnecting lines are from existing databases and pink lines are those that have been experimentally defined. Nodes that contain drawings of proteins represent proteins that have known 3D structures. Pathways highlighted are those involving ribosomal biogenesis, rRNA processing, actin cytoskeleton remodelling and cell assembly.

Proteins of interest (that featured in the functional enrichment table produced by STRING not shown) included: Protein S100-A8 which plays a prominent role in the regulation of inflammatory processes and immune response. Importantly, this protein is a member of the S100 proteins that activate the NLRP3 inflammasome complex [268]. The significance of the NLRP3 inflammasome is discussed later in this chapter. Another enriched protein included WDR36 which is involved in T-cell activation. Reassuringly, these results reflect those that I obtained from my volcano plot analysis.

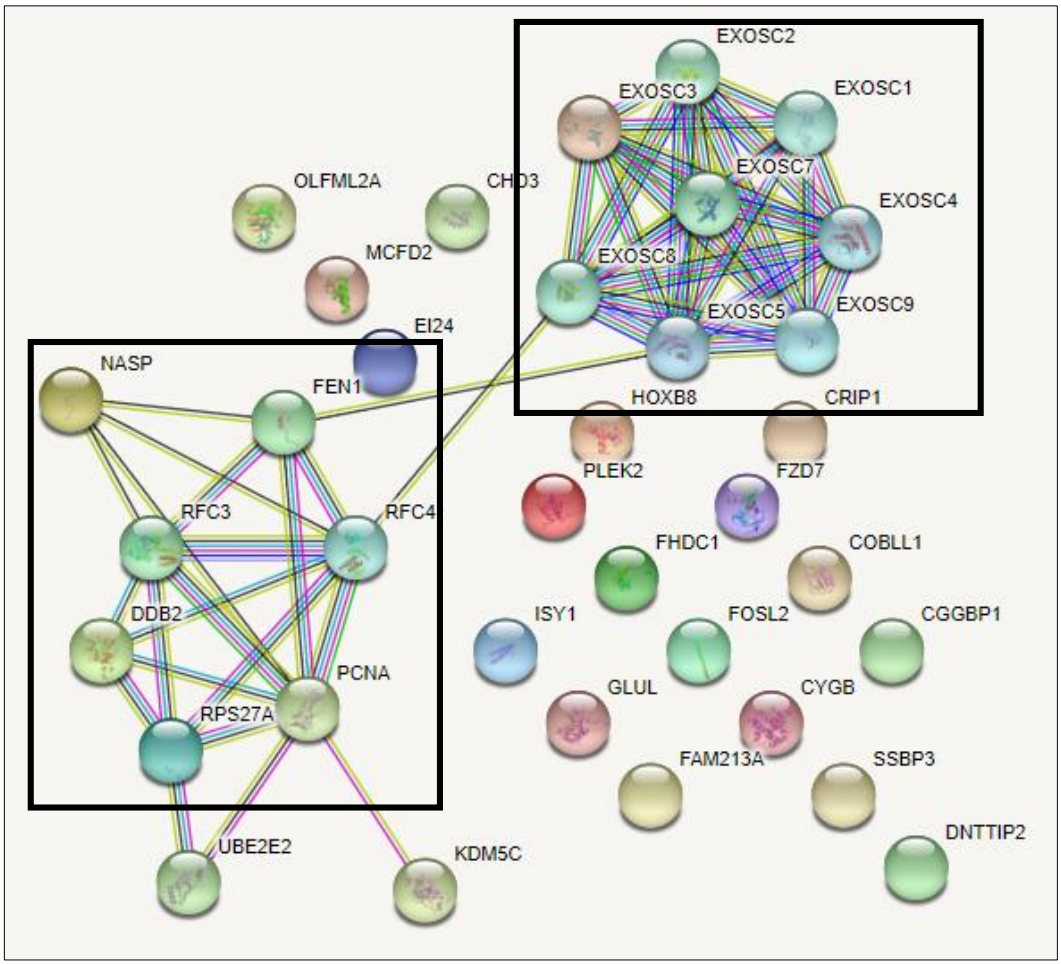

Figure 5-10: STRING network diagram of total proteins with a fold change of > -2 in WT vs. A4GALT knockdown podocytes treated with Stx 0.5hrs

STRING network diagram showing the significant nodes and protein interactions that are altered in the wild type podocytes vs. the A4GALT knockdown podocytes treated with Shiga toxin for 0.5hrs. Proteins were filtered on an abundance of > -2 fold change. Pathways highlighted are those involving RNA degradation and DNA replication; which are reflective of the changes identified in my volcano plot analysis.

A

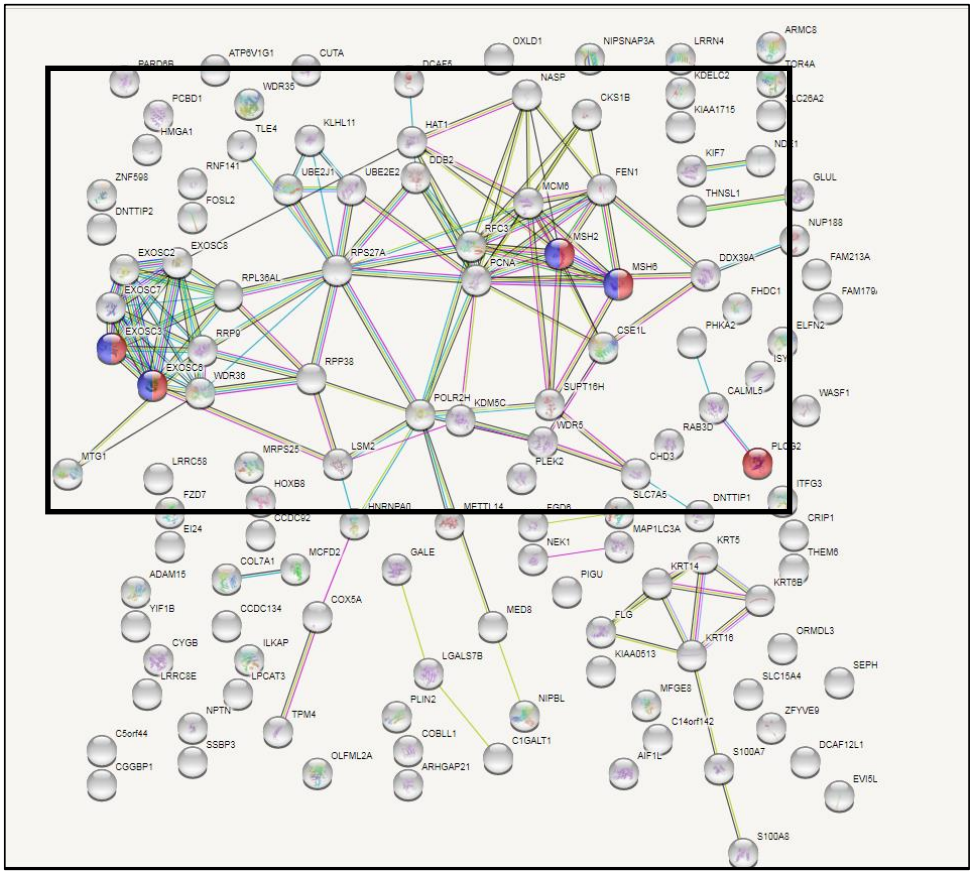
ATP6V1G1
CUTA
OXLD1
NIPSNAP3A
LRRN4
ARMC8
PCBD1
WDR35
NASP
CKS1B
KDELC2
KIAA1715
HMGA1
TLE4
KLHL11
HAT1
KIF7
ZNF598
RNF141
UBE2J1
UBE2E2
DDB2
FEN1
GLUL
DNTTIP2
FOSL2
MCM6
THNSL1
NUP188
EXOSC2
EXOSC8
RFC3
MSH2
RPS27A
PCNA
DDX39A
FAM213A
EXOSC7
RPL36AL
MSH6
FHDC1
FAM179A
EXOSC3
RRP9
CSE1L
PHKA2
ELFN2
EXOSC5
RPP38
WDR36
POLR2H
KDM5C
SUPT16H
CALML5
WASF1
WDR5
RAB3D
MTG1
MRPS25
LSM2
CHD3
PLEK2
LRRC58
HOXB8
SLC7A5
DNTTIP1
ITFG3
FZD7
HNRNPA0
METTL14
CRIP1
EI24
CCDC92
MAP1LC3A
NEK1
KRT5
THEM6
MCFD2
GALE
KRT14
COL7A1
PIGU
KRT8B
ADAM15
COX5A
FLG
YIF1B
CCDC134
MED8
ORMDL3
CYGB
ILKAP
KIAA0513
KRT16
LGALS7B
SEPH
LRRC8E
LPCAT3
SLC15A4
MFGE8
NPTN
TPM4
PLIN2
NIPBL
ZFYVE9
C5orf44
SSBP3
COBLL1
C1GALT1
C14orf142
DCAF12L1
CGGBP1
OLFML2A
ARHGAP21
AIF1L
S100A7
EVI5L
S100A8

B

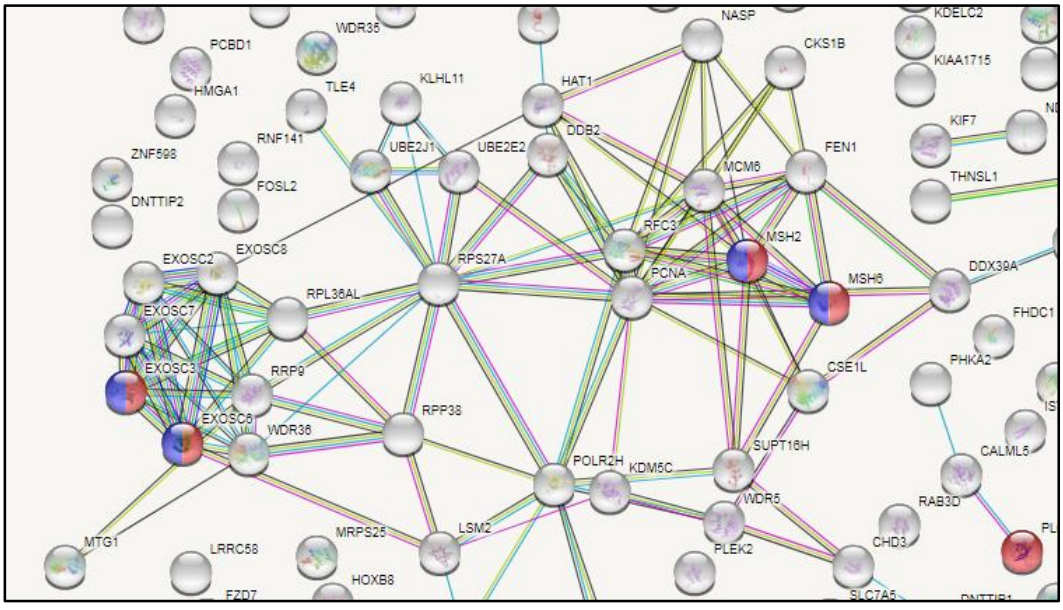
WDR35
NASP
KDELC2
PCBD1
CKS1B
KIAA1715
HMGA1
TLE4
KLHL11
HAT1
KIF7
RNF141
UBE2J1
UBE2E2
DDB2
FEN1
ZNF598
MCM6
THNSL1
FOSL2
DNTTIP2
RFC3
MSH2
EXOSC2
EXOSC8
RPS27A
PCNA
DDX39A
MSH6
RPL36AL
EXOSC7
FHDC1
EXOSC3
RRP9
CSE1L
PHKA2
RPP38
EXOSC5
WDR36
SUPT16H
CALML5
POLR2H
KDM5C
WDR5
RAB3D
MTG1
MRPS25
LSM2
CHD3
PLEK2
LRRC58
HOXB8
FZD7
SLC7A5

C

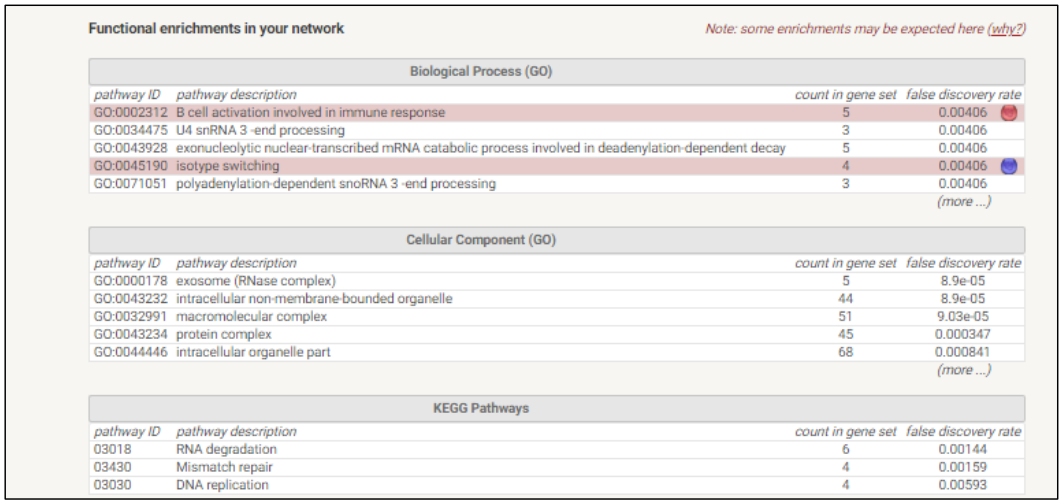

Functional enrichments in your network

Note: some enrichments may be expected here (why?)

Biological Process (GO)

pathway ID	*pathway description*	*count in gene set*	*false discovery rate*
GO:0002312	B cell activation involved in immune response	5	0.00406
GO:0034475	U4 snRNA 3'-end processing	3	0.00406
GO:0043928	exonucleolytic nuclear-transcribed mRNA catabolic process involved in deadenylation-dependent decay	5	0.00406
GO:0045190	isotype switching	4	0.00406
GO:0071051	polyadenylation-dependent snoRNA 3'-end processing	3	0.00406
			(more ...)

Cellular Component (GO)

pathway ID	*pathway description*	*count in gene set*	*false discovery rate*
GO:0000178	exosome (RNase complex)	5	8.9e-05
GO:0043232	intracellular non-membrane-bounded organelle	44	8.9e-05
GO:0032991	macromolecular complex	51	9.03e-05
GO:0043234	protein complex	45	0.000347
GO:0044446	intracellular organelle part	68	0.000841
			(more ...)

KEGG Pathways

pathway ID	*pathway description*	*count in gene set*	*false discovery rate*
03018	RNA degradation	6	0.00144
03430	Mismatch repair	4	0.00159
03030	DNA replication	4	0.00593

Figure 5-11: STRING network diagram of phospho-peptide proteins with a fold change > +/-2 in WT podocytes vs. A4GALT knockdown podocytes treated with Stx 0.5 hrs

A = STRING network diagram showing the significant nodes and phospho-peptide interactions that are altered in wild type podocytes vs. the A4GALT knockdown podocytes treated with Shiga toxin for 0.5hrs. Proteins were filtered on an abundance of > +/- 2 fold change. The black box indicates the key pathways and has been zoomed in on in panel B. C = an example output table generated by STRING detailing the GO and KEGG enrichment pathway analysis. Key pathways highlighted include immune response, RNA degradation and mismatch repair. This is in-keeping with my volcano plot data and consistent across my experimental data.

5.5.2 Ingenuity Pathway Analysis (IPA)

Another form of pathway analysis software used in proteomics is Ingenuity Pathway Analysis (IPA) which is considered the gold-standard. This is because IPA takes into consideration the effect of each protein on cell function and predicts whether it has been activated or inhibited by the change in abundance observed. It is able to do this, by drawing from a large database of published work to correlate differences in expression with differences in activation state. In the network maps generated by IPA, red and green nodes are up and down regulated proteins (respectively) within the dataset and orange and blue are up and down regulated proteins predicted by the IPA software from the expression values of related proteins.

The phospho-peptide dataset analysis is slightly more complex as phosphorylation cannot always be assumed to be a direct measurement of protein activation. Hence, the software has more difficulty predicting network regulation. However, in my analysis very similar

networks between conditions were generated across the total report and canonical pathway data generated by the IPA software and these correlated with the function / disease read-outs to give a consistent picture of the global phosphorylation state of the protein networks which was reassuring. Furthermore, IPA data analysis was in-keeping with my STRING pathway analysis which is further evidence of reproducibility of the analysis. In the case of the phospho-peptide IPA network maps, red and green nodes are proteins where the phosphorylation fold change is higher or lower than the total protein abundance fold change respectively. Orange and blue nodes are predicted up or down-regulated phosphorylation fold changes relative to the total protein abundance if phosphorylation is assumed to be activating.

It is important to note, that the data downloaded on to the IPA software was filtered, normalised and scaled as described above in the 'Protein quantification' and 'Proteomic analysis results' sections. It is vital to maintain the same methods of data processing prior to obtaining results from IPA so that they can be compared to other types of analysis I have used. These datasets were sent to Pedro Moura a PhD student working for Dr. Ash Toye in the School of Biochemistry at the University of Bristol. Pedro was familiar with the use of the IPA software and large datasets generated from proteomic experiments; he was blinded to avoid any bias in his IPA analysis. The reports generated from IPA included network maps, total reports and in-depth analysis of the diseases and functions associated with changes in total and phospho-peptides in each experimental condition. These outputs were then used together with my previous analysis in STRING to come up with key proteins and phospho-peptides for validation through western blotting, PCR, and in-situ hybridisation. Also included in the IPA analysis is a comparison of the pathways activated in wild type human podocytes treated with Shiga toxin for 6 hours versus the A4GALT knockdown podocytes treated with Shiga toxin for 0.5 hours.

A

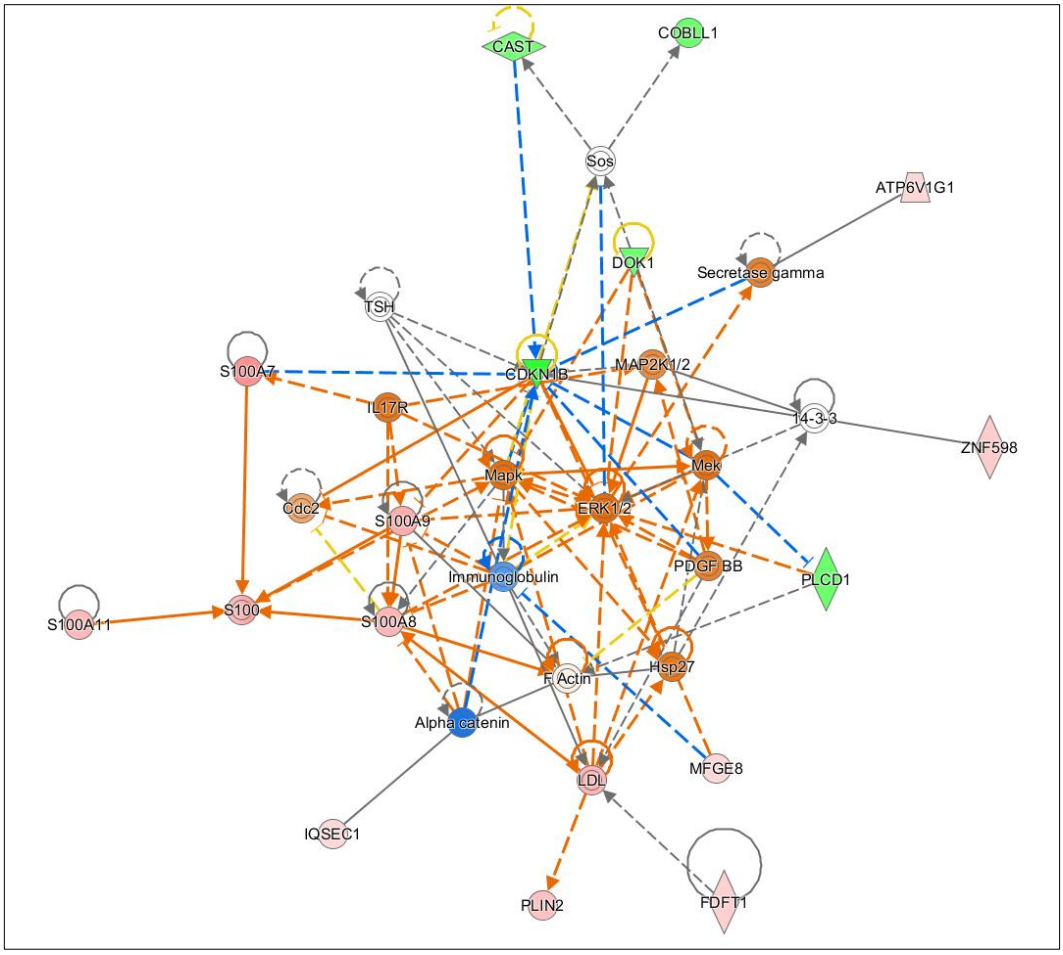

Summary of Analysis - Abundance_Total_TMT_Filtered_30m_vs_A4GALT - 2018-02-26 02 - 2018-02-26 02:42 PM

Top Canonical Pathways

Name	p-value	Overlap
Role of IL-17A in Psoriasis	3.05E-05	23.1 % 3/13
Melatonin Signaling	4.15E-04	5.6 % 4/72
BER pathway	1.49E-03	16.7 % 2/12
Synaptic Long Term Potentiation	2.95E-03	3.3 % 4/122
Sperm Motility	3.41E-03	3.1 % 4/127

Top Upstream Regulators

Upstream Regulator	p-value of overlap	Predicted Activation
TP63	7.62E-08	
indomethacin	4.19E-07	
PLA2G2E	4.31E-07	
HRAS	1.89E-06	
MYC	2.38E-06	

Top Diseases and Bio Functions

Diseases and Disorders

Name	p-value	#Molecules
Dermatological Diseases and Conditions	9.67E-03 - 1.01E-09	29
Organismal Injury and Abnormalities	9.67E-03 - 1.01E-09	102
Skeletal and Muscular Disorders	9.67E-03 - 1.01E-09	24
Developmental Disorder	9.67E-03 - 1.44E-08	33
Hereditary Disorder	9.67E-03 - 4.39E-08	34

Figure 5-12: IPA network map and summary of top canonical pathways in WT vs. A4GALT knockdown podocytes treated with Shiga toxin for 0.5hr: total protein

Human WT vs. A4GALT knockdown podocytes were treated with 0.1ng/ml Shiga toxin for 0.5hr and the protein lysates analysed by TMT LC-MS/MS. IPA software was used (as described) to generate

this protein network map which shows the key changes in total proteins that occur in the WT podocytes vs. the A4GALT knockdown podocytes treated with Shiga toxin. Key target proteins are located centrally within the protein network. Red and orange proteins are being upregulated. Blue and green proteins are being downregulated. Of interest in this dataset is the increase in ER stress markers (ERK1/2 and MAPK pathways) and pro-inflammatory cytokine IL-17 in the WT podocytes.

B

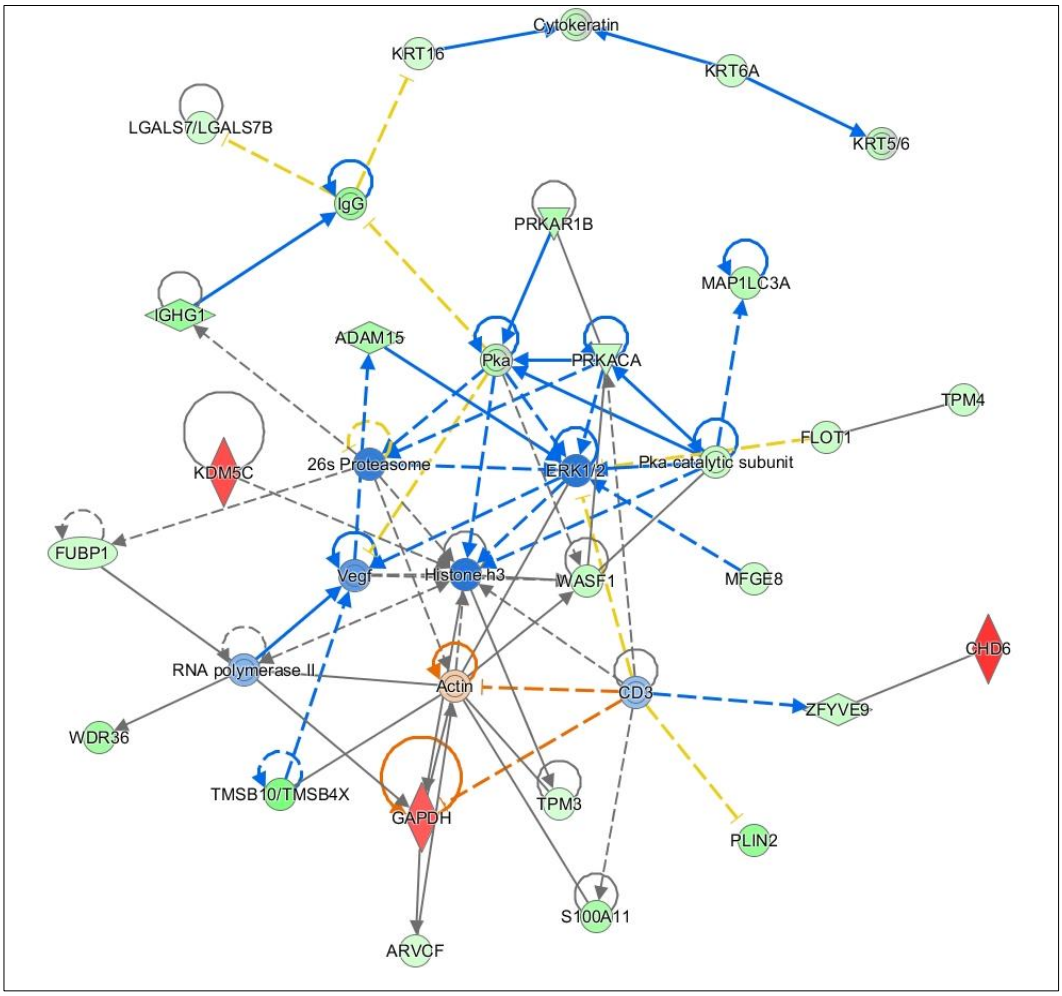

Summary of Analysis - Abundance_Total_TMTFiltered - 2018-02-26 02:38 PM - 2018-02-26 02:39 PM

Top Canonical Pathways

Name	p-value	Overlap
Dopamine Receptor Signaling	1.78E-03	3.9 % 3/77
CDK5 Signaling	3.64E-03	3.0 % 3/99
Calcium Signaling	3.88E-03	1.9 % 4/206
Sonic Hedgehog Signaling	3.91E-03	6.7 % 2/30
Glucocorticoid Receptor Signaling	4.07E-03	1.5 % 5/339

Top Upstream Regulators

Upstream Regulator	p-value of overlap	Predicted Activation
KRT14	2.79E-04	
PC-SPES	3.16E-04	
PLA2G2E	8.42E-04	
LONP1	1.42E-03	
clofazimine	3.35E-03	

Top Diseases and Bio Functions

Diseases and Disorders

Name	p-value	#Molecules
Dermatological Diseases and Conditions	4.27E-02 - 3.65E-08	14
Developmental Disorder	4.56E-02 - 3.65E-08	20
Hereditary Disorder	1.85E-02 - 3.65E-08	22
Organismal Injury and Abnormalities	4.86E-02 - 3.65E-08	66
Skeletal and Muscular Disorders	4.86E-02 - 1.15E-07	18

Figure 5-13: IPA network map and summary of top canonical pathways in WT podocytes treated with Shiga toxin for 6hrs vs. 0.5hr: total protein

Human WT podocytes were treated with 0.1ng/ml Shiga toxin for 0.5hr or 6hrs and the protein lysates analysed by TMT LC-MS/MS. IPA software was used (as described) to generate this protein

network map which shows the key changes in total proteins that occur. Key target proteins are located centrally within the protein network. Red and orange proteins are being upregulated. Blue and green proteins are being downregulated. Of interest in this dataset is the reduction in VEGF-A in the podocytes treated with Shiga toxin for 6 hrs vs. 0.5hrs.

C

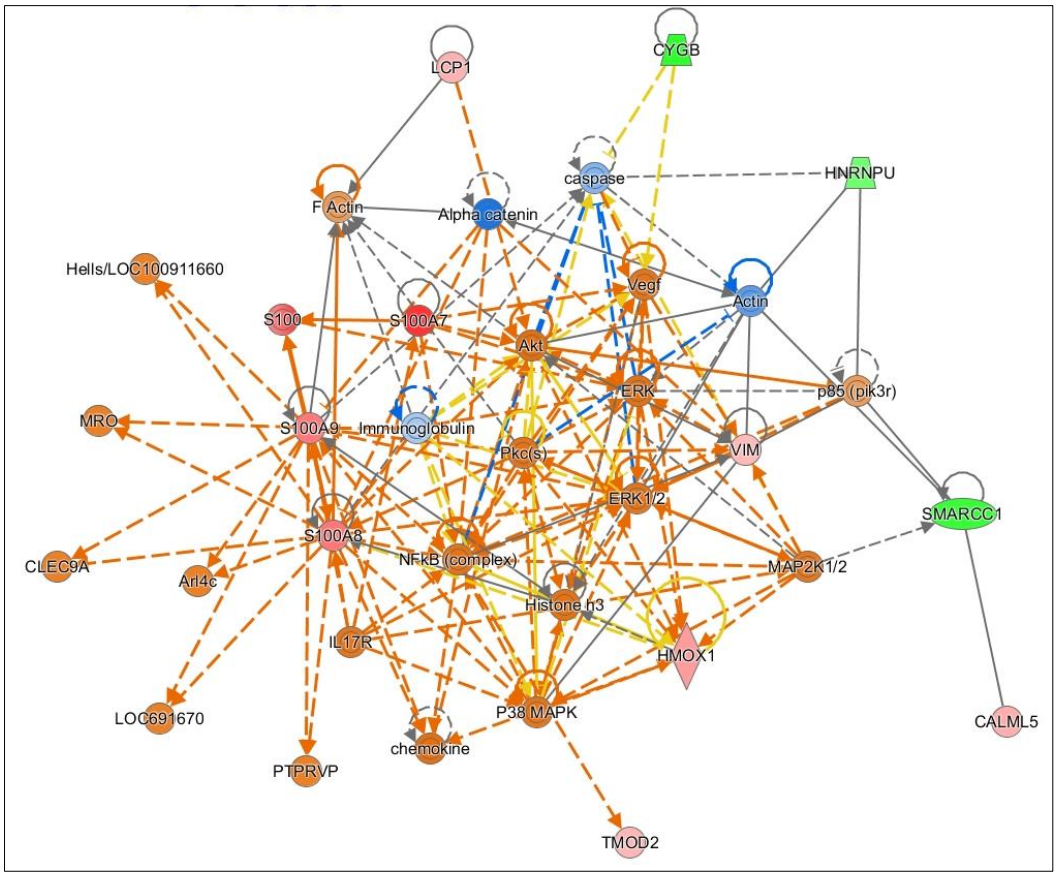

Summary of Analysis - Abundance_Total_TMT_6h_vs_A4GALT - 2018-02-26 02:41 PM - 2018-02-26 02:42 PM

Top Canonical Pathways

Name	p-value	Overlap
Role of IL-17A in Psoriasis	7.42E-08	23.1 % 3/13
Heme Degradation	2.74E-03	25.0 % 1/4
Gq Signaling	5.30E-03	1.2 % 2/161
Superoxide Radicals Degradation	5.47E-03	12.5 % 1/8
Choline Biosynthesis III	8.88E-03	7.7 % 1/13

Top Upstream Regulators

Upstream Regulator	p-value of overlap	Predicted Activation
IL22	8.86E-11	
IL17R	2.23E-07	
EHF	3.45E-07	Activated
hemozoin	7.95E-07	
IL17C	9.92E-07	

Top Diseases and Bio Functions

Diseases and Disorders

Name	p-value	#Molecules
Dermatological Diseases and Conditions	4.04E-02 - 6.36E-09	11
Immunological Disease	2.57E-02 - 6.36E-09	8
Inflammatory Disease	3.31E-02 - 6.36E-09	8
Organismal Injury and Abnormalities	4.04E-02 - 6.36E-09	15
Cancer	3.96E-02 - 9.77E-07	15

Figure 5-14: IPA network map and summary of top canonical pathways in WT podocytes treated with Shiga toxin for 6hrs vs. A4GALT knockdown podocytes treated with Shiga toxin for 0.5hr: total protein

Human WT podocytes were treated with 0.1ng/ml Shiga toxin for 6 hours and A4GALT knockdown podocytes were treated with 0.1ng/ml Shiga toxin for 0.5hr and protein lysates analysed by TMT LC-MS/MS. IPA software was used (as described) to generate this protein network map which shows the key changes in total proteins that occur in the WT podocytes vs. the A4GALT knockdown podocytes treated with Shiga toxin. Key target proteins are located centrally within the protein network. Red and orange proteins are being upregulated. Blue and green proteins are being downregulated. Of interest in this dataset is the increase in ER stress markers (ERK1/2 and MAPK pathways) and pro-inflammatory cytokines IL-17 and IL-22 in the WT podocytes vs. A4GALT knockdowns. Notably, these networks are similar to those activated in the IPA analysis of wild type podocytes treated for 0.5 hours with Shiga toxin vs. A4GALT knockdown podocytes also treated with Shiga toxin for 0.5 hours (Figure 5-12).

D

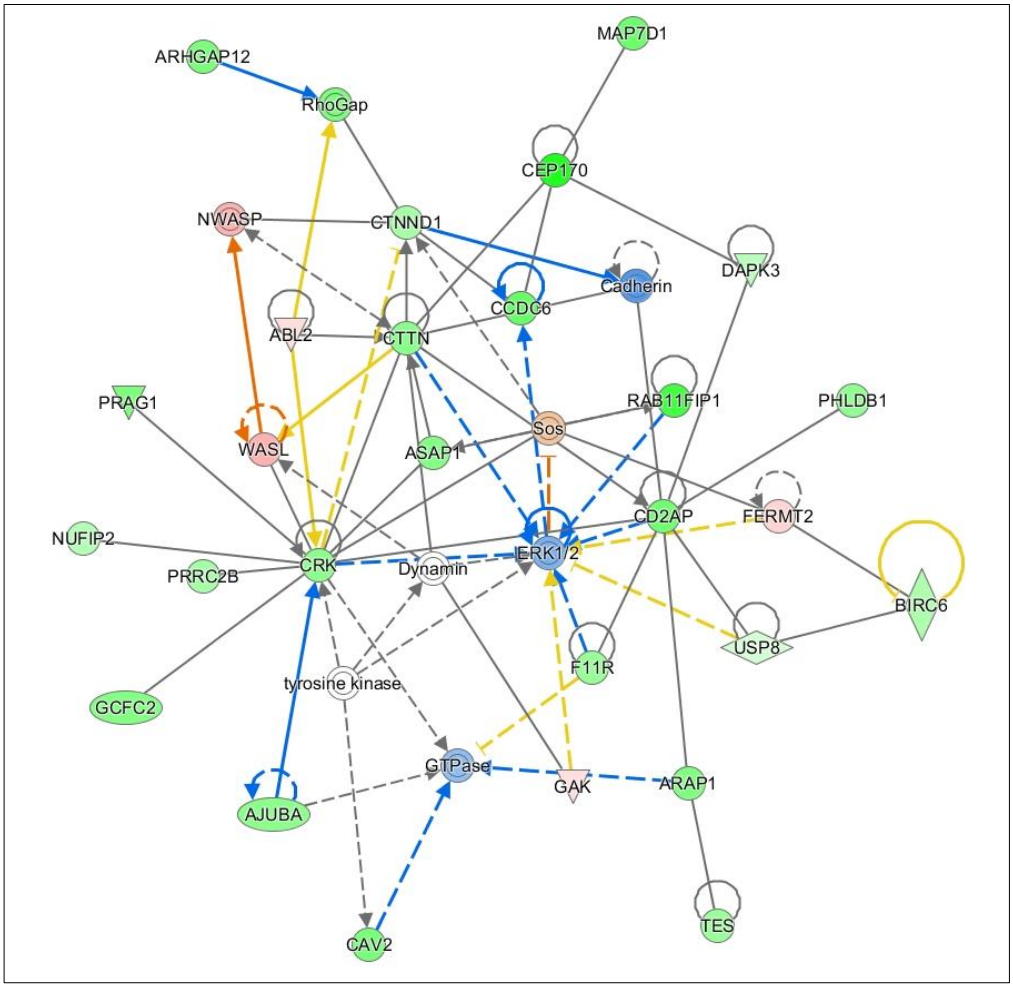

Summary of Analysis - 30m vs A4GALT

Top Canonical Pathways

Name	p-value	Overlap
Insulin Receptor Signaling	8.15E-05	5.7 % 8/141
ERK/MAPK Signaling	8.65E-04	4.0 % 8/200
HIPPO signaling	1.72E-03	5.7 % 5/87
Cardiac -adrenergic Signaling	2.71E-03	4.3 % 6/140
Mitotic Roles of Polo-Like Kinase	4.13E-03	6.1 % 4/66

Top Upstream Regulators

Upstream Regulator	p-value of overlap	Predicted Activation
CDK4/6	6.23E-12	
CST5	3.50E-09	
CCND1	8.17E-06	
mir-122	3.07E-05	
MYCN	3.15E-05	

Top Diseases and Bio Functions

Diseases and Disorders

Name	p-value	#Molecules
Cancer	4.14E-03 - 6.72E-13	203
Organismal Injury and Abnormalities	4.14E-03 - 6.72E-13	203
Gastrointestinal Disease	4.14E-03 - 2.87E-10	186
Reproductive System Disease	3.92E-03 - 4.49E-09	156
Hematological Disease	2.87E-03 - 1.62E-06	61

Figure 5-15: IPA network map and summary of top canonical pathways in WT vs. A4GALT knockdown podocytes treated with Shiga toxin for 0.5hr: phospho-peptides

Human WT vs. A4GALT knockdown podocytes were treated with 0.1ng/ml Shiga toxin for 0.5hr and the protein lysates analysed by TMT LC-MS/MS. IPA software was used (as described) to generate this protein network map which shows the key changes in phospho-peptides that occur in the WT podocytes vs. the A4GALT knockdown podocytes treated with Shiga toxin. Key target proteins are located centrally within the protein network. Red and orange proteins are being upregulated. Blue and green proteins are being downregulated. Of interest in this dataset is the apparent downregulation of ER stress pathways and adaptor protein CD2AP.

E

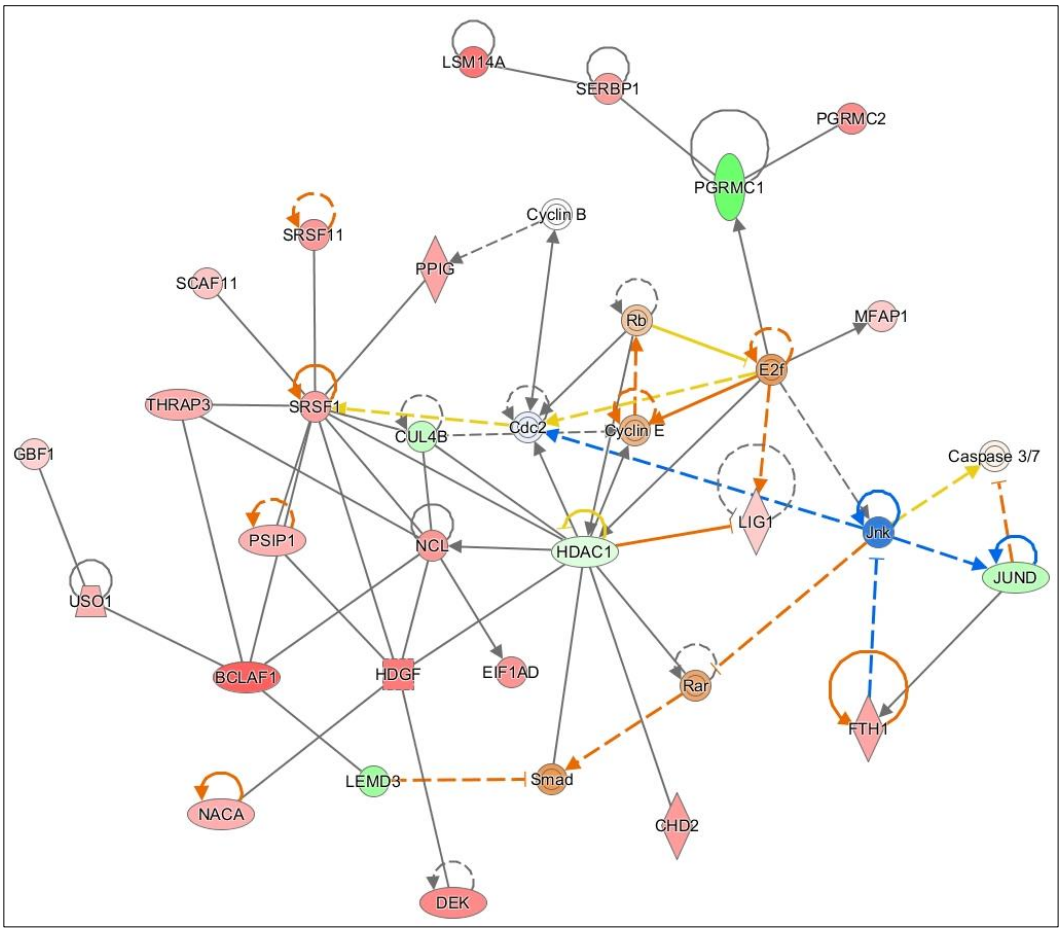

Summary of Analysis - 6h vs 30m

Top Canonical Pathways

Name	p-value	Overlap
Insulin Receptor Signaling	8.15E-05	5.7 % 8/141
ERK/MAPK Signaling	8.65E-04	4.0 % 8/200
HIPPO signaling	1.72E-03	5.7 % 5/87
Cardiac -adrenergic Signaling	2.71E-03	4.3 % 6/140
Mitotic Roles of Polo-Like Kinase	4.13E-03	6.1 % 4/66

Top Upstream Regulators

Upstream Regulator	p-value of overlap	Predicted Activation
CDK4/6	6.23E-12	
CST5	3.50E-09	
CCND1	8.17E-06	
mir-122	3.07E-05	
MYCN	3.15E-05	

Top Diseases and Bio Functions

Diseases and Disorders

Name	p-value	#Molecules
Cancer	4.14E-03 - 6.72E-13	203
Organismal Injury and Abnormalities	4.14E-03 - 6.72E-13	203
Gastrointestinal Disease	4.14E-03 - 2.87E-10	186
Reproductive System Disease	3.92E-03 - 4.49E-09	156
Hematological Disease	2.87E-03 - 1.62E-06	61

Figure 5-16: IPA network map and summary of top canonical pathways in WT podocytes treated with Shiga toxin for 6hrs vs. 0.5hr: phospho-peptides

Human WT podocytes were treated with 0.1ng/ml Shiga toxin for 0.5hr or 6hrs and the protein lysates analysed by TMT LC-MS/MS. IPA software was used (as described) to generate this protein network map which shows the key changes in phospho-peptides that occur. Key target proteins are located centrally within the protein network. Red and orange proteins are being upregulated.

Blue and green proteins are being downregulated. Of interest in this dataset is the increase in apoptosis pathways: BCLAF-1, caspases and Jnk.

F

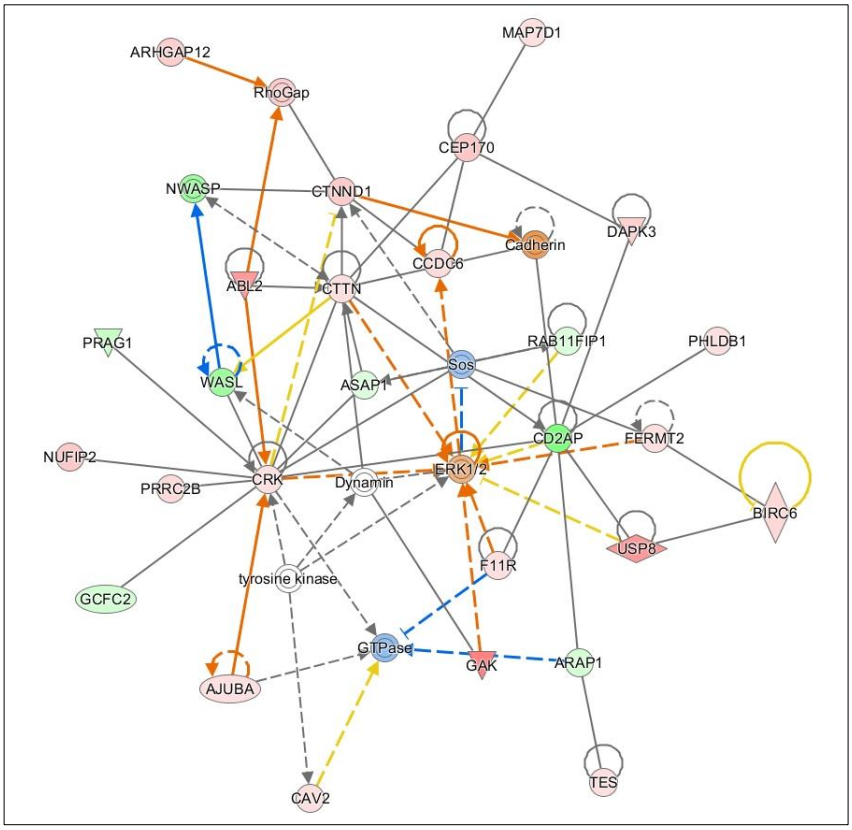

Summary of Analysis - 6h vs A4GALT

Top Canonical Pathways

Name	p-value	Overlap
Insulin Receptor Signaling	8.15E-05	5.7 % 8/141
ERK/MAPK Signaling	8.65E-04	4.0 % 8/200
HIPPO signaling	1.72E-03	5.7 % 5/87
Cardiac -adrenergic Signaling	2.71E-03	4.3 % 6/140
Mitotic Roles of Polo-Like Kinase	4.13E-03	6.1 % 4/66

Top Upstream Regulators

Upstream Regulator	p-value of overlap	Predicted Activation
CDK4/6	6.23E-12	
CST5	3.50E-09	
CCND1	8.17E-06	
mir-122	3.07E-05	
MYCN	3.15E-05	

Top Diseases and Bio Functions

Diseases and Disorders

Name	p-value	#Molecules
Cancer	4.14E-03 - 6.72E-13	203
Organismal Injury and Abnormalities	4.14E-03 - 6.72E-13	203
Gastrointestinal Disease	4.14E-03 - 2.87E-10	186
Reproductive System Disease	3.92E-03 - 4.49E-09	156
Hematological Disease	2.87E-03 - 1.62E-06	61

Figure 5-17: IPA network map and summary of top canonical pathways in WT podocytes treated with Shiga toxin for 6hrs vs. knockdown podocytes treated with Shiga toxin for 0.5hr: total protein

Human WT podocytes were treated with 0.1ng/ml Shiga toxin for 6 hours and A4GALT knockdown podocytes were treated with 0.1ng/ml Shiga toxin for 0.5hr and protein lysates analysed by TMT LC-MS/MS. IPA software was used (as described) to generate this protein network map which shows the key changes in phospho-proteins that occur in the WT podocytes vs. the A4GALT knockdown podocytes treated with Shiga toxin. Key target proteins are located centrally within the protein network. Red and orange proteins are being upregulated. Blue and green proteins are being downregulated.

Of interest in this dataset is the increase in ER stress markers (ERK1/2 and MAPK pathways) which were also a feature in the total protein IPA analysis in these cells. Interestingly, HIPPO signalling and insulin receptor signalling both feature in the top canonical pathways; just as in the IPA phospho-proteomic analysis of wild type podocytes treated for 0.5 hours with Shiga toxin vs. A4GALT knockdown podocytes also treated with Shiga toxin for 0.5 hours (Figure 5-15).

5.6 Validation of protein networks

As evident from my proteomic work, tandem mass spectrometry has the ability to generate thousands of fragment ion spectra which are then assigned to peptide and phospho-peptide sequences. The extrapolation of these data to the likely proteins they represent as well as the determination of their relative abundance in the sample analysed; represent a significant statistical and bioinformatical challenge which can be approached in many different ways [269]. In this chapter, I have outlined the methodology used to analyse my dataset. However, it is widely acknowledged by the proteomic expert community that additional experimental validation for MS derived data is necessary [269] [270]. Through the use of other protein quantification methods including western blotting and digoxigenin (DIG)-labelled RNA probe in situ hybridization, the presence of several proteins of interest identified from my LC-MS/MS experiments have been validated.

After careful review of the volcano plots, STRING networks and IPA analysis from this proteomic experiment, I decided to focus my validation work on the following key proteins and pathways: endoplasmic reticulum (ER) stress pathways which appear to increase in response to Shiga toxin in wild type human podocytes vs. A4GALT knockdown podocytes; slit diaphragm and actin cytoskeleton proteins such as CD2AP which seem to decrease in response to Shiga toxin treatment; inflammasome proteins which appear to increase in response to Shiga toxin in wild type human podocytes and VEGF-A which has been identified as decreasing in response to Shiga toxin treatment in human conditionally

immortalised podocytes. I have selected these pathways because they are likely to represent the most biologically relevant mechanisms behind Shiga toxin HUS, rather than simply choosing those proteins which were identified as being highly abundant in my samples. This serves to ensure that my results are valid and relevant – the very reason why I am performing validation work itself [270].

5.6.1 ER stress pathway validation

It is widely accepted in the published literature that Shiga toxin causes the activation of ER stress pathways and ribotoxic stress responses in eukaryotic cells [33][66]. In my proteomic dataset these pathways were activated in conditionally immortalised human podocytes vs. A4GALT knockdown podocytes treated with Shiga toxin which is perhaps unsurprising but also reassuring; indicating that Shiga toxin treatment was having an effect in my cells. This in itself provides evidence in support of any other identified pathways from this work to be 'true' responses to Shiga toxin treatment within the podocyte.

Activation of ER stress pathways within the podocyte leads to MAPK (mitogen-activated protein kinase) signalling which is known to be essential for innate immunity and regulation of apoptotic pathways [66]. Indeed, Psotka et al. have previously demonstrated that the MAPK p38 pathway is activated, along with JNK (Jun N-terminal protein kinase) in human glomerular cells in response to Shiga toxin exposure [74]. The activation of these pathways resulted in cytokine release, inflammatory kinase activity and caspase-dependant apoptosis [74]. A summary diagram of the ER stress response is shown in Figure 5-18, illustrating 3 key signalling pathways which include PERK, ATF6 and IRE1. These kinases target XBP1 and molecular chaperones such as GRP78 (BiP) to signal to the cell to either survive or undergo apoptosis. The western blots performed to identify the activation of the ER stress response in the wild type podocytes treated with Shiga toxin are shown in the subsequent figures. All densitometry calculations are based upon an n=3 unless otherwise stated.

Western blot analysis of ATF6, pIRE and GRP78 did not show any statistically significant differences between wild type human podocytes and A4GALT KD podocytes treated with Shiga toxin. However, there was a trend observed towards an increase in these markers of ER stress in the wild type podocytes treated with Shiga toxin at both 0.5 and 6 hours vs. A4GALT knockdown podocytes treated with Shiga toxin at 0.5 and 6 hours. Further 'n' numbers are likely to give rise to a statistically significance in the densitometry

measurements of these proteins. Interestingly, the transcription factor CHOP was significantly upregulated in the wild type podocytes treated with Shiga toxin for 2 hours vs. A4GALT knockdown podocytes treated with Shiga toxin at 2 and 4 hours. This is evidence in support of my proteomic analysis that ER stress pathways are activated leading to apoptosis in the human podocyte in response to Shiga toxin treatment.

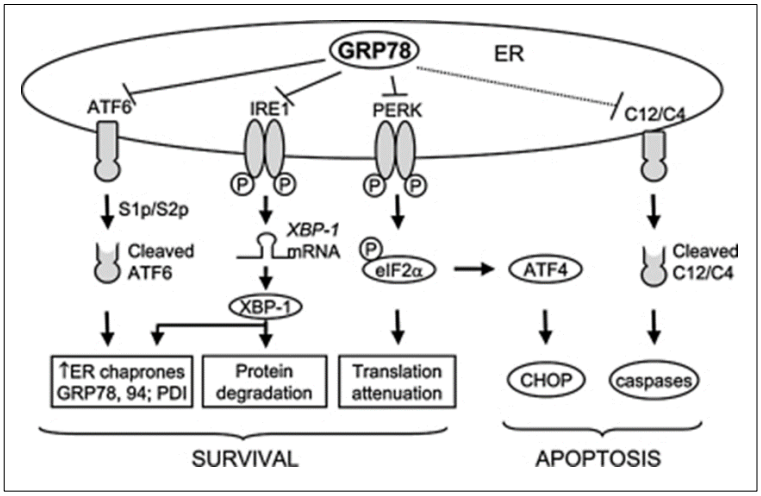

Figure 5-18: Summary of ER stress response within eukaryotic cells

Activation of ER stress (for example from Shiga toxin exposure) leads to activation of one of 3 key signalling pathways ATF6, IRE1 or ATF6. These kinases target the binding protein XBP1 which triggers the release of molecular chaperones GRP78 and PDI in an attempt to support protein folding within the cell. Increased ER stress in podocytes is known to result in cell death by apoptosis (via the transcription factor CHOP / or release of caspases) if the function of the ER cannot be restored by the cell in this way. *Figure adapted from Song et al.* [271]

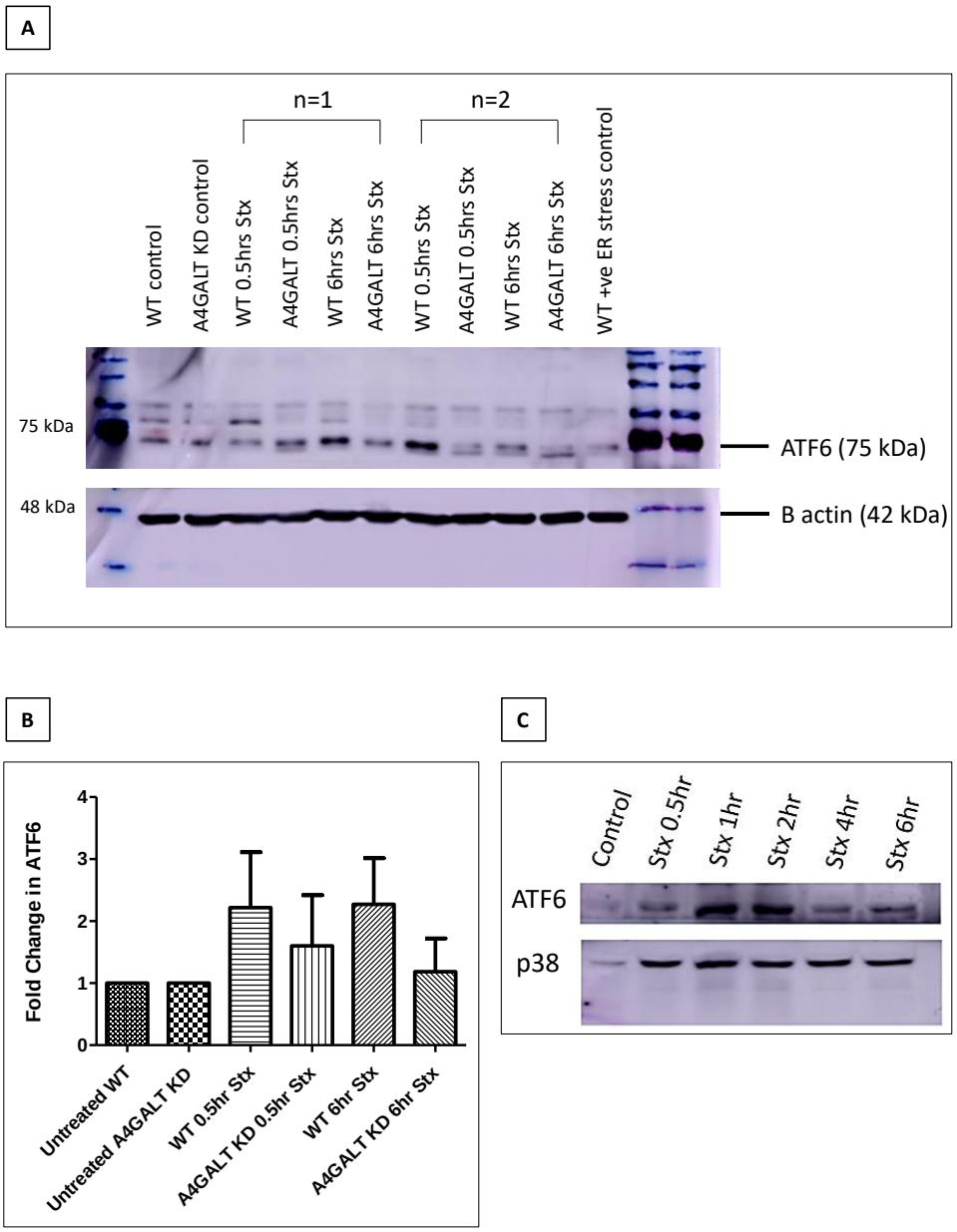

Figure 5-19: Western blot validation of ATF6 driven ER stress activation in podocytes treated with Shiga toxin

Panel A shows a representative western blot analysis (n=2 shown) for ATF6 driven ER stress activation together with β actin loading control. A concentration of 0.1ng/ml of Shiga toxin was used for each incubation. Positive control = WT podocytes treated with known ER stressor 1μM thapsigargin. Panel B shows the densitometry fold change in ATF6 across experimental conditions. Fold change has been calculated following initial normalisation of each sample to its corresponding to β actin loading control, with subsequent normalisation to untreated WT or A4GALT KD podocytes respectively (i.e. all WT lysate samples were normalised to untreated WT and all A4GALT KD samples were normalised to untreated A4GALT KD). There were no statistically significant differences between the samples on ANOVA testing. Panel C shows a representative time course

experiment where ATF6 increases within 0.5hr of Shiga toxin and further at 1 and 2 hrs of incubation. This work was used to inform the timepoints selected in my proteomic experiment.

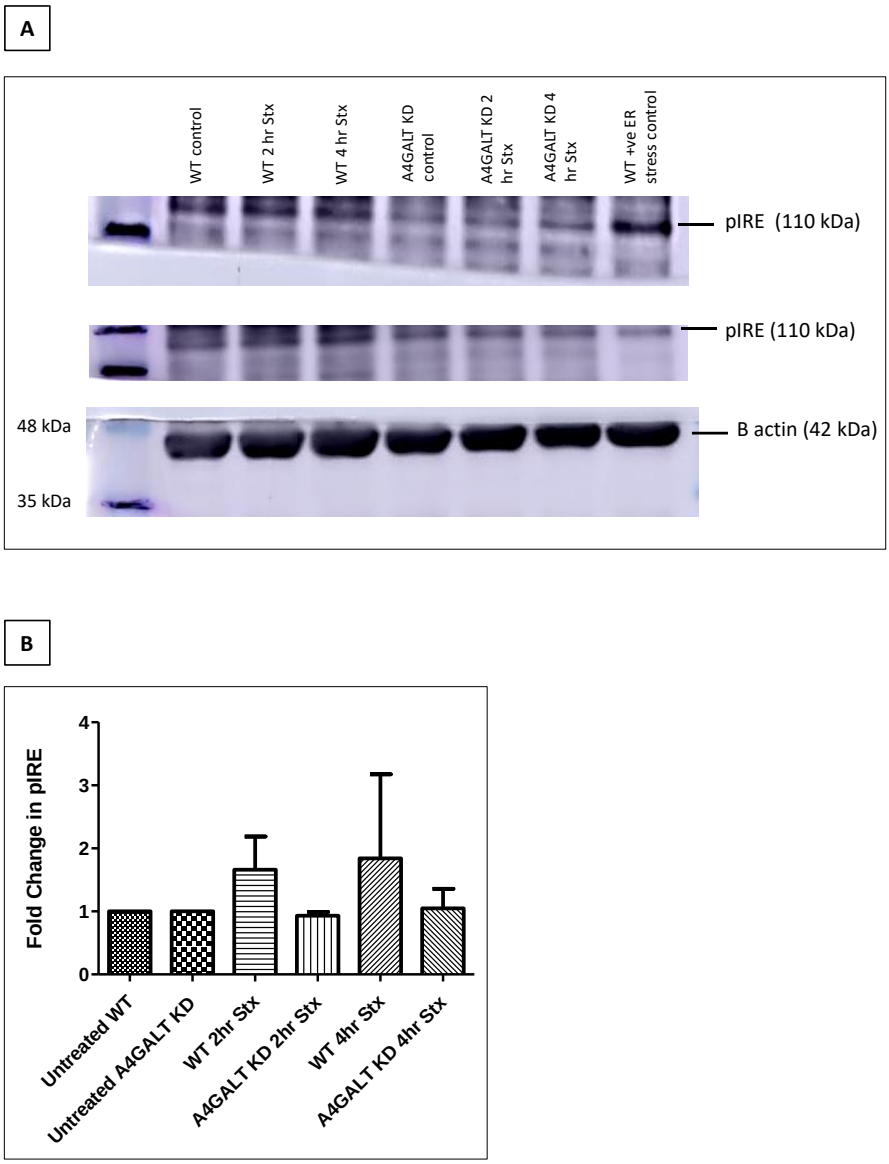

Figure 5-20: Western blot validation of pIRE driven ER stress activation in podocytes treated with Shiga toxin

Panel A shows a representative western blot analysis (n=2 shown) for pIRE driven ER stress activation together with β actin loading control (corresponding to the second pIRE blot). A concentration of 0.1ng/ml of Shiga toxin was used for each incubation. Positive control = WT podocytes treated with known ER stressor 1μM thapsigargin. Panel B shows the densitometry fold change in pIRE across experimental conditions. Fold change has been calculated following initial normalisation of each sample to its corresponding to β actin loading control, with subsequent normalisation to untreated WT or A4GALT KD podocytes, respectively. There was no statistically significant difference between the samples on ANOVA testing.

A

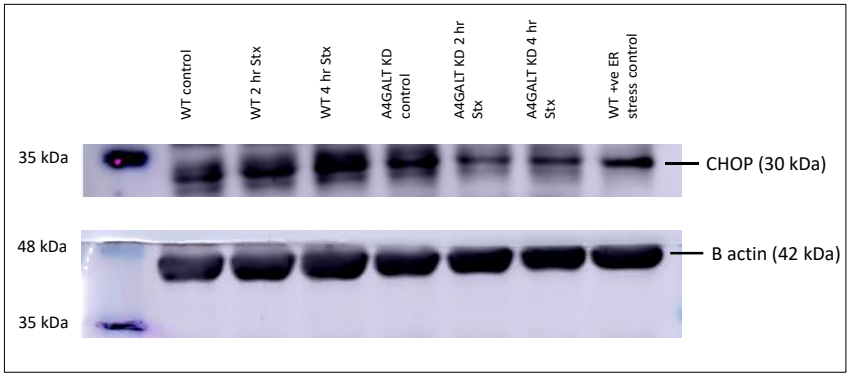

B

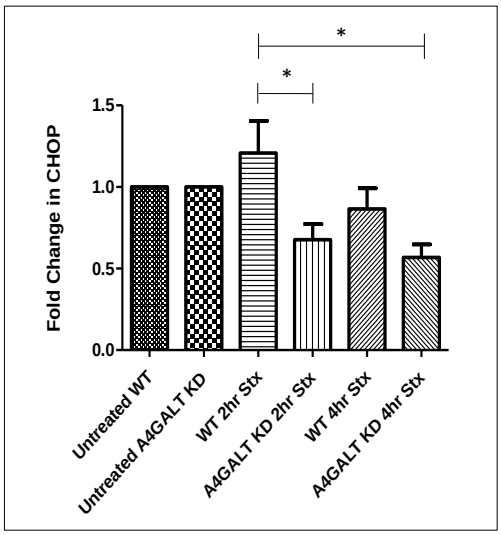

Figure 5-21: Western blot validation of CHOP driven apoptosis due to ER stress activation in podocytes treated with Shiga toxin

Panel A shows a representative western blot analysis for CHOP driven apoptosis due to ER stress activation together with β actin loading control. A concentration of 0.1ng/ml of Shiga toxin was used for each incubation. Positive control = WT podocytes treated with known ER stressor 1μM thapsigargin. Panel B shows the densitometry fold change in CHOP across experimental conditions (n=4). Fold change has been calculated following initial normalisation of each sample to its corresponding to β actin loading control, with subsequent normalisation to untreated WT or A4GALT KD podocytes, respectively. There was a statistically significant increase in CHOP between the WT podocytes treated with Shiga toxin for 2 hours vs. the A4GALT KD podocytes treated with Shiga toxin for 2 hours and 4 hours as indicated on the graph. One way ANOVA Tukey's multiple comparison test *p=0.0132.

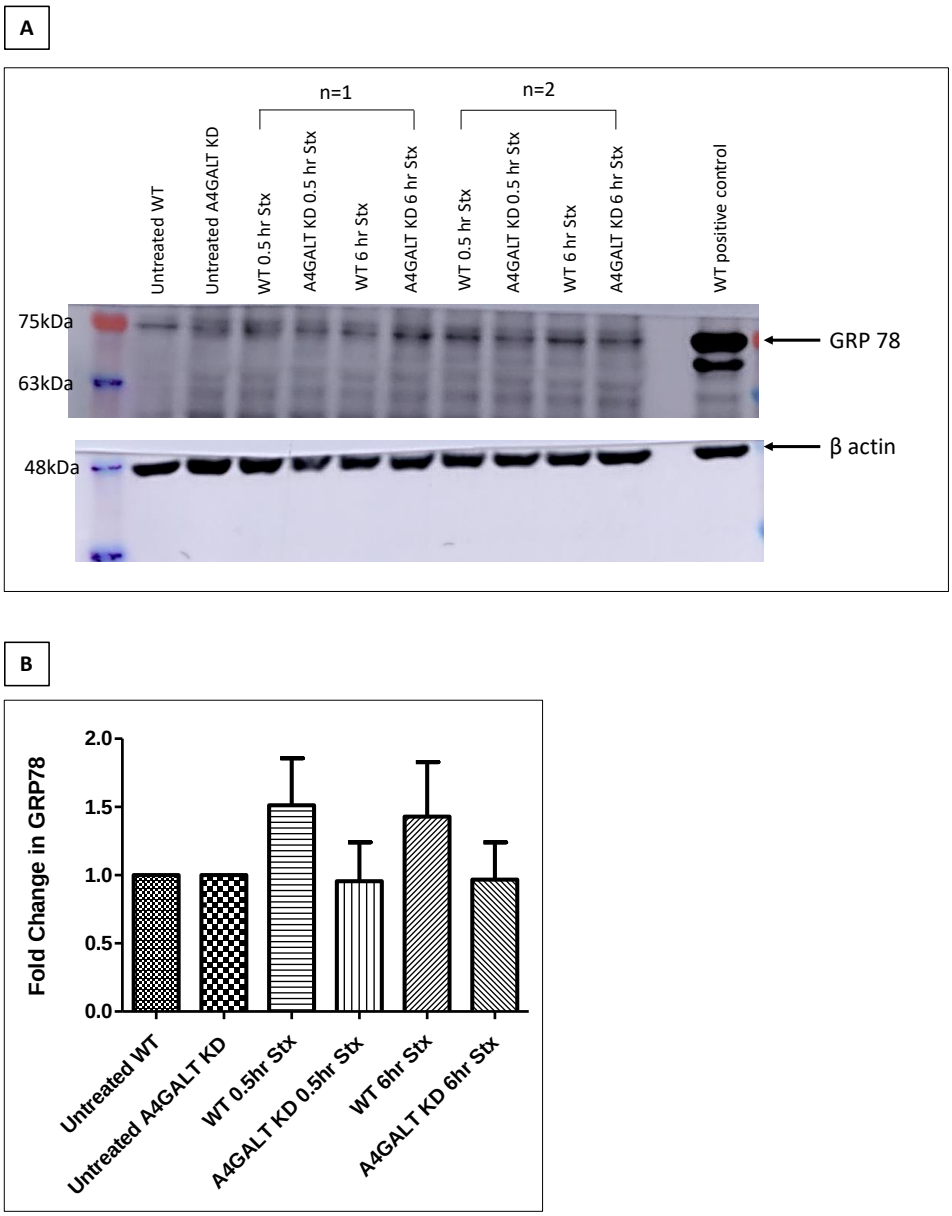

Figure 5-22: Western blot validation of GRP78 activation due to ER stress in podocytes treated with Shiga toxin

Panel A shows a representative western blot analysis (n=2 shown) for GRP78 (molecular weight 75 kDa) driven ER stress activation together with β actin loading control. A concentration of 0.1ng/ml of Shiga toxin was used for each incubation. Positive control = WT podocytes treated with known ER stressor 1μM thapsigargin. Panel B shows the densitometry fold change in GRP78 across experimental conditions. Fold change has been calculated following initial normalisation of each sample to its corresponding to β actin loading control, with subsequent normalisation to untreated WT or A4GALT KD podocytes, respectively. There was no statistically significant difference between the samples on ANOVA testing.

5.6.2 Actin cytoskeleton and cell assembly pathway validation

CD2-associated protein (CD2AP) was identified as decreasing in wild type human podocytes treated with Shiga toxin for 0.5 hr vs. A4GALT knockdown human podocytes in my proteomic analysis. CD2AP was initially characterised as a T-cell adaptor protein, until further experimental work demonstrated that it was present in the podocyte slit diaphragm and directly interacted with nephrin [272]. CD2AP knockout mouse models have shown that lack of CD2AP leads to glomerulosclerosis and lethal renal failure at 6 weeks of age [273]. This has been shown to be due to an increase in podocyte apoptosis due to activation of p38 MAPK pathway by TGF-β [273]. Furthermore, mice with a heterozygous CD2AP deficiency are more susceptible to FSGS and in humans CD2AP splice mutations have been described in focal segmental glomerulosclerosis (FSGS) patients [272]. Clearly, CD2AP is vital for normal podocyte function, but the role of this protein in human disease and how to prevent podocyte injury resulting from CD2AP deficiency is yet to be fully established [273].

To date, this is the first time that CD2AP has been shown to decrease in response to Shiga toxin treatment in podocytes. Western blotting for CD2AP confirmed that this protein is downregulated in podocytes following Shiga toxin treatment vs. A4GALT knockdown podocyte control cells. This was statistically significant on one way ANOVA testing only after the wild type podocytes had been treated with Shiga toxin for 6 hours. Further n numbers may help to demonstrate a reduction in CD2AP at 0.5 hours between these two cell lines. It is worth noting that although immunoblotting is a very useful technique to provide supportive evidence for the abundance of a particular protein or phospho-peptide identified in a proteomic dataset; it is not without its own inherent error. There are many variations in the technique that can affect the outcome, not to mention the complexities of quantification using densitometry [274]. However, taken together with my proteomic IPA pathway analysis CD2AP may well be a potential cellular target for intervention to protect podocytes against Shiga toxin damage in the future.

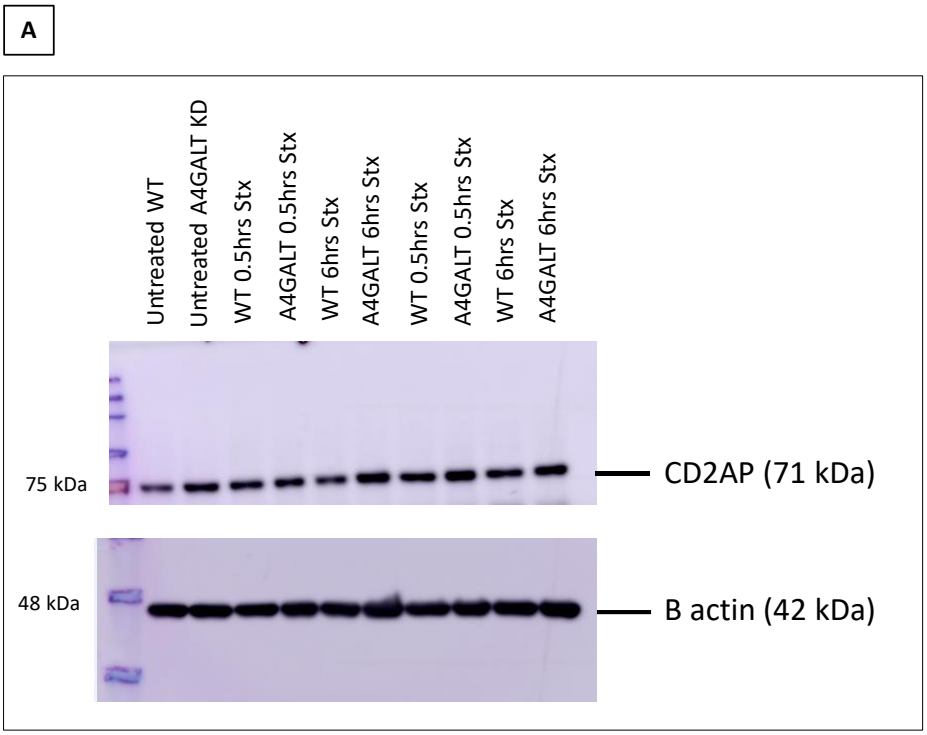

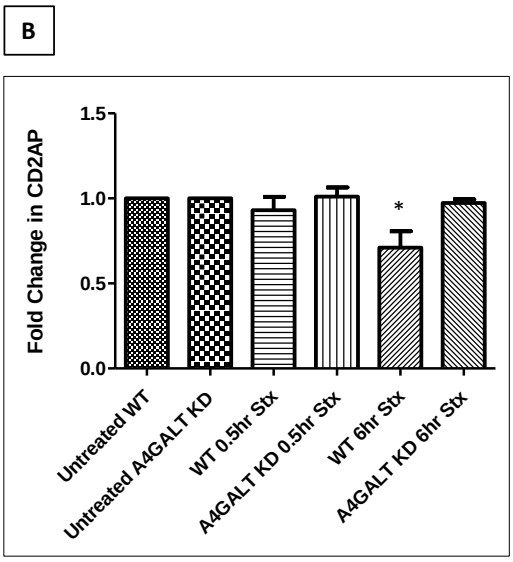

Figure 5-23: Western blot validation of CD2AP reduction in wild type podocytes treated with Shiga toxin

Panel A shows a representative western blot analysis (n=1 shown) for CD2AP together with β actin loading control. A concentration of 0.1ng/ml of Shiga toxin was used for each incubation. Panel B shows the densitometry fold change in CD2AP across experimental conditions (n=3). Fold change has been calculated following initial normalisation of each sample to its corresponding to β actin loading control, with subsequent normalisation to untreated WT or A4GALT KD podocytes respectively. There was a statistically significant reduction in CD2AP between the WT podocytes treated with Shiga toxin for 6 hours vs. untreated WT podocytes, the untreated A4GALT KD

podocytes, A4GALT KD podocytes treated with Shiga toxin for 0.5hrs and the A4GALT KD podocytes treated with Shiga toxin for 6 hrs. One way ANOVA Tukey's multiple comparison test *p=0.01.

5.6.3 Inflammasome activation validation

A recurrent theme from my proteomic dataset was an increase in proteins and phospho-peptides associated with the inflammatory response. Given that Shiga toxin originates from a bacteria and is one of the most potent biological toxins ever described this is perhaps not unexpected [63]. Of particular interest in my proteomic dataset was the x5 fold increase in protein S100-A8; also found to be enriched on STRING pathway analysis in human wild type podocytes versus A4GALT knockdown podocytes, both treated with Shiga toxin for 0.5 hours (Figure 5-9). This protein belongs to the S100 family of which are known to activate NLRP3 (NOD-like receptor family pyrin domain-containing 3) inflammasome [268]. In the last 10 years there has been great advancement in the understanding of the innate immune response to infection, most notably the discovery of the inflammasome. These are large protein complexes classified by their sensor protein [275]. Interestingly, the NLRP3 inflammasome has recently been shown to be involved in the development various acute and chronic kidney diseases through molecular pathways that regulate inflammation, apoptosis, and fibrosis [276].

Given the growing interest in NLRP3 in the nephrological community, I decided to test the samples from my experiment for NLRP3. Unfortunately, despite multiple attempts to validate the presence of this inflammasome complex in the protein lysates, I was unable to demonstrate a significant increase in NLRP3. A representative western blot is shown in Figure 5-24. In this case there is a detectable band at the correct molecular weight for NLRP3 but on repeated attempts either no band was detectable or the immunoblot required over exposure which impacts upon the accuracy of any subsequent densitometry measurements. Going forward further optimisation of western blotting for NLRP3 using this antibody or use of another will be necessary. Western blotting could also be used to detect protein S100-A8 directly.

The issues experienced with western blotting could be for several reasons including: the reactivity of the NLRP3 antibody that I was using for which western blotting is highly dependent; protein to protein interactions within the sample lysate which can cause protein aggregation and altered molecular weights that differ from those anticipated; or an erroneous assumption that the actin 'housekeeping gene' has remained relatively

unaltered in response to the cellular stress response to Shiga toxin (which may not be the case given other cytoskeletal proteins such as CD2AP have been found to change) [270]. However, the β actin loading control blot in Figure 5-24 would be against the latter. In fact, some proteomic experts believe that for all of these reasons western blotting is not a satisfactory approach to validating proteomic datasets [270].

I agree that it is important to remember that validating a single data point within a MS dataset is not the same as whole dataset authentication. To ensure the latter, what is necessary is robust statistical and bioinformatic processes which can be used to confirm the quality of the dataset overall [270]. By utilising the expertise of the bioinformaticians in the Proteomic Facility at the University of Bristol, I have been able to ensure my analysis has well defined and understood FDR values as well as confirming that the observed enrichment of proteins and phospho-peptides are due to the experimental conditions imposed [270].

Nonetheless, it remains an interesting finding that in this proteomic dataset the protein S100-A8 was found to be upregulated in human podocytes in response to Shiga toxin; suggesting that NLRP3 activation may occur in podocytes as a result of Shiga toxin treatment. This observation builds upon already published work that has reported activation of NLRP3 in a variety of acute and chronic kidney disease models including ischaemic-reperfusion injury, diabetic nephropathy and crystal-induced fibrosis [277]. Of particular interest are recent research findings from Lee et al. demonstrating Gb3-dependent Shiga toxin endocytosis activates the NLRP3 inflammasome promoting release of IL-1B, caspase 1-dependent pyroptotic cell death and activation of caspase 8/3-dependent apoptosis in Shiga toxin treated THP-1 cells [278]. This group also showed that short hairpin RNA (siRNA) knockdown of NLRP3 in THP-1 cells treated with Shiga toxin led to abolition of apoptosis and pro-inflammatory cytokine release [278]. This suggests that the cellular mechanism through which Shiga toxin regulates the increase in production of pro-inflammatory cytokines is via the NLRP3 inflammasome pathway [278]. Thus, small molecule inhibitors targeting NLRP3 and other inflammasome pathways might prove to be potential therapeutic agents in the treatment of Shiga toxin associated HUS [276].

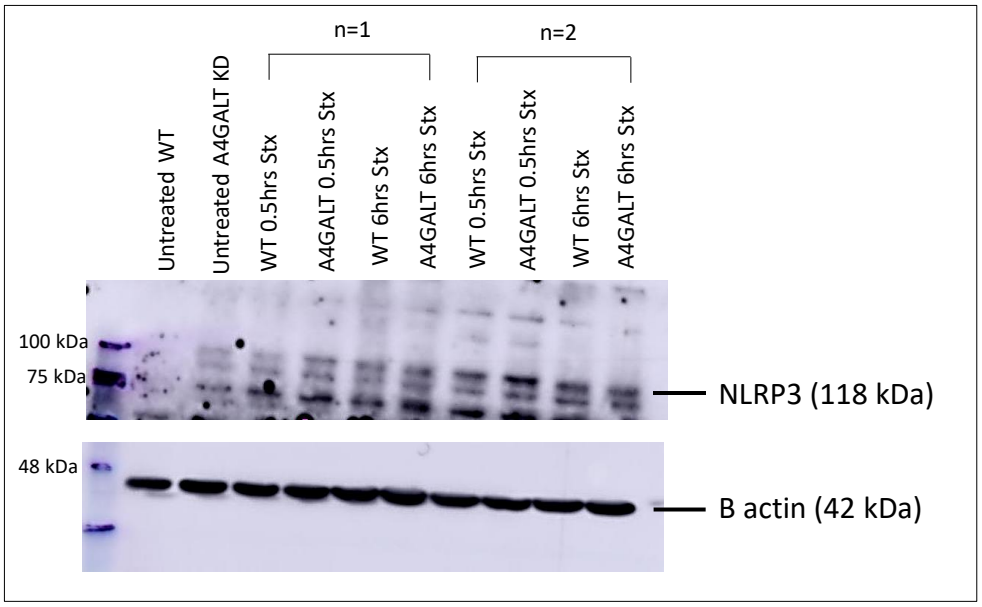

Figure 5-24: Western blot validation of NLRP3 activation in wild type podocytes treated with Shiga toxin

Western blotting for NLRP3 and β actin was performed on conditionally immortalised human podocyte protein lysate samples (both WT and A4GALT KD) incubated with 0.1ng/ml Shiga toxin for either 0.5 hr or 6 hrs as indicated. There was no statistically significant increase in the abundance of NLRP3 in wild type human podocytes treated with Shiga toxin vs. A4GALT knockdown podocytes. An n=2 is shown as indicated.

5.6.4 Decreased VEGF-A validation

IPA analysis of wild type human podocytes treated with Shiga toxin for 6 hours showed a reduction in VEGF-A in comparison to wild type human podocytes treated with Shiga toxin for 0.5 hours in my dataset. Given that it is already widely accepted that VEGF-A is critical in the regulation of angiogenesis and vascular permeability in the glomerulus this was a particularly interesting finding and one that I decided to pursue [25]. Work in recent years from Quaggin et al. has confirmed that the podocyte is the main source of VEGF-A in the glomerulus and that the glomerular endothelium is dependent upon tight regulation of VEGF signalling to function physiologically [25].

Indeed, in homozygous VEGF-A null mice lethal vascular defects are seen at 10 days of age and in mouse models of podocyte specific VEGF-A over-expression a collapsing glomerulopathy leading to end-stage renal failure occurs [214]. Of particular significance, is a seminal paper from Quaggin et al. in the New England Journal of Medicine in 2008, that reported podocyte specific VEGF-A deletion in mice resulted in a glomerular

thrombotic microangiopathy (TMA) [11]. This was presented alongside human data where cancer patients treated with the VEGF-A inhibitor bevacizumab also developed glomerular lesions consistent with TMA [11]. Hence, the finding that VEGF was reduced in human podocytes in response to Shiga toxin treatment warrants further investigation as this may prove to be important in the development of TMA in Shiga toxin HUS.

Initial work aiming to validate this finding from my proteomic dataset involved western blot analysis and immunofluorescence of human wild type podocytes treated with Shiga toxin for 0.5 and 6 hours. However, these methods failed to detect VEGF-A in my cells despite several attempts with various available commercial antibodies, different concentrations of these antibodies, and the use of various blocking agents. Published work to detect VEGF-A levels has utilised cytometric bead array analysis, ELISA and in-situ hybridisation [11][222]. Unfortunately, these techniques are difficult to employ in cell culture work. I also attempted to detect VEGF receptor 2 (VEGFR2) in human podocytes treated with Shiga toxin vs. untreated controls and normal human kidney tissue sections. VEGFR2 is the key receptor for VEGF-A as it mediates almost all of the known cellular response. Representative IF images of my attempts at detection of VEGFR2 in human podocytes and human kidney tissue are shown in Figure 5-25.

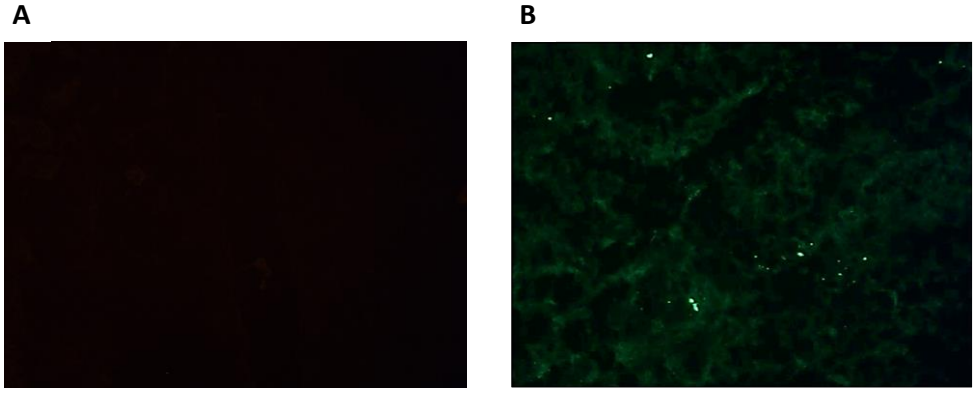

Figure 5-25: VEGFR2 immunofluorescence (x20 magnification)

Panel A shows immunofluorescence for VEGFR2 (green) in wild type, untreated human conditionally immortalised podocytes. No signal was detectable in these cells – representative image shown. Panel B shows a representative image of immunofluorescence for VEGFR2 (green) in human kidney tissue. No specific staining can be seen.

Attempts at VEGF-A ELISA on the supernatant from conditionally immortalised podocytes, glomerular endothelial cells and both cells co-cultured together in trans-well experiments have failed to detect a signal. This could be due to issues with the capture antibody, insufficient detector antibody or incorrect dilutions amongst other causes. However, the same ELISA for VEGF-A detection in plasma and urine samples from patients with Shiga toxin HUS enrolled in the ECUSTEC clinical trial (ISRCTN89553116) as well as controls performed in our laboratory have detected VEGF-A successfully. This suggests that levels of VEGF-A in cell culture may be somewhat less than those measured in patient samples or that culture conditions are influencing the detection of VEGF-A.

It is also possible that there may be no VEGF-A present in the supernatant from my cell culture experiments. It is worth noting that patient plasma samples will not reflect local VEGF-A in the glomerulus but rather systemic VEGF-A levels and so it is difficult to draw conclusions from these data. Urine samples are also difficult to interpret without normalisation to protein or albumin excretion given the effects of renal tubular secretion and uptake. Of note, most patients with Shiga toxin HUS become oligoanuric which will inevitably have an effect on the information that can be obtained from urine analysis in patients vs. controls [1]. Preliminary results from VEGF-A ELISA of patient and control plasma and urine are shown in Figure 5-26. This provides confirmation that the ELISA is able to detect VEGF-A when present.

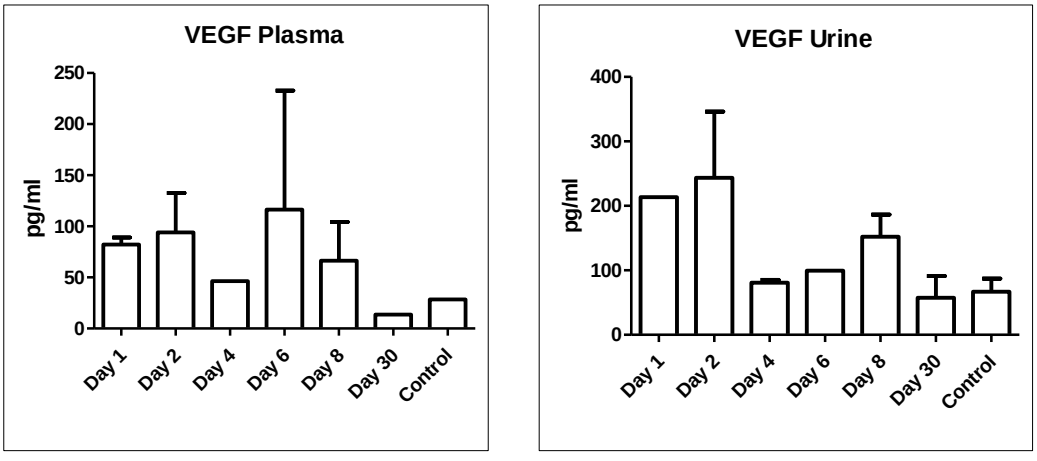

Figure 5-26: VEGF-A ELISA in patient samples preliminary ECUSTEC trial data

Shiga toxin HUS patient plasma and urine samples vs. healthy controls taken during the ongoing ECUSTEC clinical trial were analysed for VEGF-A concentration using an R&D® systems Human Quantikine ELISA kit. VEGF-A plasma levels that are considered normal are in the range of 100pg/ml

and normal VEGF-A levels for urine are 30pg/ml. Samples taken on day of presentation to secondary care (Day 1) and consecutive days thereafter. N=2 for each sample taken so no statistical analysis performed. Difficult to draw any conclusion form these data but they do demonstrate that the ELISA can detect VEGF-A. *Samples processed and analysed as part of the ECUSTEC trial by Dr Louise Farmer in our laboratory (data reproduced with permission).*

DIG-labelled in situ hybridisation is a highly sensitive and specific method that can be used to detect VEGF-A in kidney tissue sections. This technique was performed in my experimental mouse model of Shiga toxin HUS using an RNA probe kindly gifted from Professor Quaggin's laboratory (for full details of the in situ hybridisation protocol please see my methods chapter). Briefly, fresh frozen kidney sections from PodrtTA-Tet-O-Gb3 Gb3 null mice and PodrtTA-Tet-O-WT Gb3 null control mice (both of which had been given intraperitoneal Shiga toxin 10 days prior to elective termination) were assessed for expression of VEGF-A in their glomeruli. This involved the use of a VEGF-A RNA probe labelled with digoxigenin. This system utilises digoxigenin (a steroid isolated from digitalis plants) that are the only known source of digoxigenin in nature. Thus, anti-DIG antibodies will not bind to any other biological material in the experimental sample ensuring specificity of the technique. Due to this high sensitivity only a small volume of the specimen is required which is particularly well suited to nucleic acid hybridization methods [279]. Detection of the DIG-labelled probe is by anti-DIG antibodies coupled to alkaline phosphatase which will precipitate when they come into contact with BM purple solution. This purple colour can be visualised under light microscopy.

In situ hybridisation for VEGF-A in the PodrtTA-Tet-O-Gb3 Gb3 null mice given Shiga toxin showed a reduction in detectable signal compared to PodrtTA-Tet-O-WT Gb3 null control mice (Figure 5-27). This is evidence that in my mouse model of Shiga toxin HUS there was a reduction in VEGF-A, which is consistent with the IPA analysis of my proteomic experiment in human conditionally immortalised podocytes. Further work is needed to confirm this observation, through the optimisation of the VEGF-A ELISA in human cell culture work (e.g. by repeating VEGF-A ELISA experiments to include a known positive control such as patient plasma); as well as further in situ experiments in fresh frozen kidney sections from my Shiga toxin HUS mouse model.

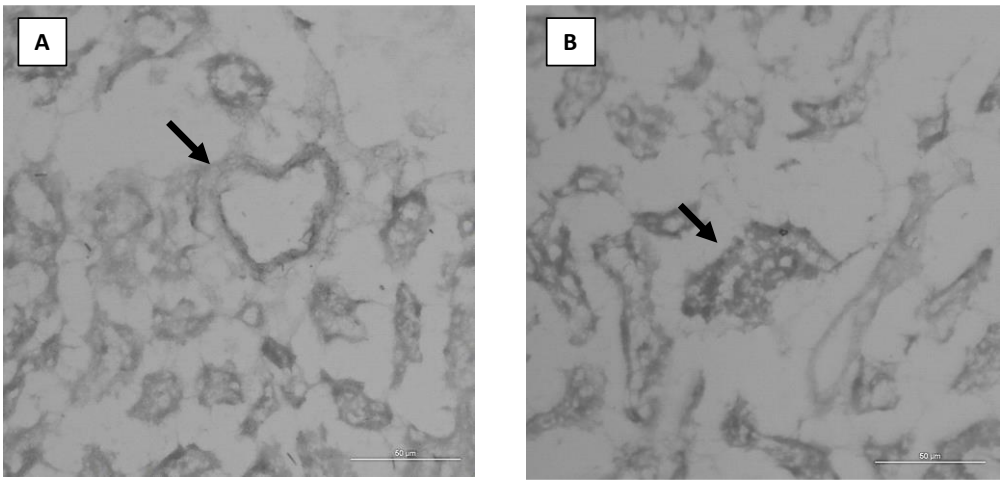

Figure 5-27: VEGF-A in situ hybridisation

In situ hybridisation using a DIG labelled VEGF-A RNA probe was performed in fresh frozen kidney tissue sections from PodrtTA-Tet-O-Gb3 Gb3 null mice given IP Shiga toxin (Panel A) vs. PodrtTA-Tet-O-WT Gb3 null control mice also given Shiga toxin (Panel B). Mice were electively terminated at Day 10 and kidneys harvested for analysis. In situ hybridisation showed a lack of VEGF-A positive staining in the glomeruli of PodrtTA-Tet-O-Gb3 Gb3 null mice vs. controls. This supports my proteomic dataset IPA work, confirming a reduction in VEGF-A in a mouse model of Shiga toxin HUS. In situ performed on an n=3 of each genotype and representative images shown.

5.7 Discussion

The aim of proteomic analysis is to identify and quantify the relative abundance of thousands of proteins and post-translational modifications in a cell or tissue [280]. These changes are then correlated to the biological processes occurring in the cell in response to an experimental stimulus [281]. Through LC-MS/MS analysis, I have been able to investigate the possible glomerular mechanisms underlying the action of Shiga toxin HUS. Using this unbiased and rigorous method, several novel pathways have been identified in human conditionally immortalised podocytes treated with Shiga toxin. Most notably, ER stress pathways and inflammasome proteins which were activated by Shiga toxin; and actin cytoskeleton, cell assembly proteins and VEGF-A signalling which were decreased by Shiga toxin. This is the first time that these pathways have been shown to change in the human podocyte in response to Shiga toxin treatment. Further investigation into how these processes interact to result in Shiga toxin HUS in patients is warranted, with the intention of identifying any potential targets amenable to pharmacological intervention in the treatment of the disease.

Unfortunately, western blot analysis for NLRP3 inflammasome activation and ER stress marker expression in wild type human podocytes treated with Shiga toxin was not able to validate the findings from my proteomic dataset. There may be several reasons for this which include: the specificity of the antibodies used, protein to protein interactions within the sample lysate, the blocking agent used to prevent non-specific binding and the antibody concentration used. All of these factors can contribute to the appearance of multiple protein band detection on the membrane (as evident in Figure 5-24) where no statistically significant changes in NLRP3 protein expression could be detected. In contrast, western blot analysis of ER stress markers (ATF6, pIRE and GRP78) did show a trend towards increased activation in the wild type podocytes treated with Shiga toxin at both 2 and 4 hours. However, this failed to reach statistical significance most likely due to a slightly raised level of baseline ER stress activation observed in several of the untreated wild type control podocyte lysate samples. This caused a reduction in the overall measurable effect of Shiga toxin treatment in these cells. The observation that CHOP driven apoptosis increased in wild type podocytes treated with Shiga toxin suggests that ER stress responses are activated in these cells. Therefore, future work to repeat these experiments alongside the appropriate controls is required to further validate these pathways in podocytes.

It must also be highlighted that major challenges exist in the interpretation of proteomic research. These have already been discussed in detail in this chapter and include: ensuring reproducibility of experimental results, careful statistical analysis using an appropriate FDR cut off, meticulous selection of reliable databases to facilitate identification of peptide and phospho-peptide sequences, appropriate normalisation and avoidance of type 1 error using a Benjamini Hochberg correction for multivariate analysis [270][280]. The expertise of the University of Bristol Proteomics Facility and bioinformatic service from Dr Phil Lewis, has been crucial to ensuring that this proteomic analysis is of high quality and representative of the biological response in the podocyte to Shiga toxin treatment. Given the large number of proteins and phospho-peptides identified in my dataset, there remains plenty of scope for further analysis and investigation of the effects of Shiga toxin on the human podocyte. Future work will involve exploration of whether the key pathways already identified are altered *in vivo* using my PodrtTA-Tet-O-Gb3 Gb3 null mouse model. I have already started this work for VEGF-A, but as discussed this requires further investigation.

Finally, it must also be acknowledged that *in vitro* cell culture work is not without limitation. This is particularly the case when studying the glomerular cells of the kidney where the interaction between podocytes and glomerular endothelial cells cannot be overlooked. Studying one cell type in isolation will not be representative of what is occurring physiologically *in vivo* at the glomerular filtration barrier. To overcome this issue, we have performed experiments involving co-culture of human conditionally immortalised podocytes and glomerular endothelial cells with some very interesting results (these are presented in later chapters of my thesis). Studies into the effects of Shiga toxin on 3D spheroids containing an outer podocyte layer and inner endothelial cell core are also in progress [282]. Regardless of these limitations, these proteomic experiments in human podocytes have provided a valuable starting point for determining the underlying cellular mechanisms that lead to Shiga toxin HUS in the glomerulus.

Chapter 6 : Generation of an A4GALT knockout mouse

6.1 Introduction

There are currently no rodent models that recapitulate Shiga toxin HUS in human disease. This represents a significant hurdle in improving our understanding of the mechanisms underlying the condition [33]. Wild type mice given intraperitoneal Shiga toxin do not develop TMA; the pathognomonic histopathological lesion seen in Shiga toxin HUS in humans. Rather, these mice die within a few days from off-target extra glomerular effects. This difference is due to species variation in kidney cellular Gb3 expression [1]. Mice express Gb3 predominantly in their renal tubules. However, humans (as well as baboons whose renal physiology more closely resembles that of Homo sapiens) express Gb3 predominantly in their glomeruli; specifically, in the glomerular endothelium and podocytes [33]. A key aim of my PhD was to investigate whether Shiga toxin can act via the Gb3 receptor in podocytes to cause HUS. In order to explore this, I needed to breed a mouse that only expresses Gb3 in the podocyte cells of the kidney. The first step in achieving this aim was to generate an A4GALT knockout (KO) mouse.

6.2 Gb3 expression *in vivo*

I have confirmed Gb3 expression in the renal tubules of wild type mice using immunofluorescence in wild type mouse kidney sections (Figure 6-1). The expression of Gb3 in different organs in the wild type mouse at different ages has been reported. This is in the context of studies in the Fabry's mouse (a Gb3 over-expressing mouse). Of note, the kidney has the greatest expression of Gb3 in the wild type mouse (Table 11) [242].

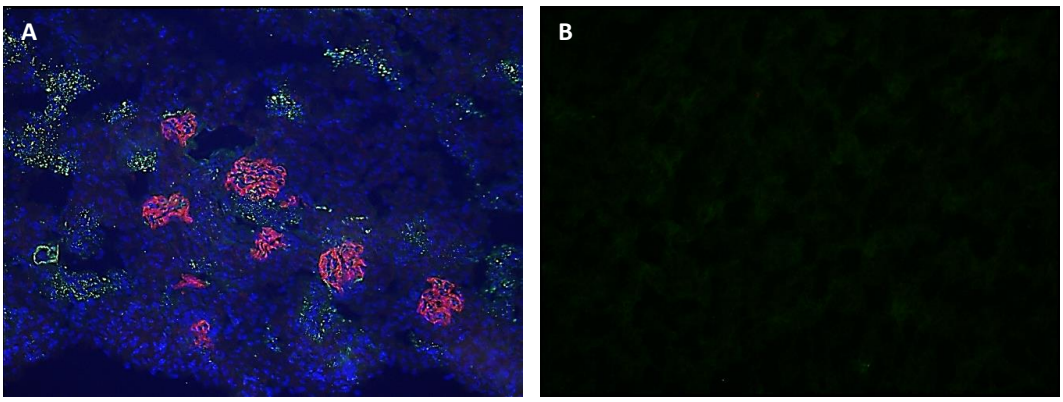

Figure 6-1: IF detection of Gb3 in wild type mouse kidney tissue x20

Fresh frozen kidney sections from wild type mice were prepared for IF as described and probed for Gb3 (green); nephrin (red – to identify podocytes outlining the glomeruli) and DAPI stained to identify nuclei (blue). Panel A shows Gb3 is located in the tubules of murine kidney and is absent from the glomeruli. The section in Panel B was prepared in the same way as Panel A, but without a primary antibody for Gb3/nephrin as an auto-fluorescence control for the secondary antibody.

		Gb_3 levels, nmol/mg protein					
Weeks	Group of mice	Liver	Kidney	Heart	Spleen	Lung	SI
4	Wild type	0.04 ± 0.0	1.03 ± 0.5	0.13 ± 0.1	0.0 ± 0.0	0.68 ± 0.0	0.21 ± 0.1
	Noninjected Fabry	3.06 ± 0.7	8.41 ± 1.5	0.85 ± 0.1	3.85 ± 0.5	4.36 ± 0.9	8.91 ± 2.7
	Injected Fabry	1.95 ± 0.5*	4.92 ± 0.4*	0.72 ± 0.1*	2.96 ± 0.2*	4.2 ± 0.2*	9.29 ± 0.7*
8	Wild type	0.15 ± 0.1	0.78 ± 0.3	0.09 ± 0.0	0.45 ± 0.0	0.33 ± 0.1	0.22 ± 0.1
	Noninjected Fabry	4.18 ± 1.2	12.7 ± 5.8	1.65 ± 0.2	9.43 ± 1.3	1.75 ± 0.6	20.1 ± 7.1
	Injected Fabry	0.21 ± 0.1*	1.52 ± 0.6*	0.22 ± 0.0†	0.55 ± 0.2†	1.23 ± 0.3*	9.01 ± 0.9*
12	Wild type	0.04 ± 0.0	0.84 ± 0.6	0.0 ± 0.0	0.47 ± 0.1	0.0 ± 0.0	0.14 ± 0.0
	Noninjected Fabry	3.06 ± 0.1	6.52 ± 1.7	0.84 ± 0.3	15.9 ± 6.6	3.37 ± 0.8	14.9 ± 1.4
	Injected Fabry	0.04 ± 0.0†	1.31 ± 0.5†	0.43 ± 0.0*	1.08 ± 0.2*	1.75 ± 0.7	8.99 ± 2.9*
24	Wild type	0.08 ± 0.0	2.31 ± 1.1	0.02 ± 0.0	0.31 ± 0.0	0.18 ± 0.0	0.39 ± 0.1
	Noninjected Fabry	4.18 ± 1.2	12.4 ± 1.2	2.24 ± 0.4	49.7 ± 10	4.85 ± 1.8	23.8 ± 4.9
	Injected Fabry	0.34 ± 0.1*	5.02 ± 2.5†	0.0 ± 0.0†	0.72 ± 0.1†	0.6 ± 0.2*	7.97 ± 2.6†

Weeks after injection of the vector are shown in the left column. Mean Gb_3 ± SEM is shown for four mice at each time point. SI, small intestine.
*$P < 0.05$ vs. noninjected Fabry mice.
†$P < 0.01$.

Table 11: Wild type mouse tissue expression of Gb3

At all stages (weeks 4-24 circled in red) mice express the most Gb3 in the kidney. This table has been taken from Park et. al who were investigating the use of adenovirus injections to correct over expression of Gb3 in the Fabry's mouse model (for our purpose the table is of relevance only for the wild type mouse – in which the kidney is the organ with the highest expression of Gb3). The amount of Gb3 has been quantified using mass spectrometry and normalised for total protein content of the organ [242].

6.3 Generation of a A4GALT knockout mouse

In 2006, Okuda et al. demonstrated that the Gb3 receptor is the receptor for Shiga toxin *in vivo* by generating a Gb3 total body knockout mouse which was resistant to intraperitoneal Shiga toxin [75]. These mice do not appear to have an obvious phenotype, other than verotoxin resistance [77]. However, a number of studies have suggested that Gb3 may be important in B cell differentiation (as it is expressed by a subset of immature B cells) [75]. Consequently, Okuda et al. performed immunological profiling of the Gb3 null mouse which showed that the number of thymocytes, spleen cells, immunoglobulin levels and ratios of lymphocytes and T cell subsets were no different to that of wild type mice of the same age (Figure 6-2) [75].

Lymphocyte populations and serum antibody levels in Gb3 null mutant mice

All analyses were carried out with 4-week-old female mice ($n = 3$). No significant differences between wild-type and Gb3 null mutant mice were found.

Organ	Genotype	
	+/+	−/−
Spleen		
No. of cells ($\times 10^8$)	0.96 ± 0.1	1.07 ± 0.11
Population (%)		
$B220^+$	38.42 ± 5.98	38.16 ± 4.12
$CD3^+$	32.10 ± 3.45	32.00 ± 1.88
$CD4^+$	21.09 ± 4.69	23.92 ± 4.86
$CD8^+$	12.28 ± 2.8	11.41 ± 0.37
Thymus		
No. of cells ($\times 10^8$)	1.60 ± 0.08	1.58 ± 0.2
Population (%)		
$CD4^+$	7.72 ± 1.08	7.15 ± 1.15
$CD8^+$	2.69 ± 0.24	2.64 ± 1.43
$CD4^+$ $CD8^+$	83.57 ± 1.32	86.92 ± 1.17
$CD4^-$ $CD8^-$	6.72 ± 0.87	4.80 ± 1.79
Serum Igs (mg/ml)		
IgG	9.81 ± 0.66	7.81 ± 0.57
IgM	0.098 ± 0.02	0.097 ± 0.01
IgA	0.81 ± 0.04	0.83 ± 0.03

Figure 6-2: Lymphocyte populations and serum antibody levels in Gb3 null mice vs. WT mice

No significant difference was observed between wild type mice and Gb3 null mice. Table taken from *Okuda et. al.* [75]

A4GALT knockout mice were generated as detailed in my *in vivo* methods chapter and transferred to the animal facility within the renal unit. They were age-matched with littermate control wild type mice. Genotyping was performed by MRC Harwell, but I repeated this prior to use in any experiments using PCR. Genotyping was performed with 2 different sets of primers (see appendix); use of the Tm1b primer pairs confirmed A4GALT knockout (Figure 6-3).

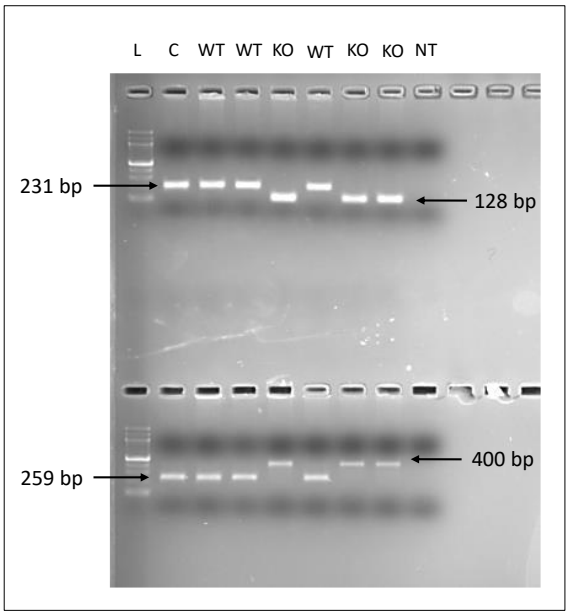

Figure 6-3: Genotyping WT vs. A4GALT KO mice

L= DNA ladder, C = wild type mouse from another background (used as a positive control), WT = littermate wild type control mice, KO = A4GALT KO mouse, NT = non-template control. Endpoint PCR was performed using both Tm1a and Tm1b primers (see appendix). Tm1a primers: WT band expected at 231 base pairs (bp) and A4GALT KO expected at 128 bp as shown in the top panel; Tm1b primers: WT band expected at 259 base pairs (bp) and A4GALT KO expected at 400 bp as shown in the bottom panel.

6.4 A4GALT knockout mice do not express Gb3

Using the Gb3 detection methods optimised *in vitro*, I confirmed that A4GALT knockdown mice do not express Gb3 their tissues. The first method used was immunofluorescence of fresh frozen kidney sections (Figure 6-4 and Figure 6-5). The second method used was endpoint PCR for Gb3 synthase mRNA (Figure 6-6). Given that wild type mice have the highest expression of Gb3 in their kidney tissue demonstrated by Park et al [242]; kidney tissue was also sent to the translational mass spectrometry department at UCL for analysis of Gb3 content. The results of the mass spectrometry analysis further confirmed that A4GALT KO had been achieved at a lipid level. i.e. knockout of Gb3 synthase resulted in a reduction in the key biologically active Gb3 isoforms (C24 and C24-1) in the mouse model (Table 12).

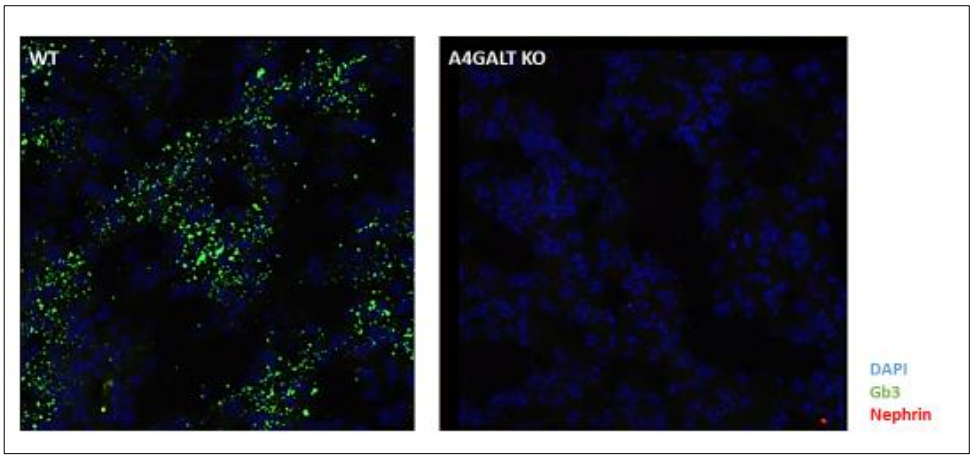

Figure 6-4: A4GALT knockout mice do not express Gb3: kidney sections renal tubules (x20)

Immunofluorescence of fresh frozen kidney sections from WT (wild type) mice and A4GALT KO (Gb3 null). The renal tubules of WT mice show expression of Gb3 (green) and A4GALT KO mice show no evidence of Gb3 expression (green). DAPI – blue, Nephrin – red. Isotype controls (not shown) confirm that Gb3 staining is specific. Images representative of n=3.

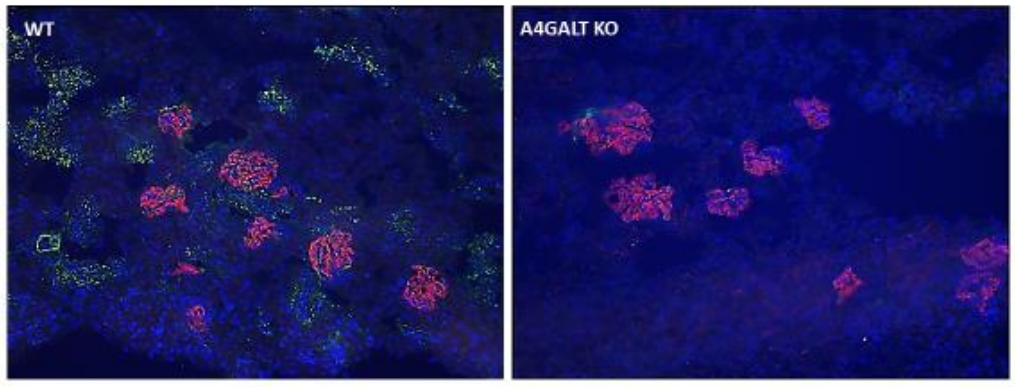

Figure 6-5: A4GALT knockout mice do not express Gb3: kidney sections with glomeruli (x20)

Immunofluorescence of fresh frozen kidney tissue sections from WT (wild type) mice and A4GALT KO (Gb3 synthase knockout) mice. There is no evidence of Gb3 expression in the A4GALT KD mouse kidney. Gb3 - green, Nephrin – red, DAPI – blue. Isotype controls (not shown) confirm that Gb3 staining is specific. Images representative of n=3.

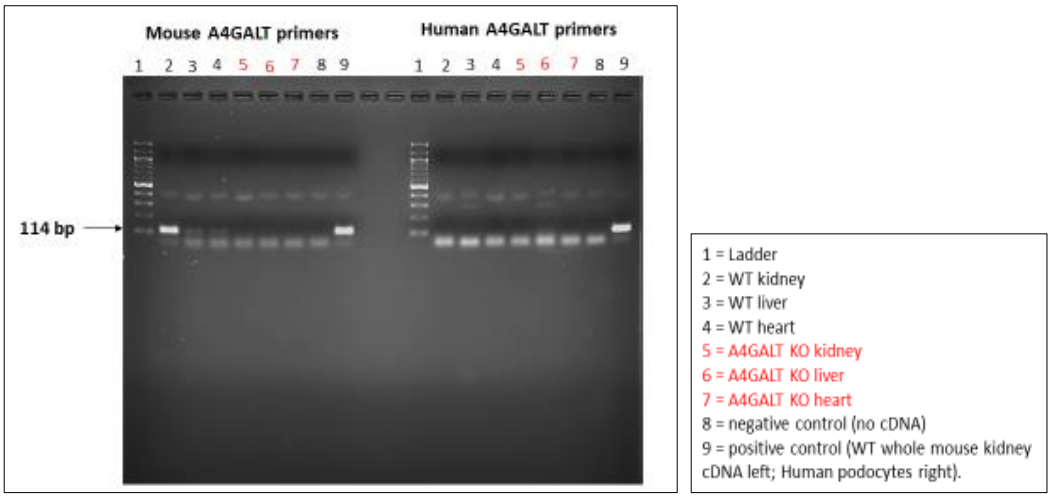

Figure 6-6: Endpoint PCR for A4GALT mRNA in WT vs. A4GALT KO mice

Mouse kidney, liver and heart tissue were analysed in both WT and A4GALT KO mice for the presence of Gb3 synthase mRNA. Results for both mouse A4GALT synthase primers and human A4GALT synthase primers are shown. Tissues from the A4GALT KO mice (red) show no evidence of Gb3 synthase expression with absence of a detectable band at 114 base pairs (corresponding to Gb3 synthase mRNA product). Human A4GALT primers appear to be species specific as there is an absence of Gb3 synthase detection in all but the positive control (human podocytes). Representative results for n=3.

A

Mouse kidney tissue WT	
Chain length	**CTH µg/mg protein**
C16-CTH	0.0591
C18-CTH	0.1031
C20-CTH	0.0127
C22:1-CTH	0.0051
C22-CTH	0.0428
C24:2-CTH	0.0073
C24:1-CTH	0.0296
C24-CTH	0.0589
C24:2-OH-CTH	0.0027
C24:1-OH-CTH	0.0084
C24-OH-CTH	0.0314
C26-CTH	0.0014
	total CTH ug/mg protein = 0.3034

B

Mouse kidney tissue A4GALT KO	
Chain length	**CTH µg/mg protein**
C16-CTH	0.0381
C18-CTH	0.0978
C20-CTH	0.0006
C22:1-CTH	0.0000
C22-CTH	0.0022
C24:2-CTH	0.0010
C24:1-CTH	0.0000
C24-CTH	0.0032
C24:2-OH-CTH	0.0014
C24:1-OH-CTH	0.0020
C24-OH-CTH	0.0040
C26-CTH	0.0022
total CTH ug/mg protein =	0.1144

Table 12: Mass spectrometry analysis of WT mouse kidney vs. A4GALT KO kidney tissue

A WT mouse (A) and an A4GALT KO mouse of the same age were terminally anaesthetised via an IP injection of pentobarbital (50mg/kg). The kidneys were dissected, removed, and the tissue sent on dry ice to the TMSC at UCL for Gb3 (CTH) mass spectrometry analysis. The A4GALT KO mouse kidney contains considerably less total Gb3 than the WT mouse.

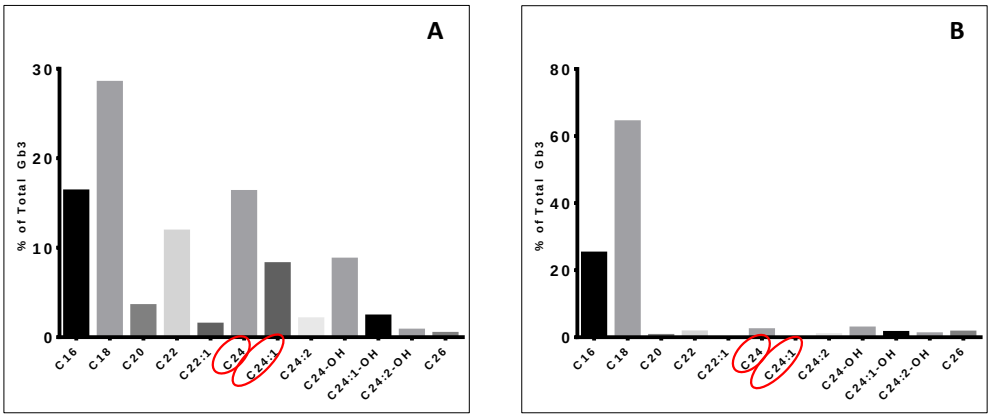

Figure 6-7: Mass spectrometry kidney profiles

The results from Table 12 (above) are graphically represented here. A = WT mouse Gb3 isoform content and B = A4GALT KO Gb3 isoform content. Of interest the C24 and C24-1 isoforms of Gb3 (circled in red) are significantly lower in the A4GALT KO mouse. These are known to be the key biologically active isoforms (as discussed in results chapter 4).

6.5 A4GALT knockout mice are resistant to Shiga toxin

Following confirmation that A4GALT KO mice showed no expression of Gb3 synthase in their tissues and lacked the key biologically active Gb3 isoform expression in their kidneys; whether this translated functionally into resistance to the lethal effects of Shiga toxin needed to be established. This would confirm the observation from Okuda et al. that Gb3 is the receptor for Shiga toxin *in vivo*. A4GALT KO mice together with age-matched WT controls (10-15 weeks of age) were given intraperitoneal Shiga toxin at a dose of 10ng/g. This dose is 40 times the LD50 dose (median dose required to kill half the population) [75]. The survival of the WT mice vs. A4GALT KO mice is shown in (Figure 6-8). All WT mice died within 5 days of Shiga toxin inoculation. Consistent with a Gb3 null phenotype, A4GALT KO mice were resistant to Shiga toxin and survived for 8 weeks following intraperitoneal Shiga toxin administration. They were electively culled under schedule 1 (via terminal IP pentobarbital anaesthesia) in order for their organs to be harvested at this timepoint for further investigation. They appeared well throughout the experimental period and gained weight as would be expected in healthy wild type mice.

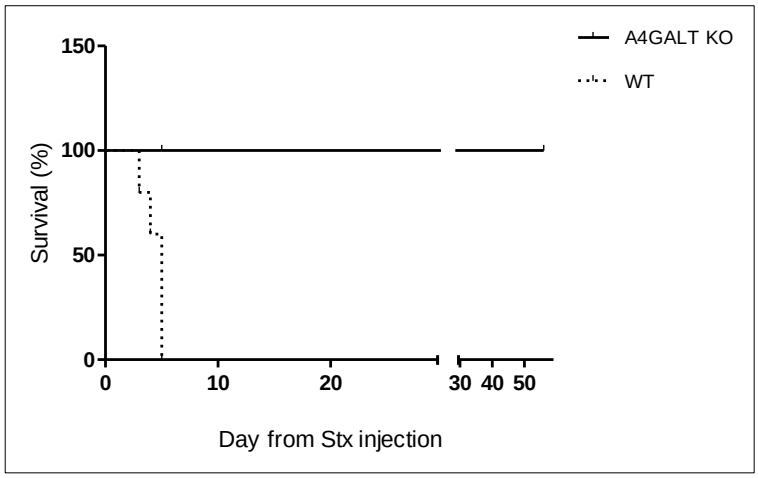

Figure 6-8: Kaplan-Meyer Survival Graph: WT mice vs. A4GALT KO mice administered 10ng/g Shiga toxin

All wild type (WT) mice died by day 5 following intraperitoneal Shiga toxin injection of 10ng/g. It is well established that there is some variation in WT mouse response to Shiga toxin *in vivo*: with variability in the time taken for the lethal effects of Shiga toxin taking between 3-5 days [75]. This reflects Shiga toxin potency, site of IP injection and hydration status of the mouse. In contrast all A4GALT KO mice survived for > 8 weeks following Shiga toxin challenge when they were culled under schedule 1 to allow tissue analysis. N=4 for each genotype.

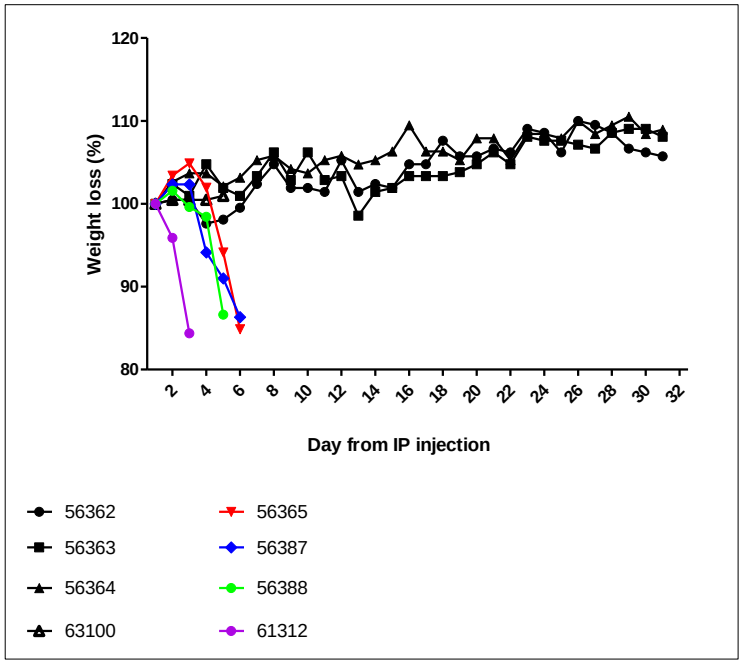

Figure 6-9: Weight chart of WT vs. A4GALT KO mice administered 10ng/g Shiga toxin

WT mice (shown in red, blue, and green) rapidly lost 15% of their body weight within days of Shiga toxin administration. A4GALT KO mice (black lines) show no evidence of weight loss and continue

to gain weight over the course of the weeks following Shiga toxin administration as would be expected in healthy mice. N=4 for each genotype.

6.5.1 A4GALT knockout mice are resistant to 100ng/g of Shiga toxin

Given that Gb3 null mice were resistant to 40 times LD50 dose of Shiga toxin, whether they remained resistant to its toxicity at 400 times the LD50 dose was tested (100ng/g). In-keeping with Okuda et al. the Gb3 null mice were resistant to 100ng/g of Shiga toxin administered by intraperitoneal injection (Figure 6-10). Again, they were culled by schedule 1 at 8 weeks following Shiga toxin administration to allow tissue analysis.

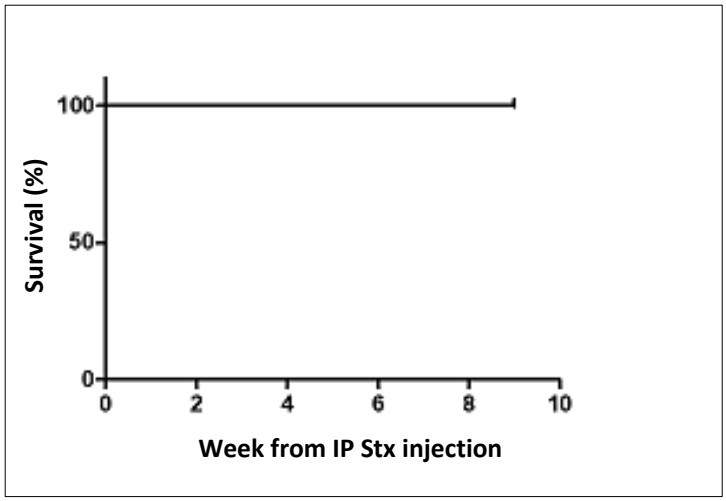

Figure 6-10: Kaplan Meyer survival graph for A4GALT KO mice following 100ng/g of Shiga toxin
A4GALT KO mice (n=2) were given 100ng/g Shiga toxin via intraperitoneal injection. All animals survived and showed no signs for concern until they were culled under schedule 1, at 8 weeks following Shiga toxin administration.

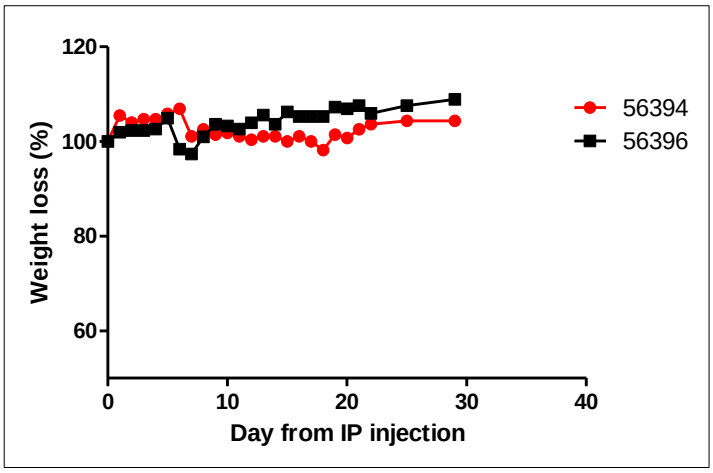

Figure 6-11: Weight chart for A4GALT KO mice following 100ng/g of Shiga toxin treatment

Both A4GALT KO mice (red and black lines – animal ID shown) showed evidence of weight gain over the 8 weeks following 100ng/g Shiga toxin challenge; indicating that they are unaffected by the toxic effects of Shiga toxin. Mice were culled under schedule 1 to allow examination of tissues.

6.5.2 A4GALT KO mice given intraperitoneal Shiga toxin do not develop renal failure or proteinuria

Blood samples were taken from all mice at the time of sacrifice and sent to the biochemistry department at Bristol Royal Infirmary for analysis. Unfortunately, the wild type mice given intraperitoneal Shiga toxin were very dehydrated at the time of terminal anaesthesia and under 100µl of blood could be obtained. This was an insufficient sample volume to be processed. However, one wild type mouse given intraperitoneal Shiga toxin was sacrificed at an earlier time point (3 days following Shiga toxin injection); prior to becoming visibly unwell and a blood sample analysed for creatinine. This result was 33µmol/L which is high; but as an isolated resulted not particularly useful, hence not included in my analysis. Serum creatinine samples taken from wild type mice and A4GALT KO mice at baseline (prior to any Shiga toxin challenge) were not statistically different. A4GALT KO mice given intraperitoneal Shiga toxin at 10ng/g and 100ng/g had no statistically significant difference in serum creatinine vs. baseline in both wild type mice and A4GALT KO mice (Figure 6-12).

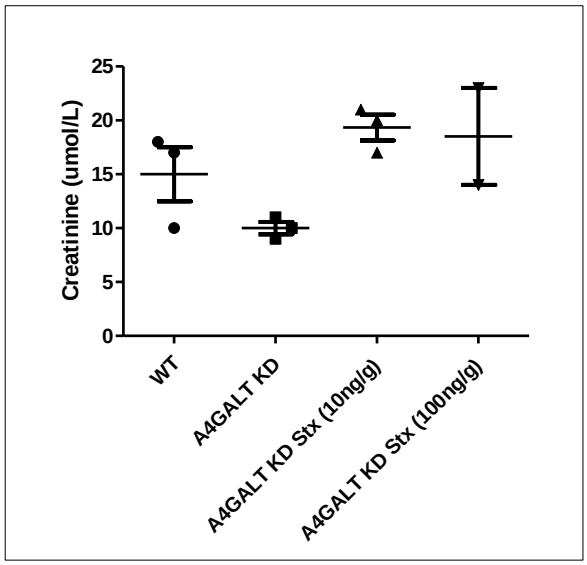

Figure 6-12: Comparison of serum creatinine WT mice vs. A4GALT KO mice

There was no statistically significant difference in serum creatinine values across all groups of mice: wild type at baseline prior to Shiga toxin administration (WT), A4GALT knockout mice at baseline (A4GALT KD), and the A4GALT KO mice given intraperitoneal Shiga toxin. n=3 in each group as shown by each data point. One way ANOVA performed comparing each group – no statistically significant difference observed.

Urine samples were collected from WT control mice, A4GALT KO mice, A4GALT KO mice after 10ng/g of Shiga toxin and A4GALT KO mice after 100ng/g of Shiga toxin treatment. Urine was collected prior to terminal anaesthesia and organ harvesting. Albumin: creatinine ratios were not statistically significant between the groups (Figure 6-13).

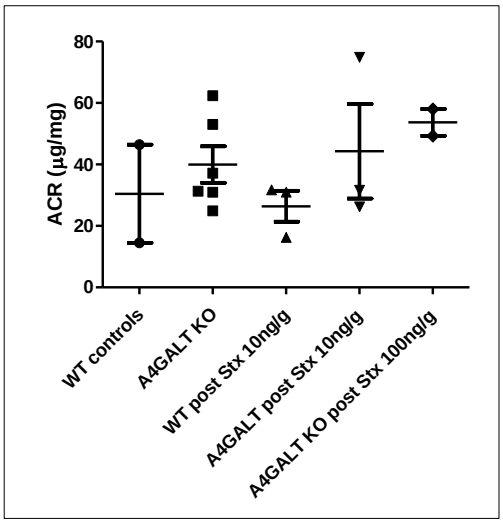

Figure 6-13: Urine albumin: creatinine ratio (ACR) is not elevated in A4GALT KO mice

Urine was collected from each of the 4 groups of mice prior to terminal anaesthesia and organ harvesting (n number indicated on the graph by each data point within each group). There was no significant difference in ACR between the groups tested. One way ANOVA: Tukey's multiple comparison test no significant difference between ACRs in each group.

6.5.3 Wild type mice show evidence of acute tubular necrosis following intraperitoneal Shiga toxin

Age-matched WT and A4GALT KO mice were given IP Shiga toxin at 10ng/g. As already described WT mice all required terminal anaesthesia by day 5 due to becoming visibly unwell; scoring a Bristol Animal Welfare Score >10 (See Appendix for details). A4GALT KO mice did not score above 0 and appeared well throughout the experiment. The A4GALT KO mice were terminally anaesthetised at 8-10 weeks and organs harvested. Mouse kidney sections were fixed in formalin at the time of dissection and paraffin embedded before being sectioned to 2-5µm thick. These were then PAS stained, to allow evaluation of renal tissue architecture. The kidneys of wild type mice showed evidence of acute tubular necrosis, with swollen oedematous tubules and areas of vacuolation. The A4GALT KO mice in contrast have no evidence of acute tubular necrosis (Figure 6-14).

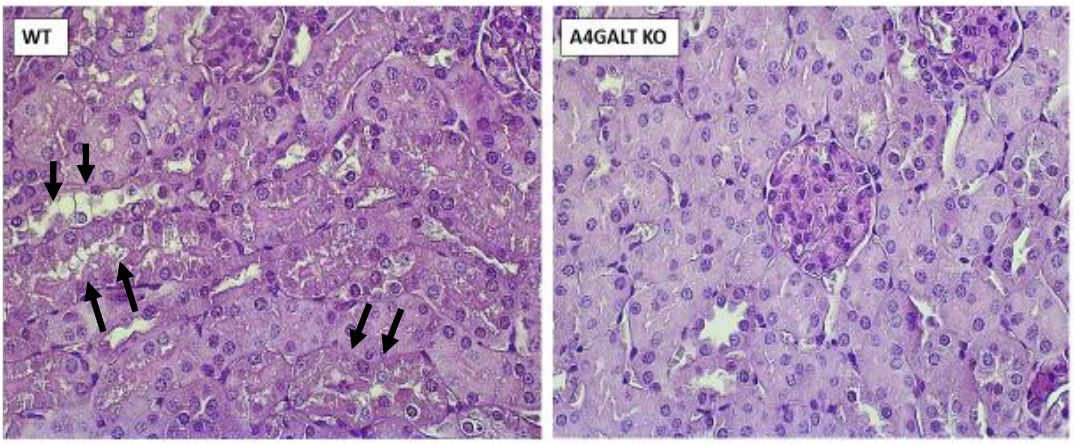

Figure 6-14: PAS stain of kidney tissue WT vs. A4GALT KO mice following 10ng/g Shiga toxin challenge (x40)

Renal tissue was fixed in formalin and paraffin embedded. Sections were cut at 2-5 µm thick and PAS (Periodic acid–Schiff–diastase) stained. Wild type (WT) mice show clear evidence of acute tubular necrosis (ATN) with oedematous tubules and vacuolations (as indicated by arrows). A4GALT KO mice show no changes in the tubular or glomerular morphology.

6.5.4 A4GALT KO mice show no evidence of renal damage on histology following intraperitoneal Shiga toxin

A4GALT KO mice given 100ng/g of intraperitoneal Shiga toxin were culled at 8 weeks post-injection and their kidneys fixed in formalin. Following paraffin embedding they were sectioned at 2-5µm thick and PAS stained as described. Representative images are shown below (Figure 6-15). There is no evidence of any renal tissue damage which is in-keeping with the serum creatinine results from these mice.

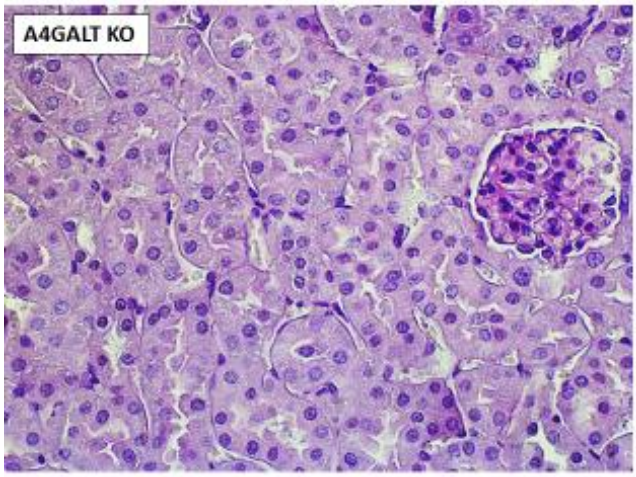

Figure 6-15: PAS stain of A4GALT KO kidney tissue following 100ng/g of intraperitoneal Shiga toxin (x40)

PAS stained renal tissue from A4GALT KO mice given 100ng/g of Shiga toxin shows normal tubular and glomerular morphology.

6.6 Generation of an inducible podocyte expressing Gb3 synthase mouse

The next step in developing a PodrtTA-Tet-OGb3 mouse on a Gb3 null background; was to breed an inducible podocyte expressing Gb3 synthase mouse on a WT background. This mouse will then be back crossed with the A4GALT KO mouse to generate a mouse that only expresses Gb3 in the podocyte (under doxycycline induction). An inducible model for Gb3 expression is required rather than a constitutive Gb3 over-expression mouse model because this mouse has a Fabry's disease phenotype.

Fabry's Disease is an X-linked lysosomal storage disorder where a deficiency in the α-galactosidase (α-GalA) enzyme results in accumulation of Gb3, lyso-Gb3 and galabiosylceramide in the kidney, brain and heart as well as biological fluids [249]. This causes acroparesthesia, hypohidrosis, angiokeratomas and psychosocial symptoms early on in the disease process. More advanced disease presents with cardiac abnormalities including arrhythmias and mitral valve disease along with progressive renal failure that eventually requires dialysis [249]. Interestingly, Fabry's mice (α-GalA–knockout mice) which over express Gb3 are resistant to the toxicity of Shiga toxin [90]. This may be due to saturation of the toxin with excess Gb3 receptor throughout the body which prevents the toxin reaching susceptible organs like the kidney. Or perhaps the Gb3 receptor itself

not being expressed on the cell surface in a functioning form preventing intracellular signalling [90].

PodrtTA-Tet-OGb3 mice (inducible podocyte expressing Gb3 synthase mice) were bred as described in my *in vivo* methods chapter at MRC Harwell and transferred to the animal unit in Bristol. These mice, together with littermate wild type controls were given either doxycycline in their drinking water for 14 days (to induce expression of Gb3 synthase in the podocyte) or standard drinking water and then sacrificed using terminal intraperitoneal anaesthesia. Tissues were harvested and assessed for expression of Gb3 using immunofluorescence and then imaged in the Wolfson Bioimaging Facility on confocal multi-laser Leica SP5II microscope. PodrtTA-Tet-OGb3 mice given doxycycline showed expression of Gb3 in their podocytes, evidenced by co-localisation with podocin (Figure 6-16 and Figure 6-17). Mice with the same genotype given standard drinking water showed no expression of Gb3 in their glomeruli. All mice were on a wild type background and therefore, expression of Gb3 was seen in their renal tubules.

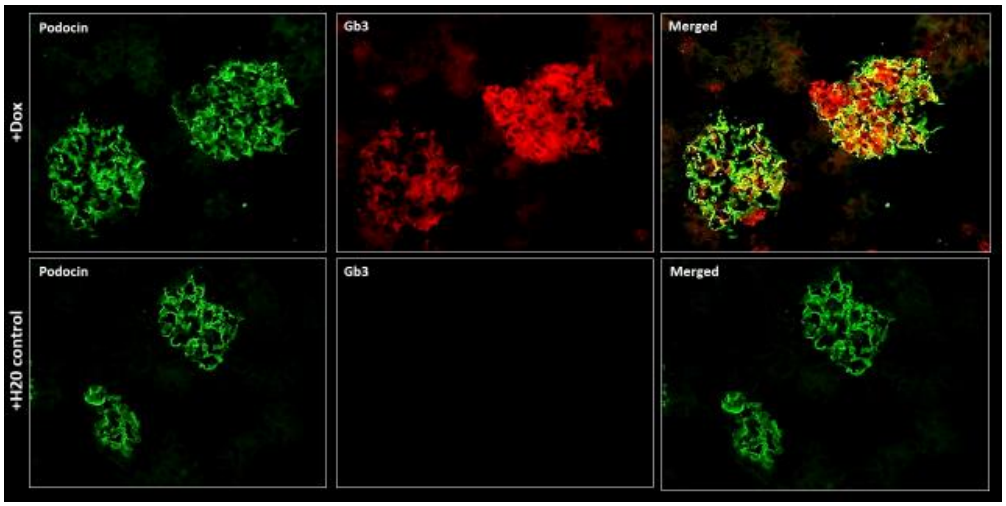

Figure 6-16: PodrtTA-Tet-O-Gb3 mice given doxycycline express Gb3 in their podocytes (x40)
Immunofluorescence of fresh frozen kidney tissue from PodrtTA-Tet-OGb3 mice given doxycycline or water for 14 days. Mice given doxycycline express Gb3 in their podocytes (evidenced by co-localisation with podocin: yellow). Mice with the same genotype given drinking water showed no expression of Gb3 in their glomeruli. Green – podocin, red – Gb3, yellow – co-localisation. Secondary antibody controls were used in isolation to confirm specificity of primary antibody – images not shown.

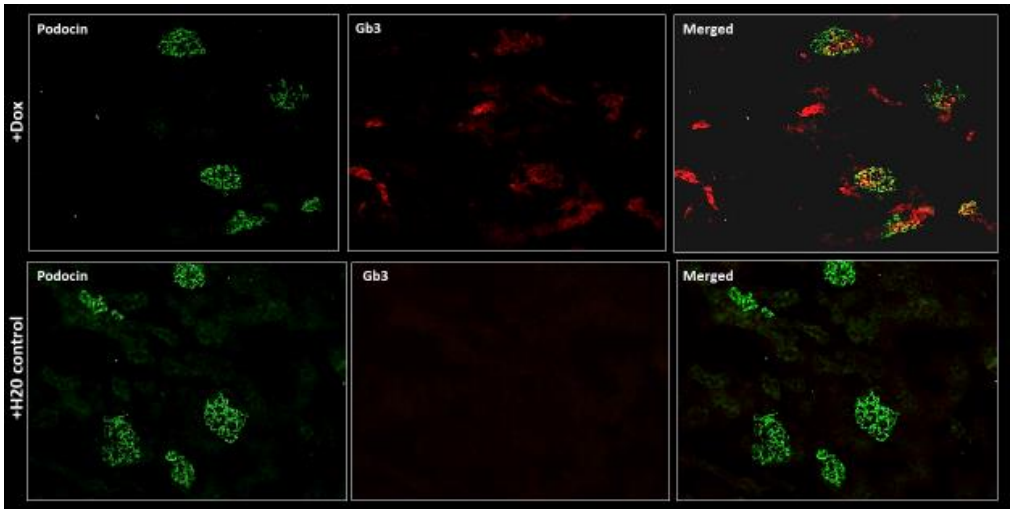

Figure 6-17: PodrtTA-Tet-O-Gb3 mice given doxycycline express Gb3 in their podocytes (x20)
Immunofluorescence of fresh frozen kidney tissue from PodrtTA-Tet-OGb3 mice given doxycycline or water for 14 days. Mice given doxycycline express Gb3 in their podocytes (evidenced by co-localisation with podocin: yellow). Mice with the same genotype given drinking water showed no expression of Gb3 in their glomeruli. Green – podocin, red – Gb3, yellow – co-localisation. Secondary antibody controls were used in isolation to confirm specificity of primary antibody – images not shown.

PodrtTA-TetO-Gb3 mice given doxycycline or standard drinking water, together with Gb3 KO mice and littermate wild type mice (WT) given standard drinking water; were culled after 14 days and a glomerular isolation using Dynabead extraction was performed. This was in an attempt to isolate the mRNA from glomeruli only to allow analysis for Gb3 synthase expression. Unfortunately, this technique is not free from contamination with renal tubular cells which in all mice (as all are on a wild type background) will express Gb3. However, quantitative real-time PCR using mouse Gb3 synthase primers did show higher expression of Gb3 synthase mRNA in the PodrtTA-TetO-Gb3 mice given doxycycline vs. standard drinking water (Figure 6-18).

This in combination with the Gb3 immunofluorescence results confirmed that the inducible model was working and not leaky. I was then happy to proceed with the next stage of the *in vivo* work: the crossing of the PodrtTA-Tet-O-Gb3 mouse with the A4GALT KO mouse; to generate an inducible podocyte specific Gb3 synthase mouse on a Gb3 null background. This mouse model will allow me to address one of my key research aims: that Shiga toxin acts via the podocyte Gb3 receptor to cause HUS.

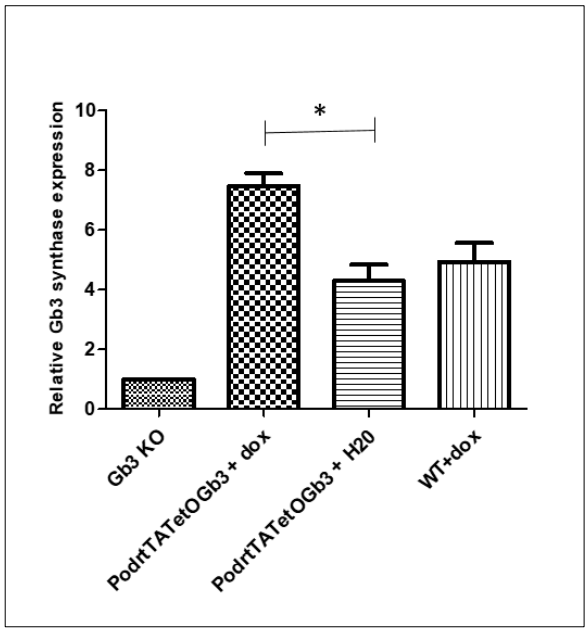

Figure 6-18: A4GALT mRNA expression in glomeruli normalised to Gb3 mice

Glomerular isolation using Dynabeads was performed on Gb3 KO, PodrtTA-TetO-Gb3 mice given doxycycline or drinking water and WT mice given doxycycline as indicated. The tissue was analysed by RT-PCR for Gb3 synthase mRNA expression. All results normalised to Gb3 KO animals (where Gb3 synthase expression was set as 1 for the purpose of relative expression – although these mice actually express no Gb3 synthase mRNA). There was a statistically significant difference between the relative expression of Gb3 synthase in PodrtTA-TetO-Gb3 mice given doxycycline vs. those given standard drinking water. *One way ANOVA performed with Tukey's multiple comparison test $p<0.05$.

6.6.1 PodrtTA-TetO-Gb3 mice on a WT background have no structural changes in their glomeruli

Previous PhD work by Dr Lindsay Keir in 2013, has already established that the PodrtTA-TetO-Gb3 mice (on a wild type background) have a normal renal histological appearance before and after doxycycline induction of Gb3 synthase so I have not repeated this work (Figure 6-19). Dr Keir also showed that urine protein: creatinine ratios in these mutant mice (irrespective of receiving doxycycline in their drinking water) was unchanged from baseline in age-matched control wild type animals (Figure 6-20).

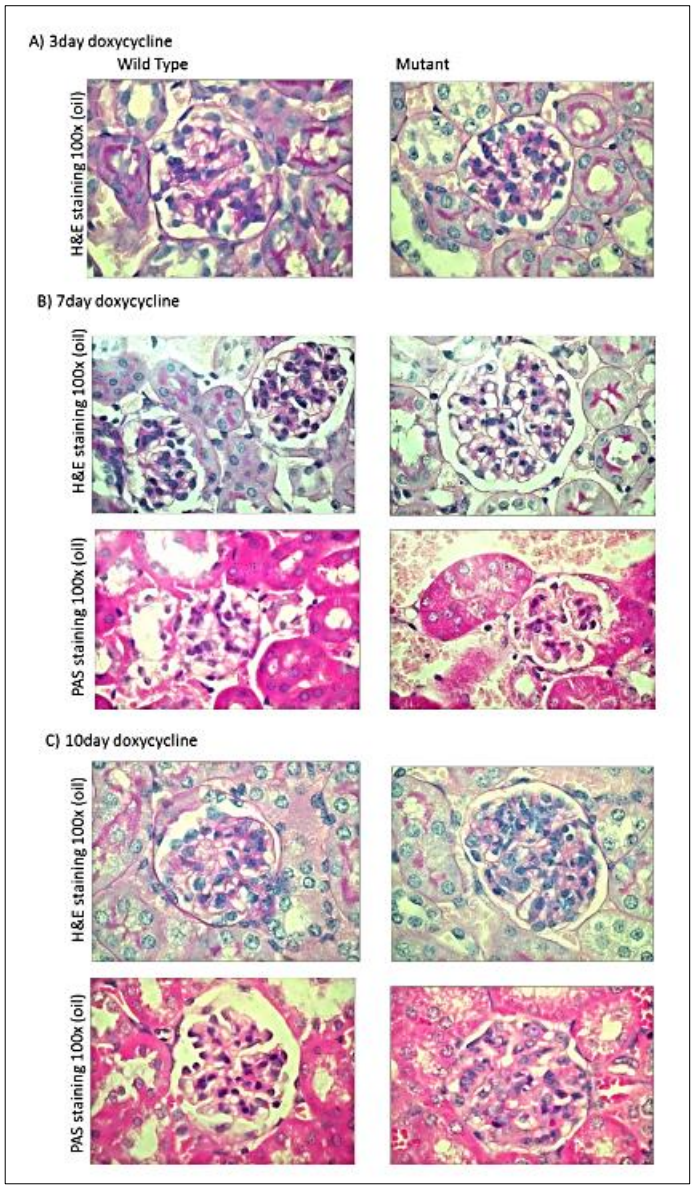

Figure 6-19: Renal histology in PodrtTA-Tet-O-Gb3 WT mice is unremarkable following Gb3 synthase induction in the podocyte

Pod rtTATet-O-Gb3 mice and WT litter mate controls were given doxycycline in their drinking for A=3 days, B=7 days and C=10 days to induce podocyte Gb3 synthase expression. The mice were then terminally anaesthetised with pentobarbitone and their kidneys harvested. After formalin fixation and paraffin embedding, sections were stained using haematoxylin and eosin (H&E) and periodic acid Schiff (PAS). There were no differences between the WT mice and mutants at all time points. *Work performed by Dr Lindsay Keir (data reproduced with permission).*

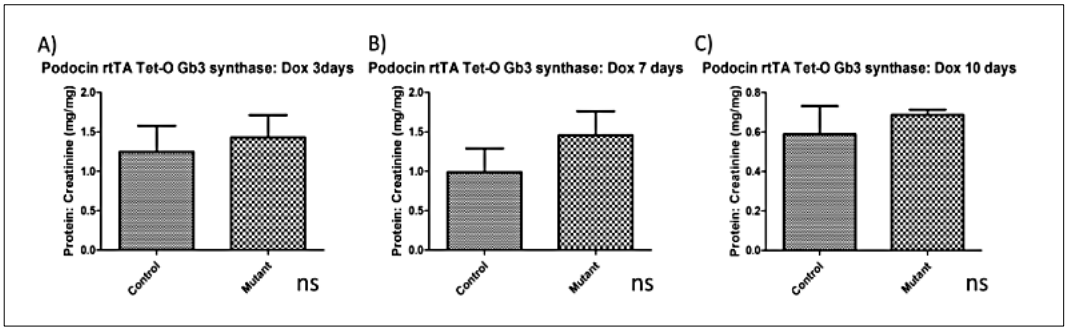

Figure 6-20: Urine protein: creatinine ratios in PodrtTA-Tet-O-Gb3 mice vs. WT controls

Urine was collected and analysed for urine protein: creatinine ratio in PodrtTA-Tet-O-Gb3 (mutant) mice and WT mice following A=3 days, B=7 days and C= 10 days of doxycycline drinking water treatment. There was no statistically significant difference between mutants and controls across all time points. *Work performed by Dr Lindsay Keir (data reproduced with permission).*

6.6.2 PodrtTA-TetO-Gb3 mice on a WT background given intraperitoneal Shiga toxin develop a TMA

PodrtTA-Tet-O-Gb3 mice on a wild type background aged 8-10 weeks were given intraperitoneal Shiga toxin at a dose of 10ng/g and monitored twice daily using the Bristol Animal Welfare Score. These mice required terminal anaesthesia with pentobarbitone within 24-48 hours following Shiga toxin challenge due to a score >10. Given that these mice express Gb3 in their podocytes and renal tubules this was not unexpected. The kidneys of these mice were harvested, and formalin fixed prior to paraffin embedding. Histological analysis using the trichrome martius scarlet blue stain demonstrated evidence of thrombi in their glomeruli (Figure 6-21). Age-matched control mice of the same genotype given intraperitoneal normal saline did not become unwell and had no evidence of TMA on histology. These lesions are in-keeping with a TMA; the histopathological hallmark of Shiga toxin HUS. This work was performed by Dr Keir and Fern Barrington prior to the start of my PhD.

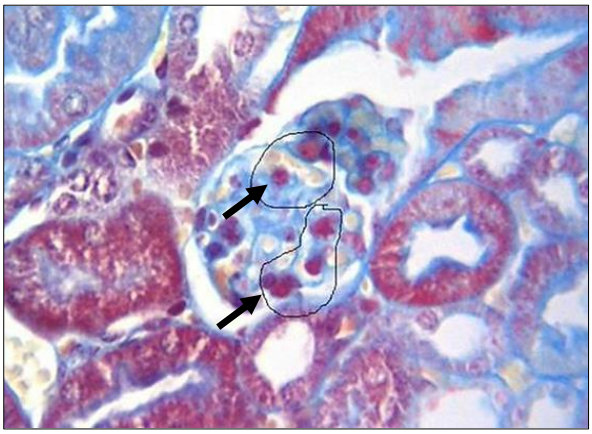

Figure 6-21: PodrtTA-Tet-O-Gb3 mice on a WT background develop a TMA following Shiga toxin challenge

Martius scarlet blue trichrome stain of renal tissue from a PodrtTA-TET-O-Gb3 mouse on a WT background following 10ng/g Shia toxin intraperitoneal injection. Fibrin thrombi are seen within the glomerular capillary loops indicated by black arrows. These appearances are characteristic of a glomerular TMA - the same histopathological lesion that is seen in humans with Shiga toxin HUS. *Work performed by Fern Barrington (data reproduced with permission).*

6.7 Discussion

This chapter has described the generation of two different mouse models. Using the Gb3 detection methods optimised under *in vitro* conditions, I have demonstrated that A4GALT KO mice do not express Gb3 synthase or the key biologically active Gb3 isoforms at a lipid level. Furthermore, these mice are resistant to the lethal effects of Shiga toxin, even at 400 times the LD50 dose (100ng/g). There can be no question that *in vivo* the receptor for Shiga toxin is Gb3 and that in the absence of this receptor mice are protected against Shiga toxin.

Of interest however, the A4GALT KO mice do express some isoforms of Gb3 as evidenced by the mass spectrometry results from the TMSC at UCL. This confirms what Dr Mills' group has already found; that not all Gb3 isoforms are biologically active *in vivo* in terms of Shiga toxin virulence. Indeed, similar findings were found in my A4GALT knockdown cell line *in vitro*. I have confirmed that A4GALT has been knocked out using the highly sensitive method of PCR. It seems counter-intuitive therefore, that any Gb3 is synthesized since A4GALT is the enzyme that catalyses this pathway. On review of the literature it is clear that glycosphingolipid biosynthesis is complex; and that there remains some

uncertainty as to the redundancy of the Gb3 synthase enzyme [249]. Indeed, the A3GALT2 enzyme catalyses the synthesis of iso-globo series and may account for the presence of Gb3 isoforms in the A4GALT KO mice [77].

The second mouse model studied is the inducible podocyte specific Gb3 synthase mouse. This mouse was generated using tetracycline controlled transcription activation of Gb3 synthase linked to a podocin promoter. In the presence of doxycycline, Gb3 is only induced in cells that possess the podocin promoter (i.e. podocytes). This is a closer representation of Gb3 expression in humans, who have the Gb3 receptor in both podocytes and glomerular endothelial cells. However, because Gb3 is expressed in the renal tubules of WT mice the PodrtTA-Tet-O-Gb3 mutants also have Gb3 in their renal tubules. Consequently, the PodrtTA-Tet-O-Gb3 mice died within 3-5 days following IP Shiga toxin challenge.

I have confirmed that the PodrtTA-Tet-O-Gb3 mice express the Gb3 receptor following 14 days of doxycycline treatment using immunofluorescence and real time PCR. It has also been established that these mice have no structural changes in their glomeruli or renal tubules following doxycycline induction. Furthermore, there was no significant increase in ACR in these mice vs. control mice. Particularly exciting was the observation that PodrtTA-Tet-O-Gb3 mice given IP Shiga toxin develop a glomerular TMA. This is the histopathological hallmark of HUS. Unfortunately, given the off target extra-glomerular effects of Shiga toxin in the renal tubules of the mutant mice I was unable to study the mechanisms behind these findings. As a result, the generation of a mouse that expresses Gb3 only in its podocyte is required; to eradicate the extra-glomerular effects and allow me to determine the role of the podocyte in the pathophysiology of Shiga toxin HUS.

Chapter 7 : Generation of an inducible podocyte specific Gb3 synthase mouse on a Gb3 null background

7.1 Introduction

In order to study the effects of Shiga toxin in the kidney *in vivo*, the lethal off-target extra glomerular effects in wild type mice needed to be eliminated and the Gb3 receptor present in glomerular cells. For the purpose of this PhD, specifically podocyte expression of Gb3 had to be induced. The previous chapter has described the generation and characterisation of the A4GALT total body KO mouse and the inducible PodrtTA-Tet-O-Gb3 mouse. By back crossing the PodrtTA-Tet-O-Gb3 mouse with the A4GALT KO mouse the PodrtTA-Tet-O-Gb3 Gb3 Null mouse was generated. This mouse only expresses Gb3 in its podocytes: breeding strategy shown in Figure 7-1.

The generation of an inducible podocyte specific Gb3 synthase mouse on a Gb3 null background results in temporal control over A4GALT gene expression providing invaluable insights into the role of the podocyte in the initiation of glomerular TMA. Should this mouse develop a HUS syndrome it will also allow investigation as to whether inhibition of the alternative complement pathway can prevent the process. This will enable testing of my hypothesis *in vivo* which is vital prior to any further translation into human studies and clinical application. To ensure that the minimum number of mice were used in each experiment whilst maintaining statistical significance; an intelligent breeding strategy was used as detailed in my *in vivo* methods chapter. All mice were genotyped at the MRC Harwell prior to use in any experiments. For details of genotyping reaction procedures see appendix.

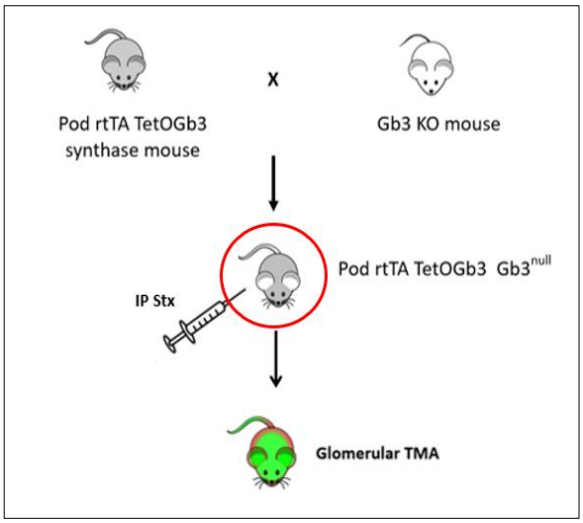

Figure 7-1: Breeding Strategy for PodrtTA-Tet-O-Gb3 Gb3 Null mice

PodrtTA-Tet-O-Gb3 mice were back-crossed over several generations with A4GALT KO mice to generate a PodrtTA-Tet-O-Gb3 Gb3 null mouse. This mouse only expresses Gb3 in the podocyte when induced with doxycycline. PodrtTA-Tet-O-Gb3 mice will then be given intraperitoneal (IP) Shiga toxin and evaluated for features of Shiga toxin HUS, including the development of a glomerular TMA.

7.2 Route of delivery of Shiga toxin

Before beginning this *in vivo* work, I had considered using the genetically modified Shiga toxin producing rodent pathogen *Citrobacter rodentium*. This was engineered by Mallick et al. as a novel murine infection model [119]. Prior to their work the only route of administration of Shiga toxin to the mouse was intraperitoneal; because oral administration of enterohaemorrhagic *E.coli* in mice does not lead to systemic illness [119]. This is an inferior route as in human disease transmission is oral. Shiga toxin is produced by *E.coli* bacteria that are ingested which cause attachment and effacement lesions in the intestinal epithelium. This leads to local inflammatory changes which progress over 7-10 days to HUS syndrome [1]. Mallick et al. describe using oral gavage to deliver the genetically modified *Citrobacter rodentium*, which resulted in attachment and effacement intestinal lesions as well as evidence of renal tubular damage on histology. No rise in serum creatinine was observed but blood urea nitrogen (BUN) was raised and oral inoculation with *Citrobacter rodentium* resulted in death of all mice 7-15 days post infection. Just as in previously described murine models of Shiga toxin HUS, infected mice showed no evidence of platelet aggregation, fibrin deposition, microcytic anaemia or

thrombocytopenia [119]. This observation is hardly surprising given that the C57BL/6 mice used in their experiment were WT mice and therefore only expressed the Shiga toxin receptor Gb3 in their renal tubules [119].

However, it was decided that genetically modified *Citrobacter rodentium* oral gavage would not be used in my experiments. This is because in the PodrtTA-Tet-O-Gb3 Gb3 null mouse model, mice require oral doxycycline to induce Gb3 receptor expression. Doxycycline administration began 14 days prior to Shiga toxin inoculation and continued throughout the experiment to ensure Gb3 synthase expression. This could potentially impact the potency of *Citrobacter rodentium*, reducing its toxicity and protecting the mice from Shiga toxin infection. As a result, intraperitoneal injection of Stx2 was used as an administration route. This method of delivery of Shiga toxin in mice is well established in published literature and oral doxycycline will not interfere with inoculation [1].

7.3 PodrtTA-Tet-O-Gb3 Gb3 null mice express Gb3 in their podocytes following doxycycline induction

PodrtTA-Tet-O-Gb3 mice on a Gb3 null background were given 14 days of oral doxycycline in their drinking water to induce A4GALT expression in the podocyte. Mice were then terminally anaesthetised using pentobarbital anaesthesia to allow organ harvest. Expression of A4GALT in the kidneys of these mice was confirmed using endpoint PCR (Figure 7-2) and expression of the Gb3 receptor was confirmed using immunofluorescence for Gb3 (Figure 7-3).

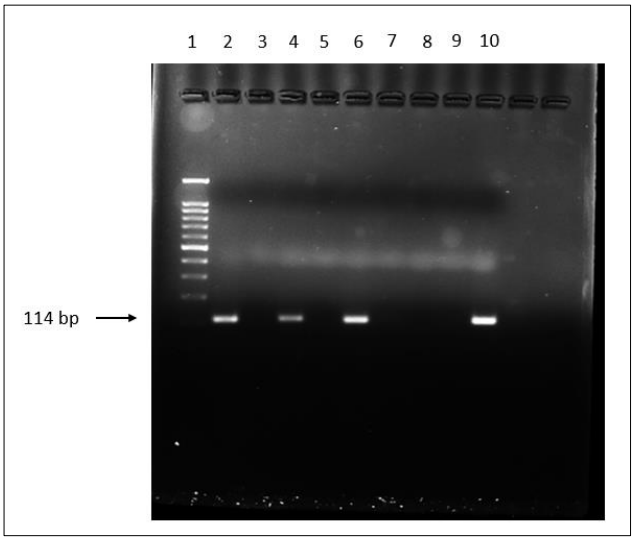

Key
1 = Ladder
2 = **Pod Gb3**
3 = PodrtTA-Tet-O-WT
4 = **Pod Gb3**
5 = PodrtTA-Tet-O-WT
6 = **Pod Gb3**
7 = PodrtTA-Tet-O-WT
8 = negative control (no cDNA)
9 = Gb3 Null control (negative control)
10 = **WT kidney** (positive control)

Figure 7-2: Endpoint PCR for Gb3 Synthase in PodrtTA-Tet-O-Gb3 Gb3 null mice vs. controls

Mouse kidney from PodrtTA-Tet-O-Gb3 Gb3 null mice (Pod Gb3) and PodrtTA-Tet-O-WT Gb3 null control mice (PodrtTA-Tet-O-WT) were analysed for Gb3 synthase expression following 14 days of doxycycline induction using endpoint PCR. As shown the Pod Gb3 mice express Gb3 synthase and the PodrtTA-Tet-O-WT mice do not. This is a highly sensitive method for detecting Gb3 synthase and confirms the phenotype of my experimental cohort. Results shown for n=3 of each genotype.

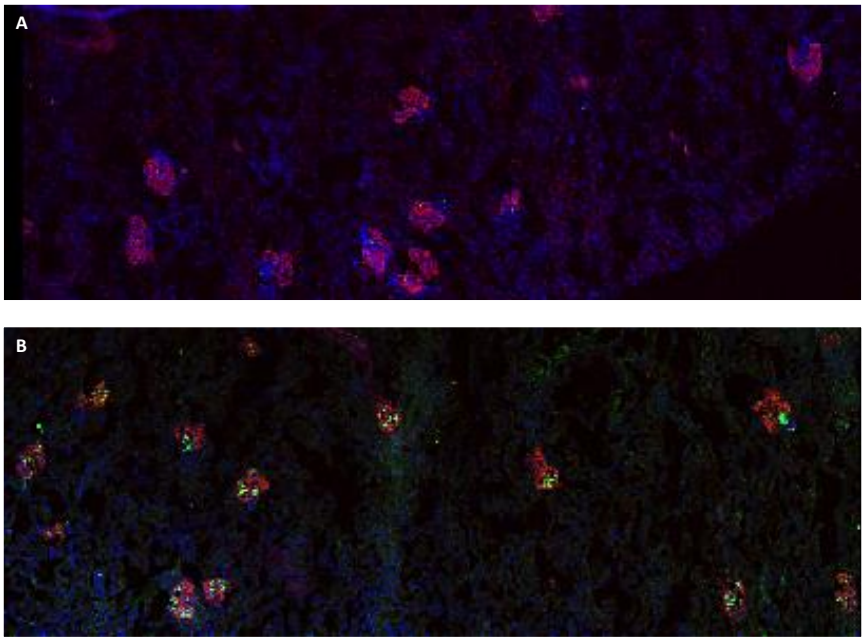

Figure 7-3: IF detection of Gb3 in PodrtTA-Tet-O-Gb3 Gb3 null mice vs. control kidney tissue x20

PodrtTA-Tet-O-WT Gb3 null mice (Panel A) and PodrtTA-Tet-O-Gb3 Gb3 null mice (Panel B) were given 14 days of doxycycline in their drinking water and then sacrificed to allow organ harvest. Renal tissue from PodrtTA-Tet-O-WT Gb3 null mice (Panel A) showed no evidence of Gb3 expression (green) whereas in PodrtTA-Tet-O-Gb3 Gb3 null mice (Panel B) Gb3 expression is seen in the glomeruli (nephrin in red). DAPI nuclear stain in blue. Images representative of n=3 animals for each genotype.

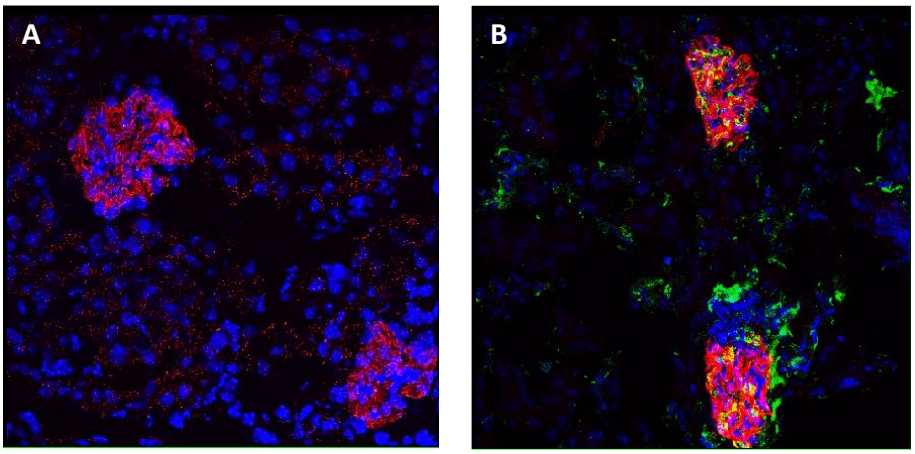

Figure 7-4: IF detection of Gb3 in PodrtTA-Tet-O-Gb3 Gb3 null mice vs. control kidney tissue x60
PodrtTA-Tet-O-WT Gb3 null mice (Panel A) and PodrtTA-Tet-O-Gb3 Gb3 null mice (Panel B) were given 14 days of doxycycline in their drinking water and then sacrificed to allow organ harvest. Renal tissue from PodrtTA-Tet-O-WT Gb3 null mice (Panel A) showed no evidence of Gb3 expression (green) whereas in PodrtTA-Tet-O-Gb3 Gb3 null mice (Panel B) Gb3 expression is seen in the glomeruli: co-localising with the podocyte marker nephrin (red) to give yellow areas. DAPI nuclear stain in blue. Gb3 is also evident in the renal tubules of the PodrtTA-Tet-O-Gb3 Gb3 null mice. The most likely explanation for this observation is Gb3 being shed from the podocyte membrane and reabsorbed by the renal tubules. Images representative of n=3 animals for each genotype.

Of note, it is evident from immunofluorescence (Figure 7-4) that there is Gb3 present in the renal tubules of the PodrtTA-Tet-O-Gb3 Gb3 null mice. The most likely explanation for this observation is Gb3 being shed from the podocyte membrane and reabsorbed by the renal tubules. Furthermore, and most importantly, the Gb3 seen in the renal tubules of the PodrtTA-Tet-O-Gb3 Gb3 null mice is not functional (see subsequent experimental findings to follow). Hence, it is highly unlikely that there is any de novo tubular Gb3 expression in these mice. Furthermore, the specificity of the podocin promoter used in the tetracycline controlled gene expression model means that only podocytes have the ability to synthesize Gb3 in the presence of doxycycline. Of note all mice were genotyped by MRC Harwell (and then genotyped on arrival at the animal unit in Bristol) prior to use to confirm the PodrtTA-Tet-O-Gb3 Gb3 null genotype.

An alternative explanation is that Shiga toxin itself has induced further expression of Gb3 in the podocyte (as seen in my *in vitro* work) which has saturated the renal tubules ability to reabsorb and filter excess Gb3 into the urine of the mice. Indeed, a recent publication

from Morace et al. has demonstrated that Gb3 is important in the regulation of proximal tubular protein reabsorption [283]. It is clear from this work that proximal tubular Gb3 expression is more important than first thought; given A4GALT KO mice were protected from AKI induced by myoglobin and gentamicin toxicity [283]. Thus, A4GALT KO itself may affect renal tubular function and explain why Gb3 is detected in the tubules of the PodrtTA-Tet-O-Gb3 Gb3 mice [284].

7.4 PodrtTA-Tet-O-Gb3 Gb3 null mice develop HUS following Shiga toxin challenge

7.4.1 Experimental plan and blood sampling

As depicted in Figure 7-5: 8-10 week old PodrtTA-Tet-O-Gb3 Gb3 null mice and age-matched control mice (PodrtTA-Tet-O-WT Gb3 null mice: effectively Gb3 null) were given 14 days of doxycycline in their drinking water. IP Shiga toxin was then administered at a dose of 10ng/g and the mice electively terminated at day 4, 8, 10, 12, 16 and 24. Blood was taken at the time of terminal anaesthesia via cannulation of the inferior vena cava (Figure 7-6). This technique was a new skill for our group, so we required training from Dr Robert Pope, as it is a technique that requires considerable manual dexterity.

A 23 gauge needle and pre-heparinised syringe was used to ensure the blood obtained did not clot as this would affect the platelet count measurement. 30 - 50 USP of heparin per ml of blood collected was used as per convention [152][285]. The blood sample was then transferred to an empty (i.e. non-coated) paediatric blood bottle. Initial attempts at blood collection was with EDTA coated blood tubes and a butterfly needle. However, the blood was clotting in the needle upon collection and very little blood could be obtained. Any clot in the blood sample meant that the platelet count was immeasurable as platelets are found within the clot itself. By using a pre-heparinised syringe this issue was circumvented. Any samples that contained a blood clot were excluded from analysis.

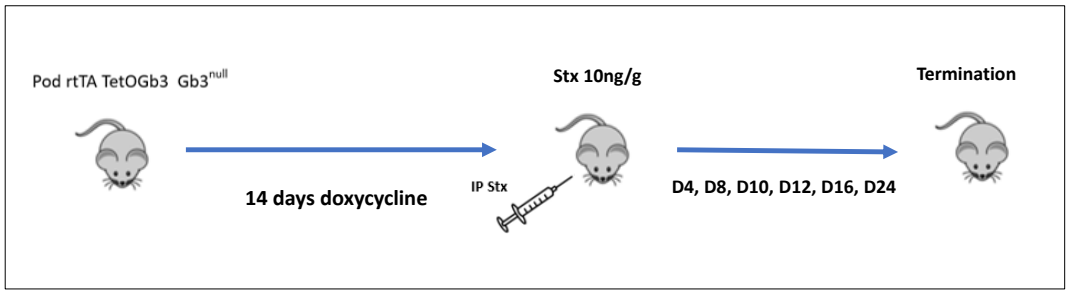

Figure 7-5: Experimental Plan for PodrtTA-Tet-O-Gb3 Gb3 null mice

PodrtTA-Tet-O-Gb3 Gb3 null mice and PodrtTA-Tet-O-WT Gb3 null control mice aged 8-10 weeks were given 14 days of doxycycline in their drinking water, followed by IP Shiga toxin challenge at 10ng/g. The mice were then electively terminated at intervals of day 4, 8,10,12, 16 and 24.

A volume of 700-1000 microlitres of blood was obtained per mouse and analysed for differential full blood count, urea, and blood film. All blood samples and blood films were coded to blind them for analysis to avoid bias. Blood films were produced by hand, taking a small drop (< 5 microlitres) of blood on a Claritex® glass histology slide using a wooden stick. Another Claritex® slide was then placed on top of the first, the short edge held at an angle of 30 degrees and the blood droplet allowed to spread across the short edge (by capillary action). The top glass slide was then swept across the bottom slide to spread the blood across it in one smooth motion; leaving a trail of blood that goes from a thicker smear through to a thinner film of blood. It is this thinner area that the blood film is analysed from; where the erythrocytes are touching but not overlapping. The glass slide with the blood smear on it was then fixed in methanol, followed by methylene blue and eosin staining on an automated fixation Sysmex SP-10® machine at Bristol Royal Infirmary Haematology laboratory. Three blood films per animal were produced and analysed for any evidence of microcytic anaemia by Dr John Moppet Consultant Paediatric Haematologist.

The remaining blood sample was then run through the Sysmex XN-20® in Bristol Royal Infirmary Haematology department to obtain a differential full blood count, under the instruction of section leader Mr Mark Nicholas. This had been calibrated to recognise the differential full blood count for mouse samples (mouse cells are of a much smaller diameter than human blood cells). Blood samples were then transported back to the laboratory and centrifuged at 2000xg at 4°C for 10-15 minutes. This separates the blood into an upper plasma layer and lower red cell layer. The upper plasma layer was carefully pipetted off, avoiding any contamination of the sample with red cells. The plasma was

then sent to Kay Burt at Langford Veterinary school for measurement of urea. All blood samples were analysed within 30 - 45 minutes from collection from the mouse to ensure accuracy.

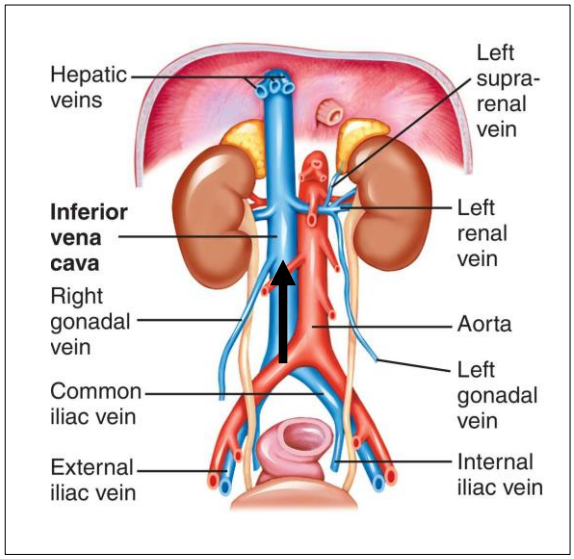

Figure 7-6: Inferior vena cava anatomy in the mouse

The inferior vena cava (IVC) was identified in terminally anaesthetised mice following a midline incision and blunt dissection down to the abdominal aorta. A 23 gauge needle pre-heparinised needle and syringe was then inserted into the vena cava (arrow) and blood aspirated into the syringe. The blood was then inverted in the syringe 10 times (to ensure mixing with heparin) before being transferred to a non-coated paediatric blood bottle. Image adapted from online source: *ivc-anatomy-y-flash-cards.*

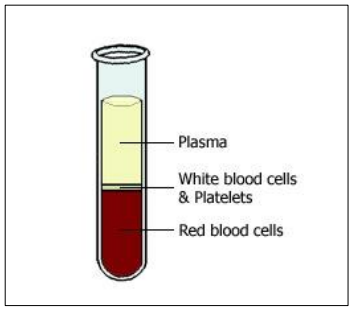

Figure 7-7: Blood sample separation into plasma

Schematic to show appearance of blood sample following centrifugation. The addition of heparin at the time of blood sample collection prevents the blood from clotting and facilitates the

separation of the sample into plasma and blood cell layers. Image taken from *Blood Groups and Red Cell Antigens 2005* [286].

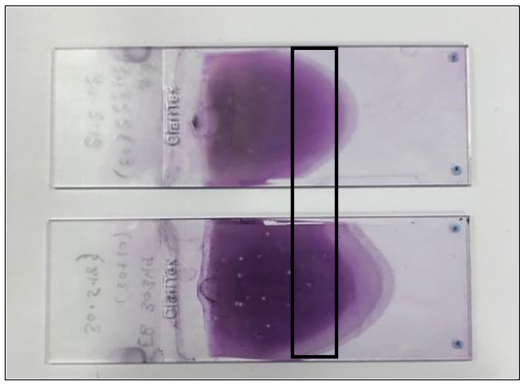

Figure 7-8: Blood film

Example of blood film slides made by hand as described in main text; subsequently fixed with methanol and stained with methylene blue and eosin on an automated slide fixation machine Sysmex SP-10® at Bristol Royal Infirmary Hospital. The thinner area of the film (boxed) is where the analysis of red cell morphology occurs.

7.4.2 PodrtTA-Tet-O-Gb3 Gb3 null mice develop thrombocytopenia following Shiga toxin challenge

PodrtTA-Tet-O-Gb3 Gb3 null mice and age-matched (8-10 week) old control mice (PodrtTA-Tet-O-WT Gb3 null) were given 14 days of oral doxycycline, followed by 10ng/g of Shiga toxin IP and electively terminated at different time points as already described. Comparison of platelet counts between each cohort of mice terminated at day 4 through to 24 are shown in Figure 7-9 and Figure 7-10. The platelet count was at its lowest 10 days following Shiga toxin IP injection in the PodrtTA-Tet-O-Gb3 Gb3 null mice. Interestingly, just as in the majority of Shiga toxin HUS patients, the platelet counts in these mice recovered by day 24. In contrast the control PodrtTA-Tet-O-WT Gb3 null mice showed no change in their platelet counts over the course of the experiment.

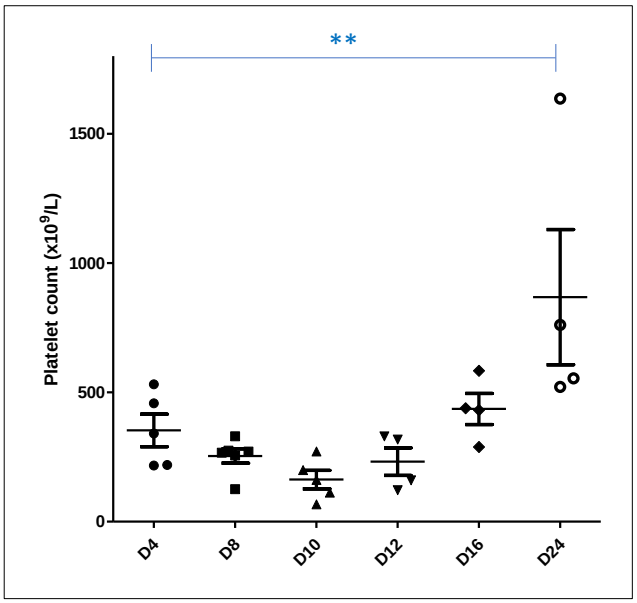

Figure 7-9: Comparison of platelet count across all time points PodrtTA-Tet-O-Gb3 Gb3 null mice

PodrtTA-Tet-O-Gb3 Gb3 null mice were given 14 days of oral doxycycline, followed by 10ng/g of Shiga toxin IP and electively terminated at different time points as already described. Comparison of platelet counts between each cohort of mice terminated at day 4 through to 24 are shown. Platelet count drops maximally at day 10 and then recovers by day 24. The observed changes were statistically significant. ** One way ANOVA with Tukey's multiple comparison test: p value 0.001.

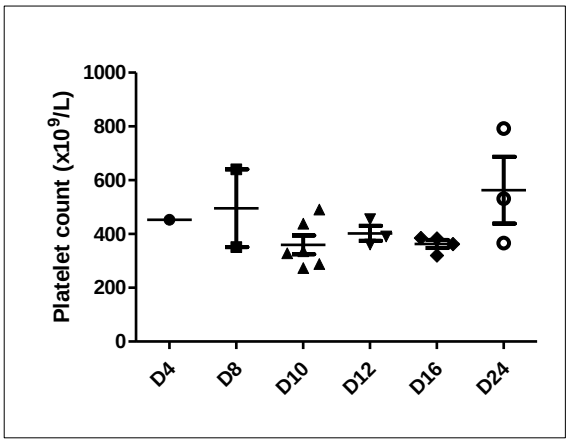

Figure 7-10: Comparison of platelet count across all time points in Gb3 null control mice

PodrtTA-Tet-O-WT Gb3 null mice were given 14 days of oral doxycycline, followed by 10ng/g of Shiga toxin IP and electively terminated at different time points as already described. Comparison of platelet counts between each cohort of mice terminated at day 4 through to 24 are shown. There was no statistically significant difference between the platelet counts at any time point.

7.4.3 PodrtTA-Tet-O-Gb3 Gb3 null mice are anaemic and uraemic at day 10 following IP Shiga toxin

Given that the PodrtTA-Tet-O-Gb3 Gb3 null mice dropped their platelet count maximally at day 10, it was decided that this time point would be used to establish whether any other features of HUS were also present. Blood samples were analysed for haemoglobin and urea as already described. At day 10 these mice had both a reduction in their haemoglobin (anaemia) and a rise in urea (uraemia). This was an exciting finding; mice that only express Gb3 in their podocytes, had developed a thrombocytopenia, anaemia and uraemia: all the features of haemolytic uraemic syndrome. The control mice (effectively Gb3 null mice) demonstrated no drop in their haemoglobin and no increase in their urea (Figure 7-11).

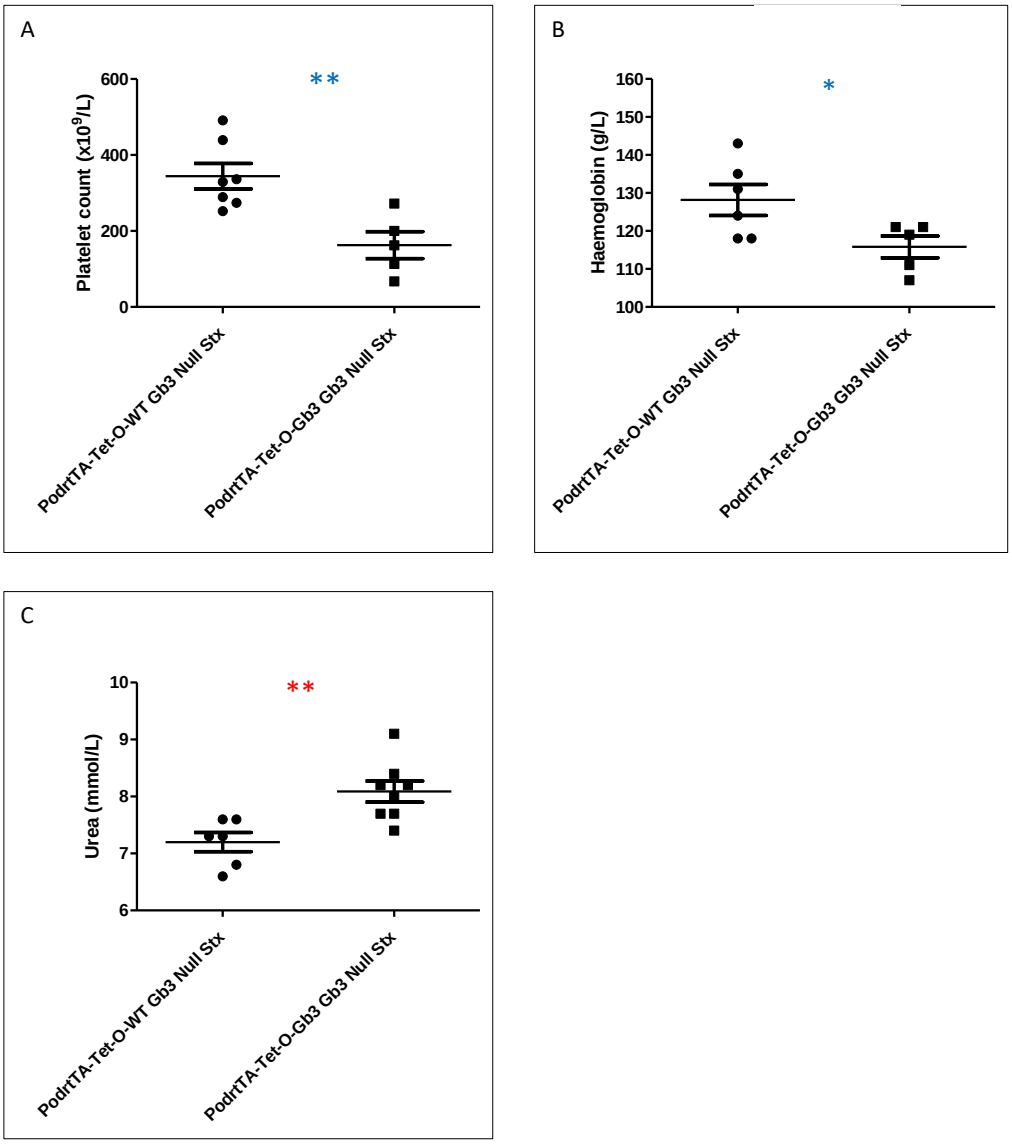

Figure 7-11: PodrtTA-Tet-O-Gb3 Gb3 null mice develop HUS following IP Shiga toxin

PodrtTA-Tet-O-Gb3 Gb3 null mice given 10ng/g of IP Shiga toxin show a drop in platelet count (A), drop in haemoglobin (B) and rise in plasma urea (C) vs. age matched control mice (PodrtTA-Tet-O-WT Gb3 null) at Day 10. These differences were statistically significant A: ** Unpaired T test p value 0.004; B: * Unpaired T test p value 0.041; C: **Unpaired T-test p value 0.0052 *Note urea results pooled from day 10 to day 16.*

7.4.4 PodrtTA-Tet-O-Gb3 Gb3 null mice develop a haemolytic anaemia at day 10 following IP Shiga toxin

The finding that podocyte expression of the Gb3 receptor in the presence of Shiga toxin could go on to cause a systemic HUS syndrome was very exciting. However, it was important to determine whether the anaemia observed at day 10 was a haemolytic anaemia such as that seen in HUS, or an anaemia due to sepsis. Sepsis can cause anaemia through reduction in serum iron levels and erythropoietin production [287]. Whereas, anaemia due to haemolysis is due to premature destruction of erythrocytes, accompanied by a rise in reticulocyte count and lactate dehydrogenase (LDH) [288].

To establish whether a microcytic haemolytic anaemia was occurring, blood films were analysed with Dr John Moppet (Consultant Paediatric Haematologist). Blood film analysis was performed whilst blinded to mouse genotype so as to avoid bias. Blood films are used in clinical practice in HUS patients to look for red cell fragmentation which indicates haemolysis [32]. Unfortunately, the volume of blood that could be collected at the time of termination was limited and so could not be used for analysis of LDH (as well as full blood count and urea). The accuracy of using the reticulocyte count (produced as part of the differential full blood count from the read out generated by the Sysmex XN-20®) was discussed with Dr Moppet; who felt this could not be accurately or reproducibly analysed. Of note, mice have a higher circulating percentage of reticulocytes in health than humans so interpretation would prove challenging given the wide range of 'normal' values [289].

Blood films demonstrated that haemolysis was occurring in the PodrtTA-Tet-O-Gb3 Gb3 null animals at day 10 following IP Shiga toxin; with no evidence of haemolysis in the control animals (Figure 7-12). An estimated 10-15% of red cells in the PodrtTA-Tet-O-Gb3 Gb3 null mice were fragmented (n=7) in each animal.

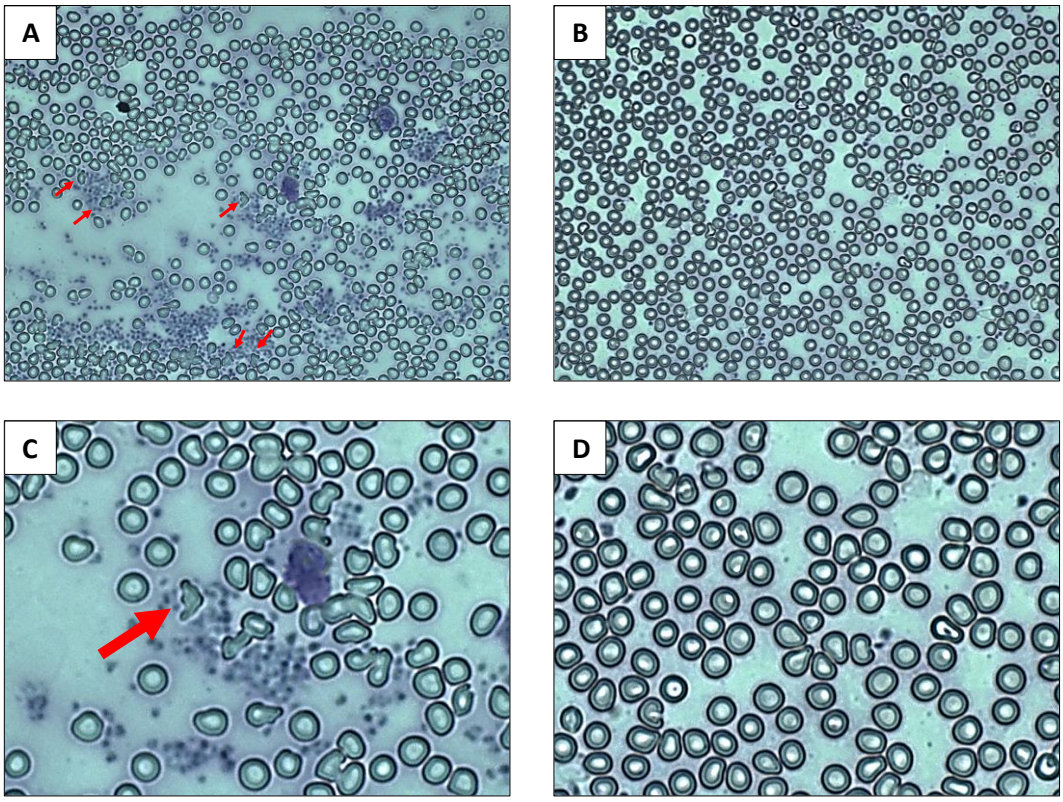

Figure 7-12: PodrtTA-Tet-O-Gb3 Gb3 null mice develop haemolysis on blood films at Day 10 following Shiga toxin IP vs. controls

Blood films for PodrtTA-Tet-O-Gb3 Gb3 null mice (A and C) and age matched controls (B and D) at day 10 following Shiga toxin IP are shown. Red arrows indicate red cell fragments which are only seen in PodrtTA-Tet-O-Gb3 Gb3 null animals. Panels C and D are the same blood films, but images are zoomed in to allow better visualisation of fragments. Magnification is x40. Blood films shown are representative of all animals analysed at day 10 (PodrtTA-Tet-O-Gb3 Gb3 null mice n=7; PodrtTA-Tet-O-WT Gb3 null controls n=5). An estimated 15-20 % of red cells in the PodrtTA-Tet-O-Gb3 Gb3 null were fragmented in each animal: representative blood films shown.

7.4.5 PodrtTA-Tet-O-Gb3 Gb3 null mice develop a TMA on renal histology at day 10 following IP Shiga toxin

The histopathological hallmark of Shiga toxin HUS is evidence of thrombotic microangiopathy (TMA) [1]. In clinical practice renal biopsy is rarely performed in Shiga toxin HUS, as patients have low platelet counts and are therefore at increased risk of bleeding complications from the procedure [1]. Renal biopsy is more often performed in patients with complement mediated atypical HUS, although it is not a requirement for diagnosis. Renal biopsy in this patient group is also used to monitor the disease response to anti-complement therapy with eculizumab [290].

The finding of TMA on biopsy reflects the kidney's response to glomerular endothelial cell injury. Endothelial swelling, mesangiolysis and fibrin platelet thrombosis are seen in acute cases and double contouring of the basement membrane seen in chronic disease [290]. However, to further complicate diagnosis, it is now recognised that overt fibrin platelet thrombosis may not be present in all renal biopsies of TMA. What is important to appreciate is that the finding of TMA on renal biopsy does not establish a cause (i.e. HUS vs. TTP) but simply signifies a final common pathway of glomerular endothelial injury [290].

The trichrome stain, martius scarlet blue (MSB) was performed on kidney sections taken from PodrtTA-Tet-O-Gb3 Gb3 null mice versus PodrtTA-Tet-O-WT Gb3 null control mice at day 10 following Shiga toxin IP challenge (Figure 7-13). In this trichrome method, fibrin clots appear red, erythrocytes yellow and collagen blue. Three mice from each genotype were analysed. Fibrin thrombi were clearly seen in the glomeruli of PodrtTA-Tet-O-Gb3 Gb3 null mice; with no evidence of thrombi in the PodrtTA-Tet-O-WT Gb3 null control mice. The percentage of glomeruli containing thrombi were quantified by selecting 10 different fields of view at random, using the Leica DMI 6000B microscope at x20 magnification in an n=3 for each genotype (Figure 7-14). The total number of glomeruli sampled in the control group was 185 and the total number in the PodrtTA-Tet-O-Gb3 Gb3 null group was 165. In the PodrtTA-Tet-o-Gb3 Gb3 null mice 20-25% of glomeruli contained thrombi.

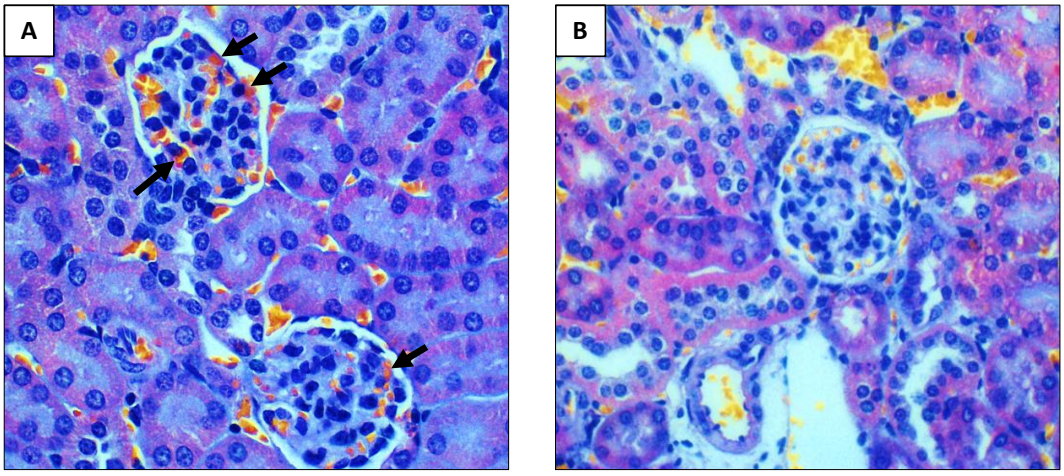

Figure 7-13: PodrtTA-Tet-O-Gb3 Gb3 null mice develop a TMA on renal histology at day 10 following IP Shiga toxin

Martius scarlet blue trichrome stain of renal tissue from a PodrtTA-Tet-O-Gb3 Gb3 null mouse vs. control following 10ng/g Shia toxin intraperitoneal injection. Panel A: fibrin thrombi (red) are seen within the glomerular capillary loops indicated by black arrows. These appearances are characteristic of a glomerular TMA, the same histopathological lesion that is seen in humans with Shiga toxin HUS. Panel B: there are no fibrin thrombi seen in the glomeruli of PodrtTA-Tet-O-WT Gb3 null control mice. Fibrin = red, collagen = blue, erythrocytes = yellow.

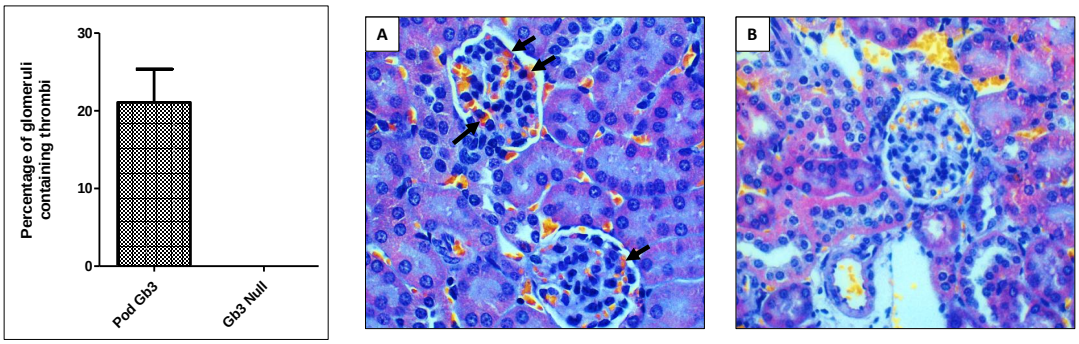

Figure 7-14: Quantification of thrombi PodrtTA-Tet-O-Gb3 Gb3 null mice vs. controls

The percentage of glomeruli containing fibrin thrombi in the PodrtTA-Tet-O-Gb3 Gb3 null mice (pod Gb3) vs. controls (Gb3 null) was calculated by selecting 10 different fields of view at random, on the Leica DMI 6000B microscope at x20 magnification in an n=3 for each genotype (graph). The total number of glomeruli sampled in the control group was 185 and the total number in the PodrtTA-Tet-O-Gb3 Gb3 null group was 165. In the PodrtTA-Tet-o-Gb3 Gb3 null mice 20-25% of glomeruli contained thrombi. No statistical test can be performed to compare the two groups because there were no thrombi seen in the control mice. Representative MSB stain shown in panel A and panel B as in Figure 7-13.

7.4.6 PodrtTA-Tet-O-Gb3 Gb3 null mice have evidence of thrombi in their glomerular capillaries on electron microscopy following IP Shiga toxin

PodrtTA-Tet-O-Gb3 Gb3 null mice develop HUS at day 10 following IP Shiga toxin and show evidence of thrombi within their glomeruli on MSB trichrome histology. Another way of demonstrating TMA in the kidney is to look at renal tissue under electron microscopy (EM). A quarter of kidney harvested from PodrtTA-Tet-O-Gb3 Gb3 null mice and controls at day 10 following IP Shiga toxin, was cut up into fine pieces and preserved in EM fix as detailed in my methods. This was then processed by the Wolfson Bioimaging Facility at the University of Bristol; and subsequently sectioned on an ultramicrotome, imaged and analysed by Dr Louise Farmer. Both myself and Dr Farmer were blinded to the genotype of the mice during sample preparation and analysis. EM images were taken on the Tecnai

12 120kV BioTwin Spirit Transmission Electron Microscope scanner in the Wolfson Institute.

TMA was evident on EM imaging in the PodrtTA-Tet-O-Gb3 Gb3 null mice at day 10 post Shiga toxin IP. Large areas of thrombus were seen in the glomerular capillaries of these mice (Figure 7-15 and Figure 7-16). Low power and high power images were taken; there were no thrombi evident in the control mice. High power images were used to calculate foot process width, slit diaphragm size and glomerular basement membrane thickness. The presence of thrombi in the capillary loops of the glomeruli seen on EM is yet further evidence of HUS developing in the PodrtTA-Tet-O-Gb3 Gb3 null mice at day 10 post Shiga toxin.

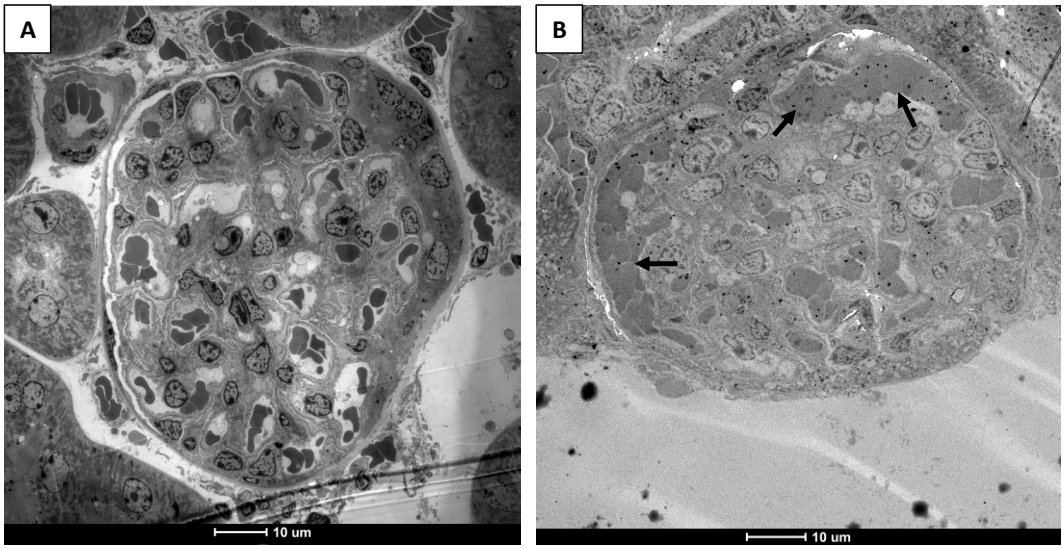

Figure 7-15: PodrtTA-Tet-O-Gb3 Gb3 null mice develop TMA on EM at day 10 following IP Shiga toxin (low power)

As described kidneys were harvested from PodrtTA-Tet-O-Gb3 Gb3 null mice and PodrtTA-Tet-O-WT Gb3 null mice under terminal anaesthesia at day 10 following IP Shiga toxin. A quarter of kidney from each animal was cut up into small pieces and preserved in EM fix. This was then processed by the Wolfson Bioimaging Facility at the University of Bristol; and subsequently sectioned on an ultramicrotome, imaged and analysed by Dr Louise Farmer. Panel A – control mouse glomerulus shows normal glomerular architecture and red blood cells in capillary loops. Panel B – PodrtTA-Tet-O-Gb3 Gb3 null mouse glomerulus: arrows indicate thrombus within the glomerular capillaries. Representative images of n=3 animals for each genotype.

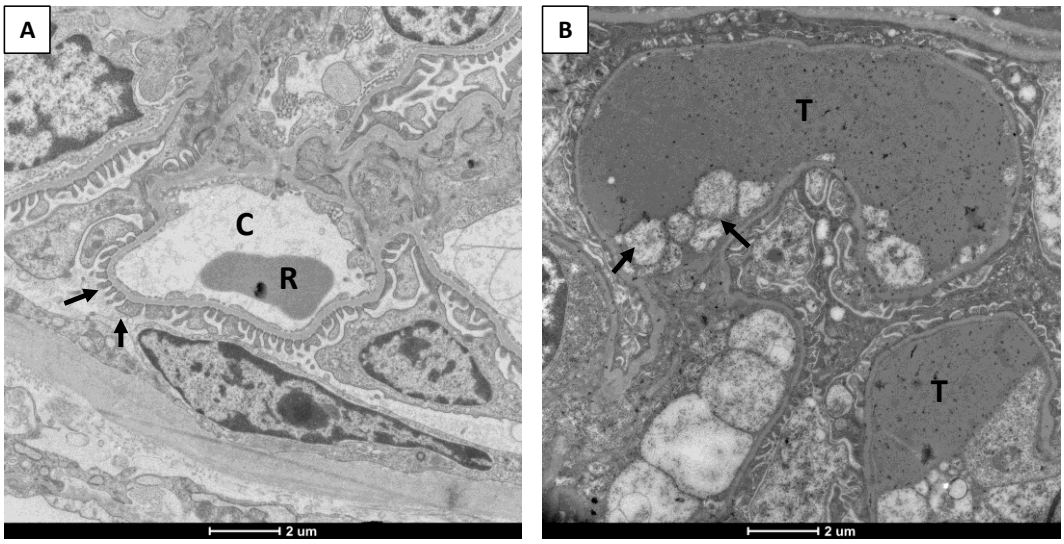

Figure 7-16: PodrtTA-Tet-O-Gb3 Gb3 null mice develop TMA on EM at day 10 following IP Shiga toxin (high power)

As described kidneys were harvested from PodrtTA-Tet-O-Gb3 Gb3 null mice and PodrtTA-Tet-O-WT Gb3 null mice under terminal anaesthesia at day 10 following IP Shiga toxin. A quarter of kidney from each animal was cut up into small pieces and preserved in EM fix. This was then processed by the Wolfson Bioimaging Facility at the University of Bristol; and subsequently sectioned on an ultramicrotome, imaged and analysed by Dr Louise Farmer. Panel A – control mouse glomerulus shows normal glomerular capillary loop (C) and red blood cell (R) within. Arrows indicate normal appearance of podocyte foot processes. Panel B – PodrtTA-Tet-O-Gb3 Gb3 null mouse glomerulus: T = thrombus completely occluding capillary loop. Arrows indicate subendothelial accumulation of electrolucent 'fluff' (i.e. flocculent material with a finely fibrillar appearance) that is characteristic of TMA. Representative images of n=3 animals for each genotype.

7.4.7 PodrtTA-Tet-O-Gb3 Gb3 null mice show no evidence of podocyte foot process effacement on electron microscopy following IP Shiga toxin

High power electron microscopy images from PodrtTA-Tet-O-Gb3 Gb3 null mice at day 10 post Shiga toxin alongside PodrtTA-Tet-O-WT Gb3 null control mice, were used to calculate foot process width, slit diaphragm width and glomerular basement membrane thickness. These measurements were taken by Dr Louise Farmer and showed no statistically significant differences between the groups in relation to podocyte morphology. There was a statistically significant difference in the thickness of the glomerular basement membrane (GBM) measurements; with the GBM slightly thinner in the PodrtTA-Tet-O-Gb3 Gb3 null mice (Figure 7-17). This was not thought to be associated with any consequence in this model, but important to document, nonetheless.

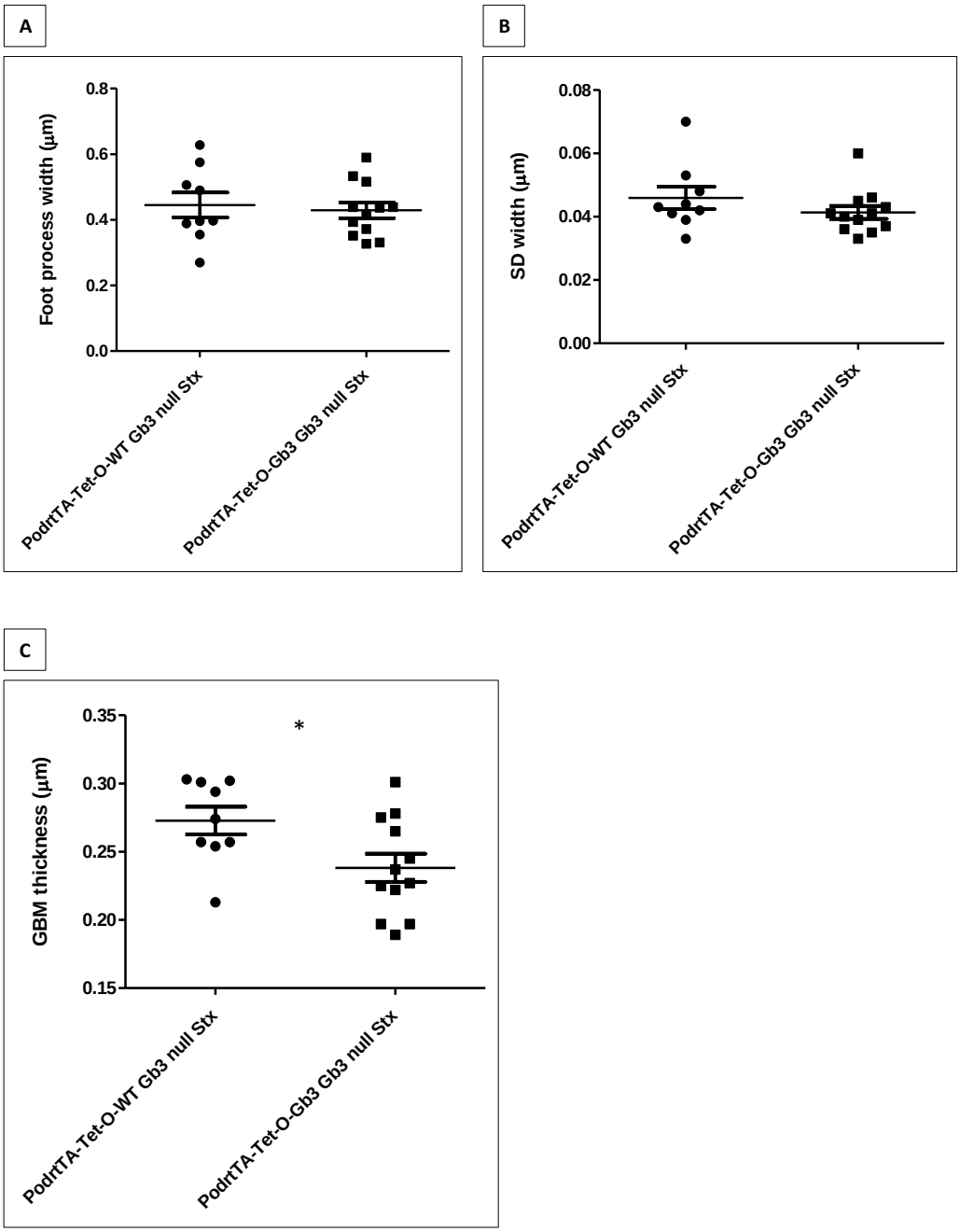

Figure 7-17: PodrtTA-Tet-O-Gb3 Gb3 null mice show no evidence of podocyte foot process effacement on electron microscopy following IP Shiga toxin at day 10

As described kidneys were harvested from PodrtTA-Tet-O-Gb3 Gb3 null mice and PodrtTA-Tet-O-WT Gb3 null mice under terminal anaesthesia at day 10 following IP Shiga toxin. A quarter of kidney from each animal was cut up into small pieces and preserved in EM fix. This was then processed by the Wolfson Bioimaging Facility at the University of Bristol; and subsequently sectioned on an ultramicrotome, imaged and analysed by Dr Louise Farmer. Graphs A and B show no statistically significant difference in podocyte foot process width or slit diaphragm (SD) width between the two groups. Graph C shows a statistically significant difference in the thickness of the glomerular

basement membrane (GBM) measurements; with the GBM slightly thinner in the PodrtTA-Tet-O-Gb3 Gb3 null mice. * Unpaired T test p value 0.03.

7.4.8 PodrtTA-Tet-O-Gb3 Gb3 null mice have no change in urine ACR following IP Shiga toxin

Although electron microscopy images taken of PodrtTA-Tet-O-Gb3 Gb3 null mice at day 10 post IP Shiga toxin challenge showed no evidence of podocyte foot process effacement; PodrtTA-Tet-O-Gb3 mice vs. age matched controls (PodrtTA-Tet-O-WT Gb3 null mice) pre-termination urine samples from day 10 to day 16 were analysed to determine if there was any significant difference in albumin creatinine ratio (ACR) between the groups (Figure 7-19). This is a standard method of measuring protein (albumin) leak from the kidney that is also used in patients. An albumin ELISA was performed on all urine samples in duplicate against albumin standards and urinary creatinine analysed at Langford Veterinary Practice. Each urine sample was also tested on urine dipstick; using Siemens Multistix 10SG Urinalysis Strips® at the time of urine collection to assess whether they were positive for blood (microscopic haematuria – which can be a marker of glomerular injury) (Figure 7-18).

Initial urine dipstick testing showed no evidence of microscopic haematuria but did show up to ++ of proteinuria. It is known that urine dipstick testing is useful as a screen for proteinuria (high specificity), but that it does not have a very good sensitivity for detection of low-end but clinically significant proteinuria. Moreover, it does not quantify the exact amount of protein in the urine [291]. Measurement of ACR also corrects for the dilution of the urine sample (i.e. creatinine concentration) which allows comparison across animals. There was no statistically significant difference in ACR between the PodrtTA-Tet-O-Gb3 Gb3 null mice and controls between days 10-16 following IP Shiga toxin. In patients with Shiga toxin HUS, acute proteinuria is not often a feature at presentation. Most are anuric and if they do develop proteinuria it is many weeks later due to the development of chronic kidney disease [292].

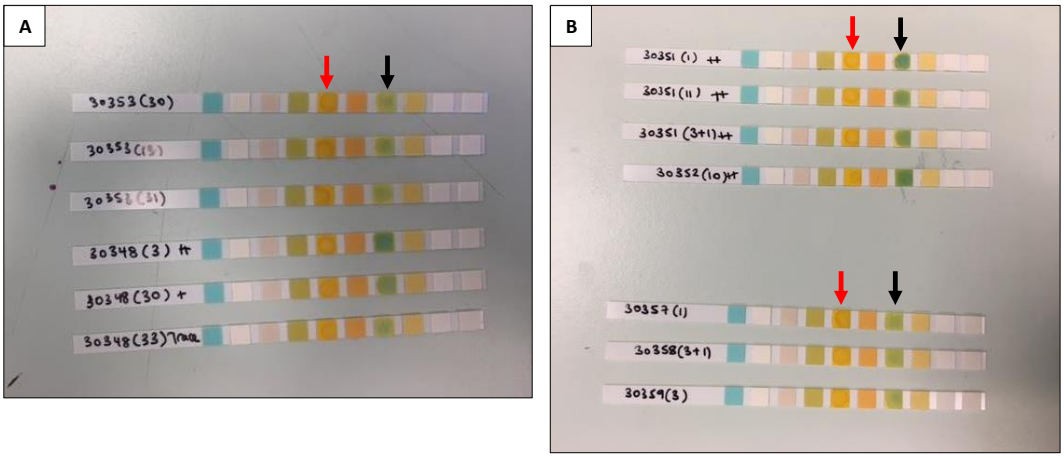

Figure 7-18: Urine dipstick testing shows proteinuria in PodrtTA-Tet-O-Gb3 Gb3 null mice following IP Shiga toxin

PodrtTA-Tet-O-Gb3 Gb3 null mice vs. control mice urine samples were tested for urinary protein and blood using Siemens Multistix 10SG Urinalysis Strips® on the day of termination. Panel A shows day 12 mice (top 3 dipstick tests are controls and show no proteinuria, bottom 3 are PodrtTA-Tet-O-Gb3 Gb3 null mice with evidence of mild proteinuria demonstrated by colour change). Panel B shows day 16 mice (top four dipstick tests show proteinuria as evidenced by dark green colour change and bottom 3 show no proteinuria). Red arrow indicates column read to detect blood and black arrow indicates column read to detect proteinuria. All urine samples negative for blood.

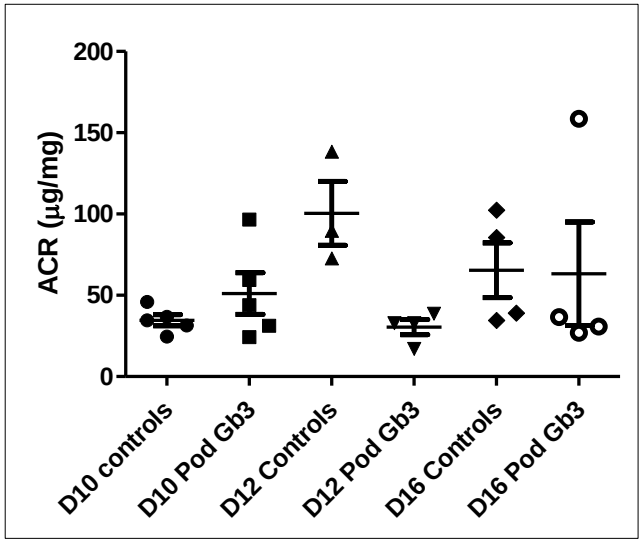

Figure 7-19: PodrtTA-Tet-O-Gb3 Gb3 null mice have no change in urine ACR following IP Shiga toxin

PodrtTA-Tet-O-Gb3 Gb3 null mice vs. control mice urine samples were analysed for ACR on days 10, 12 and 16 following IP Shiga toxin. An albumin ELISA was performed on all urine samples on the same day and urinary creatinine analysed at Langford Veterinary Practice. There was no

statistically significant difference in urine ACR between the PodrtTA-Tet-O-Gb3 Gb3 null mice vs. controls at any time point. *One way ANOVA: No significant difference between the groups.*

7.4.9 PodrtTA-Tet-O-Gb3 Gb3 null mice show increased fibrinogen deposition in their glomeruli at day 10 following IP Shiga toxin

The presence of TMA in the glomeruli of PodrtTA-Tet-O-Gb3 Gb3 null mice prompted investigation as to whether there was any evidence of fibrinogen deposition in the glomeruli using immunofluorescence. In Shiga toxin HUS, fibrin forms as an intravascular glomerular thrombi [72]. This is triggered by endothelial cell injury which results in the release of tissue factor pro-coagulants, fibrinolytic inhibitors, platelet activating factor and von Willebrand factor [293]. It is this microvascular endothelial cell injury that differentiates TMA from disseminated intravascular coagulation (DIC); where consumption of coagulation factors leads to secondary fibrinolysis [294].

The fibrin that forms in the glomerulus in Shiga toxin HUS, may be removed by phagocytic or fibrinolytic processes or persist to leave glomerular scarring - rendering the glomerulus obsolescent [293]. Thus, I could not anticipate whether or not in this model there would be an increase in glomerular fibrinogen deposition by day 10. Three mice from each group were analysed: PodrtTA-Tet-O-Gb3 Gb3 null vs. PodrtTA-Tet-O-WT Gb3 null at day 10 following Shiga toxin IP injection. The PodrtTA-Tet-O-Gb3 Gb3 null mice showed an increase in fibrinogen deposition in the glomeruli that was statistically significant versus controls. Representative immunofluorescence images are shown in Figure 7-20.

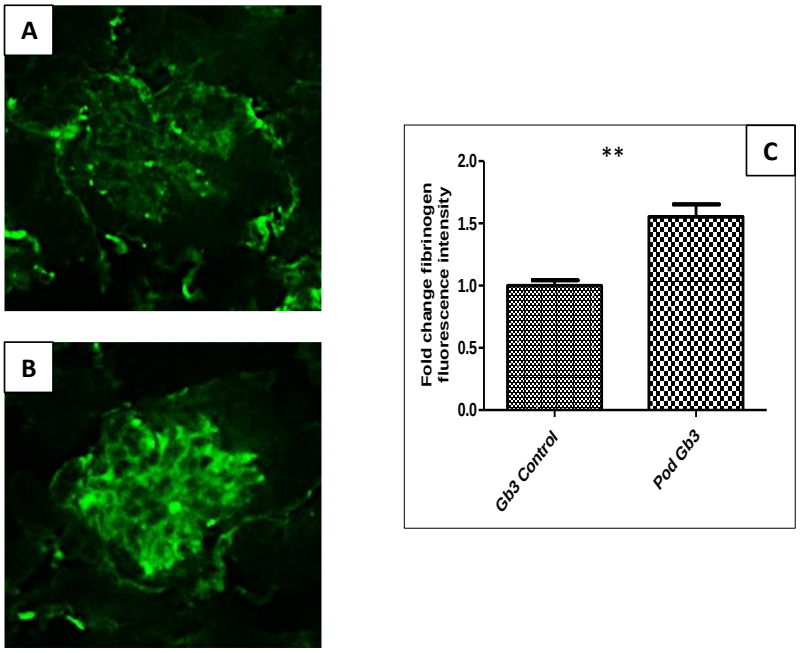

Figure 7-20: PodrtTA-Tet-O-Gb3 Gb3 null mice show an increase in glomerular fibrinogen deposition at day 10 following Shiga toxin challenge vs. control mice

Frozen kidney sections from PodrtTA-Tet-O-Gb3 Gb3 null mice and control PodrtTA-Tet-O-WT Gb3 null mice were probed for fibrinogen deposition (shown in green) using immunofluorescence. Representative images shown in panel A (PodrtTA-Tet-O-Gb3 Gb3 null mice) panel B (PodrtTA-Tet-O-WT Gb3 null controls). This demonstrated a statistically significant increase in fibrinogen deposition in the glomeruli of the PodrtTA-Tet-O-Gb3 Gb3 null mice as evidenced by the increase in fold change of fibrinogen fluorescence intensity of x1.5. Graph C: label Pod Gb3 = PodrtTA-Tet-O-Gb3 Gb3 null mice; Label Gb3 null = PodrtTA-Tet-O-WT Gb3 null mice (for clarity of figure). Results from n=3 mice of each genotype: 30 glomeruli per mouse ** Unpaired T-test p value <0.001.

7.4.10 PodrtTA-Tet-O-Gb3 Gb3 null mice have increased C3b deposition in their glomeruli at day 10 following IP Shiga toxin

Given that my central hypothesis states that the glomerular TMA seen in Shiga toxin HUS is driven by complement mediated attack on the endothelial cell, kidney sections from PodrtTA-Tet-O-Gb3 Gb3 null mice vs. controls were analysed for C3b deposition in the glomerulus (Figure 7-21). C3b was increased in the glomeruli of PodrtTA-Tet-O-Gb3 Gb3 null mice vs. controls. C3b is a cleavage product of C3 and is involved in the formation of C3 convertase when bound to Factor B; or C5 convertase when bound to C4b and C2b [2]. Cleavage of C3 can occur via all 3 complement cascade pathways: classical, lectin and alternative. It is at the point of cleavage of C3 that these pathways converge and go on to

culminate with the formation of the membrane attack complex (MAC), leading to the insertion of pores into the target cell membrane resulting in osmotic lysis and cell death.

The alternative pathway differs from the other two in that it is continually active at low levels in the plasma and is activated by spontaneous hydrolysis of a thioester bond in C3. To protect host cells from non-specific destruction, complement activation is regulated by a number of plasma (CFH, CFI) and membrane bound factors [2][153]. In the PodrtTA-Tet-O-Gb3 Gb3 null mice (n=3) vs. control PodrtTA-Tet-O-WT Gb3 null mice (n=3) there was a x2.5 fold increase in the presence of C3b in the glomeruli. Given the pattern of IF staining this appeared to be originating from the glomerular endothelial cells. This was subsequently confirmed using the endothelial cell marker PECAM (Figure 7-22 and Figure 7-23).

It was noted in these sections that C3b was also detected in Bowman's capsule and in the renal tubules of both the PodrtTA-Tet-O-Gb3 Gb3 null and PodrtTA-Tet-O-WT Gb3 null control mice. This has been published in the literature previously and appears to be at the same level of fluorescence intensity in all sections irrespective of genotype [295]. Given only C3b expression in the glomerulus is of interest (because the glomerular endothelium is where TMA occurs) any signal from outside the glomerulus was excluded from my analysis. The corrected total glomerular fluorescence (CTGF) was calculated using the following formula: CTFG = integrated density – (area of selected glomerulus x MFI of background); where background was averaged over 3 separate MFI values. The purpose of co-staining with the podocyte marker nephrin was to facilitate identification of the glomerulus accurately and calculate the C3b fluorescent signal only within this area. This allowed me to exclude the C3b located in renal tubules and Bowman's capsule and evaluate the changes occurring only within glomeruli.

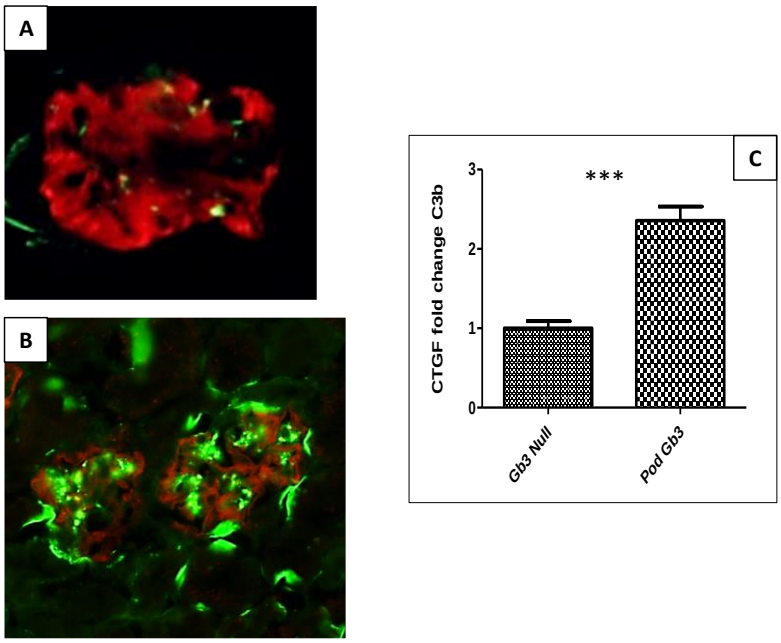

Figure 7-21: PodrtTA-Tet-O-Gb3 Gb3 null mice have increased C3b present in their glomeruli at day 10 following IP Shiga toxin

Frozen kidney sections from PodrtTA-Tet-O-Gb3 Gb3 null mice and control PodrtTA-Tet-O-WT Gb3 null mice were probed for C3b (shown in green) using immunofluorescence and co-stained with the podocyte marker nephrin (red). Representative images shown in panel A (PodrtTA-Tet-O-WT Gb3 control mice) panel B (PodrtTA-Tet-O-Gb3 Gb3 null mice). This demonstrated a statistically significant increase in C3b deposition in the glomeruli of the PodrtTA-Tet-O-Gb3 Gb3 null mice as evidenced by the increase in fold change of C3b fluorescence intensity of x2.5. Graph C: Pod Gb3 = PodrtTA-Tet-O-Gb3 Gb3 null mice; Gb3 null = PodrtTA-Tet-O-WT Gb3 null mice (for clarity of figure). Results from n=3 mice of each genotype: 30 glomeruli per mouse *** Unpaired T-test p value <0.0001.

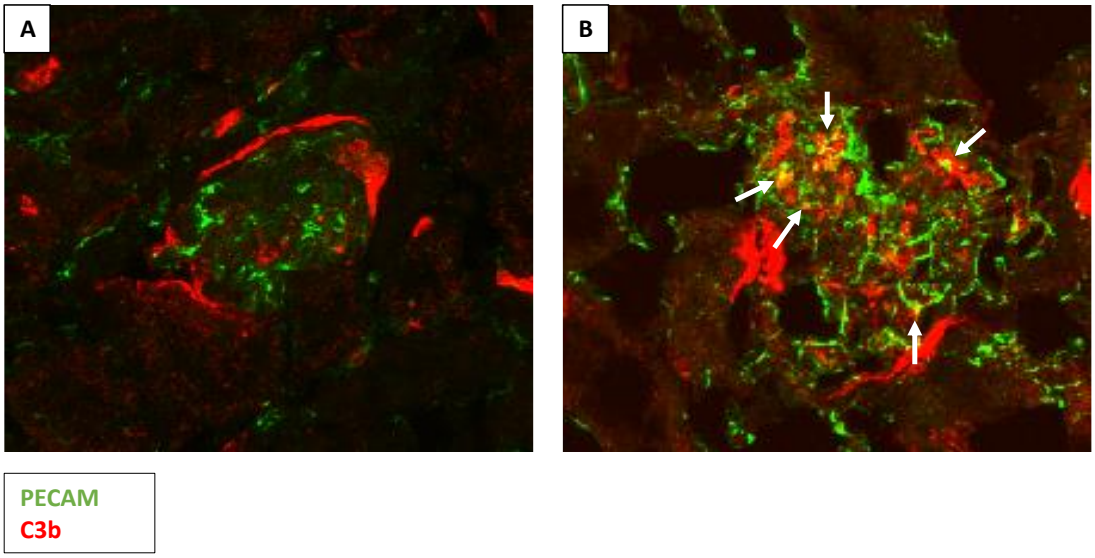

Figure 7-22: PECAM and C3b IF showing co-localisation in PodrtTA-Tet-O-Gb3 Gb3 null mice at day 10 following IP Shiga toxin

Frozen kidney sections from PodrtTA-Tet-O-Gb3 Gb3 null mice and control PodrtTA-Tet-O-WT Gb3 null mice were probed for C3b (shown in red) using immunofluorescence and co-stained with the endothelial cell marker PECAM (green). Arrows denote areas of co-localisation (yellow) suggestive that C3b is originating from the glomerular endothelial cells. Panel A shows representative section from n=3 control mice (PodrtTA-Tet-O-WT Gb3 null) and Panel B shows representative section from n=3 PodrtTA-Tet-O-Gb3 Gb3 null mice.

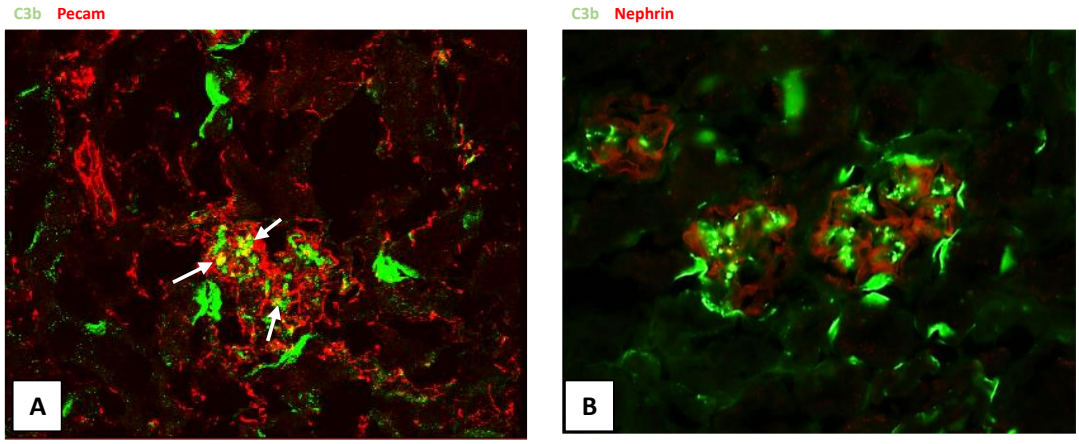

Figure 7-23: PECAM and C3b IF vs Nephrin and C3b IF in PodrtTA-Tet-O-Gb3 Gb3 mice at day 10 following IP Shiga toxin

Frozen kidney sections from PodrtTA-Tet-O-Gb3 Gb3 null mice were probed for C3b (green) and co-stained with PECAM (A) or nephrin (B) both in red. White arrows mark yellow areas of co-localisation only seen when the endothelial cell marker PECAM is used as a co-stain (A). This

demonstrates that C3b is originating from the endothelial cells. There is no evidence of co-localisation when nephrin is used as a podocyte marker. Representative images of n=3.

7.4.11 PodrtTA-Tet-O-Gb3 Gb3 null mice have reduced CFH deposition in their glomeruli at day 10 following IP Shiga toxin

It is essential that complement activation is regulated *in vivo* to prevent excessive cell injury and inflammation [138][155]. Host cells are protected by surface bound and soluble plasma complement regulatory proteins. Of particular importance are the plasma proteins Factor H and Factor I which negatively regulate the C3b amplification loop. Although found in the plasma both can act in the fluid phase and on cellular surfaces. Their role on cell surfaces that lack membrane bound complement regulators e.g. the glomerular basement membrane in the kidney is vital as they are the only defence against complement attack and thrombus formation [138][162]. The importance of Factor H is self-evident when considering atypical HUS; where mutations in CFH are associated with the worst outcomes [2].

Being a fluid phase regulator, CFH is predominantly synthesized in the liver, but there is evidence in mice and humans that platelets, podocytes and mesangial cells can produce factor H [296][297][298]. CFH has been shown to bind to C3b deposits on the cell surface and to glycosaminoglycans [296]. In the kidney, it is the binding of CFH to glomerular endothelial cells that is essential to maintain the delicate balance of compliment activation and regulation. Part of the central hypothesis of my work is that Shiga toxin targets the podocyte Gb3 receptor, resulting in a reduction in glomerular VEGF-A which predisposes the glomerular endothelium to complement attack. Our group has already demonstrated that VEGF-A inhibition reduces glomerular CFH via VEGFR2/PKC-α/CREB signalling both *in vitro* and *in vivo* [222]. Suggesting that loss of VEGF-A from podocytes results in loss of CFH protection against complement-mediated damage on the surface of the glomerular endothelial cell [222].

With this in mind, CFH expression in the glomerulus was evaluated in PodrtTA-Tet-O-Gb3 Gb3 null mice given Shiga toxin vs. controls. Immunofluorescence was used to detect CFH in glomeruli. Interestingly, the PodrTA-Tet-O-Gb3 Gb3 null mice had a 50% reduction in the level of CFH in their glomeruli vs. control animals at day 10 following IP Shiga toxin (Figure 7-24). Results were quantified by calculating CTGF (formula as previously detailed). This finding supports the hypothesis that Shiga toxin HUS is associated with a

local reduction in the regulation of the alternative complement pathway in the glomerulus.

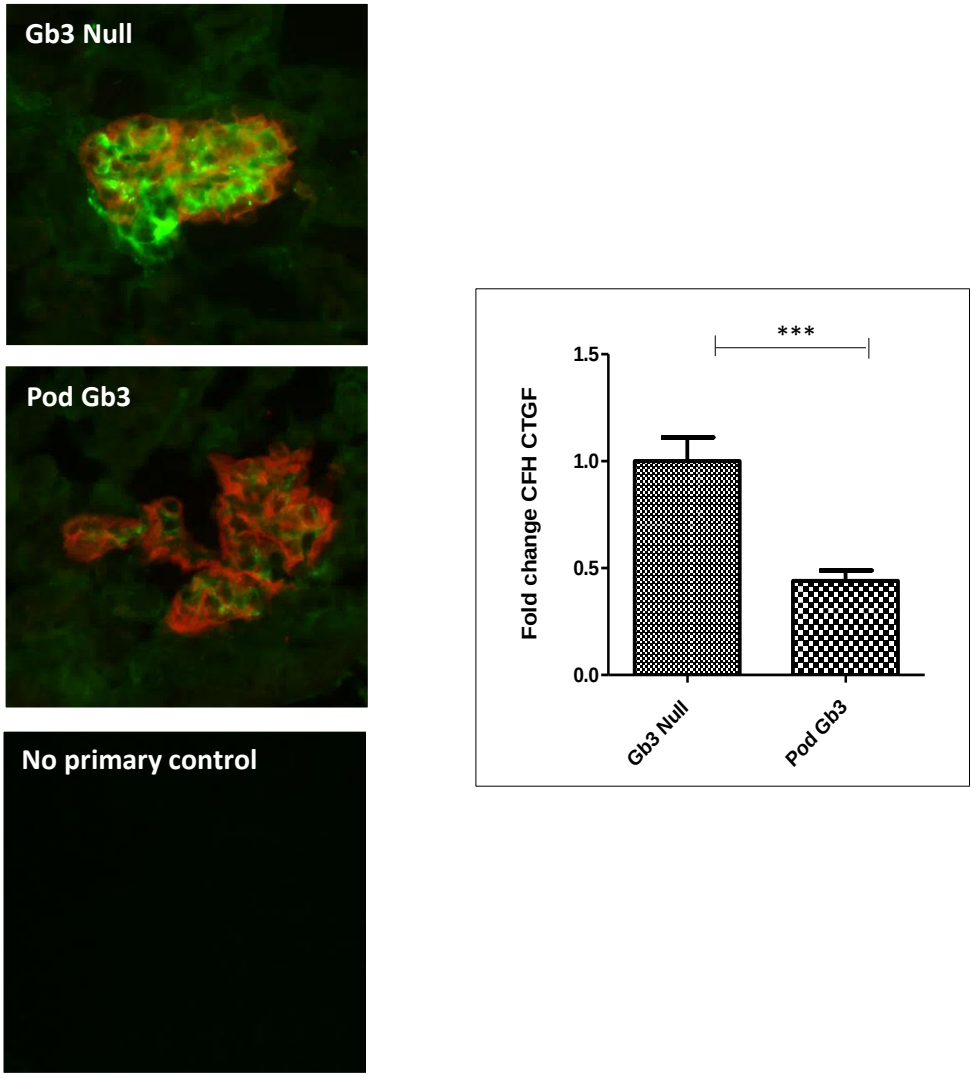

Figure 7-24: PodrtTA-Tet-O-Gb3 Gb3 null mice have reduced CFH deposition in their glomeruli at day 10 following IP Shiga toxin

Frozen kidney sections from PodrtTA-Tet-O-Gb3 Gb3 null (Pod Gb3) mice and control PodrtTA-Tet-O-WT Gb3 null mice (Gb3 null) were probed for CFH (shown in green) using immunofluorescence and co-stained with the podocyte marker nephrin (red). Representative images shown and no primary control for CFH and nephrin shown. This demonstrated a statistically significant reduction in CFH deposition in the glomeruli of the PodrtTA-Tet-O-Gb3 Gb3 null mice as evidenced by a 50% reduction in CTFG . Graph: Pod Gb3 = PodrtTA-Tet-O-Gb3 Gb3 null mice; Gb3 null = PodrtTA-Tet-O-WT Gb3 null mice (for clarity of figure). Results from n=4 mice of each genotype. *** Unpaired T-test p value <0.0001.

7.4.12 Human glomerular cell co-culture experiments confirm the importance of podocyte and endothelial cell cross-talk

The *in vivo* work presented, reflects what has been observed in co-culture human cell work. Conditionally immortalised human podocytes and glomerular endothelial cells were cultured together in transwells and treated with Shiga toxin. Endothelial cells were seeded onto coverslips on the bottom layer and podocytes were seeded into the transwell support. Cells were cultured in endothelial media without VEGF and allowed to differentiate. Shiga toxin 0.1ng/ml was added to the podocyte transwell support at intervals of 30 min to 6 hours. Images shown are from the 6 hour incubation. The Shiga toxin containing media was then removed and cells washed once with PBS. Human C7 deficient serum (40% in gelatine veronal buffer) was then added for 30 minutes. Cells were subsequently washed x3 before being fixed in 4% PFA and immunofluorescence performed for CFH or C3d and co-stained for DAPI. Endothelial cells were then imaged in the Wolfson Bioimaging Facility on confocal multi-laser Leica SP5II microscope. Of note the human anti-C3d antibody used (Abcam #ab17453) on closer inspection was not specific to C3d. It also recognised other C3 cleavage products including C3b and iC3b.

In these co-culture experiments glomerular endothelial cells showed a loss of CFH expression, that was dependent upon the presence of podocytes (Figure 7-25). C3d expression was increased in endothelial cells in these co-culture experiments when the cells were treated with Shiga toxin in the presence of podocytes (Figure 7-27). In the absence of podocytes, endothelial cells treated with Shiga toxin showed no increase in C3d expression. C3d is one of several C3 cleavage products formed when C3 is activated [2]. Clearly, cross-talk between podocytes and endothelial cells both *in vitro* and *in vivo* within the glomerulus; is vital in the development of HUS. Furthermore, it is evident from these data that CFH is an important regulator in Shiga toxin HUS and that a reduction in CFH leads to an increase in C3 activation products within the glomerulus.

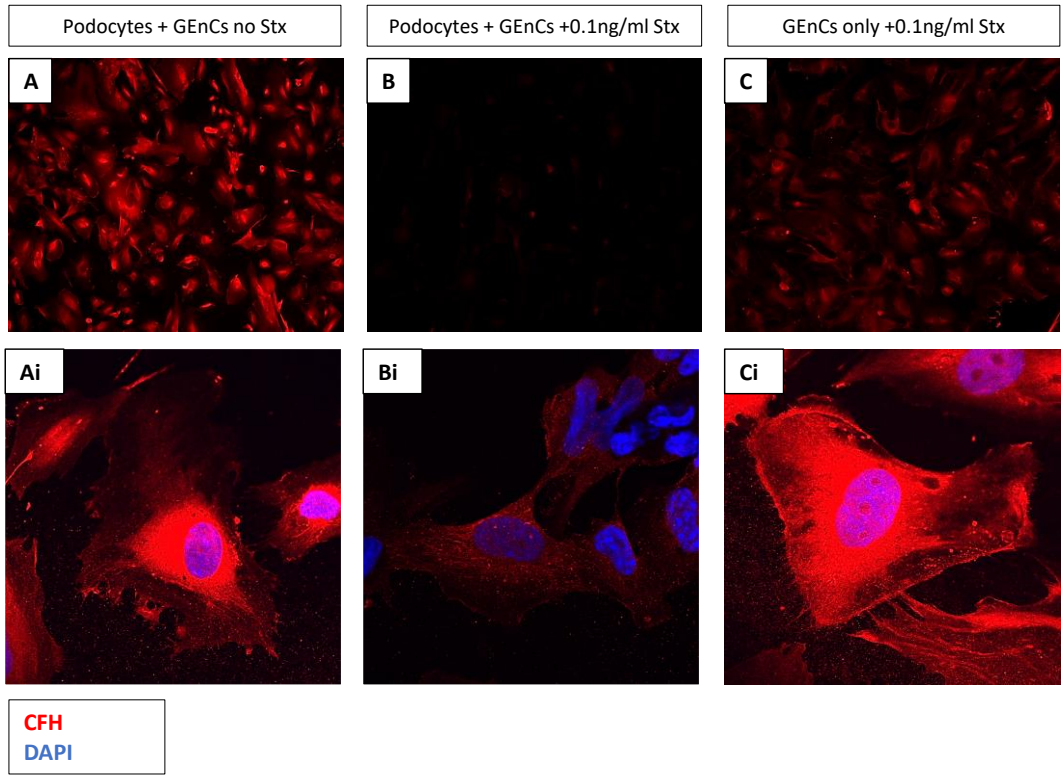

Figure 7-25: Conditionally immortalised human glomerular endothelial cells show a reduction in CFH when co-cultured with podocytes in the presence of Shiga toxin

Co-culture experiments using conditionally immortalised human podocytes and endothelial cells were set up in corning 6-well trans-well supports with 3um pores as described. Panels A and Ai show baseline CFH (red) expression in endothelial cells cultured in the presence of podocytes but no Shiga toxin. Panels B and Bi show a reduction in CFH expression in endothelial cells cultured in the presence of podocytes and Shiga toxin (6 hour incubation time). Panels C and Ci show that endothelial cells cultured alone and treated with Shiga toxin for 6 hours show no change in CFH expression. Images A-C (x10 magnification), images Ai-Ci (x60 magnification). *Experiments representative of n=3 and show DAPI (blue co-staining) performed by Dr Louise Farmer and data reproduced with permission.*

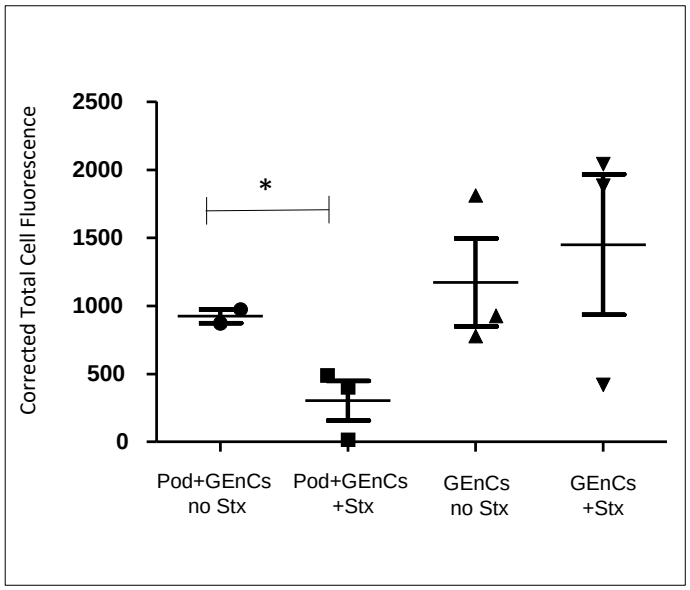

Figure 7-26: Quantification of CFH Immunofluorescence staining

Co-culture experiments using conditionally immortalised human podocytes and endothelial cells were set up in corning 6-well trans-well supports with 3um pores as described. IF images shown in Figure 7-25 were used to quantify the level CFH expression in each experimental group using corrected total cell fluorescence. When podocytes and endothelial cells are co-cultured together in the presence of Shiga toxin for 6 hours there is a statistically significant reduction in CFH expression. * Unpaired T-test $p<0.05$. *Experiments representative of n=3 as identified by each data point: experiment performed by Dr Louise Farmer and reproduced with permission.*

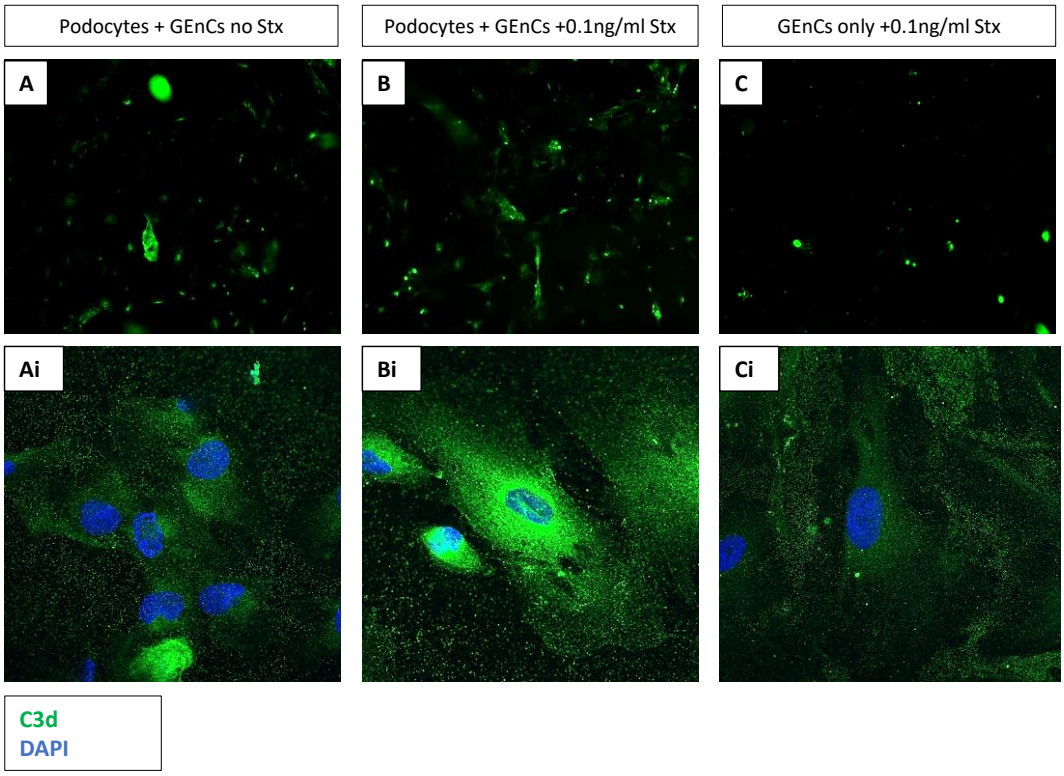

Figure 7-27: Conditionally immortalised human glomerular endothelial cells show an increase in C3d expression in the presence of podocytes and Shiga toxin

Co-culture experiments using conditionally immortalised human podocytes and endothelial cells were set up in corning 6-well trans-well supports with 3um pores as described. Cells were permeabilised prior to antibody application. Panels A and Ai show baseline C3d (green) expression in endothelial cells cultured in the presence of podocytes but no Shiga toxin. Panels B and Bi show an increase in C3d expression in endothelial cells cultured in the presence of podocytes and Shiga toxin (6 hour incubation time). Panels C and Ci show that endothelial cells cultured alone and treated with Shiga toxin for 6 hours show no change in C3d expression. Of note the human anti-C3d antibody used (Abcam #ab17453) was not specific to C3d. It also recognises other C3 cleavage products including C3b and iC3b. Images A-C (x10 magnification), images Ai-Ci (x60 magnification). *Experiments representative of n=3 and show DAPI (blue co-staining) performed by Dr Louise Farmer and data reproduced with permission.*

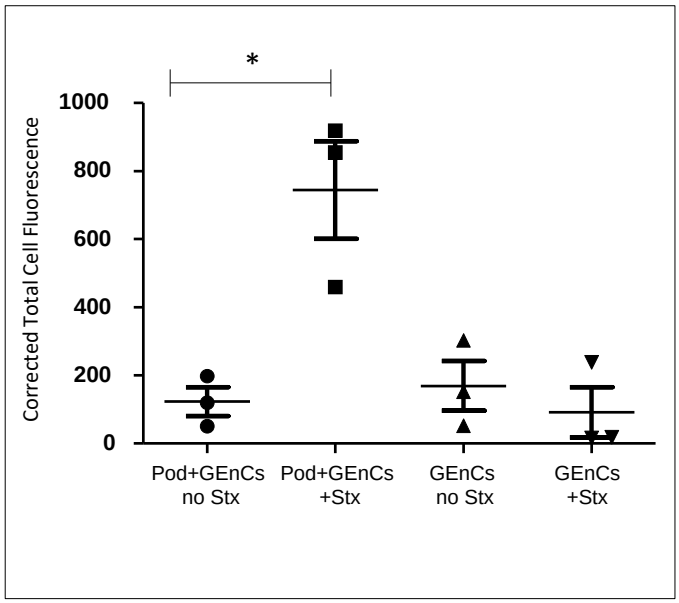

Figure 7-28: Quantification of C3d immunofluorescence staining

Co-culture experiments using conditionally immortalised human podocytes and endothelial cells were set up in corning 6-well trans-well supports with 3um pores as described. IF images shown in Figure 7-27 were used to quantify the level C3d expression in each experimental group using corrected total cell fluorescence. When podocytes and endothelial cells are co-cultured together in the presence of Shiga toxin for 6 hours there is a statistically significant increase in C3d expression. * Unpaired T-test $p<0.05$. *Experiments representative of n=3 as identified by each data point: experiment performed by Dr Louise Farmer and data reproduced with permission.*

7.5 Discussion

This chapter has described the generation of a novel mouse model: the PodrtTA-Tet-O-Gb3 Gb3 null mouse. This mouse only expresses the receptor for Shiga toxin (Gb3) in the podocyte in the presence of doxycycline due to tetracycline-controlled transcription of Gb3 synthase; allowing specific study of the role of the podocyte in HUS. Fascinatingly, when these mice were given IP Shiga toxin, they developed HUS: thrombocytopenia, haemolytic anaemia, and uraemia. This was most striking at day 10 following IP Shiga toxin treatment ($p<0.05$). This is the first time that a mouse model of Shiga toxin HUS (which recapitulates the disease in humans) has ever been described. Even more interesting, is that these animals appeared to recover by day 24 post Shiga toxin, recapitulating what is often seen in patients with Shiga toxin HUS [3]. Renal histology demonstrated glomerular TMA; the pathognomonic lesion of HUS; with intracapillary thrombus formation seen on EM. Immunofluorescence has demonstrated an increase in glomerular fibrinogen deposition and C3b vs. controls. Additionally, glomerular expression of complement

regulator Factor H was significantly reduced in PodrtTA-Tet-O-Gb3 Gb3 null mice, rendering them more susceptible to complement attack. To determine whether the increase in glomerular C3b deposition in this model is due to loss of CFH regulation; it would be interesting to see if restoration of local glomerular CFH levels rescued the phenotype and reduced C3b deposition. An alternative explanation for the apparent loss of glomerular CFH expression is that CFH binding affinity to C3b on the glomerular endothelial cell surface has been attenuated; for example, by loss of glycocalyx induced by Shiga toxin driven damage to the podocyte. Indeed, it has already been shown in Factor H binding assays that the interaction between CFH and C3b is enhanced when these molecules are bound to host cell glycocalyx [164]. Lectin staining and analysis of the glomerular endothelium in the kidneys of PodrtTA-Tet-O-Gb3 Gb3 null mice given Shiga toxin at the different experimental time points studied (days 4 through to 24) would be a relatively straightforward experiment to perform to ascertain whether glycocalyx is lost prior to STEC HUS onset in my model.

These observations were echoed in human cell co-culture experiments. Only in the presence of podocytes did glomerular endothelial cells increase C3 cleavage product (C3d, C3b, iC3b) expression and loose the protection of complement regulator FH when exposed to Shiga toxin. Glomerular endothelial cells alone (treated with Shiga toxin) showed no change in C3 cleavage product expression and did not lose CFH protection. Clearly, the crosstalk between podocytes and glomerular endothelial cells both *in vitro* and *in vivo* within the glomerulus; is vital in the development of Shiga toxin HUS. In fact, the podocyte Gb3 receptor appears to be a key initiator of the disease. The finding that the podocyte is capable of causing a systemic Shiga toxin driven syndrome, may well explain why HUS has a predilection to present in the kidney. Shiga toxin HUS does not affect every endothelial cell or vascular bed in the body; it only affects the kidney. It is only in the kidney that this highly specialised blood filtration interface between podocytes and endothelial cells exists. Suggesting that it is the unique cross-talk interaction between these glomerular cells that leads to the development of HUS.

Chapter 8 : C5 inhibition in a Shiga toxin HUS mouse model

8.1 Introduction

The PodrtTA-Tet-O-Gb3 Gb3 null mouse develops a phenotype that recapitulates the human features of Shiga toxin HUS when given IP Shiga toxin. This is the first time a small animal model of Shiga toxin HUS has ever been described. This can now be used to study the *in vivo* pathophysiology of Shiga toxin HUS and help to determine the effects of different therapeutic interventions on the development of the disease. Central to my hypothesis is that Shiga toxin targets the podocyte, which communicates with the glomerular endothelium increasing its susceptibility to complement attack. Acute inhibition of VEGF-A secretion from the podocyte is one possible mechansim driving this. In order to test this theory, a definitive experimental plan was devised to therapeutically rescue the PodrtTA-Tet-O-Gb3 Gb3 null mouse from Shiga toxin HUS using the mouse C5 inhibitor (BB5.1). This inhibitor is analogous to the C5 inhibitor eculizumab, which is already being used in humans to treat atypical HUS.

8.2 Experimental design

As summarised in Figure 8-2, PodrtTA-Tet-O-Gb3 Gb3 null mice aged between 10-12 weeks were given 14 days of oral doxycycline in their drinking water to induce Gb3 expression in their podocytes. They were then randomised to receive either 1mg of intraperitoneal (IP) mouse C5 inhibitor (mAb BB5.1 Hycult® Biotech) or IP 0.9% sterile normal saline of the same volume as a control. The following day all mice received IP Shiga toxin at a dose of 10ng/g. Three days later the mice were given either a second dose of 1mg of IP C5 inhibitor or IP 0.9% sterile normal saline control. This dosing regime was chosen due to the known half-life of BB5.1 which is 72 hours, together with the recommendation of Hycult® Biotech of twice weekly dosing which has been reported by other groups to successfully inhibit C5 *in vivo* [299][300].

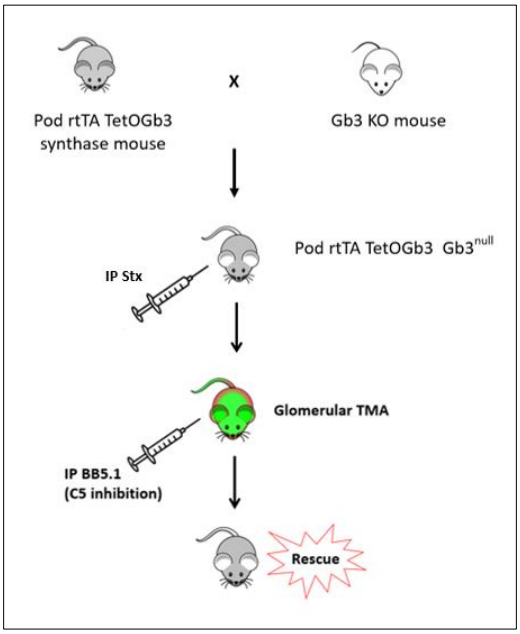

Figure 8-1: Overview of *in vivo* experimental plan with breeding strategy

PodrtTA-Tet-O-Gb3 mice on a WT background were back-crossed with Gb3 KO mice to generate the PodrtTA-Tet-O-Gb3 Gb3 null mouse. This mouse only expresses Gb3 in its podocyte following induction of Gb3 synthase by doxycycline treatment. When given IP Shiga toxin these mice develop Shiga toxin HUS (including evidence of a glomerular TMA). To determine whether this is complement driven a C5 inhibitor (BB5.1) was given IP to attempt to rescue the HUS phenotype.

Prior to starting this set of experiments, a new batch of Shiga toxin (List Biological Laboratories Inc.) was purchased. As discussed in the methods chapter, each time a new batch of Shiga toxin was purchased its virulence was assessed *in vivo* by administering an IP injection of 10ng/g to at least 2 wild type mice. From previous work, these mice were expected to die from dehydration (due to extra-glomerular off target tubular effects) within 3-4 days. However, upon testing this batch of toxin these mice died within 36 hours.

Given this observation, together with the finding that in my previous experiments PodrtTA-Tet-O-Gb3 Gb3 null mice had recovered platelet levels 24 days after IP Shiga toxin challenge; all mice in this set of experiments were electively terminated at day 7 post Shiga toxin treatment. This was to avoid missing any potential effect of the C5 inhibitor attenuating Shiga toxin HUS in light of this batch of toxin being slightly more potent in wild type mice. Interestingly, the purity of the new batch of Shiga toxin was >98% and the endotoxin content determined on kinetic chromogenic LAL assay at List Labs was <90EU/mg (the same as the previous vial supplied). Hence, I suspect that the increase

in virulence seen was attributable to the fact that the toxin was used within a few days of its arrival (rather than a few weeks) and so not kept at -20°C for very long. It is has been shown that long term storage > 6 months at -20°C will reduce the virulence of Shiga toxin [300].

As in the previous set of experiments (described in Chapter 7), blood was taken at the time of terminal anaesthesia via cannulation of the inferior vena cava. This was taken with a pre-heparinised 23 gauge needle and syringe to ensure the blood obtained did not clot. Differential full blood count (which included platelet and haemoglobin measurements) was obtained from the Sysmex XN-20® in Bristol Royal Infirmary Haematology department. Blood films were also made in the same way as before, with 3 films per mouse produced.

Any remaining blood sample was taken back to the laboratory and centrifuged (as before), to separate it into upper plasma layer and lower red cell layer. The upper plasma layer was carefully pipetted off, avoiding any contamination of the sample with red cells. The plasma was then sent to Kay Burt at Langford Veterinary school for measurement of urea. All blood samples were analysed within 30 - 45 minutes from collection from the mouse to ensure accuracy. Urine was collected and analysed as described in the methods chapter. At the time of terminal anaesthesia, organs were harvested from the mice following the protocol outlined in the methods chapter.

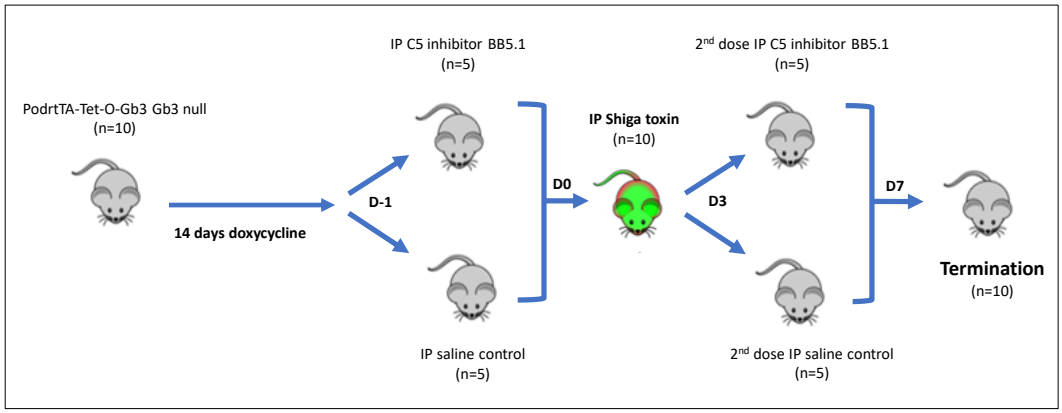

Figure 8-2: Experimental plan for C5 inhibition in Shiga toxin HUS mouse model

PodrtTA-Tet-O-Gb3 Gb3 null mice (n=10) were given 14 days of oral doxycycline in their drinking water to induce Gb3 expression in their podocytes only. They were then randomised to receive either C5 inhibitor (BB5.1) or sterile saline control via an intraperitoneal (IP) injection. The following

day they were all given IP Shiga toxin at 10ng/g and 3 days later a top up dose of either C5 inhibitor or saline IP. At day 7 (post IP Shiga toxin) all mice were electively terminated for organ harvesting and blood sampling.

8.3 C3b expression time course in Podrt-TA-Tet-O-Gb3 Gb3 null mice vs. controls

Before the decision to electively terminate mice at day 7 post Shiga toxin treatment in the C5 inhibitor experiment, the timing of the changes in C3b (complement factor 3b) were studied. This was carried out by performing C3b IF in frozen sections taken from mouse kidneys in the PodrtTA-Tet-O-Gb3 Gb3 null mice given Shiga toxin vs. control PodrtTA-Tet-O-WT Gb3 null mice. Sections were probed for C3b from mice that had been electively terminated on day 4, day 7 and day 10 post Shiga toxin IP. This work was performed by postdoctoral researcher Dr Jenny Hurcombe. The same protocol outlined in my methods was followed to obtain these results.

This work showed that as early as day 4 and certainly by day 7 post Shiga toxin, there was evidence of C3b deposition in the glomeruli of PodrtTA-Tet-O-Gb3 Gb3 null mice (Figure 8-3). This finding reinforced the decision to use day 7 post Shiga toxin as a termination point in my inhibitor experiment; as this was not only enough time post Shiga toxin challenge for complement to have been activated in the glomerulus, but it appears to peak at this time point. Hence, following two doses of the C5 inhibitor, and 7 days after Shiga toxin challenge, if there was any effect of C5 inhibition on the complement cascade I would expect to be able to observe it at this timepoint.

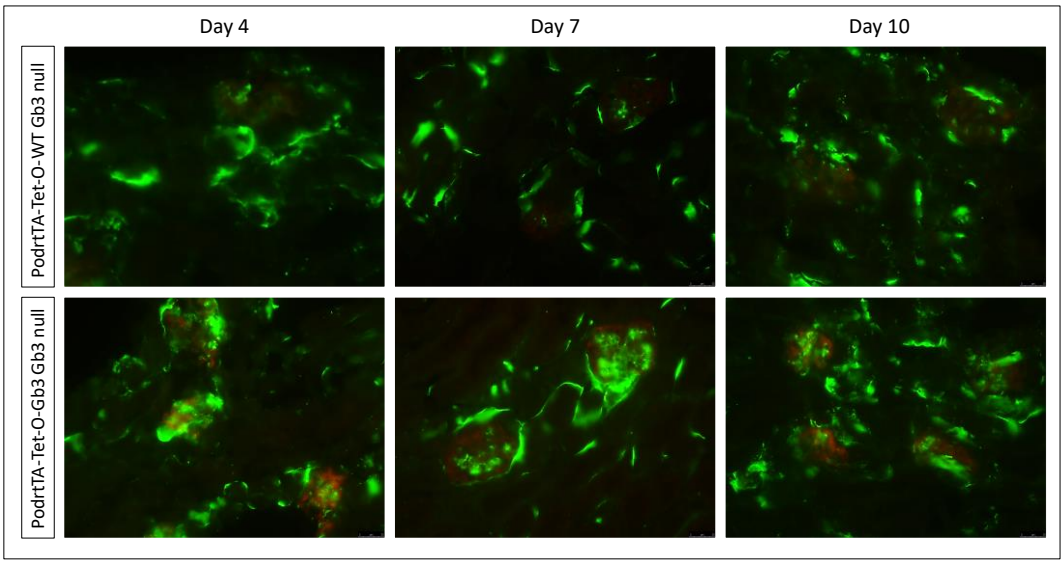

Figure 8-3: C3b IF time course in PodrtTA-Tet-O-Gb3 Gb3 null mice vs. PodrtTA-Tet-O-WT Gb3 null control mice at day 4, 7 and 10 post Shiga toxin treatment (x40 magnification).

IF for C3b was performed on frozen kidney sections in PodrtTA-Tet-O-Gb3 Gb3 null mice (bottom row) and controls (top row) following Shiga toxin challenge at day 4, 7 and 10 as indicated. C3b staining (green) can be clearly seen within the glomeruli (identified with nephrin co-staining in red) at each time point in the PodrtTA-Tet-O-Gb3 Gb3 null mice. Just as previously seen, the PodrtTA-Tet-O-Gb3 Gb3 null mice show an increase in C3b staining in their glomeruli vs. controls. This is apparent as early as day 4 post Shiga toxin treatment and in this cohort of mice C3b appears to peak at day 7 post IP Shiga toxin. Image representative of n=3 of each genotype at each timepoint. *Experiment performed by postdoctoral scientist Dr Jenny Hurcombe reproduced with permission*.

8.4 C5 inhibition prevents the development of toxin HUS

As already discussed in chapter 7, cleavage of C3 can occur via all 3 complement cascade pathways: classical, lectin and alternative. It is at the point of cleavage of C3 that these pathways converge and go on to culminate with the formation of the membrane attack complex (MAC). This leads to the insertion of pores into the target cell membrane resulting in osmotic lysis and cell death. Inhibition of C5 would not be anticipated to affect activation of C3 because this occurs upstream in the complement cascade. However, by inhibiting C5 the formation of the MAC should be prevented (Figure 8-4). Determining which of the 3 complement pathways are being activated in Shiga toxin HUS (i.e. classical, lectin or the alternative) will not be possible merely from inhibiting C5; as the pathways have already converged at this point, but it will provide evidence of whether complement blockade has any effect upon the development of the HUS phenotype in the model.

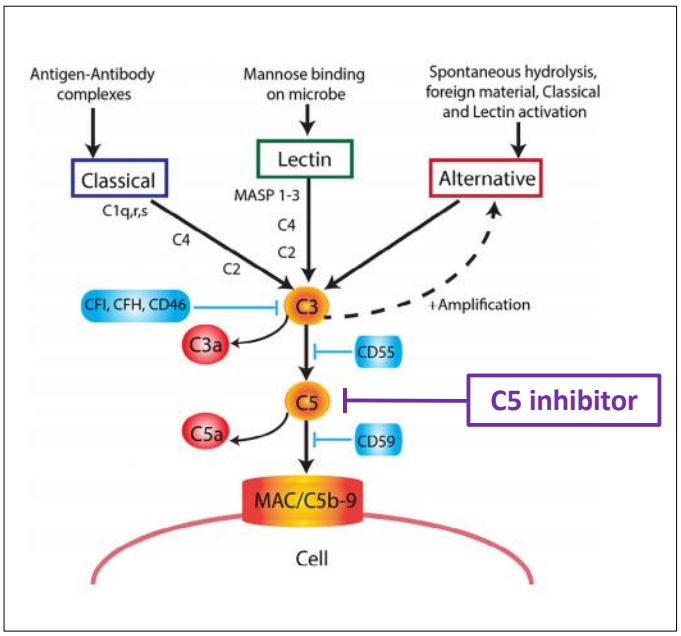

Figure 8-4: The complement cascade

The complement cascade can be activated by one of 3 pathways: the classical, lectin or alternative pathways. All 3 converge at the point of cleavage of C3 and go on to culminate with the formation of the membrane attack complex (MAC). This leads to the insertion of pores into the target cell membrane resulting in osmotic lysis and cell death. As is evident from this diagram, C5 inhibition (at the level indicated by the C5 inhibitor box) will not affect C3 activation which occurs upstream of this point in the pathway. However, C5 inhibition will prevent the formation of the MAC, thus preventing cell death occurring. *Figure adapted from Keir and Langman et al.* [30].

8.4.1 C5 inhibition in PodrtTA-Tet-O-Gb3 Gb3 null mice post IP Shiga toxin prevents thrombocytopenia

As already outlined, PodrtTA-Tet-O-Gb3 Gb3 mice (n=10) aged between 10-12 weeks of age were given 14 days of oral doxycycline, followed by 1mg/per mouse of IP C5 inhibitor (BB5.1) or 0.9% sterile normal saline of the same volume as a control. The following day all mice were given 10ng/g of Shiga toxin IP to induce a Shiga toxin HUS phenotype and 3 days later a further dose of IP C5 inhibitor or saline control. All mice were terminated at day 7 post Shiga toxin inoculation. Terminal blood sampling from these mice on day 7 showed that mice given the IP saline control dropped their platelet count to the levels seen in my previous cohort of experiments at day 7 post IP Shiga toxin (under 500 $x10^9$/L), but those given the C5 inhibitor BB5.1 were protected from this effect (Figure 8-5). This suggests a protective effect of C5 inhibition against thrombocytopenia in my Shiga Toxin HUS model.

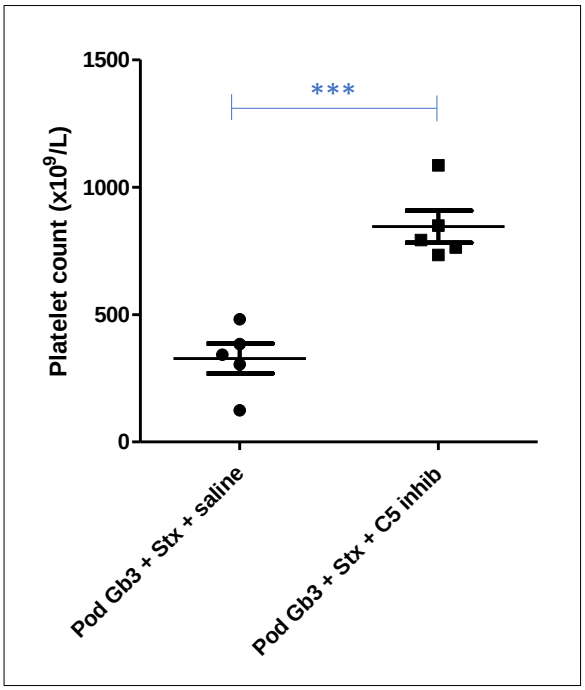

Figure 8-5: C5 inhibition prevents thrombocytopenia in Shiga toxin HUS

Comparison of platelet count in PodrtTA-Tet-O-Gb3 Gb3 null mice given IP Shiga toxin with or without C5 inhibition is shown. N=5 for each group, with individual points representing each n. Platelet count drops to under 500 x10^9/L in the mice given IP Shiga toxin and saline. In the mice given IP Shiga toxin and C5 inhibitor platelet count is preserved to almost double that of the saline group. ***Unpaired T-test p value = 0.0003.

8.4.2 C5 inhibition in PodrtTA-Tet-O-Gb3 Gb3 null mice post IP Shiga toxin prevents anaemia and uraemia

Blood samples from all PodrtTA-Tet-O-Gb3 Gb3 null mice were analysed for haemoglobin and urea at termination on day 7 post IP Shiga toxin as already described. Mice that had been given IP saline as a control showed a drop in haemoglobin and a rise in urea. Mice that were administered IP C5 inhibitor BB5.1, showed preservation of their haemoglobin and no rise in urea (Figure 8-6). These findings were both statistically significant. Together with the finding that C5 inhibition prevents thrombocytopenia in mice given IP Shiga toxin; these data suggest that C5 inhibition prevents the development of Shiga toxin HUS in my mouse model. This is the first time that complement inhibition *in vivo* has been shown to be of benefit in Shiga toxin associated HUS.

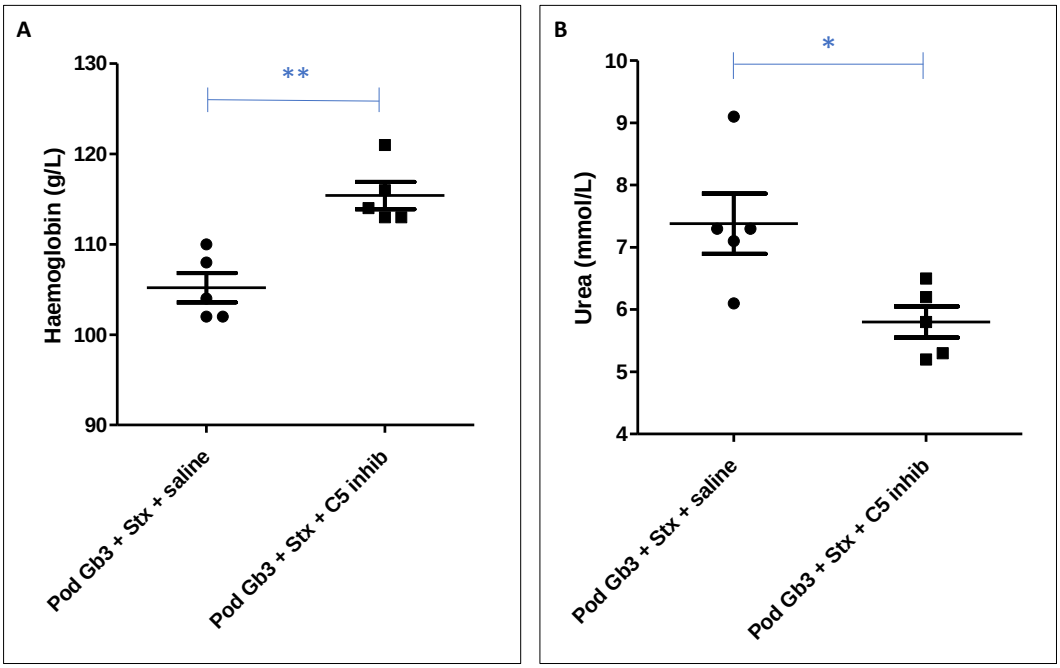

Figure 8-6: C5 inhibition prevents anaemia and uraemia in Shiga toxin HUS

Panel A shows the comparison of haemoglobin in PodrtTA-Tet-O-Gb3 Gb3 null mice given IP Shiga toxin with or without C5 inhibition. N=5 for each group, with individual points representing each n. In the mice given IP Shiga toxin and C5 inhibitor haemoglobin is preserved vs. the anaemia seen in the mice given IP Shiga toxin and normal saline control. **Unpaired T-test p value 0.0017. Panel B shows the comparison of urea in PodrtTA-Tet-O-Gb3 Gb3 null mice given IP Shiga toxin with or without C5 inhibition. N=5 for each group, with individual points representing each n. Mice given IP Shiga toxin and saline become uraemic, but mice given the IP C5 inhibitor are protected from this effect of IP Shiga toxin. *Unpaired T-test p value = 0.02.

8.4.3 C5 inhibition in PodrtTA-Tet-O-Gb3 Gb3 null mice post IP Shiga toxin prevents haemolytic anaemia

Blood films were generated, fixed, and analysed in the same way as previously described in results chapter 7. Blood films were necessary to confirm whether erythrocyte haemolysis was the cause of the anaemia seen in the mice given IP Shiga toxin and IP saline. For each mouse 3 blood films were analysed to ensure a representative sample had been obtained. Mice that received IP Shiga toxin and normal saline showed evidence of haemolytic anaemia, with fragmentation of red blood cells visible on the film. Mice given IP Shiga toxin and C5 inhibitor treatment showed no evidence of haemolysis and normal appearance of their red blood cells (Figure 8-7). An estimated 5-10% of red cells were fragmented in PodrtTA-Tet-O-Gb3 Gb3 null mice given IP Shiga toxin and saline in

each animal (n=5). This is slightly lower than the 10-15% observed in my previous cohort terminated at day 10 post Shiga toxin challenge.

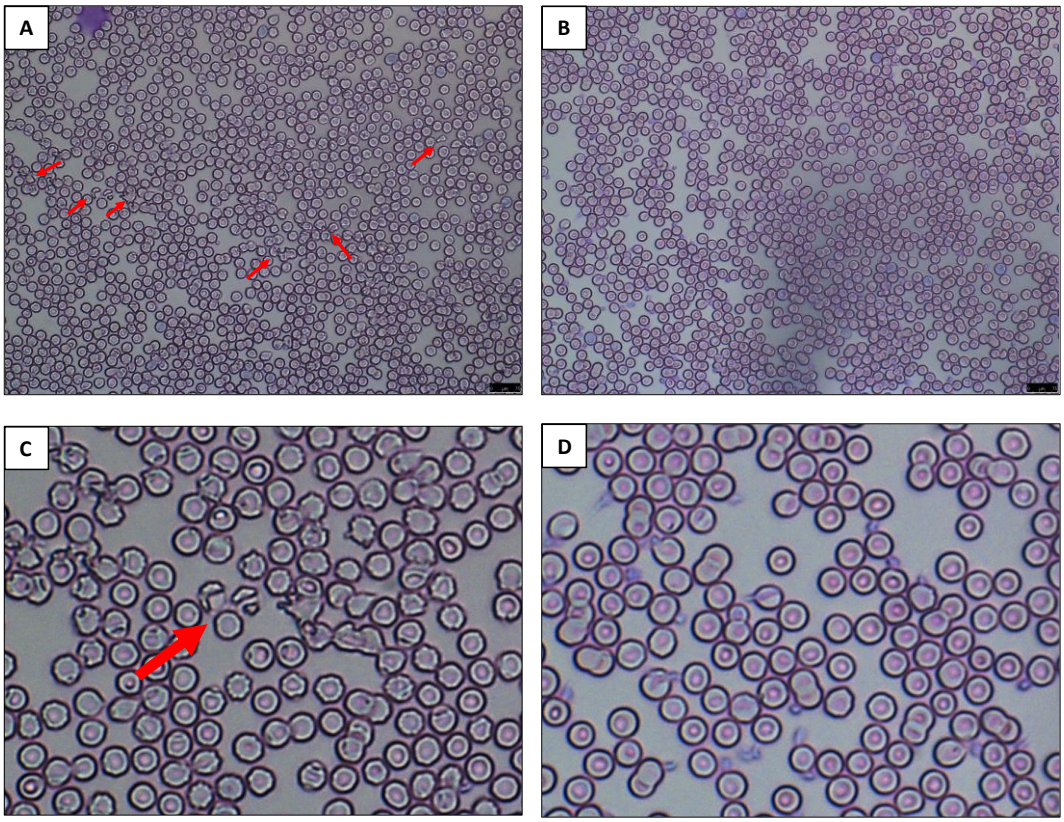

Figure 8-7: C5 inhibition prevents haemolytic anaemia in Shiga toxin HUS

Blood films for PodrtTA-Tet-O-Gb3 Gb3 null mice given IP Shiga toxin and saline (A and C) and PodrtTA-Tet-O-Gb3 Gb3 null mice given IP Shiga toxin and C5 inhibitor treatment (B and D) terminated at day 7 post Shiga toxin are shown. Red arrows indicate red cell fragments which are only seen in PodrtTA-Tet-O-Gb3 Gb3 null animals given Shiga toxin and saline. Panels C and D are the same blood films, but images are zoomed in to allow better visualisation of fragments. Magnification is x40. Blood films shown are representative of all animals analysed (n=5 in each group). An estimated 5-10 % of red cells in the PodrtTA-Tet-O-Gb3 Gb3 null mice given Shiga toxin and saline were fragmented in each animal: representative blood films shown.

8.4.4 C5 inhibition in PodrtTA-Tet-O-Gb3 Gb3 null mice post IP Shiga toxin prevents TMA

The trichrome stain martius scarlet blue (MSB) was performed on kidney sections taken from PodrtTA-Tet-O-Gb3 Gb3 null mice given IP Shiga toxin and saline or C5 inhibitor. In this trichrome stain, fibrin clots appear red, erythrocytes yellow and collagen blue. Three

mice from each experimental group were analysed. Fibrin thrombi were clearly seen in the glomeruli of PodrtTA-Tet-O-Gb3 Gb3 null mice given Shiga toxin and saline; with no evidence of thrombi in the PodrtTA-Tet-O-Gb3 Gb3 null mice given Shiga toxin and C5 inhibitor. Images shown are representative of n=3 for each experimental group and were taken using the Leica DMI 6000B microscope at x40 to x100 magnification (Figure 8-8 and Figure 8-9).

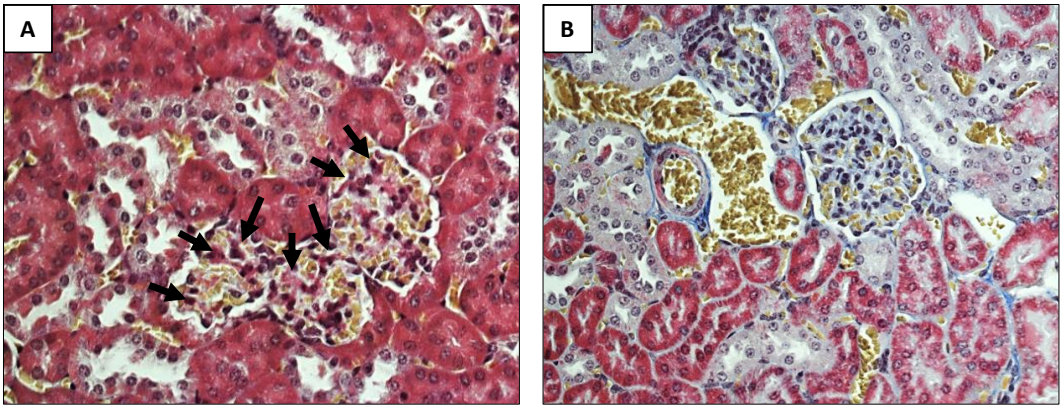

Figure 8-8: C5 inhibition prevents glomerular TMA in Shiga toxin HUS (x40 magnification)

Martius scarlet blue (MSB) trichrome stain of renal tissue from a PodrtTA-Tet-O-Gb3 Gb3 null mouse given IP Shiga toxin and normal saline (A) vs. PodrtTA-Tet-O-Gb3 Gb3 null mouse given IP Shiga toxin and C5 inhibitor (B). In panel A: fibrin thrombi (red) are seen within the glomerular capillary loops indicated by black arrows. These appearances are characteristic of a glomerular TMA, the same histopathological lesion that is seen in humans with Shiga toxin HUS. In panel B: there are no fibrin thrombi seen in the glomeruli. Fibrin = red, collagen = blue, erythrocytes = yellow. Images shown are representative of n=3 for each experimental group and were taken using the Leica DMI 6000B microscope at x40 magnification.

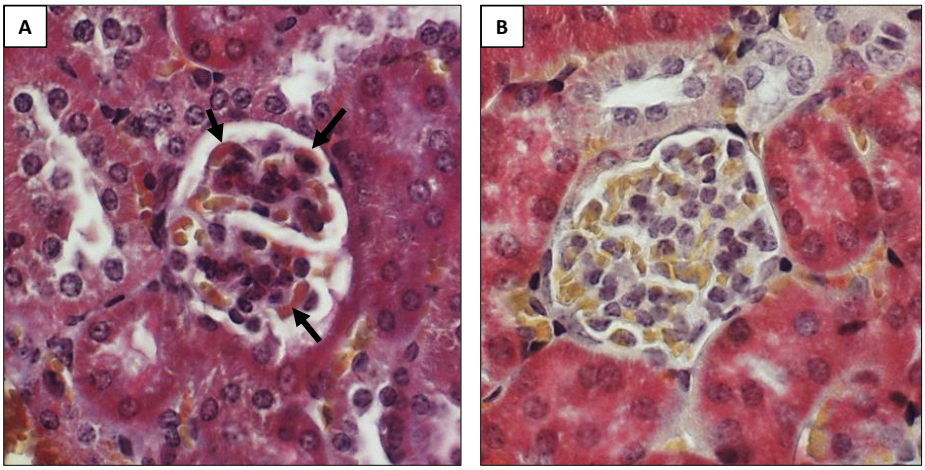

Figure 8-9: C5 inhibition prevents glomerular TMA in Shiga toxin HUS (x100 magnification)
Martius scarlet blue (MSB) trichrome stain of renal tissue from a PodrtTA-Tet-O-Gb3 Gb3 null mouse given IP Shiga toxin and normal saline (A) vs. PodrtTA-Tet-O-Gb3 Gb3 null mouse given IP Shiga toxin and C5 inhibitor (B). Glomerular fibrin thrombi are clearly seen in panel A as indicated by black arrows. There is no evidence of fibrin thrombi in the glomerulus of the PodrtTA-Tet-O-Gb3 Gb3 null mouse given Shiga toxin and the C5 inhibitor. Fibrin = red, collagen = blue, erythrocytes = yellow. Images shown are representative of n=3 for each experimental group and were taken using the Leica DMI 6000B microscope at x100 magnification.

As well as performing an MSB trichrome stain to look for evidence of TMA in both experimental groups; kidney tissue was also sent for electron microscopy analysis (EM). Kidney tissue was harvested at the time of termination and preserved in EM fixative. This was then processed by the Wolfson Bioimaging Facility at the University of Bristol and subsequently sectioned on an ultramicrotome. Unfortunately, these sections are yet to be imaged on the Tecnai 12 120kV BioTwin Spirit Transmission Electron Microscope scanner; due to the SARS-CoV-2 global pandemic the Wolfson imaging Institute had to close before this could be performed. These sections will be imaged as soon as the Wolfson Institute re-opens.

8.4.5 C5 inhibition prevents the activation of compliment factors C7 and C9

It is evident from the data presented above, that C5 inhibition prevents thrombocytopenia, haemolytic anaemia, uraemia, and glomerular TMA in this mouse model of Shiga toxin HUS. However, I wanted to be sure that C5 blockade had led to successful inhibition of MAC formation. To do so, MAC formation needed to be demonstrated in the glomeruli of the mice given Shiga toxin without the C5 inhibitor, with

absence of MAC formation in the mice administered BB5.1. Unfortunately, there are very few commercially available C5b-9 (MAC) antibodies for use in mice (see appendix for list of antibodies tested).

The immunofluorescence staining with these antibodies resulted in a high background signal in all of the samples tested, even in control Gb3 null mice that did not develop Shiga toxin HUS. Several optimisation techniques were attempted to improve this including: using normal serum from the same species as the secondary antibody (rabbit) to improve the blocking step of the protocol; incubating with the blocking solution for longer, additional washing steps and checking for secondary antibody cross-reactivity by using an isotype control antibody. The same antibodies were also used for IHC to determine whether more specific staining could be achieved using this application. Despite all of these modifications, I was unable to demonstrate specific C5b-C9 antibody staining using these antibodies (Figure 8-10).

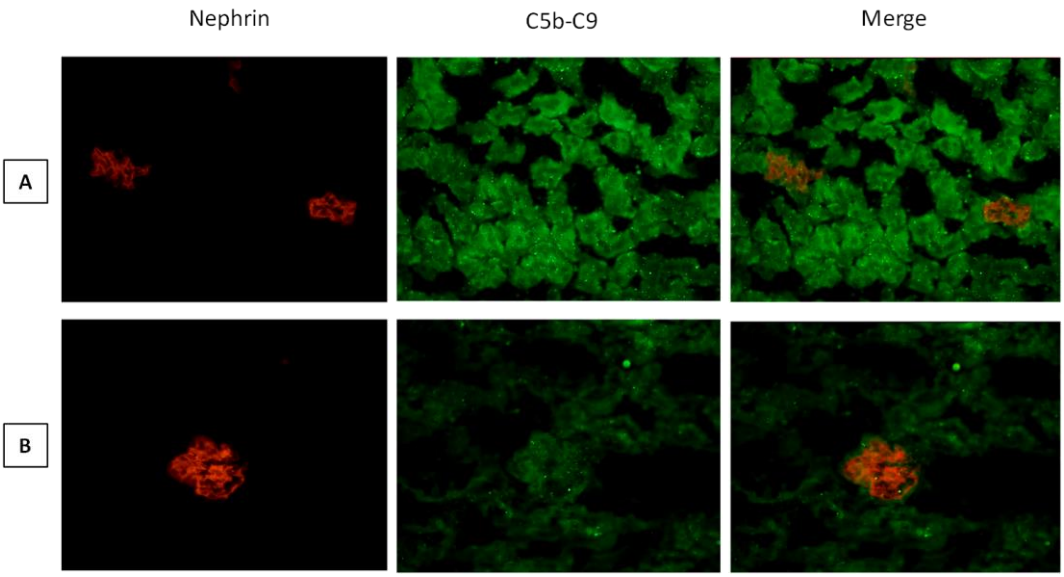

Figure 8-10: C5b-C9 Immunofluorescence optimisation

Immunofluorescence using the rabbit polyclonal anti C5b-C9 (MAC) antibody from Abcam (#ab55811). The top row (A) is a kidney section from a PodrtTA-Tet-O-Gb3 Gb3 null mouse administered IP Shiga toxin and electively terminated on day 10. The bottom row (B) is a kidney section from a PodrtTA-Tet-O-WT Gb3 null mouse (effectively Gb3 null mouse) also given IP Shiga toxin and electively terminated on day 10. In both cases there was a high background signal which meant no conclusions could be drawn. Despite the use of different blocking agents and using different antibody concentrations this could not be improved. *C5b-C9 antibody used at a*

concentration of 1 in 200 to obtain these images at a magnification of x40. Nephrin (red), C5b-C9 (green) and final image is merged as labelled.

Through a collaboration with Cardiff University Professor Paul Morgan, an expert in complement biology (with a special interest in the MAC); I was kindly gifted mouse anti-C7 and anti-C9 antibodies that had been generated by his group (see appendix for details). The anti-C9 antibody had already been used and peer reviewed in previously published work, but the anti-C7 antibody was newly developed and had only been tested in ELISAs and western blotting applications [301]. Immunofluorescence results with these antibodies were specific and reproducible on technical repeats. Immunofluorescence was performed using the standard protocol outlined in my methods chapter, with the addition of normal goat serum to the blocking solution at 10% concentration as recommended by Prof. Morgan's group. This is the first time that mouse anti-C7 antibody (clone 73D1) has been used for immunofluorescence in mouse kidney tissue.

Both C7 and C9 compliment factors were detected by immunofluorescence in PodrtTA-Tet-O-Gb3 Gb3 null mice given IP Shiga toxin and saline. Furthermore, these factors were virtually undetectable in mice given IP Shiga toxin and C5 inhibitor (Figure 8-11 and Figure 8-12). This work demonstrates the successful inhibition of C5 by BB5.1 *in vivo*, resulting in prevention of MAC formation in the kidney. Indeed, it is well established that C7 is the central regulator of the assembly of the MAC, as it is only in the presence of C7 that the stable bimolecular C5b6 complex can incorporate itself into the target cell membrane [302]. If C7 levels are insufficient locally, the C5b6 complex (formed from the activation of C5) dissociates and accumulates in the fluid phase [302].

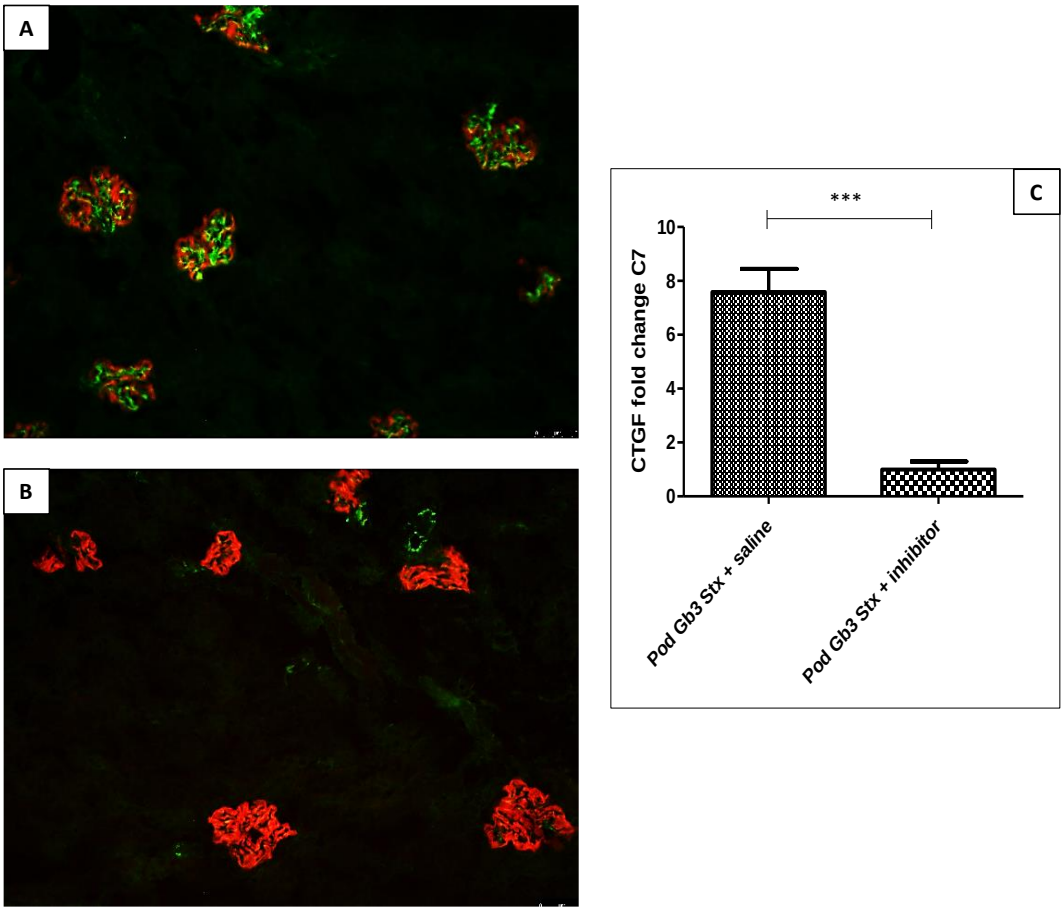

Figure 8-11: C5 inhibition prevents the activation of compliment factor C7

Frozen kidney sections from PodrtTA-Tet-O-Gb3 Gb3 null mice given IP Shiga toxin and either IP saline (panel A) or IP C5 inhibitor (panel B) were probed for C7 using IF (shown in green) and co-stained with the podocyte marker nephrin (red). This demonstrated a statistically significant increase in C7 deposition in the glomeruli of the mice administered saline vs. those given C5 inhibitor BB5.1. As evidenced by the increase in fold change of C7 fluorescence intensity of x8 fold. Graph C: Pod Gb3 = PodrtTA-Tet-O-Gb3 Gb3 null mice (for clarity of figure). Results from n=3 mice of each experimental group: 15 glomeruli per mouse at x20 magnification. *** Unpaired T-test p value <0.0001.

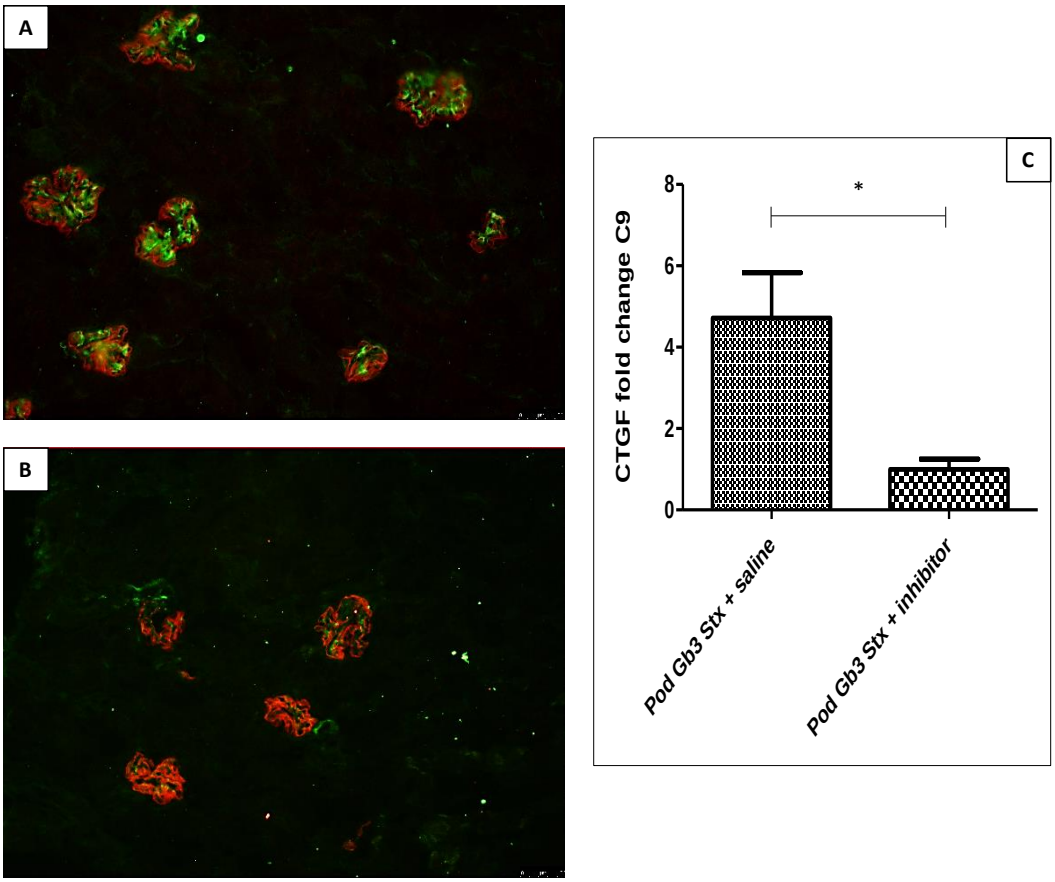

Figure 8-12: C5 inhibition prevents the activation of compliment factor C9

Frozen kidney sections from PodrtTA-Tet-O-Gb3 Gb3 null mice given IP Shiga toxin and either IP saline (panel A) or IP C5 inhibitor (panel B) were probed for C9 using IF (shown in green) and co-stained with the podocyte marker nephrin (red). This demonstrated a statistically significant increase in C9 deposition in the glomeruli of the mice administered saline vs. those given C5 inhibitor BB5.1. As evidenced by the increase in fold change of C9 fluorescence intensity of x6 fold. Graph C: Pod Gb3 = PodrtTA-Tet-O-Gb3 Gb3 null mice (for clarity of figure). Results from n=3 mice of each experimental group: 15 glomeruli per mouse at x20 magnification. *Unpaired T-test p value = 0.0143.

Once the stable trimolecular complex of C5b6 and C7 has formed, recruitment of compliment factors C8 and C9 generates a cylindrical structure that extends through the glycolipid bilayer of the target cell membrane and causes leakage with subsequent osmotic lysis of the cell [303]. Of note, after the initial enzymatic cleavage of C5, the assembly of the MAC requires no further enzymatic activity [303]. Hence, the increase in C7 (x8 fold) and in C9 (x6 fold) seen in the PodrtTA-Tet-O-Gb3 Gb3 null mice given IP Shiga toxin and saline can be used as evidence of MAC formation that is not apparent in the mice treated with the C5 inhibitor BB5.1.

C7 and C9 were also shown to co-localise with the glomerular endothelial cell marker PECAM (CD31) (Figure 8-13 and Figure 8-14). Co-staining with PECAM was performed following the observation that C7 and C9 appeared to be within the centre of the glomeruli and did not co-localise with nephrin. This is further evidence in support of Shiga toxin targeting the Gb3 receptor in podocytes, leading to activation of complement in the glomerular endothelium.

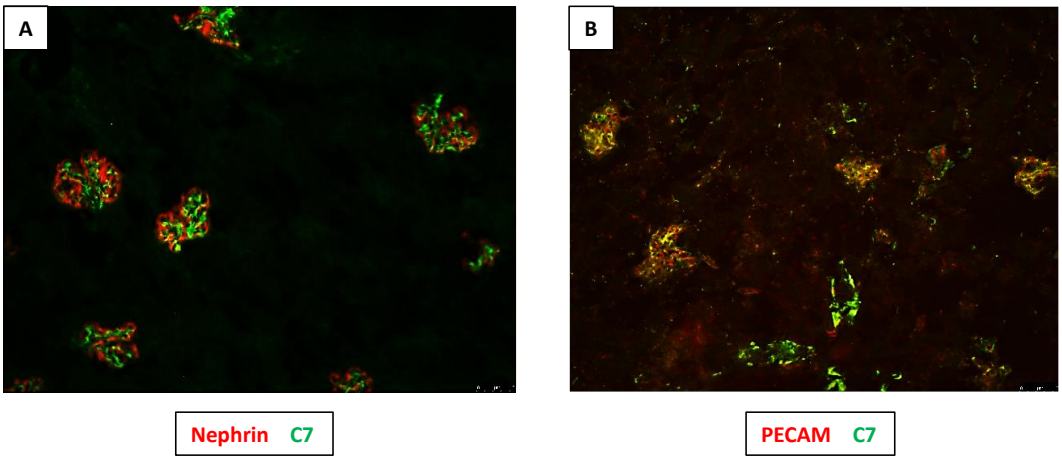

Figure 8-13: C7 co-localises with PECAM on IF

Frozen kidney sections from PodrtTA-Tet-O-Gb3 Gb3 null mice given IP Shiga toxin and saline were probed for C7 (green) and the podocyte marker nephrin (red, panel A) or the glomerular endothelial cell marker PECAM (red, panel B). This demonstrated that C7 co-localised with PECAM within the glomerulus giving a yellow appearance to the IF image, which is not seen on co-staining with nephrin.

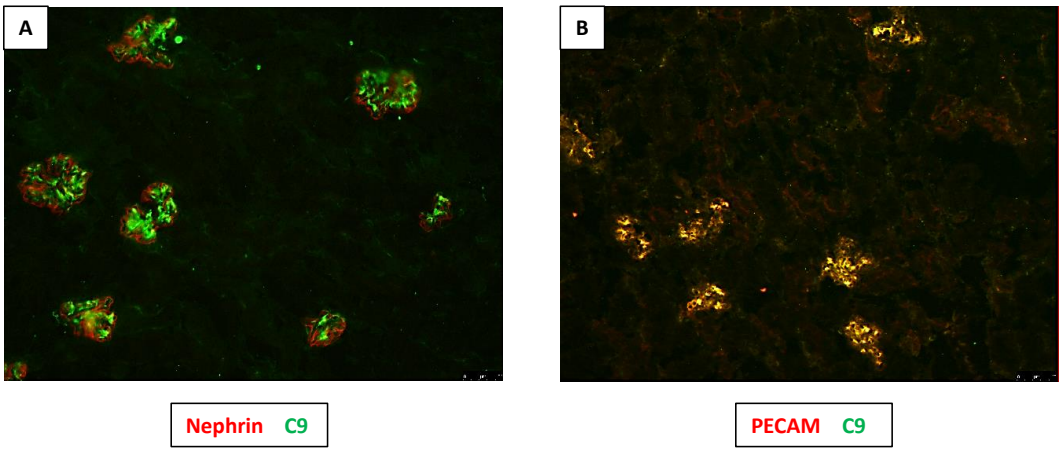

Figure 8-14: C9 co-localises with PECAM on IF

Frozen kidney sections from PodrtTA-Tet-O-Gb3 Gb3 null mice given IP Shiga toxin and saline were probed for C9 (green) and the podocyte marker nephrin (red, panel A) or the glomerular endothelial cell marker PECAM (red, panel B). This demonstrated that C9 co-localised with PECAM within the glomerulus giving a yellow appearance to the IF image, which is not seen on co-staining with nephrin.

8.4.6 C5 inhibition in PodrtTA-Tet-O-Gb3 Gb3 null mice post IP Shiga toxin reduces fibrinogen deposition in the glomerulus

It has already been established in chapter 7, that PodrtTA-Tet-O-Gb3 Gb3 null mice given IP Shiga toxin show an increase in glomerular fibrinogen deposition. This is a key feature of HUS where the classical histopathological lesion is one of glomerular TMA with glomerular thrombi staining positive for fibrinogen on immunofluorescence [304]. PodrtTA-Tet-O-Gb3 Gb3 null mice given IP Shiga toxin and saline in this experiment, also show evidence of fibrinogen deposits in their glomeruli which is attenuated by treatment with the C5 inhibitor BB5.1. Four mice were analysed from each experimental group, with at least 15 glomeruli imaged for each individual mouse (Figure 8-15).

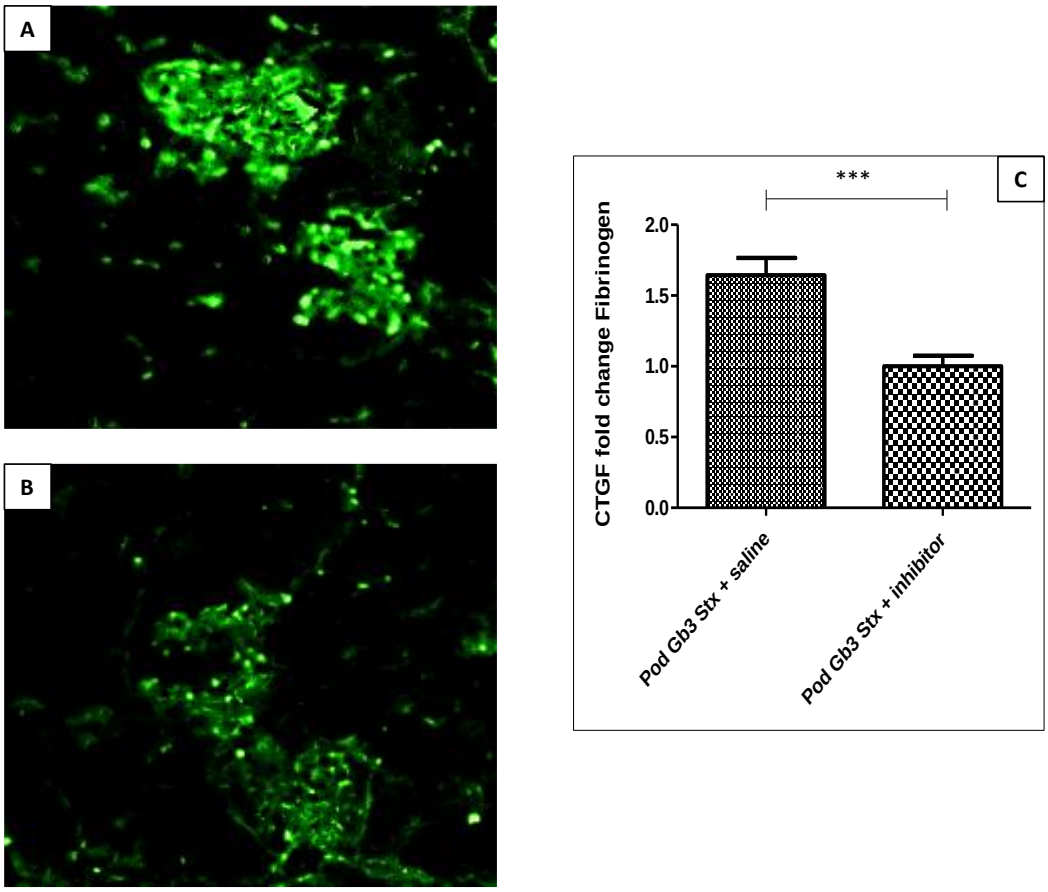

Figure 8-15: C5 inhibition reduces fibrinogen deposition in Shiga toxin HUS

Frozen kidney sections from PodrtTA-Tet-O-Gb3 Gb3 null mice given IP Shiga toxin and either IP saline (panel A) or IP C5 inhibitor (panel B) were probed for fibrinogen using IF (shown in green). This demonstrated a statistically significant increase in fibrinogen deposition in the glomeruli of the mice administered saline vs. those given C5 inhibitor BB5.1. As evidenced by the increase in fold change of fibrinogen fluorescence intensity of >x1.5 fold. Graph C: Pod Gb3 = PodrtTA-Tet-O-Gb3 Gb3 null mice (for clarity of figure). Results from n=4 mice of each experimental condition: 15 glomeruli per mouse at x20 magnification. *** Unpaired T-test p value <0.0001.

8.4.7 C5 inhibition in PodrtTA-Tet-O-Gb3 Gb3 null mice post IP Shiga toxin does not affect C3b activation in the glomerulus

As already outlined, C3b is generated upon cleavage of C3 which can occur due to activation of compliment via any of the three main pathways (Figure 8-4). C5 is located downstream of C3 in the compliment cascade and so in theory, inhibiting the pathway at this level should not affect the activation of C3b by Shiga toxin in the glomeruli of the PodrtTA-Tet-O-Gb3 Gb3 null mice. I also wanted to determine the baseline levels of C3b in the glomeruli of PodrtTA-Tet-O-Gb3 Gb3 null mice that had received oral doxycycline

in their drinking water but had not been treated with IP Shiga toxin. As this would determine if merely inducing Gb3 expression in the podocyte has an effect upon compliment activation within the glomerulus.

Fresh frozen kidney sections from PodrtTA-Tet-O-Gb3 Gb3 null mice given oral doxycycline to induce Gb3 expression in their podocytes followed by an IP saline sham injection (as a control for IP Shiga toxin) were probed for C3b on immunofluorescence. Kidney sections from PodrtTA-Tet-O-Gb3 Gb3 null mice given oral doxycycline, IP Shiga toxin and IP saline or C5 inhibitor were also probed for C3b on immunofluorescence at the same time. IF showed no statistically significant difference in glomerular deposition of C3b between the PodrtTA-Tet-O-Gb3 Gb3 null mice treated with Shiga toxin and saline vs. the PodrtTA-Tet-O-Gb3 Gb3 null mice given Shiga toxin and C5 inhibitor BB5.1 (Figure 8-16).

Of particular importance, in the PodrtTA-Tet-O-Gb3 Gb3 null mice given oral doxycycline to induce the expression of Gb3 but no IP Shiga toxin; there was no evidence of C3b activation in the glomeruli. Of note, C3b is known to be present in murine Bowman's capsule in wild type mice [305]. This was excluded in my CTFG analysis through the use of nephrin co-staining to identify podocytes which are located on the outside of the glomerulus (see methods chapter for description of image J analysis using this method). This demonstrates that C3b compliment activation in the glomerulus of PodrTA-Tet-O-Gb3 Gb3 null mice is due to Shiga toxin treatment itself and not an effect of Gb3 expression alone.

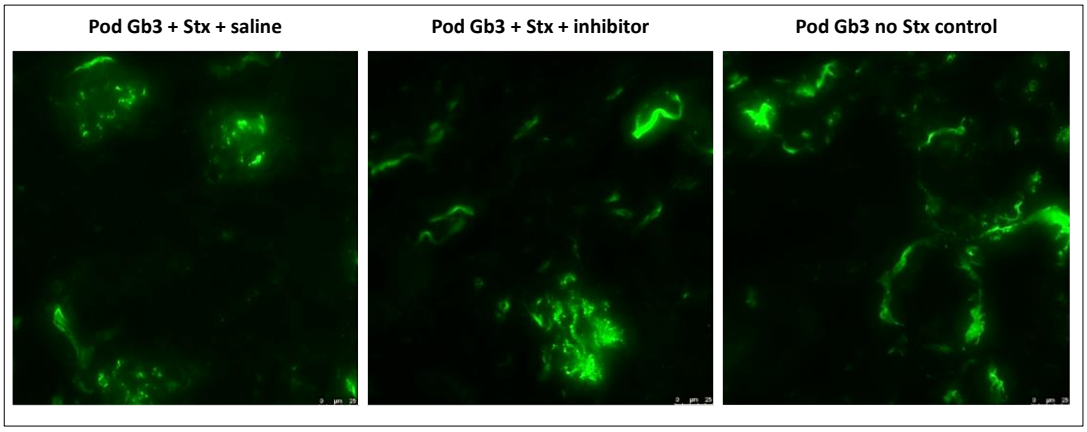

Figure 8-16: C5 inhibition does not affect C3b activation in the glomerulus following Shiga toxin challenge

Frozen kidney sections from PodrtTA-Tet-O-Gb3 Gb3 null mice given oral doxycycline for 14 days to induce Gb3 expression and IP Shiga toxin (or IP saline sham injection as a control) followed by either IP saline or IP C5 inhibitor as indicated in the figure were probed for C3b using IF (shown in green). Pod Gb3 = PodrtTA-Tet-O-Gb3 Gb3 null mice (for clarity of figure). There was no difference in the IF staining intensity of C3b between the PodrtTA-Tet-O-Gb3 Gb3 null mice treated with Shiga toxin and saline vs. the PodrtTA-Tet-O-Gb3 Gb3 null mice given Shiga toxin and C5 inhibitor BB5.1. In PodrtTA-Tet-O-Gb3 Gb3 null mice given oral doxycycline but no IP Shiga toxin; there was no evidence of C3b activation within the glomeruli. (Note C3b is known to be expressed by murine Bowman's capsule as observed here [305]). Images shown are representative of n=3 mice per experimental condition at x40 magnification.

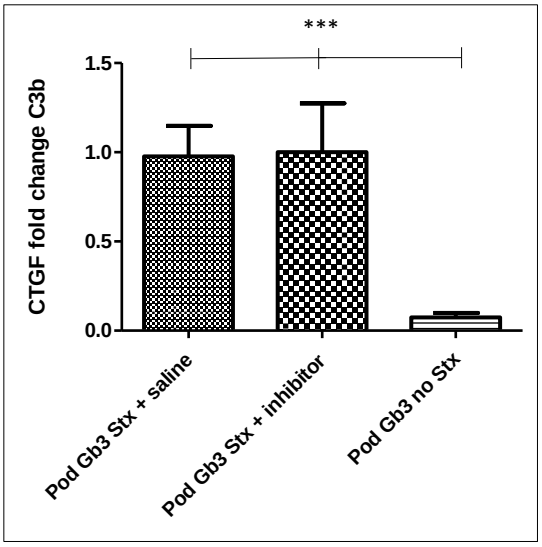

Figure 8-17: C5 inhibition does not affect C3b activation in PodrtTA-tet-O-Gb3 Gb3 null mice given IP Shiga toxin

Graphical representation of IF results: there was a statistically significant difference in glomerular deposition of C3b between the PodrtTA-Tet-O-Gb3 Gb3 null mice treated with Shiga toxin and saline vs. PodrtTA-Tet-O-Gb3 Gb3 null mice given oral doxycycline to induce the expression of Gb3 but no IP Shiga toxin. Similarly, there was a statistically significant difference between the PodrtTA-Tet-O-Gb3 Gb3 null mice given Shiga toxin and C5 inhibitor BB5.1 vs. PodrtTA-Tet-O-Gb3 Gb3 null mice given oral doxycycline to induce the expression of Gb3 but no IP Shiga toxin. In PodrtTA-Tet-O-Gb3 Gb3 null mice given oral doxycycline to induce the expression of Gb3 but no IP Shiga toxin; there was no evidence of C3b activation in the glomeruli. No statistically significant difference was detected in C3b deposition in PodrtTA-Tet-O-Gb3 Gb3 null mice treated with Shiga toxin and saline vs. PodrtTA-Tet-O-Gb3 Gb3 null mice given Shiga toxin and C5 inhibitor BB5.1. Pod Gb3 = PodrtTA-Tet-O-Gb3 Gb3 null mice (for clarity of figure). Results from n=3 mice of each experimental condition: 15 glomeruli per mouse. *** Unpaired T-test p value <0.0008.

8.4.8 C5 inhibition in PodrtTA-Tet-O-Gb3 Gb3 null mice post IP Shiga toxin restores CFH expression in the glomerulus

As illustrated in Figure 8-4, complement factor H (CFH) is a key regulator of the complement cascade ensuring that the C3b amplification loop is kept under control, preventing excessive cell injury and inflammation [30]. In the first cohort of experiments PodrtTA-Tet-O-Gb3 Gb3 null mice had a reduction of CFH deposition in their glomeruli at day 10 following IP Shiga toxin challenge. This finding was supported by human *in vitro* data from co-culture experiments where glomerular endothelial cells showed a loss of CFH expression, that was dependent upon the presence of podocytes. This suggests that in this mouse model of Shiga toxin HUS, there is a loss of CFH protection locally within the glomerulus, rendering the glomerular endothelium susceptible to complement attack.

To determine whether C5 inhibition had any effect on CFH glomerular deposition, IF was performed for CFH in frozen kidney sections from PodrtTA-Tet-O-Gb3 Gb3 null mice given IP Shiga toxin and saline vs. those given C5 inhibitor. This demonstrated a 50% reduction in CFH in the mice given IP Shiga toxin and saline, in comparison to the PodrtTA-Tet-O-Gb3 Gb3 null mice given Shiga toxin and C5 inhibitor BB5.1. IF was also performed for CFH in kidney sections from PodrtTA-Tet-O-Gb3 Gb3 null mice given doxycycline to induce Gb3 expression, but not given any Shiga toxin. This was to establish what the baseline levels of CFH were within the glomeruli of these animals. This revealed CFH staining of the same intensity as the mice given the C5 inhibitor. Thus, confirming that it is the IP Shiga toxin challenge administered to PodrTA-Tet-O-Gb3 Gb3 null mice that leads to the reduction in glomerular CFH protection (Figure 8-18).

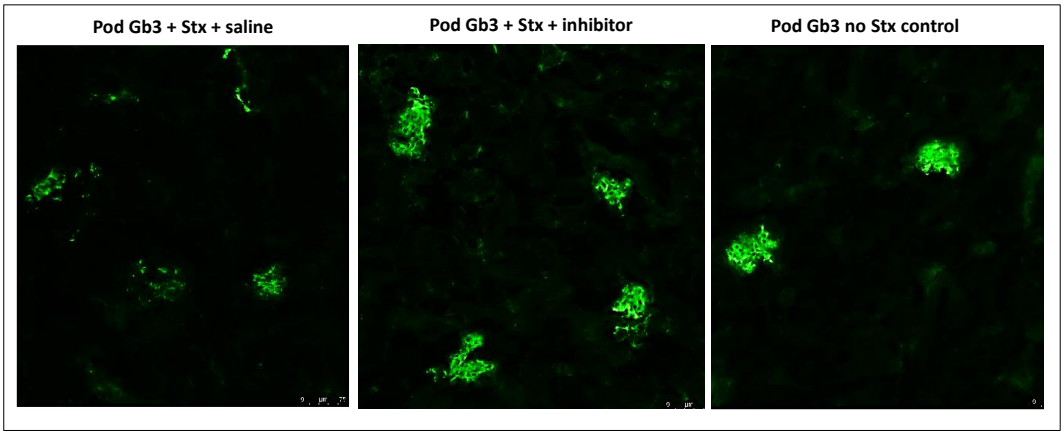

Figure 8-18: C5 inhibition restores glomerular CFH expression following Shiga toxin challenge

Frozen kidney sections from PodrtTA-Tet-O-Gb3 Gb3 null mice given oral doxycycline for 14 days to induce Gb3 expression and IP Shiga toxin (or IP saline sham injection as a control) followed by either IP saline or IP C5 inhibitor as indicated in the figure were probed for CFH using IF (shown in green). Pod Gb3 = PodrtTA-Tet-O-Gb3 Gb3 null mice (for clarity of figure). CFH expression was reduced in PodrtTA-Tet-O-Gb3 Gb3 null mice given IP Shiga toxin and saline. This was restored to baseline levels (evidenced by intensity of CFH staining in PodrtTA-Tet-O-Gb3 Gb3 null mice given no Shiga toxin challenge) when C5 inhibition treatment was administered. Images shown are representative of n=3 mice per experimental condition at x20 magnification.

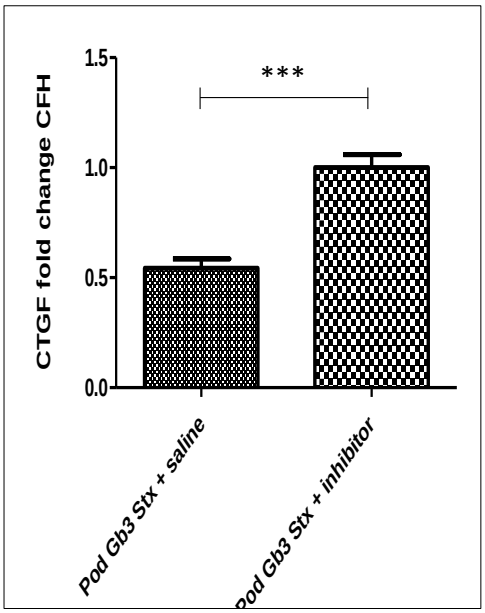

Figure 8-19: C5 inhibition restores glomerular CFH expression in PodrtTA-Tet-O-Gb3 Gb3 null mice given IP Shiga toxin

Graphical representation of IF results shown above: there was a 50% reduction in CFH expression in PodrtTA-Tet-O-Gb3 Gb3 null mice given IP Shiga toxin and saline vs. PodrtTA-Tet-O-Gb3 Gb3 null mice given Shiga toxin and C5 inhibitor BB5.1. Pod Gb3 = PodrtTA-Tet-O-Gb3 Gb3 null mice (for clarity of figure). Results from n=3 mice of each experimental condition: 15 glomeruli per mouse. *** Unpaired T-test p value <0.0001.

Together, these findings are very interesting and rather unexpected. These data suggest that C3 deposition in this model of STEC HUS, occurs due to a loss of CFH protection on the surface of the glomerular endothelial cell rather than activation of C3. To my knowledge, this is the first time that C5 inhibition has been shown to affect local glomerular levels of CFH *in vivo*. As such, further investigation is required to determine how C5 inhibition could possibly exert this effect. It is possible that there is no actual

change in the level of glomerular CFH expression, but rather a change in CFH binding affinity at the glomerular endothelial surface. This change may well be induced by Shiga toxin damage to the podocyte, possibly resulting in a change in local VEGF-A expression and loss of endothelial cell glycocalyx. Thus, what is being detected is a reduction in CFH binding rather than a true representation of glomerular CFH levels. Further work is needed to interrogate the underlying mechanism of this observation. Firstly, to assess at which timepoint following Shiga toxin inoculation there is loss of glycocalyx (if any); and then to measure systemic complement activation levels in this mouse model in the presence and absence of treatment with the C5 inhibitor. Unfortunately, in this cohort of experiments this could not be performed, as an AP50 test requires at least 200µl of blood from each mouse. This would have resulted in not enough blood for full blood count, urea, and blood film analysis. However, the AP50 test could be performed in another round of experimental mice to determine the level of systemic complement activation in this model.

8.5 Discussion

This chapter has reported the effects of C5 inhibition in a mouse model of Shiga toxin HUS. For the first time, it has been demonstrated that C5 inhibition prevents thrombocytopenia, haemolytic anaemia, uraemia, and the development of a glomerular TMA in PodrtTA-Tet-O-Gb3 Gb3 null mice given IP Shiga toxin. In this cohort of experiments all PodrtTA-Tet-O-Gb3 Gb3 null mice given IP Shiga toxin (and IP saline) developed a HUS phenotype, just as reported in the first cohort of experiments detailed in chapter 7. Furthermore, the levels of thrombocytopenia, anaemia and uraemia were comparable to those seen in my first cohort of experiments. This provides reassuring evidence of the reproducibility of the PodrtTA-Tet-O-Gb3 Gb3 null IP Shiga toxin model.

In this set of inhibitor experiments, C5 inhibition began prior to IP Shiga toxin challenge and a further dose was given 3 days later due to the short half-life of the drug (BB5.1). In clinical practice, obviously the treatment of Shiga toxin HUS cannot be given before the disease develops. Hence, future experiments in PodrtTA-Tet-O-Gb3 Gb3 null mice will need to establish whether C5 inhibition after Shiga toxin HUS develops is of benefit. From the time course experiments performed, there is evidence of C3 activation within the glomerulus as early as day 4 following IP Shiga toxin inoculation in PodrtTA-Tet-O-Gb3

Gb3 null mice. Therefore, IP C5 inhibition could be given at this timepoint to determine if it prevents glomerular TMA from occurring in my mouse model.

Extrapolating the findings from this mouse model to human Shiga toxin HUS disease will be a challenge, as there is often a delay in presentation of 7-10 days following initial infection with Shiga toxin producing bacteria [306]. However, the ECUSTEC randomised control trial (ISRCTN89553116) that is currently in progress will hopefully be able to evaluate the efficacy of C5 inhibition with eculizumab in humans with Shiga toxin HUS. A particular challenge of this trial is the recruitment of enough Shiga toxin HUS cases. The incidence in the UK was 0.24 per 100,000 cases per population in 2018, which translates to 14 cases in total in England [38]. Ensuring that all of these patients are recruited to enable statistical power to be achieved throughout the duration of the trial, requires a considerable national effort which is quite a task to coordinate. Thus, in the meantime this mouse model of Shiga toxin HUS will be vital in establishing the underlying pathophysiology of the disease and allow other compliment therapies to be trialled.

Through the use of immunofluorescence, it has been shown that formation of the MAC within the glomerulus (via activation of C7 and C9) was prevented by systemic C5 inhibition therapy in this model. Moreover, C7 and C9 expression was co-localised to the glomerular endothelium; demonstrating for the first time in Shiga toxin HUS, that glomerular cell cross-talk between the podocyte and glomerular endothelium was occurring *in vivo*. Interestingly, C3b activation remained unchanged within the glomeruli of mice given C5 inhibitor treatment, which was anticipated given that C5 is downstream of C3 in the complement cascade.

In PodrtTA-Tet-O-Gb3 Gb3 null mice given IP Shiga toxin and systemic C5 inhibition treatment, glomerular CFH levels were also found to be preserved. This was in contrast to the same mice given Shiga toxin and an IP saline control, where there was an apparent reduction in glomerular CFH expression. This observation was rather unexpected but would support my central hypothesis that Shiga toxin HUS occurs due to a loss of CFH protection against complement-mediated damage on the surface of the glomerular endothelial cell. This is the first time that this has been reported *in vivo.* These findings require further investigation as to the underlying mechanisms involved. It is likely that the change in glomerular CFH expression is more likely to reflect the binding affinity of CFH to the glomerular endothelium. Measurement of systemic complement activation through the use of functional assays such as AP50 and CH50 would be useful to delineate the

degree of systemic C5 inhibition by BB5.1 achieved in my mouse model. In support of these data, recently published work from Vernon et al. describes the development of a severe C5 dependent TMA in mice with hepatocyte CFH deficiency (i.e. partial CFH deficiency), after exposure to a complement activating trigger. This work demonstrates that partial CFH deficiency can give rise to atypical HUS, following a complement-activating trigger within the kidney that is C5 dependent. Evidently, C5 has a key role in the development of complement mediated glomerular TMA and the relationship between CFH deficiency and complement-mediated glomerular injury is extremely complex [307].

Chapter 9 : Discussion

9.1 Achievement of research aims

At the beginning of this PhD, I set out to achieve 3 main aims outlined in my original research hypothesis:

1. Prove that Shiga toxin acts through the podocyte Gb3 receptor to cause HUS.

2. Therapeutically rescue STEC-HUS with a C5 inhibitor (analogous to eculizumab).

3. Determine the cellular mechanisms underlying the action of Shiga toxin.

Through the application of an unbiased, rigorous experimental approach using total and phospho-proteomic analysis, I have been able to identify several key pathways activated in the human podocyte following Shiga toxin exposure. Further interrogation of these data has allowed me to begin to determine the cellular mechanisms underlying the action of Shiga toxin in the glomerulus. In addition, through the use of highly complex genetic mouse models, I have been able to demonstrate for the first time that Shiga toxin can act via the podocyte Gb3 receptor to cause systemic HUS. From this work it is clear that the podocyte is a key initiator in Shiga toxin HUS *in vivo*. Furthermore, by generating a small animal model that recapitulates the human phenotypical changes of STEC HUS; I have been able to demonstrate therapeutic rescue with C5 inhibition. As such, not only have I addressed the 3 key aims of my original research hypothesis; but I have also generated a novel animal model that can be taken forward to evaluate other potential therapies in the treatment of patients with this devastating disease.

9.2 Summary of key findings

9.2.1 The molecular effects of Shiga toxin on the podocyte

At the start of my research project, I optimised 3 different methods of Gb3 detection. This was vital to achieve, as the ability to confidently detect Gb3 was to form the basis of all subsequent experimental work both *in vitro* and in genetic mouse models *in vivo*. Given Gb3 is a glycosphingolipid, I needed to establish several new techniques in our laboratory. The methods I employed included immunofluorescence using an anti-Gb3 antibody; endpoint PCR detection of the enzyme responsible for Gb3 synthesis: Gb3 synthase (A4GALT); and detection of Gb3 using thin layer chromatography (TLC). Unfortunately,

although TLC proved to be both reproducible and reliable in HeLa cells, in terminally differentiated podocytes tritium labelling proved to be a challenge. Furthermore, radio-isotope labelling of sphingosine would not be possible in mouse tissues from *in vivo* experiments, rendering this TLC overlay method obsolete in this setting. This prompted me to contact Dr. Kevin Mills at the Translational Mass Spectrometry Centre (TMSC) in London. Through this collaboration I was able to use lipid mass spectrometry to accurately quantify the amount of Gb3 expressed in both podocyte cell lines and animal tissues.

Optimisation of these Gb3 detection methods confirmed that Gb3 was expressed by wild type human podocytes *in vitro,* and absent from both wild type mouse podocytes and human A4GALT knockdown podocytes; generated using short hairpin siRNA against Gb3 synthase. It is important to note that detection of the A4GALT enzyme by PCR does not necessarily equate to expression of Gb3 on the cell surface. Indeed, the fact that A4GALT mRNA was detected in small quantities in both mouse wild type podocytes and A4GALT knockdown podocytes; yet, Gb3 itself was undetectable by immunofluorescence suggests post transcriptional silencing of the enzyme. Further, evidence to support a lack of Gb3 expression in these cell lines was their resistance to the ribotoxic effects of Shiga toxin, even at several hundred times the LD50 dose. Together, these findings strongly suggest that Gb3 is the receptor required for Shiga toxin to exert its toxic effects and that cells lacking the receptor are protected from Shiga toxin cytotoxicity.

An interesting and unexpected finding from this work, was the discovery that Shiga toxin upregulated the expression of Gb3 in human podocytes *in vitro*. This effect appeared to be maximal at 6 hours and return to baseline after 24 hours. These results were replicated several times and consistent across IF and INCell analysis. This effect has not been described in podocytes before (upon review of current literature) and was not apparent in A4GALT knockdown podocytes or wild type mouse podocytes. However, it has been reported in neuronal cells of patients with Shiga toxin HUS and in dermal microvascular endothelial cells [84][248]. Pro-inflammatory cytokines such as TNF-α and IL-1β as well as bacterial lipopolysaccharide and neutral sphingomyelinase (produced by eukaryotic cells in response to stresses such as infection) have also been shown to induce Gb3 receptor expression in neurones [84]. In dermal microvascular endothelial cells, the mechanism behind upregulation of the Gb3 receptor has been found to be due to increase in intracellular ceramide; accompanied by an increase in ceramide glucosyltransferase

enzyme (the first of three enzymes involved in the Gb3 biosynthesis pathway). Notably, no evidence of an increase in A4GALT mRNA was seen in these cells [95].

Conversely, work by Hughes et al. in cultured human proximal tubule cells (known to express high levels of Gb3), has demonstrated an increase in A4GALT gene transcription and a reduction in α-galactosidase mRNA levels in response to Stx1 treatment [308]. There was no change in ceramide glucosyltransferase activity detected in this cell line. Interestingly, in human glomerular endothelial cells, upregulation of Gb3 expression is not seen in response to Shiga toxin treatment *in vitro* [95]. The finding that an upregulation of the Gb3 receptor occurs in response to Shiga toxin treatment in the podocyte, infers an increased sensitivity to Shiga toxin, that is potentiated by the toxin itself. The molecular mechanism responsible for the increase in Gb3 receptor expression in podocytes is yet to be established.

9.2.2 Proteomic Analysis

The generation of a human A4GALT knockdown podocyte cell line, provided me with a control for non-specific, non-Gb3 receptor binding which facilitated investigation of the effects of Shiga toxin treatment on the podocyte. Through LC-MS/MS analysis of the total protein and phospho-protein changes in wild type human podocytes versus A4GALT knockdown podocytes, I identified several key pathways underlying the cellular response to Shiga toxin. The most notable protein signalling networks activated were ER stress pathways and the innate immune system receptors of the NLRP3 inflammasome complex. Actin cytoskeleton and cell assembly proteins, as well as VEGF-A expression were found to be decreased in response to Shiga toxin treatment. This is the first time that the molecular effects of Shiga toxin treatment in the podocyte has been studied in detail. Further investigation into how these pathways interact to result in the development of Shiga toxin HUS in patients is warranted, with the intention of identifying novel targets amenable to pharmacological intervention in the treatment of the disease.

9.2.3 A4GALT knockdown mice are resistant to Shiga toxin effects

My *in vitro* work confirmed that expression of the Gb3 receptor correlated with the sensitivity of the podocyte to Shiga toxin. The generation of an A4GALT knockdown mouse established this association *in vivo*. Wild type mice were shown to lack expression of Gb3 in their glomeruli. The presence of the receptor in their renal tubules accounted for the severe dehydration and tubular necrosis that led to their death within 5 days of

intraperitoneal Shiga toxin administration. In stark contrast, A4GALT knockout mice were found to be resistant to the lethal effects of Shiga toxin, even at 400 times the LD50 dose. All A4GALT knockout mice survived until electively terminated for organ harvesting 8 weeks after Shiga toxin challenge. They had no change in their serum creatinine or renal histology. This model clearly illustrates that the receptor for Shiga toxin *in vivo* is Gb3 and that in the absence of this receptor mice are completely protected against the lethal effects of Shiga toxin.

9.2.4 Generation of an inducible podocyte specific Gb3 synthase mouse on a Gb3 null background

In order to address my research hypothesis that Shiga toxin acts through the podocyte Gb3 receptor to cause HUS; a mouse model with inducible podocyte Gb3 expression was generated. This was achieved using tetracycline controlled transcription activation of Gb3 synthase linked to a podocin promoter. This model needed to be inducible because the Gb3 over-expressing mouse results in a Fabry disease phenotype; which interestingly is resistant to intraperitoneal Shiga toxin challenge. PodrtTA-Tet-O-Gb3 synthase mice that given IP Shiga toxin developed evidence of glomerular TMA on histology, but unfortunately died within 3-5 days from the same off target, extra-glomerular effects that were seen in wild type mice. Consequently, to eliminate the renal tubular dehydration effects of Shiga toxin *in vivo*, the PodrtTA-Tet-O-Gb3 mouse was back-crossed with the A4GALT knockout mouse, to generate a mouse that only expressed Gb3 in its podocytes. This model allowed me to study the specific role of the podocyte in Shiga toxin HUS.

Fascinatingly, PodrtTA-Tet-O-Gb3 Gb3 null mice developed HUS: thrombocytopenia, haemolytic anaemia, and uraemia at day 10 following IP Shiga toxin. Renal histology demonstrated a glomerular TMA, the pathognomonic lesion of HUS; with intracapillary thrombus formation seen on electron microscopy. Immunofluorescence confirmed a statistically significant increase in glomerular fibrinogen deposition and C3b versus control mice. Interestingly, not all glomeruli were affected by TMA in this model; suggestive of a degree of podocyte and/or glomerular endothelial cell heterogeneity in the response to Shiga toxin treatment *in vivo*. This finding may also reflect the temporal evolution of STEC HUS with different glomeruli affected over the course of the disease. Indeed, this has been observed in renal biopsies taken from humans with HUS. In fact, in a recent 'Kidney Disease: Improving Global Outcomes' (KDIGO) meeting it was even suggested that consideration be given to re-classification of HUS as with or without overt

fibrin platelet thrombosis, given the fact that this may be absent altogether from renal biopsies of patients with TMA [141].

In addition, glomerular expression of complement regulator factor H, was significantly reduced in PodrtTA-Tet-O-Gb3 Gb3 null mice, rendering them more susceptible to complement attack. This is the first time that a mouse model of Shiga toxin HUS which recapitulates the disease in humans has ever been described. Even more interesting, is that in this model mice appear to recover by day 24 post Shiga toxin, recapitulating the clinical sequelae that is often seen in STEC HUS patients [3].

9.2.5 C5 inhibition protects against glomerular TMA in STEC HUS

Using the PodrtTA-Tet-O-Gb3 Gb3 null mouse model of STEC HUS, I was able to rescue the HUS phenotype with the C5 inhibitor BB5.1. This is a mouse C5 inhibitor, analogous to the C5 inhibitor eculizumab used in humans with atypical HUS. Confirmation of C5 inhibition was confirmed by the finding that C7 and C9 activation was significantly reduced in the glomeruli of animals treated with the inhibitor versus those treated with a saline control. Reassuringly, C3b activation was unchanged in the glomeruli of mice given C5 inhibitor treatment, in-keeping with the fact that C5 is downstream of C3 in the complement pathway. However, the finding that the complement regulator factor H was restored in PodrtTA-Tet-O-Gb3 Gb3 null mice given the C5 inhibitor (versus mice given an IP saline control) was rather unexpected and difficult to explain.

Further investigation is required to determine how C5 inhibition could possibly exert this effect. It is conceivable that there is no change in the actual level of glomerular CFH expression, but rather a change in CFH binding affinity at the glomerular endothelial surface. This change may well be induced by Shiga toxin damage to the podocyte, possibly resulting in a change in local VEGF-A expression and loss of endothelial cell glycocalyx. Indeed, it has already been established that binding of CFH to C3b is enhanced when these molecules are bound to host cell glycocalyx [164]. Thus, the immunofluorescence findings may well reflect a reduction in CFH binding rather than a true representation of glomerular CFH levels. Further work to assess whether glomerular endothelial cells loose glycocalyx in this STEC HUS model; and to measure systemic complement activation levels in mice treated with the C5 inhibitor is required to interrogate the precise sequence of pathological events that are occurring.

9.3 Implications of this work

9.3.1 Insights into the pathogenesis of STEC HUS

The work performed throughout the course of my PhD, has led to a greater understanding of the pathogenesis of Shiga toxin HUS. Through the use of *in vitro* and *in vivo* A4GALT knockdown models I have demonstrated that the receptor for Shiga toxin is Gb3; and that in the absence of this receptor, cells and tissues are protected against the lethal effects of Shiga toxin. Furthermore, the generation of the PodrtTa-Tet-O-Gb3 Gb3 null mouse has led to the development of a STEC HUS small animal model that recapitulates the disease in humans. Through interrogation of this model, I have shown that local complement activation occurs in the kidney in response to Shiga toxin exposure and that complement regulatory factor H protection is lost from the glomerular endothelial cell surface. Together this led to an increase in the susceptibility of the glomerular endothelium to complement attack with formation of the MAC on the glomerular endothelial cell surface. For the first time *in vivo*, I have demonstrated that Shiga toxin HUS is associated with local complement activation in the kidney.

In support of this work, my observations *in vivo* were echoed in human glomerular cell co-culture experiments. Only in the presence of podocytes did glomerular endothelial cells show an increase in C3 cleavage product deposition (C3b, iC3b and C3d) and loose the protection of complement factor H. In view of these findings, a potential sequence of pathological events in STEC HUS could be; Shiga toxin binding to the podocyte Gb3 receptor resulting in disruption of glomerular homeostasis due to a reduction in VEGF-A production. This leads to loss of glomerular endothelial glycocalyx and a reduction in complement factor H binding affinity to the glomerular endothelial cell surface, resulting in loss of local complement regulation and TMA. Further work is needed to determine whether there is also activation of C3 in the glomerulus or if the increase in C3b deposition is solely due to loss of regulation. Clearly, cross-talk between podocytes and glomerular endothelial cells both *in vitro* and *in vivo*, is vital in the development of Shiga toxin HUS. In fact, the podocyte Gb3 receptor appears to be a key initiator of the disease.

9.3.2 Direct clinical implications

The finding that in the STEC HUS mouse model, C5 inhibition resulted in rescue of the glomerular TMA phenotype; further supports the hypothesis that STEC HUS is a result of complement activation in the kidney. Particularly exciting is the prospect that a C5

inhibitor (eculizumab) is already available for use in humans. With over a decade of safety data for its use in atypical HUS patients, it is theoretically plausible to test its efficacy in human STEC HUS imminently. Of note, the concept of complement blockade in the treatment of STEC HUS is not new. Several case series have been reported in paediatric patients suggesting benefit from eculizumab treatment. However, retrospective analysis of C5 inhibition in adults with STEC HUS have been inconclusive [199]. My experimental findings further support the need for a randomised controlled trial to definitively evaluate whether C5 inhibition with eculizumab is beneficial in the treatment of STEC HUS in humans.

It is also important to highlight that in the STEC HUS animal experiments performed, C5 inhibition began prior to IP Shiga toxin challenge. In the clinical setting, the mean interval from exposure to Shiga toxin producing bacteria and onset of symptoms is 3 days, with almost all cases diagnosed within 2 weeks of onset of diarrhoea [31][41]. Hence, future experiments using the STEC HUS mouse model, would need to establish whether C5 inhibition after IP Shiga toxin challenge (i.e. following disease induction) is of benefit. Additionally, the discovery that C5 inhibition in the STEC HUS mouse model protected against the development of the disease, has demonstrated that terminal complement pathway activation is important in the pathogenesis of STEC HUS. Given that the classical, lectin and alternative complement pathways all culminate in the formation of the MAC, further work would also need to be performed to delineate precisely which pathways are active in the model.

9.3.3 Clinical trial data

During the course of my PhD, a national randomised, double-blind, placebo controlled trial 'ECUSTEC' (international trial no: ISRCTN89553116) opened in the United Kingdom [201]. This trial is ongoing, with the aim to establish whether eculizumab treatment in children with STEC HUS is of benefit. The Bristol Renal research group (under supervision of Professor Moin Saleem) has been receiving blood and urine samples from the ECUSTEC trial. These are taken as optional, additional samples to allow the investigation of several key areas of interest that fall outside of the primary and secondary outcomes of the main trial. A particular challenge of the ECUSTEC trial has been in the recruitment of sufficient STEC HUS cases to ensure statistical power is reached. Thus, until enough cases are recruited and randomised into the trial with publication of its results, the STEC HUS mouse model will be crucial in establishing the underlying pathophysiology of the disease; and in

the assessment of any new therapeutic targets that may be of benefit in the treatment of STEC HUS patients.

Chapter 10 : Future work

The work presented in this thesis has provided evidence in support of a key role for the podocyte in the pathogenesis of Shiga toxin HUS. However, several unanswered questions remain which could form the basis of future studies as outlined below.

10.1 Further investigation into the pathogenesis of STEC HUS

My *in vitro* work has found that in the human podocyte, upregulation of the Gb3 receptor occurs in response to Shiga toxin treatment. The mechanism behind this observation in podocytes is yet to be elucidated. This phenomenon has been reported in several cell types and attributed to changes in the gene transcription of different enzymes within the Gb3 synthesis pathway in each cell line studied. Thus, an initial line of investigation would be to measure A4GALT mRNA levels in human podocytes treated with Shiga toxin, versus untreated controls over time. Analysis of ceramide glucosyltransferase and α-galactosidase mRNA levels would also be of interest and relatively straight forward to perform. Not only would this provide an insight into the cellular processes leading to an increase in Gb3 receptor expression in podocytes; but could also lead to the identification of intracellular pathways that might be potential therapeutic targets in STEC HUS patients. For example, if a reduction of α-galactosidase mRNA levels were found in podocytes treated with Shiga toxin, the effect of restoring this enzyme could be evaluated against the level of expression of Gb3 and podocyte susceptibility to Shiga toxin induced cytotoxicity.

To date, *in vitro* studies into the host inflammatory response to infection with STEC, have focused upon the glomerular endothelial cell. This work has shown that in culture, glomerular endothelial cells upregulate Gb3 receptor expression only when treated with Shiga toxin in the presence of pro-inflammatory cytokines TNFα and IL-1β [72][98]. Therefore, it would be interesting to evaluate the effect of these cytokines in the podocyte; both in the presence and absence of Shiga toxin, to investigate any associated changes in Shiga toxin sensitivity. The INCell and immunofluorescence assays that I have already set up during my PhD would mean that these experiments could be fairly easily performed. Equally, the local glomerular inflammatory response in STEC HUS would be interesting to evaluate in my STEC HUS mouse model. Initial investigation would involve RT-PCR analysis of whole kidney tissue in these mice to ascertain whether there is any

increase in pro-inflammatory cytokine mRNA and at which time points in the development of the disease.

The *in vivo* STEC HUS mouse model described in this project, recapitulated the disease seen in humans but does not entirely reflect human disease. STEC HUS in humans is caused by ingestion of infected food and water or exposure to contamination from animal faeces [46][47]. However, in PodrtTA-Tet-O-Gb3 Gb3 null mice, Shiga toxin HUS was induced via intraperitoneal inoculation with Stx2. This represents a somewhat artificial method of infection with direct entry of the toxin into the circulation; bypassing the need for ingestion of Shiga toxin producing bacteria and gastrointestinal absorption. Thus, the mechanism behind Shiga toxin translocation from the large intestine into the bloodstream cannot be addressed by this STEC HUS animal model and remains unknown.

Of note, my initial experimental plan had been to use the genetically modified Shiga toxin producing rodent pathogen *Citrobacter rodentium* that has been described by Mallick et al [119]. These bacteria are known to cause attaching and effacing lesions on the intestinal epithelium in mice, reflecting those seen in STEC HUS in the human gut [119]. Furthermore, wild type mice infected by oral gavage with genetically modified Shiga toxin producing *Citrobacter rodentium*, were reported develop renal tubular disease reminiscent of that seen in mice administered intraperitoneal Shiga toxin and LPS [119]. Thus, theoretically this method of infection is a much better representation of STEC HUS human infection. However, in PodrtTA-Tet-O-Gb3 Gb3 null mice, induction of Gb3 expression in the podocyte is dependent upon oral doxycycline treatment for 14 days. Thus, I was concerned that co-administration of oral *Citrobacter rodentium* and doxycycline would impact upon the toxicity of the bacteria; potentially reducing its effect in this model. Hence, the decision was made to opt for intraperitoneal injection of Stx2 which would not be affected by oral doxycycline; accepting that this modality of inoculation was somewhat unrepresentative of human infection [1].

However, the STEC HUS mouse model developed during my PhD could be used to investigate how Shiga toxin is transported in the circulation to target organs. This would require labelling of the toxin prior to mouse inoculation and a way of tracing its journey to the kidney. This is not a new concept; the B subunit of cholera toxin has been used as a retrograde tracer in neurones since the 1980s [309]. In fact, there are now commercially available cholera toxin subunit B probes that are Alexa fluor™ conjugated, enabling tracing of neuronal projections in animals [310]. To date, there are no such available

labelled Shiga toxin subunits to facilitate tracing of the toxin *in vivo*. However, the finding that Gb3 is over-expressed in colorectal, breast and ovarian tumours has led to work investigating the potential use of Shiga toxin as a method of delivering cytotoxic chemotherapy compounds directly to cancer cells. Studies in this field have also reported coupling of the Shiga toxin B subunit to contrast agents to facilitate non-invasive tumour imaging using confocal fluorescence endoscopy and positron emission tomography (PET) scanning [69]. The use of these contrast labelling technologies in my model of STEC HUS would be fascinating; and may lead to insights into how Shiga toxin is transported in the circulation to target organs such as the kidney.

10.2 Development of a mouse endothelial cell Gb3 expression model

The PodrtTA-Tet-O-Gb3 Gb3 null mouse model generated during my PhD has shown that the podocyte is capable of causing a systemic Shiga toxin driven HUS. In this mouse model, only the podocyte expresses the Shiga toxin receptor Gb3. This suggests that carriage of Shiga toxin in the circulation to the kidney (at least in this model) is independent of Gb3 expression on blood cells. This would support recent studies demonstrating Shiga toxin carriage by TLR4 receptors on neutrophils in the circulation in humans [123]. As such, the PodrtTA-Tet-O-Gb3 Gb3 null mouse model is a somewhat purest model, designed specifically to determine the role of the podocyte in STEC HUS. In humans however, the Gb3 receptor is present throughout the nephron and highly expressed in glomerular endothelial cells. Thus, the generation of a mouse that expresses Gb3 in both the podocyte and glomerular endothelial cell would represent a more humanised model in which to study the disease.

This genetic mouse model could be generated using similar targeted, cell specific techniques that have been utilised in this project. The endothelial cell promoter Tie-2 could be used in place of the podocin promoter construct PodrtTA, to induce expression of the Gb3 receptor in the glomerular endothelial cell in the presence of doxycycline. The Tie-2rtTA-Tet-O-Gb3 Gb3 null mouse could then be administered Shiga toxin and the effects studied. Following this, the PodrtTA-Tet-O-Gb3 Gb3 null mouse could be crossed with the Tie-2rtTA-Tet-O-Gb3 Gb3 null mouse to generate a mouse expressing Gb3 both in the podocyte and glomerular endothelium. One would anticipate that this mouse might display a more severe phenotype than either model alone, when administered intraperitoneal Shiga toxin. However, of note the Tie-2 promoter is not specific to

glomerular endothelium. This promoter encodes an angiopoietin receptor that is expressed in all endothelial cells from embryogenesis through to adulthood [311]. Therefore, study of the specific effects of Shiga toxin in the glomerular endothelium would not be possible using this promoter. Tie-2 is also expressed in megakaryocytes, B and T lymphocytes, macrophages, and granulocytes. Given that thrombocytopenia is a key feature of STEC HUS, the induction of Gb3 expression in megakaryocytes is also likely to be an issue in this model. Nevertheless, this mouse would arguably be a more representative model of Gb3 expression in humans (versus Gb3 expression in the podocyte alone); as in humans Gb3 is found in other microvascular endothelial beds including the brain, skin and lungs [93][96][97]. Hence, this model may well provide further insight into the mechanisms underlying STEC HUS pathogenesis.

A further avenue of investigation would be the application of rtTA-Tet-O-Gb3 gene technology to induce Gb3 expression in other organs in the mouse model, that are known to be affected in humans with STEC HUS. Indeed, it is well documented that extra-renal manifestations affecting the brain, pancreas, heart, and skin occur in human disease [32][42]. This model would require a specific promoter for each organ in order to delineate the tissue specific effects of Shiga toxin *in vivo*.

10.3 Determining the role of VEGF-A in the development of TMA

The link between VEGF-A and the development of glomerular TMA was first highlighted in a seminal paper from Eremina et al. that observed the phenotype in a podocyte specific VEGF-A knockout mouse model [11]. More recently published work by Keir et al. went on to interrogate the mechanism behind this finding and reported a reduction in glomerular factor H expression in both podocytes and glomerular endothelial cells. Loss of factor H protection in the glomerulus was also shown to be associated with an increase in C3 deposition [222]. In STEC HUS patients, studies of renal biopsy samples have also confirmed that glomerular VEGF-A expression was reduced [220]. Together, these findings demonstrate a link between VEGF-A, complement regulation and the development of glomerular TMA. This is of particular relevance to my work as the podocyte is the major source of VEGF-A in the glomerulus [11].

In fact, in my original research hypothesis it was postulated that following binding of Shiga toxin to Gb3 in the podocyte there is a reduction in local glomerular VEGF-A production; which results in an increase in glomerular endothelial cell susceptibity to complement

attack. I have started to address this theory in my STEC HUS mouse model, using in situ hybridisation to quantify VEGF-A expression (Figure 5-27). However, due to the recent global SARS-CoV-2 virus outbreak, my work was prematurely halted as a result of laboratory closure. Mouse kidney sections from PodrtTA-Tet-O-Gb3 Gb3 null mice given Shiga toxin, are ready to be imaged on light microscopy and analysed once the laboratory reopens. Evidence of a reduction in glomerular VEGF-A expression in my STEC HUS mouse model would be fascinating; and further support the link between VEGF-A expression in the glomerulus, loss of local complement factor H protection and the development of glomerular TMA.

In further support of the importance of local complement factor H regulation in the development of glomerular TMA in STEC HUS, C5 inhibition was found to restore glomerular factor H in PodrTA-Tet-O-Gb3 Gb3 null mice given Shiga toxin. In situ hybridisation for VEGF-A in kidney sections from these mice, to determine if glomerular VEGF-A levels are also preserved would be of particular interest. Confirmation of VEGF-A preservation in the inhibitor treated mice (versus control mice), would provide strong evidence in support of a fundamental role for not only VEGF-A, but also the podocyte in the pathogenesis of STEC HUS.

10.4 Final Conclusion

The work presented in this thesis has led to the generation of a STEC HUS mouse model, that recapitulates the phenotypical changes seen in human disease. The discovery that the podocyte is capable of causing STEC HUS, with activation of complement observed on the glomerular endothelium; is compelling evidence for the importance of glomerular cell cross-talk within the kidney in the development of this disease. Indeed, this model may well explain why HUS has a predilection to present in the kidney; as it is only here that this highly specialised blood-filtration interface between podocytes and endothelial cells exist. Many questions remain, but I hope that the STEC HUS mouse model together with the techniques developed in this PhD, will go on to prove useful in advancing our understanding of this devastating disease.

Chapter 11 : References

[1] E. E. Bowen and R. J. Coward, “Advances in our understanding of the pathogenesis of hemolytic uremic syndromes,” *American Journal of Physiology - Renal Physiology*, vol. 314, no. 3. pp. F454–F461, 2018.

[2] M. Noris, F. Mescia, and G. Remuzzi, “STEC-HUS, atypical HUS and TTP are all diseases of complement activation,” *Nat. Rev. Nephrol*, vol. 8, no. 10, pp. 622–633, 2012.

[3] L. Keir and R. J. M. Coward, “Advances in our understanding of the pathogenesis of glomerular thrombotic microangiopathy,” *Pediatr. Nephrol.*, vol. 26, pp. 523–533, 2011.

[4] Kidney Research UK, “www.kidneyresearchuk.org/health-information/resources/the-kidneys-a-basic-guide.” 2018.

[5] National Kidney Foundation, “How the kidneys work,” *https://www.kidney.org/howkidneyswrk*. 2020.

[6] Encyclopaedia Britannica, “Nephron Anatomy,” *https://www.britannica.com/science/nephron*. 2010.

[7] H. D. Field M, Pollock C, *The Renal System: Basic science and clinical conditions.*, 2nd ed. Churchill Livingstone, 2010.

[8] F. J. Johnson RJ, Feehally J, *Comprehensive Clinical Nephrology*, 5th ed. Elsevier Saunders, 2015.

[9] Khan Academy, “Renal physiology: Glomerular filtration,” *www.khanacademy.org*. 2020.

[10] M. C. Menon, P. Y. Chuang, and C. J. He, “The glomerular filtration barrier: Components and crosstalk,” *International Journal of Nephrology*. pp. 1–9, 2012.

[11] V. Eremina *et al.*, “VEGF Inhibition and Renal Thrombotic Microangiopathy,” *N Engl J Med*, vol. 358, pp. 1129–36, 2008.

[12] National Institute of Diabetes and Renal Disease, “Kidney Disease,” *https://www.niddk.nih.gov/health-information/kidney-disease*. 2020.

[13] M. Nagata, “Podocyte injury and its consequences,” *Kidney Int.*, vol. 89, no. 6, pp. 1221–1230, 2016.

[14] W. Kriz and K. V. Lemley, “A potential role for mechanical forces in the detachment of podocytes and the progression of CKD,” *J. Am. Soc. Nephrol.*, vol. 26, no. 2, pp. 258–269, 2015.

[15] N. Hill *et al.*, “Glomerular endothelial derived vesicles mediate podocyte dysfunction: A potential role for miRNA,” *PLoS One*, vol. 15, no. 3, pp. 1–18, 2020.

[16] Q. S. Bartlett CS, Jeansson M, “Vascular Growth Factors and Glomerular Disease,” *Annu Rev Physiol*, vol. 78, pp. 437–461, 2016.

[17] A. S. Li, J. F. Ingham, and R. Lennon, “Genetic Disorders of the Glomerular Filtration

Barrier," *Clin. J. Am. Soc. Nephrol.*, vol. 15, pp. 1–11, 2020.

[18] S. Weinbaum, J. M. Tarbell, and E. R. Damiano, "The Structure and Function of the Endothelial Glycocalyx Layer," *Annu. Rev. Biomed. Eng.*, vol. 9, no. 1, pp. 121–167, 2007.

[19] M. J. Butler, C. J. Down, R. R. Foster, and S. C. Satchell, "The Pathological Relevance of Increased Endothelial Glycocalyx Permeability," *Am. J. Pathol.*, vol. 190, no. 4, pp. 742–751, 2020.

[20] J. M. Tarbell and L. M. Cancel, "The glycocalyx and its significance in human medicine," *Journal of Internal Medicine*, vol. 280, no. 1. pp. 97–113, 2016.

[21] R. D. Ramnath *et al.*, "Blocking matrix metalloproteinase-mediated syndecan-4 shedding restores the endothelial glycocalyx and glomerular filtration barrier function in early diabetic kidney disease," *Kidney Int.*, vol. 97, no. 5, pp. 951–965, 2020.

[22] S. C. Satchell, "The glomerular endothelium emerges as a key player in diabetic nephropathy," *Kidney Int.*, vol. 82, no. 9, pp. 949–951, 2012.

[23] T. L. Weissgerber *et al.*, "Early onset preeclampsia is associated with glycocalyx degradation and reduced microvascular perfusion," *J. Am. Heart Assoc.*, vol. 8, no. 4, 2019.

[24] Q. S. Dimke H, Maezawa Y, "Crosstalk in Glomerular Injury and Repair," *Curr Opin Nephrol Hypertens.*, vol. 24, no. 3, pp. 231–238, 2015.

[25] V. Eremina, H. J. Baelde, and S. E. Quaggin, "Role of the VEGF-A signaling pathway in the glomerulus: Evidence for crosstalk between components of the glomerular filtration barrier," *Nephron - Physiology*, vol. 106. pp. 32–37, 2007.

[26] P. Ruggenenti, M. Noris, and G. Remuzzi, "Thrombotic microangiopathy, hemolytic uremic syndrome, and thrombotic thrombocytopenic purpura," *Kidney Int.*, vol. 60, pp. 831–846, 2001.

[27] L. Byrne, C. Jenkins, N. Launders, R. Elson, and G. K. Adak, "The epidemiology, microbiology and clinical impact of Shiga toxin-producing Escherichia coli in England, 2009-2012," *Epidemiol. Infect.*, vol. 143, pp. 3475–3487, 2015.

[28] D. Karpman, S. Loos, R. Tati, and I. Arvidsson, "Haemolytic uraemic syndrome," *J. Intern. Med.*, vol. 281, pp. 123–148, 2017.

[29] C. M. Legendre *et al.*, "Terminal Complement Inhibitor Eculizumab in Atypical Hemolytic–Uremic Syndrome," *N Engl J Med*, vol. 23368, no. 6, pp. 2169–81, 2013.

[30] L. S. Keir and C. B. Langman, "Complement and the kidney in the setting of Shiga-toxin hemolytic uremic syndrome, organ transplantation, and C3 glomerulonephritis," *Transfus. Apher. Sci.*, vol. 54, pp. 203–211, 2016.

[31] P. I. Tarr, "Shiga toxin-associated hemolytic uremic syndrome and thrombotic thrombocytopenic purpura: Distinct mechanisms of pathogenesis," *Kidney Int.*, vol. 75, pp. S29–S32, 2009.

[32] F. Fakhouri, J. Zuber, V. Frémeaux-Bacchi, and C. Loirat, "Haemolytic uraemic

syndrome," *Lancet*, vol. 390, no. 10095, pp. 681–696, 2017.

[33] T. G. Obrig, "Escherichia coli shiga toxin mechanisms of action in renal disease," *Toxins (Basel).*, vol. 2, pp. 2769–2794, 2010.

[34] V. der K. N. Davin JC, "Advances and challenges in the management of complement-mediated thrombotic microangiopathies," *Ther Adv Hematol* , vol. 6, pp. 171–185, 2015.

[35] Á. Szilágyi *et al.*, "The role of complement in Streptococcus pneumoniae-associated haemolytic uraemic syndrome," *Nephrol. Dial. Transplant.*, vol. 28, pp. 2237–2245, 2013.

[36] K. L. Wijnsma *et al.*, "Fecal diagnostics in combination with serology: best test to establish STEC-HUS," *Pediatr. Nephrol.*, vol. 31, pp. 2163–2170, 2016.

[37] W. F. Clark, S.-H. S. Huang, M. W. Walsh, M. Farah, A. M. Hildebrand, and J. M. Sontrop, "Plasmapheresis for the treatment of kidney diseases," *Kidney Int.*, vol. 90, pp. 974–984, 2016.

[38] National Enhanced Surveillance System for STEC infection in England (NESSS), "Shiga toxin-producing Escherichia coli (STEC) data," *https://www.gov.uk/government/publications/escherichia-coli-e-coli-o157-annual-totals*, 2020. .

[39] T. Shimizu, Y. Ohta, and M. Noda, "Shiga toxin 2 is specifically released from bacterial cells by two different mechanisms," *Infect. Immun.*, vol. 77, no. 7, pp. 2813–2823, 2009.

[40] D. Werber *et al.*, "Associations of age and sex with the clinical outcome and incubation period of Shiga toxin-producing Escherichia coli O104:H4 infections, 2011.," *Am. J. Epidemiol.*, vol. 178, no. 6, pp. 984–992, 2013.

[41] M. Noris and G. Remuzzi, "Hemolytic uremic syndrome," *J. Am. Soc. Nephrol.*, vol. 16, no. 4, pp. 1035–1050, 2005.

[42] M. Fitzpatrick, "Haemolytic uraemic syndrome and E coli 0157: Prevention rests with sound public health measures D," *BMJ*, vol. 318, no. March, pp. 684–685, 1999.

[43] S. Nathanson *et al.*, "Acute neurological involvement in diarrhea-associated hemolytic uremic syndrome," *Clin. J. Am. Soc. Nephrol.*, vol. 5, no. 7, pp. 1218–1228, 2010.

[44] B. S. Kaplan, R. L. Ruebner, J. M. Spinale, and L. Copelovitch, "Current treatment of atypical hemolytic uremic syndrome," *Intractable Rare Dis. Res.*, vol. 3, no. 2, pp. 34–45, 2014.

[45] A. Rosales *et al.*, "Need for long-term follow-up in enterohemorrhagic Escherichia coli-Associated hemolytic uremic syndrome due to late-emerging sequelae," *Clin. Infect. Dis.*, vol. 54, no. 10, pp. 1413–1421, 2012.

[46] L. Byrne, C. Jenkins, N. Launders, R. Elson, and G. K. Adak, "The epidemiology, microbiology and clinical impact of Shiga toxin-producing Escherichia coli in England, 2009-2012," *Epidemiol. Infect.*, vol. 143, no. 16, pp. 3475–3487, 2015.

[47] D. Mackenzie, “Bean sprouts to blame for ‘decade-old’ E. coli,” *New Sci.*, vol. 210, no. 2817, p. 6, 2011.

[48] M. A. Rivero, J. A. Passucci, E. M. Rodríguez, and A. E. Parma, “Seasonal variation of HUS occurrence and VTEC infection in children with acute diarrhoea from Argentina,” *Eur. J. Clin. Microbiol. Infect. Dis.*, vol. 31, no. 6, pp. 1131–1135, 2012.

[49] K. Stanford, R. P. Johnson, T. W. Alexander, T. A. McAllister, and T. Reuter, “Influence of season and feedlot location on prevalence and virulence factors of seven serogroups of Escherichia coli in feces of western-Canadian slaughter cattle,” *PLoS One*, vol. 11, no. 8, pp. 1–18, 2016.

[50] O. Tenaillon, D. Skurnik, B. Picard, and E. Denamur, “The population genetics of commensal Escherichia coli,” *Nat. Rev. Microbiol.*, vol. 8, no. 3, pp. 207–217, 2010.

[51] K. Todar, “Pathogenic E. coli,” *http://textbookofbacteriology.net/e.coli.html*. pp. 1–4, 2012.

[52] Z. R. Stromberg, A. Van Goor, G. A. J. Redweik, M. J. Wymore Brand, M. J. Wannemuehler, and M. Mellata, “Pathogenic and non-pathogenic Escherichia coli colonization and host inflammatory response in a defined microbiota mouse model,” *DMM Disease Models and Mechanisms*, vol. 11. 2018.

[53] A. M. Valdes, J. Walter, E. Segal, and T. D. Spector, “Role of the gut microbiota in nutrition and health,” *BMJ*, vol. 361, pp. 36–44, 2018.

[54] S. M. Jandhyala, R. Talukdar, C. Subramanyam, H. Vuyyuru, M. Sasikala, and D. N. Reddy, “Role of the normal gut microbiota,” *World J. Gastroenterol.*, vol. 21, no. 29, pp. 8836–8847, 2015.

[55] A. M. Gorecki *et al.*, “Altered gut microbiome in Parkinson’s disease and the influence of lipopolysaccharide in a human α-synuclein over-expressing mouse model,” *Front. Neurosci.*, vol. 13, pp. 1–13, 2019.

[56] S. Cho, C. R. Jackson, and J. G. Frye, “The prevalence and antimicrobial resistance phenotypes of Salmonella , Escherichia coli , and Enterococcus sp. in surface water,” *Lett. Appl. Microbiol.*, vol. 71, pp. 3–25, 2020.

[57] P. M. Fratamico, C. DebRoy, Y. Liu, D. S. Needleman, G. M. Baranzoni, and P. Feng, “Advances in molecular serotyping and subtyping of Escherichia coli,” *Front. Microbiol.*, vol. 7, pp. 1–8, 2016.

[58] K. S. Baker, “Demystifying Escherichia coli pathovars,” *Nat. Rev. Microbiol.*, vol. 13, p. 5, 2015.

[59] S. Lu *et al.*, “Insights into the evolution of pathogenicity of Escherichia coli from genomic analysis of intestinal E. coli of Marmota himalayana in Qinghai-Tibet plateau of China,” *Emerg. Microbes Infect.*, vol. 5, no. 12, pp. 1–9, 2016.

[60] S. Delannoy, L. Beutin, and P. Fach, “Discrimination of enterohemorrhagic Escherichia coli (EHEC) from Non-EHEC strains based on detection of various combinations of Type III effector genes,” *J. Clin. Microbiol.*, vol. 51, no. 10, pp. 3257–3262, 2013.

[61] L. Keir, “Understanding the Renal Pathogenesis of Diarrhoea Associated

Haemolytic Uraemic Syndrome (PhD Thesis).” pp. 1–348, 2013.

[62] J. E. Alouf, “A 116-year story of bacterial protein toxins (1888-2004): From ‘diphtheritic poison’ to molecular toxinology,” *The Comprehensive Sourcebook of Bacterial Protein Toxins*. pp. 3–21, 2006.

[63] A. R. Melton-Celsa, “Shiga Toxin (Stx) Classification, Structure, and Function,” *Microbiol. Spectr.*, vol. 2, no. 4, pp. 1–21, 2014.

[64] L. Johannes and W. Römer, “Shiga toxins — from cell biology to biomedical applications,” *Nat. Rev. Microbiol.*, vol. 8, pp. 105–116, 2009.

[65] A. D. Thorpe C, Ritchie JM, “Enterphemorrhagic and Other Shiga toxin-producing Escherichia Coli,” *Escherichia coli: Virulence Mechansisms of a Versatile Pathogen*. Elsevier Inc., pp. 119–154, 2002.

[66] V. L. Tesh, “Activation of cell stress response pathways by Shiga toxins,” *Cell. Microbiol.*, vol. 14, pp. 1–9, 2012.

[67] S. D. Gamage, J. E. Strasser, C. L. Chalk, and A. A. Weiss, “Nonpathogenic Escherichia coli can contribute to the production of Shiga toxin,” *Infect. Immun.*, vol. 71, no. 6, pp. 3107–3115, 2003.

[68] K. Westman *et al.*, “Shiga Toxin-induced complement mediated hemolysis and release of complement-coated red blood cell derived microvesicles in HUS,” *J. Immunol.*, vol. 194, pp. 2309–2318, 2015.

[69] L. Johannes and W. Römer, “Shiga toxins from cell biology to biomedical applications,” *Nat. Rev. Microbiol.*, vol. 8, no. 2, pp. 105–116, 2010.

[70] S. Oyadomari and M. Mori, “Roles of CHOP/GADD153 in endoplasmic reticulum stress,” *Cell Death Differ.*, vol. 11, no. 4, pp. 381–389, 2004.

[71] A. R. Safa, “Roles of c-FLIP in Apoptosis, Necroptosis, and Autophagy,” *J Carcinog Mutagen.*, vol. 6, pp. 1–19, 2013.

[72] T. G. Obrig and D. Karpman, “Shiga toxin pathogenesis: Kidney complications and renal failure,” *Curr. Top. Microbiol. Immunol.*, vol. 357, pp. 105–136, 2012.

[73] L. B. Márquez, A. Araoz, H. A. Repetto, F. R. Ibarra, and C. Silberstein, “Effects of shiga toxin 2 on cellular regeneration mechanisms in primary and three-dimensional cultures of human renal tubular epithelial cells,” *Microb. Pathog.*, vol. 99, pp. 87–94, 2016.

[74] M. A. Psotka *et al.*, “Shiga toxin 2 targets the murine renal collecting duct epithelium,” *Infect. Immun.*, vol. 77, pp. 959–969, 2009.

[75] T. Okuda *et al.*, “Targeted disruption of Gb3/CD77 synthase gene resulted in the complete deletion of globo-series glycosphingolipids and loss of sensitivity to verotoxins,” *J. Biol. Chem.*, vol. 281, pp. 10230–10235, 2006.

[76] I. Van Die and R. Geyer, “Glycobiology: Sphingolipid Metabolism and Cell Signalling,” in *Methods in enzymology*, 2010, pp. 117–140.

[77] M. L. Allende and R. L. Proia, “Simplifying complexity: Genetically resculpting glycosphingolipid synthesis pathways in mice to reveal function,” *Glycoconj. J.*, vol.

31, pp. 613–622, 2014.

[78] D. Hammache, N. Yahi, M. Maresca, G. Piéroni, and J. Fantini, “Human Erythrocyte Glycosphingolipids as Alternative Cofactors for Human Immunodeficiency Virus Type 1 (HIV-1) Entry: Evidence for CD4-Induced Interactions between HIV-1 gp120 and Reconstituted Membrane Microdomains of Glycosphingolipids (Gb3 and GM3),” *J. Virol.*, vol. 73, no. 6, pp. 5244–5248, 1999.

[79] A. Puri *et al.*, “The neutral glycosphingolipid globotriaosylceramide promotes fusion mediated by a CD4-dependent CXCR4-utilizing HIV type 1 envelope glycoprotein,” *PNAS*, vol. 95, pp. 14435–14440, 1998.

[80] A. Kiarash, B. Boyd, and C. A. Lingwood, “Glycosphingolipid receptor function is modified by fatty acid content,” *J. Biol. Chem.*, vol. 269, no. 15, pp. 11138–11146, 1994.

[81] H. O. Yosief, S. S. Iyer, and A. A. Weissc, “Binding of pk-trisaccharide analogs of globotriaosylceramide to shiga toxin variants,” *Infect. Immun.*, vol. 81, no. 8, pp. 2753–2760, 2013.

[82] K. M. Gallegos, D. G. Conrady, S. S. Karve, T. S. Gunasekera, A. B. Herr, and A. A. Weiss, “Shiga toxin binding to glycolipids and glycans,” *PLoS One*, vol. 7, pp. 1–10, 2012.

[83] T. D. Simons Kai, “Lipid rafts and signal transduction,” *Nat. Rev. Mol. Cell Biol.*, vol. 1, no. 1, pp. 31–41, 2000.

[84] T. G. Obrig *et al.*, “Induction by Sphingomyelinase of Shiga Toxin Receptor and Shiga Toxin 2 Sensitivity in Human Microvascular Endothelial Cells,” *Infect. Immun.*, vol. 71, no. 2, pp. 845–849, 2003.

[85] W. C. Butler R, Williams M, “Fabry Disease Service,” *North Bristol NHS*, no. 9307. p. 1, 2019.

[86] J. A. Shayman and P. D. Killen, “Fabry disease,” in *Molecular and Genetic Basis of Renal Disease*, First Edit., Elsevier Inc., 2008, pp. 195–199.

[87] T. D. Butters, R. A. Dwek, and F. M. Platt, “Imino sugar inhibitors for treating the lysosomal glycosphingolipidoses,” *Glycobiology*, vol. 15, no. 10, pp. 43–52, 2005.

[88] R. Schiffmann *et al.*, “Screening, diagnosis, and management of patients with Fabry disease: conclusions from a ‘Kidney Disease: Improving Global Outcomes’ (KDIGO) Controversies Conference,” *Kidney Int.*, vol. 91, no. 2, pp. 284–293, 2017.

[89] T. Ohshima *et al.*, “α-Galactosidase A deficient mice: A model of fabry disease,” *PNAS*, vol. 94, no. 6, pp. 2540–2544, 1997.

[90] S. A. Cilmi, B. J. Karalius, W. Choy, R. N. Smith, and J. R. Butterton, “ Fabry Disease in Mice Protects against Lethal Disease Caused by Shiga Toxin–Expressing Enterohemorrhagic Escherichia coli ,” *J. Infect. Dis.*, vol. 194, no. 8, pp. 1135–1140, 2006.

[91] S. D. Zumbrun *et al.*, “Human intestinal tissue and cultured colonic cells contain globotriaosylceramide synthase mRNA and the alternate shiga toxin receptor globotetraosylceramide,” *Infect. Immun.*, vol. 78, no. 11, pp. 4488–4499, 2010.

[92] T. Okuda and K. I. Nakayama, “Identification and characterization of the human Gb3/CD77 synthase gene promoter,” *Glycobiology*, vol. 18, no. 12, pp. 1028–1035, 2008.

[93] H. Uchida, N. Kiyokawa, T. Taguchi, H. Horie, J. Fujimoto, and T. Takeda, “Shiga Toxins Induce Apoptosis in Pulmonary Epithelium–Derived Cells,” *J. Infect. Dis.*, vol. 180, no. 6, pp. 1902–1911, 1999.

[94] C. A. Lingwood, B. Binnington, A. Manis, and D. R. Branch, “Globotriaosyl ceramide receptor function - Where membrane structure and pathology intersect,” *FEBS Lett.*, vol. 584, no. 9, pp. 1879–1886, 2010.

[95] D. T. Obrig TG, Louise CB, Lingwood CA, Boyd B, Barley-Maloney L, “Endothelial Heterogeneity in Shiga Toxin Receptors and Responses,” *J. Biol. Chem.*, vol. 268, pp. 15484–15488, 1993.

[96] A. Bauwens *et al.*, “Differential cytotoxic actions of Shiga toxin 1 and Shiga toxin 2 on microvascular and macrovascular endothelial cells,” *Thromb. Haemost.*, vol. 105, no. 3, pp. 515–528, 2011.

[97] T. G. Obrig *et al.*, “Induction by sphingomyelinase of Shiga toxin receptor and Shiga toxin 2 sensitivity in human microvascular endothelial cells,” *Infect. Immun.*, vol. 71, pp. 845–849, 2003.

[98] C. Zoja, S. Buelli, and M. Morigi, “Shiga toxin-associated hemolytic uremic syndrome: Pathophysiology of endothelial dysfunction,” *Pediatr. Nephrol.*, vol. 25, no. 11, pp. 2231–2240, 2010.

[99] D. Karpman, A. Andreasson, H. Thysell, B. S. Kaplan, and C. Svanborg, “Cytokines in childhood hemolytic uremic syndrome and thrombotic thrombocytopenic purpura,” *Pediatric Nephrology*, vol. 9, no. 6. pp. 694–699, 1995.

[100] A. K. Hughes, P. K. Stricklett, and D. E. Kohan, “Shiga toxin-1 regulation of cytokine production by human proximal tubule cells,” *Kidney Int.*, vol. 54, no. 4, pp. 1093–1106, 1998.

[101] P. A. Van Setten, L. A. H. Monnens, R. G. G. Verstraten, L. P. W. J. Van Den Heuvel, and V. W. M. Van Hinsbergh, “Effects of verocytotoxin-1 on nonadherent human monocytes: Binding characteristics, protein synthesis, and induction of cytokine release,” *Blood*, vol. 88, no. 1. pp. 174–183, 1996.

[102] R. Hirschberg, S. Wang, and G. M. Mitu, “Functional symbiosis between endothelium and epithelial cells in glomeruli,” *Cell Tissue Res.*, vol. 331, no. 2, pp. 485–493, 2008.

[103] M. E. Penning *et al.*, “Association of preeclampsia with podocyte turnover,” *Clin. J. Am. Soc. Nephrol.*, vol. 9, no. 8, pp. 1377–1385, 2014.

[104] V. D. Garovic, “The role of the podocyte in preeclampsia,” *Clin. J. Am. Soc. Nephrol.*, vol. 9, no. 8, pp. 1337–1340, 2014.

[105] I. M. Craici *et al.*, “Advances in the pathophysiology of pre-eclampsia and related podocyte injury,” *Kidney Int.*, vol. 86, no. 2, pp. 275–285, 2015.

[106] L. De Petris *et al.*, “Urinary Podocyte mRNA Excretion in Children with D + HUS : A

Potential Marker of Long-Term Outcome Urinary Podocyte mRNA Excretion in Children with D + HUS : A Potential Marker of Long-Term Outcome," *Ren. Fail.*, vol. 28, pp. 475–482, 2009.

[107] H. Trachtman *et al.*, "Urinary neutrophil gelatinase-associated lipocalcin in D + HUS : a novel marker of renal injury," *Pediatr. Nephrol.*, vol. 21, pp. 989–994, 2006.

[108] Y. Sun *et al.*, "The expression and significance of neuronal iconic proteins in podocytes," *PLoS One*, vol. 9, no. 4, pp. 3–10, 2014.

[109] T. Weide and T. B. Huber, "Signaling at the Slit : Podocytes Chat by Synaptic Transmission," *J. Am. Soc. Nephrol.*, vol. 20, pp. 1860–1870, 2009.

[110] A. Richard Kitching and H. L. Hutton, "The players: Cells involved in glomerular disease," *Clinical Journal of the American Society of Nephrology*, vol. 11, no. 9. pp. 1664–1674, 2016.

[111] N. P. Curthoys and O. W. Moe, "Proximal tubule function and response to acidosis," *Clin. J. Am. Soc. Nephrol.*, vol. 9, no. 9, pp. 1627–1638, 2014.

[112] T. R. Keepers, M. A. Psotka, L. K. Gross, and T. G. Obrig, "A Murine Model of HUS: Shiga Toxin with Lipopolysaccharide Mimics the Renal Damage and Physiologic Response of Human Disease," *J Am Soc Nephrol*, vol. 17, pp. 3404–3414, 2006.

[113] S. Dennhardt *et al.*, "Modeling hemolytic-uremic syndrome: In-depth characterization of distinct murine models reflecting different features of human disease," *Front. Immunol.*, vol. 9, pp. 1–19, 2018.

[114] M. Locatelli *et al.*, "Shiga toxin promotes podocyte injury in experimental hemolytic uremic syndrome via activation of the alternative pathway of complement," *J. Am. Soc. Nephrol.*, vol. 25, no. 8, pp. 1786–1798, 2014.

[115] T. R. Keepers, L. K. Gross, and T. G. Obrig, "Monocyte chemoattractant protein 1, macrophage inflammatory protein 1α, and RANTES recruit macrophages to the kidney in a mouse model of hemolytic-uremic syndrome," *Infect. Immun.*, vol. 75, no. 3, pp. 1229–1236, 2007.

[116] Z. G. Laszik and G. L. Blakey, "Searching for a Valid Animal Model of Hemolytic Uremic Syndrome," *Am J Clin Pathol*, vol. 118, pp. 323–325, 2002.

[117] B. C. Lee, C. L. Mayer, C. S. Leibowitz, D. J. Stearns-Kurosawa, and S. Kurosawa, "Quiescent complement in nonhuman primates during E coli Shiga toxin-induced hemolytic uremic syndrome and thrombotic microangiopathy," *Blood*, vol. 122, pp. 803–806, 2013.

[118] T. Sursal *et al.*, "Plasma Bacterial and Mitochondrial DNA Distinguish Bacterial Sepsis from Sterile SIRS and Quantify Inflammatory Tissue Injury in Nonhuman Primates," *Shock*, vol. 39, pp. 55–62, 2013.

[119] E. M. Mallick *et al.*, "A novel murine infection model for Shiga toxin-producing Escherichia coli," *J. Clin. Invest.*, vol. 122, pp. 4012–4024, 2012.

[120] A. Serna IV and E. C. Boedeker, "Pathogenesis and treatment of Shiga toxin-producing Escherichia coli infections," *Curr. Opin. Gastroenterol.*, vol. 24, no. 1, pp. 38–47, 2008.

[121] J. Holgersson, P. Jovall, and M. E. Breimer, “Glycosphingolipids of Human Large Intestine: detailed structural characterisation with special reference to blood group compounds and bacterial receptor structures,” *J. Biochem.*, vol. 110, pp. 120–131, 1991.

[122] O. Kovbasnjuk, “New insights into the role of Shiga toxins in intestinal disease,” *Gastroenterology*, vol. 129, no. 4, pp. 1354–1355, 2005.

[123] C. Zoja, S. Buelli, and M. Morigi, “Shiga toxin triggers endothelial and podocyte injury: the role of complement activation,” *Pediatr. Nephrol.*, vol. 34, pp. 379–388, 2017.

[124] S. Buelli, C. Zoja, G. Remuzzi, and M. Morigi, “Complement activation contributes to the pathophysiology of shiga toxin-associated hemolytic uremic syndrome,” *Microorganisms*, vol. 7, pp. 1–16, 2019.

[125] A. J. King, S. Sundaram, M. Cendoroglo, D. W. K. Acheson, and G. T. Keusch, “Shiga Toxin Induces Superoxide Production in Polymorphonuclear Cells with Subsequent Impairment of Phagocytosis and Responsiveness to Phorbol Esters,” *J. Infect. Dis.*, vol. 179, no. 2, pp. 503–507, 1999.

[126] J. Liu *et al.*, “Inhibition of neutrophil apoptosis by verotoxin 2 derived from Escherichia coli O157:H7,” *Infect. Immun.*, vol. 67, no. 11, pp. 6203–6205, 1999.

[127] V. Cheung and H. Trachtman, “Hemolytic uremic syndrome: Toxins, vessels, and inflammation,” *Front. Med.*, vol. 1, pp. 1–7, 2014.

[128] P. D. Ziakas, M. L. Prodromou, J. El Khoury, E. Zintzaras, and E. Mylonakis, “The role of TLR4 896 A>G and 1196 C>T in susceptibility to infections: A review and meta-analysis of genetic association studies,” *PLoS One*, vol. 8, no. 11, pp. 1–13, 2013.

[129] M. Brigotti *et al.*, “Soluble Toll-like receptor 4 impairs the interaction of Shiga toxin 2a with human serum amyloid P component,” *Toxins (Basel).*, vol. 10, no. 9, pp. 1–9, 2018.

[130] A. Ståhl *et al.*, “A Novel Mechanism of Bacterial Toxin Transfer within Host Blood Cell-Derived Microvesicles,” *PLoS Pathog.*, vol. 11, no. 2, pp. 1–22, 2015.

[131] S. A. Ghosh, R. K. Polanowska-Grabowska, J. Fujii, T. Obrig, and A. R. L. Gear, “Shiga toxin binds to activated platelets,” *J. Thromb. Haemost.*, vol. 2, no. 3, pp. 499–506, 2004.

[132] M. Morigi *et al.*, “Verotoxin-1-induced up-regulation of adhesive molecules renders microvascular endothelial cells thrombogenic at high shear stress,” *Blood*, vol. 98, no. 6, pp. 1828–1835, 2001.

[133] M. Mor and S. Ashkenazi, “The dilemma of antimicrobial treatment of shiga toxin-producing escherichia coli,” *Pediatr. Infect. Dis. J.*, vol. 33, no. 9, pp. 979–981, 2014.

[134] G. Hall, S. Kurosawa, and D. J. Stearns-Kurosawa, “Shiga toxin therapeutics: Beyond neutralization,” *Toxins (Basel).*, vol. 9, pp. 1–18, 2017.

[135] J. Mukherjee *et al.*, “Human Stx2-specific monoclonal antibodies prevent systemic complications of Escherichia coli O157:H7 infection,” *Infect. Immun.*, vol. 70, no. 2, pp. 612–619, 2002.

[136] S. Tzipori, A. Sheoran, D. Akiyoshi, A. Donohue-Rolfe, and H. Trachtman, “Antibody therapy in the management of Shiga toxin-induced hemolytic uremic syndrome,” *Clin. Microbiol. Rev.*, vol. 17, no. 4, pp. 926–941, 2004.

[137] E. L. López *et al.*, “Safety and pharmacokinetics of urtoxazumab, a humanized monoclonal antibody, against Shiga-like toxin 2 in healthy adults and in pediatric patients infected with Shiga-like toxin-producing Escherichia coli,” *Antimicrob. Agents Chemother.*, vol. 54, no. 1, pp. 239–243, 2010.

[138] N. R. Medjeral-Thomas *et al.*, “Circulating complement factor H-related proteins 1 and 5 correlate with disease activity in IgA nephropathy,” *Kidney Int.*, vol. 92, pp. 942–952, 2017.

[139] M. Crowley, “NHS England aHUS Service specification 2017,” *https://www.england.nhs.uk/wp-content/uploads/2017*. pp. 1–7, 2017.

[140] K. Yan, K. Desai, L. Gullapalli, E. Druyts, and C. Balijepalli, “Epidemiology of atypical hemolytic uremic syndrome: A systematic literature review,” *Clin. Epidemiol.*, vol. 12, pp. 295–305, 2020.

[141] T. H. J. Goodship *et al.*, “Atypical hemolytic uremic syndrome and C3 glomerulopathy: conclusions from a ‘Kidney Disease: Improving Global Outcomes’ (KDIGO) Controversies Conference,” *Kidney Int.*, vol. 91, no. 3, pp. 539–551, 2017.

[142] W. J. C. Feitz, N. C. A. J. van de Kar, D. Orth-Höller, L. P. J. W. van den Heuvel, and C. Licht, “The genetics of atypical hemolytic uremic syndrome,” *Medizinische Genet.*, vol. 30, no. 4, pp. 400–409, 2018.

[143] D. Kavanagh, T. H. J. Goodship, and A. Richards, “Atypical haemolytic uraemic syndrome,” *Br. Med. Bull.*, vol. 77–78, no. 1, pp. 5–22, 2006.

[144] R. A. Kavanagh D, Goodship TH, “Seminars in Atypical Haemolytic Uraemic Syndrome,” *Semin. Nephrol.*, vol. 33, no. 6, pp. 508–530, 2013.

[145] National Renal Complement Therapeutics Centre, “The Annual Report of the National Renal Complement Therapeutics Centre 2018/19,” *www.atypicalhus.co.uk*. pp. 1–52, 2019.

[146] A. M. Durkan, S. Kim, J. Craig, and E. Elliott, “The long - term outcomes of atypical haemolytic uraemic syndrome : a national surveillance study,” *Arch. Dis. Child.*, vol. 0, pp. 1–5, 2016.

[147] Quaggin SE., “DGKE and atypical HUS.,” *Nat Genet*, vol. 45, pp. 475–476, 2013.

[148] S. Bruneau *et al.*, “Loss of DGKε induces endothelial cell activation and death independently of complement activation,” *Blood*, vol. 125, pp. 1038–1046, 2015.

[149] L. Q. M. et al. Lemaire M, Frémeaux-Bacchi V, Schaefer F, Choi M, Tang WH, “Recessive mutations in DGKE cause atypical hemolytic-uremic syndrome.,” *Nat. Genet.*, vol. 45, no. 5, pp. 531–536, 2013.

[150] S. P. Berger, A. Roos, and M. R. Daha, “Complement and the kidney: What the nephrologist needs to know in 2006?,” *Nephrol Dial Transpl.*, vol. 20, pp. 2613–2619, 2005.

[151] E. B. Volokhina, D. Westra, T. J. A. M. Van Der Velden, N. C. A. J. Van De Kar, T. E. Mollnes, and L. P. Van Den Heuvel, "Complement activation patterns in atypical haemolytic uraemic syndrome during acute phase and in remission," *Clin. Exp. Immunol.*, vol. 181, pp. 306–313, 2015.

[152] M. Ozaki *et al.*, "Human mannose-binding lectin inhibitor prevents Shiga toxin induced renal injury," *Kidney Int.*, vol. 90, pp. 774–782, 2016.

[153] L. T. Roumenina, J. Rayes, M. Frimat, and V. Fremeaux-Bacchi, "Endothelial cells: source, barrier, and target of defensive mediators," *Immunol. Rev.*, vol. 274, pp. 307–329, 2016.

[154] C. Joseph and J. Gattineni, "Complement disorders and hemolytic uremic syndrome," *Curr. Opin. Pediatr.*, vol. 25, no. 2, pp. 209–215, 2013.

[155] A. Z. Blatt, S. Pathan, and V. P. Ferreira, "Properdin: a tightly regulated critical inflammatory modulator," *Immunol. Rev.*, vol. 274, pp. 172–190, 2016.

[156] J. R. Dunkelberger and W. C. Song, "Complement and its role in innate and adaptive immune responses," *Cell Res.*, vol. 20, no. 1, pp. 34–50, 2010.

[157] C. A. Janeway, P. Travers, M. Walport, and M. J. Shlomchik, "Principles of innate and adaptive immunity: Chapter 1-5," in *Immunobiology: The Immune System in Health and Disease.*, 2001.

[158] T. H. Mogensen, "Pathogen recognition and inflammatory signaling in innate immune defenses," *Clin. Microbiol. Rev.*, vol. 22, no. 2, pp. 240–273, 2009.

[159] Z. A. Chen *et al.*, "Structure of complement C3(H2O) revealed by quantitative cross-linking/mass spectrometry and modeling," *Mol. Cell. Proteomics*, vol. 15, no. 8, pp. 2730–2743, 2016.

[160] P. G. and J. D. L. Daniel Ricklin, Edimara S. Reis, Dimitrios C. Mastellos, "Complement component C3 - The 'Swiss Army Knife' of innate immunity and host defense," *Immunol. Rev.*, vol. 274, no. 1, pp. 33–58, 2016.

[161] E. Jacobs, C. Ortiz, and C. Licht, "The Role of Complement in the Pathogenesis of HUS and the TMA Spectrum Disorders," *Curr. Pediatr. Rep.*, vol. 7, no. 1, pp. 1–11, 2019.

[162] C. Q. Schmidt, J. D. Lambris, and D. Ricklin, "Protection of host cells by complement regulators," *Immunol. Rev.*, vol. 274, pp. 152–171, 2016.

[163] D. Kavanagh and T. Goodship, "Genetics and complement in atypical HUS," *Pediatr. Nephrol.*, vol. 25, no. 12, pp. 2431–2442, 2010.

[164] H. P. Morgan *et al.*, "Structural basis for engagement by complement factor H of C3b on a self surface," *Nat. Struct. Mol. Biol.*, vol. 18, no. 4, pp. 463–471, 2011.

[165] M. Józsi, "Factor H family proteins in complement evasion of microorganisms," *Front. Immunol.*, vol. 8, pp. 1–8, 2017.

[166] S. Meri and M. K. Pangburn, "Regulation of alternative pathway complement activation by glycosaminoglycans: Specificity of the polyanion binding site on factor H," *Biochemical and Biophysical Research Communications*, vol. 198, no. 1.

pp. 52–59, 1994.

[167] A. L. Ståhl *et al.*, “Factor H dysfunction in patients with atypical hemolytic uremic syndrome contributes to complement deposition on platelets and their activation,” *Blood*, vol. 111, no. 11, pp. 5307–5315, 2008.

[168] M. C. Pickering *et al.*, “Spontaneous hemolytic uremic syndrome triggered by complement factor H lacking surface recognition domains,” *J. Exp. Med.*, vol. 204, no. 6, pp. 1249–1256, 2007.

[169] E. G. De Jorge *et al.*, “The development of atypical hemolytic uremic syndrome depends on complement C5,” *J. Am. Soc. Nephrol.*, vol. 22, no. 1, pp. 137–145, 2011.

[170] R. B. Pouw, M. C. Brouwer, A. E. van Beek, M. Józsi, D. Wouters, and T. W. Kuijpers, “Complement factor H-related protein 4A is the dominant circulating splice variant of CFHR4,” *Front. Immunol.*, vol. 9, no. APR, 2018.

[171] M. Józsi and P. F. Zipfel, “Factor H family proteins and human diseases,” *Trends Immunol.*, vol. 29, no. 8, pp. 380–387, 2008.

[172] M. K. Liszewski and J. P. Atkinson, “Complement regulator CD46: genetic variants and disease associations,” *Hum. Genomics*, vol. 9, p. 7, 2015.

[173] S. J. Clark, C. Q. Schmidt, A. M. White, S. Hakobyan, B. P. Morgan, and P. N. Bishop, “Identification of Factor H–like Protein 1 as the Predominant Complement Regulator in Bruch’s Membrane: Implications for Age-Related Macular Degeneration,” *J. Immunol.*, vol. 193, no. 10, pp. 4962–4970, 2014.

[174] M. Cserhalmi, A. Papp, B. Brandus, B. Uzonyi, and M. Józsi, “Regulation of regulators: Role of the complement factor H-related proteins,” *Semin. Immunol.*, vol. 45, pp. 1–13, 2019.

[175] J. M. Thurman and V. M. Holers, “The Central Role of the Alternative Complement Pathway in Human Disease,” *J. Immunol.*, vol. 176, no. 3, pp. 1305–1310, 2006.

[176] G. B. Appel *et al.*, “Membranoproliferative glomerulonephritis type II (dense deposit disease): An update,” *J. Am. Soc. Nephrol.*, vol. 16, no. 5, pp. 1392–1403, 2005.

[177] M. S. Józsi M, “Factor H-Related Proteins: The Complement System.,” *Methods in Molecular Biology*, vol. 1100. pp. 225–236, 2014.

[178] A. M. Shields, A. T. Pagnamenta, A. J. Pollard, J. C. Taylor, H. Allroggen, and S. Y. Patel, “Classical and Non-classical Presentations of Complement Factor I Deficiency: Two contrasting cases diagnosed via genetic and genomic methods,” *Front. Immunol.*, vol. 10, pp. 1–10, 2019.

[179] P. Roversi *et al.*, “Structural basis for complement factor I control and its disease-associated sequence polymorphisms,” *PNAS*, vol. 108, no. 31, pp. 12839–12844, 2011.

[180] M. M. Brodbeck WG, Kuttner-Kondo L, Mold C, “Structure/function studies of human decay-accelerating factor,” *Immunology*, vol. 101, pp. 104–111, 2000.

[181] A. Hill, A. E. Dezern, T. Kinoshita, and R. A. Brodsky, “Paroxysmal nocturnal haemoglobinuria,” *Nat. Rev. Dis. Prim.*, vol. 3, pp. 1–14, 2017.

[182] D. Kavanagh *et al.*, “The decay accelerating factor mutation I197V found in hemolytic uraemic syndrome does not impair complement regulation,” *Mol. Immunol.*, vol. 44, no. 12, pp. 3162–3167, 2007.

[183] X. Sun, C. D. Funk, C. Deng, A. Sahu, J. D. Lambris, and W. C. Song, “Role of decay-accelerating factor in regulating complement activation on the erythrocyte surface as revealed by gene targeting,” *Proc. Natl. Acad. Sci. U. S. A.*, vol. 96, no. 2, pp. 628–633, 1999.

[184] Y. Huang, F. Qiao, R. Abagyan, S. Hazard, C. Davies, and S. Tomlinson, “Defining the CD59–C9 binding interaction,” *Molecular Immunology*, vol. 44, no. 1–3. p. 187, 2007.

[185] C. Parker *et al.*, “Review in translational hematology Diagnosis and management of paroxysmal nocturnal hemoglobinuria,” *Rev. Transl. Hematol.*, vol. 106, no. 12, pp. 3699–3709, 2005.

[186] R. Martínez-Barricarte *et al.*, “The molecular and structural bases for the association of complement C3 mutations with atypical hemolytic uremic syndrome,” *Mol. Immunol.*, vol. 66, no. 2, pp. 263–273, 2015.

[187] F. Bu *et al.*, “Comprehensive genetic analysis of complement and coagulation genes in atypical hemolytic uremic syndrome,” *J. Am. Soc. Nephrol.*, vol. 25, no. 1, pp. 55–64, 2014.

[188] The Human Protein Atlas, “Tissue expression of SLC2A2,” *https://www.proteinatlas.org/SLC2A2/tissue*, 2018. [Online]. Available: https://www.proteinatlas.org/ENSG00000163581-SLC2A2/tissue.

[189] A. Java, M. K. Liszewski, D. E. Hourcade, F. Zhang, and J. P. Atkinson, “Role of complement receptor 1 (CR1; CD35) on epithelial cells: A model for understanding complement-mediated damage in the kidney,” *Mol. Immunol.*, vol. 67, pp. 584–595, 2015.

[190] G. R. Andersen, “Mutations in complement C3 from aHUS patients,” *Blood*, vol. 125, no. 15, pp. 2316–2318, 2015.

[191] E. K. S. Wong, T. H. J. Goodship, and D. Kavanagh, “Complement therapy in atypical haemolytic uraemic syndrome (aHUS),” *Molecular Immunology*, vol. 56, no. 3. pp. 199–212, 2013.

[192] S. Faguer, A. Huart, V. Frémeaux-Bacchi, D. Ribes, and D. Chauveau, “Eculizumab and drug-induced haemolytic-uraemic syndrome,” *Clin. Kidney J.*, vol. 6, pp. 484–485, 2013.

[193] A. F. Saad, J. Roman, A. Wyble, and L. D. Pacheco, “Pregnancy-Associated Atypical Hemolytic- Uremic Syndrome,” *Am J Perinatol Rep*, vol. 6, pp. 125–128, 2016.

[194] NICE, “Final evaluation determination Eculizumab for treating atypical haemolytic uraemic syndrome,” *nice.org.uk/guidance/hst1/documents/atypical-haemolytic-uraemic-syndrom*. pp. 1–43, 2014.

[195] J. Menne *et al.*, “Outcomes in patients with atypical hemolytic uremic syndrome treated with eculizumab in a long-term observational study,” *BMC Nephrol.*, vol. 20, no. 1, pp. 1–12, 2019.

[196] T. J. Hoerger, N. R. Burrows, and M. E. Pavkov, “Discontinuation of Eculizumab Treatment in Atypical Hemolytic Uremic Syndrome: An Update,” *YAJKD*, vol. 66, pp. 172–173, 2015.

[197] National Renal Complement Therapeutics Centre, “Clinical Trials,” *http://www.atypicalhus.co.uk/clinical-trials/*. 2020.

[198] P. R. Walsh and S. Johnson, “Eculizumab in the treatment of Shiga toxin haemolytic uraemic syndrome,” *Pediatr. Nephrol.*, vol. 34, no. 9, pp. 1485–1492, 2019.

[199] E. M. Conway, “HUS and the case for complement,” *Blood*, vol. 126, no. 18, pp. 2085–2090, 2015.

[200] J. Menne *et al.*, “Validation of treatment strategies for enterohaemorrhagic Escherichia coli O104:H4 induced haemolytic uraemic syndrome:case-control study,” *BMJ*, vol. 345, pp. 1–13, 2012.

[201] European Medicines Agency, “Clinical Trials Register,” *https://www.clinicaltrialsregister.eu/*, 2017. [Online]. Available: https://www.clinicaltrialsregister.eu/ctr-search/search.

[202] H. I. Kenawy, I. Boral, and A. Bevington, “Complement-coagulation cross-talk: A potential mediator of the physiological activation of complement by low pH,” *Front. Immunol.*, vol. 6, pp. 1–10, 2015.

[203] C. K. Lupu F, Keshari R, Lambris J, “Crosstalk between the coagulation and complement systems in sepsis,” *Thromb Res.*, vol. 133, no. 0 1, pp. S28–S31, 2014.

[204] M. Huber-Lang *et al.*, “Generation of C5a in the absence of C3: A new complement activation pathway,” *Nat. Med.*, vol. 12, no. 6, pp. 682–687, 2006.

[205] U. Amara *et al.*, “Molecular Intercommunication between the Complement and Coagulation Systems,” *J. Immunol.*, vol. 185, no. 9, pp. 5628–5636, 2010.

[206] A. Krarup, R. Wallis, J. S. Presanis, P. Gál, and R. B. Sim, “Simultaneous activation of complement and coagulation by MBL-associated serine protease 2,” *PLoS One*, vol. 2, no. 7, pp. 1–8, 2007.

[207] K. Ikeda, K. Nagasawa, T. Horiuchi, T. Tsuru, H. Nishizaka, and Y. Niho, “C5a induces tissue factor activity on endothelial cells,” *Thrombosis and Haemostasis*, vol. 77, no. 2. pp. 394–398, 1997.

[208] M. Morigi *et al.*, “Alternative Pathway Activation of Complement by Shiga Toxin Promotes Exuberant C3a Formation That Triggers Microvascular Thrombosis,” *J. Immunol.*, vol. 187, no. 1, pp. 172–180, 2011.

[209] M. Riedl Khursigara *et al.*, “Vascular endothelial cells evade complement-mediated membrane injury via Weibel-Palade body mobilization,” *J. Thromb. Haemost.*, vol. 18, pp. 1484–1494, 2020.

[210] A. K. Pandey *et al.*, “Mechanisms of VEGF (vascular endothelial growth factor)

inhibitor-associated hypertension and vascular disease," *Hypertension*, vol. 71, no. 2, pp. E1–E8, 2018.

[211] W. G. Roberts and G. E. Palade, "Increased microvascular permeability and endothelial fenestration induced by vascular endothelial growth factor," *J. Cell Sci.*, vol. 108, no. 6, pp. 2369–2379, 1995.

[212] E. Liu *et al.*, "Increased expression of vascular endothelial growth factor in kidney leads to progressive impairment of glomerular functions," *J. Am. Soc. Nephrol.*, vol. 18, no. 7, pp. 2094–2104, 2007.

[213] B. F. Schrijvers, A. Flyvbjerg, and A. S. De Vriese, "The role of vascular endothelial growth factor (VEGF) in renal pathophysiology," *Kidney Int.*, vol. 65, no. 6, pp. 2003–2017, 2004.

[214] V. Eremina *et al.*, "Glomerular-specific alterations of VEGF-A expression lead to distinct congenital and acquired renal diseases," *J. Clin. Invest.*, vol. 111, no. 5, pp. 707–716, 2003.

[215] R. M. McFee, T. G. Rozell, and A. S. Cupp, "The balance of proangiogenic and antiangiogenic VEGFA isoforms regulate follicle development," *Cell Tissue Res.*, vol. 349, no. 3, pp. 635–647, 2012.

[216] D. I. R. Holmes and I. Zachary, "The vascular endothelial growth factor (VEGF) family: Angiogenic factors in health and disease," *Genome Biol.*, vol. 6, no. 209, pp. 1–10, 2005.

[217] V. Eremina and S. E. Quaggin, "The role of VEGF-A in glomerular development and function : Current Opinion in Nephrology and Hypertension," *Curr Opin Nephrol Hypertens.*, pp. 9–15, 2004.

[218] J. Jin *et al.*, "Soluble FLT1 binds lipid microdomains in podocytes to control cell morphology and glomerular barrier function," *Cell*, vol. 151, pp. 349–399, 2012.

[219] S. A. Robertson and D. Ph, "Preventing Preeclampsia by Silencing Soluble Flt-1?," *N. Engl. J. Med.*, vol. 380, pp. 1080–1082, 2019.

[220] D. M. te Loo *et al.*, "Elevated levels of vascular endothelial growth factor in serum of patients with D+ HUS," *Pediatr. Nephrol.*, vol. 19, no. 7, pp. 754–760, 2004.

[221] Y. G. Kim *et al.*, "Vascular endothelial growth factor accelerates renal recovery in experimental thrombotic microangiopathy," *Kidney Int.*, vol. 58, no. 6, pp. 2390–2399, 2000.

[222] L. S. Keir *et al.*, "VEGF regulates local inhibitory complement proteins in the eye and kidney," *J. Clin. Invest.*, vol. 127, no. 1, pp. 199–214, 2017.

[223] M. A. Saleem *et al.*, "A conditionally immortalized human podocyte cell line demonstrating nephrin and podocin expression.," *J. Am. Soc. Nephrol.*, vol. 13, no. 3, pp. 630–8, 2002.

[224] L. S. Keir, R. Firth, C. May, L. Ni, G. I. Welsh, and M. A. Saleem, "Generating Conditionally Immortalised Podocyte Cell Lines from Wild-Type Mice," *Nephron*, vol. 129, no. 2, pp. 128–136, 2015.

[225] S. C. Satchell *et al.*, “Conditionally immortalized human glomerular endothelial cells expressing fenestrations in response to VEGF.,” *Kidney Int.*, vol. 69, no. 9, pp. 1633–40, 2006.

[226] L. Ni, M. Saleem, and P. W. Mathieson, “Podocyte culture: Tricks of the trade,” *Nephrology*, vol. 17, pp. 525–531, 2012.

[227] G. M. Baranzoni *et al.*, “Characterization of shiga toxin subtypes and virulence genes in porcine shiga toxin-producing Escherichia coli,” *Front. Microbiol.*, vol. 7, no. 574, pp. 1–10, 2016.

[228] Thermoscientific, “NanoDrop Lite: Interpretation of Nucleic Acid 260/280 Ratios,” *Protocols and Product Manuals: Technical bulletin T123. http://tools.thermofisher.com/content/sfs/brochures/T123-NanoDrop-Lite-Interpretation-of-Nucleic-Acid-260-280-Ratios*. 2012.

[229] C. W. Dieffenbach, T. M. J. Lowe, and G. S. Dveksler, “General concepts for PCR primer design,” *Genome Res.*, vol. 3, no. 3, pp. 30–37, 1993.

[230] J. Haimes and M. Kelley, “Demonstration of a ΔΔCq Calculation Method to Compute Relative Gene Expression from qPCR Data,” *GE Healthcare: https://horizondiscovery.com/Technical-manuals/delta-cq*. pp. 1–4, 2014.

[231] Dharmacon, “GIPZ ™ Lentiviral shRNA,” *Technical Manual: https://horizondiscovery.com/en/products/gene-modulation/knockdown-reagents*. pp. 1–17, 2017.

[232] M. Rabe and F. Schaefer, “Non-transgenic mouse models of kidney disease,” *Nephron*, vol. 133, no. 1, pp. 53–61, 2016.

[233] R. S. Sellers, C. B. Clifford, P. M. Treuting, and C. Brayton, “Immunological variation between inbred laboratory mouse strains: Points to consider in phenotyping genetically immunomodified mice,” *Vet. Pathol.*, vol. 49, no. 1, pp. 32–43, 2012.

[234] A. K. Beery, “Inclusion of females does not increase variability in rodent research studies,” *Curr. Opin. Behav. Sci.*, vol. 23, pp. 143–149, 2018.

[235] J. Tannenbaum and B. T. Bennett, “Russell and Burch’s 3Rs then and now: The need for clarity in definition and purpose,” *J. Am. Assoc. Lab. Anim. Sci.*, vol. 54, no. 2, pp. 120–132, 2015.

[236] MRC Harwell, “Mouse Genetics Research Institute,” *https://www.har.mrc.ac.uk/resources*. 2020.

[237] W. C. Skarnes *et al.*, “A conditional knockout resource for the genome-wide study of mouse gene function,” *Nature*, vol. 474, no. 7351, pp. 337–344, 2011.

[238] G. L. Kolling, F. Obata, L. K. Gross, and T. G. Obrig, “Immunohistologic techniques for detecting the glycolipid Gb3 in the mouse kidney and nervous system,” *Histochem Cell Biol*, vol. 130, pp. 157–164, 2008.

[239] S. J. Shankland, J. W. Pippin, J. Reiser, and P. Mundel, “Podocytes in culture: Past, present, and future,” *Kidney Int.*, vol. 72, no. 1, pp. 26–36, 2007.

[240] L. S. Keir, R. Firth, C. May, L. Ni, G. I. Welsh, and M. A. Saleem, “Generating

Conditionally Immortalised Podocyte Cell Lines from Wild-Type Mice," *Nephron*, vol. 129, no. 2. pp. 128–136, 2015.

[241] D. J. Montefusco, A. E. Asinas, and R. M. Weis, "Liposome-Mediated Assembly of Receptor Signaling Complexes," *Methods Enzymol.*, vol. 423, no. 7, pp. 267–298, 2007.

[242] J. Park *et al.*, "Long-term correction of globotriaosylceramide storage in Fabry mice by recombinant adeno- associated virus-mediated gene transfer," *PNAS*, vol. 100, no. 6, pp. 3450–3454, 2003.

[243] E. E. Bowen, R. Hangartner, and I. Macdougall, "Campylobacter-Associated Hemolytic Uremic Syndrome Associated with Pulmonary-Renal Syndrome," *J Gen Intern Med*, vol. 31, no. 3, pp. 353–6.

[244] G. Kaur and J. M. Dufour, "Cell lines: valuable tools or useless artefacts?," *Spermatogenesis*, vol. 2, no. 1, pp. 1–5, 2012.

[245] R&D Systems, "Dot Blot Protocol," *https://www.rndsystems.com/resources/protocols/dot-blot-protocol*. 2020.

[246] I. D. Doykov *et al.*, "Rapid, proteomic urine assay for monitoring progressive organ disease in Fabry disease," *J. Med. Genet.*, vol. 0, pp. 1–10, 2019.

[247] R.-B. R. O'Loughlin EV, "Effect of Shiga toxin and Shiga-like toxins on eukaryotic cells," *Microbes Infect.*, vol. 3, no. 6, pp. 493–507, May 2001.

[248] C. Hagel, S. Krasemann, J. Löffler, K. Püschel, T. Magnus, and M. Glatzel, "Upregulation of shiga toxin receptor CD77/Gb3 and interleukin-1β expression in the brain of EHEC patients with hemolytic uremic syndrome and neurologic symptoms," *Brain Pathol.*, vol. 25, pp. 146–156, 2015.

[249] A. Toupin *et al.*, "Analysis of globotriaosylceramide (Gb3) isoforms/analogs in unfractionated leukocytes, B lymphocytes and monocytes from Fabry patients using ultra-high performance liquid chromatography/tandem mass spectrometry," *Anal. Chim. Acta*, vol. 1015, pp. 35–49, 2018.

[250] S. S. Karve and A. A. Weiss, "Glycolipid binding preferences of shiga toxin variants," *PLoS ONE*, vol. 9, no. 7. 2014.

[251] L. De Petris, J. Patrick, E. Christen, and H. Trachtman, "Urinary podocyte mRNA excretion in children with D+HUS: A potential marker of long-term outcome," *Ren. Fail.*, vol. 28, no. 6, pp. 475–482, 2006.

[252] L. R. Yu, N. A. Stewart, and T. D. Veenstra, "Proteomics: The Deciphering of the Functional Genome," *Genomic and Personalized Medicine, Two-Vol Set*. pp. 173–179, 2009.

[253] E. S. Lander *et al.*, "Initial sequencing and analysis of the human genome," *Nature*, vol. 412, pp. 565–566, 2001.

[254] A. F. M. Altelaar, J. Munoz, and A. J. R. Heck, "Next-generation proteomics: Towards an integrative view of proteome dynamics," *Nat. Rev. Genet.*, vol. 14, no. 1, pp. 35–48, 2013.

[255] J. C. Chuang and P. A. Jones, “Epigenetics and microRNAs,” *Pediatr. Res.*, vol. 61, no. 5, pp. 24–29, 2007.

[256] J. Saba, “High Throughput Quantitative Proteomics Using Isobaric Tags,” *thermofisher.com/Reference-Materials/wp-65593-quantitative-proteomics-isobaric-tags*, 2018. .

[257] Bristol University, “Quantitative proteomics,” *https://www.bristol.ac.uk/life-sciences/research/facilities/proteomics*, 2020. .

[258] L. Ting, R. Rad, S. P. Gygi, and W. Haas, “MS3 eliminates ratio distortion in isobaric multiplexed quantitative proteomics,” *Nat. Methods*, vol. 8, no. 11, pp. 937–940, 2011.

[259] NIH (National Institutes of Health), “Ingenuity Pathways Analysis (IPA),” *https://www.nihlibrary.nih.gov/resources/tools/ingenuity-pathways-analysis-ipa*. 2020.

[260] Qiagen, “Ingenuity Pathway Analysis Knowledge Base,” *https://digitalinsights.qiagen.com/products-overview/clinical-insights-portfolio*. 2015.

[261] K. Hodge, S. Ten Have, L. Hutton, and A. I. Lamond, “Cleaning up the masses: Exclusion lists to reduce contamination with HPLC-MS/MS,” *J. Proteomics*, vol. 88, pp. 92–103, 2013.

[262] E. Torban *et al.*, “From podocyte biology to novel cures for glomerular disease,” *Kidney Int.*, vol. 96, no. 4, pp. 850–861, 2019.

[263] E. M. Campion, S. T. Loughran, and D. Walls, “Protein quantitation and analysis of purity,” *Methods in Molecular Biology*, vol. 1485. pp. 225–255, 2017.

[264] S. Lakshmanan, “How, When and Why Should You Normalize / Standardize / Rescale Your Data?,” *https://towardsai.net/p/data-science/how-when-and-why-should-you-normalize-standardize-rescale-your-data*. 2017.

[265] Y. H. W, Haynes, Dubitzky W., Wolkenhauer O., Cho KH., “Benjamini–Hochberg Method in Encyclopedia of Systems Biology. Springer, New York, NY.” Springer, pp. 9863–9867, 2013.

[266] D. Szklarczyk *et al.*, “STRING v11: Protein-protein association networks with increased coverage, supporting functional discovery in genome-wide experimental datasets,” *Nucleic Acids Res.*, vol. 47, no. D1, pp. D607–D613, 2019.

[267] A. C. Müller *et al.*, “Pathway enrichment analysis and visualization of omics data using g:Profiler, GSEA, Cytoscape and EnrichmentMap,” *Nat. Protoc.*, vol. 22, no. 1, pp. 924–934, 2019.

[268] S. Wang, R. Song, Z. Wang, Z. Jing, S. Wang, and J. Ma, “S100A8/A9 in inflammation,” *Front. Immunol.*, vol. 9, no. 1298, pp. 1–14, 2018.

[269] A. I. Nesvizhskii, O. Vitek, and R. Aebersold, “Analysis and validation of proteomic data generated by tandem mass spectrometry,” *Nat. Methods*, vol. 4, no. 10, pp. 787–797, 2007.

[270] D. C. Handler, D. Pascovici, M. Mirzaei, V. Gupta, G. H. Salekdeh, and P. A. Haynes, "The Art of Validating Quantitative Proteomics Data," *Proteomics*, vol. 18, no. 23, pp. 1–6, 2018.

[271] J. Song, X. Wang, Z. Zhang, L. Che, B. Fan, and G. Li, "Endoplasmic reticulum stress and the protein degradation system in ophthalmic diseases," *Peer J*, vol. 1, pp. 1–21, 2020.

[272] A. Weins, M. R. Pollak, and G. Basis, "CD2AP Inherited Nephroses," *Mol. Genet. Basis Ren. Dis.*, vol. 9, pp. 141–150, 2008.

[273] P. Saurus *et al.*, "Inhibition of SHIP2 in CD2AP-deficient podocytes ameliorates reactive oxygen species generation but aggravates apoptosis," *Sci. Rep.*, vol. 7, no. 1, pp. 1–14, 2017.

[274] K. A. Janes, "An analysis of critical factors for quantitative immunoblotting," *Sci. Signal.*, vol. 8, no. 371, pp. 1–12, 2015.

[275] S. Chei *et al.*, "Spirulina maxima extract prevents activation of the NLRP3 inflammasome by inhibiting ERK signaling," *Sci. Rep.*, vol. 10, no. 1, pp. 1–10, 2020.

[276] T. Komada and D. A. Muruve, "The role of inflammasomes in kidney disease," *Nature Reviews Nephrology*, vol. 15, no. 8. pp. 501–520, 2019.

[277] S. M. Kim *et al.*, "Inflammasome-independent role of NLRP3 mediates mitochondrial regulation in renal injury," *Front. Immunol.*, vol. 9, no. NOV, pp. 1–14, 2018.

[278] M. S. Lee *et al.*, "Shiga toxins activate the NLRP3 inflammasome pathway to promote both production of the proinflammatory cytokine interleukin-1β and apoptotic cell death," *Infect. Immun.*, vol. 84, no. 1, pp. 172–186, 2015.

[279] Sigma, "DIG Labeling Methods," *https://www.sigmaaldrich.com/technical-documents/articles/biology/roche/dig-labeling-methods.html*. 2020.

[280] A. Wolf-Yadlin, A. Hu, and W. S. Noble, "Technical advances in proteomics: New developments in data-independent acquisition," *F1000Research*, vol. 5, pp. 1–12, 2016.

[281] E. E. Gulcicek, C. M. Colangelo, W. Mcmurray, K. Stone, H. Spratt, and A. Kurosky, "Proteomics and the Analysis of Proteomic Data: An Overview of Current Protein-Profiling Technologies," *Curr. Protoc. Bioinforma.*, vol. 10, no. 1, pp. 1–31, 2005.

[282] J. Tuffin *et al.*, "A Composite Hydrogel Scaffold Permits Self-Organization and Matrix Deposition by Cocultured Human Glomerular Cells," *Advanced Healthcare Materials*, vol. 8, no. 17. 2019.

[283] I. Morace *et al.*, "Renal globotriaosylceramide facilitates tubular albumin absorption and its inhibition protects against acute kidney injury," *Kidney Int.*, vol. 96, no. 2, pp. 327–341, 2019.

[284] A. Labilloy and O. A. Weisz, "Lose the lipid: renoprotection conferred by Gb3 synthase knockout," *Kidney Int.*, vol. 96, no. 2, pp. 270–272, 2019.

[285] G. Dimeski, P. P. Masci, M. Trabi, M. F. Lavin, and J. De Jersey, "Evaluation of the

Becton-Dickinson rapid serum tube: Does it provide a suitable alternative to lithium heparin plasma tubes?," *Clin. Chem. Lab. Med.*, vol. 48, no. 5, pp. 651–657, 2010.

[286] L. Dean, "Blood Groups and Red Cell Antigens," in *The ABO blood group*, 2005, pp. 31–41.

[287] G. Jansma *et al.*, "Sepsis-related anemia is absent at hospital presentation; a retrospective cohort analysis," *BMC Anesthesiol.*, vol. 15, no. 1, pp. 1–6, 2015.

[288] W. Barcellini and B. Fattizzo, "Clinical Applications of Hemolytic Markers in the Differential Diagnosis and Management of Hemolytic Anemia," *Dis. Markers*, vol. 15, pp. 1–7, 2015.

[289] K. E. O'Connell *et al.*, "Practical murine hematopathology: A comparative review and implications for research," *Comp. Med.*, vol. 65, no. 2, pp. 96–113, 2015.

[290] P. Warwicker, "Thrombotic microangiopathies and the kidney," *Medicine*, vol. 47, no. 10. pp. 661–665, 2019.

[291] J. I. Park, H. Baek, B. R. Kim, and H. H. Jung, "Comparison of urine dipstick and albumin: Creatinine ratio for chronic kidney disease screening: A population-based study," *PLoS One*, vol. 12, no. 2, pp. 1–12, 2017.

[292] J. M. Spinale, R. L. Ruebner, L. Copelovitch, and B. S. Kaplan, "Long-term outcomes of Shiga toxin hemolytic uremic syndrome," *Pediatr. Nephrol.*, vol. 28, no. 11, pp. 2097–2105, 2013.

[293] J. Bergstein, "Glomerular fibrin deposition and removal," *Pediatr. Nephrol.*, vol. 4, pp. 78–87, 1990.

[294] H. Wada *et al.*, "Differences and similarities between disseminated intravascular coagulation and thrombotic microangiopathy," *Thromb. J.*, vol. 16, no. 1, pp. 1–7, 2018.

[295] M. Morigi *et al.*, "A previously unrecognized role of C3a in proteinuric progressive nephropathy," *Sci. Rep.*, vol. 6, no. June, pp. 1–13, 2016.

[296] S. W. Lesher AM, "Review: Complement and its regulatory proteins in kidney diseases," *Nephrology*, vol. 15, no. 7, pp. 663–675, 2010.

[297] M. E. A. Dobblesteen *et al.*, "Regulation of C3 and factor H synthesis of human glomerular mesangial cells by IL-1 and interferon-gamma," *Clin. Exp. Immunol.*, vol. 95, no. 1, pp. 173–180, 2008.

[298] T. Zoshima *et al.*, "Possible role of complement factor H in podocytes in clearing glomerular subendothelial immune complex deposits," *Sci. Rep.*, vol. 9, no. 1, pp. 1–9, 2019.

[299] H. Wang *et al.*, "Inhibition of Terminal Complement Components in Presensitised Transplant Recipients Prevents Antibody-Mediated Rejection Leading to Long-Term Graft Survival and Accomodation," *J. Immunol.*, vol. 179, pp. 4451–4463, 2020.

[300] D. Huugen *et al.*, "Inhibition of complement factor C5 protects against

glomerulonephritis in mice," *Kidney Int.*, vol. 71, no. 7, pp. 646–654, 2007.

[301] W. M. Zelek, P. R. Taylor, and B. P. Morgan, "Development and characterization of novel anti-C5 monoclonal antibodies capable of inhibiting complement in multiple species," *Immunology*, vol. 157, no. 4, pp. 283–295, 2019.

[302] R. Würzner, "Modulation of complement membrane attack by local C7 synthesis," *Clin. Exp. Immunol.*, vol. 121, no. 1, pp. 8–10, 2000.

[303] A. Devine, "Principles of the complement system," in *Blood Banking and Transfusion Medicine*, 2007, pp. 30–42.

[304] M. A. Lusco, A. B. Fogo, B. Najafian, and C. E. Alpers, "AJKD Atlas of Renal Pathology: Thrombotic Microangiopathy," *Am. J. Kidney Dis.*, vol. 68, no. 6, pp. e33–e34, 2016.

[305] D. Turnberg, M. Lewis, J. Moss, Y. Xu, M. Botto, and H. T. Cook, "Complement Activation Contributes to Both Glomerular and Tubulointerstitial Damage in Adriamycin Nephropathy in Mice," *J. Immunol.*, vol. 177, no. 6, pp. 4094–4102, 2006.

[306] V. J. Harkins, D. A. McAllister, and B. C. Reynolds, "Shiga-Toxin E. coli Hemolytic Uremic Syndrome: Review of Management and Long-term Outcome," *Curr. Pediatr. Rep.*, vol. 8, no. 1, pp. 16–25, 2020.

[307] K. A. Vernon, M. M. Ruseva, H. T. Cook, M. Botto, T. H. Malik, and M. C. Pickering, "Partial complement factor H deficiency associates with C3 glomerulopathy and thrombotic microangiopathy," *Journal of the American Society of Nephrology*, vol. 27, no. 5. pp. 1334–1342, 2016.

[308] A. K. Hughes, Z. Ergonal, P. K. Stricklett, and D. E. Kohan, "Molecular basis for high renal cell sensitivity to the cytotoxic effects of shigatoxin-1: Upregulation of globotriaosylceramide expression," *J. Am. Soc. Nephrol.*, vol. 13, no. 9, pp. 2239–2245, 2002.

[309] A. Angelucci, F. Clascá, and M. Sur, "Anterograde axonal tracing with the subunit B of cholera toxin: A highly sensitive immunohistochemical protocol for revealing fine axonal morphology in adult and neonatal brains," *J. Neurosci. Methods*, vol. 65, no. 1, pp. 101–112, 1996.

[310] A. Fluor, "Cholera Toxin Subunit B (CT-B) Conjugates," *J. Cell Biol.*, vol. 1252, no. 1980, pp. 34775–34776, 2003.

[311] S. Payne, S. De Val, and A. Neal, "Endothelial-specific cre mouse models is your cre CREdibile?," *Arterioscler. Thromb. Vasc. Biol.*, vol. 38, no. 11, pp. 2550–2561, 2018.

Chapter 12 : Appendix

All reagents are from Sigma-Aldrich unless stated.

12.1 *In vitro* work reagents

12.1.1 Cell culture work

Podocyte cell media:

RPMI-1640 (500ml) with L-glutamine and sodium bicarbonate (Sigma-Aldrich)

Heat inactivated Fetal Bovine Serum (FBS 50ml) (Life technologies)

Penicillin and Streptomycin (10ml) (Sigma-Aldrich)

Endothelial cell media:

EGM-2V Basal Medium (500mls) (Lonza Biologics PLC)

EGM-2V Bullet kit™ (Lonza Biologics PLC) – added as supplied except for VEGF which was discarded.

HeLa cell media:

DMEM/F12 (500mls) (Fisher Scientific)

Freezing Solution:

FBS (5mls) (Life technologies)

Cell specific media made up as above (4mls)

Dimethyl sulphoxide (DMSO) (1ml) (Sigma-Aldrich)

Basic Reagents:

- Trypsin-EDTA 0.25% - 1% (Sigma-Aldrich)
- Trypan blue 0.4% (Biosystems)
- 4% paraformaldehyde (PFA) in PBS (Santa Cruz)
- Phosphate buffered saline (PBS): *made up in 10L of distilled water*: 80g sodium chloride, 2g potassium chloride, 14.4g of disodium hydrogen phosphate and 2.4g potassium hydrogen phosphate. Stir and adjust pH to 7.4.

- Bovine Serum Albumin 5% solution: add 2.5g to 50mls distilled water (for IF) or TBST (for western blotting).

12.1.2 Western blotting reagents

RIPA Buffer:

For 250mls (make up in distilled water):

2.2g sodium chloride (150mM)

2.5ml Triton X 100 (1%)

1.25g sodium deoxycholate (0.5%)

0.25g sodium dodecyl sulphate (0.1%)

1.51g Tris (pH 8 with HCl, 50mM)

Cell lysis buffer for protein extraction:

For 500µL of cell lysis buffer (required per T75 flask of cells):

485µL of cold RIPA buffer (made as above) with 5µL of phosphatise inhibitor cocktail A, 5µl phosphatise inhibitor cocktail B and 5µl protease inhibitor (all Sigma-Aldrich)

Sample buffer: (x2)

Add to 3.4ml of distilled water: 1ml of 0.5M Tris, 2ml glycerol, 1.6ml 10% SDS, 50µl mercaptoethanol and sprinkle of bromophenol blue for blue colour to facilitate easy sample loading.

Reducing gel recipe for western blotting: x2 gels (all reagents from Fisher Scientific)

	Stacking gel (4%)	7.5% Running	10% Running	15% Running
Acrylamide (30%) (ml)	1.25	5	6.7	10
dH20 (ml)	5.65	11.3	9.6	6.3
0.5M Tris pH 6.8 (ml)	2.5	-	-	-
3M Tris pH 8.8 (ml)	-	2.5	2.5	2.5
SDS (10%) (µl)	100	200	200	200

APS (100mg/ml) (ml)	0.5	1	1	1
TEMED (µl)	5	10	10	10

Non-reducing gel recipe for western blotting:

As above but all gels made without SDS

Sample buffer made without SDS or beta mercaptoethanol

Running buffer made without SDS

Running buffer (10x stock):

30.3g Tris base, 144g Glycine, 10g SDS. 100ml diluted in 900ml of distilled water to make 1L of 1x running buffer.

Transfer buffer (10x stock):

30g Tris base, 144g Glycine. 100ml diluted with 100ml methanol in 800ml of distilled water to make 1L of 1x transfer buffer.

Tris buffered saline plus Tween (TBST) (10x stock):

24.33g Tris base, 80.06g sodium chloride, pH 7.5 with HCl. Dilute 100mls with 10ml Tween 20 in 890ml distilled water.

0.5M Tris pH 6.8: 6.057g Tris base in 100ml dH2O make to pH 6.8 with HCl.

3M Tris pH 8.8: 36.342g Tris base in 100ml dH2O make to pH 8.8 with HCl.

Ammonium persulphate (APS): 0.6g added to 2ml

Western ECL substrate (Biorad)

Luminol Enhancer solution / Peroxidase (Biorad)

Primary antibodies used for western blotting:

Name	Species	Supplier	Concentration
Nephrin	Guinea pig IgG	Progen (#GP-N2)	1 in 1000
Synaptopodin	Rabbit IgG	Santa Cruz (#sc-50459)	1 in 1000

β-actin	Mouse IgG	Sigma Aldrich (#A1978)	1 in 10,000
ATF6	Rabbit IgG	Abcam (#ab37149)	1 in 1000
p38	Rabbit IgG	Abcam (#ab197348)	1 in 1000
pIRE	Rabbit IgG	Abcam (#ab48187)	1 in 1000
CHOP	Mouse IgG	Abcam (#ab11419)	1 in 1000
GRP78	Rabbit IgG	Cell Signalling (#31775)	1 in 1000
CD2AP	Rabbit IgG	Cell Signalling (#2135)	1 in 1000
NLRP3	Rabbit IgG	Cell Signalling (#15101)	1 in 1000

Secondary Antibodies for western blotting: all HRP conjugated.

Anti-rabbit IgG (Sigma) used at 1 in 10,000 (used for all primary antibody rabbit IgG species in table above).

Anti-mouse IgG (Sigma) used at 1 in 10,000 (used for all primary antibody mouse IgG species in the table above).

Anti-guinea pig IgG (Sigma) used at 1 in 10,000 (used for primary nephrin antibody in table above).

12.1.3 Immunofluorescence antibodies

Primary Antibodies:

Name	Species	Supplier	Concentration
Gb3 / CD77	Rat IgM	Beckman Coulter (#IM0175)	1 in 100
Nephrin	Guinea pig IgG	2B Scientific (#BP5030)	1 in 400
Podocin	Rabbit IgG	Sigma Aldrich (#P0372)	1 in 400
PECAM / CD31	Rabbit IgG	Abcam (#ab124432)	1 in 50
PECAM/ CD31	Rat IgG	BD Bioscience (#553370)	1 in 200
C3b (Mouse)	Rat IgG	Hycult Biotech (#HM1065)	1 in 100
C3d (Human) *non-specific for C3d also detects C3b and iC3b.	Mouse IgG	Abcam (#ab17453)	1 in 100
Complement factor H (Mouse)	Mouse IgG	Hycult Biotech (#HM1119)	1 in 100

Complement factor H (Human)	Goat IgG	Quidel (#A312)	1 in 100
Fibrinogen (FITC conjugated)	Rabbit IgG	Dako (F0111)	1 in 100
C5b-C9	Rabbit IgG	Abcam (#ab55811)	1 in 50
C7	Rat IgG	Gift from Prof. Paul Morgan (Cardiff)	1 in 100
C9	Mouse IgG	Gift from Prof. Paul Morgan (Cardiff)	1 in 100

Secondary Antibodies:

All fluorescently labelled secondary antibodies used in IF were Alexa Fluor conjugated and from Life Technologies.

All were used at a concentration of 1 in 200.

Primary Antibody (see table above)	**Secondary Antibody pairing**	**Fluorophore**
PECAM from BD Bioscience / C3b (Mouse) / C7	Anti-rat IgG	AF 488 or AF 568
Gb3 / CD77	Anti-rat IgM	AF488
Nephrin	Anti-guinea pig IgG	AF 546 or AF 568 or AF 647
Podocin / PECAM from Abcam / C5b-C9	Anti-rabbit IgG	AF 488 or AF 546
C3d (human) / CFH (mouse) / C9	Anti-mouse IgG	AF 488 or AF 594
CFH (human)	Anti-goat IgG	AF 594

DAPI stain used for IN Cell work was used at a concentration of 1 in 10,000 (Sigma Aldrich).

Vecta Shield hard setting mount with DAPI was used for IF on coverslips (Vector Labs, Maravai Life Sciences).

12.2 *In vivo* work reagents

12.2.1 Genotyping

PCR reaction mix: Hotmaster Taq polymerase from 5 prime (#2200410)

Reaction set-up:

1ul - 10uM F and R Primer

2.5ul - 10x HotMaster Taq Buffer

0.5ul - 10mM dNTPs

0.25ul - HotMaster Taq DNA Polymerase

18.75ul - dH_2O

Primers:

A4GALT KO mice:

TM1a assay

A4galt 5arm-WTF	CTAAGCCCAGGTCTTCATGC
A4galt Crit-WTR	GGACCAGAAGCGATGTGTCT
A4galt 5mut-R1	GAACTTCGGAATAGGAACTTCG

Programme:

95ºC 1min

95ºC 10sec}

60ºC 10sec} 30 cycles

72ºC 1sec}

72ºC 30sec

WT band – 231

KO band – 128

Primers:

TM1b assay

A4galt Crit-WTF TTCCACAGATGGGAACAGGC

A4galt 3arm-WTR GGCTGTGGCTAGCACCTATT

A4galt LacZ-F CCAGTTGGTCTGGTGTCA

Programme:

95ºC 1min

95ºC 10sec}

58ºC 10sec} 30 cycles

72ºC 1sec}

72ºC 30sec

WT band – 259

KO band – ~400

PodrtTA-Tet-O-Gb3 mice:

Primers Podocin rtTA (product size 400 bp)

Forward 5' CGCACTTCAGTTACTTCAGGTCCTC 3'

Reverse 5' GCTTATGCCTGATGTTGATGATGC 3'

TetO-GB3 synthase (product size 513 bp)

Forward 5': ATAGAAGACACCGGGACCGA 3’

Reverse 5’: CTTGCAAGTCCAGAGGTCGT 3’

Programmes:

Podocin rtTA

Denature 95°C 1min

Denature 94°C 45s

Anneal 51°C 45s

Elongation 72°C 1m

Repeat steps 2-4 38 times

Elongation 72°C 7 m Hold 15°C forever

Tet-O Gb3 Synthase

Denature 94°C 2minutes

Denature 94°C 30 seconds

Anneal 46°C 30s

Elongation 68°C 1m 25s

Repeat steps 2-4 35 times

Elongation 68°C 10mins

Hold 15°C forever

Touch down

Denature 94°C 2m

Denature 94°C 30s

Anneal 68°C 20s-reduce by 2°C ever cycle

Elongation 68°C 1m 15s

Repeat steps 2-4 10 times

Denature 94°C 30s Anneal 46°C 30s

Elongation 68°C 1m 30s

Repeat steps 5-7 25 times

Elongation 68°C 10m

Hold 15°C forever

12.2.2 Endpoint PCR Primers

Human A4GALT: (109 bp product)

Forward 5’ GTCTGCACCCTGTTCATCATC 3’

Reverse 5’ GCAGGTTATAGAGCTGCCCT 3’

Mouse A4GALT: (114 bp product)

Forward 5’ TCTTCTTCCTAGAGACATCGGAC 3’

Reverse 5’ CCCTTTCATCAGCACAACCA 3’

12.2.3 Quantitative PCR

From the Sigma SYBR green website the master mix is made up with:

10µl of SYBR green (SYBR Green JumpStart Taq Ready Mix, #S9194),

0.4µl of forward primer (at 10nM concentration)

0.4µl of reverse primer (at 10nM concentration)

4.2µl of RNAse/DNAse free water

Total volume of 15µl of master mix – keep on ice.

Note: to this mastermix add diluted cDNA sample from stock of prepared cDNA: optimal dilution of your sample for the primer you are using will have been calculated from a standard curve experiment see main methods.

Cycle steps:

Denaturation temperature 95°C 20s

Annealing temperature 60°C 20s

Elongation temperature 72°C 20s

12.2.4 Restriction Digest Reaction Mix:

Enzyme 1 µL (used either Ecor1 or XbaI)

DNA plasmid 3 µL

*Buffer (10x) 5 µL

DPEC water = make up to 50 µL final reaction volume

*Buffer is determined by restriction enzymes used.

All enzymes and buffers used were bought from New England biolabs (NEB).

The NEB website provides a table indicating which buffer is best to use with each enzyme.

12.2.5 Agarose Gels

Ingredient (100 ml gel)	1%	2%
1x TRIS-acetate-EDTA buffer	100mls	100mls
Agarose	1g	2g

This mix is heated in a microwave on full power until clear.

It is then cooled until it is 'hand hot' and Midori green advance (Geneflow #S6-0222) DNA stain is added to allow visualisation of DNA. The gel is then poured in to moulds and left to set.

Gels are run in 1x Tris Acetate (TAE) buffer (Severn Biotech #20-6001-10)

12.2.6 Lysogeny Broth (LB) Agar

LB To make 1L (add to distilled water):

10g Trypton (#T7293)

5g yeast (#51475)

10g of sodium chloride (#S3014)

Aliquot the broth into glass bottles, seal and autoclave them. Then store at room temperature until use.

Agar plates:

Make the LB as above add 15g/L prior to autoclaving the solution.

To prepare the plates: heat the solution to 55°C in the microwave.

Allow to cool at room temperature and add antibiotic (Ampicillin 100ug/ml) to the solution and pour into plates. Allow to cool and solidify at room temperature prior to use.

12.2.7 Glomerular isolation

Dynabeads® for glomerular isolation were from Invitrogen (Thermofisher Scientific)

DNASe I (Life technologies)

HBSS-Hank's Balanced Salt Solution (Fisher Scientific)

Collagenase A (Roche) stock solution made up in HBSS (10mg/ml)

RNA Later™ – RNA stabilisation agent (Qiagen)

12.2.8 Immunohistochemistry (IHC) of formalin fixed tissue

De-paraffinisation Protocol:

Tissue sections are treated with in a step wise process:

Xylene (histoclear) 100% 5 minutes x2

Ethanol 100% 5 minutes x1

Ethanol 90% 5 minutes x1

Ethanol 70% 5 minutes x1

Ethanol 50% 5 minutes x1

Distilled H_20 5 minutes x1

100mM Citrate Buffer: (pH 6 – correct with 1M HCL)

29.4g of Tri-sodium citrate to 1L distilled water.

10mM Citrate Buffer:

Dilute 100mM stock buffer 1 in 10 with distilled water and add 500µL of Tween 20 to each 1L.

Primary Antibodies:

Rabbit IgG Fibrinogen antibody (Abcam #ab34269) used at 1 in 50.

Rat IgM Gb3 antibody (Beckman Coulter #IM0175) used at 1 in 100.

Secondary Antibodies:

SignalStain® Boost detection Reagent anti-rabbit (Cell Signalling #8114) 1-3 drops

SignalStain® DAB chromogen concentrate (Cell Signalling #8059P)

SignalStain® DAB diluent (Cell signalling #8059P)

Biotinylated anti rat IgM secondary (Abcam #97178) used at 1 in 200.

Streptavidin was from (Sigma) used at 1 in 20.

Haematoxylin (Sigma #H3136)

12.2.9 In Situ Hybridisation Buffers and Reagents

DIG labelling mix reagents: (for riboprobe DIG labelling)

Reagent	1x	3x	6x
DEPC H_20 (Thermosfisher #AM9922)	10.5 µl	31.5 µl	63 µl
10x transcription buffer (Sigma: included in DIG labelling kit)	2 µl	6 µl	12 µl

100mM DTT (Promega #P1171)	2 µl	6 µl	12 µl
10x DIG labelling mix (Sigma #11175025910)	2 µl	6 µl	12 µl
Ribonuclease inhibitor (100U/µl) (Promega #N2111)	1 µl	3 µl	6 µl
T3/T7 RNA polymerase (10U/µl) (Sigma #11031163001)	2 µl	6 µl	12 µl
Linearised plasmid (1µg/µl) *VEGF-A gifted from Dr M Stevens*	1 µl	3 µl	6 µl

1x DEPC Phosphate buffer saline (PBS):

8 g NaCl

0.2 g KCl

1.44 g Na2HPO4

0.24 g KH2PO4

Add to 1L DEPC H2O, pH 7 with HCl

Hybridisation buffer:

Reagent	**Final concentration**	**50ml**	**100ml**
Formamide (Sigma #47671)	50%	25ml	50ml
20x SSC (pH 7.0) (Sigma #S6639)	5X	12.5ml	25ml
20% CHAPS	0.5%	1.25ml	2.5ml
10% triton X-100	0.1%	500ul	1ml
10mg/ml yeast RNA (Sigma #10109223001)	50ug/ml	250ul	500ul
20 mg/ml heparin (Sigma #H4784)	50ug/ml	125ul	250ul
0.5 EDTA	5mM	500ul	1ml
Blocking powder (Sigma #11096176001)	2%	1g	2g
DEPC H_20 (Thermosfisher #AM9922)	-	6ml	12ml

NT buffer: (pH 7.5)

Total volume	200ml
H_20	187.3ml
3M Tris pH 7.5	6.67ml
5M NaCl	6ml

For NT blocking buffer:

10x solution: 1g of blocking reagent (Sigma # 11096176001) added to 10mls of NT wash buffer, agitate to dissolve.

Dilute to 1x prior to use with freshly made NT buffer.

APB Buffer:

Total volume	200ml	400ml
1M Tris (pH 9.5)	20 ml	40ml
5M NaCl	4ml	8ml
1M $MgCl_2$	10ml	20ml
10% Tween 20	2ml	4ml
2M Levamisole (Sigma #L9756)	200ul	400ul
H_20	164ml	328ml

12.2.10 Bristol animal welfare score (BAWS):

All animal experiments undertaken during this PhD involved at least twice daily scoring of mice according to the generic Bristol animal welfare scoring system shown below:

Appearance:

Description	Score
Normal	0
General lack of grooming	2
Coat stirring, ocular and nasal discharge	4
Piloerection, hunched up	6

Weight:

Description	Score
No weight loss	0
<5% loss	1
10-15% loss	2

>15% loss over 3 days	3

Clinical Signs:

Description	Score
Normal temperature, pulse, respiration (TPR)	0
Slight change in TPR	1
T+/-1°C, PR+/-30%	2
T+/-2°C, PR+/-50%	3

Natural behaviour:

Description	Score
Normal	0
Minor changes	1
Less active	2
Very still or restless, self-mutilation, vocalisation	3

Provoked behaviour:

Description	Score
Normal	0
Minor depression/exaggeration in response	1
Moderate change in expected behaviour	2
Reacts violently / weak and comatose	3

Scoring and action to be taken:

If any parameters score 3 more than once, then add 3 extra points to total score.

Normal = 0-4

Monitor carefully = 5-9

Observe more frequently and discuss with named vet = 9-14

Substantial adverse effects, terminate and consider experimental design change = 15-20

Awards and Achievements

Awards:

Best Scientific Abstract Award – UK Kidney Week (UKKW) 2020

Young Investigator of the Year Award – The Renal Association 2018

First author abstracts selected for presentation at the following meetings:

'The Role of the Podocyte in Shiga Toxin Associated Haemolytic Uraemic Syndrome.' **Renal Association Meeting UK Kidney Week**, Birmingham, June 2020.

'The Role of complement in Shiga Toxin Associated Haemolytic Uraemic Syndrome.' **Clinical Academy of Medical Sciences: Clinical Academics in Training Annual Conference**, Bristol, May 2020.

'The Role of complement in Shiga Toxin Associated Haemolytic Uraemic Syndrome.' **6th Complement UK Symposium**, Cardiff, March 2020.

'The Role of the Podocyte in Shiga toxin Associated Haemolytic Syndrome.' **Kidney Research UK Fellows Day**, Leicester, September 2019.

'The Role of the Podocyte in Shiga Toxin Associated Haemolytic Uraemic Syndrome.' **Renal Association Meeting UK Kidney Week**, Harrogate, June 2018.

Publications:

Bowen EE, Hangartner R, Macdougall I. 'Campylobacter Associated Hemolytic Uremic Syndrome Associated with Pulmonary Renal Syndrome'. *Journal of General Internal Medicine* 2016, 353-356. PMID 26001543.

Bowen EE, Coward RJC. 'Advances in our Understanding of the Pathogenesis of Hemolytic Uremic Syndromes'. *Am Journal Physiology Renal Physiol* 2018, 314(3) F454-F461. PMID 29167171.

Grants awarded for students under my supervision during this PhD:

Kidney Research UK (KRUK) intercalated BSc studentship 2018/2019

For 3rd year medical student Eva Larkai at the University of Bristol to 'Investigate the role of the podocyte in Shiga toxin associated HUS.' Student obtained a 1st Class Honours degree and completed a basic science project.

INSPIRE Academy of Medical Sciences Grant 2018

For 2nd year medical student Eva Larkai at the University of Bristol to perform proteomic validation work. Student went on to continue with her interest in basic Science by completing an intercalated BSc in our laboratory under my supervision.